THROUGH A GLASS, DARKLY: THE INFLUENCE OF THE EEG REFERENCE ON INFERENCE ABOUT BRAIN FUNCTION AND DISORDERS

EDITED BY: Pedro Antonio Valdes-Sosa, Paul L. Nunez, Jorge J. Riera, Maria L. Bringas and Rui Zhang

PUBLISHED IN: Frontiers in Neuroscience

frontiers Research Topics

frontiers

ISSN 1664-8714
ISBN 978-2-88963-440-8
DOI 10.3389/978-2-88963-440-8

About Frontiers

Frontiers is more than just an open-access publisher of scholarly articles: it is a pioneering approach to the world of academia, radically improving the way scholarly research is managed. The grand vision of Frontiers is a world where all people have an equal opportunity to seek, share and generate knowledge. Frontiers provides immediate and permanent online open access to all its publications, but this alone is not enough to realize our grand goals.

Frontiers Journal Series

The Frontiers Journal Series is a multi-tier and interdisciplinary set of open-access, online journals, promising a paradigm shift from the current review, selection and dissemination processes in academic publishing. All Frontiers journals are driven by researchers for researchers; therefore, they constitute a service to the scholarly community. At the same time, the Frontiers Journal Series operates on a revolutionary invention, the tiered publishing system, initially addressing specific communities of scholars, and gradually climbing up to broader public understanding, thus serving the interests of the lay society, too.

Dedication to Quality

Each Frontiers article is a landmark of the highest quality, thanks to genuinely collaborative interactions between authors and review editors, who include some of the world's best academicians. Research must be certified by peers before entering a stream of knowledge that may eventually reach the public - and shape society; therefore, Frontiers only applies the most rigorous and unbiased reviews.
Frontiers revolutionizes research publishing by freely delivering the most outstanding research, evaluated with no bias from both the academic and social point of view. By applying the most advanced information technologies, Frontiers is catapulting scholarly publishing into a new generation.

What are Frontiers Research Topics?

Frontiers Research Topics are very popular trademarks of the Frontiers Journals Series: they are collections of at least ten articles, all centered on a particular subject. With their unique mix of varied contributions from Original Research to Review Articles, Frontiers Research Topics unify the most influential researchers, the latest key findings and historical advances in a hot research area! Find out more on how to host your own Frontiers Research Topic or contribute to one as an author by contacting the Frontiers Editorial Office: researchtopics@frontiersin.org

THROUGH A GLASS, DARKLY: THE INFLUENCE OF THE EEG REFERENCE ON INFERENCE ABOUT BRAIN FUNCTION AND DISORDERS

Topic Editors:
Pedro Antonio Valdes-Sosa, Clinical Hospital of Chengdu Brain Science Institute, China
Paul L. Nunez, Tulane University, United States
Jorge J. Riera, Florida International University, United States
Maria L. Bringas, Clinical Hospital of Chengdu Brain Science Institute, China
Rui Zhang, Zhengzhou University, China

Citation: Valdes-Sosa, P. A., Nunez, P. L., Riera, J. J., Bringas, M. L., Zhang, R., eds. (2020). Through a Glass, Darkly: The Influence of the EEG Reference on Inference About Brain Function and Disorders. Lausanne: Frontiers Media SA. doi: 10.3389/978-2-88963-440-8

Table of Contents

frontiers in Neuroscience

EDITORIAL
published: 12 December 2019
doi: 10.3389/fnins.2019.01341

Editorial: Through a Glass, Darkly: The Influence of the EEG Reference on Inference About Brain Function and Disorders

Maria L. Bringas Vega[1], *Paul Nunez*[2], *Jorge Riera*[3], *Rui Zhang*[4] and *Pedro A. Valdes-Sosa*[1,5]*

[1] The Clinical Hospital of Chengdu Brain Science Institute, MOE Key Lab for Neuroinformation, University of Electronic Science and Technology of China, Chengdu, China, [2] Tulane University, New Orleans, LA, United States, [3] Department of Biomedical Engineering, Florida International University, Miami, FL, United States, [4] Henan Key Laboratory of Brain Science and Brain-Computer Interface Technology, School of Electrical Engineering, Zhengzhou University, Zhengzhou, China, [5] Neuroinformatics Department, Cuban Neuroscience Center, Havana, Cuba

Keywords: reference, EEG, ERPs, inference, Laplacian, average, rest

Editorial on the Research Topic

Through a Glass, Darkly: The Influence of the EEG Reference on Inference About Brain Function and Disorders

This Research Topic summarizes recent advances in a conflictive and controversy laden topic in neurophysiology: the selection of the electroencephalographic reference that is best for inference about brain function. Since its discovery, the human EEG has proven itself an indispensable tool for brain research. Despite this success story, there is a fundamental technical issue that has yet to be solve: selection of the correct EEG reference. Ideally one would like to measure neural activity restricted to certain brain regions. Since EEG amplifiers measure potential difference between the activities recorded by two electrodes, in addition to the active electrode, one must employ a reference electrode which should ideally be at zero. In theory, this might be achieved by placing the reference at a point infinitely far away. Yet the "infinite reference," in practice, is an antenna for ambient noise which would pre-empt brain measurements—for example cephalic references that minimize unwanted signal pickup. Examples of such references are the unilateral-mastoid, ear, linked mastoids or ears, vertex, the tip of the nose, neck ring, etc. Unfortunately, all such references are doomed to fail since there is no point on the scalp or body surface where the potential is actually zero or a constant. This has serious consequences since the non-neutral reference may itself reflect physiological dynamic processes that will be inevitably embedded into all EEG recordings. Without solving the reference issue, we are looking at brain activity, as it were, "through a glass, darkly."

This Research Topic focused the comparison of the effect that various EEG references may have on inference about brain function and disorders—with respect to both physical and computational issues. The crucial point is to determine the reference that best identifies neural activity and therefore be the basis of improved estimates of various linear and non-linear EEG features. These include spectra, amplitude, latency, coherence/correlation, network, symmetry/asymmetry, fractal dimension, complexity, covariance, and related statistical tests. If a single reference can be finally recognized universally as the optimal one for general use, we will have indeed rendered the "glass less opaque" and thus "know in part" more about brain function.

Recent attempts to make this "glass" more transparent have been based on mathematically constructing a reference based on physical principles and subtracting it from all EEG recordings.

OPEN ACCESS

Edited and reviewed by:
Srikantan S. Nagarajan, University of California, San Francisco, United States

***Correspondence:**
Pedro A. Valdes-Sosa
pedro.valdes.sosa@gmail.com

Specialty section:
This article was submitted to Brain Imaging Methods, a section of the journal Frontiers in Neuroscience

Received: *28 August 2019*
Accepted: *28 November 2019*
Published: *12 December 2019*

Citation:
Bringas Vega ML, Nunez P, Riera J, Zhang R and Valdes-Sosa PA (2019) Editorial: Through a Glass, Darkly: The Influence of the EEG Reference on Inference About Brain Function and Disorders. Front. Neurosci. 13:1341. doi: 10.3389/fnins.2019.01341

The best-known example is the average reference (AVE). Originally proposed with an analog implementation, it was heuristically espoused by Lehman (1971) and later theoretically justified since the average of a dipole potential over a spherical surface is zero. Consequently, the AVE might be a good choice when a dense and whole brain coverage of an EEG montage is available, which explains why it is widely accepted. Nevertheless, AVE has poor performance with a lower number of electrodes.

An alternative is the Reference Electrode Standardization Technique (REST; Yao, 2001) which used a re-referencing method to reconstruct the desired zero or neutral reference, based on the fact that the underlying neural sources are the same no matter what a reference is actually adopted.

Here we present contributions related to methodological and theoretical aspects of the influence of the reference in the continuous EEG (8 papers), at different electrophysiological experimental situations using event-related potentials and fMRI-EEG simultaneous recordings (9 papers), in pathological populations (2 papers), and the proposal of an open source toolbox to implement and estimate REST (1 paper). All of them, providing evidences about the scenarios where one reference can be more reliable than others.

Regarding the methodological and theoretical aspects, we want to highlight the original theoretical framework proposed by Hu et al. where the reference is conceptualized as a unified inverse problem that can be solved via bayesian techniques, employing a regularization method to estimate the potential referenced to infinity. They demonstrated that (REST) and (AVE) are special cases of the unified estimator with different EEG spatial covariance priors and after regularization have superior performance for both simulation and real data (rREST and rAVE). Other paper discussed the role of two references AR and REST (Zheng et al.) but during using three brain states, closed and open eyes and listening to music, from the perspective of alpha blocking, brain lateralization effects, functional connectivity density and weighted small-world network characteristics. They didn't find differences in the alpha blocking, but REST exhibited greater effects than AR for the lateralization effect, for the small-world network parameters, for all frequency bands and for functional connectivity density in closed eyes condition. Music also was employed by Wu, using music on the scalp derived from data in the brain (simulated and real) from three different references REST, average (AR) and linked mastoids (LM). They found in the simulation for only one source, different references do not change the music/waveform; for two sources or more, REST provide the most faithful music/waveform to the original ones inside the brain, and the distortions caused by AR and LM influenced spatial locations of both source and scalp electrode.

Olejarczyk et al. directed their research to the phenomenological origins of the alpha peak, testing the impact of window size and choice of reference electrode (REST or AR) on the identification of two or more peaks with close frequencies in the spectral power distribution, so called "split alpha." She found that for the occipital alpha wave generators, the presence of occipital split alpha peaks may be associated with variation in inter-hemispheric connectivity, which leads to relatively independent activity of occipital alpha wave generators in left and right hemispheres. The re-referenced data using the REST technique suggested that the split alpha effect may be driven by an interaction between the occipital and temporo-parietal areas, rather than between left and right occipital lobes. Current spectral density (CSD), frequently used to reduce the effect of volume conduction, was employed because its transform is free from reference effects, so the highest correlation between CSD and REST should be expected, but this paper showed that CSD correlated better with AR than with REST, which may be due to the use of low-density EEG data. In sum, this results suggest that recording montage, duration of the analytical window, and EEG activity dynamics should be considered when collecting and analyzing EEG data.

Trujillo et al. performed a comprehensive investigation into the effect of the EEG using information-theoretic measures of integration I(X), which are relatively robust to volume-conduction artifacts across all four EEG references (REST, AR, Laplacian, and LM) when comparing resting state condition differences. The authors found that measuring EEG complexity and integration during resting states or similar tasks that involve ongoing, relatively stationary EEG signals, is better to use the Laplacian-transformation due to its positive impact on EEG signal quality, sharpening of source topography, reduction of volume-conduction effects, and the resultant positive effect these have on the measurement of complexity and integration. On the other comparison, surface Laplacian was more suitable (Wong et al.) when compared with average mastoid, common average and REST on the spatial filter, timing and scalp distribution of ERP elicited during task-switching. The surface Laplacian transformation characterized better the EEG signatures from the complex spatiotemporal networks involved in cognitive control.

Related to estimation of functional connectivity (Huang et al.) emphasized the influence of the reference and tested this comparing REST, AR, and LM using two simulations with 300 or 20 dipole pairs located on the superficial cortex with a radial source direction. The relative error and hamming distance were employed as metrics of scalp functional connectivity graph (FCG) and found that REST not only achieves excellent performance for superficial and radial dipolar sources, but also achieves a stable and robust performance with variable source locations and orientations. Benefitting from the stable and robust performance of REST vs. other reference methods, REST might best recover the real FCG of EEG.

For the analysis of the non-linear features of EEG signals through bicoherence (Chella et al.) investigated the effects of the reference choice [vertex electrode (Cz), the digitally linked mastoids, the average and REST] for the estimation of cross-frequency EEG connectivity through two different non-linear measures, i.e., the cross-bicoherence and the antisymmetric cross-bicoherence. The results in simulations and real EEG experiment demonstrated the superior performance of REST than all the other references.

A system perspective of the influence of EEG reference was provided by Lei and Liao who examined the EEG signals associated with the locations from a common network parcellation of the human brain function. He performed

simulations, vertices uniformly distributed in eight large-scale brain networks: visual, somatomotor, dorsal attention, ventral attention, limbic, frontoparietal, default networks, and the deep brain structure, were adopted to generate the scalp EEG. Simulated data were referenced at the FCz, the Oz, the mean mastoids (MM), the average (AVE), and (REST) and using the relative error from the theoretical potential and the re-referenced potential followed the pattern REST<AVE<MM<(FCz, Oz), regardless of the number of electrodes and signal-to-noise ratios. This suggested that REST was a potentially preferable reference for all large-scale networks and AVE virtually performed as REST under several conditions. A group of contributions are presented related to electrophysiological experimental situations using event-related potentials (ERPs) and fMRI-EEG. Tian et al. designed a ERP experiment using the time-varying network analysis to study the flow of information from right to left hemisphere in the N170 component elicited by a face recognition task, comparing REST and AR both with simulation and experimental data. She found that AR induced changes in amplitude and latency, but REST obtained more precise outcomes. Li et al. using ERP and semantic and gambling tasks, with an intrasubject approach, studied which reference was optimal to identify the N400 and the feedback-related negativity (FRN) components, the later preferably studied using linked mastoid (LM) reference method. In this approach, the authors did the systematic comparison with REST and AR. The results confirmed that LM exhibits the higher magnitude of the components, followed by REST and AR.

In the particular case of the readiness potential (RP) (Hu et al.) analyzed its waveform and voltage topographies under the influence of REST, AR, and Cz references. Since the Cz channel is near the primary motor cortex, where the source of RP is located, this reference was not recommended. REST and Common AR references getting the more accurate RP waveforms and voltage topographies.

Liang et al. studied the auditory event-related potential (AEP) in children with cochlear implants comparing the common references employed in AEP: nose reference (NR), mastoid reference (MR), and montage average reference (MAR) to identify their advantages. The results showed how the P1 amplitude is significantly larger with contralateral MR than with NR and MAR and has a greater ability to distinguish control healthy children from children with ear malformation, with less of a chance to make a type I error. MAR and MR can distinguish the difference of two groups on P1 latency, and MAR is less likely to make type I errors. They recommended contralateral MR or MAR as an acceptable reference in the AEP P1 component study in cochlear implant patients. Considering that MR also showed greater P1 amplitude, contralateral MR is a more ideal choice for a general AEP study.

The effect of different references on auditory mismatch negativity (MMN) was tested by Mahajan et al. who demonstrated that (1) the experimental effect of magnitude of frequency deviance on MMN amplitude and latency do not depend on the choice of referencing procedure (LM, AVG, or REST). (2) Auditory MMN will be largest if the EEG data is referenced with LM followed by REST and then AVG referencing. (3) MMN amplitude computed using REST referencing depends on the number of electrodes used in the montage with 64-channel montage producing largest MMN amplitude. (4) The MMN amplitude elicited using average AVG referencing did not depend on the electrode montage.

Liang et al. described the electrophysiological correlates of change detection during delayed matching tasks according to the reference. They found that the N270 task-relevant is more positive posterior P2 in REST and AR but not in LM. SPM results showed a left posterior distribution for AR anterior distribution for LM and both for REST. They concluded that different references may provide distinct cognitive interpretations. Only SPM of REST was consistent with previous fMRI findings.

Qin et al. compared the influence of different references (LM, AR, REST) in the dynamic EEG center of mass (CM) approach in simulated and visual oddball paradigm real ERP. CM is a metric of the dynamic pattern of EEG spatiotemporal activity. CM and the traveling velocity extend the exploration of these cognitive mechanisms their results indicated that REST introduced less error than the AR, LM, and CZ references and was less affected by dipole location and orientation.

Yang et al. compared the reference effect of AR, LM, and REST on task-related ERP results of a working memory task during an fMRI scan. They found that the adopted reference did not change the topography map of ERP components (N1 and P300 in the present study), but it did alter the task-related effect on ERP components. LM decreased or eliminated the visual working memory (VWM) load effect on P300, and the AR distorted the distribution of VWM location-related effect at left posterior electrodes as shown in the statistical parametric scalp mapping (SPSM) of N1. ERP cortical source estimates, which are independent of the EEG reference choice, were used as the golden standard to infer the relative utility of different references on the ERP task-related effect. By comparison, REST reference provided a more integrated and reasonable result. These results were further confirmed by the results of fMRI activations and a corresponding EEG-only study. Thus, they recommend the REST, especially with a realistic head model, as the optimal reference method for ERP data analysis in simultaneous EEG-fMRI studies.

About the applications in pathological populations, Anastasiadou et al. demonstrated that the scalp- EEG-based functional brain networks in epilepsy, exhibit clear periodic patterns at different time scales but they highlighted how these patterns were not affected by the choice of the reference comparing "bipolar" and "common Cz." More importantly, they found out other factors affecting the perform of the reference such as cross-correlation, coherence, imaginary coherence and phase lag index, and also how the low number and inadequate electrode coverage of the scalp can disrupt this estimation. On the other hand, She et al. reported in Schizophrenia patients how the dysfunction of schematic facial expression varied depending of the reference employed (average or REST). They found that REST was more precise than AVE to locate the temporo-occipital distribution of the visual Mismatch Negativity, also for the discrimination of different emotional valence (happy and sad stimuli) in patients.

Finally, one of the most practical contributions of this Research Topic is coming from Dong et al. who developed a Toolbox of REST open-source Matlab for scalp EEG. http://www.neuro.uestc.edu.cn/rest/Down.html giving the opportunity to the people to test all the benefits of this reference.

One apparent limitation of this group of contributions, could be the dissimilarity of the results, where the comparison between different references are not following the same design or common modeling techniques. For that reason, the results seem to be contradictory at first glance, but on the contrary, the reader can find suggestions and valuable recommendations for reference selection in clinical and basic researches. For example, different references may provide distinct cognitive interpretations; the Reference Electrode Standardization Technique REST showed its superiority in many scenarios but not in others. The Laplacian references could be more robust when employed in specific situations, the linked-mastoid reference for the computation of EEG complexity and integration measures is not the ideal choice, due to its greater noise levels and tendency to induce artifactual correlations among scalp electrodes. The clarification about the specific conditions where one reference is superior to others needs to be tested in special experimental designs. We hope that this special research issue helped to gain a deeper insight of the reference. Now the glass is less dark than before, but more theoretical studies are needed to complement the present knowledge.

AUTHOR CONTRIBUTIONS

PV-S, PN, JR, RZ, and MB contributed equally to the conceptualization and editing of the Research Topic. MB, RZ, and PV-S wrote the editorial together. JR and PN revised the final version.

ACKNOWLEDGMENTS

The authors would like to thank for the support from the National Nature and Science Foundation of China NSFC with the China-Cuba-Canada project (Nos. 81861128001, 61871105, 61673090, 81330032, and 61603344), and the CNS Programme of UESTC (No. Y0301902610100201).

REFERENCES

Lehman, D. (1971). Multichannel topography of human alpha EEG fields. *Electroencefalogr. Clin. Neurophysiol.* 31, 439–449.

Yao, D. (2001). A method to standardize a reference of scalp EEG recordings to a point at infinity. *Physiol. Meas.* 22, 693–711. doi: 10.1088/0967-3334/22/4/305

Conflict of Interest: The authors declare that the research was conducted in the absence of any commercial or financial relationships that could be construed as a potential conflict of interest.

frontiers in Neuroscience

ORIGINAL RESEARCH
published: 13 April 2017
doi: 10.3389/fnins.2017.00205

Understanding the Influences of EEG Reference: A Large-Scale Brain Network Perspective

Xu Lei[1,2]* *and Keren Liao*[1,2]

[1] Sleep and NeuroImaging Center, Faculty of Psychology, Southwest University, Chongqing, China, [2] Key Laboratory of Cognition and Personality of Ministry of Education, Chongqing, China

The influence of reference is a critical issue for the electroencephalography (EEG) and event-related potentials (ERPs) studies. However, previous investigations concentrated less on the location of source at a systematic neuroscience level. Our goal was to examine the EEG signal associated with the locations from a common network parcellation of the human brain function, offering a system perspective of the influence of EEG reference. In our simulation, vertices uniformly distributed in eight large-scale brain networks were adopted to generate the scalp EEG. The brain networks contain the visual, somatomotor, dorsal attention, ventral attention, limbic, frontoparietal, default networks, and the deep brain structure. The distributions of the most sensitive and neutral electrodes were calculated for each network based on the lead-field matrix. While the most sensitive electrode had a network-specific symmetric pattern, the electrodes in scalp surface had approximately equal chance to be the most neutral electrode. Simulated data were referenced at the FCz, the Oz, the mean mastoids (MM), the average (AVE), and the infinity reference obtained by the reference electrode standardization technique (REST). Intriguingly, the relative error followed the pattern REST<AVE<MM<(FCz, Oz), regardless of the number of electrodes and signal-to-noise ratios. Our findings suggested that REST was a potentially preferable reference for all large-scale networks and AVE virtually performed as REST under several conditions. As EEG and ERPs experiments within the same behavioral domain always have activations in some specific brain networks, the comparisons revealed here may provide a valuable recommendation for reference selection in clinical and basic researches.

Keywords: EEG reference, large-scale networks, average reference, reference electrode standardization technique

OPEN ACCESS

Edited by:
Pedro Antonio Valdes-Sosa, Joint China-Cuba Laboratory for Frontier Research in Translational Neurotechnology, China

Reviewed by:
Quanying Liu, ETH Zurich, Switzerland
Eduardo Martínez-Montes, Cuban Neuroscience Center, Cuba

***Correspondence:**
Xu Lei
xlei@swu.edu.cn

Specialty section:
This article was submitted to Brain Imaging Methods, a section of the journal Frontiers in Neuroscience

Received: *15 December 2016*
Accepted: *27 March 2017*
Published: *13 April 2017*

Citation:
Lei X and Liao K (2017) Understanding the Influences of EEG Reference: A Large-Scale Brain Network Perspective. Front. Neurosci. 11:205. doi: 10.3389/fnins.2017.00205

INTRODUCTION

Electroencephalography (EEG) is a real-time, noninvasive measure of neuronal activity, which is considered as a valuable and cost-effective tool for the study of brain function in a wide range of clinical and basic research. The recent developments of EEG have allowed an increased topographic accuracy with high-density montage systems, the improved data quality with hardware updating and the reduced preparation time with dry electrode (Kleffner-Canucci et al., 2012; Mullen et al., 2015). Additionally, the opportunities to combine scalp EEG with other imaging modalities, as well as with robotics or neurostimulation, have made this technique more attractive for many emerging research fields.

However, an unsolved critical issue for the EEG studies is the choice of the EEG reference. In fact, both the evoked and spontaneous potentials of neural activities are influenced by reference, because each EEG electrode only yields information about the difference of electrical activity between two positions on the head (Nunez, 1981; Hagemann et al., 2001; Yao, 2001). It is indispensable to set a physical reference during EEG recordings and the signal in each electrode is obtained as the difference between the electric potentials in its location and in the location of the reference electrode. Here, the physical references used during recording is different from the computational references used during re-reference. The former includes the FCz, Oz, linked ears, nose, and neck ring, while the latter includes the mean mastoids, the average and the reference electrode standardization technique (REST) (Yao, 2001). If the neural electric potential near the reference electrode is not neutral, the measurement will be contaminated inevitably at all the other electrode sites, and further distorts the temporal dynamic analysis and power spectra analysis of the EEG recording. As a result, the preferential use of different reference schemes has evolved for individual research teams and led to de facto conventions for specific research fields or clinical practice (Kayser and Tenke, 2010).

Currently, there is no universally accepted reference scheme, hindering across-study comparability (Kayser and Tenke, 2010; Nunez, 2010). One commonly applied reference is the mean mastoids, which assumed the sites around the mastoids are free from activity of neural source. This assumption is always violated, because there is no single location where the potential can be considered to be completely neutral. The average reference has obtained large consensus thanks to its assumption of that the surface integral of the electric potential over a volume conductor containing all the current sources is zero (Bertrand et al., 1985). As the number of electrodes is increased and the coverage of the whole brain is approachable, it is increasingly believed that the average potential over all the electrodes provides a virtual zero-potential point. An alternative approach latter proposed by Yao was REST (Yao, 2001). REST transforms the EEG potentials referenced at any scalp points into the potentials referenced to a point located at infinity, far from all the possible neuronal sources and thus acting as an ideal neutral reference location. The merit of REST has been proved in event-related potentials (ERPs) (Tian and Yao, 2013), EEG spectrum (Yao et al., 2005), EEG coherence (Marzetti et al., 2007), and network analysis (Qin et al., 2010; Chella et al., 2016).

Previous investigations are confined to associating the selection of reference with some experiment paradigms (Hagemann et al., 2001) or source configurations (Marzetti et al., 2007), and rare has investigated the impact of the localization of EEG source on reference selection, due to lack of large-scale brain functional network templates. Fortunately, Yeo et al. (2011) adopted a data-driven clustering approach using 1,000 resting-state fMRI studies and segmented seven cortical neuronal networks from the cerebral cortex: the visual, somatomotor, dorsal attention, ventral attention, limbic, frontoparietal, and default mode networks. Based on the general assumption that EEG and ERPs experiments on the same psychological process normally activates certain brain networks, comparing the effects of different references within a template of brain network may unravel the potentially effective choice of reference in each behavioral domain. Our goal was to examine the EEG signal associated with the locations from a common network parcellation of the human brain function, offering a systems-neuroscience perspective of effect of the EEG reference.

We utilized a high-density canonical cortical mesh with 8,196 vertices to simulate the scalp EEG signal and each vertex was uniformly distributed in eight large-scale brain networks. The simulated signal was referenced to FCz, Oz, the mean mastoids (MM), the common average (AVE) of all electrodes and the infinity reference recovered by the Reference Electrode Standardization Technique (REST). The number of electrodes with 32, 64, and 128 and the signal-to-noise ratios with 2, 4, 8, 16, and 32 were included as influencing factors for the effect of reference electrode. Our systematic neuroscience comparisons among large-scale brain networks may provide valuable recommendations of reference selection for EEG and ERP studies.

METHODS

The influence of reference electrodes (FCz, Oz, MM, AVE) and the infinity reference recovered by the REST method were investigated through the simulated EEG potentials under different densities of electrode and signal-to-noise ratios. The spatial distribution and the time course for each large-scale brain functional network are described in the following.

Spatial Distribution of EEG Source and the Head Model

The EEG forward model is restricted to a high-density canonical cortical mesh (**Figure 1**). The mesh has 8,196 vertices and was extracted from a structural MRI of a neurotypical male in Fieldtrip software (http://fieldtrip.fcdonders.nl/download.php). Vertices were uniformly distributed on the gray-white matter interface, and assumed as potential dipoles oriented perpendicular to the surface. The electrodes of EEG system were registered to the scalp surface, and the lead-field matrix was calculated analytically using a three-shell spherical head model including scalp, skull, and brain (de Munck, 1988). As the EEG forward problems was solved by using the analytic expansion, an implicit assumption is that the lead field is based on the reference at infinity. The normalized radii of the three-shell spheres were 0.87 (inner radius of the skull), 0.92 (outer radius of the skull) and 1.0 (radius of the scalp). The normalized conductivities were 1.0, 0.0125, and 1.0 for the brain, skull and scalp, respectively. For the number of electrodes n, the lead-field $\boldsymbol{L}$ was a matrix with dimension $n \times 8{,}196$.

Each vertex was adopted to generate the scalp EEG recording per simulation. As the vertex belongs to one of the eight large-scale brain networks, we averaged all the performance of the vertices belonging to a network to evaluate the influence of the network parcellation on the EEG data. Seven large-scale networks were identified based on 1000 resting-state functional

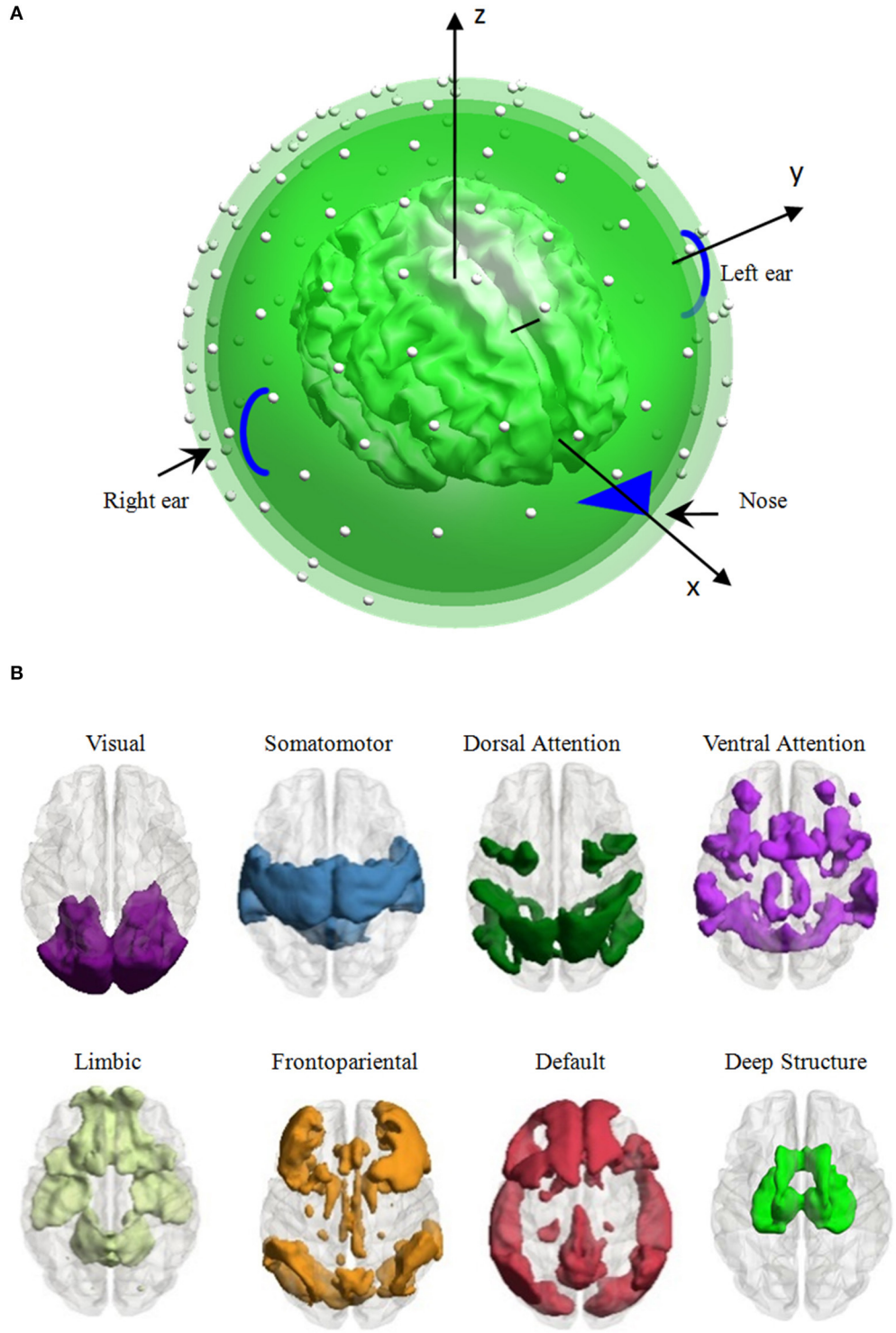

FIGURE 1 | Head model and the distribution of eight large-scale brain functional networks. (A) Head model: a high-density canonical cortical mesh (inner irregular object) with 8,196 vertices within a concentric three-sphere head model, with electrodes (the white dots) on the upper surface. **(B)** Vertex, which was used to generate EEG signal per simulation, is distributed in one of the eight large-scale brain networks, i.e., the visual, somatomotor, dorsal attention, ventral attention, limbic, frontoparietal, default networks, and the deep brain structure.

connectivity, including the visual, somatomotor, dorsal attention, ventral attention, limbic, frontoparietal, and default networks (Yeo et al., 2011). Considering the importance of the deep brain structure (thalamus, caudate, hippocampus, amygdala and olfactory), we used the automated anatomical labeling (AAL) parcellation atlas (Tzourio-Mazoyer et al., 2002) to construct an eighth large-scale network comprising these structures. The 8,196 vertices were separated to eight subsets depended on its nearest neighbor voxel in the large-scale brain network templates. The number of vertices of each network ranged from 428 to 1,572 (1,255 vertices in the visual network, 1,539 vertices in the somatomotor network, 979 vertices in the dorsal attention network, 842 vertices in the ventral attention network, 513 vertices in the limbic network, 1,068 vertices in the frontoparietal network, 1,572 vertices in the default network, and 428 vertices in the deep brain structure, see **Figure 1B** for the spatial pattern of each network).

Signal Strength and the Sensitive/Neutral Electrode

As the lead-field matrix $\boldsymbol{L}$ was calculated for each dipole with a unit strength, the ith column $\boldsymbol{L}_i$ (corresponding to the ith dipole and $i = 1, ..., 8{,}196$) is a measurement for how strong the signal of the source can be observed from every electrode on the scalp surface. The relative strengths in $\boldsymbol{L}_i$ have direct relation with the sensitivity of electrodes (Rush and Driscoll, 1969). For example, if the absolute value of $\boldsymbol{L}_{im}$ (the mth row in $\boldsymbol{L}_i$) is larger than the absolute value of $\boldsymbol{L}_{in}$ (the nth row in $\boldsymbol{L}_i$), it means the mth electrode is more sensitive than the nth electrode. The reciprocity theorem shows that the sensitivity of the electrode is maximum to the dipolar sources oriented in the direction of the lead-field (perpendicular to the lines), and falls off as the cosine of the angle between the source and lead-field directions (Rush and Driscoll, 1969). We defined the electrodes corresponding to the maximum and minimum absolute values in $\boldsymbol{L}_i$ as the most sensitive and neutral electrodes, respectively. We calculated the global sensitivity of the ith dipole to be reflected in the scalp as:

$$S_i = \frac{1}{\sqrt{n}} \parallel L_i \parallel \tag{1}$$

where $||\boldsymbol{L}_i||$ is the Frobenius norm of the lead-field column corresponding to the ith dipole and n is the number of electrodes. We will use the averaged of the global sensitivity in the kth network for comparison among the montages with different number of electrodes.

Because 64-electrode is widely applied in experimental study, we focused our analysis on the electrode level with the lead-field matrix of 64-electrode. As the maximum or minimum absolute value in $\boldsymbol{L}_i$ corresponds to the most sensitive or neutral electrode to reflect the source activity, we counted the times of electrode j that was selected as the most sensitive or neutral electrode for network k.

$$\mathrm{S}_{\mathrm{k}}^{\mathrm{j}} = \frac{1}{m_k} \sum\nolimits_{(i \in \textit{network } k)} b_i \tag{2}$$

$$\mathrm{N}_{\mathrm{k}}^{\mathrm{j}} = \frac{1}{m_k} \sum\nolimits_{(i \in \textit{network } k)} w_i \tag{3}$$

where $b_i = 1$ ($w_i = 1$) if the jth row in vector $\boldsymbol{L}_i$ has the maximum (minimum) absolute value, otherwise $b_i = 0$ ($w_i = 0$). m_k is the number of vertices in brain network k. Notice that S_k^j or N_k^j would be equal to 1/64 if all the electrodes have the same chance to be the most sensitive or neutral electrode.

Simulation Description

We simulated the temporal process of a dipolar neural source by employing a damped Gaussian function:

$$\begin{aligned} \mathrm{y_k} &= \exp(-2\pi\tau \times \mathrm{k} \times \mathrm{dt}) \\ &\quad \times \cos(2\pi f \times \mathrm{k} \times \mathrm{dt}), \mathrm{k} = 1, ..., 500 \end{aligned} \tag{4}$$

where dt = 2 ms, τ = 2 Hz, and f = 10 Hz. We chose this function because it looks like an evoked potential and was utilized in previous simulations (Yao, 2001). Using the function y and the lead-field $\boldsymbol{L}$, we derived the spatiotemporal recordings of ith vertex ($i = 1, ..., 8{,}196$ and each simulation used one vertex to generate signal): $\boldsymbol{V}_{\mathrm{sim}} = \boldsymbol{L}_i \mathrm{y}$ with size $n \times 500$, where $\boldsymbol{L}_i$ is the ith column of $\boldsymbol{L}$.

We examined the effect of the number of electrodes n by comparing the performance of electrode configuration with 32, 64, and 128 electrodes. All electrode configurations were down-sampled from the standard 10-5 system (Oostenveld and Praamstra, 2001) to obtain an approximate uniform sample of the upper head. For each configuration, FCz, Oz, TP9, and TP10 were included, in order to simulate the reference electrodes. TP9 and TP10 were averaged to construct the mean mastoids (MM) reference. The effects of Gaussian white noise Σ was investigated by varying the signal-to-noise ratio with values of 2, 4, 8, 16, and 32, which were calculated as the ratio between the mean variance across channels of the signal $\boldsymbol{V}_{\mathrm{sim}}$ and the variance of noise Σ. In other words, the scalp EEG recording are $\boldsymbol{V}_{\mathrm{rec}} = \boldsymbol{V}_{\mathrm{sim}} + \Sigma$ with size $n \times 500$, which is the input of the following reference techniques. Obviously, the reference of this simulated data $\boldsymbol{V}_{\mathrm{sim}}$ is at infinity.

The EEG References

The potentials referenced to the cephalic (FCz), the occipital (Oz), the mean mastoids (MM) and the average (AVE) references, indicated by $\boldsymbol{V}_{\mathrm{FCz}}$, $\boldsymbol{V}_{\mathrm{Oz}}$, $\boldsymbol{V}_{\mathrm{MM}}$, and $\boldsymbol{V}_{\mathrm{AVE}}$ respectively, have been derived from the simulated EEG $\boldsymbol{V}_{\mathrm{rec}}$ according to the appropriate linear transformation (Yao, 2001). In particular, the MM reference signal has been modeled by the average of the TP9 and TP10 electrodes that are located in the proximity of the mastoids. The simulated EEG recording has been transformed according to the REST method (Yao, 2001), and a reconstruction of the infinity reference potential $\boldsymbol{V}_{\mathrm{REST}}$ was derived from $\boldsymbol{V}_{\mathrm{AVE}}$ based on the free software of REST (http://www.neuro.uestc.edu.cn/rest).

Relative Error for Evaluation

The re-referenced potentials $\boldsymbol{V}^*$ were compared to the theoretical potential $\boldsymbol{V}_{\mathrm{sim}}$ to assess the effects of different references, and $\boldsymbol{V}^*$ was an alternative denotation of the recording $\boldsymbol{V}_{\mathrm{FCz}}$, $\boldsymbol{V}_{\mathrm{Oz}}$, $\boldsymbol{V}_{\mathrm{MM}}$, $\boldsymbol{V}_{\mathrm{AVE}}$ as well as $\boldsymbol{V}_{\mathrm{REST}}$. The degree of similarity between the re-referenced potentials and the theoretical simulation potential has

been assessed by calculating the relative error (RE) according to the formula:

$$\mathrm{RE} = ||\boldsymbol{V}_{\mathrm{sim}} - \boldsymbol{V}^*||/||\boldsymbol{V}_{\mathrm{sim}}|| \quad (5)$$

where $||\cdot||$ denotes the matrix Frobenius norm. As the transformations of references are linear operations, we only simulated the performance according to the potential of a single vertex in each simulation, and the performance according to various dipole combinations can be deduced according to the linearity of the operation. We conducted 128 realizations with different the random seeds of the Gaussian white noise Σ for each dipole, in each signal-to-noise ratio and each number of electrodes. And the RE was averaged in these 128 realizations to obtain the performance of a single vertex. Then all the dipoles belonging to a large-scale brain network were averaged to obtain the performance of a single network.

RESULTS

Signal Strength and the Sensitive/Neutral Electrode

Based on the averaged Frobenius norm of the lead-field matrix, we obtained the global sensitivity of each large-scale network for each electrode configuration. We found the increased number of electrodes did not mean the increasing of the global sensitivity of a large-scale network that can be observed from the scalp surface, as the averaged norm was consistent with the same level (see **Figure 2**). Another interesting pattern was that visual network always had the largest sensitivity (0.1171, averaged for all electrode configuration), while limbic system had the smallest (0.0882).

For widely employed 64-electrode, we further considered the sensitivity to observe the large-scale networks in electrode level. **Figure 3** illustrated the percentage topography of each electrode that was selected as the most sensitive or neutral electrode. Notice it would be 1/64 (marked in the legend of **Figure 3**) if each electrode had the same chance to be the most sensitive or neutral electrode. For the most sensitive electrode, the topography had a left-right symmetric pattern and the largest percentage electrodes neighbored to the superficial regions of a network. This phenomenon was apparent for the visual (PO3, PO4, and POz), the somatomotor (C3 and C4), the dorsal attention (P3 and P4), the ventral attention (FC3 and FC4), the limbic (FT9, FT10, TP9, and TP10) networks and the deep brain structure (FC5 and FC6). The above listed electrodes had percentage larger than 5%, which was triple of the random chance. We did not find any specific sensitive electrode for the frontoparietal or the default network, as neither had any percentage of electrode larger than 4.2%.

It was hard to find the neutral electrode in the scalp surface, except in the deep brain structure. For the visual, somatomotor, dorsal attention, ventral attention, limbic, frontoparietal, and default networks, all the electrodes had the chance to be selected as the most neutral electrode with percentage less than 3.5%. For the deep brain structure, Oz and FCz had percentage of 6.8% and 6.1%, respectively, implying they were potential good reference for the study of the deep brain structure.

The relative error of the re-reference signal to the theoretical true signal was calculated in each signal-to-noise ratio and electrode configuration, for each large-scale network. As illustrated in **Figure 4**, the relative error followed the pattern REST<AVE<MM<(FCz, Oz), as the number of electrodes and the signal-to-noise ratio constituted the coordinates (see **Table 1** for an example dataset of 64-electrode). REST always had the best performance compared with any other reference system. For example, its relative error was less than 3% in the signal-to-noise ratio of 32 in 64-electrode (the fifth row of **Table 1**). However,

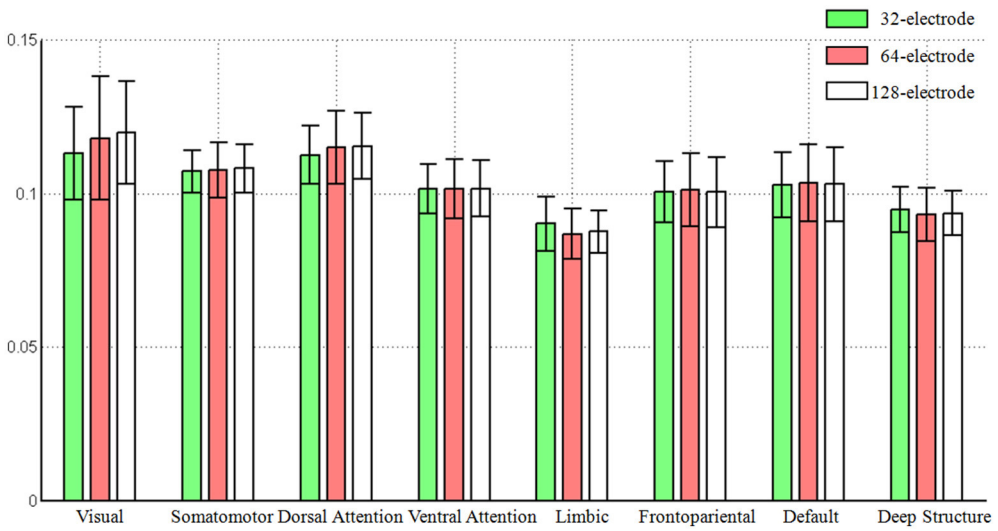

FIGURE 2 | The global sensitivity (averaged Frobenius norm) of large-scale network that can be observed in the scalp EEG. The Frobenius norm of vertices were averaged across each large-scale brain network and the standard error was also calculated. The number of electrodes included 32, 64, and 128.

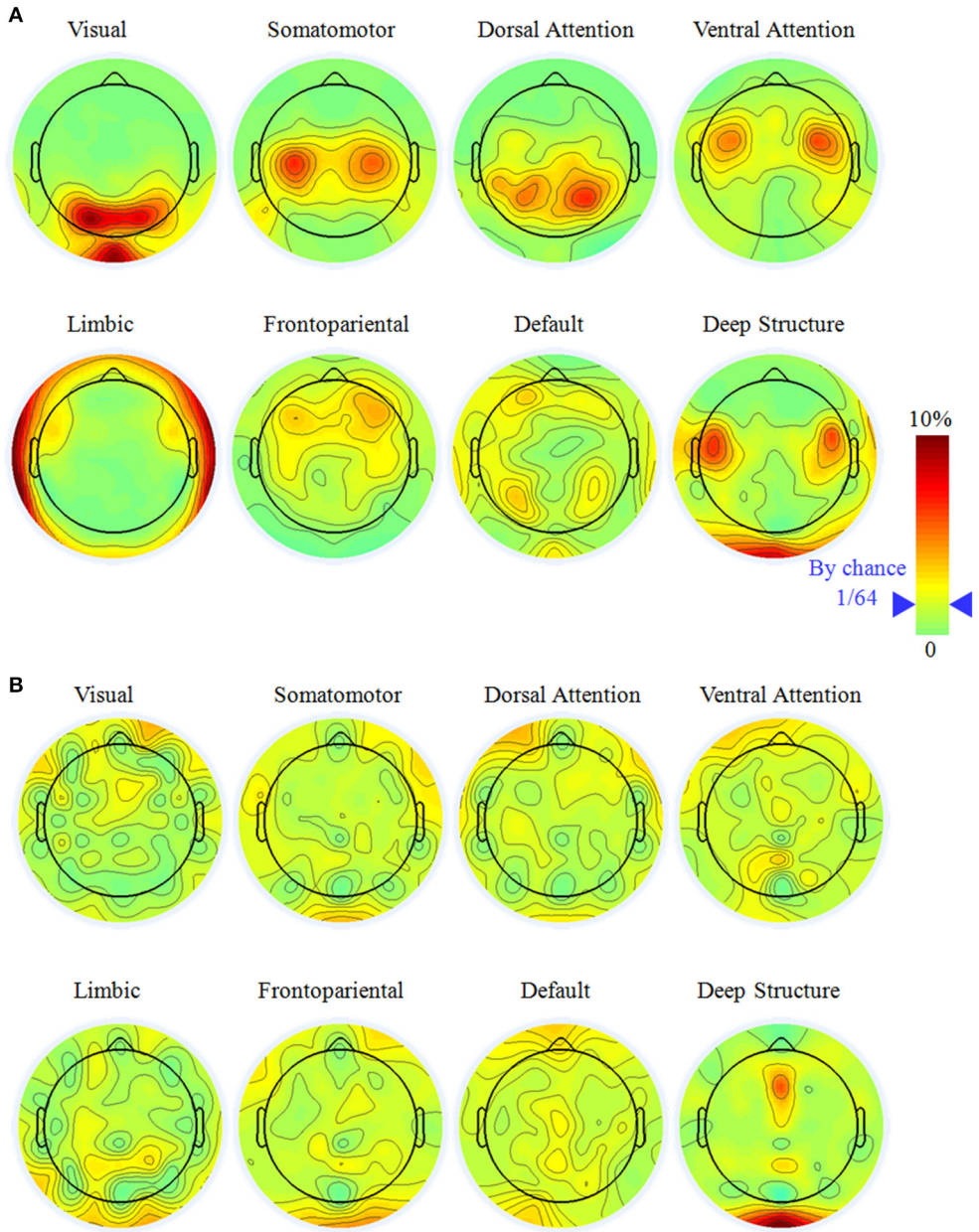

FIGURE 3 | The most sensitive (A) and neutral electrodes **(B)** for each large-scale brain network with the electrode number of 64. Notice it would be 1/64 (marked in the color bar) if all the electrodes have equal chance to be the most sensitive or neutral electrode. The most sensitive electrode had a symmetric distribution and concentrated on specific electrode while the most neutral electrode was random.

the other references all had relative errors larger than 15% (the first to fourth rows of **Table 1**). For the dataset of 64-electrode, we conducted a 2-factor analysis of variance (ANOVA) in each large-scale network, with factors of signal-to-noise ratio (6) and reference electrode (5). All large-scale networks had significant main effect of reference electrode ($p < 0.0001$), and F values ranged from 342.51 (the deep brain structure) to 2,106.78 (the somatomotor network).

A strong contender is AVE, which had much closer performance to REST, especially for small signal-to-noise ratio and high density of electrode. In the worst condition of signal-to-noise ratio of 2, REST decreased its performance greatly with the relative error larger than 40% in 64-electrode (the last bold row of **Table 1**). When comparing with AVE in signal-to-noise ratio of 2, though REST (39.11%) was better than AVE (41.18%) in 32-electrode, it became worse when density increased to 64-electrode (REST: 49.02% vs. AVE 43.3) and even twice the relative error in 128-electrode (REST: 81.38% vs. AVE 43.31%). Our statistical analysis in each brain network with signal-to-noise ratio of 2 and the number of electrodes of 64 further confirmed

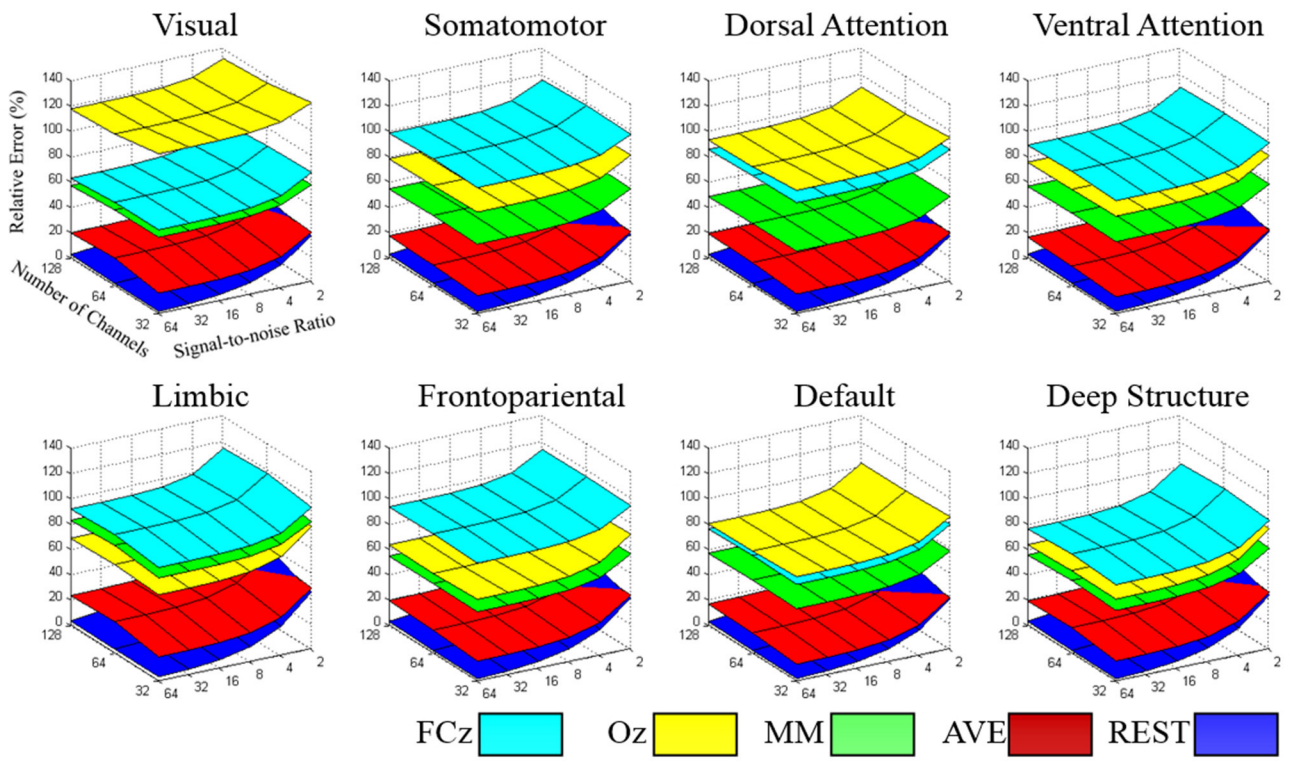

FIGURE 4 | The relative error of the re-reference signal to the theoretical true signal was calculated in each signal-to-noise level and electrode configuration, for each large-scale network. The value of the relative error followed the pattern REST<AVE<MM<(FCz, Oz), which each network had its specific characteristic in reference selection.

the poor performance of REST, as all the paired t-tests between REST and AVE had $p < 0.0001$ and the t value were ranged from −55.43 (the somatomotor network) to −11.49 (the visual network).

Though each reference had relative constant performance for different number of electrodes and signal-to-noise ratio, we found each brain network had its distinct pattern in the relative error. In the worst condition with the number of electrodes of 32 and signal-to-noise ratio of 2, the relative error was ranged from 100.7% (deep brain structure) to 140.5% (visual), implying the importance of reference selection. Intriguingly, when comparing the reference of FCz and Oz, FCz was better in the visual, dorsal attention and default networks, while Oz was better in the somatomotor, ventral attention, limbic, frontoparietal networks and the deep brain structure.

DISCUSSION

In current study, the effect of reference was examined under a common network parcellation of the human brain function containing eight large-scale networks. Based on the lead-field matrix, we found the distribution of the most sensitive electrode had a symmetric pattern, and each network preferred some specific electrodes. In contrast, the electrodes in scalp surface had approximately equal chance to be the most neutral electrode. We focused our simulations on some reference systems, including FCz, Oz, MM, AVE, and REST. The results showed that the magnitude of relative error followed the pattern of REST<AVE<MM<(FCz, Oz), regardless of the number of electrodes and the signal-to-noise ratio. Our findings suggested that REST was the most outstanding reference for all large-scale networks and AVE had much closer performance to REST than any other references. As ERPs and EEG experiments within the same behavioral domain always concern certain components relating to specific brain networks, our systems neuroscience comparisons revealed here may provide a valuable recommendation about reference selection for clinical and basic researches.

Sensitive/Neutral Electrode for Large-Scale Network

For the widely adopted density of 64-electrode, we investigated the probability of each electrode that can be selected as the most sensitive or neutral electrode. In fact, the lead-field matrix provided a pure measure of activity that a dipole with a unit strength can be represented with electrode in the scalp surface and the probability would be 1/64 if each electrode had equal chance to be selected. For the most sensitive electrode, the topography had a hemisphere symmetric pattern and the largest probability electrodes neighbored to the superficial regions of

TABLE 1 | The relative error of the re-reference signal to the theoretical true signal was calculated in each signal-to-noise level, for each large-scale network, with the number of electrodes of 64.

SNR	Reference	The averaged relative error in each large-scale network, mean ± SE (%)							
		Visual	Somato-motor	Dorsal attention	Ventral attention	Limbic	Fronto pariental	Default	Deep structure
64	FCz	65.4 ± 1.2	99.8 ± 1.5	86.4 ± 1.7	90.0 ± 2.1	93.1 ± 2.1	93.7 ± 1.9	76.7 ± 1.3	77.9 ± 2.7
	Oz	119.2 ± 2.3	78.5 ± 1.2	93.4 ± 1.8	75.6 ± 1.6	69.5 ± 1.9	62.5 ± 1.4	80.2 ± 1.4	64.7 ± 2.7
	MM	59.4 ± 1.1	55.1 ± 0.9	48.8 ± 1.0	57.0 ± 1.3	84.7 ± 2.2	54.5 ± 1.1	57.3 ± 1.1	57.0 ± 2.2
	AVE	21.6 ± 0.4	16.0 ± 0.3	18.0 ± 0.3	15.2 ± 0.4	24.6 ± 0.7	17.9 ± 0.4	15.7 ± 0.3	19.8 ± 0.7
	REST	1.5 ± 0.0	1.6 ± 0.0	1.4 ± 0.0	1.6 ± 0.0	2.9 ± 0.1	1.7 ± 0.0	1.8 ± 0.0	1.8 ± 0.0
32	FCz	65.6 ± 1.2	99.9 ± 1.5	86.5 ± 1.7	90.1 ± 2.1	93.2 ± 2.1	93.8 ± 1.9	76.8 ± 1.3	78.1 ± 2.7
	Oz	119.3 ± 2.3	78.7 ± 1.2	93.5 ± 1.8	75.7 ± 1.6	69.7 ± 1.9	62.7 ± 1.4	80.3 ± 1.4	65.0 ± 2.7
	MM	59.5 ± 1.1	55.2 ± 0.9	48.9 ± 1.0	57.1 ± 1.3	84.8 ± 2.2	54.6 ± 1.1	57.4 ± 1.1	57.2 ± 2.2
	AVE	21.8 ± 0.4	16.2 ± 0.3	18.1 ± 0.3	15.4 ± 0.4	24.9 ± 0.7	18.1 ± 0.4	15.9 ± 0.3	20.1 ± 0.7
	REST	2.8 ± 0.0	3.0 ± 0.0	2.8 ± 0.0	3.1 ± 0.0	4.3 ± 0.0	3.2 ± 0.0	3.2 ± 0.0	3.4 ± 0.0
16	FCz	66.0 ± 1.2	100.2 ± 1.5	86.8 ± 1.7	90.5 ± 2.1	93.6 ± 2.1	94.2 ± 1.9	77.3 ± 1.3	78.7 ± 2.7
	Oz	119.6 ± 2.3	79.1 ± 1.1	93.9 ± 1.8	76.3 ± 1.6	70.4 ± 1.9	63.3 ± 1.3	80.8 ± 1.4	65.8 ± 2.7
	MM	59.8 ± 1.1	55.6 ± 0.9	49.3 ± 1.0	57.6 ± 1.3	85.2 ± 2.2	55.1 ± 1.0	57.9 ± 1.0	57.8 ± 2.2
	AVE	22.3 ± 0.3	16.9 ± 0.2	18.7 ± 0.3	16.3 ± 0.4	25.6 ± 0.7	18.8 ± 0.4	16.8 ± 0.3	20.9 ± 0.7
	REST	5.5 ± 0.0	5.8 ± 0.0	5.5 ± 0.0	6.2 ± 0.0	7.6 ± 0.0	6.3 ± 0.0	6.2 ± 0.0	6.8 ± 0.0
8	FCz	67.3 ± 1.2	101.3 ± 1.5	87.9 ± 1.7	91.9 ± 2.1	95.1 ± 2.0	95.6 ± 1.9	78.8 ± 1.3	80.7 ± 2.6
	Oz	120.6 ± 2.2	80.4 ± 1.1	95.0 ± 1.7	77.9 ± 1.6	72.6 ± 1.8	65.3 ± 1.3	82.4 ± 1.3	68.5 ± 2.6
	MM	60.9 ± 1.1	56.9 ± 0.9	50.5 ± 1.0	59.1 ± 1.3	86.6 ± 2.1	56.5 ± 1.0	59.4 ± 1.0	59.8 ± 2.1
	AVE	23.9 ± 0.3	19.1 ± 0.2	20.5 ± 0.3	18.8 ± 0.3	27.9 ± 0.7	21.1 ± 0.3	19.2 ± 0.3	23.4 ± 0.7
	REST	10.8 ± 0.1	11.6 ± 0.0	10.9 ± 0.0	12.3 ± 0.0	14.6 ± 0.1	12.4 ± 0.0	12.2 ± 0.0	13.4 ± 0.1
4	FCz	71.5 ± 1.2	104.9 ± 1.4	91.4 ± 1.6	96.4 ± 2.0	100.0 ± 1.9	99.9 ± 1.8	83.7 ± 1.2	86.6 ± 2.5
	Oz	123.8 ± 2.2	84.8 ± 1.0	98.6 ± 1.6	83.0 ± 1.5	79.3 ± 1.6	71.4 ± 1.2	87.4 ± 1.3	75.8 ± 2.4
	MM	64.3 ± 1.1	61.1 ± 0.9	54.5 ± 0.9	63.7 ± 1.2	91.0 ± 2.0	61.1 ± 0.9	64.0 ± 1.0	65.6 ± 2.0
	AVE	28.5 ± 0.3	25.1 ± 0.2	25.6 ± 0.2	25.5 ± 0.3	34.6 ± 0.6	27.4 ± 0.3	25.8 ± 0.2	30.3 ± 0.6
	REST	21.6 ± 0.1	23.2 ± 0.1	21.8 ± 0.1	24.6 ± 0.1	28.9 ± 0.1	24.8 ± 0.1	24.4 ± 0.1	26.9 ± 0.1
2	FCz	84.2 ± 1.1	116.1 ± 1.3	102.5 ± 1.5	109.9 ± 1.8	115.8 ± 1.7	113.1 ± 1.7	98.1 ± 1.1	103.4 ± 2.2
	Oz	133.7 ± 2.0	97.9 ± 0.9	109.5 ± 1.5	97.9 ± 1.2	98.8 ± 1.4	88.3 ± 1.0	102.0 ± 1.1	95.1 ± 2.0
	MM	74.8 ± 1.0	73.4 ± 0.8	66.3 ± 0.8	77.1 ± 1.0	104.5 ± 1.8	74.7 ± 0.8	77.3 ± 0.9	81.2 ± 1.7
	AVE	41.1 ± 0.3	40.1 ± 0.1	39.1 ± 0.2	41.8 ± 0.2	52.2 ± 0.5	43.3 ± 0.2	41.7 ± 0.2	47.4 ± 0.5
	REST	43.3 ± 0.2	46.4 ± 0.1	43.6 ± 0.1	49.2 ± 0.2	57.7 ± 0.2	49.6 ± 0.2	48.7 ± 0.1	53.7 ± 0.3

a network. These electrodes provided a potential observing window for experimental studies concentrating on a specific brain network.

Based on the minimum absolute value of the lead-field matrix, we proposed a quantitative measure for the relatively neutral or "quiet" reference location. Previous studies had mentioned that the neutral reference location did not exist anywhere on the body (Kayser and Tenke, 2010; Nunez, 2010), it seemed to be true as all the electrodes for seven large-scale networks have the percentage less than 3.5%. One exception is the deep brain structure, which has the highest probability of neutral electrodes around OIz and FCz.

The electrodes near the parietal-occipital junction (PO3, PO4, and POz) had the high probability to be the most sensitive electrode for the visual network. For example, visual evoked potential such as P100 component, is observed over the electrode around parietal-occipital region (Hillyard and Anllo-Vento, 1998). In classical experiment paradigm of spatial selective attention, attention to the stimulus location increased amplitude of the P100. Another widely utilized paradigm concentrated on the visual network is steady state visually evoked potentials (SSVEP), which are signals that are responses to visual stimulation at specific frequencies ranging from 3.5 to 75 Hz (Herrmann, 2001). The electrode around parietal-occipital junction would record the electrical activity at the same frequency of the visual stimuli.

The electrodes near the central (C3 and C4) had the high probability to be the most sensitive electrode for the somatomotor network (**Figure 3A**). In the brain-computer interface based on motor imagery, C3 and C4 are utilized to

record the Mu and Beta rhythms during motor imaging (Lei et al., 2009). They were proved to have strong signal as overlaying the sensorimotor areas. Another potential concentrated on the somatomotor network is the lateralized readiness potential (LRP), which is considered as the representation of the activation of response-related processes, starting after response hand selection and at the beginning of motor programming (Coles, 1989). LRP are extracted from an array of electrodes located over central and neighboring areas.

The electrodes near the parietal lobe (P3 and P4) had the high probability to be the most sensitive electrodes for the dorsal attention network. These dorsal parietal electrodes are close to the intra parietal sulcus and superior parietal lobe, which are the basic structures of the dorsal attention network (Yeo et al., 2011). In the goal-directed attention paradigm, P300 recorded during effortful attention correlated significantly with parietal, effortful processes under the subject's active control (Ford et al., 1994). FC3 and FC4 had the high probability to be the most sensitive electrode for the ventral attention network. We should emphasize that the ventral attention network is an aggregate of multiple networks such as the salience and the cingulo-opercular networks in the literature (Yeo et al., 2011).

Choice of Reference for Large-Scale Network

We had a systematic simulation for the reference of FCz, Oz, the mean mastoids, the average and the infinity reference, with the number of electrodes from 32 to 128 and signal-to-noise level from 2 to 32. Our simulations demonstrated that the off-line re-reference techniques has distinct performance for different large-scale network, and always followed the pattern REST<AVE<MM<(FCz, Oz). In addition, the infinity reference performed by REST can substantially reduce the relative error.

Because FCz and Oz are always an electrically sensitive positions, there is some consensus in the literature that all cephalic reference such as FCz and Oz may be not a preferential choice for the measurement of local activity at cephalic target position (Hagemann et al., 2001). We found both FCz and Oz references may substantially distort the EEG potentials. In worst condition with 32-electrode and the signal-to-noise ratio of 2, both references had relative error larger than 100% in some networks. As FCz and Oz were close to frontal eye field and occipital regions respectively, the large-scale networks around these regions had been affected. We found FCz was better in visual, dorsal attention, default, while Oz was better in somatomotor, ventral attention, limbic, frontoparietal, and deep brain structure. In simultaneous EEG-fMRI study, FCz was frequently served as online reference in a nonmagnetic MRI-compatible EEG system (Lei et al., 2014). This may because it is easy to be affixed to the surface of the scalp and it has typical MRI imaging artifact, and the latter is crucial in off-line process to remove gradient and ballistocardiographic (BCG) artifacts.

Although it has been argued that the mastoids are relatively inactive, this has been persuasively shown to be false (Hagemann et al., 2001). In our simulation, the mean mastoids (MM) was always better than FCz and Oz because the average of bilateral mastoids regions was substantially less active for most networks. However, there was an exception for the limbic network, which followed the pattern Oz<MM<FCz in relative error. In the condition of signal-to-noise ratio of 64 and number of electrodes of 64, the relative errors of MM was 84.7% while that of Oz was 69.5% in the limbic network.

The average reference is commonly recommended reference, and it assumed that the average across all scalp electrodes at each time point is substantially less active than the target sites. Theoretically, if the head is assumed to be a concentric sphere structure with homogenous conductivities within each sphere, then an ensemble of dipoles inside the sphere would generate an electric field such that the integral of the potential on the surface of the sphere is zero at any given time point (Bertrand et al., 1985). This is valid only with sufficient electrode density and full coverage of the head surface (Yao, 2017). Otherwise the AVE reference was not completely free of biases as the spatial sampling being limited to the upper part of the head (Nunez and Srinivasan, 2006). Our simulation proved that the AVE reference was quite a neutral reference, and had the best performance when compared with FCz, Oz, or MM. More importantly, the performance of AVE can even be better than REST for high density electrode, and we will back to this point hereinafter.

With the application of high density electrode and modern computation technique, a better reference, named infinity reference, was developed based on a reference electrode standardization technique (REST) (Yao, 2001). As it approximately reconstructed a point far away from all the scalp electrodes, REST provided a neutral reference. Previous studies of simulation and experiments showed that REST is very effective for most important superficial cortical region. We specified this simulation to the whole brain, with the common network parcellation of the human brain function, offering a system perspective of the performance of REST. Previous studies have shown the availability of high-density EEG systems and an accurate knowledge of the head model are crucial elements to improve REST performance (Zhai and Yao, 2004; Liu et al., 2015; Chella et al., 2016).

In this work, a particular emphasis has been placed on the comparison between the REST and AVE references, the superiority of one method over the other having been the subject of some debates (Kayser and Tenke, 2010; Nunez, 2010). Based on the findings of our simulation, we concluded that REST can provide superior performance than AVE in reducing the reference bias even when the signal-to-noise ratio decreased to 4. However, when noise was extremely large, or the electrodes were high-density, AVE may be a strong rival to REST. This is in line with previous finding that REST was sensitive to noise and the number of electrodes (Liu et al., 2015). Though REST (38.3%) was better than AVE (40.3%) when the number of electrodes was 32, it was worse when electrode is increase to 64 (REST: 47.8% vs. AVE 42.1%) and 128 (REST: 79.4% vs. AVE 42.2%). This is essentially due to REST assuming the sources of the EEG recordings lying inside the equivalent source distribution (ESD). Since the instrumental noise is not generated by sources inside the ESD, the effectiveness of the standardization to a reference point at infinity becomes less accurate in comparison to the noiseless case (Zhai and Yao, 2004).

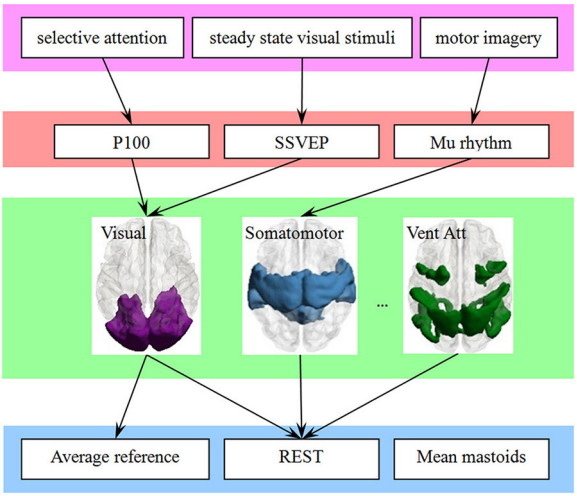

FIGURE 5 | The large-scale brain network is a bridge to link the behavioral paradigm to the EEG studies, which may simplify the choice of reference. A behavioral paradigm (first row) often engages several EEG or ERPs components (second row) that are in turn supported by multiple brain regions, which constructed a large-scale network (third row). In addition, each large-scale network has its specific sensitive or neutral electrodes. The choice of electrode is simplified if the link from electrophysiological components (fourth row) to large-scale network is finite and consistent.

EEG Reference under the Perspective of Large-Scale Network

The choice of reference has substantial effects on analysis and interpretation, and the optimal choice of reference site depended on the study domain and purpose of the analysis. In our current study, we considered a special application scenario: behavioral paradigm focused on some special large-scale brain networks. This is rational for most model-driving experiments because brain regions are always included in the assumptions before the EEG or ERPs studies. Both the evoked and the spontaneous potentials of neural activities are currently interpreted in terms of components generated by distinct large-scale network. Because of the complex influence of the spatiotemporal characteristics of skull volume conduction on the EEG signal, it is still hard to estimate the related large-scale networks from the signal in scalp surface (Lei et al., 2011). However, the application of the high-density EEG, especially the wide application of fMRI, makes it acceptable and even normal to include some assumptions about the localization of source before an EEG or ERPs study.

The large-scale brain networks, which are constructed from the intrinsic spontaneous activity of resting-state function MRI, were found have a constant spatial pattern in task conditions (Smith et al., 2009; Yeo et al., 2015). As illustrated in **Figure 5**, we thought the large-scale brain network might be a bridge to link EEG and ERP components in one hand, and the choice of EEG reference in another hand. Previous neuroimaging studies have revealed that each network is functional specialization, and we thought this will lead to a many-to-one mapping between electrophysiological components and the large-scale network.

The attribution of functional specialization illustrated in **Figure 5** may be considered at different spatial scales (Gilbert et al., 2010). For example, at the macro-scale, the visual network can be described as being specialized for visual processing, and the reference scheme of visual ERPs such as P100 or N170 may be inferred at this macro-scale. At a finer scale, sub-regions of the visual network may be distinguished based on their sensitivity to different visual features. A fine-resolution parcellation of the cerebral cortex can increase the accuracy of the choice of electrode. For example, N170 may indicate its reference scheme from the sub-network around the lateral visual areas. The template we utilized also has a fine-resolution with 17-network parcellation of the human cerebral cortex based on 1,000 subjects (Yeo et al., 2011). This detailed parcellation corresponded to a hierarchical behavioral domain classification (Poldrack and Yarkoni, 2016), and may lead to a more relevant reference selection.

Our current simulations have several limitations, especially separating a vertex to a specific large-scale network. In fact, the same vertex can belong to different networks. In addition, if all or majority of vertices in a network are active simultaneously, the most sensitivity\neutral electrodes and the relative error of each re-reference method would be extremely different from the current results. More important, it is in this way that the results can be interpreted in terms of what happens when a particular network is functioning. And experiments may find a guide on which reference and what type of analysis are adequate when the activity of interest is related with/generated from a particular brain network.

SUMMARY AND CONCLUSION

The choice of an EEG reference is an important initial step for EEG analysis, and the findings of different reference schemes should be treated as interchangeable (Hagemann et al., 2001). Our findings suggested that REST was a potential reference for all the large-scale networks and AVE was much closer in performance to REST. This large-scale network approach, based on a large sample of published neuroimaging studies, can reassign large bodies of EEG and ERPs signal of distinct tasks with novel organizational features at the systems level, thereby offering potential reference electrode for clinical studies and research studies using EEG and ERPs.

AUTHOR CONTRIBUTIONS

Conceived and designed the experiments, performed the experiments and analyzed the data: XL. Contributed reagents/materials/analysis tools: XL and KL.

ACKNOWLEDGMENTS

This research was supported by grants from the National Nature Science Foundation of China (31571111), Fundamental Research Funds for the Central Universities (SWU1609109) and Specialized Research Fund for the Doctoral Program of Higher Education of China (20120182120001).

REFERENCES

Bertrand, O., Perrin, F., and Pernier, J. (1985). A theoretical justification of the average reference in topographic evoked potential studies. *Electroencephalogr. Clin. Neurophysiol.* 62, 462–464. doi: 10.1016/0168-5597(85)90058-9

Chella, F., Pizzella, V., Zappasodi, F., and Marzetti, L. (2016). Impact of the reference choice on scalp EEG connectivity estimation. *J. Neural Eng.* 13:036016. doi: 10.1088/1741-2560/13/3/036016

Coles, M. G. (1989). Modern mind-brain reading: psychophysiology, physiology, and cognition. *Psychophysiology* 26, 251–269. doi: 10.1111/j.1469-8986.1989.tb01916.x

de Munck, J. C. (1988). The potential distribution in a layered anisotropic spheroidal volume conductor. *J. Appl. Phys.* 64, 464–470. doi: 10.1063/1.341983

Ford, J. M., Sullivan, E. V., Marsh, L., White, P. M., Lim, K. O., and Pfefferbaum, A. (1994). The relationship between P300 amplitude and regional gray matter volumes depends upon the attentional system engaged. *Electroencephalogr. Clin. Neurophysiol.* 90, 214–228. doi: 10.1016/0013-4694(94)90093-0

Gilbert, S. J., Henson, R. N. A., and Simons, J. S. (2010). The Scale of functional specialization within human prefrontal cortex. *J. Neurosci.* 30, 1233–1237. doi: 10.1523/JNEUROSCI.3220-09.2010

Hagemann, D., Naumann, E., and Thayer, J. F. (2001). The quest for the EEG reference revisited: a glance from brain asymmetry research. *Psychophysiology* 38, 847–857. doi: 10.1111/1469-8986.3850847

Herrmann, C. S. (2001). Human EEG responses to 1-100 Hz flicker: resonance phenomena in visual cortex and their potential correlation to cognitive phenomena. *Exp. Brain Res.* 137, 346–353. doi: 10.1007/s002210100682

Hillyard, S. A., and Anllo-Vento, L. (1998). Event-related brain potentials in the study of visual selective attention. *Proc. Natl. Acad. Sci. U.S.A.* 95, 781–787. doi: 10.1073/pnas.95.3.781

Kayser, J., and Tenke, C. E. (2010). In search of the Rosetta stone for scalp EEG: converging on reference-free techniques. *Clin. Neurophysiol.* 121, 1973–1975. doi: 10.1016/j.clinph.2010.04.030

Kleffner-Canucci, K., Luu, P., Naleway, J., and Tucker, D. M. (2012). A novel hydrogel electrolyte extender for rapid application of EEG sensors and extended recordings. *J. Neurosci. Methods* 206, 83–87. doi: 10.1016/j.jneumeth.2011.11.021

Lei, X., Wang, Y., Yuan, H., and Mantini, D. (2014). Neuronal oscillations and functional interactions between resting state networks: effects of alcohol intoxication. *Hum. Brain Mapp.* 35, 3517–3528. doi: 10.1002/hbm.22418

Lei, X., Xu, P., Luo, C., Zhao, J., Zhou, D., and Yao, D. (2011). fMRI Functional networks for EEG source imaging. *Hum. Brain Mapp.* 32, 1141–1160. doi: 10.1002/hbm.21098

Lei, X., Yang, P., and Yao, D. (2009). An empirical bayesian framework for brain-computer interfaces. *IEEE Trans. Neural Syst. Rehabil. Eng.* 17, 521–529. doi: 10.1109/TNSRE.2009.2027705

Liu, Q., Balsters, J. H., Baechinger, M., van der Groen, O., Wenderoth, N., and Mantini, D. (2015). Estimating a neutral reference for electroencephalographic recordings: the importance of using a high-density montage and a realistic head model. *J. Neural Eng.* 12:056012. doi: 10.1088/1741-2560/12/5/056012

Marzetti, L., Nolte, G., Perrucci, M. G., Romani, G. L., and Del Gratta, C. (2007). The use of standardized infinity reference in EEG coherency studies. *Neuroimage* 36, 48–63. doi: 10.1016/j.neuroimage.2007.02.034

Mullen, T. R., Kothe, C. A., Chi, Y. M., Ojeda, A., Kerth, T., Makeig, S., et al. (2015). Real-time neuroimaging and cognitive monitoring using wearable dry, EEG. *IEEE Trans. Biomed. Eng.* 62, 2553–2567. doi: 10.1109/TBME.2015.2481482

Nunez, P. L. (1981). A study of origins of the time dependencies of scalp EEG: i–theoretical basis. *IEEE Trans. Biomed. Eng.* 28, 271–280. doi: 10.1109/TBME.1981.324700

Nunez, P. L. (2010). REST: A good idea but not the gold standard. *Clin. Neurophysiol.* 121, 2177–2180. doi: 10.1016/j.clinph.2010.04.029

Nunez, P. L., and Srinivasan, R. (2006). A theoretical basis for standing and traveling brain waves measured with human EEG with implications for an integrated consciousness. *Clin. Neurophysiol.* 117, 2424–2435. doi: 10.1016/j.clinph.2006.06.754

Oostenveld, R., and Praamstra, P. (2001). The five percent electrode system for high-resolution EEG and ERP measurements. *Clin. Neurophysiol.* 112, 713–719. doi: 10.1016/S1388-2457(00)00527-7

Poldrack, R. A., and Yarkoni, T. (2016). From brain maps to cognitive ontologies: informatics and the search for mental structure. *Annu. Rev. Psychol.* 67, 587–612. doi: 10.1146/annurev-psych-122414-033729

Qin, Y., Xu, P., and Yao, D. (2010). A comparative study of different references for EEG default mode network: the use of the infinity reference. *Clin. Neurophysiol.* 121, 1981–1991. doi: 10.1016/j.clinph.2010.03.056

Rush, S., and Driscoll, D. A. (1969). EEG electrode sensitivity-an application of reciprocity. *IEEE Trans. Biomed. Eng.* 16, 15–22. doi: 10.1109/TBME.1969.4502598

Smith, S. M., Fox, P. T., Miller, K. L., Glahn, D. C., Fox, P. M., Mackay, C. E., et al. (2009). Correspondence of the brain's functional architecture during activation and rest. *Proc. Natl. Acad. Sci. U.S.A.* 106, 13040–13045. doi: 10.1073/pnas.0905267106

Tian, Y., and Yao, D. (2013). Why do we need to use a zero reference? Reference influences on the ERPs of audiovisual effects. *Psychophysiology* 5, 1282–1290. doi: 10.1111/psyp.12130

Tzourio-Mazoyer, N., Landeau, B., Papathanassiou, D., Crivello, F., Etard, O., Delcroix, N., et al. (2002). Automated anatomical labeling of activations in SPM using a macroscopic anatomical parcellation of the MNI MRI single-subject brain. *Neuroimage* 15, 273–289. doi: 10.1006/nimg.2001.0978

Yao, D. (2001). A method to standardize a reference of scalp EEG recordings to a point at infinity. *Physiol. Meas.* 22, 693–711. doi: 10.1088/0967-3334/22/4/305

Yao, D. (2017). Is the surface potential integral of a dipole in a volume conductor always zero? A cloud over the average reference of EEG and ERP. *Brain Topogr.* 30, 161–171. doi: 10.1007/s10548-016-0543-x

Yao, D., Wang, L., Oostenveld, R., Nielsen, K. D., Arendt-Nielsen, L., and Chen, A. C. (2005). A comparative study of different references for EEG spectral mapping: the issue of the neutral reference and the use of the infinity reference. *Physiol. Meas.* 26, 173–184. doi: 10.1088/0967-3334/26/3/003

Yeo, B. T., Krienen, F. M., Eickhoff, S. B., Yaakub, S. N., Fox, P. T., Buckner, R. L., et al. (2015). Functional specialization and flexibility in human association cortex. *Cereb. Cortex* 25, 3654–3672. doi: 10.1093/cercor/bhu217

Yeo, B. T., Krienen, F. M., Sepulcre, J., Sabuncu, M. R., Lashkari, D., Hollinshead, M., et al. (2011). The organization of the human cerebral cortex estimated by intrinsic functional connectivity. *J. Neurophysiol.* 106, 1125–1165. doi: 10.1152/jn.00338.2011

Zhai, Y., and Yao, D. (2004). A study on the reference electrode standardization technique for a realistic head model. *Comput. Methods Programs Biomed.* 76, 229–238. doi: 10.1016/j.cmpb.2004.07.002

Conflict of Interest Statement: The authors declare that the research was conducted in the absence of any commercial or financial relationships that could be construed as a potential conflict of interest.

frontiers in Neuroscience

ORIGINAL RESEARCH
published: 05 May 2017
doi: 10.3389/fnins.2017.00247

A Comparative Study of Average, Linked Mastoid, and REST References for ERP Components Acquired during fMRI

*Ping Yang, Chenggui Fan, Min Wang and Ling Li **

Key Laboratory for NeuroInformation of Ministry of Education, High-Field Magnetic Resonance Brain Imaging Key Laboratory of Sichuan Province, Center for Information in Medicine, School of Life Science and Technology, University of Electronic Science and Technology of China, Chengdu, China

In simultaneous electroencephalogram (EEG) and functional magnetic resonance imaging (fMRI) studies, average reference (AR), and digitally linked mastoid (LM) are popular re-referencing techniques in event-related potential (ERP) analyses. However, they may introduce their own physiological signals and alter the EEG/ERP outcome. A reference electrode standardization technique (REST) that calculated a reference point at infinity was proposed to solve this problem. To confirm the advantage of REST in ERP analyses of synchronous EEG-fMRI studies, we compared the reference effect of AR, LM, and REST on task-related ERP results of a working memory task during an fMRI scan. As we hypothesized, we found that the adopted reference did not change the topography map of ERP components (N1 and P300 in the present study), but it did alter the task-related effect on ERP components. LM decreased or eliminated the visual working memory (VWM) load effect on P300, and the AR distorted the distribution of VWM location-related effect at left posterior electrodes as shown in the statistical parametric scalp mapping (SPSM) of N1. ERP cortical source estimates, which are independent of the EEG reference choice, were used as the golden standard to infer the relative utility of different references on the ERP task-related effect. By comparison, REST reference provided a more integrated and reasonable result. These results were further confirmed by the results of fMRI activations and a corresponding EEG-only study. Thus, we recommend the REST, especially with a realistic head model, as the optimal reference method for ERP data analysis in simultaneous EEG-fMRI studies.

Keywords: ERP, REST reference, average reference, linked mastoid, N1, P300, statistical parametric scalp mapping (SPSM)

OPEN ACCESS

Edited by:
Maria L. Bringas, University of Electronic Sciences and Technology of China, China

Reviewed by:
Claudio Babiloni, Sapienza University of Rome, Italy
Laura Marzetti, University of Chieti-Pescara, Italy

****Correspondence:***
Ling Li
liling@uestc.edu.cn

Specialty section:
This article was submitted to Brain Imaging Methods, a section of the journal Frontiers in Neuroscience

Received: *31 August 2016*
Accepted: *18 April 2017*
Published: *05 May 2017*

Citation:
Yang P, Fan C, Wang M and Li L (2017) A Comparative Study of Average, Linked Mastoid, and REST References for ERP Components Acquired during fMRI. Front. Neurosci. 11:247. doi: 10.3389/fnins.2017.00247

INTRODUCTION

In electroencephalogram (EEG) and event-related potential (ERP) research, the reference issue is an important problem. Previous studies investigated the effects of different references on simulated or real EEG/ERP data, showing that the voltage of the scalp potentials, power spectra, EEG coherence, connectivity configuration, DMN configuration, and even the polarity of some electrodes were changed by the adopted reference methods (Joyce and Rossion, 2005; Marzetti et al., 2007; Yao et al., 2007; Qin et al., 2010). Moreover, the statistical parametric scalp mapping (SPSM), which is the

scalp distribution of the significant statistical difference between two conditions, varied depending on the adopted references (Tian and Yao, 2013). Therefore, the choice of different references might cause data misinterpretation within the same experiment.

Typically, the EEG/ERP references include average reference (AR), digitally linked mastoid (LM), vertex reference (CZ), and REST reference (Yao, 2001). AR is the most popular choice in ERP studies, since it uses the average of channels as reference and it is unbiased to any electrode position. However, an inadequate spatial sampling (e.g., sparse electrode array) can affect the AR data and the underlying source estimation (Lantz et al., 2003). LM, with the average of left and right mastoids as reference, is another popular reference method for ERP studies, since the LM is suggested to be far from all brain sources and thus could be treated as a zero potential point. Also, LM is independent of electrode montages, which facilitates the comparison of results from different laboratories with different electrode caps. However, using simulated data, previous studies showed that AR and LM references lead to significant distortion of scalp power distribution and scalp network structure (Yao et al., 2005; Qin et al., 2010). This occurs because using scalp recordings as reference, like AR and LM, would bring their own physiological dynamic signals into the EEG signal and thus affect the spatial and temporal aspects of the EEG signal (Yao, 2001; Thatcher, 2012). To minimize the effect of physical reference on EEG signals, Yao proposed a reference electrode standardization technique (REST) which calculated a reference point at infinity (Yao, 2001).

The REST is based on the fact that the EEG source estimates are reference-free (Geselowitz, 1998; Yao, 2001; Michel et al., 2004), so the scalp potential topography can be unambiguously reconstructed by a set of known generator sources for a given head model (forward solution). Therefore, Yao proposed a non-unique equivalent dipole source model, which assumed an equivalent source distribution (ESD) on the cortical surface. The ESD and a proposed three-concentric-sphere head model were used to compute a transfer matrix. Then, the transfer matrix can be used to rereference scalp potentials to an infinity reference (Yao, 2001). Please note that, the non-unique equivalent dipole source model is used to calculate the transfer matrix rather than to solve the EEG inverse problem. So that the transfer matrix is independent of the actual neuronal generators, and the REST reference is independent of the actual EEG data. Furthermore, this infinity reference (REST) is considered to be located far from all brain sources and scalp electrodes, and thus it induces a small effect on EEG signals. Previous studies have demonstrated that REST reference can approximately recover the EEG temporal waveform, power spectrum (Yao, 2001), EEG coherence (Marzetti et al., 2007), EEG connectivity patterns (Chella et al., 2016), and EEG network configuration (Qin et al., 2010). Also, simulation studies using a concentric three-sphere head model and a realistic head model (Zhai and Yao, 2004) have confirmed the accurateness of the REST reconstruction, even when a low-density montage was used (Liu et al., 2015). According to the REST calculation, its validity depends on the leadfield matrix. Thus, the limitations of REST are the electrode density and the accuracy of the head model (Yao, 2001; Nunez, 2010).

In the present study, we collected simultaneous electroencephalography and functional magnetic resonance imaging (EEG-fMRI) data with a classical working memory paradigm. To determine the reference that best identifies neural activity and therefore be the basis of improved estimates of ERP features in the present EEG-fMRI recordings, we compared the reference effects of AR, LM, REST with the sphere head model (RESTs), and REST with the realistic head model (RESTr) on the task-related ERP effects and its distribution (e.g., discrimination-related posterior N1, VWM load-related parietal P300, and so on), which is the most concern in cognitive neuroscience research and was confirmed to be affected by the reference choice (Kayser et al., 2007; Tian and Yao, 2013). We hypothesized the change of reference methods would alter the task-related ERP effect itself (measured by statistical significance) and especially its scalp distribution (measured by SPSM).

ERP cortical source estimations were used as the golden standard in this comparison, since the underlying neural sources are the same no matter what reference is actually adopted (Geselowitz, 1998; Yao, 2001; Michel et al., 2004). Please note that, the REST approach is independent of the actual EEG data, thus the REST does not give any special advantage over the other electrode references when EEG source estimation is performed. In more detail, we localized the ERP of interest source generators and got source activities for each source region (inverse solution), then the source activities can be projected back to scalp voltage (forward solution). According to scalp topographical maps at the respective latency of the peak source intensities, we can indicate the contribution of a given source to the scalp responses at specific electrode sites (Bledowski, 2004; Bledowski et al., 2006). Thus, the observed task-related differences in the peak source intensities can be considered responsible for task-related differences in the ERP at that electrode sites (Mitzdorf, 1985; Bledowski, 2004; Bledowski et al., 2006; Kayser et al., 2007). So, we computed the distribution of the task-related ERP effect on the scalp (SPSM) for each reference method, and compared them to the distribution of the task-related source activities acquired from ERP source regions and the corresponding fMRI activations. In addition, we assessed the reference effect on the EEG-only data analysis which was collected during the same task but without active fMRI recordings. This could provide supportive evidence for reference selection in EEG-fMRI studies.

Although, AR and LM are the most popular reference methods for the ERP analysis of simultaneous EEG-fMRI studies (Huettel et al., 2004; Bledowski et al., 2006; Novitskiy et al., 2011; Castelhano et al., 2014; Chun et al., 2016), they might alter the ERP results by bringing physical interference into the EEG signal as previously mentioned. The REST overcomes this problem by calculating a reference point at infinity but is limited with the electrode density and the accuracy of the head model. Since the individual structure image and realistic electrode positions were available, and the number of electrodes is sufficient (64-channels), we speculate that REST with the realistic head model (RESTr) is the best option in simultaneous EEG-fMRI studies.

MATERIALS AND METHODS

Subjects

Eighteen right-handed subjects (9 females), age 19–27 (mean age = 21.9 years, standard deviation = 2 years), participated in the EEG-fMRI study for monetary compensation. Another group of 14 right-handed subjects (3 females), age 21–28 (mean age = 23 years), were recruited for the EEG-only study. Subjects were recruited at the University of Electronic Science and Technology of China. All the subjects had no history of neurological problems and had normal color vision. An informed consent form was signed by each subject before the experiment. The study was approved by the local ethics committee for the Protection of Human Subjects for the University of Electronic Science and Technology of China. The methods were carried out in accordance with the approved guidelines and all experiments conformed to the declaration of Helsinki.

Procedure

The stimuli consisted of nine disks with highly discriminable colors, including red, yellow, blue, green, cyan, purple, pink, orange, and carmine. The diameter of each disk was 2.2 cm and the distance between disks was at least 3.8° (center to center). **Figure 1** illustrates an example of the change detection paradigm (Li et al., 2011). The trial began with a 200-ms black fixation cross and an arrow, which instructed subjects to attend and memorize the items in the corresponding visual field. A fixation cross was then presented alone for 200 ms. Following that, subjects were presented with a memory array for 500 ms, consisting of the same number of disks in the left and right visual fields, with 2 or 4 disks per hemi-field. Within each hemi-field, the disks were randomly selected without repetition from the nine potential disk colors. The disks were randomly located on an invisible 4 × 3 matrix (5.5° × 4.2°) in both visual fields. After the memory array presentation, a black fixation cross was presented for the duration of the 6,000 ms maintenance interval which allowed us to separate the activation related to the encoding, maintenance, and retrieval phases of the VWM task (Pessoa et al., 2002; Ranganath, 2006). Subsequently, the test array remained on the screen for up to 1,500 ms, during which subjects responded with a button press, indicating whether the colors of the disks in the attended hemi-field were the same or different from those in the memory array regardless of object locations. Only one colored disk changed its location from the memory to the test array for the *location change condition* and none of the objects changed their original location for the *location repeat condition*. After the test array, the inter-trial interval (ITI) varied between 800 and 1,400 ms (average ITI was 1.1 s).

In the present experiment, subjects were instructed to remember the color and disregard the location of the disks in the attended hemi-field. Subjects were required to maintain central fixation throughout the recordings and to respond as quickly as possible. Subjects used their right hands to press button 1 when the color of all the disks in the memory array was the same as that of the test array in the attended visual field, and button 2 when the color of a disk was changed.

The EEG-only study used the same paradigm, but the VWM maintenance interval was changed from 6,000 to 900 ms (Li et al., 2011).

EEG and fMRI Recording

Subjects performed the task inside the MRI scanner (GE Signa 3.0 T) with simultaneous EEG and MRI recordings. The sampling clocks of the EEG and MRI systems were synchronized by means of the Syncbox (BrainProducts).

EEG signals were collected using a 64-channel fMRI-compatible Neuroscan Maglink System with Ag/AgCl electrodes placed according to the international 10/20 electrode placement standard. Vertical and horizontal electrooculogram (EOG) were recorded with electrodes above and on the outer canthi of the left eye. The electrocardiograms (ECGs) were recorded with a pair of electrodes above and below the left sternum. EEG data were sampled at 1,000 Hz and the electrode impedances were kept under 10 KΩ throughout the experiment. The amplifier gain was 150 and the analogic bandpass filter was set at 0–200 Hz. The AFz electrode site served as the ground electrode and an electrode between Cz and Pz served as reference.

Functional MR images were acquired with a gradient echo planar imaging (EPI) sequence with the following scanning parameters: TR = 2,000 ms; TE = 30 ms; FA = 90°; FOV = 240 mm; matrix size = 64 × 64; voxel size = 3.75 × 3.75 × 4.4 mm^3; 35 slices. The structural images were acquired with a high-resolution T1-weighted scan (voxel size = 1 × 1 × 1 mm^3).

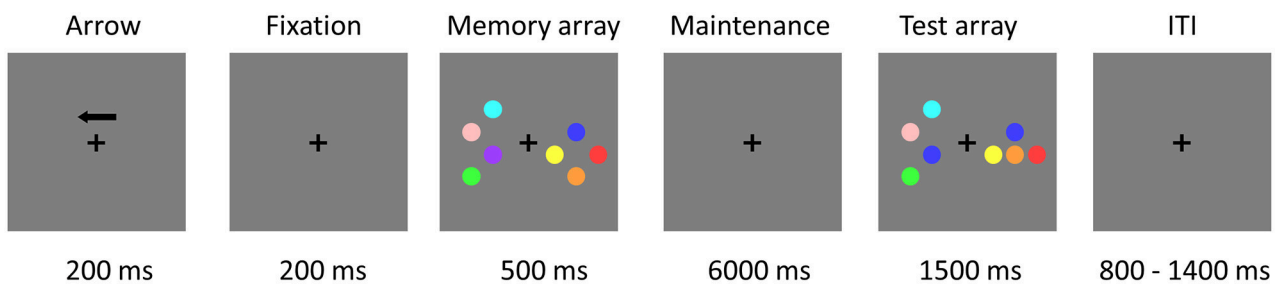

FIGURE 1 | Trial demonstration of the change detection task in the EEG-fMRI study. Subjects were asked to maintain two or four objects in an attended visual side for 6 s and then to indicate whether the test array matched or mismatched the object colors in the memory array, regardless of object location. Independent EEG study without simultaneous fMRI recordings used the same paradigm, but the VWM maintenance interval was changed from 6,000 to 900 ms.

EEG Data Preprocess and Re-Reference

EEG data preprocessing was performed using the CURRY 7 Neuroimaging Suite. The preprocessing step included filtering between 0.1 Hz (slope, which is the frequency range from complete attenuation to complete transfer, is 0.2 Hz) and 48 Hz (slope is 9.6 Hz), removing gradient artifacts (using average subtraction during each TR interval), removing ballistocardiogram artifacts (PCA based correction) and removing EOG artifacts (amplitude exceeding a ± 60 μv threshold). Artifact-free EEG data was exported to MATLAB and EEGlab for further analysis.

The continuous EEG data were segmented into test array locked epochs (from −200 to 1,000 ms relative to the test array onset). Trials in which the EEG activities exceeded 100 μV and contained incorrect responses were rejected. The remaining trials were re-referenced to AR, LM, RESTs, and RESTr references. The AR reference used the average of all channels as reference, whereas the LM used the average of left and right mastoid as reference.

For the RESTs reference, a three-concentric-sphere head model was reconstructed with the radii of the three concentric spheres: 0.87 (inner radius of the skull), 0.92 (outer radius of the skull), and 1.0 (radius of the head). The conductivities were 1.0 (brain and scalp) and 0.0125 (skull). The coordinates of the electrodes are automatically normalized to the spherical surface with radius 1.0. The lead field matrix was calculated from 3,000 radical cortical dipoles distributing on the spherical surface using the LeadField.exe (in REST software). Finally, EEG data, electrode positions and lead field matrix were imported into REST software (http://www.neuro.uestc.edu.cn) and then the REST reference was applied to the EEG data.

For the RESTr reference, (1) we extracted the cortex surface from subject's MRI images using the BrainVISA (version 4.3 http://brainvisa.info/); (2) we then reconstructed a 3-shell realistic BEM head model on the cortex surface, by means of Brainstorm (http://neuroimage.usc.edu/brainstorm); (3) projected the electrode positions on the scalp surface, and then modified the electrode positions based on the head shape and EEG gel artifact observed in the structural image; (4) the cortex surface was down-sampled to 3,000 vertices; (5) the transfer lead field matrix was calculated by the above-mentioned electrode positions and head model using the OpenMEEG boundary element method (Gramfort et al., 2010), where conductivities for the scalp, skull, and brain were 1.0, 1/80, and 1.0 separately. Sample dipoles were positioned at each vertex, with their directions constrained to be perpendicular to the cortical surface; (6) EEG data, electrode positions and lead field matrix are imported into REST software and then the REST reference was applied to the EEG data. Above steps were perform for each subject.

ERP Analysis

By inspecting the grand average ERP waveforms and the topographic maps, two ERP components of interest were examined. N1 was defined as a negative deflection in the 150–200 ms time window and P300 was defined as a positive deflection in the 300–600 ms time window after the test array onset. The N1 peak amplitude and latency were measured and averaged across the left (P5, P3, P1) and right (P2, P4, P6) parietal electrodes sites as two separate clusters. P300 mean amplitudes were measured between 300 and 600 ms and averaged across the central-parietal electrode cluster (CP1, CP2, P1, PZ, P2).

To evaluate the reference effects on ERP components, we applied a four-way repeated measure analysis of variance (ANOVA) with reference method, memory load, cue side, and location change/repeat as factors for N1 and P300 components, separately. After that, for each reference data, we applied a three-way repeated ANOVA with memory load, cue side, and location change/repeat as factors for N1 and P300 components, separately. Such analysis investigates whether the experimental effect (significant differences across experimental conditions) would be changed by the adopted references.

SPSM Analysis

We computed a *t*-test of the N1 amplitude (peak value between 150 and 200 ms) between *location repeat* and *location change* condition for each electrode. The resulting *P*-value was described on a topography map with a threshold of 0.05 to form the statistical parametric scalp mapping (SPSM). The above processes were performed for each reference data. Such analysis seeks to investigate whether the scalp distributions of experimental effect (significant differences across experimental conditions) would be changed by the adopted references.

Source Analysis

Source reconstruction of individual ERP data was performed using the Brainstorm 3.0 software. We used the standard MNI template ICBM152, which is consistent with the MNI template used in the fMRI analysis, to create the head model by using the boundary element method. The cortical current maps were computed from the ERP time series using the weighted minimum norm estimate (wMNE) inverse solution for each condition in each subject separately, as well as for the grand average condition (combined for eight conditions) in each subject. The source orientation was constrained to be normal to the cortical surface. Subject-wise cortical current maps were normalized (*z*-score) with the baseline period (−200 to −1 ms). The group-wise cortical maps were computed by the average of *z*-score across all subjects in each condition and the grand averaged condition, and then spatially smoothed with a 6 mm FWHM Gaussian filter.

For each potential source, we extracted the source activities for *location repeat* and *location change* conditions. Furthermore, the source activities were projected back to scalp voltage, and the topographical maps were calculated at the respective peak latency in order to assess the contribution of the current source to the scalp voltage. To assess whether the sources responsible for the location-related effect as measured on the posterior N1 component, the mean source intensities (± 10 ms around the peak) were calculated for each condition in each subject and then compared using a three-way ANOVA. The location-related fMRI activations were also treated as the potential sources of N1 and were processed using the above-stated steps.

Please note that we did not calculate the P300 source nor extract the P300 source waveforms. This was because the

generators of P300 are widely distributed in space and time (Kok, 2001), thus it is hard to use the P300 sources to verify the distribution pattern of VWM load-related effect on P300. Our fMRI results also showed the VWM load-related activations were widely distributed at frontal, parietal, temporal, and occipital cortices.

fMRI Preprocessing and Analysis

fMRI data preprocessing was performed using statistical parametric mapping software (SPM12, http://www.fil.ion.ucl.ac.uk/spm) for each subject. The first five EPI volumes of the fMRI images were discarded for signal stabilization. fMRI data preprocessing included slice timing correction, three-dimensional motion correction, co-registration to individual anatomical images, normalization to the Montreal Neurological Institute (MNI) reference space ($3 \times 3 \times 3$ mm^3), and spatial smoothing with an 8 mm Gaussian kernel (full-width at half-maximum). One session from one subject with a total vector motion >2 mm or rotation >2° was excluded from further analysis.

For the first level statistical analyses, a general linear model (GLM) was constructed for each subject's observed fMRI time course. Three time points (representing the onsets of arrow, delay, and test arrays) were defined for each condition and convolved with a canonical hemodynamic response function (HRF) to form regressors of the design matrix (Gazzaley et al., 2007; Robitaille et al., 2010; Passaro et al., 2013). Moreover, six additional spatial movement regressors were added to the design matrix. The memory array period was not modeled in the design matrix since the time interval between the arrow and the memory array was too small. Thus, the regressor of the arrow was used to represent both the arrow and memory periods in the present study. The data and models for each individual subject were high-pass filtered to a cutoff of 1/128 Hz and pre-whitened with a fitted autoregressive model [AR (1)].

For the second level statistical analyses, VWM retrieval-related maps were compared using a one-sample *t*-test, contrasting the combined activation across conditions during the retrieval phase with the fixation baseline. The retrieval-related map was thresholded at $P < 0.05$ (FDR corrected) and cluster size >45 voxels, and then used as a prior mask for the following statistics. Individual subject contrast images for each condition, during the VWM retrieval phase, were entered into a random-effect model with a 2 (load 2 vs. 4) × 2 (left vs. right visual field) × 2 (location repeat vs. change) ANOVA using GLM_Flex2 (http://mrtools.mgh.harvard.edu/index.php/GLM_Flex). Masked by the retrieval-related map, we reported clusters >15 contiguous voxels, at a voxel-wise threshold of $P < 0.005$ (uncorrected, cluster size corrected to $P < 0.01$ using the AlphaSim; Forman et al., 1995), for location effects.

Regions of interest (ROIs) were defined based on the multi-subject statistical maps. A 6-mm radius sphere (centered around the peak activation of each cluster) was drawn as a ROI, by means of MarsBar software (http://marsbar.sourceforge.net). The values of each ROI were analyzed using a three-way repeated-measures ANOVA as described above.

We used the fMRI location-related clusters as regional sources to obtain the source waveform and scalp projection. The peak intensities were calculated for each condition in each subject and then compared using a three-way ANOVA, for each ROI (same process in Source Analysis).

EEG-Only Recordings (Collection, Preprocessing, and Analysis)

EEG-only was recorded using a 128-channel EGI HydroCel GSN (EGI, Eugene, OR, USA) electrode cap with electrodes placed according to the international 10/20 electrode placement standard. EEG signals were recorded using NetStation 4.1.2 with a Net Amps 300 amplifier (Electrical Geodesic Inc., EGI, Eugene, Oregon, USA). The online reference electrode was the Cz (129th) and the ground reference had a centroparietal location. All electrode impedances were kept well below 50 kΩ. EEG was digitized at 1,000 Hz with an amplifier band-pass of 0.1–48 Hz.

EEG data were processed off-line using Net Station Waveform Tools and Matlab. The continuous EEG data were filtered by a two-way FIR bandpass filter from 0.1 to 48 Hz (eegfilt.m from EEGLAB toolbox), and were segmented into test array locked epochs (from −200 to 1,000 ms relative to the test array onset). For each segments, channels with amplitudes exceeding 200 μV were marked as undesirable and replaced through the interpolation of neighboring electrodes. EOG and significant muscle artifacts were excluded by automatic artifact rejection (±100 μV). EEG epochs containing incorrect button presses and eye movements were excluded. The data was baseline corrected using the 200 ms before the onset of the memory array. EEG epochs were then averaged across trials according to load (two and four), visual side (left and right), and location repeat/change conditions. For each subject, at least 32 trials were included for each condition. The remaining trials were re-referenced to AR, LM, and RESTs reference. Since LM reference distorted the grand-average ERP shape, it will not be used for subsequent analyses.

ERP analysis refers to the analysis of ERP data in the EEG-fMRI study. N1 and P300 were selected as the ERP components of interest. The N1 peak amplitude and latency were measured and averaged across the left (P7, P3, PO3, and 66) and right (P8, P4, PO4, and 84) parietal electrode sites as two separate clusters. P300 mean amplitudes were measured between 300 and 600 ms and averaged across the central-parietal electrode cluster (CP1, CP2, C1, CZ, C2, 7, 106, 31, 80). SPSM analysis for the N1 component measured by the *t*-test between *location repeat* and *location change* conditions using the peak N1 amplitude (150–200 ms interval), for each electrode separately. Source analysis refers to the Source Analysis in the EEG-fMRI study.

Statistical Analysis

Statistical analyses were performed using SPSS Statistics Release 19 (IBM, Somers, NY, USA) General Linear Model. Bonferroni corrections were performed for multiple comparisons, and Greenhouse-Geisser corrections were performed for non-sphericity data where necessary. *Post-hoc* multiple-comparison tests were performed where appropriate.

RESULTS

ERP Effects

Figure 2A depicts the topographic map of the test array locked to the N1 component at 187 ms, which was defined by the peak of the grand-average ERP data, for AR, LM, RESTs, and RESTr references separately. Consistent with previous studies, the choice of different references would not change the spatial distribution pattern of the voltages (Yao et al., 2007). **Figures 2B,C** depict the test array locked ERPs for the *location repeat* and *location change* conditions at left and right electrode clusters, calculated for four references separately.

For the N1 amplitude at left electrode clusters, a four-way repeated measures ANOVA revealed a location effect [$F_{(1, 17)} = 20.5$, $P < 0.001$], as well as an interaction between reference method and location effect [$F_{(3, 15)} = 3.9$, $P < 0.05$]. For the N1 amplitude at right electrode clusters, we detected a location effect [$F_{(1, 17)} = 7.0$, $P < 0.05$] and an interaction between reference method and location effect [$F_{(3, 15)} = 3.9$, $P < 0.05$].

After that, we performed three-way repeated measures ANOVAs for N1 amplitude at the left and right electrode clusters, calculated for the four references separately. N1 amplitude was significantly larger during the *location repeat* compared with the *location change* condition at both left and right electrode clusters, with corresponding *F*- and *P*-values for different references described in **Figure 2**.

For the N1 latency, neither reference effects nor interaction effects between reference and other factors were detected, both at left or right electrode clusters (all Ps > 0.1). When we examined each type of reference data, we detected delayed N1 latency for left-view stimuli compared to right-view stimuli at left electrode clusters, for AR [$F_{(1, 17)} = 10.6$, $P = 0.005$], RESTs [$F_{(1, 17)} = 6.3$, $P = 0.022$], and RESTr [$F_{(1, 17)} = 5.8$, $P = 0.028$]. Furthermore, we detected delayed N1 latency for load 2 compared with load 4 at right electrode clusters, for AR [$F_{(1, 17)} = 11.5$, $P = 0.003$], MM [$F_{(1, 17)} = 34.9$, $P < 0.001$], RESTs [$F_{(1, 17)} = 13.8$, $P = 0.002$], and RESTr [$F_{(1, 17)} = 9.3$, $P = 0.007$].

For the P300 amplitude, a four-way repeated measures ANOVA revealed a load effect [$F_{(1, 17)} = 2.4$, $P < 0.05$] and a marginally significant main effect of reference [$F_{(3, 15)} = 2.8$, $P = 0.077$]. After that, we performed a three-way repeated measures ANOVA for each type of reference data. P300 amplitude revealed a significant main effect of VWM load for AR and two REST data but a marginally significant load effect for LM data. The corresponding *F*- and *P*-values are described in **Figure 3**.

SPSM Results

Since the N1 amplitude (peak value between 150 and 200 ms) revealed a significant difference between *location repeat* and *location change* conditions, we computed the significance level (*P*-value) for each electrode and presented the *P*-value on the topography map with a threshold of 0.05 (see **Figure 4**). For AR, the significant location effect was distributed at left posterior (P3, P5), right posterior (P2, P4, P6, CP2, CP4, CP6), frontal (FZ,

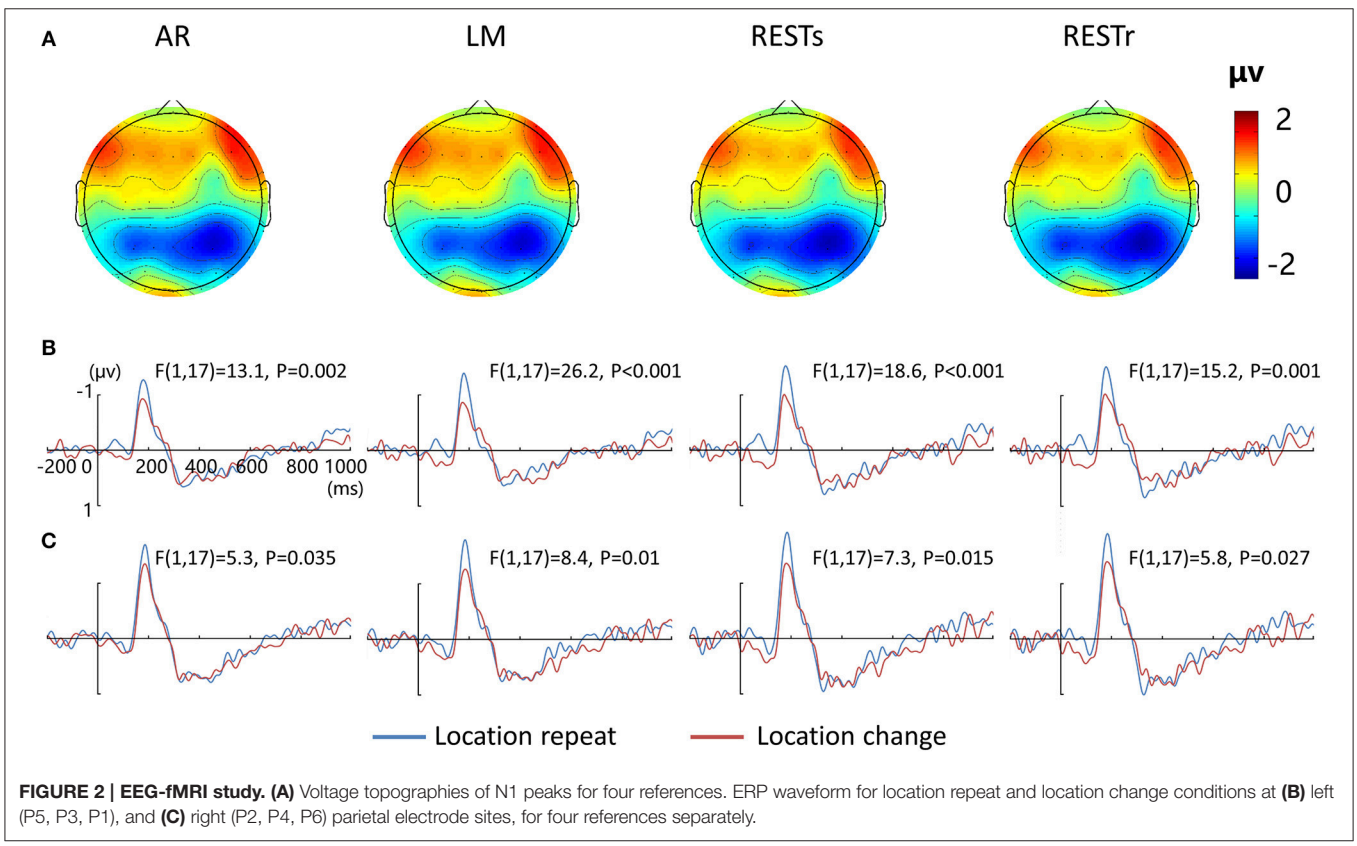

FIGURE 2 | EEG-fMRI study. (A) Voltage topographies of N1 peaks for four references. ERP waveform for location repeat and location change conditions at **(B)** left (P5, P3, P1), and **(C)** right (P2, P4, P6) parietal electrode sites, for four references separately.

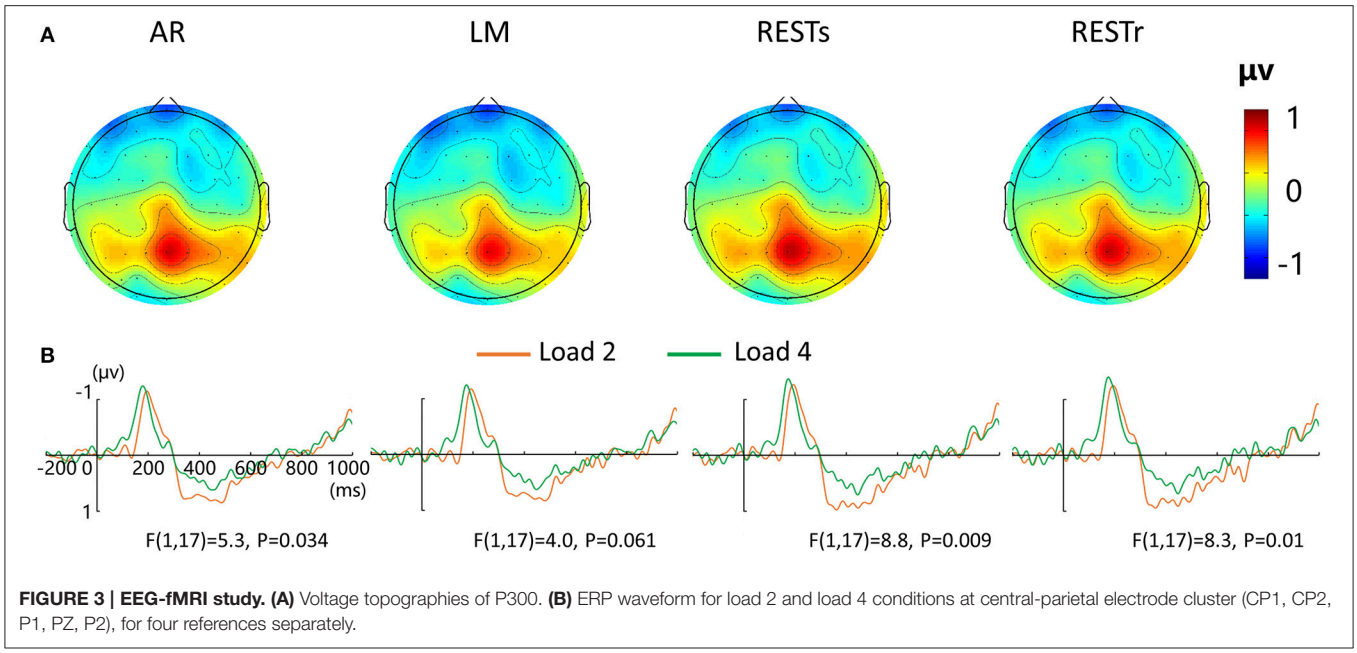

FIGURE 3 | EEG-fMRI study. (A) Voltage topographies of P300. **(B)** ERP waveform for load 2 and load 4 conditions at central-parietal electrode cluster (CP1, CP2, P1, PZ, P2), for four references separately.

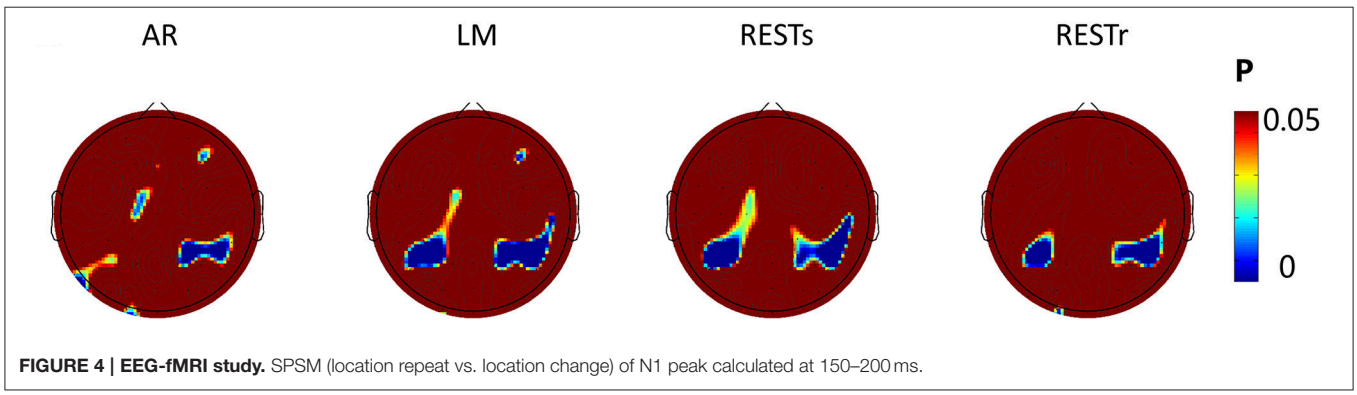

FIGURE 4 | EEG-fMRI study. SPSM (location repeat vs. location change) of N1 peak calculated at 150–200 ms.

F4), and left center (C1) electrodes sites. For LM, the significant location effect was distributed at left posterior (P3, P5, CP3, CP1), right posterior (P2, P4, P6, CP2, CP4, CP6, C6), left center (C1), and right frontal (F4) electrodes sites. For RESTs, the significant location effect was distributed at left posterior (P3, P5, CP3, CP1), right posterior (P2, P4, P6, CP2, CP4, CP6, C6), and left center (C1) electrodes sites. For RESTr, the significant location effect was distributed at left posterior (P3, P5, CP3, CP1) and right posterior (P2, P4, P6, CP2, CP4, CP6, C6) electrodes sites.

Source Results

Figure 5 illustrates the group-wise cortical maps in the N1 time range. Active sources were defined as those containing at least 15 adjacent vertices exceeding a z-score of 2. The results revealed bilateral activations in postcentral gyrus (PC), superior temporal gyrus (STG), middle temporal gyrus (MT), and superior occipital gyrus (SOG), as well as left hemisphere activations in superior parietal lobule (SPL), and right hemisphere activations in supramarginal gyrus (SMG), and insula (INS; **Table 1**).

Analysis of the scalp projection indicated these sources contribute to a negative scalp ERP at bilateral parieto-occipital electrodes sites and a positive scalp ERP at bilateral fronto-central electrodes sites. Three-way ANOVAs showed significant location effects in bilateral PC and STG, as well as left SPL and right SMG (see **Figure 5**).

fMRI Results

To localize the location-related brain regions, we contrasted activations of the *location repeat* with the *location change* conditions. The results showed significantly greater activations during the *location repeat* condition in the right SMG (BA 40) and right IFG (BA 45) compared to the *location change* condition. The results were projected onto a 3D surface using BrainNet (Xia et al., 2013) (**Figure 6A**).

The source in the right SMG revealed a negative deflection at 187 ms and the corresponding scalp projection indicated the right SMG source activity contributed mainly to the right posterior N1 component (**Figure 6B**). A three-way ANOVA showed a significant location effect [$F_{(1, 17)} = 5.14$, $P < 0.05$]

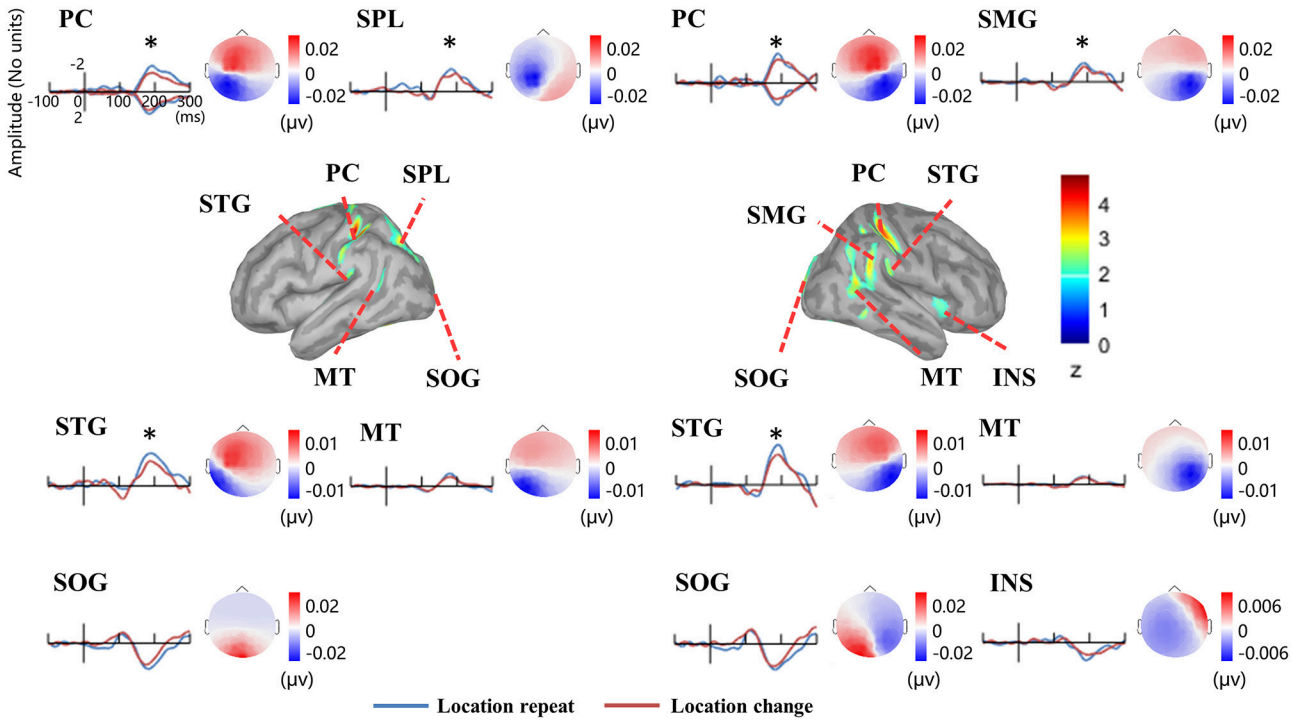

FIGURE 5 | EEG-fMRI study. Time courses of the regional source activity for *location repeat* and *location change*, and the scalp projection at the peak intensity. Cortical sources of the posterior N1 component on the ICBM152 MNI template (middle). *$P < 0.05$.

TABLE 1 | Sources of the N1 ERP component in the EEG-fMRI study.

Sources	H	x	Y	z
Postcentral gyrus	L	−44	−34	55
	R	34	−36	59
Middle temporal gyrus	L	−47	−54	8
	R	47	−51	16
Superior temporal gyrus	L	−52	−33	17
	R	52	−29	20
SupraMarginal gyrus	R	57	−48	27
Insula	R	39	18	3
Superior parietal lobule	L	−22	−66	45
Superior occipital gyrus	L	−6	−103	12
	R	7	−92	18

Regions showing the center of sources of the N1 component. Active sources with z-score >2 and adjacent vertices >15 are listed. (L, left; R, right; MNI coordinates are presented).

on the source intensities. The source in the right IFG revealed a positive deflection at 187 ms, and this source activity contributed mainly to the right frontal positivity of ERP (**Figure 6B**). No significant main effects for location were detected ($P > 0.1$).

Results of EEG-Only Study

Figure 7A depicts the topographic map of the test array locked to the N1 component at 187 ms, which was defined by the peak of the grand-average ERP data, for AR and RESTs separately. **Figures 7B,C** depict the test array locked ERPs for the *location repeat* and *location change* conditions at left and right electrode clusters, calculated for each reference separately.

N1 amplitude was significantly larger during the *location repeat* compared with the *location change* condition at both left and right electrode clusters, with corresponding *F*- and *P*-values for different references described in **Figure 7**. For the N1 latency at the left posterior electrode cluster, we detected delayed N1 latency for low load compared to high load conditions [AR data: $F_{(1, 17)} = 15.3$, $P = 0.002$; RESTs data: $F_{(1, 17)} = 17.4$, $P = 0.001$], and for *location change* than *location repeat* conditions [AR data: $F_{(1, 17)} = 20$, $P = 0.001$; RESTs data: $F_{(1, 17)} = 21.2$, $P < 0.001$]. For the N1 latency at the right posterior electrode cluster, we detected delayed N1 latency for low load compared to high load conditions [AR data: $F_{(1, 17)} = 32.6$, $P < 0.001$; RESTs data: $F_{(1, 17)} = 43$, $P < 0.001$], and for *location change* than *location repeat* conditions [AR data: $F_{(1, 17)} = 8$, $P = 0.014$; RESTs data: $F_{(1, 17)} = 5.2$, $P = 0.041$].

The central P300 component showed higher amplitude for load 2 compared to load 4 conditions [AR data: $F_{(1, 17)} = 68.5$, $P < 0.001$; RESTs data: $F_{(1, 17)} = 76.5$, $P < 0.001$]. Furthermore, the *location change* elicted higher P300 amplitude load compared to *location repeat* conditions [AR data: $F_{(1, 17)} = 5.1$, $P = 0.043$; RESTs data: $F_{(1, 17)} = 8.1$, $P = 0.14$].

SPSM of N1 showed significant location effect at left frontal (19, F3, 39, 44) and bilateral posterior electrode sites (50–52, 56–60, 63–72, 74–77, 82–84, 89–90 electrodes), both for AR and RESTs data.

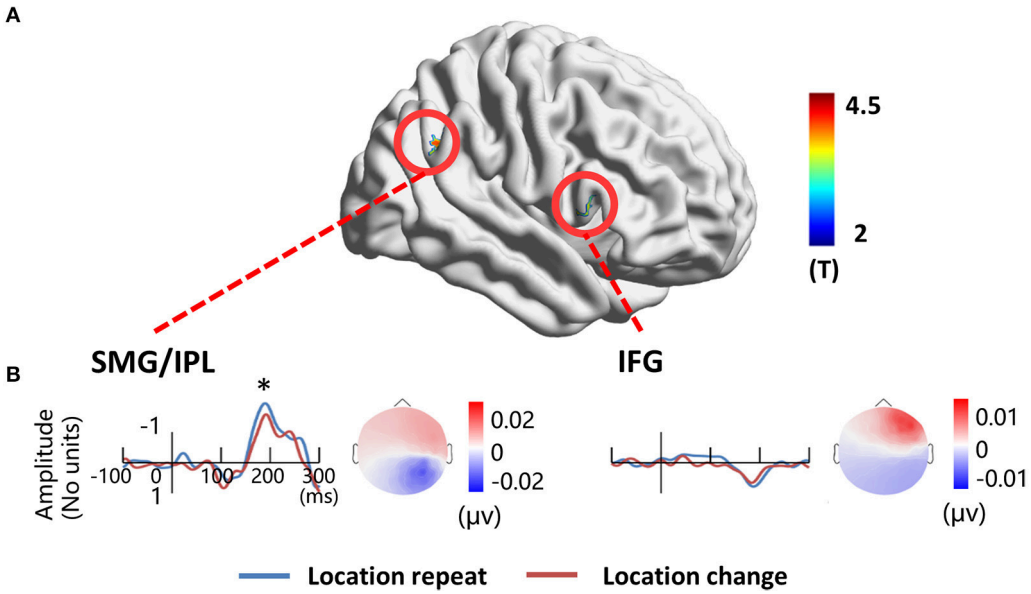

FIGURE 6 | EEG-fMRI study. (A) location-related fMRI activation regions. **(B)** Source time courses of the right SMG/IPL and the right IFG for the *location repeat* and *location change* conditions, and the corresponding scalp projection at the peak latency. *$P < 0.05$.

Source analysis showed the N1 component generated in bilateral PC, SPL, and SOG, left MOG, as well as right SMA (**Figure 8**, **Table 2**). Analysis of the scalp projection indicated these sources, except right SMA, contribute to a negative scalp ERP at bilateral parieto-occipital electrode sites. Three-way ANOVAs showed location repeated enhancement in the peak source activities in bilateral SPL, SOG, left MOG, and right PC, as showed in **Figure 8**.

DISCUSSION

The current study sought to identify the optimal referencing electrode procedure to study scalp ERPs recorded during fMRI scanning. We applied AR, LM, RESTs, and RESTr references to the ERP analysis within a simultaneous EEG-fMRI study and compared the reference effects on task-related ERP results which is a concern in cognitive neuroscience research and was confirmed to be affected by the reference choice (Kayser et al., 2007; Tian and Yao, 2013). ERP cortical source estimates were used as the golden standard in this comparison. It is because that the source localization of ERP components is reference-free, and also the implementation of the REST reference is independent of the actual EEG data. Results showed that the two REST references provided more integrated and reasonable results than that of AR and LM reference methods. These results were further confirmed by task-related fMRI activations and a corresponding EEG-only study.

Reference Effect on the ERP Amplitude and Latency

Similar topographic maps of N1 and P300 components were observed across four reference methods, which is consistent with previous studies reporting that the choice of different references would not change the spatial distribution pattern of the scalp voltages (Yao et al., 2007; Tian and Yao, 2013). However, in the present study, we did not find a main effect of reference methods on the N1 amplitude and latency, only a marginally significant main effect of reference methods on the P300 amplitude was observed. This is partly inconsistent with previous evidence showing that the ERP amplitude would be significantly altered by the adopted references (Kayser et al., 2007; Yao et al., 2007; Tian and Yao, 2013; Liu et al., 2015).

Actually, the amplitudes of N1 or P300 were small (about −1.3 uv for N1 and about 1 uv for P300) and showed high similarity across different references (**Figures 2**, **3**). This may be due to the static magnetic field interference on the EEG signal collected in the MRI scanner (Toyomaki and Yamamoto, 2007). Additionally, MRI gradient artifacts and ballistocardiogram artifacts result in small voltages of EEG signal after a series of preprocessing compared to that collected outside the scanner (Srivastava et al., 2005). Since the original signal is very weak, it is difficult to detect the difference across different references.

Reference Effect on the Task-Related ERP

Although, the reference choice does not change the spatial distribution of ERP component, it might change the significant difference between two experimental conditions. For example, a prominent occipital vision vs. audition attentional effect was observed in REST and AR reference, but not in LM reference (Tian and Yao, 2013). Consistent with above findings, we observed an interaction between reference choice and location effect both at left and right electrode clusters for N1 amplitude. As shown in **Figures 2B,C**, although location repeated enhancement was observed at both left and right electrode clusters at each

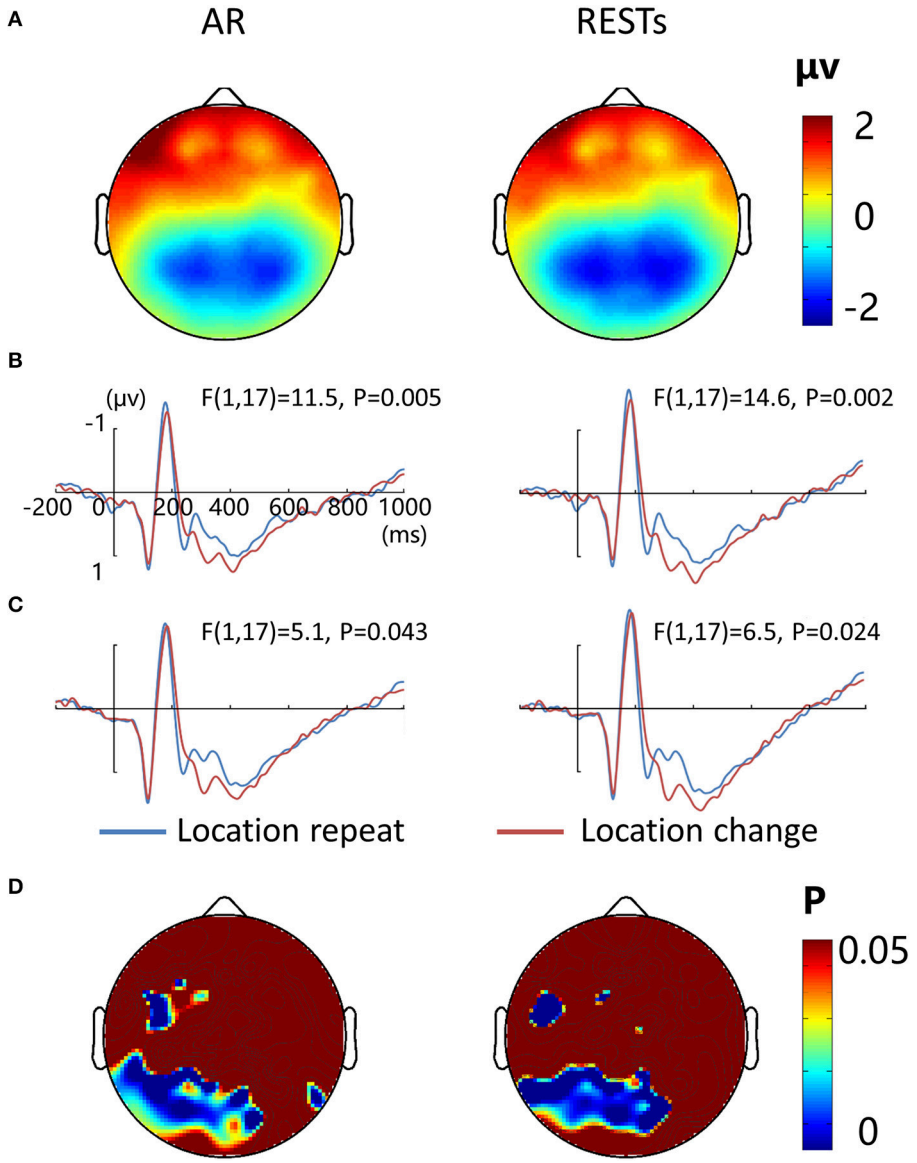

FIGURE 7 | EEG-only study. (A) Voltage topographies of N1 peaks for AR and RESTs references. ERP waveform for *location repeat* and *location change* conditions at **(B)** left (P7, P3, PO3, and 66), and **(C)** right (P8, P4, PO4, and 84) parietal electrodes sites, for two references separately. **(D)** SPSM (location repeat vs. location change) of N1 peak calculated at 150–200 ms.

reference method, the significance level (p-value) had a slight difference with different reference methods.

For the load-related P300 amplitude, although no interaction between reference choice and VWM load was observed, the significance level of VWM load effect was altered by the adopted references (**Figure 3B**). Compared with AR data, two REST references increased the VWM load effect while the LM decreased or eliminated the VWM load effect [$F_{(1,\ 17)} = 4.0$, $P = 0.061$].

More importantly, we used multiple adjacent electrodes as ROI and used the mean value of ROI to test the task-related effect, which improves the signal-to-noise ratio (Keil et al., 2014) of data. This may be the possible reason why these different references showed slight effect on the outcome.

Reference Effect on the Distribution of the Task-Related ERP

To assess the distribution of the experimental effects over the electrode sites, we performed the t-test of N1 amplitude between object location repeat and object location change conditions for each electrode and used the p-value to form the SPSM (statistical parametric scalp mapping) of N1 (Tian and Yao, 2013). The SPSM of N1 showed a distribution that is mostly the same but with a few differences, when using different references (**Figure 4**). In particular, we observed a significant

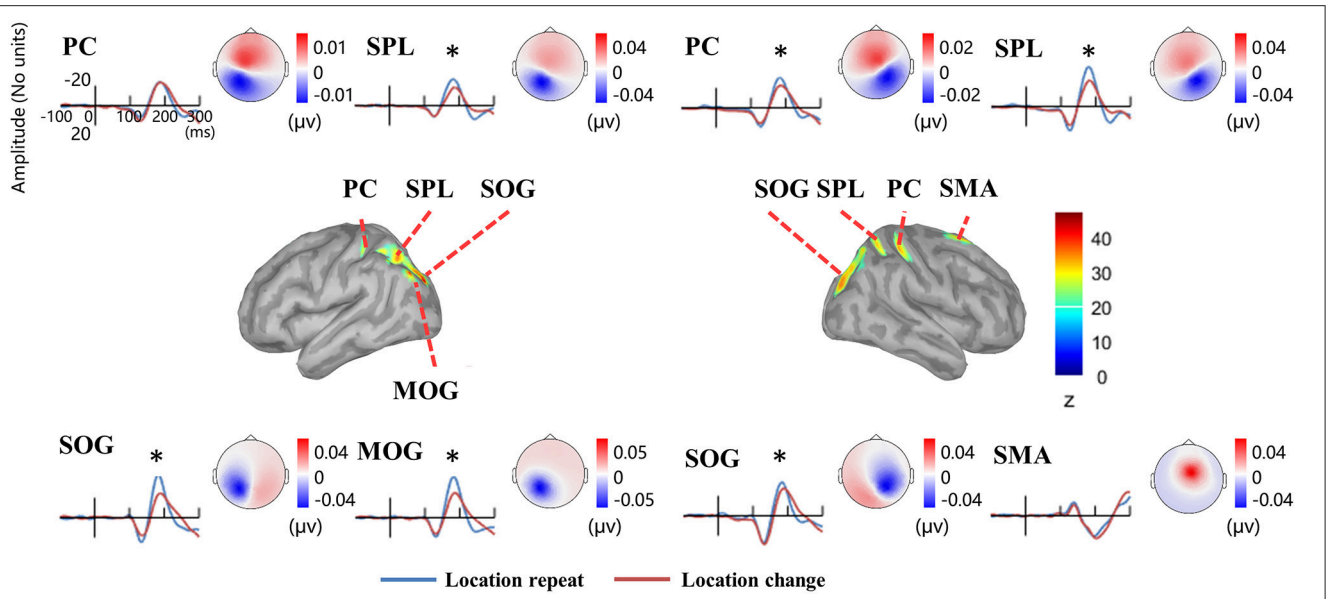

FIGURE 8 | EEG-only study. Time courses of the regional source activity for location repeat and location change, and the scalp projection at the peak intensity. Cortical sources of the posterior N1 component on the ICBM152 MNI template (middle). *$P < 0.05$.

TABLE 2 | Sources of the N1 ERP component in the EEG-only study.

Sources	H	*x*	*y*	*z*
Postcentral gyrus	L	−38	−37	56
	R	35	−39	62
Superior occipital gyrus	L	−24	−84	31
	R	24	−80	30
Superior parietal lobule	L	−32	−67	49
	R	33	−58	64
Middle occipital gyrus	L	−43	−75	36
Supplementary motor area	R	15	14	66

Regions showing the center of sources of the N1 component. Active sources with z-score >20 and adjacent vertices >15 are listed. (L, left; R, right; MNI coordinates are presented).

location effect at the right posterior sites for four types of reference data, while less significance at left posterior sites for AR data. C1 and CP1 showed significant location effect for AR, LM, and RESTs data, but not for RESTr data. F4 showed a significant location effect for AR and LM data, but not for REST data.

To verify the distribution of the location effect, we localized the N1 sources and detected the generators related to the location effect as measured on the scalp. As several researchers stated that the EEG source estimates are independent of the EEG reference (Pascual-Marqui and Lehamann, 1993; Geselowitz, 1998; Yao, 2001), so it is reasonable to use the source distribution and source activities as the golden standard to infer the relative utility of different references. According to the scalp projection, source waveform, peak intensities latency, and the location effect on the peak intensities, we suggest that the generators in bilateral PC, SPL, STG, and right SMG were mainly responsible for the location effect for the bilateral posterior N1 component (**Figure 5**). These results suggest that LM and the two REST references provide the closest distribution pattern of the N1 SPSM to the source analysis. The relatively credible results of N1 SPSM from the LM referenced data may be due to the phenomenon that the potentials of two mastoids are actually near zero at the N1 topographic map (**Figure 2A**). In the source analysis, we did not detect the location effect at C1 and CP1 electrode for AR, LM, and RESTs data, and the location effect at the F4 electrode for AR and LM data.

By inspecting the SPSM of N1 in RESTs data and RESTr data, the RESTr seem provided a closer distribution to the location-related source distribution since the RESTs still revealed some significant points at C1 and CP1. Such result may support the improvement of accuracy of the REST reconstruction when a realistic head model (volume conductor) was used (Zhai and Yao, 2004; Liu et al., 2015).

It is worth noting that the head volume conduction effects can confound the topography and amplitude of ERPs at the scalp electrode. Thus, to accurately evaluate the cortical activity under the scalp EEG electrodes, a researcher should be encouraged to perform a source analysis which is able to take into account at least in part the head volume conduction effects. In the previous simulation studies, researchers have demonstrated the validity of REST even when the volume conductor differs from the true head model and even when the conductivity ratio was varied, showing that the relative error between the simulated EEG recordings and the EEG recordings referenced at infinity is greater reduced by REST compared with other commonly used references (Yao, 2001; Qin et al., 2010; Liu et al., 2015). However, even when the realistic MRI head model was used, it cannot mitigate the overlapping effects of the neural ionic currents at the scalp electrodes.

fMRI Supports

Since EEG and fMRI are two modalities related to the same neuronal activity (Logothetis et al., 2001), we used the task-related fMRI brain regions as sources to test if these sources contribute to the task-related ERPs as measured on the scalp. The results indicated that the right SMG contributes to the location-related effect on the N1 component at right posterior sites. Most interestingly, the right SMG activated in the fMRI is consistent with the N1 source analysis. Since four reference data types showed the location effect at the right posterior sites (**Figure 4**), the fMRI result here is insufficient to verify which reference is preferable.

Although, the ERP and source analysis showed a location effect on both sides of posterior areas, fMRI showed a location effect only on the right SMG. These incongruent results on ERP and BOLD measures are common in simultaneous EEG and fMRI studies (Bledowski et al., 2006). This is because the ERP and fMRI BOLD signal are related directly and indirectly to neural activity separately (Ogawa et al., 1990; Nunez and Silberstein, 2000; Logothetis et al., 2001). Thus, the different sensitivity of the two modalities leads to activity visible in one modality but invisible in the other modality (Nunez and Silberstein, 2000).

In Comparison with EEG-Only Study

In order to confirm the results in the present simultaneous EEG-fMRI study, we used the ERP data collected in the same task but without active fMRI recordings to evaluate the effects of different reference procedures on task-related ERP results.

The results showed that the location repeated enhancement was reflected at bilateral posterior N1 and the VWM load suppression was reflected at central P300, which is consistent with the ERP results in the present EEG-fMRI study when using AR and two REST references. SPSM and source analysis of the N1 component confirmed that the bilateral posterior sources contribute to the bilateral posterior scalp N1 component, showing location repeated enhancement effects. These results are more closer to the LM and two REST references data in the present EEG-fMRI study. In general, the two REST references provide more consistent results between the simultaneous EEG-fMRI study and the EEG-only study.

The Effectiveness of ERP Result

In the present study, we found that the N1 amplitudes were insensitive to VWM load and the visual side of the presented stimulus, indicating that the N1 component may reflect a discriminative process rather than a sensory-perceptual process of attention allocation (Vogel and Luck, 2000). Furthermore, we observed larger N1 amplitudes for the object location repeated condition compared to the object location changed condition. This is in line with previous studies reporting repetition priming effects in posterior N1, such as enhanced N1 amplitudes for the repeated stimuli (Ji et al., 1998; Soldan et al., 2006; Frings and Groh-Bordin, 2007). This result can be interpreted as the attention-based rehearsal for the memorized location facilitated the perceptual process of the probe appearing at the same location (Awh et al., 2000; Jha, 2002).

The P300 component has been shown to be associated with memory retrieval, stimulus evaluation, decision making (e.g., whether template matching the test array matches the memorial representations or not; Murphy et al., 2009). We found that P300 amplitudes decreased with increasing VWM load, implying that more processing resources, which are related to memory retrieval and the comparison between the test array and the memorial representations, were required and thus less "central resources" remained (Kok, 2001; Pinal et al., 2014). These findings are consistent with a previous study showing larger P300 amplitudes in VWM load 1 compared to that in load 3 (Bledowski et al., 2006).

CONCLUSION

We found that the adopted reference did not change the topography map of N1 and P300 components, but it did alter the task-related effect on ERP components. LM decreased or eliminated the visual working memory (VWM) load effect on P300, and the AR distorted the distribution of VWM location-related effect at left posterior electrodes as shown in the SPSM of N1. For the RESTs and RESTr, they both revealed object location effects on N1 and VWM load effects on P300. The SPSM of N1 revealed a bilateral posterior distribution. This result is consistent with the source analysis (e.g., source distribution and source activities) of N1, which estimates are independent of the adopted references (e.g., AR, LM, RESTs, and RESTr). Furthermore, in comparison with the EEG-only study, the two REST references in the EEG-fMRI study provide closer results to the independent ERP study. Taken together, the two REST references revealed more integrated and reasonable results than AR and LM in the EEG-fMRI study. Furthermore, with the data of individual structured MRI and realistic electrode positions, we recommend the RESTr as the reference method for EEG data in the simultaneous EEG-fMRI study.

LIMITATIONS

Previous studies have reported the effects of reference choice on EEG band analysis, using measures of power spectra, coherence, and network connectivity (Yao et al., 2005; Marzetti et al., 2007; Qin et al., 2010; Chella et al., 2016). However, in our practical experiment, we are only interested in the task-related effect on ERP and fMRI results, which is a major concern in cognitive neuroscience research. Thus, we care more if the reference method would alter the "what" and "where" of task-related effects on ERP components.

We hoped to use the task-related fMRI activations to inform the ERP sources, and in turn to verify the distribution of the task-related effect measured on the scalp (ERP). Due to the sensitivity difference of the two modalities in neuronal activity, the experimental effect was detected at bilateral posterior electrodes for ERP but only at right posterior

cortex for fMRI. Since four reference data types showed the location effect at the right posterior (**Figure 4**), the fMRI result here is insufficient to verify which reference is the best option.

The independent ERP study used a 128-channel EGI system, which is inconsistent with the 64-channel Neuroscan system used in the EEG-fMRI study. This will not provide the precise pairwise comparison between these two studies. However, the independent ERP study provides the what and where of task-related ERP effects that can help to evaluate the closest results in the EEG-fMRI study when using different reference methods.

AUTHOR CONTRIBUTIONS

PY and LL conceived and designed the experiments. PY, CF, and MW performed the experiments and analyzed the data. PY wrote the main manuscript text. All authors reviewed the manuscript.

ACKNOWLEDGMENTS

This research was supported by grants from the National Natural Science Foundation of China projects (NSFC, Nos. 61473062, 61403066), 111 Project (B12027), and the Fundamental Research Funds for the Central Universities.

REFERENCES

Awh, E., Anllo-Vento, L., and Hillyard, S. (2000). The role of spatial selective attention in working memory for locations: evidence from event-related potentials. *J. Cogn. Neurosci.* 12, 840–847. doi: 10.1162/089892900562444

Bledowski, C. (2004). Localizing P300 generators in visual target and distractor processing: a combined event-related potential and functional magnetic resonance imaging study. *J. Neurosci.* 24, 9353–9360. doi: 10.1523/JNEUROSCI.1897-04.2004

Bledowski, C., Cohen Kadosh, K., Wibral, M., Rahm, B., Bittner, R. A., Hoechstetter, K., et al. (2006). Mental chronometry of working memory retrieval: a combined functional magnetic resonance imaging and event-related potentials approach. *J. Neurosci.* 26, 821–829. doi: 10.1523/JNEUROSCI.3542-05.2006

Castelhano, J., Duarte, I. C., Wibral, M., Rodriguez, E., and Castelo-Branco, M. (2014). The dual facet of gamma oscillations: separate visual and decision making circuits as revealed by simultaneous EEG/fMRI. *Hum. Brain Mapp.* 35, 5219–5235. doi: 10.1002/hbm.22545

Chella, F., Pizzella, V., Zappasodi, F., and Marzetti, L. (2016). Impact of the reference choice on scalp EEG connectivity estimation. *J. Neural Eng.* 13:36016. doi: 10.1088/1741-2560/13/3/036016

Chun, J., Peltier, S. J., Yoon, D., Manschreck, T. C., and Deldin, P. J. (2016). Prolongation of ERP latency and reaction time (RT) in simultaneous EEG/fMRI data acquisition. *J. Neurosci. Methods* 268, 78–86. doi: 10.1016/j.jneumeth.2016.05.011

Forman, S. D., Cohen, J. D., Fitzgerald, M., Eddy, W. F., Mintun, M. A., and Noll, D. C. (1995). Improved assessment of significant activation in functional magnetic resonance imaging (fMRI): use of a cluster-size threshold. *Magn. Reson. Med.* 33, 636–647. doi: 10.1002/mrm.1910330508

Frings, C., and Groh-Bordin, C. (2007). Electrophysiological correlates of visual identity negative priming. *Brain Res.* 1176, 82–91. doi: 10.1016/j.brainres.2007.07.093

Gazzaley, A., Rissman, J., Cooney, J., Rutman, A., Seibert, T., Clapp, W., et al. (2007). Functional interactions between prefrontal and visual association cortex contribute to top-down modulation of visual processing. *Cereb. Cortex* 17, 125–135. doi: 10.1093/cercor/bhm113

Geselowitz, D. B. (1998). The zero of potential. *IEEE Eng. Med. Biol. Mag.* 17, 128–132. doi: 10.1109/51.646230

Gramfort, A., Papadopoulo, T., Olivi, E., and Clerc, M. (2010). OpenMEEG: opensource software for quasistatic bioelectromagnetics. *Biomed. Eng. Online* 9:45. doi: 10.1186/1475-925x-9-45

Huettel, S. A., McKeown, M. J., Song, A. W., Hart, S., Spencer, D. D., Allison, T., et al. (2004). Linking hemodynamic and electrophysiological measures of brain activity: evidence from functional MRI and intracranial field potentials. *Cereb. Cortex* 14, 165–173. doi: 10.1093/cercor/bhg115

Jha, A. P. (2002). Tracking the time-course of attentional involvement in spatial working memory: an event-related potential investigation. *Cogn. Brain Res.* 15, 61–69. doi: 10.1016/S0926-6410(02)00216-1

Ji, J., Porjesz, B., and Begleiter, H. (1998). ERP components in category matching tasks. *Electroencephalogr. Clin. Neurophysiol.* 108, 380–389. doi: 10.1016/S0168-5597(97)00103-2

Joyce, C., and Rossion, B. (2005). The face-sensitive N170 and VPP components manifest the same brain processes: the effect of reference electrode site. *Clin. Neurophysiol.* 116, 2613–2631. doi: 10.1016/j.clinph.2005.07.005

Kayser, J., Tenke, C. E., Gates, N. A., and Bruder, G. E. (2007). Reference-independent ERP old/new effects of auditory and visual word recognition memory: joint extraction of stimulus- and response-locked neuronal generator patterns. *Psychophysiology* 44, 949–967. doi: 10.1111/j.1469-8986.2007.00562.x

Keil, A., Debener, S., Gratton, G., Junghöfer, M., Kappenman, E. S., Luck, S. J., et al. (2014). Committee report: publication guidelines and recommendations for studies using electroencephalography and magnetoencephalography. *Psychophysiology* 51, 1–21. doi: 10.1111/psyp.12147

Kok, A. (2001). On the utility of P3 amplitude as a measure of processing capacity. *Psychophysiology* 38, 557–577. doi: 10.1017/S0048577201990559

Lantz, G., Grave de Peralta, R., Spinelli, L., Seeck, M., and Michel, C. M. (2003). Epileptic source localization with high density EEG: How many electrodes are needed? *Clin. Neurophysiol.* 114, 63–69. doi: 10.1016/S1388-2457(02)00337-1

Li, L., Zhang, J.-X., and Jiang, T. (2011). Visual working memory load-related changes in neural activity and functional connectivity. *PLoS ONE* 6:e22357. doi: 10.1371/journal.pone.0022357

Liu, Q., Balsters, J. H., Baechinger, M., van der Groen, O., Wenderoth, N., and Mantini, D. (2015). Estimating a neutral reference for electroencephalographic recordings: the importance of using a high-density montage and a realistic head model. *J. Neural Eng.* 12:56012. doi: 10.1088/1741-2560/12/5/056012

Logothetis, N. K., Pauls, J., Augath, M., Trinath, T., and Oeltermann, A. (2001). Neurophysiological investigation of the basis of the fMRI signal. *Nature* 412, 150–157. doi: 10.1038/35084005

Marzetti, L., Nolte, G., Perrucci, M. G., Romani, G. L., and Del Gratta, C. (2007). The use of standardized infinity reference in EEG coherency studies. *Neuroimage* 36, 48–63. doi: 10.1016/j.neuroimage.2007.02.034

Michel, C. M., Murray, M. M., Lantz, G., Gonzalez, S., Spinelli, L., and Grave De Peralta, R. (2004). EEG source imaging. *Clin. Neurophysiol.* 115, 2195–2222. doi: 10.1016/j.clinph.2004.06.001

Mitzdorf, U. (1985). Current source-density method and application in cat cerebral cortex: investigation of evoked potentials and EEG phenomena. *Physiol. Rev.* 65, 37–100.

Murphy, J. S., Wynne, C. E., O'Rourke, E. M., Commins, S., and Roche, R. A. P. (2009). High-resolution ERP mapping of cortical activation related to implicit object-location memory. *Biol. Psychol.* 82, 234–245. doi: 10.1016/j.biopsycho.2009.08.002

Nunez, P. L. (2010). REST: a good idea but not the gold standard. *Clin. Neurophysiol.* 121, 2177–2180. doi: 10.1016/j.clinph.2010.04.029

Novitskiy, N., Ramautar, J. R., Vanderperren, K., De Vos, M., Mennes, M., Mijovic, B., et al. (2011). The BOLD correlates of the visual P1 and N1 in single-trial analysis of simultaneous EEG-fMRI recordings during a spatial detection task. *Neuroimage* 54, 824–835. doi: 10.1016/j.neuroimage.2010.09.041

Nunez, P. L., and Silberstein, R. B. (2000). On the relationship of synaptic activity to macroscopic measurements: does co-registration of EEG with fMRI make sense? *Brain Topogr.* 13, 79–96. doi: 10.1023/A:1026683200895

Ogawa, S., Lee, T. M., Kay, A. R., and Tank, D. W. (1990). Brain magnetic resonance imaging with contrast dependent on blood oxygenation. *Proc. Natl. Acad. Sci. U.S.A.* 87, 9868–9872. doi: 10.1073/pnas.87.24.9868

Pascual-Marqui, R. D., and Lehamann, D. (1993). Topographic maps, source localization inference, and the reference electrode: comments on a paper by Desmedt et al. *Electroencephalogr. Clin. Neurophysiol.* 88, 532–533. doi: 10.1016/0168-5597(93)90043-O

Passaro, A. D., Elmore, L. C., Ellmore, T. M., Leising, K. J., Papanicolaou, A. C., and Wright, A. A. (2013). Explorations of object and location memory using fMRI. *Front. Behav. Neurosci.* 7:105. doi: 10.3389/fnbeh.2013.00105

Pessoa, L., Gutierrez, E., Bandettini, P. A., and Ungerleider, L. (2002). Neural correlates of visual working memory: fMRI amplitude predicts task performance. *Neuron* 35, 975–987. doi: 10.1016/S0896-6273(02)00817-6

Pinal, D., Zurrón, M., and Díaz, F. (2014). Effects of load and maintenance duration on the time course of information encoding and retrieval in working memory: from perceptual analysis to post-categorization processes. *Front. Hum. Neurosci.* 8:165. doi: 10.3389/fnhum.2014.00165

Qin, Y., Xu, P., and Yao, D. (2010). A comparative study of different references for EEG default mode network: the use of the infinity reference. *Clin. Neurophysiol.* 121, 1981–1991. doi: 10.1016/j.clinph.2010.03.056

Ranganath, C. (2006). Working memory for visual objects: complementary roles of inferior temporal, medial temporal, and prefrontal cortex. *Neuroscience* 139, 277–289. doi: 10.1016/j.neuroscience.2005.06.092

Robitaille, N., Marois, R., Todd, J., Grimault, S., Cheyne, D., and Jolicoeur, P. (2010). Distinguishing between lateralized and nonlateralized brain activity associated with visual short-term memory: fMRI, MEG, and EEG evidence from the same observers. *Neuroimage* 53, 1334–1345. doi: 10.1016/j.neuroimage.2010.07.027

Soldan, A., Mangels, J. A., and Cooper, L. A. (2006). Evaluating models of object-decision priming: evidence from event-related potential repetition effects. *J. Exp. Psychol. Learn. Mem. Cogn.* 32, 230–248. doi: 10.1037/0278-7393.32.2.230

Srivastava, G., Crottaz-Herbette, S., Lau, K. M., Glover, G. H., and Menon, V. (2005). ICA-based procedures for removing ballistocardiogram artifacts from EEG data acquired in the MRI scanner. *Neuroimage* 24, 50–60. doi: 10.1016/j.neuroimage.2004.09.041

Thatcher, R. W. (2012). Coherence, phase differences, phase shift, and phase lock in EEG/ERP analyses. *Dev. Neuropsychol.* 37, 476–496. doi: 10.1080/87565641.2011.619241

Tian, Y., and Yao, D. (2013). Why do we need to use a zero reference? Reference influences on the ERPs of audiovisual effects. *Psychophysiology* 50, 1282–1290. doi: 10.1111/psyp.12130

Toyomaki, A., and Yamamoto, T. (2007). Observation of changes in neural activity due to the static magnetic field of an MRI scanner. *J. Magn. Reson. Imaging* 26, 1216–1221. doi: 10.1002/jmri.21151

Vogel, E. K., and Luck, S. J. (2000). The visual N1 component as an index of a discrimination process. *Psychophysiology* 37, 190–203. doi: 10.1111/1469-8986.3720190

Xia, M., Wang, J., and He, Y. (2013). BrainNet viewer: a network visualization tool for human brain connectomics. *PLos ONE* 8:e68910. doi: 10.1371/journal.pone.0068910

Yao, D. (2001). A method to standardize a reference of scalp EEG recordings to a point at infinity. *Physiol. Meas.* 22, 693–711. doi: 10.1088/0967-3334/22/4/305

Yao, D., Wang, L., Arendt-Nielsen, L. N., and Chen, A. C. (2007). The effect of reference choices on the spatio-temporal analysis of brain evoked potentials: the use of infinite reference. *Comput. Biol. Med.* 37, 1529–1538. doi: 10.1016/j.compbiomed.2007.02.002

Yao, D., Wang, L., Oostenveld, R., Nielsen, K. D., Arendt-Nielsen, L., and Chen, A. C. N. (2005). A comparative study of different references for EEG spectral mapping: the issue of the neutral reference and the use of the infinity reference. *Physiol. Meas.* 26, 173–184. doi: 10.1088/0967-3334/26/3/003

Zhai, Y., and Yao, D. (2004). A study on the reference electrode standardization technique for a realistic head model. *Comput. Methods Programs Biomed.* 76, 229–238. doi: 10.1016/j.cmpb.2004.07.002

Conflict of Interest Statement: The authors declare that the research was conducted in the absence of any commercial or financial relationships that could be construed as a potential conflict of interest.

The handling Editor declared a shared affiliation, though no other collaboration, with the authors and states that the process nevertheless met the standards of a fair and objective review.

frontiers in Neuroscience

ORIGINAL RESEARCH
published: 16 May 2017
doi: 10.3389/fnins.2017.00262

Non-linear Analysis of Scalp EEG by Using Bispectra: The Effect of the Reference Choice

Federico Chella[1,2]*, *Antea D'Andrea*[1], *Alessio Basti*[1], *Vittorio Pizzella*[1,2] and *Laura Marzetti*[1,2]*

[1] Department of Neuroscience, Imaging and Clinical Sciences, G. d'Annunzio University of Chieti-Pescara, Chieti, Italy,
[2] Institute for Advanced Biomedical Technologies, G. d'Annunzio University of Chieti-Pescara, Chieti, Italy

OPEN ACCESS

Edited by:
Maria L. Bringas,
University of Electronic Sciences and Technology of China, China

Reviewed by:
Forooz Shahbazi Avarvand,
Heinrich Hertz Institute (FHG), Germany
Dante Mantini,
KU Leuven, Belgium

***Correspondence:**
Federico Chella
federico.chella@unich.it
Laura Marzetti
laura.marzetti@unich.it

Specialty section:
This article was submitted to Brain Imaging Methods, a section of the journal Frontiers in Neuroscience

Received: 24 February 2017
Accepted: 24 April 2017
Published: 16 May 2017

Citation:
Chella F, D'Andrea A, Basti A, Pizzella V and Marzetti L (2017) Non-linear Analysis of Scalp EEG by Using Bispectra: The Effect of the Reference Choice. Front. Neurosci. 11:262. doi: 10.3389/fnins.2017.00262

Bispectral analysis is a signal processing technique that makes it possible to capture the non-linear and non-Gaussian properties of the EEG signals. It has found various applications in EEG research and clinical practice, including the assessment of anesthetic depth, the identification of epileptic seizures, and more recently, the evaluation of non-linear cross-frequency brain functional connectivity. However, the validity and reliability of the indices drawn from bispectral analysis of EEG signals are potentially biased by the use of a non-neutral EEG reference. The present study aims at investigating the effects of the reference choice on the analysis of the non-linear features of EEG signals through bicoherence, as well as on the estimation of cross-frequency EEG connectivity through two different non-linear measures, i.e., the cross-bicoherence and the antisymmetric cross-bicoherence. To this end, four commonly used reference schemes were considered: the vertex electrode (Cz), the digitally linked mastoids, the average reference, and the Reference Electrode Standardization Technique (REST). The reference effects were assessed both in simulations and in a real EEG experiment. The simulations allowed to investigated: (i) the effects of the electrode density on the performance of the above references in the estimation of bispectral measures; and (ii) the effects of the head model accuracy in the performance of the REST. For real data, the EEG signals recorded from 10 subjects during eyes open resting state were examined, and the distortions induced by the reference choice in the patterns of alpha-beta bicoherence, cross-bicoherence, and antisymmetric cross-bicoherence were assessed. The results showed significant differences in the findings depending on the chosen reference, with the REST providing superior performance than all the other references in approximating the ideal neutral reference. In conclusion, this study highlights the importance of considering the effects of the reference choice in the interpretation and comparison of the results of bispectral analysis of scalp EEG.

Keywords: EEG reference, EEG functional connectivity, non-linear connectivity, bispectral analysis, bicoherence, antisymmetric cross-bispectrum

1. INTRODUCTION

How synchronization affects communication between groups of neurons represents one of the central issues of neuroscience. Several studies have been conducted to investigate neuronal functional communication, postulating a model of the human brain as a complex integrated system (Fries, 2005, 2015; Friston, 2011). It is now clear that, among the different neuroimaging techniques, electroencephalography (EEG) can be considered as an excellent tool for the study of neuronal interactions in both research and clinical practice (Friston and Frith, 1995; Stam et al., 2007; Fogelson et al., 2013; Frantzidis et al., 2014). Indeed, thanks to its high temporal resolution, EEG can provide insights into coupling of cortical oscillations hypothesized as the mechanism that underpins local and long-range neuronal communication (Tallon-Baudry et al., 1996; Womelsdorf and Fries, 2006; Fries, 2015).

In this framework, local and long-range synchronization can occur either in selected frequency bands (e.g., Palva and Palva, 2007; Hipp et al., 2012; Engel et al., 2013; Marzetti et al., 2013) or in a more sophisticated fashion which involves the interaction between different frequencies, i.e., non-linear synchronization. The latter possibly serves as a carrier mechanism for the integration of spectrally distributed processing (Varela et al., 2001; Palva et al., 2005; Jensen and Colgin, 2007; Canolty and Knight, 2010), providing a plausible physiological mechanism for linking activity at different temporal rates. Bispectral analysis has proven to be an effective tool to assess non-linear synchronization in human EEG (Dumermuth et al., 1971; Sigl and Chamoun, 1994; Darvas et al., 2009a,b; Chella et al., 2014, 2016b; Özkurt, 2016). Notably, bispectral measures such as bicoherence (Dumermuth et al., 1971; Sigl and Chamoun, 1994) were successfully used to detect non-linear long-range coupling from scalp EEG data in healthy subjects (ShilS et al., 1996; Schack et al., 2002; Isler et al., 2008; Chella et al., 2014). Moreover, the information from bispectral analysis of the EEG signals is highly used in clinical applications, such as in the determination of consciousness states and anesthetic depth levels (Freye and Levy, 2005; Pritchett et al., 2010), or in the identification and prediction of epileptic seizures (Bullock et al., 1997; Mormann et al., 2005; Chua et al., 2009). Indeed, changes in scalp EEG bicoherence have been shown to index the effects of the different drugs used to induce clinical anesthesia (Pritchett et al., 2010), as well as to indicate anesthesia vs. conscious states (Pritchett et al., 2010; Hayashi et al., 2014). Moreover, in epileptology the clinical markers of local hypersynchronous activity of the neuronal pools can be identified through information on higher order spectra extracted from EEG data (Chua et al., 2009).

Of note, all the above studies directly rely on bispectral indices derived from channel level EEG data. Nevertheless, since EEG measures only electric potential differences, it is implicitly assumed that signals at a given EEG electrode are referred to a neutral reference. Previous works have investigated different options in the attempt to find a neutral reference location. Several referencing schemes have been suggested like the vertex (Lehmann et al., 1998; Hesse et al., 2004), unimastoid (Başar et al., 1998; Thatcher et al., 2001), linked mastoids (Gevins and Smith, 2000; Croft et al., 2002), or nose (Andrew and Pfurtscheller, 1996; Essl and Rappelsberger, 1998), but no true neutral location has been found (Nunez and Srinivasan, 2006). Moreover, the average reference (Offner, 1950; Nunez et al., 2001) and the Reference Electrode Standardization Technique (REST) (Yao, 2001) have been shown to be valid solutions. Despite the proven advantages of the latter strategies, these are not completely free from biases (Desmedt et al., 1990; Dien, 1998; Zhai and Yao, 2004). Thus, it has to be kept in mind that a non-neutral reference affects the spatial and temporal features of EEG recordings, leading to possible distortions in the results. Recent works, through simulated and real data, provided a quantitative overview of the perturbation generated by the reference choice on the estimation of EEG voltage waveforms or scalp distributions (Joyce and Rossion, 2005; Yao et al., 2007; Tian and Yao, 2013; Liu et al., 2015), spectral power (Yao et al., 2005), correlation and coherence (Andrew and Pfurtscheller, 1996; Essl and Rappelsberger, 1998; Rummel et al., 2007; Müller et al., 2014), and linear functional connectivity (Guevara et al., 2005; Marzetti et al., 2007; Qin et al., 2010; Chella et al., 2016a).

To date, despite the wide use of bispectral analysis in EEG as above documented, no quantification of the effects of the use of different referencing schemes on these indices has been provided. The aim of this paper is to provide such quantification through simulated and real data, for local synchrony assessment through bicoherence as well as for long range synchrony characterization through two different non-linear metrics: (i) cross-bicoherence, (ii) antisymmetric cross-bicoherence. To this end, the vertex electrode (Cz), the digitally linked mastoids, the average reference, and the REST transformation were considered and different electrode densities were taken into account. In addition, the effects of the accuracy in the head model used to build the REST transformation have been assessed.

2. MATERIALS AND METHODS

2.1. Theoretical Background

2.1.1. Bispectral Analysis

This subsection recalls the basic principles and properties of bispectral analysis of EEG signals used in this study. Let, v_i be the time series of the signal recorded by the ith EEG channel. The auto-bispectrum of v_i can be estimated as (Nikias and Petropulu, 1993):

$$B_i(f_1, f_2) = \left\langle \hat{v}_i(f_1)\, \hat{v}_i(f_2)\, \hat{v}_i^*(f_1 + f_2) \right\rangle \tag{1}$$

where $\hat{v}_i(f_1)$, $\hat{v}_i(f_2)$, and $\hat{v}_i(f_1 + f_2)$ are the Fourier coefficients of the signal components at frequencies f_1, f_2, and $f_1 + f_2$, and the symbols * and $\langle\cdot\rangle$ denote the complex conjugation and the expectation value, respectively. In practice, the expectation value is replaced by the average over a sufficiently large number of signal realizations, or data segments. The auto-bispectrum of a signal is a measure of the non-linear cross-frequency coupling between signal components at three different frequencies, i.e., f_1, f_2, and $f_3 = f_1 + f_2$. In particular, the third frequency is set to the sum of the other two because all the other choices lead to vanishing bispectra for stationary processes, or also for non-stationary processes if the experimental design is not

appropriate (Chella et al., 2016b). The non-linear coupling essentially means the synchronization of the phases of the above frequency components, i.e., $\varphi_i(f_1)$, $\varphi_i(f_2)$, and $\varphi_i(f_1+f_2)$, in such a way that the generalized phase difference $\Delta\varphi_i = \varphi_i(f_1)+\varphi_i(f_2)-\varphi_i(f_1+f_2)$ stays close to a constant value. This kind of interaction is usually termed quadratic phase coupling (Kim and Powers, 1978; Nikias and Petropulu, 1993).

The auto-bicoherence, simply referred to as bicoherence in this study, is the normalized version of the auto-bispectrum in Equation (1), i.e.,

$$b_i(f_1,f_2) = \frac{B_i(f_1,f_2)}{\mathcal{N}_i(f_1,f_2)} \tag{2}$$

with $\mathcal{N}_i(f_1,f_2)$ being a normalization factor. There are a number of expressions for bicoherence (Brillinger, 1965; Kim and Powers, 1979; Hinich and Wolinsky, 2005; Helbig et al., 2006), which essentially differ only by the normalization factor used. In the present study, the normalization factor suggested by Shahbazi et al. (2014) is used, i.e.,

$$\mathcal{N}_i(f_1,f_2) = Q_i(f_1)\,Q_i(f_2)\,Q_i(f_1+f_2) \tag{3}$$

with

$$Q_i(f) = \left(\frac{1}{L}\sum_l \left|\hat{v}_i(f,l)\right|^3\right)^{1/3} \tag{4}$$

being [apart a multiplicative factor $(1/L)^{1/3}$] the three-norm of a L-length vector $\hat{v}_i(f,l)$, whose elements are the Fourier coefficients of the signal in channel i at frequency f estimated from the segment l. Of note, this normalization factor guarantees that the magnitude of the bicoherence is bounded between 0 (i.e., no interaction) and 1 (i.e., maximum interaction).

Following the definition of bicoherence, the cross-bicoherence is used to determine the non-linear phase synchronization between the frequency components of signals measured at three different channels, i.e., v_i, v_j, and v_k, and it reads:

$$cb_{ijk}(f_1,f_2) = \frac{B_{ijk}(f_1,f_2)}{\mathcal{N}_{ijk}(f_1,f_2)} = \frac{\left\langle \hat{v}_i(f_1)\,\hat{v}_j(f_2)\,\hat{v}_k^*(f_1+f_2)\right\rangle}{Q_i(f_1)\,Q_j(f_2)\,Q_k(f_1+f_2)}. \tag{5}$$

For this reason, the cross-bicoherence is used as a measure of non-linear functional relationships between EEG channels, i.e., a measure of EEG non-linear functional connectivity (ShilS et al., 1996; Schack et al., 2002; Isler et al., 2008).

The estimation of functional connectivity from EEG signals has to face the problem of the artifacts due to volume conduction (Nunez et al., 1997; Nolte et al., 2004; Srinivasan et al., 2007). These are essentially due to the widespread representation of brain source activity over the scalp and are especially relevant for nearby channels (Winter et al., 2007; Schoffelen and Gross, 2009). For instance, two EEG channels can record, with some weights, from the same neural population, opening the possibility for spurious interactions between channels even in the absence of actual brain interactions. Almost all the measures of linear and non-linear connectivity, including the cross-bispectra and the cross-bicoherence, are sensitive to these artifacts (Schoffelen and Gross, 2009). In order to address this problem in relation to bispectral analysis of EEG signals, in Chella et al. (2016b) it has been suggested to use the antisymmetric cross-bicoherence, i.e.,

$$acb_{ijk}(f_1,f_2) = \frac{B_{ijk}(f_1,f_2) - B_{kji}(f_1,f_2)}{\mathcal{N}_{ijk}(f_1,f_2) + \mathcal{N}_{kji}(f_1,f_2)} \tag{6}$$

namely the normalized difference between two cross-bispectra where two of the channel indices have been switched. Indeed, this quantity cannot be generated by a superposition of independent sources and, thus, necessarily reflects genuine brain interactions as opposite to the artifacts due to volume conduction (Chella et al., 2014).

Finally, it can be noted that the bicoherence, the cross-bicoherence, and the antisymmetric cross-bicoherence are complex-valued quantities. In this paper, however, in order to be interpreted as indices of non-linear properties and functional relationships of the EEG signals, these quantities will be considered in magnitude.

2.1.2. EEG Reference Schemes

In this subsection, notations and formulas for the re-referencing transformations used in this paper are introduced. Let V_m be a $N \times M$ matrix, with N being the number of channels and M being the number of time samples, containing the EEG recordings measured by using a given reference scheme. The re-referencing to a different EEG reference scheme, here generically labeled as X, can be performed by using the following transformation:

$$V_{\mathrm{X}} = V_m - V_{\mathrm{ref_X}} = T_{\mathrm{X}} V_m \tag{7}$$

where V_{X} is the matrix containing the re-referenced EEG recordings, $V_{\mathrm{ref_X}}$ is the matrix containing N copies of the reference signal, and T_{X} is a $N \times N$ transformation matrix.

Along this line, the reference to the physical electrode Cz is obtained by subtracting from each channel and for each time sample the potential measured at Cz. The corresponding transformation matrix is:

$$T_{\mathrm{Cz}} = \mathbb{I} - R_{\mathrm{Cz}} \tag{8}$$

with $\mathbb{I}$ being the $N \times N$ identity matrix, and R_{Cz} being a $N \times N$ matrix with all the elements equal to 0 except for those of the column corresponding to the Cz channel, which are equal to 1.

The reference signal for the digitally linked mastoid (DLM) reference is the average between the signals recorded at the electrodes located over (or in proximity of) the left and right mastoids. Then, the re-referencing transformation can be written as:

$$T_{\mathrm{DLM}} = \mathbb{I} - R_{\mathrm{DLM}} \tag{9}$$

with R_{DLM} having all the elements equal to 0 except for those of the columns corresponding to left and right mastoid channels, which are equal to 0.5.

The average reference (AVE) is performed by subtracting, for each time sample, the average of all the electrodes from each channel. The corresponding transformation matrix is:

$$T_{\mathrm{AVE}} = \mathbb{I} - R_{\mathrm{AVE}} \tag{10}$$

with R_{AVE} having all the elements equal to $1/N$.

The REST (Yao, 2001) aims at constructing a virtual reference to a point located at infinity. The REST exploits the fact that the EEG potentials measured with any original reference and those referenced to a point at infinity are generated by the same neuronal sources, i.e.,

$$V_m = G_m S \tag{11}$$

$$V_{\mathrm{REST}} = G_{\mathrm{REST}} S \tag{12}$$

with S being the matrix of the source activities, and G_m and G_{REST} being the transfer matrices from these sources to EEG sensors, i.e, the lead field matrices. Since the inverse problem solution is not affected by the choice of the EEG reference, at least for noiseless potentials (Pascual-Marqui and Lehamann, 1993; Geselowitz, 1998), an estimate of S can be obtained by inverting Equation (11), i.e.,

$$S = G_m^{+} V_m \tag{13}$$

with $(\cdot)^{+}$ denoting the Moore-Penrose generalized inverse. Then, by combining Equations (12, 13), the transformation matrix for REST can be derived as follows:

$$T_{\mathrm{REST}} = G_{\mathrm{REST}} G_m^{+} \tag{14}$$

A key feature of REST is that, since only the transfer matrices G_{REST} and G_m are needed to built the transformation matrix, the actual sources S do not need to be found explicitly. Indeed, based on the equivalent source technique (Yao, 1996, 2000, 2003), it is sufficient to assume an equivalent source distribution (ESD) and calculate G_{REST} and G_m for this ESD rather than for the actual sources. In this study, the ESD was assumed consisting in a discrete layer of current dipoles forming a closed surface, in analogy with previous studies (Yao, 2001; Yao et al., 2005; Marzetti et al., 2007; Chella et al., 2016a). This also has the advantage that the transformation matrix does not depend on the actual data, thus allowing, for instance, to re-reference different sessions of the same EEG acquisition by using the same transformation matrix. However, the transformation matrix still depends on the accuracy of the EEG forward solution in the calculation of the transfer matrices, which in turn depends on a number of choices including, e.g., the volume conductor model, the EEG forward solver, the EEG electrode density or locations. Some of these aspects will be investigated in this paper.

2.2. Simulations

The effects of the reference choice on the estimation of non-linear features of scalp EEG data were first assessed by using simulations. Indeed, differently from real world experiments, in simulations it is possible to measure the potential difference between any point over the scalp and a reference point located infinitely far from the head, where the electric field generated by brain sources vanishes, thus allowing to simulate an "ideal" neutral reference and, thus, unbiased EEG recordings. The simulations performed in this work followed an approach similar to the one used in our previous study (Chella et al., 2016a) to assess the changes induced by the EEG reference in linear connectivity patterns of EEG imaginary coherency (Nolte et al., 2004; Marzetti et al., 2008). In brief, in the present work, the analyses of bicoherence and non-linear connectivity based on either cross-bicoherence or antisymmetric cross-bicoherence were performed on various simulated datasets referenced to a point at infinity, as well as on the re-referenced datasets derived from the former by applying each of the reference schemes presented in Section 2.1.2. The effects of the reference choice were then assessed through the comparison between the results obtained prior and after re-referencing, considering as gold standard the results for the datasets referenced to a point at infinity.

2.2.1. Generation of Simulated EEG Data

Ten realistic head models, with different head shapes to account for inter-subject anatomical variability, were built based on the segmentation of high resolution whole-head anatomical magnetic resonance images (MRIs) acquired from the 10 subjects participating to the real data experiment described in this paper (see Section 2.3.1). The MRI segmentation was performed by using the Curry 6.0 software package (Neuroscan Compumedics USA, Charlotte, NC, USA), and resulted in the generation of triangulated meshes for the boundaries between gray matter and CSF (cortex), CSF and skull (inner skull), skull and skin (outer skull), and for the outer surface of the head (skin). For each head model, a three-shell volume conductor model, i.e., including the brain, the skull and the scalp, was built using the shapes of the inner skull, outer skull, and skin meshes. Conductivities were set equal to 0.33 S/m for the brain and scalp, and 0.0066 S/m for the skull. The source space consisted in a regular grid with 5 mm step inside the volume bounded by the cortical mesh. A 128-channel EEG sensor net was registered to the head models, with the electrodes located at the standard positions of the 10-5 system (Oostenveld and Praamstra, 2001).

Given a set of current dipole sources, 5 min simulated EEG recordings referenced to a point at infinity, sampled at 500 Hz, were generated from source time courses by solving the EEG forward problem. The set of sources included two non-linear coupled sources and four uncorrelated sources of noise, the latter aiming to mimic background brain activity. All of these sources were randomly located and oriented over the source space. The time courses for the two non-linear coupled sources were generated by using a time-delayed interaction model, i.e.,

$$s_2(t) = s_1(t - \tau) \tag{15}$$

with s_1 and s_2 being two non-linear sources with quadratic non-linearity, and τ being equal to 10 ms. This model was previously used in Chella et al. (2014, 2016b) for testing the properties of antisymmetric bispectral measures. In the present study, s_1 was generated by summing the time courses of three quadratically

phase coupled oscillators centered at 6, 10, and 16 Hz. The former two oscillators were obtained by band-pass filtering two i.i.d. white Gaussian processes around 6 and 10 Hz, respectively. The latter oscillator was generated by a multiplicative interaction (i.e., a time-point by time-point multiplication) between the other two oscillators, followed by filtering around 16 Hz. A Butterworth filter with 1 Hz bandwidth was used for the filtering at the above three frequencies, performing filtering in both the forward and the reverse directions to ensure zero phase distortion. The time courses for the four uncorrelated sources of noise were simulated as broadband white Gaussian processes filtered between 0.5 and 100 Hz.

By using the information about the realistically shaped head model and the EEG electrode locations, the lead field matrix for the simulated sources with the reference to a point at infinity was computed according to Nolte and Dassios (2005). The EEG recordings were then generated by multiplying the time courses of the simulated sources with the lead field matrix. The signal-to-noise ratio (SNR) was set equal to 1, with the SNR being defined as the ratio between the mean variance across channels of the signals generated by the interacting sources and the mean variance of the signals generated by the sources of noise. A low level of uncorrelated white Gaussian noise was also added to sensor signals to mimic instrumental noise. One-hundred different dataset were generated for each of the 10 realistic head models by randomizing source locations and orientations, resulting in a total amount of 1,000 different dataset on which the various reference schemes were tested.

2.2.2. Re-referencing of Simulated EEG Recordings

From the datasets referenced to a point at infinity, the datasets re-referenced to Cz, DLM, and AVE were obtained by applying the transformations in Equations (8–10). The datasets re-referenced using REST were obtained by applying the transformation in Equation (14) to data previously re-referenced to the physical reference Cz.

To investigate the effectiveness of REST in dependence on the head modeling accuracy, the REST transformation was calculated for three different volume conductor models with increasing complexity levels: (i) a three-concentric-shell *spherical* model (Yao, 2001; Yao et al., 2005; Marzetti et al., 2007; Zappasodi et al., 2014, 2015; Liu et al., 2015; Chella et al., 2016a), whose dimensions were based on the dimensions of a standard head provided by the MNI-152 template (Fonov et al., 2009, 2011); (ii) a three-shell *realistic standard* model (Chella et al., 2014, 2016a) obtained from the segmentation of the MNI-152 template (Fonov et al., 2009, 2011); and (iii) a three-shell *realistic individual* model (Zhai and Yao, 2004; Liu et al., 2015; Chella et al., 2016a) obtained from the segmentation of subject individual MRI. Notably, the latter model was similar but not exactly the same model used for the generation of simulated EEG recordings. Specifically, in order to fulfill independence between the two models, the one used for the REST re-referencing was derived from the one used to generate the EEG datasets after re-sampling of the boundary meshes of head compartments. Tissue conductivities were set to 0.33 S/m for the innermost (brain) and outermost (scalp) compartments, and to 0.0066 S/m for the intermediate compartment (skull). The equivalent source distribution consisted in 4,000 current dipoles uniformly distributed and normally oriented over a closed surface. Specifically, for the spherical model (i.e., case i), the closed surface was formed by a spherical cap closed on the bottom by a transverse plane (Marzetti et al., 2007; Chella et al., 2016a). For the realistic models (i.e., cases ii and iii), the closed surface was constructed by contracting the brain mesh to 95% of its size (Zhai and Yao, 2004). The REST transformations using the spherical, realistic standard and realistic individual models were labeled as $\mathrm{REST}_{\mathrm{sph}}$, $\mathrm{REST}_{\mathrm{std}}$, and $\mathrm{REST}_{\mathrm{ind}}$, respectively.

2.2.3. Bicoherence and Cross-Bicoherence Analysis

The simulated datasets were divided into 1 s non-overlapping segments. Within each segment, data were Hanning windowed, and the Fourier coefficients were evaluated using conventional FFT algorithms. Bicoherence and cross-bicoherence analyses were then restricted to the three frequencies of interest considered for the generation of simulated recordings, i.e., $f_1 = 6\mathrm{Hz}$, $f_2 = 10\mathrm{Hz}$, and $f_3 = f_1 + f_2 = 16\,\mathrm{Hz}$. The bicoherence $b_i(f_1, f_2)$ was estimated for each channel i according to Equation (2). Cross-bicoherence $cb_{ijk}(f_1, f_2)$ and antisymmetric cross-bicoherence $acb_{ijk}(f_1, f_2)$ were estimated for each possible triplet of channels denoted by indices i, j and k according to Equations (5, 6), respectively.

2.2.4. Performance Measures

To assess the performances of the various reference schemes, the estimates of bicoherence, cross-bicoherence, and antisymmetric cross-bicoherence obtained from the original datasets referenced to a point at infinity were compared to those obtained after re-referencing in terms of relative error (RE) (Yao, 2001; Zhai and Yao, 2004; Marzetti et al., 2007; Liu et al., 2015; Chella et al., 2016a), i.e.,

$$RE_b^{\mathrm{X}} = \frac{\sqrt{\sum_i \left| b_i^{\mathrm{X}} - b_i^{\mathrm{INF}} \right|^2}}{\sqrt{\sum_i \left| b_i^{\mathrm{INF}} \right|^2}} \tag{16}$$

$$RE_{cb}^{\mathrm{X}} = \frac{\sqrt{\sum_{i,j,k} \left| cb_{ijk}^{\mathrm{X}} - cb_{ijk}^{\mathrm{INF}} \right|^2}}{\sqrt{\sum_{i,j,k} \left| cb_{ijk}^{\mathrm{INF}} \right|^2}} \tag{17}$$

$$RE_{acb}^{\mathrm{X}} = \frac{\sqrt{\sum_{i,j,k} \left| acb_{ijk}^{\mathrm{X}} - acb_{ijk}^{\mathrm{INF}} \right|^2}}{\sqrt{\sum_{i,j,k} \left| acb_{ijk}^{\mathrm{INF}} \right|^2}} \tag{18}$$

where the superscript INF denotes the reference to a point at infinity, the superscript X is an alternative among Cz, DLM, AVE, $\mathrm{REST}_{\mathrm{sph}}$, $\mathrm{REST}_{\mathrm{std}}$, or $\mathrm{REST}_{\mathrm{ind}}$, and the subscripts i, j, and k run over $1, \ldots, N$, with N being the number of channels. The contrast between the different EEG reference schemes was performed

by looking at the distributions of the RE from all simulation repetitions.

In order to investigate the effects of EEG electrode density, the above analyses were repeated for three subsets of the 128 simulated recordings, corresponding to the following EEG sensor layouts: (i) a 21-channel system, including to the 19 electrodes of the 10–20 International system (Jasper, 1958) with the addition of TP9 and TP10 electrodes; (ii) a 34-channel system, including a selection of the electrodes of the 10–10 system (Chatrian et al., 1985); and (iii) a 74-channel system, i.e., the full 10–10 system (Chatrian et al., 1985).

2.3. Real EEG Data

A real EEG experiment was carried out to provide an example of the effects of the EEG reference choice in actual experimental situations. In particular, our experiment aimed at evaluating the changes in the patterns of resting state EEG bicoherence and bispectrum-based non-linear connectivity induced by the chosen reference scheme.

2.3.1. Data Acquisition and Preprocessing

Ten healthy adults subjects (age 20–29 years; gender 2 F, 8 M) were recruited for the experiment. The study was approved by the Ethics Committee for Biomedical Research of the Provinces of Chieti and Pescara and of the G. d'Annunzio University of Chieti-Pescara. All subjects gave written informed consent in accordance with the Declaration of Helsinki. Experiments were performed in a quiet room with soft natural light. Subjects were requested to sit in a comfortable chair, relax and fix a cross in front of them. Measurement consisted of 10 min of continuous eyes-open resting state activity. The EEG signals were recorded using a 128-channel HydroCel GSN net (Electrical Geodesics, Inc., Eugene, OR, USA) referenced to Cz. The electrode impedance was kept below 100 kΩ. Data were sampled at 1 kHz. The locations of EEG electrodes on the scalp and of three anatomical landmarks (nasion, left, and right pre-auricolar points) were measured using a 3D digitizer (Polhemus, Colchester, VT, USA).

For each subject, high resolution whole-head anatomical MRIs were also acquired in order to construct a realistic individual head model for the re-referencing using REST. MRIs were acquired by using a 3 T Philips Achieva scanner (Philips Medical Systems, Best, The Netherlands) via a 3D fast field echo T1-weighted sequence (MP-RAGE; voxel size 1 mm isotropic; repetition time 8.1 ms; echo time 3.7 ms; flip angle 8°; SENSE factor 2). The coregistration of EEG electrode locations with the MRI volume was performed based on the match between anatomical landmark locations identified in the two imaging modalities.

As a preprocessing step, the signals from the electrodes located over the face and neck were excluded from the analysis because highly contaminated by muscular activity. The number of available recording channels was thus reduced to 110. Raw data were band-pass filtered at 0.5–100 Hz and a visual inspection was carried out to remove the segments of signals containing spikes, eye blinks or horizontal movements. An independent component analysis (ICA) was then performed to remove biological and instrumental artifacts. Specifically, ICA was performed by using the FastICA algorithm with deflationary orthogonalization and tanh non-linearity (Hyvärinen and Oja, 2000). The extracted independent components were visually inspected and classified as artifactual components or as components of brain origin on the basis of their topographies, power spectral density and time courses. The independent components classified as artifactual were rejected. Particular attention was paid to the removal of hearth related activity. In order to allow for across-subject averaging or comparison between subjects, a few missing channels (i.e., one channel in 3 out of 10 subjects and two channels in 2 out of 10 subjects), excluded from the set of 110 channels prior to ICA because extremely noisy or damaged, were interpolated from clean signals by using the spherical interpolation method (Perrin et al., 1989) implemented in the FieldTrip software package (Oostenveld et al., 2011).

2.3.2. EEG Data Re-referencing

The EEG signals were acquired with Cz as a physical reference. The other reference schemes (i.e., DLM, AVE, REST_{sph}, REST_{std}, or REST_{ind}) were applied to preprocessed signals using the transformations in Equations (9, 10, 14). Analogously to the re-referencing of simulated EEG data discussed in Section 2.2.2, the REST transformations were calculated by assuming an equivalent source distribution consisting of 4,000 current dipoles uniformly distributed and normally oriented over a closed surface encompassing the brain volume. Conductivities for the brain, the skull and the scalp were set equal to 0.33, 0.0066, and 0.33 S/m, respectively. Forward solutions based on a spherical, realistic standard or realistic individual three-shell volume conductor model were computed according to Nolte and Dassios (2005).

2.3.3. EEG Data Analysis

The analysis was first focused on the estimation of EEG bicoherence. Signals were divided into 1 s non-overlapping segments. Within each segment, data were Hanning windowed and Fourier transformed, and the bicoherence $b_i(f_1, f_2)$ was estimated for each channel $i = 1, ..., N$ according to Equation (2). The resulting frequency resolution was 1 Hz on both the f_1 and the f_2 axis. This analysis was performed for all the combinations of frequencies (f_1, f_2) up to $f_1 + f_2 = 40$ Hz, but it was then restricted to a single frequency pair corresponding to the individual peak of bicoherence. In particular, a peak of bicoherence was observed at around $(f_1, f_2) = (10, 10\,\text{Hz})$ in all the subjects (shown in Figure S1 of the Supplementary Material), which reflects a non-linear coupling between EEG signal components in the alpha ($f_1 = f_2 = 10$ Hz) and beta ($f_3 = f_1 + f_2 = 20$ Hz) bands. Scalp distributions of bicoherence at the individual frequency pair and from the different reference schemes were used to assess the effects of the reference choice. Moreover, in order to assess whether the latter affects a global measure of bicoherence, the maximum value of bicoherence over channels was considered for each subject, i.e.,

$$b^{max} = \max_{i\,=\,1,\ldots,N} b_i \tag{19}$$

This index essentially aims at measuring the maximum level of bicoherence regardless of the location over the scalp, and it has been used in some clinical practice, e.g., to investigate the changes related to anesthetic concentration in bicoherence measurements (Hagihira et al., 2002, 2004; Morimoto et al., 2006; Pritchett et al., 2010).

In order to perform connectivity analysis, we chose two seed channels [60 and 85 in the EGI's sensor net, equivalent to P1 and P2 in the 10-10 system (Luu and Ferree, 2005)] overlying the left and right medial-parietal areas, i.e., two regions where the observed bicoherence was rather prominent regardless of the reference scheme used. We then considered the cross-bicoherence and the antisymmetric cross-bicoherence with respect to each of the two seed channels as metrics of interest to evaluate functional connectivity. In particular, the connectivity of a generic channel i to the seed channel was assessed by using a bivariate version of Equations (5, 6), i.e., obtained by setting the second channel index equal to the first, as follows:

$$cb_{\mathrm{P1}\text{-}i}(f_1,f_2) \triangleq cb_{\mathrm{P1\,P1}\,i}(f_1,f_2) \tag{20}$$

$$acb_{\mathrm{P1}\text{-}i}(f_1,f_2) \triangleq acb_{\mathrm{P1\,P1}\,i}(f_1,f_2) \tag{21}$$

for P1, and similarly for P2.

2.3.4. Group Analysis and Statistics

Topographical maps of bicoherence, cross-bicoherence, and antisymmetric cross-bicoherence were evaluated for each subject and for each re-referenced dataset separately. Group-level results were obtained by across-subject averaging. A paired sample t-test was used to assess the differences between the investigated reference schemes. The statistical significance of t-values was assessed through the non-parametric permutation test implemented in the FieldTrip software package (Oostenveld et al., 2011). This approach aims at evaluating the p-values associated to the observed t-values by comparison with an empirical reference distribution constructed from data which do not violate the null hypothesis (Maris and Oostenveld, 2007). To this purpose, for each observed t-value from pairwise comparisons between the different reference schemes, say reference 1 vs. reference 2, we generated 10,000 random partitions of the data by randomly shuffling the two references in each subject. The paired sample t-test was then applied to each of the 10,000 random partitions. As the random partitions do not violate the null hypothesis by construction, the respective t-values provide the distribution for the test statistic under the null hypothesis. The p-value associated to the observed t-value was finally evaluated as the proportion of random partitions that resulted in t-values larger than the observed one in absolute value.

3. RESULTS

3.1. Simulation Results

The effects of the different reference schemes, i.e., Cz, DLM, AVE, $\mathrm{REST_{sph}}$, $\mathrm{REST_{std}}$, and $\mathrm{REST_{ind}}$, on the estimation of bicoherence, cross-bicoherence, and antisymmetric cross-bicoherence were assessed in terms of relative error (RE) between the estimates obtained from the datasets referenced to a point at infinity and those obtained from the re-referenced datasets, as defined in Equations (16–18). As the point at infinity behaves as an ideal neutral reference, the best reference scheme is the one that yields the smallest RE.

The box plots in **Figure 1** show the dependence of the RE for bicoherence on the reference scheme and on the EEG electrode density. In particular, each box plot displays the distribution of the RE-values obtained from the 1,000 simulation repetitions: the rectangular box denotes the range from the 25th to the 75th percentile; the whiskers extend 1.5 times this range, such that they roughly cover the 99.3% of the data in case of normal distribution; the black dot denotes the median value; the two horizontal lines denote the notches for assessing the significance of difference of medians, i.e., two medians are significantly different at the 5% level if their notch intervals do not overlap. It can be noted that, among the investigated reference schemes, the reference to Cz is the one that shows the largest RE, as demonstrated by the median values being larger than 70%. Lower values of RE can be achieved by using the DLM reference (i.e., median RE of about 34%), although these values are still larger than those obtained for the REST, or for the AVE reference (except for the case of 128 channels, when the median RE obtained from DLM and AVE do not show significant differences). Notably, the RE-values for Cz and DLM references are not noticeably affected by the EEG electrode density. The AVE reference performs better than the Cz and DLM references, as demonstrated by the RE being effectively reduced. Interestingly, the RE for AVE reference slightly increases with increasing electrode number (i.e., median RE of about 18% for 21 channels, 20% for 34 channels, 23% for 74 channels, and 34% for 128 channels). The REST performs better than all the other reference schemes, with the lowest RE being achieved when using a realistic individual head model and high density EEG (i.e., median RE of about 7% for 21 channels, and 5% for 34-, 74- and 128-channels). In general, the more realistic the head model is, the better the REST performance is. Indeed, even if a realistic standard model is used in place of a realistic individual model, the median RE is lower than 10%, regardless of the number of channels, while significantly larger errors occur if a spherical head model is used, especially for increasing electrode density. It must be noted, however, that even in the case of a spherical head model, the REST performance is better than the ones of AVE, DLM, or Cz.

A similar scenario can be found when assessing the performances of the different reference schemes in the estimation of scalp EEG connectivity based on either cross-bicoherence (**Figure 2**) or antisymmetric cross-bicoherence (**Figure 3**). Indeed, although a significant and systematic increase of median RE can be observed for both of the connectivity measures as compared to bicoherence (**Figure 1**), such an increase does not affect the contrast between the different EEG reference performances. In particular, the REST still remains the best choice of EEG reference scheme, especially when using a high density EEG system and a realistic individual head model (i.e., for cross-bicoherence: median RE of about 10% for 21 channels, and 7% for 34-, 74- and 128-channels; for antisymmetric cross-bicoherence: median RE of about 14% for 21 channels, and

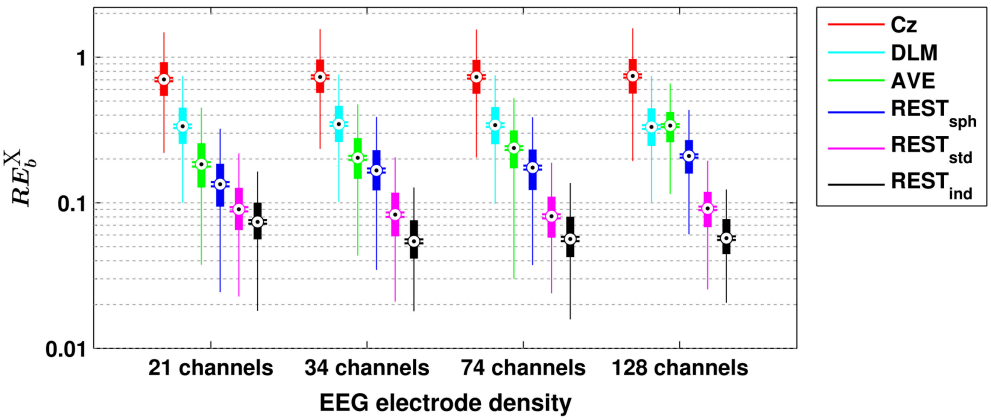

FIGURE 1 | Box plots for the relative error for bicoherence (RE_b^X) evaluated with different EEG reference schemes and with different EEG electrode densities. The ordinate axis is logarithmically scaled. Each box plot displays the RE-values from 1,000 simulation repetitions.

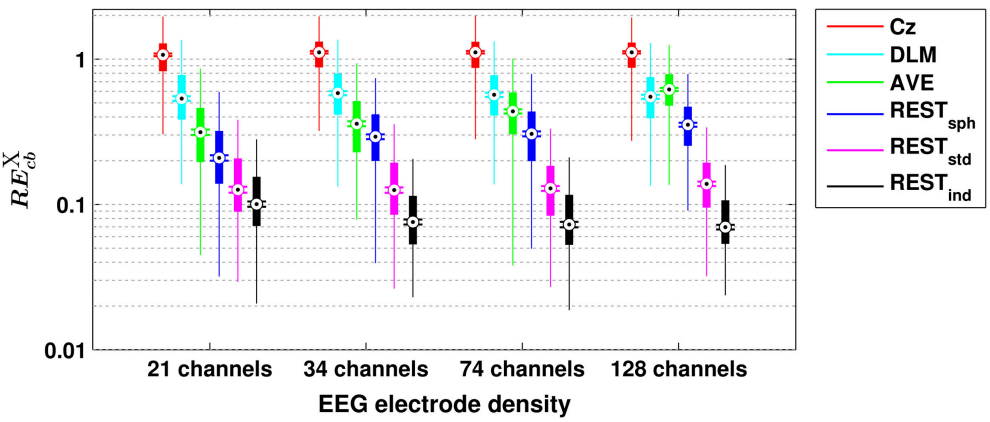

FIGURE 2 | Box plots for the relative error for cross-bicoherence (RE_{cb}^X) evaluated with different EEG reference schemes and with different EEG electrode densities. The ordinate axis is logarithmically scaled. Each box plot displays the RE-values from 1,000 simulation repetitions.

11% for 34-, 74- and 128-channels). If the latter is not available, REST still performs better than the other reference schemes, but the dependence of RE on the EEG density is negligible (i.e., for REST_{std}) or even the opposite (i.e., for REST_{sph}). The AVE reference performs worse than REST (i.e., median RE $>$ 30%), while the largest RE is obtained when using DLM (i.e., median RE $>$ 50%) or Cz (i.e., median RE $>$ 100%). Finally, in the comparison between the two connectivity measures, it can be noted that the median RE for antisymmetric cross-bicoherence is generally larger than the respective values for cross-bicoherence.

3.2. Real Data Results

3.2.1. Bicoherence

The bicoherence was estimated for each channel and for each combination of frequencies (f_1, f_2) up to $f_1 + f_2 = 40$ Hz. For all subjects, a prominent peak of bicoherence was found at around $(f_1, f_2) = (10, 10\text{ Hz})$ (shown in Figure S1 of the Supplementary Material), which essentially means that the EEG signals in the alpha band (i.e., at $f_1 = f_2 = 10$ Hz) have a strong non-linear coupling with their first harmonically related components in the beta band (i.e., at $f_3 = f_1 + f_2 = 20$ Hz). The analysis was then restricted to bicoherence at the individual frequency pair where such a peak occurred.

Figure 4 shows the patterns of bicoherence obtained for the different EEG reference schemes. In particular, the maps on the main diagonal show the average bicoherence across subjects obtained for each of the EEG reference. The off-diagonal maps show the t-values resulting from pairwise contrasts between bicoherence maps using a paired-sample t-test; here, the channels showing significant differences at the $p < 0.05$ level were marked with a cross. First, all the bicoherence maps reveal a strong level of bicoherence in a wide area roughly extending from the centro-parietal to the occipito-parietal channels. However, both the values and spatial distribution of bicoherence in this area change according to the chosen reference scheme. Second, there are a number of other significant differences in these maps, which can be better appreciated by looking at the t-value maps in the same figure. Indeed, the reference to Cz induces a systematic increase

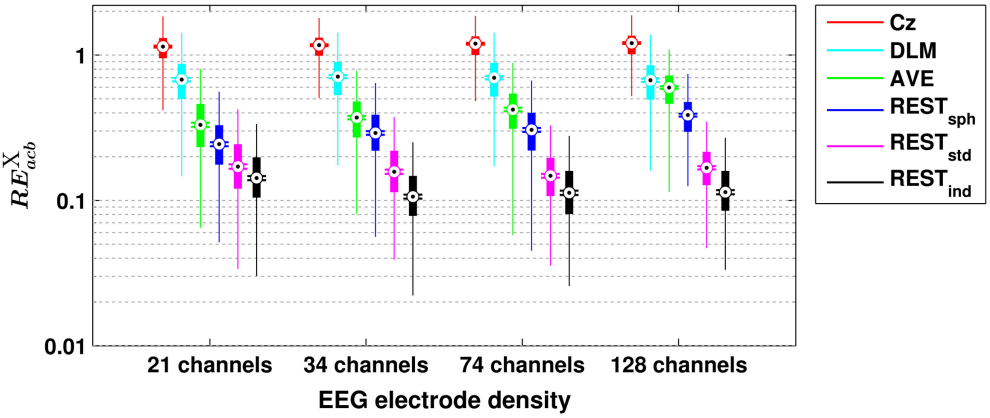

FIGURE 3 | Box plots for the relative error for antisymmetric cross-bicoherence (RE^{X}_{acb}) evaluated with different EEG reference schemes and with different EEG electrode densities. The ordinate axis is logarithmically scaled. Each box plot displays the RE-values from 1,000 simulation repetitions.

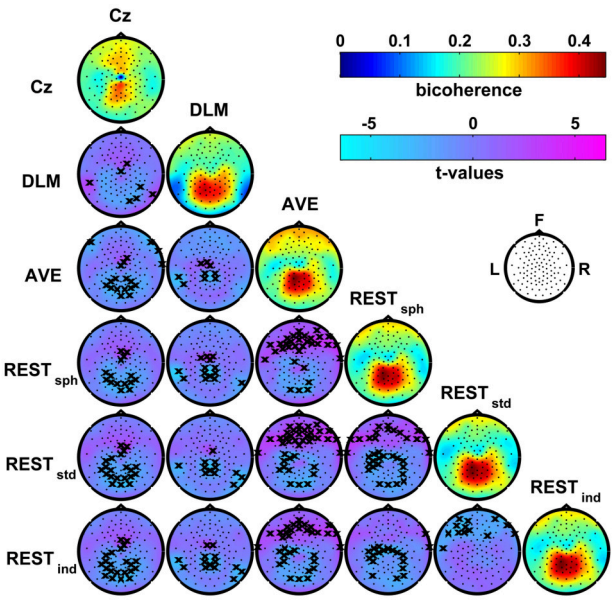

FIGURE 4 | Effects of the EEG reference choice on alpha-beta bicoherence patterns estimated from resting state EEG data. Main diagonal: maps of the average bicoherence across subjects obtained for the different EEG reference schemes. Off-diagonal: maps of *t*-values for pairwise contrasts between bicoherence maps from different EEG reference schemes using a paired-sample *t*-test; the black crosses mark the channels showing significant differences at the $p < 0.05$ level (two-tailed) based on a permutation test (10,000 randomizations).

of bicoherence in the fronto-central channels as compared to all the other references. At the same time, Cz suppresses the values of bicoherence in proximity of the reference electrode and, if compared to AVE and REST reference, over the parietal regions. The DLM reference scheme is characterized by an overall increase of bicoherence in the central channels, and by a decrease of bicoherence in the parietal channels and in proximity of the left and right mastoids used for the reference signal. Although the bicoherence maps obtained with the AVE and the REST reference look similar based on a qualitative evaluation, our analysis highlighted systematic and significant differences in these patterns. In particular, the AVE reference causes an increase of bicoherence in the frontal channels as compared to REST, along with a decrease of bicoherence in the occipital and in some of the parietal and central channels. Finally, the bicoherence maps obtained with REST significantly change according to the head model used for the data standardization as revealed by the *t*-values, although the differences can be poorly appreciated from a visual contrast between these map.

In order to asses whether the choice of the EEG reference affects a global measure of bicoherence, the maximum value of bicoherence over channels, i.e., b^{max}, was considered for each subjects. The results are summarized in **Figure 5**, where the bar plot shows the average b^{max} across subjects and its standard error, in dependence of the reference scheme. Notably, this analysis revealed that the Cz and DLM references yield a significantly lower b^{max} than the AVE and REST references, with the statistical significance being determined by permutation testing.

3.2.2. Non-linear Connectivity Analysis

Connectivity with respect to two seed channels located over the left and right medial-parietal areas, i.e., P1 and P2, was estimated using both the cross-bicoherence and the antisymmetric cross-bicoherence. The obtained results are summarized below.

Figure 6 shows the group average maps of the cross-bicoherence with seed channels P1 (**Figure 6A**) and P2 (**Figure 6B**) for each of the EEG reference schemes. The *t*-value maps are also shown for the contrast between the different reference conditions. The cross-bicoherence maps reveal a main pattern of interaction where the seed channel is primarily coupled to its neighbor channels. Beside this finding, the pairwise contrasts between these maps reveal a number of significant differences which, as similarly discussed above for bicoherence mapping, are only due to the choice of the particular EEG reference scheme. In particular, the Cz reference shows lower connectivity with the central channels as compared to DLM,

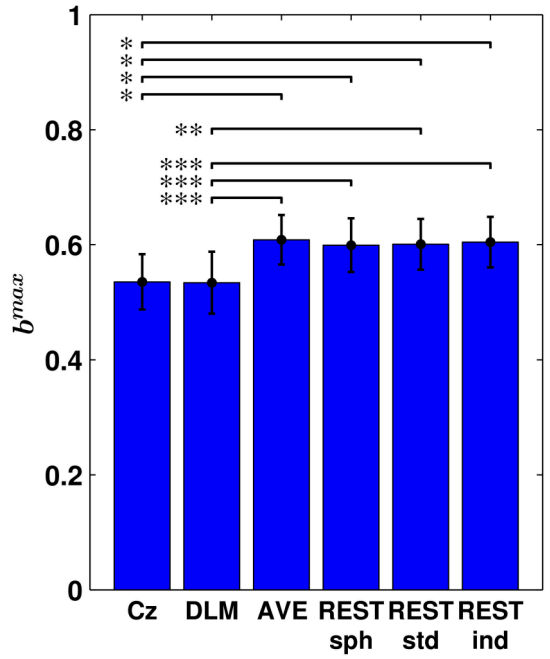

FIGURE 5 | Maximum bicoherence (b^{max}) obtained for the different EEG reference schemes. The bar plot shows the average b^{max} across subjects and its standard error. Statistical comparison between the different reference schemes was performed by using a paired sampled *t*-test (*$p < 0.05$; **$p < 0.01$; ***$p < 0.001$; two-tailed; fdr-corrected; permutation test).

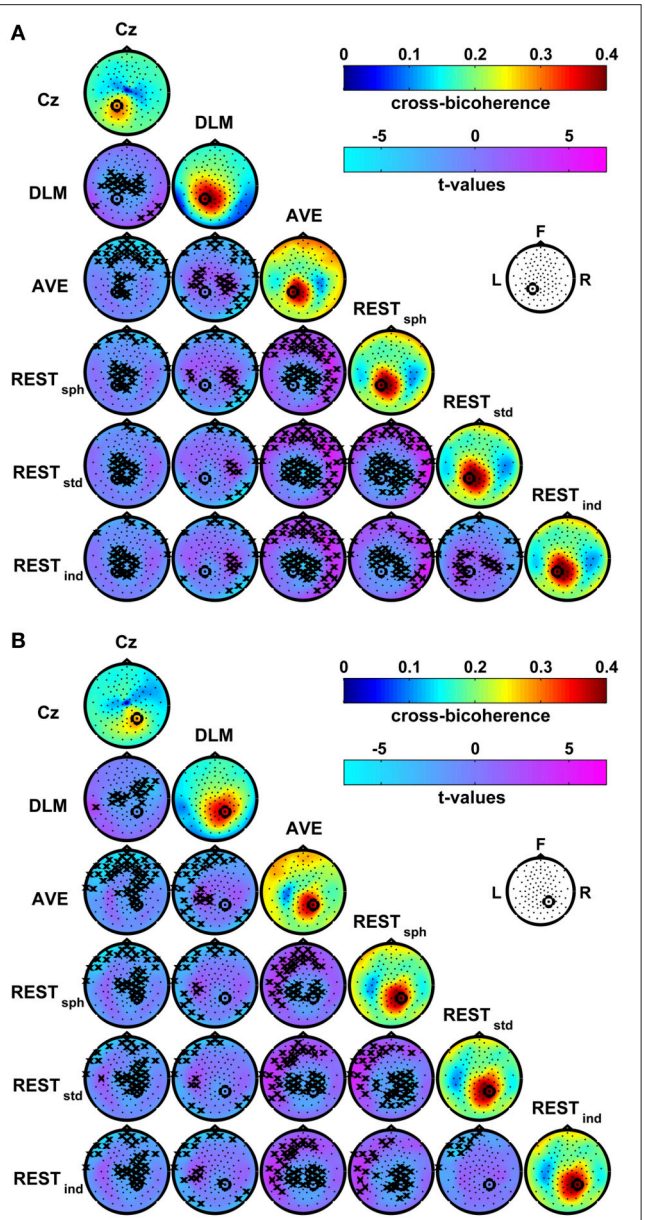

FIGURE 6 | Effects of the EEG reference choice on the estimation of alpha-beta connectivity using cross-bicoherence. Panel **(A)**: maps of connectivity with seed channel P1. Panel **(B)**: maps of connectivity with seed channel P2. The seed channels have been marked by a black circle. Main diagonals: maps of the average cross-bicoherence across subjects obtained for the different EEG reference schemes. Off-diagonals: maps of *t*-values for pairwise contrasts between cross-bicoherence maps from different EEG reference schemes using a paired-sample *t*-test; the black crosses mark the channels showing significant differences at the $p < 0.05$ level (two-tailed) based on a permutation test (10,000 randomizations).

and with the central and frontal channels as compared to AVE and REST. The DLM reference shows lower connectivity with the frontal channels, but higher connectivity with the central channels as compared to AVE or REST. At the same time, the DLM reference suppresses the connectivity with the channels located over the left and right mastoids as compared to all the other references. In the comparison between AVE and REST, the AVE reference shows lower connectivity with central channels, and higher connectivity with the fronto-central channels or with the temporal channels controlateral to the seed. Finally, for the REST, the head model accuracy has a significant impact on the estimation of the connectivity patterns. Specifically, if a spherical model is used (i.e., $REST_{sph}$) instead of a realistic one (i.e., $REST_{std}$ or $REST_{ind}$), the connectivity with the central channels and with the channels located in proximity of the seed is lower, whilst the connectivity with the fronto-temporal and temporal channels controlateral to the seed is higher. A few significant differences also arise in $REST_{std}$ as compared to $REST_{ind}$, consisting in a lower connectivity with the frontal channels and, only for the connectivity with P1, in higher connectivity with the centro-parietal channels.

A different pattern of interaction arises when the connectivity is estimated by using the antisymmetric cross-bicoherence. **Figure 7** shows the maps of the antisymmetric cross-bicoherence with P1 (panel A) and P2 (panel B) obtained for the different EEG reference schemes and their respective contrasts. Notably, contrarily to the cross-bicoherence, the antisymmetric cross-bicoherence reveals a pattern of long range interaction between channels, which clearly results from this measure being not biased by the artifacts of EEG volume conduction. Moreover, large differences can be observed in the comparison between

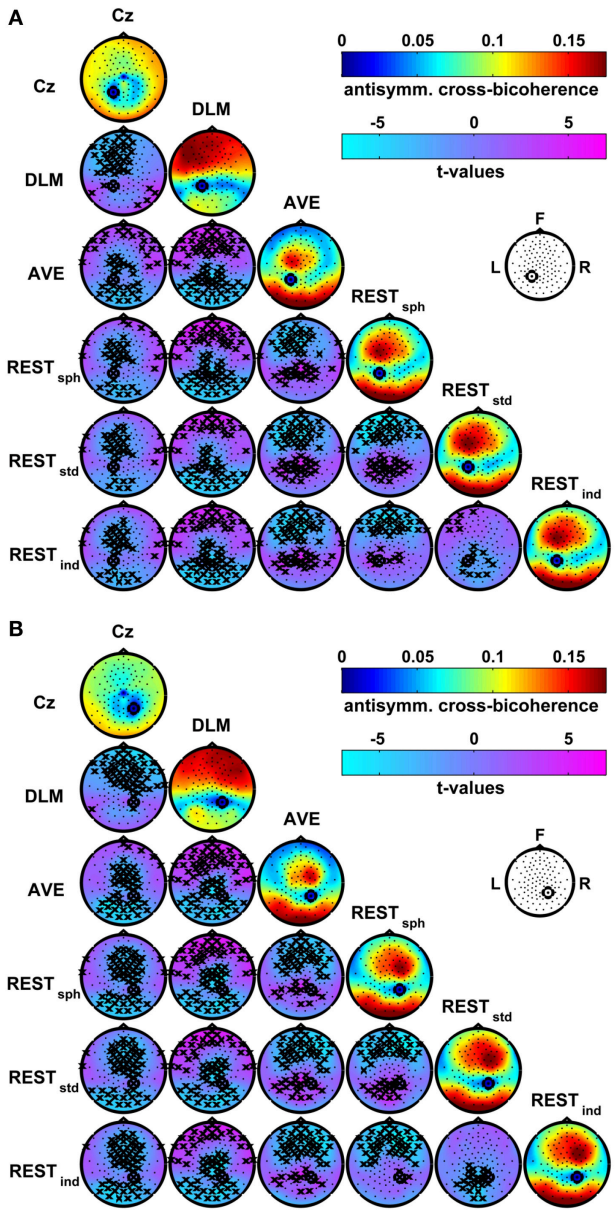

FIGURE 7 | Effects of the EEG reference choice on the estimation of alpha-beta connectivity using the antisymmetric cross-bicoherence. Panel **(A)**: maps of connectivity with seed channel P1. Panel **(B)**: maps of connectivity with seed channel P2. The seed channels have been marked by a black circle. Main diagonals: maps of the average antisymmetric cross-bicoherence across subjects obtained for the different EEG reference schemes. Off-diagonals: maps of *t*-values for pairwise contrasts between antisymmetric cross-bicoherence maps from different EEG reference schemes using a paired-sample *t*-test; the black crosses mark the channels showing significant differences at the $p < 0.05$ level (two-tailed) based on a permutation test (10,000 randomizations).

the different reference schemes, especially when contrasting Cz and DLM to AVE and REST. Indeed, for the Cz reference, the interaction is mainly with the occipital channels. For the DLM reference, the interaction is mainly with the frontal and central channels in the hemisphere ipsilateral to the seed. On the other hand, the AVE and REST references reveal a clear pattern of interaction of the seed channels, which we recall to be located in the medial-parietal left and right areas, with the channels in the fronto-central area ipsilateral to the seed and with channels in the left and right occipital areas. As discussed above for bicoherence and cross-bicoherence mapping, the *t*-value maps in **Figure 7** reveal significant differences in the antisymmetric cross-bicoherence depending on the reference scheme, with specific spatial topographies. In particular, the Cz reference mainly shows a lower interaction with the frontal and fronto-central channels as compared to DLM, and with the fronto-central and occipital channels as compared to AVE and REST. The DLM shows larger connectivity with the frontal channels, and lower connectivity with the parietal and occipital channels as compared to AVE and REST. As compared to REST, the AVE reference shows lower connectivity with the frontal channels, and higher connectivity with the parietal and occipital channels. A similar distortion can be observed when contrasting $REST_{sph}$ and $REST_{std}$ or $REST_{ind}$. Finally, the differences between $REST_{std}$ and $REST_{ind}$ are mainly located in the parietal and occipital channels, with the $REST_{std}$ showing lower connectivity than $REST_{ind}$.

4. DISCUSSION

In the present study, the effects of four commonly used EEG reference schemes, i.e., Cz, DLM, AVE, and REST, on bispectral measures derived from EEG signals were investigated. To this purpose, the following bispectral measures were considered: (i) the bicoherence, which is a measure of the local degree of non-linear coupling within each of the EEG channels, reflecting the non-linear and non-Gaussian features of the underlying brain processes (Sigl and Chamoun, 1994; Bullock et al., 1997; Schack et al., 2002); and (ii) the cross-bicoherence and the antisymmetric cross-bicoherence, which are both measures of non-linear cross-frequency connectivity between different EEG channels, possibly reflecting long-range non-linear synchronization between neuronal populations (ShilS et al., 1996; Schack et al., 2002; Isler et al., 2008; Jirsa and Müller, 2013; Chella et al., 2016b). Particularly relevant for the estimation of connectivity from scalp EEG data is the antisymmetric cross-bicoherence, which, as opposed to the cross-bicoherence, is not biased by the artifacts due to volume conduction (Chella et al., 2014, 2016b).

The reference effects were first assessed by using simulations, where the above mentioned reference schemes were compared to the ideal case of the reference to a true neutral location, i.e., a point located at infinity (Kayser and Tenke, 2010; Nunez, 2010). In particular, the simulations examined the accuracy in estimating the bispectral measures in relation to EEG electrode density and, since the REST requires the solution of the EEG forward problem, to the head model accuracy. Notably, previous studies investigated the effects of the electrode density on the analysis of EEG potentials or power by using different reference schemes (Nunez and Srinivasan, 2006). Yao (2001), Zhai and Yao (2004), and Liu et al. (2015) also highlighted the importance of

using an accurate head model as a key factor to improve the performance of REST. Marzetti et al. (2007), Qin et al. (2010), and Chella et al. (2016a) performed a comparative assessment of different EEG reference schemes in the estimation of linear scalp EEG connectivity based on coherency or imaginary part of coherency, demonstrating the validity of REST in data re-referencing. Along this line, this simulation study expands upon these previous findings by characterizing the effects of the reference choice on bispectrum-based non-linear EEG measures, an issue which is particularly relevant for several of applications, especially clinical, relying on bispectral analysis of the EEG (Freye and Levy, 2005; Mormann et al., 2005; Chua et al., 2009; Pritchett et al., 2010; Hayashi et al., 2014).

Our simulations showed that, as compared to all the other reference schemes, the reference to the physical electrode Cz induces the largest distortion in the estimates of bicoherence, cross-bicoherence, and antisymmetric cross-bicoherence. This is conceivably due to the reference electrode being in a location, i.e., the vertex, which is highly contaminated by the electrical activity of brain sources. Even though the mastoids are often regarded to as electrically inactive locations, the distortion induced by the DLM reference is also substantially large. Notably, the performances of the Cz and DLM references are not affected by the EEG electrode density, proving that indeed the observed distortion is only due to the electrical contamination of the reference signal. These results are consistent with previous findings (Dien, 1998; Hagemann et al., 2001; Nunez and Srinivasan, 2006; Chella et al., 2016a) and are particularly relevant for those studies using linked mastoids or a single cephalic electrode as a reference scheme for bicoherence and cross-bicoherence estimation (e.g., Hagihira et al., 2002; Schack et al., 2002; Hagihira et al., 2002; Schack et al., 2005).

Overall, the AVE reference provides better results as compared to Cz and DLM, although it is not completely free of biases. Most notably, the distortion induced by the AVE reference increases for increasing electrode density. This effect was already observed by Chella et al. (2016a) in the estimates of EEG imaginary coherency, thus confirming that an increased electrode density may be not a key factor to improve the performance of the AVE reference. Indeed, it is well-known that the actual accuracy of the AVE reference in approximating a theoretical zero-potential reference depends not only on the electrode density, but also on the electrode scalp coverage, i.e., which is limited to the upper part of the head (Tomberg et al., 1990; Dien, 1998; Nunez, 2010) or, as recently shown by Yao (2017), even on the head geometry.

The REST reference significantly reduces the above reference-induced distortion, with median values for relative errors being around 5% for the bicoherence, 7% for the cross-bicoherence, and 11% for the antisymmetric cross-bicoherence if a realistic individual head model and more than 34 EEG channels are used. In line with previous findings (Zhai and Yao, 2004; Liu et al., 2015; Chella et al., 2016a), this study shows that an accurate knowledge of the head model is crucial to improve the performance of REST standardization. Indeed, the distortion substantially increases if the head model is not sufficiently accurate, i.e., when using a realistic standard or spherical head model. However, it must be noted that, for a given sensor density, the REST still remains better choice than all the other reference schemes. In addition, these results demonstrate that the REST benefits from high density EEG only if used in combination with a realistic individual head model, whilst, if used in combination with a realistic standard or spherical head model, the effects of an increased electrode density are negligible or even the opposite.

The analysis of real EEG data provided further evidence of the reference effects on bispectral measures derived from EEG signals. This analysis was primarily focused on the contrast between the patterns of alpha-beta bicoherence as well as of bispectrum-based alpha-beta connectivities obtained from resting state EEG data with the different reference schemes. The results show that, indeed, there are systematic and significant differences in these patterns, which only depend on the use of the chosen reference scheme. In particular, the differences are larger for the Cz reference as compared to all the other reference schemes. This is conceivably due to the fact that the alpha and beta rhythms in the resting state EEG have a dominant activity in the occipito-parietal and central areas, which are in close proximity to the reference electrode. Substantial differences were also observed for DLM as compared to AVE and REST, while it should be noted that the differences between the AVE and REST are considerably small, although statistically significant. As for the analysis of connectivity patterns, this study shows that the antisymmetric bicoherence in combination with REST can provide patterns of long-range connectivity which can be directly interpreted in terms of functional interactions between the underlying brain sources. In particular, our findings (**Figure 7**) show an alpha-beta interaction between the left and right medial-parietal cortices with the ipsilateral frontal cortices, as well as with bilateral occipital cortices. Indeed, there is abundant evidence of this frequency specific signature of occipito-parietal and frontal areas in the resting state (Palva et al., 2005; Nikulin and Brismar, 2006; Sauseng and Klimesch, 2008; Marzetti et al., 2013; Hillebrand et al., 2016; Siebenhühner et al., 2016). It is thus conceivable that a circuit comprising occipito-parietal and frontal areas is recruited through an alpha-beta cross-frequency synchronization mechanism. The above findings could not be argued from the analysis of cross-bicoherence (**Figure 6**) which, in fact, seems to be mainly biased by volume conduction effects.

Besides the methods concerned in this paper, when dealing with the issue of the EEG reference, the possibility of getting rid of the reference effects by performing the analysis at the source level should also be considered. Indeed, it has been shown that the choice of the EEG reference does not affect the reconstruction of neural active sources, at least for noiseless potentials (Pascual-Marqui and Lehamann, 1993; Geselowitz, 1998). Thus, once a solution to the EEG inverse problem has been provided, bispectral analysis can be performed directly on reconstructed source time courses. However, in practice this approach still depends on a number of factors including, e.g., the accuracy in the knowledge of the head model, the EEG sensor density, or the choice of the inverse solver, which may affect the accuracy of source reconstruction. The advantages and disadvantages of source-level analysis over sensor-level analysis will not be addressed here, as they go beyond the scope of this work. The aim of our study was to show how the choice of the EEG reference affects bispectral analysis of sensor-level EEG data, which is a standard practice for many

research or clinical applications (e.g., Chua et al., 2009; Pritchett et al., 2010; Hayashi et al., 2014; Chella et al., 2016b; Özkurt, 2016).

In conclusion, the present study provides evidence that, also in the analysis of non-linear features of EEG signals and interactions, the choice of the reference may significantly affect the study results and the derived conclusions. To minimize this effect, we recommend the use of the REST reference, which guarantees less biased results and a straightforward comparison across different laboratories or databases, with a clear impact for research and clinical practice.

AUTHOR CONTRIBUTIONS

FC, VP, and LM conceived and designed the study. FC acquired the data and performed the analysis. All the authors interpreted the results. FC, AD, and LM wrote the manuscript. All the authors critically reviewed the manuscript.

FUNDING

The author FC has received funding from the European Commission Horizon 2020 research and innovation program under Grant Agreement No. 686865 (BREAKBEN—H2020-FETOPEN-2014-2015/H2020-FETOPEN-2014-2015-RIA). The content reflects only the author's view and the European Commission is not responsible for the content. This work was partially supported by the University of Chieti-Pescara Faculty Resources Grant 2016 of author LM, entitled "Methods for the study of functional connectivity with MEG and EEG and applications to neuroscience."

SUPPLEMENTARY MATERIAL

The Supplementary Material for this article can be found online at: http://journal.frontiersin.org/article/10.3389/fnins.2017.00262/full#supplementary-material

REFERENCES

Andrew, C., and Pfurtscheller, G. (1996). Dependence of coherence measurements on EEG derivation type. *Med. Biol. Eng. Comput.* 34, 232–238. doi: 10.1007/BF02520079

Başar, E., Rahn, E., Demiralp, T., and Schürmann, M. (1998). Spontaneous EEG theta activity controls frontal visual evoked potential amplitudes. *Electroencephalogr. Clin. Neurophysiol.* 108, 101–109. doi: 10.1016/S0168-5597(97)00039-7

Brillinger, D. R. (1965). An introduction to polyspectra. *Ann. Math. Stat.* 36, 1351–1374. doi: 10.1214/aoms/1177699896

Bullock, T. H., Achimowicz, J. Z., Duckrow, R. B., Spencer, S. S., and Iragui-Madoz, V. J. (1997). Bicoherence of intracranial EEG in sleep, wakefulness and seizures. *Electroencephalogr. Clin. Neurophysiol.* 103, 661–678. doi: 10.1016/S0013-4694(97)00087-4

Canolty, R. T., and Knight, R. T. (2010). The functional role of cross-frequency coupling. *Trends Cogn. Sci.* 14, 506–515. doi: 10.1016/j.tics.2010.09.001

Chatrian, G. E., Lettich, E., and Nelson, P. L. (1985). Ten percent electrode system for topographic studies of spontaneous and evoked EEG activities. *Am. J. EEG Technol.* 25, 83–92.

Chella, F., Marzetti, L., Pizzella, V., Zappasodi, F., and Nolte, G. (2014). Third order spectral analysis robust to mixing artifacts for mapping cross-frequency interactions in EEG/MEG. *NeuroImage* 91, 146–161. doi: 10.1016/j.neuroimage.2013.12.064

Chella, F., Pizzella, V., Zappasodi, F., and Marzetti, L. (2016a). Impact of the reference choice on scalp EEG connectivity estimation. *J. Neural Eng.* 13:036016. doi: 10.1088/1741-2560/13/3/036016

Chella, F., Pizzella, V., Zappasodi, F., Nolte, G., and Marzetti, L. (2016b). Bispectral pairwise interacting source analysis for identifying systems of cross-frequency interacting brain sources from electroencephalographic or magnetoencephalographic signals. *Phys. Rev. E* 93:052420. doi: 10.1103/PhysRevE.93.052420

Chua, K. C., Chandran, V., Acharya, U. R., and Lim, C. M. (2009). Analysis of epileptic EEG signals using higher order spectra. *J. Med. Eng. Technol.* 33, 42–50. doi: 10.1080/03091900701559408

Croft, R. J., Chandler, J. S., Burgess, A. P., Barry, R. J., Williams, J. D., and Clarke, A. R. (2002). Acute mobile phone operation affects neural function in humans. *Clin. Neurophysiol.* 113, 1623–1632. doi: 10.1016/S1388-2457(02)00215-8

Darvas, F., Miller, K. J., Rao, R. P., and Ojemann, J. G. (2009a). Nonlinear phase-phase cross-frequency coupling mediates communication between distant sites in human neocortex. *J. Neurosci.* 29, 426–435. doi: 10.1523/JNEUROSCI.3688-08.2009

Darvas, F., Ojemann, J. G., and Sorensen, L. B. (2009b). Bi-phase locking - a tool for probing non-linear interaction in the human brain. *NeuroImage* 46, 123–132. doi: 10.1016/j.neuroimage.2009.01.034

Desmedt, J. E., Chalklin, V., and Tomberg, C. (1990). Emulation of somatosensory evoked potential (SEP) components with the 3-shell head model and the problem of 'ghost potential fields' when using an average reference in brain mapping. *Electroencephalogr. Clin. Neurophysiol.* 77, 243–258. doi: 10.1016/0168-5597(90)90063-J

Dien, J. (1998). Issues in the application of the average reference: review, critiques, and recommendations. *Behav. Res. Methods Instrum. Comp.* 30, 34–43. doi: 10.3758/BF03209414

Dumermuth, G., Huber, P. J., Kleiner, B., and Gasser, T. (1971). Analysis of the interrelations between frequency bands of the EEG by means of the bispectrum a preliminary study. *Electroencephalogr. Clin. Neurophysiol.* 31, 137–148. doi: 10.1016/0013-4694(71)90183-0

Engel, A. K., Gerloff, C., Hilgetag, C. C., and Nolte, G. (2013). Intrinsic coupling modes: multiscale interactions in ongoing brain activity. *Neuron* 80, 867–886. doi: 10.1016/j.neuron.2013.09.038

Essl, M., and Rappelsberger, P. (1998). EEG coherence and reference signals: experimental results and mathematical explanations. *Med. Biol. Eng. Comput.* 36, 399–406. doi: 10.1007/BF02523206

Fogelson, N., Li, L., Li, Y., del Olmo, M. F., Santos-Garcia, D., and Peled, A. (2013). Functional connectivity abnormalities during contextual processing in schizophrenia and in parkinson's disease. *Brain Cogn.* 82, 243–253. doi: 10.1016/j.bandc.2013.05.001

Fonov, V., Evans, A. C., Botteron, K., Almli, C. R., McKinstry, R. C., and Collins, D. L. (2011). Unbiased average age-appropriate atlases for pediatric studies. *NeuroImage* 54, 313–327. doi: 10.1016/j.neuroimage.2010.07.033

Fonov, V. S., Evans, A. C., McKinstry, R. C., Almli, C. R., and Collins, D. L. (2009). Unbiased nonlinear average age-appropriate brain templates from birth to adulthood. *NeuroImage* 47(Suppl. 1), S102. doi: 10.1016/S1053-8119(09)70884-5

Frantzidis, C. A., Vivas, A. B., Tsolaki, A., Klados, M. A., Tsolaki, M., and Bamidis, P. D. (2014). Functional disorganization of small-world brain networks in mild Alzheimer's disease and amnestic mild cognitive impairment: an EEG study using relative wavelet entropy (rwe). *Front. Aging Neurosci.* 6:224. doi: 10.3389/fnagi.2014.00224

Freye, E. and Levy, J. V. (2005). Cerebral monitoring in the operating room and the intensive care unit: an introductory for the clinician and a guide for the novice wanting to open a window to the brain. *J. Clin. Monit. Comput.* 19, 1–76. doi: 10.1007/s10877-005-0712-z

Fries, P. (2005). A mechanism for cognitive dynamics: neuronal communication through neuronal coherence. *Trends Cogn. Sci.* 9, 474–480. doi: 10.1016/j.tics.2005.08.011

Fries, P. (2015). Rhythms for cognition: communication through coherence. *Neuron* 88, 220–235. doi: 10.1016/j.neuron.2015.09.034

Friston, K. J. (2011). Functional and effective connectivity: a review. *Brain Connect.* 1, 13–36. doi: 10.1089/brain.2011.0008

Friston, K. J., and Frith, C. D. (1995). Schizophrenia: a disconnection syndrome? *Clin. Neurosci.* 3, 89–97.

Geselowitz, D. B. (1998). The zero of potential. *IEEE Eng. Med. Biol. Mag.* 17, 128–136. doi: 10.1109/51.646230

Gevins, A., and Smith, M. E. (2000). Neurophysiological measures of working memory and individual differences in cognitive ability and cognitive style. *Cereb. Cortex* 10, 829–839. doi: 10.1093/cercor/10.9.829

Guevara, R., Velazquez, J. L., Nenadovic, V., Wennberg, R., Senjanović, G., and Dominguez, L. G. (2005). Phase synchronization measurements using electroencephalographic recordings. *Neuroinformatics* 3, 301–313. doi: 10.1385/NI:3:4:301

Hagemann, D., Naumann, E., and Thayer, J. F. (2001). The quest for the EEG reference revisited: a glance from brain asymmetry research. *Psychophysiology* 38, 847–857. doi: 10.1111/1469-8986.3850847

Hagihira, S., Takashina, M., Mori, T., Mashimo, T., and Yoshiya, I. (2002). Changes of electroencephalographic bicoherence during isoflurane anesthesia combined with epidural anesthesia. *J. Am. Soc. Anesthesiol.* 97, 1409–1415. Available online at: http://anesthesiology.pubs.asahq.org/article.aspx?articleid=1943876

Hagihira, S., Takashina, M., Mori, T., Ueyama, H., and Mashimo, T. (2004). Electroencephalographic bicoherence is sensitive to noxious stimuli during isoflurane or sevoflurane anesthesia. *J. Am. Soc. Anesthesiol.* 100, 818–825. doi: 10.1097/00000542-200404000-00011

Hayashi, K., Mukai, N., and Sawa, T. (2014). Simultaneous bicoherence analysis of occipital and frontal electroencephalograms in awake and anesthetized subjects. *Clin. Neurophysiol.* 125, 194–201. doi: 10.1016/j.clinph.2013.06.024

Helbig, M., Schwab, K., Leistritz, L., Eiselt, M., and Witte, H. (2006). Analysis of time-variant quadratic phase couplings in the tracé alternant EEG by recursive estimation of 3rd-order time-frequency distributions. *J. Neurosci. Methods* 157, 168–177. doi: 10.1016/j.jneumeth.2006.04.012

Hesse, C., Seiss, E., Bracewell, R., and Praamstra, P. (2004). Absence of gaze direction effects on EEG measures of sensorimotor function. *Clin. Neurophysiol.* 115, 29–38. doi: 10.1016/S1388-2457(03)00302-X

Hillebrand, A., Tewarie, P., van Dellen, E., Yu, M., Carbo, E. W. S., Douw, L., et al. (2016). Direction of information flow in large-scale resting-state networks is frequency-dependent. *Proc. Natl. Acad. Sci. U.S.A.* 113, 3867–3872. doi: 10.1073/pnas.1515657113

Hinich, M. J., and Wolinsky, M. (2005). Normalizing bispectra. *J. Stat. Plan. Infer.* 130, 405–411. doi: 10.1016/j.jspi.2003.12.022

Hipp, J. F., Hawellek, D. J., Corbetta, M., Siegel, M., and Engel, A. K. (2012). Large-scale cortical correlation structure of spontaneous oscillatory activity. *Nat. Neurosci.* 15, 884–890. doi: 10.1038/nn.3101

Hyvärinen, A., and Oja, E. (2000). Independent component analysis: algorithms and applications. *Neural Netw.* 13, 411–430. doi: 10.1016/S0893-6080(00)00026-5

Isler, J. R., Grieve, P. G., Czernochowski, D., Stark, R. I., and Friedman, D. (2008). Cross-frequency phase coupling of brain rhythms during the orienting response. *Brain Res.* 1232, 163–172. doi: 10.1016/j.brainres.2008.07.030

Jasper, H. H. (1958). The ten-twenty electrode system of the international federation. *Electroencephalogr. Clin. Neurophysiol.* 10, 371–375.

Jensen, O., and Colgin, L. L. (2007). Cross-frequency coupling between neuronal oscillations. *Trends Cogn. Sci.* 11, 267–269. doi: 10.1016/j.tics.2007.05.003

Jirsa, V., and Müller, V. (2013). Cross-frequency coupling in real and virtual brain networks. *Front. Comput. Neurosci.* 7:78. doi: 10.3389/fncom.2013.00078

Joyce, C., and Rossion, B. (2005). The face-sensitive N170 and VPP components manifest the same brain processes: the effect of reference electrode site. *Clin. Neurophysiol.* 116, 2613–2631. doi: 10.1016/j.clinph.2005.07.005

Kayser, J., and Tenke, C. E. (2010). In search of the rosetta stone for scalp EEG: converging on reference-free techniques. *Clin. Neurophysiol.* 121, 1973–1975. doi: 10.1016/j.clinph.2010.04.030

Kim, Y. C., and Powers, E. J. (1978). Digital bispectral analysis of self-excited fluctuation spectra. *Phys. Fluids* 21, 1452–1453. doi: 10.1063/1.862365

Kim, Y. C., and Powers, E. J. (1979). Digital bispectral analysis and its applications to nonlinear wave interactions. *IEEE Trans. Plasma Sci.* 7, 120–131. doi: 10.1109/TPS.1979.4317207

Lehmann, D., Strik, W., Henggeler, B., Koenig, T., and Koukkou, M. (1998). Brain electric microstates and momentary conscious mind states as building blocks of spontaneous thinking: I. visual imagery and abstract thoughts. *Int. J. Psychophysiol.* 29, 1–11. doi: 10.1109/TPS.1979.4317207

Liu, Q., Balsters, J. H., Baechinger, M., van der Groen, O., Wenderoth, N., and Mantini, D. (2015). Estimating a neutral reference for electroencephalographic recordings: the importance of using a high-density montage and a realistic head model. *J. Neural Eng.* 12:056012. doi: 10.1088/1741-2560/12/5/056012

Luu, P., and Ferree, T. (2005). *Determination of the Hydrocel Geodesic Sensor Nets Average Electrode Positions and Their 10–10 International Equivalents*. Technical Note, Electrical Geodesic, Inc.

Maris, E., and Oostenveld, R. (2007). Nonparametric statistical testing of EEG- and MEG-data. *J. Neurosci. Methods* 164, 177–190. doi: 10.1016/j.jneumeth.2007.03.024

Marzetti, L., Del Gratta, C., and Nolte, G. (2008). Understanding brain connectivity from EEG data by identifying systems composed of interacting sources. *NeuroImage* 42, 87–98. doi: 10.1016/j.neuroimage.2008.04.250

Marzetti, L., Della Penna, S., Snyder, A., Pizzella, V., Nolte, G., de Pasquale, F., et al. (2013). Frequency specific interactions of MEG resting state activity within and across brain networks as revealed by the multivariate interaction measure. *NeuroImage* 79, 172–183. doi: 10.1016/j.neuroimage.2013.04.062

Marzetti, L., Nolte, G., Perrucci, M. G., Romani, G. L., and Del Gratta, C. (2007). The use of standardized infinity reference in EEG coherency studies. *NeuroImage* 36, 48–63. doi: 10.1016/j.neuroimage.2007.02.034

Morimoto, Y., Hagihira, S., Yamashita, S., Iida, Y., Matsumoto, M., Tsuruta, S., et al. (2006). Changes in electroencephalographic bicoherence during sevoflurane anesthesia combined with intravenous fentanyl. *Anesth. Analg.* 103, 641–645. doi: 10.1213/01.ane.0000229699.99371.3c

Mormann, F., Kreuz, T., Rieke, C., Andrzejak, R. G., Kraskov, A., David, P., et al. (2005). On the predictability of epileptic seizures. *Clin. Neurophysiol.* 116, 569–587. doi: 10.1016/j.clinph.2004.08.025

Müller, M. F., Rummel, C., Goodfellow, M., and Schindler, K. (2014). Standing waves as an explanation for generic stationary correlation patterns in noninvasive EEG of focal onset seizures. *Brain Connect.* 4, 131–144. doi: 10.1089/brain.2013.0192

Nikias, C. L., and Petropulu, A. P. (1993). *Higher-Order Spectra Analysis: A Nonlinear Signal Processing Framework*. Prentice Hall signal processing series. Englewood Cliffs, NJ: PTR Prentice Hall.

Nikulin, V. V., and Brismar, T. (2006). Phase synchronization between alpha and beta oscillations in the human electroencephalogram. *Neuroscience* 137, 647–657. doi: 10.1016/j.neuroscience.2005.10.031

Nolte, G., Bai, O., Wheaton, L., Mari, Z., Vorbach, S., and Hallett, M. (2004). Identifying true brain interaction from EEG data using the imaginary part of coherency. *Clin. Neurophysiol.* 115, 2292–2307. doi: 10.1016/j.clinph.2004.04.029

Nolte, G., and Dassios, G. (2005). Analytic expansion of the EEG lead field for realistic volume conductors. *Phys. Med. Biol.* 50, 3807. doi: 10.1088/0031-9155/50/16/010

Nunez, P. L. (2010). REST: a good idea but not the gold standard. *Clin. Neurophysiol.* 121, 2177–2180. doi: 10.1016/j.clinph.2010.04.029

Nunez, P. L., and Srinivasan, R. (2006). *Electric Fields of the Brain: The Neurophysics of EEG*. New York, NY: Oxford University Press. doi: 10.1093/acprof:oso/9780195050387.001.0001

Nunez, P. L., Srinivasan, R., Westdorp, A. F., Wijesinghe, R. S., Tucker, D. M., Silberstein, R. B., et al. (1997). EEG coherency: I: statistics, reference electrode, volume conduction, laplacians, cortical imaging, and interpretation at multiple scales. *Electroencephalogr. Clin. Neurophysiol.* 103, 499–515. doi: 10.1016/S0013-4694(97)00066-7

Nunez, P. L., Wingeier, B. M., and Silberstein, R. B. (2001). Spatial-temporal structures of human alpha rhythms: theory, microcurrent sources, multiscale measurements, and global binding of local networks. *Hum. Brain Mapp.* 13, 125–164. doi: 10.1002/hbm.1030

Offner, F. F. (1950). The EEG as potential mapping: the value of the average monopolar reference. *Electroencephalogr. Clin. Neurophysiol.* 2, 213–214. doi: 10.1016/0013-4694(50)90040-X

Oostenveld, R., Fries, P., Maris, E., and Schoffelen, J.-M. (2011). Fieldtrip: open source software for advanced analysis of MEG, EEG, and

invasive electrophysiological data. *Intell. Neurosci.* 2011:156869. doi: 10.1155/2011/156869

Oostenveld, R., and Praamstra, P. (2001). The five percent electrode system for high-resolution EEG and ERP measurements. *Clin. Neurophysiol.* 112, 713–719. doi: 10.1016/S1388-2457(00)00527-7

Özkurt, T. E. (2016). Estimation of nonlinear neural source interactions via sliced bicoherence. *Biomed. Signal Process. Control* 30, 43–52. doi: 10.1016/j.bspc.2016.05.001

Palva, J. M., Palva, S., and Kaila, K. (2005). Phase synchrony among neuronal oscillations in the human cortex. *J. Neurosci.* 25, 3962–3972. doi: 10.1523/JNEUROSCI.4250-04.2005

Palva, S., and Palva, J. M. (2007). New vistas for α-frequency band oscillations. *Trends Neurosci.* 30, 150–158. doi: 10.1016/j.tins.2007.02.001

Pascual-Marqui, R. D., and Lehamann, D. (1993). Topographic maps, source localization inference, and the reference electrode: comments on a paper by desmedt et al. *Electroencephalogr. Clin. Neurophysiol.* 88, 532–533. doi: 10.1016/0168-5597(93)90043-O

Perrin, F., Pernier, J., Bertrand, O., and Echallier, J. (1989). Spherical splines for scalp potential and current density mapping. *Electroencephalogr. Clin. Neurophysiol.* 72, 184–187. doi: 10.1016/0013-4694(89)90180-6

Pritchett, S., Zilberg, E., Xu, Z. M., Myles, P., Brown, I., and Burton, D. (2010). Peak and averaged bicoherence for different EEG patterns during general anaesthesia. *Biomed. Eng. Online* 9:76. doi: 10.1186/1475-925X-9-76

Qin, Y., Xu, P., and Yao, D. (2010). A comparative study of different references for {EEG} default mode network: the use of the infinity reference. *Clin. Neurophysiol.* 121, 1981–1991. doi: 10.1016/j.clinph.2010.03.056

Rummel, C., Baier, G., and Müller, M. (2007). The influence of static correlations on multivariate correlation analysis of the EEG. *J. Neurosci. Methods* 166, 138–157. doi: 10.1016/j.jneumeth.2007.06.023

Sauseng, P., and Klimesch, W. (2008). What does phase information of oscillatory brain activity tell us about cognitive processes? *Neurosci. Biobehav. Rev.* 32, 1001–1013. doi: 10.1016/j.neubiorev.2008.03.014

Schack, B., Klimesch, W., and Sauseng, P. (2005). Phase synchronization between theta and upper alpha oscillations in a working memory task. *Int. J. Psychophysiol.* 57, 105–114. doi: 10.1016/j.ijpsycho.2005.03.016

Schack, B., Vath, N., Petsche, H., Geissler, H.-G., and Müller, E. (2002). Phase-coupling of theta-gamma EEG rhythms during short-term memory processing. *Int. J. Psychophysiol.* 44, 143–163. doi: 10.1016/S0167-8760(01)00199-4

Schoffelen, J.-M., and Gross, J. (2009). Source connectivity analysis with MEG and EEG. *Hum. Brain Mapp.* 30, 1857–1865. doi: 10.1002/hbm.20745

Shahbazi, F., Ewald, A., and Nolte, G. (2014). Univariate normalization of bispectrum using Hölder's inequality. *J. Neurosci. Methods* 233, 177–186. doi: 10.1016/j.jneumeth.2014.05.030

ShilS, J. L., Litt, M., Skolnick, B. E., and Stecker, M. M. (1996). Bispectral analysis of visual interactions in humans. *Electroencephalogr. Clin. Neurophysiol.* 98, 113–125. doi: 10.1016/0013-4694(95)00230-8

Siebenhühner, F., Wang, S. H., Palva, J. M., and Palva, S. (2016). Cross-frequency synchronization connects networks of fast and slow oscillations during visual working memory maintenance. *eLife* 5:e13451. doi: 10.7554/elife.13451

Sigl, J. C., and Chamoun, N. G. (1994). An introduction to bispectral analysis for the electroencephalogram. *J. Clin. Monitor.* 10, 392–404. doi: 10.1007/BF01618421

Srinivasan, R., Winter, W. R., Ding, J., and Nunez, P. L. (2007). EEG and MEG coherence: measures of functional connectivity at distinct spatial scales of neocortical dynamics. *J. Neurosci. Methods* 166, 41–52. doi: 10.1016/j.jneumeth.2007.06.026

Stam, C. J., Jones, B. F., Nolte, G., Breakspear, M., and Scheltens, P. (2007). Small-world networks and functional connectivity in Alzheimer's disease. *Cereb. Cortex* 17, 92–99. doi: 10.1093/cercor/bhj127

Tallon-Baudry, C., Bertrand, O., Delpuech, C., and Pernier, J. (1996). Stimulus specificity of phase-locked and non-phase-locked 40 hz visual responses in human. *J. Neurosci.* 16, 4240–4249.

Thatcher, R. W., Biver, C., Gomez, J. F., North, D., Curtin, R., Walker, R. A., et al. (2001). Estimation of the EEG power spectrum using MRI T2 relaxation time in traumatic brain injury. *Clin. Neurophysiol.* 112, 1729–1745. doi: 10.1016/S1388-2457(01)00609-5

Tian, Y., and Yao, D. (2013). Why do we need to use a zero reference? Reference influences on the ERPs of audiovisual effects. *Psychophysiology* 50, 1282–1290. doi: 10.1111/psyp.12130

Tomberg, C., Noël, P., Ozaki, I., and Desmedt, J. E. (1990). Inadequacy of the average reference for the topographic mapping of focal enhancements of brain potentials. *Electroencephalogr. Clin. Neurophysiol.* 77, 259–265. doi: 10.1016/0168-5597(90)90064-K

Varela, F., Lachaux, J.-P., Rodriguez, E., and Martinerie, J. (2001). The brainweb: phase synchronization and large-scale integration. *Nat. Rev. Neurosci.* 2, 229–239. doi: 10.1038/35067550

Winter, W. R., Nunez, P. L., Ding, J., and Srinivasan, R. (2007). Comparison of the effect of volume conduction on EEG coherence with the effect of field spread on MEG coherence. *Stat. Med.* 26, 3946–3957. doi: 10.1002/sim.2978

Womelsdorf, T., and Fries, P. (2006). Neuronal coherence during selective attentional processing and sensory-motor integration. *J. Physiol. Paris* 100, 182–193. doi: 10.1002/sim.2978

Yao, D. (1996). The equivalent source technique and cortical imaging. *Electroencephalogr. Clin. Neurophysiol.* 98, 478–483. doi: 10.1016/0013-4694(96)94694-5

Yao, D. (2000). High-resolution EEG mappings: a spherical harmonic spectra theory and simulation results. *Clin. Neurophysiol.* 111, 81–92. doi: 10.1016/S1388-2457(99)00205-9

Yao, D. (2001). A method to standardize a reference of scalp EEG recordings to a point at infinity. *Physiol. Meas.* 22, 693. doi: 10.1088/0967-3334/22/4/305

Yao, D. (2003). High-resolution EEG mapping: an equivalent charge-layer approach. *Phys. Med. Biol.* 48, 1997. doi: 10.1088/0031-9155/48/13/311

Yao, D. (2017). Is the surface potential integral of a dipole in a volume conductor always zero? a cloud over the average reference of EEG and ERP. *Brain Topogr.* 30, 161–171. doi: 10.1007/s10548-016-0543-x

Yao, D., Wang, L., Arendt-Nielsen, L., and Chen, A. C. N. (2007). The effect of reference choices on the spatio-temporal analysis of brain evoked potentials: the use of infinite reference. *Comput. Biol. Med.* 37, 1529–1538. doi: 10.1016/j.compbiomed.2007.02.002

Yao, D., Wang, L., Oostenveld, R., Nielsen, K. D., Arendt-Nielsen, L., and Chen, A. C. N. (2005). A comparative study of different references for EEG spectral mapping: the issue of the neutral reference and the use of the infinity reference. *Physiol. Meas.* 26, 173. doi: 10.1088/0967-3334/26/3/003

Zappasodi, F., Marzetti, L., Olejarczyk, E., Tecchio, F., and Pizzella, V. (2015). Age-related changes in electroencephalographic signal complexity. *PLoS ONE* 10:e141995. doi: 10.1371/journal.pone.0141995.

Zappasodi, F., Olejarczyk, E., Marzetti, L., Assenza, G., Pizzella, V., and Tecchio, F. (2014). Fractal dimension of EEG activity senses neuronal impairment in acute stroke. *PLoS ONE* 9:e100199. doi: 10.1371/journal.pone.0100199

Zhai, Y., and Yao, D. (2004). A study on the reference electrode standardization technique for a realistic head model. *Comp. Methods Prog. Biomed.* 76, 229–238. doi: 10.1016/j.cmpb.2004.07.002

Conflict of Interest Statement: The authors declare that the research was conducted in the absence of any commercial or financial relationships that could be construed as a potential conflict of interest.

frontiers in Neuroscience

ORIGINAL RESEARCH
published: 31 May 2017
doi: 10.3389/fnins.2017.00314

Revealing the Dysfunction of Schematic Facial-Expression Processing in Schizophrenia: A Comparative Study of Different References

Shenglin She[1†], Haijing Li[1†], Yuping Ning[1], Jianjuan Ren[1], Zhangying Wu[1], Rongcheng Huang[1], Jingping Zhao[1,2], Qian Wang[3*] and Yingjun Zheng[1*]*

[1] Department of General Psychiatry, The Affiliated Brain Hospital of Guangzhou Medical University (Guangzhou Huiai Hospital), Guangzhou, China, [2] National Clinical Research Center for Mental Disorders, Mental Health Institute, The Second Xiangya Hospital of Central South University, Changsha, China, [3] Beijing Key Laboratory of Epilepsy, Department of Functional Neurosurgery, Epilepsy Center, Sanbo Brain Hospital, Capital Medical University, Beijing, China

OPEN ACCESS

Edited by:
Maria L. Bringas,
University of Electronic Sciences and Technology of China, China

Reviewed by:
Elisabetta C. Del Re,
Harvard Medical School, United States
Dezhong Yao,
University of Electronic Science and Technology of China, China

***Correspondence:**
Jingping Zhao
zhaojingpingcsu@163.com
Qian Wang
aleinwangba@126.com
Yingjun Zheng
shenglitougao@163.com

[†] These authors have contributed equally to this work.

Specialty section:
This article was submitted to Brain Imaging Methods, a section of the journal Frontiers in Neuroscience

Received: 28 February 2017
Accepted: 18 May 2017
Published: 31 May 2017

Citation:
She S, Li H, Ning Y, Ren J, Wu Z, Huang R, Zhao J, Wang Q and Zheng Y (2017) Revealing the Dysfunction of Schematic Facial-Expression Processing in Schizophrenia: A Comparative Study of Different References. Front. Neurosci. 11:314. doi: 10.3389/fnins.2017.00314

The use of event-related potential (ERP) recording technology during perceptual and cognitive processing has been studied in order to develop objective diagnostic indexes for people with neuropsychiatric disorders. For example, patients with schizophrenia exhibit consistent abnormalities in face-evoked early components of ERPs and mismatch negativities (MMNs). In most studies, the choice of reference has been the average reference (AVE), but whether this is the most suitable choice is still unknown. The aim of this study was to systematically compare the AVE and reference electrode standardization technique (REST) methods for assessing expressional face-evoked early visual ERPs and visual MMNs (vMMNs) in patients with schizophrenia and healthy controls. The results showed that both the AVE and REST methods could: (1) obtain primary visual-evoked ERPs in the two groups, (2) reveal the neutral and emotional expression discrimination deficit of the P1 component in the patients, which was normal in the healthy controls, (3) reflect reductions of happy vMMNs in the patients compared to the healthy controls, and (4) show right-dominant sad vMMNs only in the patients. On the other hand, compared to the energy distributions of the AVE-obtained potentials, those of REST-obtained early visual ERPs and vMMNs were more concentrated around the temporo-occipital areas. Furthermore, only the REST-obtained vMMNs revealed a significant difference between happy and sad mismatch stimuli in patients with schizophrenia. These results demonstrate that REST technology might provide new insights into neurophysiological factors associated with neuropsychiatric disorders.

Keywords: schizophrenia, facial expression, visual mismatch negativity (vMMN), average reference (AVE), reference electrode standardization technique (REST)

INTRODUCTION

Schizophrenia is a psychiatric disorder that is associated with various clinical symptoms such as auditory hallucinations, paranoid delusional thoughts, disorganized thinking, and disturbances of self (Diagnostic and Statistical Manual of Mental Disorders, Fourth Edition) (American Psychiatry Association, 1994; Onitsuka et al., 2013). One of the cognitive dysfunctions in people with schizophrenia is facial processing at both the behavioral (Chen, 2011; Maher et al., 2015, 2016) and physiological levels (Herrmann et al., 2004; Onitsuka et al., 2006; Tsunoda et al., 2012; Maher et al., 2016; Zheng et al., 2016). Many recent studies have shown that people with diagnosis of schizophrenia often exhibit impairments in facial expression recognition, which are suggested to be related to poor social functioning (Michalopoulou et al., 2008; Kohler et al., 2009; Mendoza et al., 2011; Csukly et al., 2013; McCleery et al., 2015). The perception of facial expressions, which provides a fundamental emotional analysis of the mental intention of a person, is found to be abnormal in people with schizophrenia (for review see McCleery et al., 2015). Previous studies have mainly focused on the recognition or memory of facial expressions in patients with schizophrenia (Guillaume et al., 2012). However, a recent study reveals that the visual mismatch negativities (vMMNs) evoked by changes of facial expressions could also be abnormal in schizophrenia (Csukly et al., 2013).

Related to automatic processing, MMN is defined as the difference between the potentials evoked by deviant (infrequent) and standard (frequent) stimuli (Näätänen et al., 2004). Accumulating evidence has suggested that the variation of not only the low-level features of visual stimuli such as color, motion, or spatial frequency, but also high-level facial expressions could effectively evoke vMMN (Pazo-Alvarez et al., 2003; Susac et al., 2004; Zhao and Li, 2006; Czigler, 2007; Astikainen and Hietanen, 2009; Li et al., 2012). Previous studies have shown that a right-posterior facial expression vMMN elicited by sad and happy faces rather than neutral ones (Zhao and Li, 2006) was possibly generated from the combination of occipital, temporal, and frontal areas (Kimura et al., 2012; Stefanics et al., 2012).

Recently, new studies investigating vMMN in patients with psychiatric disorders have been conducted (for review see Kremláček et al., 2016). For example, a previous study has shown that deviant motion direction could elicit a reduction of vMMN signals in patients with schizophrenia, indicating the impairment of early processing of visual information (Urban et al., 2008). In an investigation that is particularly relevant to the current study, Csukly et al. (2013) studied the deficit in vMMN toward irregular expression in patients with schizophrenia and found that, compared to healthy people, neither happy nor fearful faces elicited any mismatch responses in the patients with schizophrenia. This indicates that patients with schizophrenia have insufficient automatic processing of emotions, which correlates with emotional recognition deficits. As patients with schizophrenia frequently show abnormal processing of emotional expressions, it should be emphasized on the neurophysiological evidences in schizophrenic population.

Technologically, many of the clinical studies prefer lower number of recording electrodes, which raises the question of whether the choice of electroencephalogram (EEG) reference electrodes could affect the results. Whether the reference methods could significantly affect the EEG are still under debate. The previous facial expression vMMN study (Csukly et al., 2013) used averaged reference (AVE) method. However, accumulating evidences suggest that a neutral reference such as the reference electrode standardization technique (REST) should be used in EEG studies (Yao, 2001; Zhai and Yao, 2004; Liu et al., 2015; Chella et al., 2016). Although the previous vMMN studies with AVE are broadly accepted, a recent study claims that REST shows a more reliable scalp signal reconstruction with low-density montage than AVE (Liu et al., 2015). Therefore, it should be essential to find whether some new insight could be gained when REST is adopted. Thus, in the current study, AVE and REST methods were both conducted to study expressional face-evoked early visual event-related potentials (ERPs) and vMMNs in schizophrenic patients and healthy controls. Faces with sad and happy expressions were used as deviant stimuli, and faces with neutral expressions as standard stimuli under situations (Chang et al., 2010). To avoid the variance inherent with images of actual faces, schematic emotional faces were used, because faces that are formed using simple lines are sufficient to arouse face-specific activity (Sagiv and Bentin, 2001; Wright et al., 2002). It is hypothesized that; (1) there is early visual dysfunction in processing emotional faces, (2) a reduced vMMN will occur in patients with schizophrenia in comparison with healthy participants, and (3) REST-obtained potential might be better in revealing the neurophysiological differences between patients with schizophrenia and healthy participants.

METHODS

Participants

Twenty-three patients with schizophrenia (11 females, mean age 32.3 ± 11.1 years old) and 23 age-matched healthy controls (11 females, mean age 32.6 ± 11.3 years old) participated in the current study. All the participants had normal or corrected-to-normal binocular visual acuity. They could read all "E" orientations correctly at line 5.0/1.0 in a visual acuity chart (from 3 meters) using each eye. Each patient was diagnosed with schizophrenia in accordance with the Diagnostic and Statistical Manual of Mental Disorders, Fourth Edition. None of them were first-episode patients, and the time relative to their first diagnosis was at least 2 years. None of the included patients had a history of severe medical disorder or severe neurological disorder. An experienced psychiatrist or psychologist evaluated clinical symptoms using the Positive and Negative Syndrome Scale (PANSS) (Kay et al., 1987). The basic demographic and descriptive characteristics of the participants are showed in **Table 1**.

No history of any serious mental illnesses was reported among the healthy volunteers, and they did not use any medications that affected the central nervous system. No neurological illness or brain injury, addiction, or visual impairment existed in either of the groups. The Institutional Review Board of Guangzhou Brain Hospital approved all the experimental procedures. All

TABLE 1 | Basic demographic and descriptive characteristics in both groups.

	Patients with schizophrenia ($n = 23$)	Healthy control subjects ($n = 23$)	*P*
Gender (male/female)	12/11	12/11	1.0[a]
Education (years)	12.9 (2.6)	12.5 (3.5)	0.707[b]
Average family income (RMB/per year)	5079.2 (3724.9)	6291.67 (3473.2)	0.249[b]
Handedness (right/left)	23/0	23/0	
Schizophrenia subtypes: Paranoid/Undifferentiated	16/7	N/A	
Duration of illness (years)	8.7 (6.3)	N/A	
PANSS total	52.4 (12.4)	32.3 (1.5)	0.000[b]
PANSS positive symptoms	13.3 (5.4)	7.4 (0.7)	0.000[b]
PANSS negative symptoms	11.2 (4.2)	7.2 (0.4)	0.000[b]
PANSS general symptoms	27.9 (6.2)	17.7 (1.2)	0.000[b]
Antipsychotic medication (Atypical/Typical)	21/2	N/A	
Chlorpromazine equivalent (mg)	556.5 (350.2)	N/A	
PSP	60.5 (9.9)	89.1 (4.3)	0.000[b]

[a] *Binomial.*
[b] *T-test.*
PANSS, Positive and Negative Syndrome Scale.

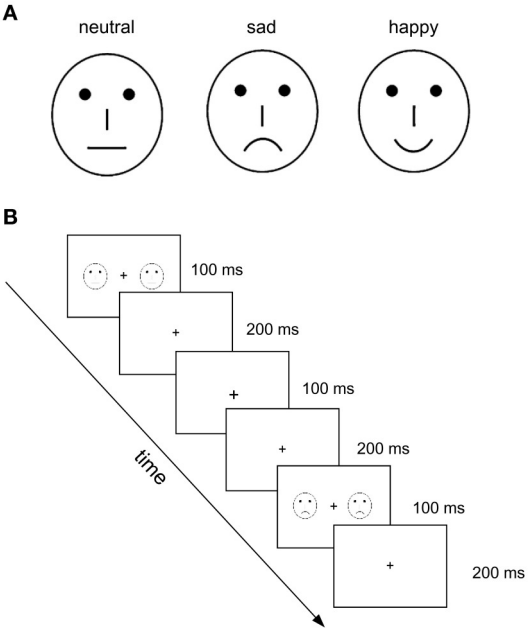

FIGURE 1 | Illustration of experimental stimuli and procedure used in the present study. **(A)** Examples of schematic face stimuli that contain three facial expressions: neutral, sad, and happy. **(B)** Illustration of the experimental procedure. The neutral faces served as standard stimuli and happy and sad faces as deviant stimuli. The task was to judge the change in size of the fixation cross ("+") in the visual center.

participants received payments and provided written informed consent for their participation.

Stimuli and Procedure

As presented in a previous study conducted by this research group (Xu et al., 2013), to reduce the effect of low-level features, 54 different schematic faces with neutral, sad, and happy expressions were used, and 18 individual schematic faces were included for each stimulus type (see an example in **Figure 1A**). Modulated by changing the shape of and the distance between the facial features, each type of stimulus included 18 models. The visual stimuli were presented on both sides of the fixation, and the duration of exposure was 100 ms, with a 500 ms inter-stimulus interval, and a visual angle of 3.68° × 3.42°.

The three-stimulus oddball paradigm was used. **Figure 1B** shows the experimental procedure. The neutral faces served as standard stimuli, and happy and sad faces as deviant stimuli. To establish a sensory memory pattern, 10 standard stimuli (neutral faces) were presented at the beginning of a stimulus sequence, and with no less than two standards between consecutive deviants. The participants were asked to focus on the fixation crosses with a changed size, which were always presented without faces to avoid motor-generated artifacts. Four blocks were conducted with 250 trials for each (standard: 200 neutral faces; deviant: 25 happy and 25 sad faces). The task performed by the participants was to judge the change in size of the fixation cross ("+") in the visual center. Practice trials were conducted before the test trials. There was a 1-min break between blocks.

Electrophysiological Recording

EEG was recorded continuously by a set of 16 Ag/AgCl electrodes placed according to the 10/20 system, including F3, Fz, F4, C3, Cz, C4, P7, P3, Pz, P4, P8, PO7, PO8, O1, Oz, and O2. Electrooculography (EOG) was recorded via electrodes placed on the bilateral external canthi and the left infraorbital and supraorbital areas to monitor for eye movements and blinks. Both EEG and EOG were sampled at 1,000 Hz, with a 0.1–100 Hz band pass using a Neuroscan NuAmps digital amplifiers system (Neuroscan Labs, El Paso, TX). The tip of the nose was used as reference during recording. Impedances of all electrodes were kept below 5 kΩ.

Data Analyses

The pre-processing of the electrophysiological data was conducted by the functions of the EEGLAB toolbox (Delorme and Makeig, 2004) in MATLAB environment. Both average reference (AVE) and approximate zero reference (REST) (Yao, 2001) were conducted off-line to generate two long-term EEGs. The AVE was conducted by the *reref* function from EEGLAB toolbox (Delorme and Makeig, 2004) and the REST was conducted by the *rest_refer* function from www.neuro.uestc.edu.cn/rest. These long-term EEGs of each electrode were firstly filtered by a band pass filter (0.5 - 40 Hz) and then segmented into epochs from -100 to 500 ms around the onset. The baseline correction was conducted within the time window of -100 to 0 ms. The epochs that contained more

than ±150 μV EOG potential were rejected as artifacts. The rest of the epochs were then averaged and low-pass filtered (cut-off frequency = 15 Hz) to obtain two groups of ERPs for AVE and REST methods, respectively. The amplitudes of early visual ERP components (P1 and N170) were analyzed to compare the primary sensory processing in the two groups. The vMMNs were obtained by subtracting ERPs to standard stimuli (neutral faces) from ERPs to deviant stimuli (sad or happy faces) for each facial expression.

Statistical analyses were performed with IBM SPSS Statistics 20 (SPSS Inc., Chicago, Illinois 60606). Analyses of variance (ANOVAs), *post-hoc* tests and *t*-tests were conducted. *P* values were corrected by *Bonferoni* adjustment to avoid multiple comparisons. The null-hypothesis rejection level was set at 0.05.

RESULTS

The results of behavioral data showed that, for healthy controls, the mean reaction time and accuracy rate were 368 ms ($SD = 80$ ms) and 96.6 % ($SD = 3.5\%$), respectively, while for schizophrenic patients, the mean reaction time and accuracy rate were 375 ms ($SD = 75$ ms) and 96.2 % ($SD = 4.2\%$), respectively. Independent *t*-tests found no significant difference between the two groups (both $p > 0.05$).

Face Evoked P1 and N170 Components

After the artifact rejection, the mean numbers of epochs under neutral face conditions were 220.92 ($SD = 11.61$) and 221.88 ($SD = 11.96$), sad face conditions were 86.24 ($SD = 4.21$) and 85.92 ($SD = 4.67$), and happy face conditions were 85.24 ($SD = 5.43$) and 85.88($SD = 5.15$), in control and patient groups, respectively. Independent *t*-tests showed no significant differences between epochs of the two groups under any of the conditions.

Figure 2 shows the grand average ERPs at the temporo-occipital electrodes (PO7 and PO8) and central electrode (CZ) evoked by deviant and standard faces in both groups. The primary visual processing components including P1 and N170 were observed in both schizophrenic patients and healthy controls. After comparing the AVE and REST results, the REST gave higher evoked potentials around the temporo-occipital electrodes (PO7 and PO8) and lower evoked potentials in CZ. This observation was further confirmed in topographic analyses. The results showed that, compared to AVE-obtained components, the absolute amplitudes of REST-obtained P1 component (110 to 130 ms, **Figure 3A**) were higher around the temporo-occipital areas (more positive) and lower around the central areas (less negative), while those of REST-obtained N170 component (175 to 195 ms, **Figure 3B**) were also higher around the temporo-occipital areas (more negative) and lower around the central areas (less positive), under all conditions. These results indicated that REST-obtained visual evoked ERPs gave significant temporo-occipital distributions in both schizophrenic patients and healthy controls.

In order to evaluate the group and stimulation effects on P1 and N170 potentials with different reference technologies, 2 (Group: patient and control) × 3 (Facial expression: neutral, happy, and sad) × 2 (Reference type: AVE and REST) three-way

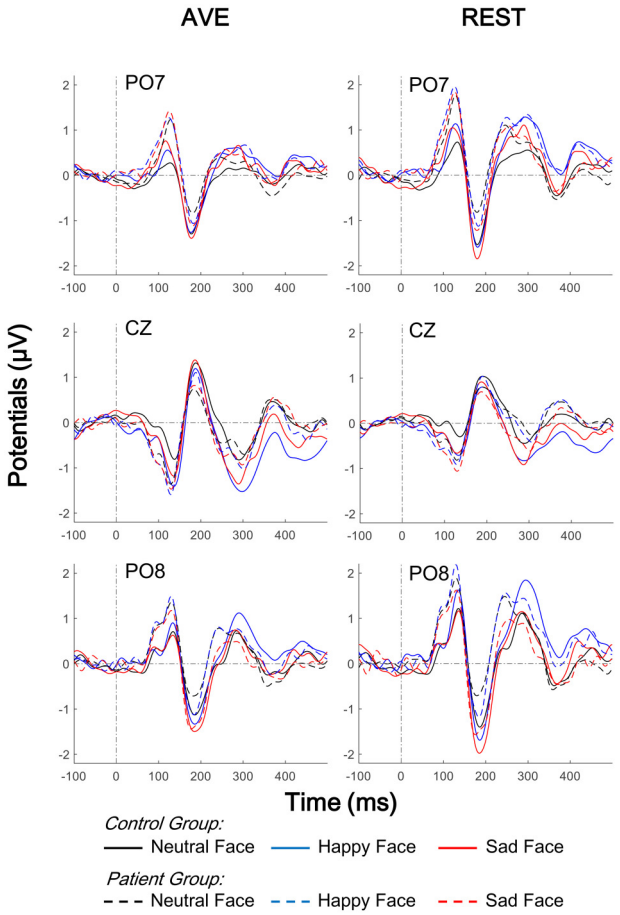

FIGURE 2 | Comparison of face evoked ERPs using two reference-modes (AVE and REST). Waveforms of temporo-occipital electrodes (PO7, PO8) and central electrode (CZ) ERPs evoked using three stimulus conditions (neutral, happy, and sad facial expressions) in both control and patient groups are also compared. Solid lines, control group; Broken lines, patient group; AVE, average reference; REST, reference electrode standardization technique; ERP, event-related potential.

mixed-measured ANOVAs were conducted, respectively. The P1 amplitude was defined as the averaged amplitude from 110 to 130 ms after stimulus onset, while the N170 amplitude was defined as the averaged amplitude from 175 to 195 ms. Three electrodes, PO7, PO8, and CZ were involved in the analysis, representing the temporo-occipital and central areas, respectively.

For P1 amplitudes, neither main effect of Group nor Reference type was significant (all $p > 0.05$). Significant Facial expression effect was found in central electrode [CZ: $F_{(1, 42)} = 9.054$, $p = 0.004$] but not in temporo-occipital electrodes [PO7: $F_{(1, 42)} = 2.547$, $p = 0.118$; PO8: $F_{(1, 42)} = 0.195$, $p = 0.661$]. No interaction effect was found (all $p > 0.05$). *Post-hoc* results with *Bonferoni* adjustment showed that the REST-obtained P1 amplitude was significantly more positive than the AVE-obtained ones in PO7 and PO8, and less negative in CZ (all $p < 0.05$) in both groups and all stimulus conditions (**Figures 2**, **4A**). *Post-hoc* results also showed that in the control group, both AVE-obtained (CZ: neutral vs. happy, $p = 0.001$; neutral vs.

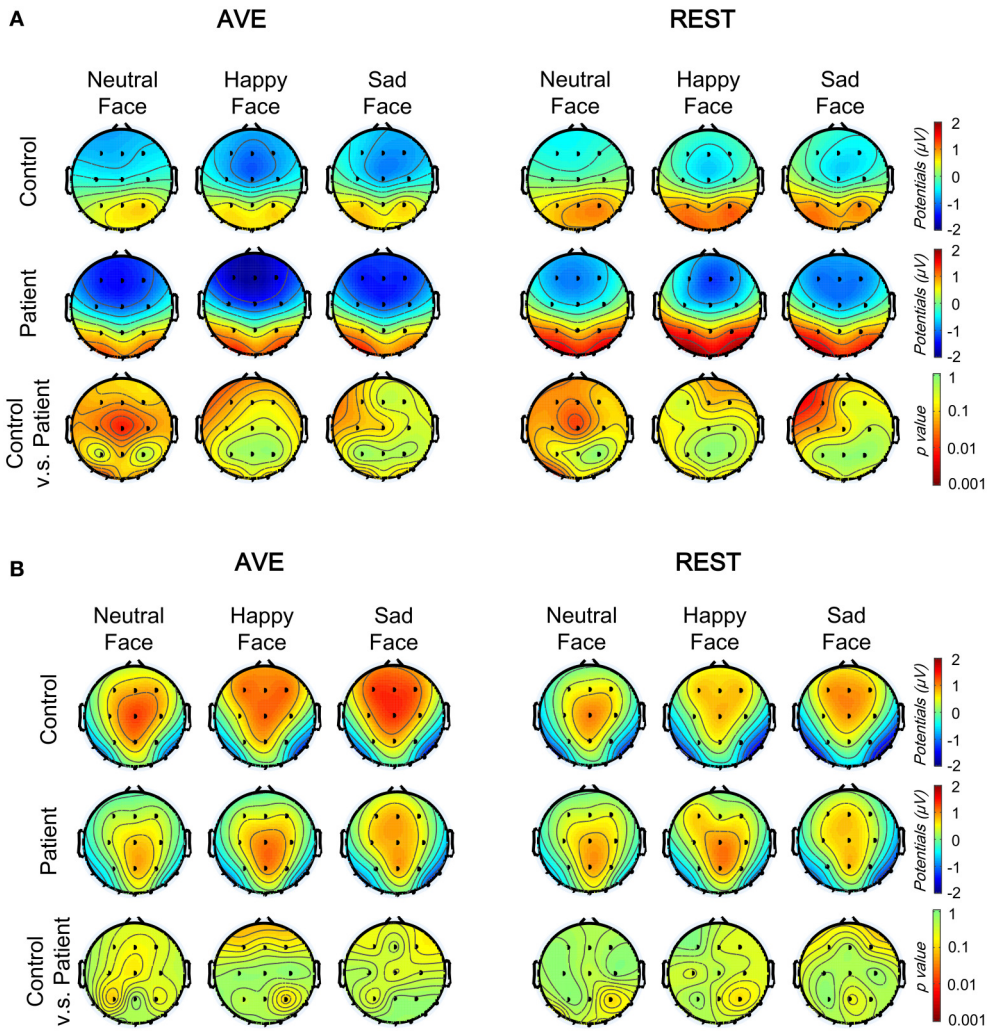

FIGURE 3 | Comparison of face evoked topographic distributions using two reference-modes (AVE and REST). **(A)** The topographic distributions of the P1 mean amplitudes (110–130 ms) under three conditions in control (top) and patient (middle) groups, and between group significance analyses (bottom, with *Bonferoni* correction). **(B)** The topographic distributions of the N170 mean amplitudes (175–195 ms) under three conditions in control (top) and patient (middle) groups, and between group significance analyses (bottom, with Bonferoni correction). AVE, average reference; REST, reference electrode standardization technique.

sad, $p = 0.004$; happy vs. sad, $p = 1.000$; PO7 and PO8: no significance) and REST-obtained (CZ: neutral vs. happy, $p = 0.008$; neutral vs. sad, $p = 0.002$; happy vs. sad, $p = 1.000$; PO7 and PO8: no significance) P1 amplitude had significant difference between neutral and emotional expressions; while in the patient group, no significance between neutral and emotional expressions was found. No other significant *post-hoc* results were found. These results demonstrated that both the REST and AVE methods could reveal a central dominant face expression specific P1 component in healthy controls, which failed to distinguish neutral and emotional expressions in schizophrenic patients.

For N170 amplitudes, no significance of any main effect or interaction effect was found (all $p > 0.05$). *Post-hoc* results with *Bonferoni* adjustment showed that in the control group, the REST-obtained N170 amplitude was significantly more negative than the AVE-obtained ones in PO7 and PO8, and less positive in CZ under sad expression condition (all $p < 0.05$), but not under neutral and happy expression conditions (all $p > 0.05$) (**Figures 2**, **4B**). These significances did not exist in patient group (all $p > 0.05$). No other significant *post-hoc* results were found.

In sum, these results demonstrated that, compared to the AVE-obtained visual processing ERPs, the energy of REST-obtained ERPs were more concentrated around temporo-occipital areas. Both REST and AVE methods could effectively discriminate early visual processing ERPs between healthy controls and schizophrenic patients.

Visual Mismatch Negativity (vMMN)

Both happy and sad vMMN were calculated by subtracting ERPs of neutral faces from ERPs of sad and happy faces, respectively. **Figure 5** shows the grand average vMMNs at

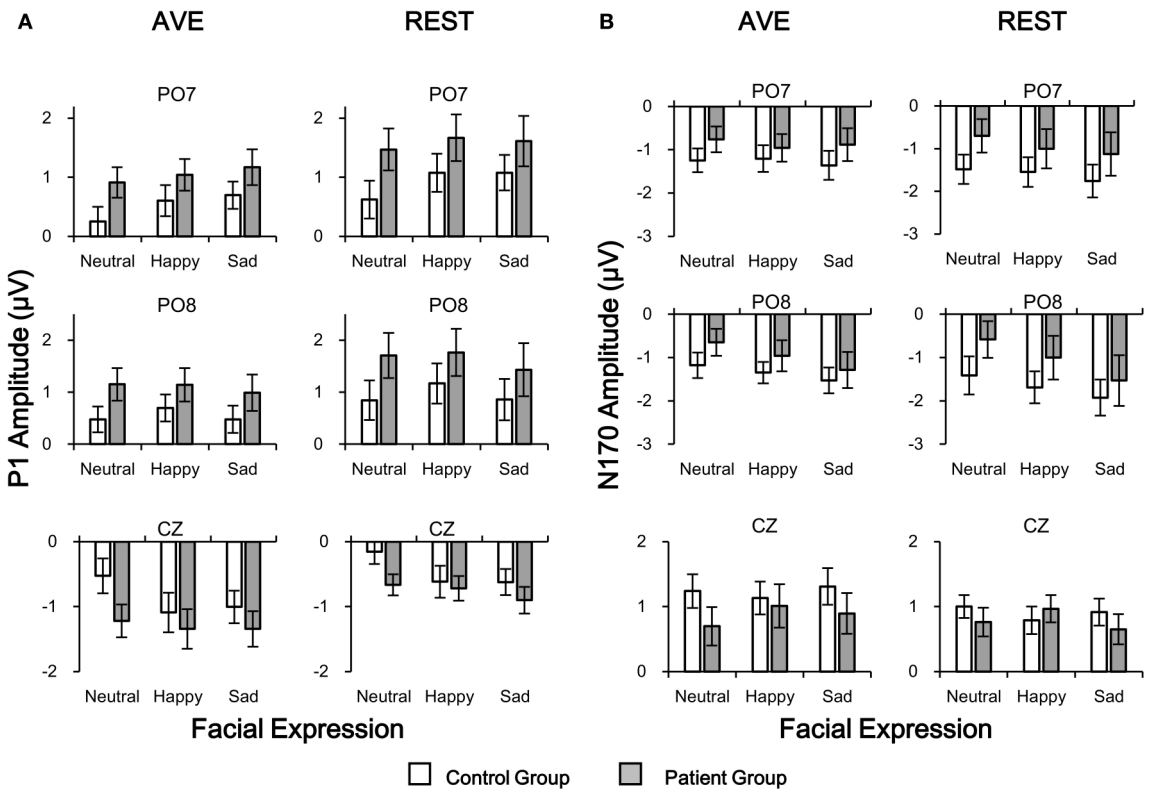

FIGURE 4 | Comparisons of P1 **(A)** and N170 **(B)** amplitudes in patient and control groups in temporo-occipital electrodes (PO7 and PO8) and central electrode (CZ) using two reference-modes (AVE and REST). White bars, control group; Gray bars, patient group. AVE, average reference; REST, reference electrode standardization technique.

the temporo-occipital electrodes (PO7 and PO8) and central electrode (CZ). Compared to the AVE-obtained vMMN, the REST-obtained vMMN gave higher evoked potentials around temporo-occipital electrodes (PO7 and PO8), and lower evoked potentials in CZ. The results of topographic analyses showed that for both reference methods, the distributions of vMMN were concentrated in the central areas in control group but not in patient group (100 to 450 ms, **Figure 6**). Furthermore, the differences between topographic distributions of controls and patients were also concentrated in the central areas (**Figure 6**, bottom panels).

To evaluate the group and stimulation effects on the vMMN potential with different reference technologies, 2 (Group: patient and control) × 2 (Mismatched facial expression: happy and sad) × 2 (Reference type: AVE and REST) three-way mixed-measured ANOVAs were conducted, respectively. Three electrodes, PO7, PO8, and CZ were involved in the analysis, representing the temporo-occipital and central areas, respectively.

The results showed that neither main effect of Mismatched facial expression nor Reference type was significant (all $p > 0.05$). Significant Group effect was found in central electrode [CZ: $F_{(1, 42)} = 4.112$, $p = 0.049$] but not in temporo-occipital electrodes [PO7: $F_{(1, 42)} = 0.653$, $p = 0.424$; PO8: $F_{(1, 42)} = 3.052$, $p = 0.088$]. No interaction effect was found (all $p > 0.05$). *Post-hoc* results with *Bonferoni* adjustment also showed that in patient group, the REST-obtained sad vMMN was significantly more negative that happy vMMN (CZ: $p = 0.045$; PO7 and PO8: no significance), but no significant difference between AVE-obtained sad and happy vMMN (CZ: $p = 0.973$; PO7 and PO8: no significance). *Post-hoc* results also showed that the happy vMMNs in patients were significantly lower than those in controls using both the AVE (CZ: $p = 0.021$; PO7 and PO8: no significance) and REST (CZ: $p = 0.032$; PO7 and PO8: no significance) methods. No other significant *post-hoc* results were found. These results demonstrated that both the REST and AVE methods could reveal significant differences between happy vMMNs in healthy controls and schizophrenic patients. Furthermore, only the REST-obtained vMMN revealed a significant difference between happy and sad mismatch stimuli in the patient group.

To evaluate the hemisphere effects on the vMMN potential of different stimulation and group, 2 [Group: patient and control) × 2 (Mismatched facial expression: happy and sad) × 2 (Hemisphere: Left (PO7) and Right (PO8)] three-way mixed-measured ANOVAs and *post-hoc* tests were conducted for AVE and REST, respectively. Interestingly, although no significant main effect or interaction effect was found, the *post-hoc* tests showed that the sad MMN in PO8 was significantly negative than

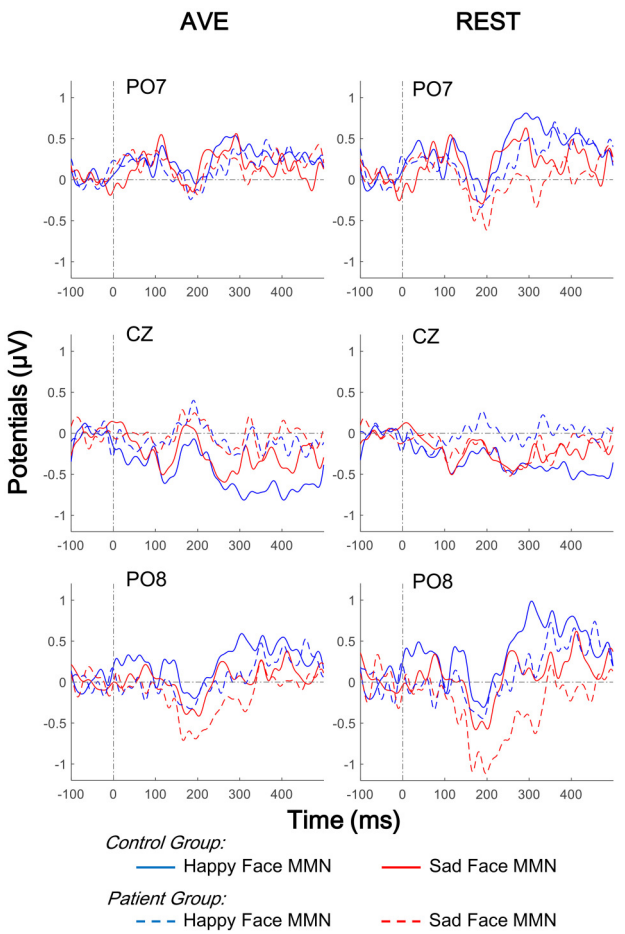

FIGURE 5 | Comparison of face evoked vMMNs using two reference-modes (AVE and REST). Waveforms of temporo-occipital electrodes (PO7 and PO8) and central electrode (CZ) ERPs evoked using three stimulus conditions (neutral, happy, and sad facial expressions) in both control and patient groups are also compared. Solid lines, control group; Broken lines, patient group; AVE, average reference; REST, reference electrode standardization technique; vMMN, visual mismatch negativity.

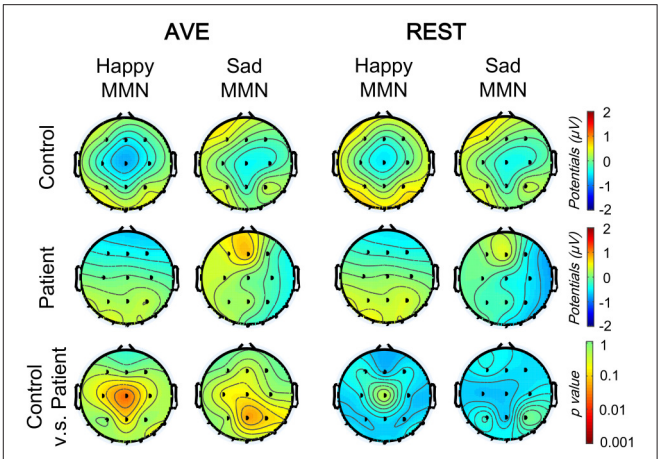

FIGURE 6 | Comparison of vMMN topographic distributions using two reference-modes (AVE and REST). The topographic distributions of facial expression vMMNs (100–400 ms) under two conditions (happy and sad deviant) in control (top) and patient (middle) groups, and between group significance analyses (bottom, with Bonferoni correction). AVE, average reference; REST, reference electrode standardization technique.

that in PO7 in only the patient group ($p = 0.018$ for both AVE and REST). These results suggested a right hemisphere dominance of sad MMN in people with schizophrenia.

DISCUSSION

Face processing dysfunction has been widely explored in previous studies (Herrmann et al., 2004; Onitsuka et al., 2006; Chen, 2011; Tsunoda et al., 2012; Maher et al., 2015, 2016; Zheng et al., 2016); however, only a few have compared visual mismatch responses elicited by task-irrelevant facial expressions between healthy controls and patients with schizophrenia (Urban et al., 2008; Csukly et al., 2013). In the current study, although the performance in the detection task did not differ between the two groups of participants, both the AVE- and REST-obtained early visual ERPs and vMMN were different between the patient and control groups. Our hypotheses were clarified by the findings that; (1) early visual dysfunction in processing emotional faces existed in people with schizophrenia, (2) vMMN significantly reduced in people with schizophrenia in comparison to healthy participants, which had a right hemisphere dominance, and (3) generally, REST was as good as AVE in revealing the neurophysiological differences between people with schizophrenia and healthy people, while only the REST-obtain vMMN revealed a significant difference between happy and sad mismatch stimuli in schizophrenic patients.

Expressional Face-Evoked P1 and vMMN Dysfunction in Schizophrenia

Generally, in the current study, both AVE and REST methods could effectively distinguish the expressional face-evoked P1 and vMMNs between healthy controls and schizophrenic patients, which were in accordance with previous studies of early visual ERPs (Herrmann et al., 2004; Onitsuka et al., 2006; Tsunoda et al., 2012; Maher et al., 2016; Zheng et al., 2016) and vMMNs (Urban et al., 2008; Csukly et al., 2013) using AVE reference.

A recent study has suggested that the underlying processes of early vMMN reflect the neuronal refractory effect, while vMMN reflects the memory-comparison-based change detection effect (Kimura et al., 2009). Supporting this issue, there is evidence that the earlier vMMN components could be evoked under task-irrelevant stimuli, representing an automatic change detection mechanism (Astikainen and Hietanen, 2009; Maekawa et al., 2012). The results of the current study indicated a functional difference in automatic detection of changes in facial expression in schizophrenic patients.

Importantly, the vMMNs were significantly reduced in patients with schizophrenia compared to healthy controls, indicating the dysfunction of processing task-irrelevant facial

expressions, when happy expressions acted as mismatch stimuli. Csukly et al. (2013) investigated the abnormality in the vMMN elicited by unexpected facial expressions in patients with schizophrenia, and found that mismatch responses to both fearful and happy emotional faces were significantly impaired in patients compared to age-matched controls. Although the conclusion of the Csukly et al. (2013) study is similar to that of the present study, there are several methodological differences. For instance, in this study, only paranoid and undifferentiated schizophrenic patients with emotional abnormity were recruited to more reliably investigate the processes underlying facial recognition.

It should be noted that emotional recognition was not required in the present study. Csukly et al. (2013) proposed that processing deficits of emotion might mediate the association between automatic information processing deficits in the daily lives of people with schizophrenia (Csukly et al., 2013). However, this issue needs further investigation. In addition, schematic emotional faces were used as experimental stimuli to minimize the variations of actual faces, including low processing-level facial features, as well as the possibility of gender effects. Previous findings have indicated that schematic faces may be useful for clinical study and application because of their simplicity compared to actual human faces (Wright et al., 2002). Although schematic emotional faces have been used in several studies (Chang et al., 2010; Xu et al., 2013) and similar vMMN results have been reported with real faces, it is necessary to use real faces to further investigate this issue.

In addition, the current study also revealed that the sad vMMN was significantly larger in the right than the left temporo-occipital area in schizophrenic patients. Because previous neuropsychological studies have suggested that the right hemisphere is relatively superior to the left in the perception of facial expression (Mandal and Singh, 1990; Borod, 1992; Mandal et al., 1993), especially negative ones (Davidson et al., 1990; Mandal et al., 1991), these evidences imply that automatically processing of negative facial emotion might be impaired in schizophrenic patients with dominant right hemispheres.

Choice of Reference in Clinical ERP Study

This study systematically investigated the face-expression neurophysiological markers in people with diagnosis of schizophrenia and healthy controls by comparing AVE and REST referencing methods. As a commonly recommended reference, AVE is conducted by averaging all the scalp electrodes. However, recent studies show that REST is more reliable with low-density montage (Liu et al., 2015; Yao, 2017). Considering the time costs and operational difficulties, most of the clinical studies that aimed at finding a reliable and effective biomarker to distinguish neuropsychiatric patients from the healthy population prefer a low-density montage design. In the current study, both AVE and REST methods could effectively distinguish the facial expression evoked ERPs and MMNs between schizophrenic patients and healthy controls in our low-density montage design, suggesting REST is an appropriate approach in clinical neurophysiological studies, which could be applied to large populations.

An interesting result from the current study was the finding that only the REST-obtained vMMN, but not the AVE-obtained vMMN revealed a significant difference between happy and sad mismatch stimuli in schizophrenic patients, but not in healthy controls (**Figure 7**). Critically, this finding dose not directly suggest that REST is superior to AVE. Approximately reconstructing a point far away from all the scalp electrodes, REST was suggested to be a neutral reference (Yao, 2001; Zhai and Yao, 2004; Liu et al., 2015; Chella et al., 2016). Therefore, REST usually achieves more objective results, which could possibly flip the significance of a result from the other references including AVE (Tian and Yao, 2013). Although the main purpose of the clinical ERP studies was to reveal neurophysiological difference between patients and controls, previous results obtained with a non-zero reference such as AVE need more confirmatory evidence, and so we recommend applications of REST in neurophysiological studies of neuropsychiatric disorders in the future.

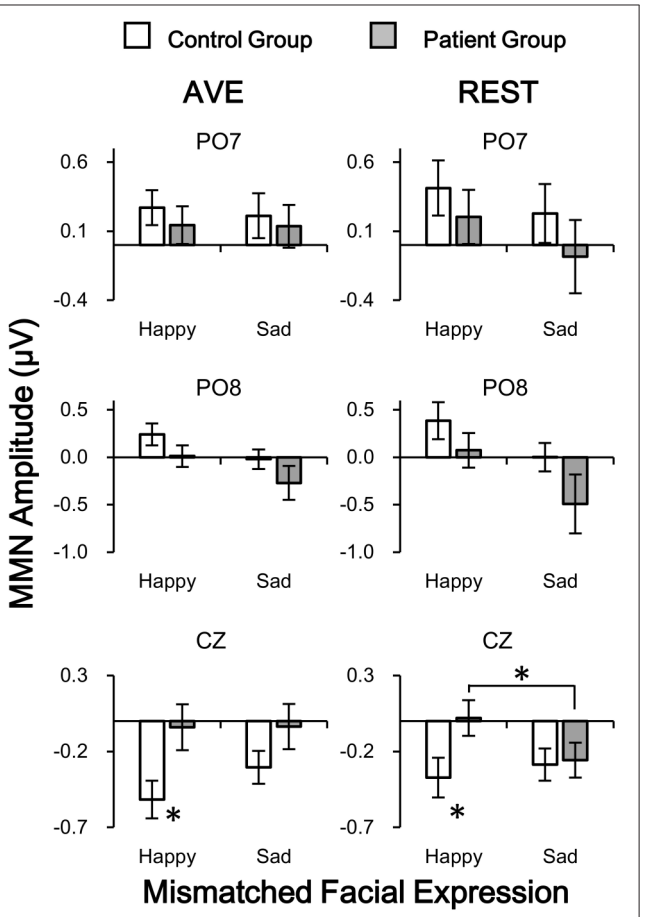

FIGURE 7 | Comparisons of vMMN amplitudes in patient and control groups in temporo-occipital electrodes (PO7 and PO8) and central electrode (CZ) using two reference-modes (AVE and REST). White bars, control group; Gray bars, patient group. AVE, average reference; REST, reference electrode standardization technique. *$p < 0.05$.

AUTHOR CONTRIBUTIONS

Each of the authors, SS, HL, YN, JR, RH, ZW, RH, JZ, QW, and YZ designed the study and wrote the protocol. SS, HL, and YZ performed the experiments. QW wrote the first draft of the manuscript. All authors contributed to and have approved the final manuscript.

ACKNOWLEDGMENTS

This work was supported by National Natural Science Foundation of China (81671334, 31400960, 81571275), the National Science and Technologic Program of China (2015BAI13B02), Planned science and technology projects of Guangzhou (2014Y2-00105), and China Postdoctoral Science Foundation (2016M601066).

REFERENCES

American Psychiatry Association, (1994). *DSM-IV: Diagnostic and Statistical Manual of Mental Disorders, 4th Edn.* Washington, DC: American Psychiatry Association

Astikainen, P., and Hietanen, J. K. (2009). Event-related potentials to task-irrelevant changes in facial expressions. *Behav. Brain Funct.* 5:30. doi: 10.1186/1744-9081-5-30

Borod, J. C. (1992). Interhemispheric and intrahemispheric control of emotion: a focus on unilateral brain damage. *J. Consult. Clin. Psychol.* 60:339. doi: 10.1037/0022-006X.60.3.339

Chang, Y., Xu, J., Shi, N., Zhang, B., and Zhao, L. (2010). Dysfunction of processing task-irrelevant emotional faces in major depressive disorder patients revealed by expression-related visual MMN. *Neurosci. Lett.* 472, 33–37. doi: 10.1016/j.neulet.2010.01.050

Chella, F., Pizzella, V., Zappasodi, F., and Marzetti, L. (2016). Impact of the reference choice on scalp EEG connectivity estimation. *J. Neural Eng.* 13:036016 doi: 10.1088/1741-2560/13/3/036016

Chen, Y. (2011). Abnormal visual motion processing in schizophrenia: a review of research progress. *Schizophr. Bull.* 37, 709–715. doi: 10.1093/schbul/sbr020

Csukly, G., Stefanics, G., Komlósi, C., and Czobor, P. (2013). Emotion-related visual mismatch responses in Schizophrenia: impairments and correlations with emotion recognition. *PLoS ONE* 8:e75444. doi: 10.1371/journal.pone.0075444

Czigler, I. (2007). Visual mismatch negativity: violation of nonattended environmental regularities. *J. Psychophysiol.* 21, 224–230. doi: 10.1027/0269-8803.21.34.224

Davidson, R. J., Ekman, P., Saron, C. D., Senulis, J. A., and Friesen, W. V. (1990). Approach-withdrawal and cerebral asymmetry: emotional expression and brain physiology: I. *J. Pers. Soc. Psychol.* 58:330. doi: 10.1037/0022-3514.58.2.330

Delorme, A., and Makeig, S. (2004). EEGLAB: an open source toolbox for analysis of single-trial EEG dynamics including independent component analysis. *J. Neurosci. Methods* 134, 9–21. doi: 10.1016/j.jneumeth.2003.10.009

Guillaume, F., Guillem, F., Tiberghien, G., and Stip, E. (2012). ERP investigation of study-test background mismatch during face recognition in schizophrenia. *Schizophr. Res.* 134, 101–109. doi: 10.1016/j.schres.2011.10.010

Herrmann, M. J., Ellgring, H., and Fallgatter, A. J. (2004). Early-stage face processing dysfunction in patients with schizophrenia. *Am. J. Psychiatry* 161, 915–917. doi: 10.1176/appi.ajp.161.5.915

Kay, S. R., Fiszbein, A., and Opler, L. A. (1987). The positive and negative syndrome scale (PANSS) for schizophrenia. *Schizophr. Bull.* 13, 261–276. doi: 10.1093/schbul/13.2.261

Kimura, M., Katayama, J., Ohira, H., and Schroger, E. (2009). Visual mismatch negativity: new evidence from the equiprobable paradigm. *Psychophysiology* 46, 402–409. doi: 10.1111/j.1469-8986.2008.00767.x

Kimura, M., Kondo, H., Ohira, H., and Schröger, E. (2012). Unintentional temporal context-based prediction of emotional faces: an electrophysiological study. *Cereb. Cortex* 22, 1774–1785. doi: 10.1093/cercor/bhr244

Kohler, C. G., Walker, J. B., Martin, E. A., Healey, K. M., and Moberg, P. J. (2009). Facial emotion perception in schizophrenia: a meta-analytic review. *Schizophr. Bull.* 36, 1009–1019. doi: 10.1093/schbul/sbn192

Kremláček, J., Kreegipuu, K., Tales, A., Astikainen, P., Põldver, N., Näätänen, R., et al. (2016). Visual mismatch negativity (vMMN): a review and meta-analysis of studies in psychiatric and neurological disorders. *Cortex* 80, 76–112. doi: 10.1016/j.cortex.2016.03.017

Li, X., Lu, Y., Sun, G., Gao, L., and Zhao, L. (2012). Visual mismatch negativity elicited by facial expressions: new evidence from the equiprobable paradigm. *Behav. Brain Funct.* 8:7. doi: 10.1186/1744-9081-8-7

Liu, Q., Balsters, J. H., Baechinger, M., van der Groen, O., Wenderoth, N., and Mantini, D. (2015). Estimating a neutral reference for electroencephalographic recordings: the importance of using a high-density montage and a realistic head model. *J. Neural Eng.* 12:056012. doi: 10.1088/1741-2560/12/5/056012

Maekawa, T., Hirano, S., and Onitsuka, T. (2012). Auditory and visual mismatch negativity in psychiatric disorders: a review. *Curr. Psychiatry Rev.* 8, 97–105. doi: 10.2174/157340051120802009 7

Maher, S., Mashhoon, Y., Ekstrom, T., Lukas, S., Chen, Y., et al. (2016). Deficient cortical face-sensitive N170 responses and basic visual processing in schizophrenia. *Schizophr. Res.* 170, 87–94. doi: 10.1016/j.schres.2015.12.005

Maher, S., Ekstrom, T., Holt, D., Ongur, D., and Chen, Y. (2015). The core brain region for face processing in Schizophrenia lacks face selectivity. *Schizophr. Bull.* 42, 666–674. doi: 10.1093/schbul/sbv140

Mandal, M. K., Asthana, H. S., and Tandon, S. C. (1993). Judgment of facial expression of emotion in unilateral brain-damaged patients. *Arch. Clin. Neuropsychol.* 8, 171–183. doi: 10.1093/arclin/8.2.171

Mandal, M. K., and Singh, S. K. (1990). Lateral asymmetry in identification and expression of facial emotions. *Cogn. Emot.* 4, 61–69. doi: 10.1080/02699939008406765

Mandal, M. K., Tandon, S. C., and Asthana, H. S. (1991). Right brain damage impairs recognition of negative emotions. *Cortex* 27, 247–253. doi: 10.1016/S0010-9452(13)80129-3

McCleery, A., Lee, J., Joshi, A., Wynn, J. K., Hellemann, G. S., and Green, M. F. (2015). Meta-analysis of face processing event-related potentials in schizophrenia. *Biol. Psychiatry* 77, 116–126. doi: 10.1016/j.biopsych.2014.04.015

Mendoza, R., Cabral-Calderin, Y., Domînguez, M., Garcia, A., Borrego, M., Caballero, A., et al. (2011). Impairment of emotional expression recognition in schizophrenia: A Cuban familial association study. *Psychiatry Res.* 185, 44–48. doi: 10.1016/j.psychres.2009.10.006

Michalopoulou, P. G., Surguladze, S., Morley, L. A., Giampietro, V. P., Murray, R. M., and Shergill, S. S. (2008). Facial fear processing and psychotic symptoms in schizophrenia: functional magnetic resonance imaging study. *Br. J. Psychiatry* 192, 191–196. doi: 10.1192/bjp.bp.106.032649

Näätänen, R., Pakarinen, S., Rinne, T., and Takegata, R. (2004). The mismatch negativity (MMN): towards the optimal paradigm. *Clin. Neurophysiol.* 115, 140–144. doi: 10.1016/j.clinph.2003.04.001

Onitsuka, T., Niznikiewicz, M. A., Spencer, K. M., Frumin, M., Kuroki, N., Lucia, L. C., et al. (2006). Functional and structural deficits in brain regions subserving face perception in schizophrenia. *Am. J. Psychiatry* 163, 455–462. doi: 10.1176/appi.ajp.163.3.455

Onitsuka, T., Oribe, N., Nakamura, I., and Kanba, S. (2013). Review of neurophysiological findings in patients with schizophrenia. *Psychiatry Clin. Neurosci.* 67, 461–470. doi: 10.1111/pcn.12090

Pazo-Alvarez, P., Cadaveira, F., and Amenedo, E. (2003). MMN in the visual modality: a review. *Biol. Psychol.* 63, 199–236. doi: 10.1016/S0301-0511(03)00049-8

Sagiv, N., and Bentin, S. (2001). Structural encoding of human and schematic faces: holistic and part-based processes. *J. Cogn. Neurosci.* 13, 937–995. doi: 10.1162/089892901753165854

Stefanics, G., Csukly, G., Komlósi, S., Czobor, P., and Czigler, I., (2012). Processing of unattended facial emotions: a visual mismatch negativity study. *Neuroimage* 59, 3042–3049. doi: 10.1016/j.neuroimage.2011.10.041

Susac, A., Ilmoniemi, R. J., Pihko, E., and Supek, S. (2004). Neurodynamic studies on emotional and inverted faces in an oddball paradigm. *Brain Topogr.* 16, 265–268. doi: 10.1023/B:BRAT.0000032863.39907.cb

Tian, Y., and Yao, D. (2013). Why do we need to use a zero reference? Reference influences on the ERPs of audiovisual effects. *Psychophysiology* 50, 1282–1290. doi: 10.1111/psyp.12130

Tsunoda, T., Kanba, S., Ueno, T., Hirano, Y., Hirano. S., Maekawa. T., et al. (2012). Altered face inversion effect and association between face N170 reduction and social dysfunction in patients with schizophrenia. *Clin. Neurophysiol.* 123, 1762–1768. doi: 10.1016/j.clinph.2012.01.024

Urban, A., Kremlacek, J., Masopust, J., and Libiger, J. (2008). Visual mismatch negativity among patients with schizophrenia. *Schizophr. Res.* 102, 320–328. doi: 10.1016/j.schres.2008.03.014

Wright, C. I., Martis, B., Shin, L. M., Fischer, H., and Rauch, S. L. (2002). Enhanced amygdala responses to emotional versus neutral schematic facial expressions. *Neuroreport* 13, 785–790. doi: 10.1097/00001756-200205070-00010

Xu, Q., Yang, Y., Wang, P., Sun, G., and Zhao, L. (2013). Gender differences in preattentive processing of facial expressions: an ERP Study. *Brain Topogr.* 26, 488–500. doi: 10.1007/s10548-013-0275-0

Yao, D. (2001). A method to standardize a reference of scalp EEG recordings to a point at infinity. *Physiol. Meas.* 22:693. doi: 10.1088/0967-3334/22/4/305

Yao, D. (2017). Is the surface potential integral of a dipole in a volume conductor always zero? A cloud over the average reference of EEG and ERP. *Brain Topogr.* 30, 161–171. doi: 10.1007/s10548-016-0543-x

Zhai, Y., and Yao, D. (2004). A study on the reference electrode standardization technique for a realistic head model. *Comput. Methods Programs Biomed.* 76, 229–238. doi: 10.1016/j.cmpb.2004.07.002

Zhao, L., and Li, J. (2006). Visual mismatch negativity elicited by facial expressions under non-attentional condition. *Neurosci. Lett.* 410, 126–131. doi: 10.1016/j.neulet.2006.09.081

Zheng, Y., Li, H., Ning, Y., Ren, J., Wu, Z., Huang, R., et al. (2016). Sluggishness of early-stage face processing (n170) is correlated with negative and general psychiatric symptoms in schizophrenia. *Front. Hum. Neurosci.* 10:615. doi: 10.3389/fnhum.2016.00615

Conflict of Interest Statement: The authors declare that the research was conducted in the absence of any commercial or financial relationships that could be construed as a potential conflict of interest.

The reviewer DY and handling Editor declared their shared affiliation, and the handling Editor states that the process nevertheless met the standards of a fair and objective review.

frontiers in Neuroscience

ORIGINAL RESEARCH
published: 05 July 2017
doi: 10.3389/fnins.2017.00368

How Different EEG References Influence Sensor Level Functional Connectivity Graphs

Yunzhi Huang[1,2], Junpeng Zhang[2], Yuan Cui[3], Gang Yang[2], Ling He[2], Qi Liu[2]* and Guangfu Yin[1]*

[1] Department of Biomedical Engineering, College of Materials Science and Engineering, Sichuan University, Chengdu, China, [2] School of Electrical Engineering and Information, Sichuan University, Chengdu, China, [3] Department of Biomedical Engineering, Chengdu Medical College, Chengdu, China

Highlights:

- Hamming Distance is applied to distinguish the difference of functional connectivity network
- The orientations of sources are testified to influence the scalp Functional Connectivity Graph (FCG) from different references significantly
- REST, the reference electrode standardization technique, is proved to have an overall stable and excellent performance in variable situations.

The choice of an electroencephalograph (EEG) reference is a practical issue for the study of brain functional connectivity. To study how EEG reference influence functional connectivity estimation (FCE), this study compares the differences of FCE resulting from the different references such as REST (the reference electrode standardization technique), average reference (AR), linked mastoids (LM), and left mastoid references (LR). Simulations involve two parts. One is based on 300 dipolar pairs, which are located on the superficial cortex with a radial source direction. The other part is based on 20 dipolar pairs. In each pair, the dipoles have various orientation combinations. The relative error (RE) and Hamming distance (HD) between functional connectivity matrices of ideal recordings and that of recordings obtained with different references, are metrics to compare the differences of the scalp functional connectivity graph (FCG) derived from those two kinds of recordings. Lower RE and HD values imply more similarity between the two FCGs. Using the ideal recording (IR) as a standard, the results show that AR, LM and LR perform well only in specific conditions, i.e., AR performs stable when there is no upward component in sources' orientation. LR achieves desirable results when the sources' locations are away from left ear. LM achieves an indistinct difference with IR, i.e., when the distribution of source locations is symmetric along the line linking the two ears. However, REST not only achieves excellent performance for superficial and radial dipolar sources, but also achieves a stable and robust performance with variable source

OPEN ACCESS

Edited by:
Rui Zhang,
Zhengzhou University, China

Reviewed by:
Dezhong Yao,
University of Electronic Science and Technology of China, China
Xu Lei,
Southwest University, China

***Correspondence:**
Junpeng Zhang
junpeng.zhang@gmail.com
Qi Liu
liuqi@scu.edu.cn

Specialty section:
This article was submitted to Brain Imaging Methods, a section of the journal Frontiers in Neuroscience

Received: *18 April 2017*
Accepted: *12 June 2017*
Published: *05 July 2017*

Citation:
Huang Y, Zhang J, Cui Y, Yang G, He L, Liu Q and Yin G (2017) How Different EEG References Influence Sensor Level Functional Connectivity Graphs. Front. Neurosci. 11:368. doi: 10.3389/fnins.2017.00368

locations and orientations. Benefitting from the stable and robust performance of REST vs. other reference methods, REST might best recover the real FCG of EEG. Thus, REST based FCG may be a good candidate to compare the FCG of EEG based on different references from different labs.

Keywords: electroencephalograph references, scalp functional connectivity graph, relative error, hamming distance, REST

INTRODUCTION

Electroencephalography (EEG) has excellent temporal resolution and is a valuable and cost effective tool for the study of brain functional interactions across a wide range of clinical and research applications (Friston and Frith, 1995; Courchesne and Pierce, 2005; Stam and Reijneveld, 2007; Fogelson et al., 2013; Frantzidis et al., 2014; Van Schependom et al., 2014). It offers a window into the spatiotemporal structure of phase-coupled cortical oscillations that underlie neuronal communication (Tallon-Baudry et al., 1996; Gross et al., 2006; Womelsdorf and Fries, 2006; Fries, 2009; Miller et al., 2009). However, the EEG scalp recording can only provide the potential difference between two points meaning that the use of an appropriate reference is vital (Geselowitz, 1998). This is a problem because no neutral locations exist on the human body (Nunez et al., 1997), and any choice for the reference location inevitably affects the EEG measurements. To minimize this effect, a number of different reference schemes have been proposed including the vertex (Lehmann et al., 1998; Hesse et al., 2004), nose (Andrew and Pfurtscheller, 1996; Essl and Rappelsberger, 1998), unimastoid or ear (Basar et al., 1998; Thatcher et al., 2001), linked mastoids or ears (Gevins and Smith, 2000; Croft et al., 2002), and average reference (i.e., average potential over all EEG electrodes) (Offner, 1950; Nunez et al., 2001). These can provide a relatively neutral reference at least with respect to the signal of interest. Specific laboratories, research fields, or clinical practices have various preferences, and the least biased reference site remains controversial (Nunez and Srinivasan, 2006; Kayser and Tenke, 2010). The lack of a universally accepted reference scheme also represents a major obstacle for cross-study comparability (Kayser and Tenke, 2010).

A neutral potential is required to resolve the problems inherent to using body surface points as a reference. Theoretically, a point at infinity is far from brain sources and has an ideal neutral potential. Therefore, a point at infinity constitutes an ideal reference (infinity reference, IR). Unlike the channel-based methods, such as AR, LR, and LM, Yao (Yao, 2001; Yao et al., 2007) proposed a "reference electrode standardization technique (REST)" to approximately transform EEG data recorded with a scalp point reference to recordings using an infinity reference (IR).

REST has recently been quantitatively validated via simulation studies with assumed neural sources in both a concentric three-sphere head model (Yao, 2001) and a realistic head model (Zhai and Yao, 2004). These studies have shown that data referenced with REST are more consistent with physiology than data referenced using traditional scalp references. This has been shown with a variety of techniques including EEG spectral imaging (Yao, 2017), EEG coherence (Marzetti et al., 2007; Qin et al., 2010), brain evoked potentials (EP) and spatiotemporal analysis (Yao and He, 2003). Previously studies on EEG electrode reference effects have predominantly focused on the power spectra or spatiotemporal analysis; however, there are few reports focusing on EEG reference effects from the perspective of graph theory. This is a significant method to evaluate functional connectivity (FC) networks (Singer and Gray, 1995; De Vico Fallani et al., 2014; Garces et al., 2016). In the realm of FC, Qin (Qin et al., 2010) and Chella (Chella et al., 2016) reported a relatively comprehensive changes on network pattern with different reference schemes. The relative error (RE) (Pereda et al., 2005; Nunez, 2010; Qin et al., 2010) is a metric to evaluate the difference of coherence matrices between each reference scheme and IR. Strictly speaking, instead of describing the FCG similarity (Garces et al., 2016) intuitively, the RE can only detect the global difference between the two matrices. To further evaluate the quantized similarity between FCGs, this study exploited HD as another metric to differentiate the two graphs via the transformed times (Makram Talih, 2005; Medkour et al., 2010; van Wijk et al., 2010; Garces et al., 2016).

One aim of this paper is to get deeper insight into the reference effects on FCGs of EEG with simulated data. Another goal is to determine how the source orientations and locations influence the FCGs from different EEG references. All simulations use an ideal three-shell spherical head model (Yao, 2001, 2017). Four regular references are involved for performance comparison including average reference (AR), the digitally linked mastoid (LM), left mastoid references (LR), and the REST transformation. A coherence matrix (Pereda et al., 2005; Srinivasan et al., 2007; Nunez, 2010) can nicely represent the relationship among EEG channels, and it is utilized to construct a FCG. The reference effects are then evaluated at the matrix level and the graph level. In the matrix level, RE detects the global difference between different references. In the intuitive graph level, HD assesses the difference between connective networks (Makram Talih, 2005; Medkour et al., 2010; van Wijk et al., 2010).

METHODS

Referencing Techniques of EEG

Here, we summarize the most commonly used reference schemes.

Reference Electrode Standardization Technique

There are two key points exploited in REST (Yao, 2001, 2017), one is the fact that an approximate neutral reference can be achieved at an infinity point that is far from brain sources, and the other

is that activated neuronal sources in the brain are always the same no matter what kind of the reference schemes are utilized (Pascual-Marqui and Lehmann, 1993). Therefore, if we denote S as the unknown matrix of the source activities and G_{REST} as the transfer matrix from these sources to sensors with REST scheme, we have

$$V_{REST} = G_{REST}S \tag{1}$$

where V_{REST} is the scalp EEG recording with a reference at infinity generated by S. Similarly, with the same source activities, the scalp EEG recordings measured with any original reference can be expressed as in

$$V_{REF} = G_{REF}S \tag{2}$$

where G_{REF} denotes the corresponding transfer matrix of any original reference. Thereby, a linear transformation T_{REST} can be derived, by combining the above equations, that derives a directly estimate V_{REST} from V_{REF} as follows

$$V_{REST} = G_{REST}S = G_{REST}(G^{+}_{REF}V_{REF}) = T_{REST}V_{REF} \tag{3}$$

where G^{+}_{REF} denotes the Moore-Penrose generalized inverse and

$$T_{REST} = G_{REST}G^{+}_{REF} \tag{4}$$

From Equation (4), one significant advantage of REST is that EEG inverse problem is not necessary to solve explicitly, that is, the transformation matrix T_{REST} can be computed without the need to know the actual sources S. In fact, only transfer matrices G_{REST} and G_{REF} are imperative to construct T_{REST}.

We can calculate G_{REST} and G_{REF} based on this ESD rather than on the actual sources because the potential originated by any source can be equivalently produced by a source distribution enclosing the actual sources (Yao, 2003; Yao et al., 2005) and an equivalent source distribution (ESD) on the cortical surface encloses all the possible neural sources. The other main advantage of REST is that, rather than depending on actual EEG data, can only rely on the characteristic of the assumed ESD including the head model, electrode montage, original reference, and spatial geometric. In this study, the ESD is assumed to be a discrete layer of current dipoles forming a closed surface analogous to previous studies (Yao, 2001, 2017; Marzetti et al., 2007; Zappasodi et al., 2014).

AR Reference, LM Reference and LR Reference

The reference electrodes should ideally be placed on a presumed "inactive" zone to ensure an arbitrarily "zero level." The option of the reference depends on the goal of the recording. Frequently, the AR reference, LM reference, and LR reference are adopted. LR uses the right earlobe as a reference, and LM uses the average of both earlobes as a reference. AR, as the name implies, takes the mean of all electrodes as the reference similar to the CZ transformation (vertex) electrode (Lehmann et al., 1998; Hesse et al., 2004). The transfer of data to recordings with reference AR, LR, and LM is easy. A perfect example can be seen in the simulated data derived from an original IR. The results of each reference can be obtained by subtracting the respective reference channel signal from the other channel (Yao, 2017).

Coherence and Network Construction

Coherence

Coherence is a frequently utilized measure in the analysis of co-operative, synchrony-defined, cortical neuronal assemblies (Pereda et al., 2005; Nunez, 2010). Coherence represents the linear relationship at a specific frequency between two signals $x(t)$ and $y(t)$, which can be expressed as:

$$C(f) = \frac{\left|C_{xy}(f)\right|^2}{C_{xx}(f)C_{xy}(f)} \tag{5}$$

where $C_{xy}(f)$ denotes cross-spectral density between $x(t)$ and $y(t)$, $C_{xx}(f)$ and $C_{yy}(f)$ denote the auto-spectral density of $x(t)$ and $y(t)$ respectively.

Construct the Functional Connectivity Topography

FCG plays an increasingly important role in offering a plausible mechanism for information transfer among neurons (Singer and Gray, 1995; Thatcher et al., 2001; Garces et al., 2016). According to its definition, FCG describes how different brain regions interact with each other while recording signals interact simultaneously (Stephan et al., 2000). A reliable FCG can reproduce the synchronous changes and the interactions between the two brain areas. In this study, a scalp FCG based on EEG is constructed with a coherence matrix, i.e., the coherence among the channels is deemed as the weight of connectivity. To give an efficient representation of network connectivity topography, a connectivity threshold is set to remove weak links between nodes by gradually increasing the connectivity threshold until the degree of each network corresponding to different references reaches four. Therefore, we produce a binary-weighted network.

Affected by the effect of volume conduction (van den Broek et al., 1998), a dense intensity of electrodes may introduce unnecessary or fake links while analyzing the interactions between brain areas. Therefore, 19 nodes are selected from the 129 channels in the EGI montage. These nodes were labeled Ch9, Ch14, Ch20, Ch27, Ch34, Ch36, Ch42, Ch44, Ch62, Ch65, Ch68, Ch73, Ch88, Ch94, Ch96, Ch103, Ch110, Ch116, and Ch121 to approximate the 20 standard electrode locations (Fp1, Fp2, Fz, F3, F4, F7, F8, C3, C4, Cz, T3, T4, T5, T6, Pz, P3, P4, O1, and O2) in the 10–20 system.

Simulations

Simulated Source Signals

To investigate the robustness and stability of each reference scheme, an EEG connectivity network for each reference was reconstructed by conducting a simulation study. To avoid the effect of volume conduction as much as possible—as well as to better visualize the data—a low-density EEG montage consisting of 19 electrodes from the EGI (Electrical Geodesics, Inc.) 129 system approximating the standard 10–20 system locations was selected.

EEG is mainly used to detect the neuronal activity on the cortex; therefore, rather than deep-level source activity, EEG accurately records the active cortex active from the radial oriented and superficial located dipolar pairs. To clearly confirm the difference between each reference overall, 300 simulated

dipole-pair configurations [each consisting of two unit radial dipoles randomly positioned within the upper hemisphere (radius 0.87)] were analyzed. To further determine the feasibility of each EEG reference scheme, 20 dipole pair configurations (each containing two unit radial dipoles with a specific position and 12 different orientations) were analyzed.

Figure 1 shows that two coherent dipolar neural source are generated using a damped Gaussian function, which can be expressed as

$$y(t_i) = e^{(-(2\pi \frac{t_i - t_0}{\gamma})^2)} cos(2\pi f(t_i - t_0) + \alpha) \quad i = 1, 2 \cdots, k \quad (6)$$

Where, $t_0 = 100^* dt, f = 30Hz, \gamma = 5, \alpha = \frac{\pi}{4}$ for one dipole in the pair, and $t_0 = 200^* dt, f = 30Hz, \gamma = 10, \alpha = \frac{\pi}{2}$ for the other.

Evaluation Metrics

Relative error for coherence

RE calculates the overall difference between the two matrices, which can be utilized as a holistic approach to evaluate the effectiveness of each reference. Smaller RE values are closer to the reference with IR. Here, RE is calculated as:

$$RE = \frac{\|C - C_*\|}{\|C\|} \quad (7)$$

where denotes the coefficient matrix of coherence (19*19) between channel pairs in specific frequency referenced at infinity, and denotes the coherence coefficient matrix C_{AR}; C_{LM}, C_L , C_{REST} and are calculated with an alternative reference scheme. The matrix norm $\|*\|$ is the Frobenius norm defined as

$$\|C\| = \sqrt{\sum_{i=1}^{N}\sum_{j=1}^{N} C_{ij}^2} \quad (8)$$

where N denotes to the total electrode number, and C_{ij} refers to the coherence between channel i and channel j.

Hamming distance for similarity

Although RE can measure the entire relationship between two coherence matrices from two methods, the accurate relationship of the two elements, which share the same location in two matrices, cannot be measured sometimes due to the effect of square operator. Therefore, another more efficient metric should be considered to measure FCG.

HD is usually used to measure the distance between graphs (Makram Talih, 2005; Medkour et al., 2010; van Wijk et al., 2010). In recent studies on FCG (Singer and Gray, 1995; De Vico Fallani et al., 2014; Garces et al., 2016), HD is introduced to measure the percentage of vector entries that differ. Compared to RE for coherence, the HD can recognize the similarity between two graphs in a more direct way. Given the number of elements of two graphs G_1 and G_2 with adjacency matrices $N^{(1)}$ and $N^{(2)}$ that disagree, HD is defined formally as follows.

$$dist(G_1, G_2) = \frac{\sum_{i \neq j}^{N} [N_{ij}^{(1)} \neq N_{ij}^{(2)}]}{N} \quad (9)$$

The square bracket notation here reflects an indicator function that is equal to one if its argument is true and zero otherwise. The Hamming distance may also be viewed of as the number of addition/deletion operations required to turn the set of edges of into. Smaller HD values results in more similar distances between two FCGs.

Comparison between HD and RE

HD is an excellent complement for RE. Assuming that there are three nodes, the 3 × 3 coherence matrices from three different methods are listed in **Figure 2**. For each node, the coherence for itself is equal to 1. Here, we take matrix A as a standard reference and use RE and HD to evaluate the difference of B and C. According to Equation (7), matrix B and matrix C share the same RE (both are equal to 0.1172). However, B and C are not the same. Especially, in the perspective of connective graph, the two matrices are indeed different from each other. The topographies from matrix B and C—which are combined by the satisfied connections—are quite different when setting the threshold to 0.55 (**Figures 2B,C**). This difference can then be detected by HD, and the HD for matrices B and C are 0.4444 and 0, respectively. Therefore, despite the similar RE of matrix B and C, matrix C has a smaller value than matrix B. Thus, matrix C is more similar to matrix A than matrix B.

The signal is inevitably mixed with noise in each collection channel. Thus, a good metric should be insensitive to noise. We used 10 groups of data, and each group consists of three matrices—all of which are 5 × 5. In each group, matrix A represents the reference and the other two matrices B and C are used for comparison. B and C can obtain their RE and HD separately by comparison with A. To better investigate the

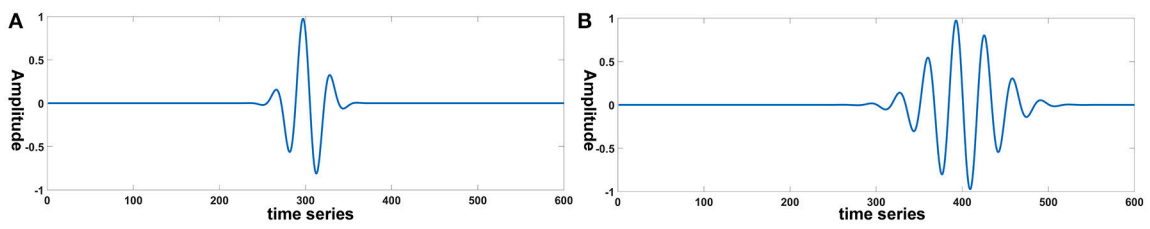

FIGURE 1 | Simulated signal generating two coherent sources where the X-axis represents the sample points, and the Y-axis presents the amplitude of signal. **(A)** The waveform of source 1. **(B)** The waveform of source 2.

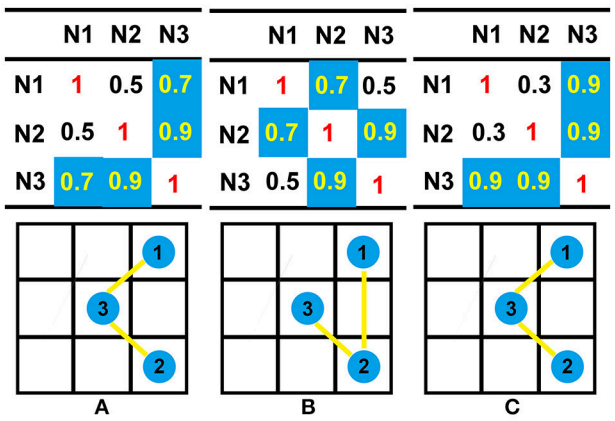

FIGURE 2 | Illustrations of the differences between RE and HD. Here, a coherence matrix of a three-node connection is used as an example. To compare the differences in the matrices from different methods, we set a threshold of 0.55; all connections larger than the threshold are colored with blue, and the connectivity graphs are then calculated from the original coherence matrices. According to Equation (7), the RE between matrix A and B, as well as the RE between matrix A and C, share the same value (0.1172). According to Equation (9), the HD between matrix A and B is 0.4444, while the HD between matrix A and C is zero. The topographies of each matrix are shown in bottom subfigure of **(A)**, **(B)**, or **(C)**; the blue circle denote the nodes, and the yellow lines denote the binary connections between two nodes.

influence of noise on HD and RE, we suppose that B and C in each group have the same overall difference with matrix A but they have different inner connectivity. That is, they share the same RE but different HD. The results of HD and RE are analyzed statistically in different SNR values ranging from 1 to 9. The HD and RE from 10 groups are recorded under specific signal-to-noise (SNR) ratios. Firstly, normal distribution test is exposed on HD and RE to determine whether the two vectors come from normal distribution, Then, the Bartlett test is utilized to determine whether the two vectors own the homogeneity of variance. Finally, if two vectors have the same variance, then a paired test is then exploited to conduct a test decision whether two vectors share the same equal mean. The Bartlett test results of HD and RE illustrate that by adding noise with specific SNR, the intragroup HD and RE can maintain the normal distributions with the same variance (p-value $>$ 0.05). Paired-test results show that; intragroup HD can hold the stability in distinguishing matrices with various SNRs (p-value $<$ 0.05), while intragroup RE cannot recognize the difference between matrices even in high SNRs (p-value $>$ 0.05). The Appendix discusses in more detail the effects of HD and RE on evaluating the similarities between two FCGs (Supplementary Material).

Configurations of Simulations

Simulation 1: Reference Effects on Two Fixed Dipoles

A general case is shown in two fixed dipoles, and the configuration of the corresponding sources are set as follows: one dipolar is set in with orientation vector, and the other is set inwith the orientation vector. Both the simulated source signal is in the form of a damped Gaussian without any noise (see **Figure 1**).

Simulation 2: Reference Effects on Superficial and Radial Dipoles

To explore the influence of orientation on difference references, various orientation combinations were used for the simulations. Source orientations in the human brain are dynamic, and thus a good reference scheme should be insensitive to changes in source orientations. To investigate the stability and robustness of each reference scheme, different orientations that contain almost all of the possible combinations of basic orientation components of sources should be applied to each simulated dipolar pair.

Inspired by Qin et al. (2010), the performance of each reference scheme with 300 random distributed dipolar pairs was investigated. However, in their work, the factor of source orientations was discussed only in passing. Their results from deep sources have not yet been clearly detailed. Therefore, we further explored the source direction in this study. Twenty dipolar pairs were considered, and each pair contained 12 orientations.

In this simulation, we used 20 dipolar pairs with a large scale of variations on orientations and locations. While the variation between each dipolar pair is distinct, the distributions cover almost the entire possible active area in the cortex. These are primarily located in four situations including bottom-up, left, right, central, and left-right (**Table 1**).

To evaluate the stability of the different reference schemes in all possible directions, 12 orientation combinations were applied to each dipolar pair, respectively. The vector of each orientation is represented in the three unit components, i.e., the unit along the X-axis, Y-axis, and Z-axis. The combinations are listed in **Table 2**.

All the electrodes and the simulated dipolar pairs were projected into the central transverse section in simulations. This better reveals the relative temporal relationship of each electrode in one plane. To give a better representation of the network connectivity topography, a connectivity threshold was used to remove weak links between nodes. The threshold was increased by decreasing the network degree (mean number of links per node across the network) until the degree of each network reached two.

RESULTS

Simulation 1: Reference Effects on Positions Fixed Two Dipoles

To illuminate the source location vividly, a standard three-view MRI structure was used from an anatomy template ICBM512 in Brainstorm. Sources location in *Simulation* 2 are shown in **Figure 3A**, and the corresponding FCGs are shown in **Figure 3B**. The RE and HD statistics are shown in **Figure 3C**. Taking the FCG of IR as a standard, REST obviously has the most similarity with IR at the first sight, and AR FCG is the most disordered (**Figure 3B**). Here, HD is used to evaluate the graph similarity, and the quantized performance of each method is $HD_{REST} = 7.2\%$, $HD_{AR} = 16.96\%$, $HD_{LM} = 9.94\%$, $HD_{LR} = 14.62\%$. This agrees with the exhibited connectivity topographies.

In no-noise simulation, RE is an efficient metric to illustrate the accuracy of different schemes quantitatively. However, the

TABLE 1 | Illustrative Maps of Distribution of the 20 Dipolar Pairs [colorful solid points (green and yellow) denote the simulated sources].

Source distribution types	Illustrative maps
Bottom-Up	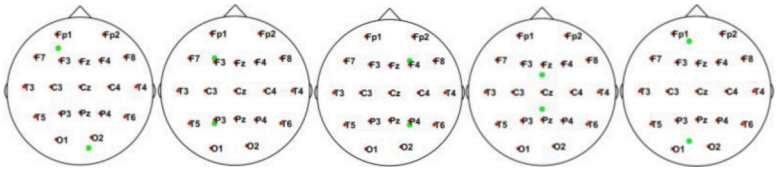
Left	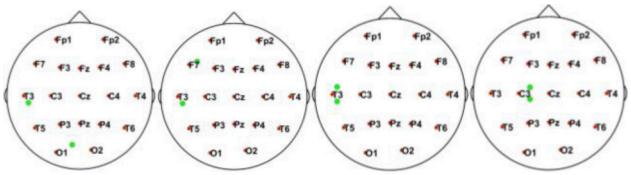
Central	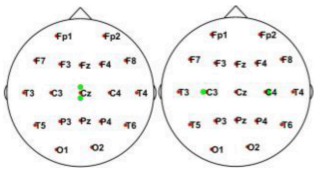
Right	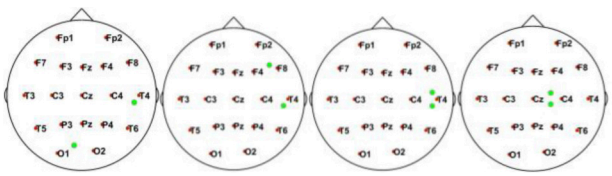
Left-right	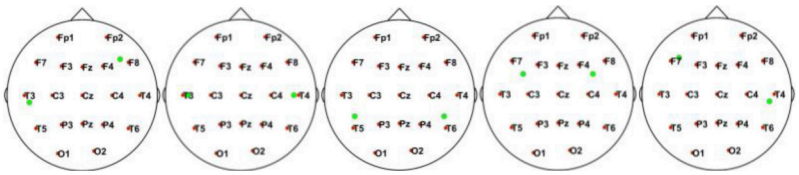

Source is projected on the z = 0 plane.

TABLE 2 | Orientation combinations used in each dipolar pair (applicable for 20 dipolar pairs with complicated orientations).

No. of orientation combinations	Source 1	Source 2
1	(1,0,0)	(1,0,0)
2	(1,0,0)	(0,1,0)
3	(1,0,0)	(0,0,1)
4	(0,1,0)	(0,1,0)
5	(0,1,0)	(0,0,1)
6	(0,0,1)	(0,0,1)
7	(1,0,0)	(−1,0,0)
8	(1,0,0)	(0, −1,0)
9	(0,1,0)	(0, −1,0)
10	(1,0,1)	(1,0,1)
11	(1,0,1)	(0,1,1)
12	(1,0,1)	(−1,0,1)

persuasiveness of RE in FCG is not that intuitive. HD is a complementary metric, and it can measure the distance between each reference schemes and IR with respect to graph similarity. Theoretically, for each reference, smaller HD and RE values result in values that are more similar to the IR. This further improves the method. On the fixed location, the results of different combinations of orientation are shown **Figure 3C**, and REST is closer to zero than the other three reference schemes from the perspective of average HD and RE. While the standard REST is higher than that of LM, the entire range of REST is closer to zero than LM.

Simulation 2: Reference Effects on Superficial and Radial Dipoles

Theoretically, if the active source is located on the superficial cortex and the source direction is radial, then EEG can detect and

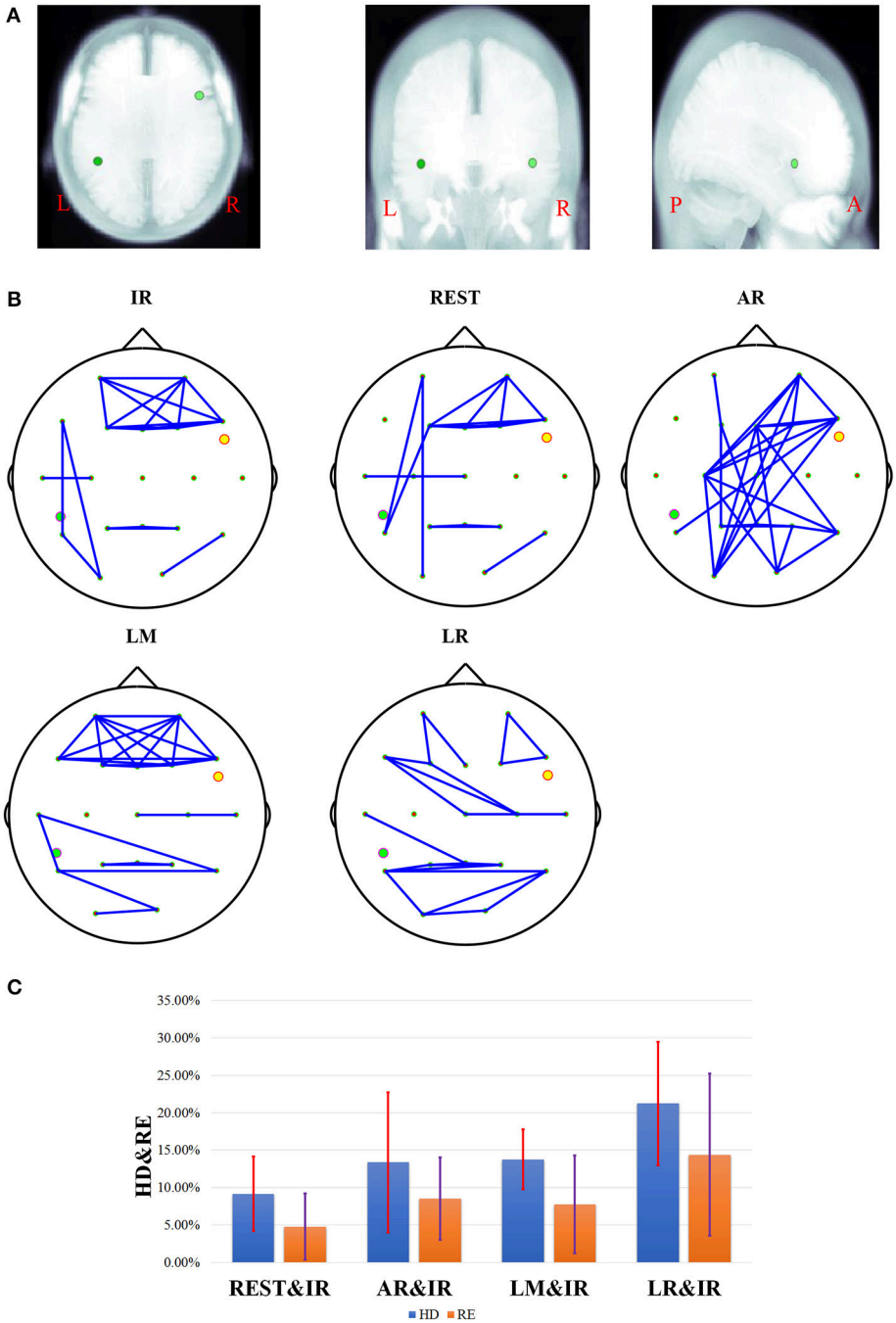

FIGURE 3 | The results of one fixed dipolar pair, one dipolar is set in [−0.6, −0.3, −0.4] with orientation vector. The other is set in [0.6, 0.3, 0.4] with the orientation vector (0,1,1). Here, **(A)** is the location of the dipolar pair overlaid on MRI structure images. The MRI structure comes from Brainstorm anatomy template ICBM512. From left to right, this shows the location of the two simulated sources under the view of axial, coronal, and sagittal respectively. Here, L denotes the left, R denotes the right, P denotes the posterior, and A denotes the anterior. In **(B)**, the network connectivity topography is a dipolar pair with different references. **(C)** Results of different references on one fixed dipolar pair involving 12 orientations. The blue bar represents the results of HD, and the orange bar represents the results of RE. The red and violet segments denote errors sources from different references in HD from 12 different orientations and RE results from 12 different orientations, respectively.

recover active signals very well. Therefore, a good EEG reference must have an excellent reflection of the source activation—especially the superficial and radial cortex source. The RE and HD metrics are utilized to evaluate the difference for each reference from the perspective of coherence matrix and the similarity of FCG.

The histogram can reflect the distribution of results at different levels. **Figure 4A** shows RE histograms of each reference in a noisy situation (SNR of 5). There are 300 dipoles with REs between REST and IR, 200 diploes are nearly zero, and almost 75 dipoles are around 0.1. However, for REs between AR and IR, only ∼125 dipoles are nearly zero. A comparative number of dipoles are around 0.1. The remaining dipoles are distributed across a relatively large scale of variation. The LR situation shows a worse result—fewer than 100 dipoles are obtained from the nearly zero RE. There are fewer than 200 dipoles with RE values of 0.1. As for LM, the distribution scale is larger than REST, and the number of RE that is less than 0.1. These only occupy half of the total.

During EEG measurements, the electronic disturbance from noise must be considered. A good reference should have a stable performance at different noise levels. **Figures 4B,C** shows that when the noise is difficult to distinguish from signal, then SNR equals 1. Here, the EEG measurements at all references lose efficacy. However, when SNR is greater than 1, REST is much better. Clearly, the averages of REST RE in different SNRs (≥2) from 300 dipoles are all around 0.1. The REST HD are all below 0.025. The RE and HD of other references are almost twice as high in terms of average and variation. The REST RE and REST HD have relatively smaller values and vary on a smaller and more stable scale. AR in particular varies more sharply than other references in different SNRs.

Simulation 3: Reference Effects on 20 Dipoles with Various Orientation Combinations

Figure 5 shows the overall statistical results of HD and RE. These are consistent, i.e., RE tends to be similar to HD at each reference. While these are affected by the distributed form of sources, REST also shows a better performance than the other methods. Statistically, REST has the smallest average RE and HD as well as the smallest fluctuation (**Table 3**). The HD and RE variations of REST are both about 5%; other references are much greater. Thus, REST seems to be a better reference choice. **Figure 5** shows that LR is obviously the worst choice. It has a high average and variance; the performance of AR and LM is moderate.

The results in **Figure 5** do not consider noise. However, scalp electrodes always contain real EEG and noise. Thus, to verify the robustness of the different methods in a real situation, we simulated the signals with different SNRs by adding random Gaussian noise considering both poor and good situations. Once the location of each dipolar pair is determined, random Gaussian noise is added to the ideal source signal. This is repeated 100 times. **Figure 6** shows both high SNR (SNR = 5) and low SNR (SNR = 1) vs. other methods. The average and standard deviation of HD and RE from REST is the minimum. Thus, in a noisy situation, REST achieves relatively higher robustness.

In ideal (no-noise) situations, the orientation of the dipolar pair significantly affects the performance, in addition to the

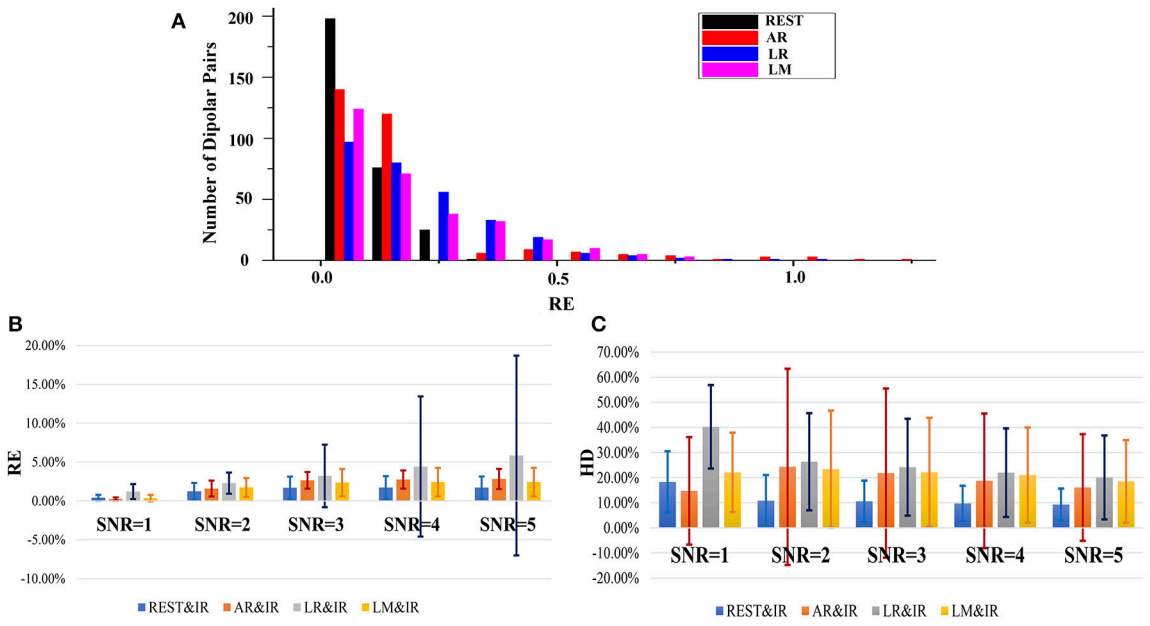

FIGURE 4 | Statistical results of RE and HD based on 300 radial and superficial dipoles. **(A)** Relative error histogram of each reference where the SNR of each dipolar pair is 5. The black bars denote the number of the results from REST in different RE values, and the red, blue and magenta bars represent the results of AR, LR and LM, respectively. **(B)** The results of RE between each reference and IR on 300 dipolar pairs. The results are shown for different SNR conditions where the blue bars denote the RE results for different SNRs. The orange, gray, and yellow represent the RE results of AR, LR, and LM, respectively. **(C)** HD results between each reference and IR based on 300 dipolar pairs. The results are seen for different SNR conditions where the blue bars denote the RE results for different SNRs, and the orange, gray, yellow represent the RE results of AR, LR, and LM, respectively.

positional influence on each method. To investigate the stability of each reference scheme with these inevitable variable factors, the results in each orientation are considered separately by exploiting HD as a direct metric.

In fact, the real orientation of the dipolar pair is usually complicated; therefore, a good zero-reference scheme should be promising with a stable tolerance in many possible orientations. **Figure 7** shows that even though REST may not always have the best performance, it is the most stable. AR, LM, and LR have good performance in limited. According to **Figure 3**, REST should achieve excellent performance when the source active is superficial and radial, but it is affected by the deeper simulated source (**Figure 7**). The REST has undesirable performance in ORI*6* (orientations of two source that are both radial). Although REST has poor performance in ORI*6*, REST is better in AR.

AR operates better than REST under certain orientations, but it performs worse in many orientations like *ORI3*, *ORI5, ORI6, ORI10,* and *ORI12* that contain the upward component in dipolar pair. Since AR fluctuates largely with the change of orientation, AR maybe not a good choice for zero-reference. LR and LM are limited by their own strategy and are largely affected by the source position. In the simulated 20 dipolar pairs, the amount of symmetry distribution is larger than the asymmetry distribution. Therefore, LM performs better than LR.

TABLE 3 | Statistical results of HD and RE on each reference in a noise free situation (20 dipolar pairs; each pair with 12 orientations).

	Hamming distance (%)	Relative error (%)
REST	11.18 ± 7.60	5.93 ± 4.51
AR	13.98 ± 9.04	7.97 ± 5.73
LM	14.87 ± 9.87	6.45 ± 5.4
LR	21.66 ± 12.69	10.11 ± 8.99

DISCUSSION

EEG results from different reference sometimes vary widely. They are influenced by the inevitable reference issue and are limited by the principle of EEG. Here, we studied EEG reference effects on FCG with AR, LR, LM, and REST. Each reference has specific zero-reference schemes. The LR systematic decreases the EEG amplitude in the electrodes, and these are closer to the reference side. Although the LM reference makes use of "linked" earlobes, asymmetry from LR reference is avoided, but this distorts the EEG mapping because the electric current flows inside the linking wire. This affects the intracranial currents that form the EEG potentials. AR avoids asymmetry from LR or LM. However, vs. REST, the AR reference needs several strict conditions to gain zero integral assumptions: (1) sufficiently dense electrodes, (2) complete electrode coverage (sampling both the upper and lower part of head), and (3) the head must be spherical (Nunez and Srinivasan, 2006; Yao et al., 2007). Such ideal conditions are rarely realized. in contrast to REST, the AR reference, LM reference, and LR reference are all theoretically based on the channel transformation. The unexpected activity would be largely induced to the referenced recordings because the specific channels are not electrically active. Therefore, channel-based references are not that recommended (Yao and He, 2003).

It must be acknowledged that RE (Pereda et al., 2005; Nunez, 2010; Qin et al., 2010) can well reflect the overall difference between the two matrices and has its irreplaceable superiority on measuring the difference between graphs, thus RE has been widely adopted to evaluate the difference between coherence matrices from EEG references. However, evaluations on EEG references which only depend on RE are not sufficient. A perfect example can be found that, if two graphs share the same whole difference but their inner networks are changed, RE cannot detect the difference between the two graphs. To complete RE, HD (Makram Talih, 2005; Medkour et al., 2010; van Wijk et al., 2010) is induced as a new metric, which can well evaluate the

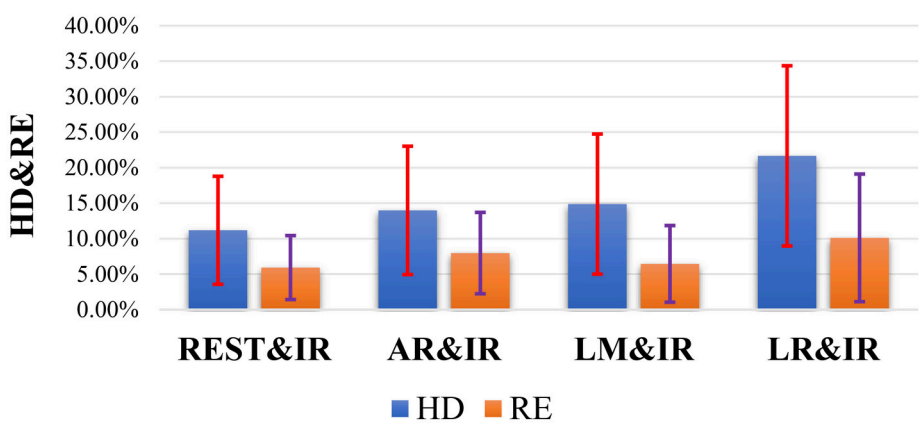

FIGURE 5 | Results of HD and RE on 20 dipolar pairs in a noise free situation. The blue bar represents the results of HD, and the orange bar represents the results of RE.

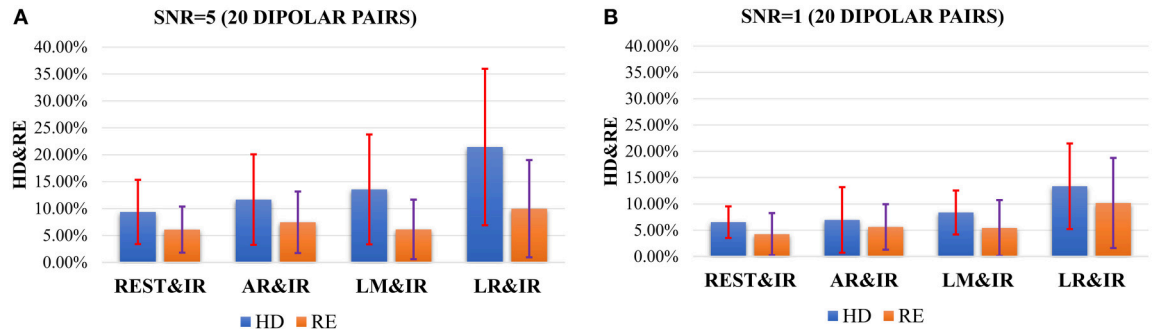

FIGURE 6 | HD and RE results of 4 references with different SNRs. The blue bar represents the results of HD, and the orange bar represents the results of RE. **(A)** Results in the case of SNR = 5; **(B)** Results in the case of SNR = 1.

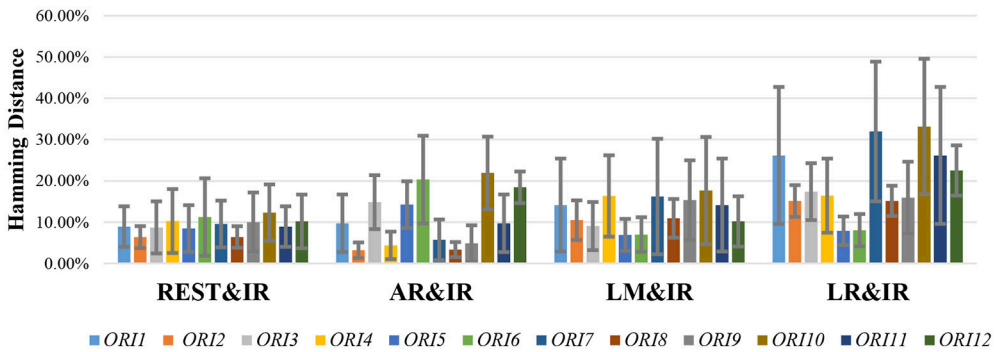

FIGURE 7 | HD results of different references on 20 dipolar pairs. Each pair contains 12 orientations. Color bars represent the average value of 20 dipolar pairs on each orientation, respectively, and the error bars represent the standard deviation of 20 dipolar pairs on each orientation.

difference in topographies. Derived from graph theory, HD can effectively detect the edge changes in networks. Even though, unlike RE, HD cannot measure the entire difference of weights, it is relative intuitive and objective to detect alterations in FCG. Thus, as a complementary, HD contributes to helping complete the detection of RE by measuring the alterations in networks. For example, in *Simulation* 1, the difference of RE between LM and REST is too subtle to detect. But by combing the two metrics, we can evaluate the similarity of graphs more precisely, so that we can better study reference effects on FCG. The two metrics have their unique superiority, and they can make their respective advantages complementary to each other. Therefore, we should choose the appropriate evaluate metrics according to the practical issues.

The results of RE and HD validates that REST performs well in terms of both stability and robustness. REST works because it grasps the essence of the zero-reference. AR can average the signal and noise from each electrode; thus, it achieves good performance when the orientation of the source is along with the axial plane or under noisy situations. However, once there is an upward component in the source orientation, the baseline of AR is abnormally high. Thus, thus performance of AR is unsatisfactory. Although LM and L are insensitive to the orientation of sources, the results depend significantly on the distribution of sources. LM would achieve a stable performance especially for of bilateral symmetry of sources. LR requires rigorous conditions to achieve good results, i.e., LR is close to IR only when the location of the source is far from the left ear. We conclude that REST can achieve stable performance under diverse situations, while AR, LM, and LR can achieve satisfactory results only in a few situations.

CONCLUSIONS

In this study, we investigated how different reference choices influence FCG using simulated EEG data with various SNR values that were generated from different source combinations. The simulation shows that reference choices have a significant effect on coherence—a measure that indicates synchronization and interaction. As a result, the FCGs also differ across reference schemes. The RE or HD between REST and IR had the smallest values relative to AR, LM, and LR references as well as IR. This means that REST reconstructs FCG better than IR. Moreover, the results revealed that REST could perform stably even when the sources vary on orientations compared to other reference schemes. These findings indicate that the choice of reference plays a crucial role in functional network studies in the brain. It is

critical to consider this thoughtfully. REST is the recommended reference technique for objective comparisons as well as cross-laboratory studies and clinical practice.

AUTHOR CONTRIBUTIONS

YH: Simulate the designed experiments and evaluate the results, Write the whole manuscript. JZ and QL: Design the whole experiments and Revise the entire framework of the manuscript. YC, LH, GaY, and GuY takes part in analyzing the logic and checking the grammar error of the manuscript.

ACKNOWLEDGMENTS

This work was supported by National Nature Science Foundation of China (Contract Grants Nos. 81470085, 312 71204).

SUPPLEMENTARY MATERIAL

The Supplementary Material for this article can be found online at: http://journal.frontiersin.org/article/10.3389/fnins.2017.00368/full#supplementary-material

REFERENCES

Andrew, C., and Pfurtscheller, G. (1996). Dependence of coherence measurements on EEG derivation type. *Med. Biol. Eng. Comput.* 34, 232–238. doi: 10.1007/BF02520079

Basar, E., Rahn, E., Demiralp, T., and Schurmann, M. (1998). Spontaneous EEG theta activity controls frontal visual evoked potential amplitudes. *Electroencephalogr. Clin. Neurophysiol.* 108, 101–109. doi: 10.1016/S0168-5597(97)00039-7

Chella, F., Pizzella, V., Zappasodi, F., and Marzetti, L. (2016). Impact of the reference choice on scalp EEG connectivity estimation. *J. Neural Eng.* 13, 036016.

Courchesne, E., and Pierce, K. (2005). Why the frontal cortex in autism might be talking only to itself: local over-connectivity but long-distance disconnection. *Curr. Opin. Neurobiol.* 15, 225–230. doi: 10.1016/j.conb.2005.03.001

Croft, R. J., Chandler, J. S., Burgess, A. P., Barry, R. J., Williams, J. D., and Clarke, A. R. (2002). Acute mobile phone operation affects neural function in humans. *Clin. Neurophysiol.* 113, 1623–1632. doi: 10.1016/S1388-2457(02)00215-8

De Vico Fallani, F., Richiardi, J., Chavez, M., and Achard, S. (2014). Graph analysis of functional brain networks: practical issues in translational neuroscience. *Philos. Trans. R. Soc. B Biol. Sci.* 369, 20130521.

Essl, M., and Rappelsberger, P. (1998). EEG coherence and reference signals: experimental results and mathematical explanations. *Med. Biol. Eng. Comput.* 36, 399–406. doi: 10.1007/BF02523206

Fogelson, N., Li, L., Li, Y., Fernandez-Del-Olmo, M., Santos-Garcia, D., and Peled, A. (2013). Functional connectivity abnormalities during contextual processing in schizophrenia and in Parkinson's disease. *Brain Cogn.* 82, 243–253. doi: 10.1016/j.bandc.2013.05.001

Frantzidis, C. A., Vivas, A. B., Tsolaki, A., Klados, M. A., Tsolaki, M., and Bamidis, P. D. (2014). Functional disorganization of small-world brain networks in mild Alzheimer's Disease and amnestic Mild Cognitive Impairment: an EEG study using Relative Wavelet Entropy (RWE). *Front. Aging Neurosci.* 6:224. doi: 10.3389/fnagi.2014.00224

Fries, P. (2009). Neuronal gamma-band synchronization as a fundamental process in cortical computation. *Annu. Rev. Neurosci.* 32, 209–224. doi: 10.1146/annurev.neuro.051508.135603

Friston, K. J., and Frith, C. D. (1995). Schizophrenia: a disconnection syndrome? *Clin. Neurosci.* 3, 89–97.

Garces, P., Pereda, E., Hernandez-Tamames, J. A., Del-Pozo, F., Maestu, F., and Pineda-Pardo, J. A. (2016). Multimodal Description of Whole Brain Connectivity: A Comparison of Resting State MEG(,) fMRI(,) and DWI. *Hum. Brain Mapp.* 37, 20–34. doi: 10.1002/hbm.22995

Geselowitz, D. B. (1998). The zero of potential. *IEEE Eng. Med. Biol. Mag.* 17, 128–132. doi: 10.1109/51.646230

Gevins, A., and Smith, M. E. (2000). Neurophysiological measures of working memory and individual differences in cognitive ability and cognitive style. *Cereb. Cortex* 10, 829–839. doi: 10.1093/cercor/10.9.829

Gross, J., Schmitz, F., Schnitzler, I., Kessler, K., Shapiro, K., Hommel, B., et al. (2006). Anticipatory control of long-range phase synchronization. *Eur. J. Neurosci.* 24, 2057–2060. doi: 10.1111/j.1460-9568.2006.05082.x

Hesse, C. W., Seiss, E., Bracewell, R. M., and Praamstra, P. (2004). Absence of gaze direction effects on EEG measures of sensorimotor function. *Clin. Neurophysiol.* 115, 29–38. doi: 10.1016/S1388-2457(03)00302-X

Kayser, J., and Tenke, C. E. (2010). In search of the Rosetta Stone for scalp EEG: converging on reference-free techniques. *Clin. Neurophysiol.* 121, 1973–1975. doi: 10.1016/j.clinph.2010.04.030

Lehmann, D., Strik, W. K., Henggeler, B., Koenig, T., and Koukkou, M. (1998). Brain electric microstates and momentary conscious mind states as building blocks of spontaneous thinking: I. Visual imagery and abstract thoughts. *Int. J. Psychophysiol.* 29, 1–11. doi: 10.1016/S0167-8760(97)00098-6

Makram Talih, N. H. (2005). Structural learning with time-varying components: tracking the cross-section of financial time series. *R. Stat. Soc.* 67, 321–341. doi: 10.1111/j.1467-9868.2005.00504.x

Marzetti, L., Nolte, G., Perrucci, M. G., Romani, G. L., and Del Gratta, C. (2007). The use of standardized infinity reference in EEG coherency studies. *Neuroimage* 36, 48–63. doi: 10.1016/j.neuroimage.2007.02.034

Medkour, T., Walden, A. T., Burgess, A. P., and Strelets, V. B. (2010). Brain connectivity in positive and negative syndrome schizophrenia. *Neuroscience* 169, 1779–1788. doi: 10.1016/j.neuroscience.2010.05.060

Miller, K. J., Weaver, K. E., and Ojemann, J. G. (2009). Direct electrophysiological measurement of human default network areas. *Proc. Natl. Acad. Sci. U.S.A.* 106, 12174–12177. doi: 10.1073/pnas.0902071106

Nunez, P. L. (2010). REST: a good idea but not the gold standard. *Clin. Neurophysiol.* 121, 2177–2180. doi: 10.1016/j.clinph.2010.04.029

Nunez, P. L., and Srinivasan, R. (2006). *Electric Fields of the Brain: The Neurophysics of EEG*. Oxford; New York: Oxford University Press.

Nunez, P. L., Srinivasan, R., Westdorp, A. F., Wijesinghe, R. S., Tucker, D. M., Silberstein, R. B., et al. (1997). EEG coherency. I: Statistics, reference electrode, volume conduction, Laplacians, cortical imaging, and interpretation at multiple scales. *Electroencephal. Clin. Neurophysiol.* 103, 499–515. doi: 10.1016/S0013-4694(97)00066-7

Nunez, P. L., Wingeier, B. M., and Silberstein, R. B. (2001). Spatial-temporal structures of human alpha rhythms: theory, microcurrent sources, multiscale measurements, and global binding of local networks. *Hum. Brain Mapp.* 13, 125–164. doi: 10.1002/hbm.1030

Offner, F. F. (1950). The EEG as potential mapping: the value of the average monopolar reference. *Electroencephalogr. Clin. Neurophysiol.* 2, 213–214. doi: 10.1016/0013-4694(50)90040-X

Pascual-Marqui, R. D., and Lehmann, D. (1993). Topographic maps, source localization inference, and the reference electrode: comments on a paper by Desmedt et al. *Electroencephalogr. Clin. Neurophysiol.* 88, 532–536. doi: 10.1016/0168-5597(93)90043-O

Pereda, E., Quiroga, R. Q., and Bhattacharya, J. (2005). Nonlinear multivariate analysis of neurophysiological signals. *Prog. Neurobiol.* 77, 1–37. doi: 10.1016/j.pneurobio.2005.10.003

Qin, Y., Xu, P., and Yao, D. (2010). A comparative study of different references for EEG default mode network: the use of the infinity reference. *Clin. Neurophysiol.* 121, 1981–1991. doi: 10.1016/j.clinph.2010.03.056

Singer, W., and Gray, C. M. (1995). Visual Feature Integration and the Temporal Correlation Hypothesis. *Annu. Rev. Neurosci.* 18, 555–586. doi: 10.1146/annurev.ne.18.030195.003011

Srinivasan, R., Winter, W. R., Ding, J., and Nunez, P. L. (2007). EEG and MEG coherence: measures of functional connectivity at distinct spatial scales of neocortical dynamics. *J. Neurosci. Methods* 166, 41–52. doi: 10.1016/j.jneumeth.2007.06.026

Stam, C. J., and Reijneveld, J. C. (2007). Graph theoretical analysis of complex networks in the brain. *Nonlinear Biomed. Phys.* 1:3. doi: 10.1186/1753-4631-1-3

Stephan, K. E., Hilgetag, C. C., Burns, G. A., O'Neill, M. A., Young, M. P., and Kötter, R. (2000). Computational analysis of functional connectivity between areas of primate cerebral cortex. *Philos. Trans. R. Soc. B Biol. Sci.* 355, 111–126. doi: 10.1098/rstb.2000.0552

Tallon-Baudry, C., Bertrand, O., Delpuech, C., and Pernier, J. (1996). Stimulus specificity of phase-locked and non-phase-locked 40 Hz visual responses in human. *J. Neurosci.* 16, 4240–4249.

Thatcher, R. W., Biver, C., Gomez, J. F., North, D., Curtin, R., Walker, R. A., et al. (2001). Estimation of the EEG power spectrum using MRI T(2) relaxation time in traumatic brain injury. *Clin. Neurophysiol.* 112, 1729–1745. doi: 10.1016/S1388-2457(01)00609-5

van den Broek, S. P., Reinders, F., Donderwinkel, M., and Peters, M. J. (1998). Volume conduction effects in EEG and MEG. *Electroencephalography. Clin. Neurophysiol.* 106, 522–534. doi: 10.1016/S0013-4694(97)00147-8

Van Schependom, J., Gielen, J., Laton, J., D'Hooghe, M. B., De Keyser, J., and Nagels, G. (2014). Graph theoretical analysis indicates cognitive impairment in MS stems from neural disconnection. *Neuroimage Clin.* 4, 403–410. doi: 10.1016/j.nicl.2014.01.012

van Wijk, B. C., Stam, C. J., and Daffertshofer, A. (2010). Comparing brain networks of different size and connectivity density using graph theory. *PLoS ONE* 5:e13701. doi: 10.1371/journal.pone.0013701

Womelsdorf, T., and Fries, P. (2006). Neuronal coherence during selective attentional processing and sensory-motor integration. *J. Physiol. Paris* 100, 182–193. doi: 10.1016/j.jphysparis.2007.01.005

Yao, D. (2001). A method to standardize a reference of scalp EEG recordings to a point at infinity. *Physiol. Meas.* 22, 693–711. doi: 10.1088/0967-3334/22/4/305

Yao, D. (2003). High-resolution EEG mapping: an equivalent charge-layer approach. *Phys. Med. Biol.* 48, 1997–2011. doi: 10.1088/0031-9155/48/13/311

Yao, D. (2017). Is the Surface Potential Integral of a Dipole in a Volume Conductor Always Zero? A Cloud Over the Average Reference of EEG and ERP. *Brain Topogr.* 30, 161–171. doi: 10.1007/s10548-016-0543-x

Yao, D., and He, B. (2003). Equivalent physical models and formulation of equivalent source layer in high-resolution EEG imaging. *Phys. Med. Biol.* 48, 3475–3483. doi: 10.1088/0031-9155/48/21/002

Yao, D., Wang, L., Arendt-Nielsen, L., and Chen, A. C. (2007). The effect of reference choices on the spatio-temporal analysis of brain evoked potentials: the use of infinite reference. *Comput. Biol. Med.* 37, 1529–1538. doi: 10.1016/j.compbiomed.2007.02.002

Yao, D., Wang, L., Oostenveld, R., Nielsen, K. D., Arendt-Nielsen, L., and Chen, A. C. (2005). A comparative study of different references for EEG spectral mapping: the issue of the neutral reference and the use of the infinity reference. *Physiol. Meas.* 26, 173–184. doi: 10.1088/0967-3334/26/3/003

Zappasodi, F., Olejarczyk, E., Marzetti, L., Assenza, G., Pizzella, V., and Tecchio, F. (2014). Fractal dimension of EEG activity senses neuronal impairment in acute stroke. *PLoS ONE* 9:e100199. doi: 10.1371/journal.pone.0100199

Zhai, Y., and Yao, D. (2004). A study on the reference electrode standardization technique for a realistic head model. *Comput. Methods Programs Biomed.* 76, 229–238. doi: 10.1016/j.cmpb.2004.07.00

Conflict of Interest Statement: The authors declare that the research was conducted in the absence of any commercial or financial relationships that could be construed as a potential conflict of interest.

frontiers in Neuroscience

ORIGINAL RESEARCH
published: 25 July 2017
doi: 10.3389/fnins.2017.00425

The Effect of Electroencephalogram (EEG) Reference Choice on Information-Theoretic Measures of the Complexity and Integration of EEG Signals

*Logan T. Trujillo *, Candice T. Stanfield and Ruben D. Vela*

Department of Psychology, Texas State University, San Marcos, TX, United States

OPEN ACCESS

Edited by:
Maria L. Bringas, University of Electronic Sciences and Technology of China, China

Reviewed by:
Uncheol Lee, University of Michigan, United States
Stefan Haufe, Technische Universität Berlin, Germany

****Correspondence:***
Logan T. Trujillo
logant@txstate.edu

Specialty section:
This article was submitted to Brain Imaging Methods, a section of the journal Frontiers in Neuroscience

Received: *21 February 2017*
Accepted: *07 July 2017*
Published: *25 July 2017*

Citation:
Trujillo LT, Stanfield CT and Vela RD (2017) The Effect of Electroencephalogram (EEG) Reference Choice on Information-Theoretic Measures of the Complexity and Integration of EEG Signals. Front. Neurosci. 11:425. doi: 10.3389/fnins.2017.00425

Converging evidence suggests that human cognition and behavior emerge from functional brain networks interacting on local and global scales. We investigated two information-theoretic measures of functional brain segregation and integration—interaction complexity $C_I(X)$, and integration $I(X)$—as applied to electroencephalographic (EEG) signals and how these measures are affected by choice of EEG reference. $C_I(X)$ is a statistical measure of the system entropy accounted for by interactions among its elements, whereas $I(X)$ indexes the overall deviation from statistical independence of the individual elements of a system. We recorded 72 channels of scalp EEG from human participants who sat in a wakeful resting state (interleaved counterbalanced eyes-open and eyes-closed blocks). $C_I(X)$ and $I(X)$ of the EEG signals were computed using four different EEG references: linked-mastoids (LM) reference, average (AVG) reference, a Laplacian (LAP) "reference-free" transformation, and an infinity (INF) reference estimated via the Reference Electrode Standardization Technique (REST). Fourier-based power spectral density (PSD), a standard measure of resting state activity, was computed for comparison and as a check of data integrity and quality. We also performed dipole source modeling in order to assess the accuracy of neural source $C_I(X)$ and $I(X)$ estimates obtained from scalp-level EEG signals. $C_I(X)$ was largest for the LAP transformation, smallest for the LM reference, and at intermediate values for the AVG and INF references. $I(X)$ was smallest for the LAP transformation, largest for the LM reference, and at intermediate values for the AVG and INF references. Furthermore, across all references, $C_I(X)$ and $I(X)$ reliably distinguished between resting-state conditions (larger values for eyes-open vs. eyes-closed). These findings occurred in the context of the overall expected pattern of resting state PSD. Dipole modeling showed that simulated scalp EEG-level $C_I(X)$ and $I(X)$ reflected changes in underlying neural source dependencies, but only for higher levels of integration and with highest accuracy for the LAP transformation. Our observations suggest that the

Laplacian-transformation should be preferred for the computation of scalp-level $C_I(X)$ and I(X) due to its positive impact on EEG signal quality and statistics, reduction of volume-conduction, and the higher accuracy this provides when estimating scalp-level EEG complexity and integration.

Keywords: electroencephalography, EEG complexity, EEG integration, EEG spectral power density, EEG reference, resting state EEG

INTRODUCTION

Converging evidence suggests that human cognition and behavior emerge from brain networks interacting on local and global scales. These different scales of neural activity reflect the functional *segregation* (specialized information processing within regional groups of brain regions) and *integration* (the combination of that specialized information across distributed brain regions) of the brain networks (Tononi et al., 1994, 1996, 1998a,b; Bullmore and Sporns, 2009; Fair et al., 2009; Rubinov and Sporns, 2010). Moreover, the organization of these brain networks is highly complex due to the dynamic interplay of segregation and integration. This *neural complexity* reflects a large number of coordinated interactions among brain elements engaged in various levels of subordination that are neither fully regular nor random (Tononi et al., 1998a). One approach to quantifying segregation, integration, and complexity in the brain utilizes information theory to characterize neural activity in terms of "deviations from statistical independence among components of a neural system" (Tononi et al., 1994, p. 5033). In this paper, we consider two such information-theoretic measures as applied to the analysis of electroencephalographic (EEG) data. The first measure, called *integration I(X)*, is a multivariate index of the overall deviation from statistical independence of the individual elements in a system. The second measure, called *interaction complexity* $C_I(X)$, is a statistical measure of a system's information content that results from the interactions among the system's elements. The relationship between complexity and integration follows an "inverted-U" non-monotonic function (Tononi et al., 1994; see **Figure 1**). Complexity is low at low integration values when system components are fully statistically independent; complexity is high at intermediate integration values when there is heterogenous statistical dependence among system components (i.e., when a system is highly integrated and specialized; Tononi et al., 1998a), and complexity is low at high integration values when system components are fully statistically dependent. These measures are, in part, the precursors to the segregation and integration measures used in the current integrated information theory of consciousness and brain function (Tononi, 2004; Tononi and Koch, 2016).

In order for $C_I(X)$ and I(X) to provide useful insight into the brain networks underlying cognition and behavior, it is important to understand how they are influenced by the various parameters of EEG measurements. This allows one to assess the reliability and validity of $C_I(X)$ and I(X) under different measurement scenarios. One crucial EEG measurement parameter is the reference scheme or montage. The EEG signal represents a difference between two voltages, one located at an electrode site of interest and another at a location that is as electrically neutral as possible with respect to the signal of interest. The choice of EEG reference is well-known to affect signal quality (Gencer et al., 1996), as different reference choices may or may not be electrically neutral depending on location, participant behavior, and the neurocognitive process under investigation (Wolpaw and Wood, 1982; Desmedt et al., 1990; Dien, 1998; Yao, 2001; Trujillo et al., 2005). The impact of EEG reference on signal quality should also affect the reliability of the signal statistics from which these $C_I(X)$ and I(X) measures are derived. Furthermore, $C_I(X)$ and I(X) index the interaction between different brain signal elements, interdependencies that can be artificially-inflated at the level of the scalp due to the effects of volume conduction of cortical EEG source signals throughout the head (Nunez et al., 1997, 1999; Nunez and Srinivasan, 2006). Scalp EEG measurements made with respect to different reference schemes may be affected by volume conduction to different degrees, and this in turn should affect the degree to which these complexity measures reflect true or artifactual complexity and integration.

Thus, if such complexity and integration measures are to be useful when applied to scalp-recorded EEG data, it is first necessary to ascertain the reliability and stability of these measures with respect to different EEG references. Unfortunately, such studies are lacking in the current literature. To our knowledge, only one previous study (van Putten and Stam, 2001) has compared the effect of EEG reference on information-theoretic measures of integration and complexity. Van Putten and Stam applied I(X) and another EEG complexity measure called neural complexity $C_N(X)$ (which is related, but not identical, to interaction complexity) to the analysis of scalp-recorded EEG signals collected during a resting state task (eyes-closed and eyes-open condition). In this study, the EEG data were referenced to an average reference and a source reference (computed as the voltage difference between the recording site and the mean voltage of 3–4 neighboring recording sites) that served to reduce idiosyncratic reference effects and effects of volume conduction. The magnitude of I(X) and $C_N(X)$ were lower for the source reference compared to the average reference, although the overall between-condition pattern was the same for both references (greater I(X) and $C_I(X)$ for eyes closed than eyes open).

The goal of the present study was to perform a more comprehensive investigation into the effect of EEG reference on the quantification of EEG integration and complexity. We recorded 72 channels of scalp EEG from human participants who sat in a wakeful resting state (interleaved counterbalanced

eyes-open and eyes-closed blocks). We then computed $C_I(X)$ and I(X) of the EEG signals, as well as a conventional EEG measure of resting state activity—Fourier-based power spectral density (PSD)—for comparison and as a check of data integrity and quality. We computed the information-theoretic and spectral power measures using four different EEG reference schemes. The first was the linked-mastoids (LM) reference, which consists of the mathematical average of the signals from electrodes located at the mastoid bones of each ear. The second scheme was the average (AVG) reference (Bertrand et al., 1985), computed by averaging the signals from all electrodes and then subtracting the averaged signal from each electrode individually. The third scheme was a Laplacian (LAP) "reference-free" transformation of the raw EEG potentials into a measure of the radial current density at the scalp (Law et al., 1993; Yao, 2002). Finally, the fourth reference scheme was an infinity (INF) reference, which uses the Reference Electrode Standardization Technique (REST; Yao, 2001) to approximately transform a scalp point reference (or the average reference) to a reference point at infinity. REST achieves this by computing the actual or equivalent neural sources for a set of EEG signals and then implementing a forward computation of the obtained sources to a point at infinity.

In order to assist interpretation of the observed EEG complexity and integration, we simulated oscillatory resting state EEG data at the scalp via a concentric 4-shell spherical head forward volume-conduction model (Cuffin and Cohen, 1979; Mosher et al., 1993; Tenke and Kayser, 2015). These simulations were based on oscillating, fixed-location intracranial dipole sources with pre-determined complexity and integration. This allowed us to investigate how accurately EEG source complexity and integration patterns could be estimated at the scalp, given the known mixing effects of volume conduction (Nunez and Srinivasan, 2006). We addressed four specific questions in this study: (1) what, if any, difference does choice of EEG reference make for empirical assessments of $C_I(X)$ and I(X); (2) how accurately does scalp EEG recordings reflect the complexity and integration of underlying sources; (3) can these measures reliably distinguish between neurocognitive conditions in which, in theory, complexity and integration should be different; and (4) does this between-condition sensitivity vary according to EEG reference scheme?

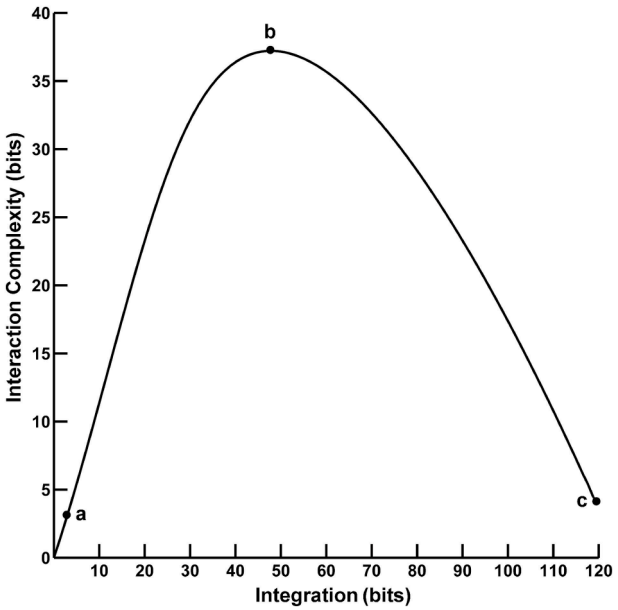

FIGURE 1 | The functional relationship between interaction complexity $C_I(X)$ and integration I(X). In this example, interaction complexity $C_I(X)$ and integration I(X) were computed from constant mean Gaussian Toeplitz covariance matrices ($n = 72$) with increasing σ and 10% uncorrelated Gaussian noise added to the matrix diagonal (following Tononi et al., 1994). For low values of I(X) (case a), $C_I(X)$ is also low and all system components are fully statistically independent. For intermediate values of I(X) (case b), $C_I(X)$ is high; some system components are statistically dependent, others are not. For high values of I(X) (case c), $C_I(X)$ is low; the system components are fully dependent.

MATERIALS AND METHODS

Participants

Twenty two Texas State University undergraduates (11 female, 11 male, mean age = 21.1 ± 0.52 years, age range = 18—26) participated in this study for course credit or monetary payment. This study was carried out in accordance with the recommendations of the Human Subjects Institutional Review Board (IRB) at Texas State University with written informed consent from all participants. All participants gave written informed consent in accordance with the Declaration of Helsinki. The protocol was approved by the Texas State University IRB.

Stimuli and Procedure

After consent, participants underwent setup for EEG recording. During the setup, participants completed several questionnaires indexing demographic and health information, sleep quality and quantity, emotion and mood states, and current attentional states. However, the results of these questionnaires are not relevant to the topic of this paper and are not reported here.

Resting State EEG

After completion of the EEG setup, participants underwent 8 min of resting state EEG recording while sitting quietly in a comfortable padded chair in a darkened room (4 min eyes open and 4 min eyes closed interleaved in 1-min intervals; eyes open/closed order was balanced across participants). (Due to a technical recording error, one participant only received 4 min of recording time.) Subjects were instructed to remain relaxed, yet alert and awake at all times during recording. After completion of the resting state EEG recording, participants then performed a visual categorization task, the results of which are not relevant to the topic of this paper and thus are not reported here.

EEG Recording and Pre-processing

We recorded 72 channels of continuous EEG signals using active Ag/AgCl electrodes either mounted in a BioSemi electrode cap or via freestanding electrodes. Recording sites included

international 10/5 system locations (Jurcak et al., 2007) and the inferior orbits of the eyes (**Figure 2**). All channels were amplified by a BioSemi Active II amplifier system in 24-bit DC mode at an initial sampling rate of 2,048 Hz (400-Hz bandwidth) downsampled online to 256 Hz, with EEG signals recorded with respect to a common mode sense (CMS) electrode located between sites PO3 and POZ. Half-cell potentials of the electrode/gel/skin interface were kept between ± 40 mV, following standard recommendations for the Active II system. EEG data were imported offline into the MATLAB computing software environment (The Math Works, Inc., Natick, MA, USA) using the EEGLAB toolbox (Delorme and Makeig, 2004) for MATLAB, where all subsequent analysis was performed via in-house scripts that utilized EEGLAB functions.

Resting EEG baseline data were divided into 1 s (256 sample) epochs with 50% overlap, initially producing 480 epochs for each of the two resting task conditions. Next, we created a copy of the resting EEG trials that were transformed to an average reference for the purpose of identifying bad channels and muscle and signal artifacts from the EEG record by visual inspection. Once identified, we then removed artifact-contaminated trials from, and replaced bad channels in, the original non-average-referenced EEG trials. Bad EEG channels were replaced using an EEGLAB-based spherical spline interpolation algorithm (Perrin et al., 1987; $m = 50$, 50 term expansion). No more than 3.5% of channels on average were interpolated for any given subject.

Blink and saccade-related electroocular (EOG) artifacts were removed by first computing two EOG channels: one formed from the bipolar montage of site NZ and the average of the two electrodes located at the inferior orbits of the eyes (sensitive to blinks and vertical saccades) and a second formed from the bipolar montage of AF9 and AF10 (sensitive to horizontal saccades). Next, EEG trials containing EOG amplitudes higher than 50 μV or lower than −50 μV (after removal of the constant direct current offset from the EOG signals) were rejected from the analysis in MATLAB via automatic algorithm. These rejection criteria were applied over the full epoch interval for resting EEG data. Then, a second round of manual artifact scoring was performed because the ocular artifact rejection algorithm occasionally failed to identify trials with ocular artifacts. The derived horizontal and vertical EOG channels were removed from the data after elimination of the EOG artifact-contaminated trials.

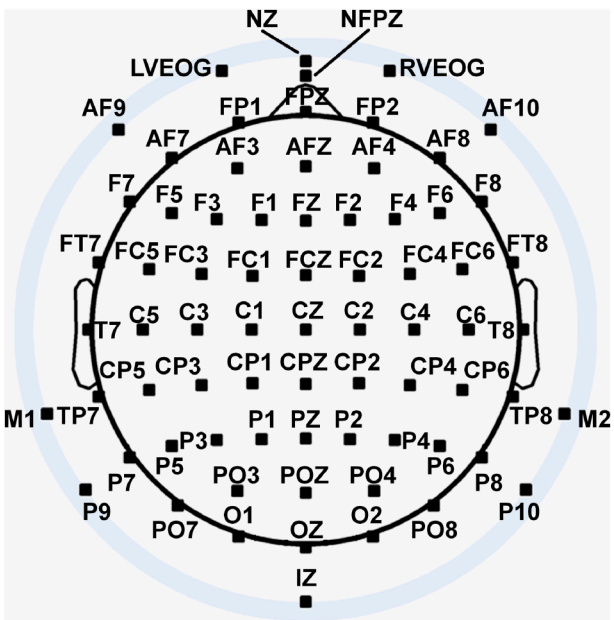

FIGURE 2 | Extended 10–20 scalp locations of EEG recording electrodes. Note that sites outside the radius of the head represent locations that are below the equatorial plane (FPZ-T7-T8-OZ plane) of the (assumed spherical) head model. Sites LVEOG and HEOG were located below the eyes approximately at the same longitude as sites M1 and M2.

On average 314 ± 16 and 299 ± 20 trials remained for the eyes closed and open resting state conditions after artifact rejection. However, in order to avoid any potential between-condition differences in information bias (Pola et al., 2003; Misra et al., 2005; Magri et al., 2009; Ince et al., 2017) that might arise during the computation of the complexity and integration measures (see Computation of EEG Complexity and Integration section, below), the number of EEG trials were matched between resting state conditions. For each participant, we randomly sampled trials (without replacement) from the condition with the larger number of trials to match the smaller number of trials for the other condition. Thus, the final number of trials entering into each resting state condition was 270 ± 18 on average. Trials were also matched in this manner for computation of EEG spectral power for a cleaner comparison with the EEG complexity and integration analyses.

EEG trials were then converted into four reference montages examined in this study: linked-mastoids (LM) reference, average (AVG) reference, Laplacian (LAP) "reference free" transformation, and an infinity (INF) reference estimated via the Reference Electrode Standardization Technique (REST). LM and AVG references were created via standard derivations (Yao et al., 2007). The LAP transformation ($\mu V/m^2$ units; unit sphere; 50 iterations; $m = 4$; $\lambda = 10^{-5}$) was achieved using a spherical spline algorithm (Perrin et al., 1989, 1990) implemented in the CSD Toolbox for MATLAB (Kayser and Tenke, 2006a,b; Kayser, 2009; http://psychophysiology.cpmc.columbia.edu/Software/CSDtoolbox). The INF was estimated using the REST software for MATLAB (Tian and Yao, 2013; www.neuro.uestc.edu.cn/rest). All 72 electrodes were entered into the computation of the LAP transformation and the average- and infinite-references.

Computation of Resting EEG Power Spectral Density

Resting EEG power spectral density (PSD; $\mu V^2/Hz$) was computed on unfiltered data via Fast Fourier Transformation (FFT) tapered by a 1 s Hamming window (Kornguth et al., 2013; Witkowski et al., 2015). For each subject and resting state condition, mean PSD was computed and then converted into decibels (dB). The latter conversion allowed for direct

comparison between the PSD computed for the LAP-transformed data (in units of $\mu V^2/m^4/Hz$), and the PSD computed for the data referenced to the other EEG references (in units of $\mu V^2/Hz$). Additionally, the logarithmic transformation of the data during the process of conversion to dB units served to transform the PSD values toward a Gaussian statistical distribution, thus allowing application of parametric statistical tests (see Statistical Analysis of EEG Measures, below). For each participant and condition, mean PSD values were computed over two EEG frequency bands: theta/alpha (4–13 Hz) and beta (14–25 Hz). Mean PSD was computed over bilateral posterior scalp sites (PO7, PO8) demonstrating maximal PSD responses in each frequency band. These specific scalp sites and frequency bands were chosen based on the observed ranges of prominent differences in PSD of the resting EEG data (see Results, below).

Computation of EEG Complexity and Integration

The complexity and integration measures utilized here are based in information theory, which views information as an ordered sequence of symbols. The information in a signal is then quantified in terms of its entropy H:

$$H = \sum_{i=1}^{N} p_i \log_2 p_i$$

where p_i is the probability of occurrence of the *ith* possible value of a symbol. H indexes the uncertainty of a symbol sequence and thus how informative the sequence is. The integration $I(X)$ and interaction complexity $C_I(X)$ of a set of signals X are then computed as Tononi et al. (1998a):

$$I(X) = \sum_{i=1}^{N} H(X_i) - H(X)$$

$$C_I(X) = H(X) - \sum_{i=1}^{N} H(X_i|X - X_i)$$

Here, X_i is the state of an individual EEG channel, $H(X_i)$ is the entropy of the channel, $H(X)$ is the joint entropy of the coincident patterns X of binary states across all N EEG channels, and $H(X_i|X–X_i)$ is the conditional entropy of a single EEG channel X_i, given the state of the remaining multi-channels $X–X_i$. If all EEG channels are statistically independent, then $I(X) = 0$, otherwise it is maximal when EEG activity is fully dependent across channels. In contrast, $C_I(X)$ is minimal for fully independent or dependent channels and is maximal when the channels are neither completely independent nor completely dependent; see **Figure 1**.

We computed the single-channel, joint, and conditional entropies of the EEG signals via explicit analytic expressions for the entropies based on the assumption that the EEG amplitudes realize continuous univariate and multivariate Gaussian processes with variances σ_{ii}^2 and covariance matrix K (Norwich, 1993; Tononi et al., 1994; van Putten and Stam, 2001; Ince et al., 2017):

$$H(X_i) = \frac{1}{2\ln(2)} \cdot \ln(2\pi e\sigma_{ii}^2)$$

$$H(X) = \frac{1}{2\ln(2)} \cdot \ln\left\{(2\pi e)^N |K|\right\}$$

$$H(X_i|X - X_i) = H(X) - H(X - X_i)$$

Continuous Gaussian univariate and multivariate entropies are *differential entropies* that are not independent of data units or scale; however, entropy differences—such as those that define $C_I(X)$, $I(X)$, and $H(X_i|\ X–X_i)$—are data unit-/scale-independent (Norwich, 1993). All entropy functions were computed using the Information Breakdown Toolbox for MATLAB (Magri et al., 2009) with a correction for any information bias that may arise due to the estimation of the covariance matrices from limited data (Pola et al., 2003; Misra et al., 2005; Magri et al., 2009; Ince et al., 2017). The two mastoid sites could not be included in the entropy computations for the linked-mastoids reference due to the fact that, in this case, their linear dependence rendered the covariance matrix determinant |K| to be zero (Lay, 2005); hence, mastoid sites were also not included in the entropy calculations for the other EEG references in order to facilitate between-reference comparisons. All entropies were computed in terms of binary units (bits) of information.

Before computing the entropy functions, we first bandpass-filtered the resting EEG into two separate frequency ranges, the theta/alpha range (4–13 Hz) and the beta range (14–30 Hz), using a 424 point zero-phase shift FIR filter with 2 Hz transition bands. These specific frequency bands were chosen based on the observed ranges and scalp patterns of prominent differences in the spectral power of the resting EEG data (see Results, below). We performed this filtering step based on evidence that information-theoretic computations are more accurate when performed on data with a narrower frequency range (van Cappellen van Walsum et al., 2003).

Moreover, we took steps to ensure the filtered EEG signal distributions were approximately Gaussian, as assumed by the analytic expressions for $H(X_i)$, $H(X)$, and $H(X_i|X–X_i)$ above (see Discussion section for further elaboration of this requirement). First, we assessed the univariate and multivariate normality of the channels via Jarque-Bera tests (Jarque and Bera, 1987) and Royston's Test of Multivariate Normality (Royston, 1983), respectively, for each trial, condition, reference scheme, and participant. (Note that Royston's Test was computed via a publically available MATLAB script; Trujillo-Ortiz et al., 2007.) These tests indicated that, for the theta/alpha-range filtered data, the statistical distributions of approximately 49% of electrodes on average (collapsed across conditions and EEG reference schemes) violated the univariate normality assumption on any given trial, whereas the multivariate normality assumption was violated on 100% of trials on average. In the beta-range filtered data, the statistical distribution of 1% of electrodes on average (collapsed across conditions and EEG reference schemes) violated the univariate normality assumption on any given trial, whereas the

multivariate normality assumption was violated on 99% of trials on average.

It is possible that our use of short (1 s), low sample number (256 samples) trials may have contributed, in part, to the rejection of the Gaussian-hypothesis for these trials. However, as will be argued in the Discussion section, we believe the pattern of results we observed in our data rule this out as a main origin of this rejection. In addition, the shorter EEG epochs utilized here better meet the assumptions of statistical stationarity, which is an important factor in the accurate assessment of the distribution of a time series data segment and EEG complexity (Branston et al., 2005); data epochs longer than 2 s yield poor assessments of goodness-of-fit (Elul, 1969). Use of short EEG trials also reduced the possibility that violations of stationarity across long data samples may distort complexity and integration calculations. (We note that we used 1-s trial lengths in order to minimize the number of trials that needed to be rejected due to muscle, signal, and ocular artifacts in the EEG. The latter were especially problematic, and we did not apply an ocular correction algorithm in order to avoid the possible effects of that algorithm on measurement of EEG complexity and integration.)

Hence, prior to calculation of $C_I(X)$ and I(X), we applied a method to transform non-normal distributions to Gaussian that have been successfully used before with EEG data (van Albada and Robinson, 2007). We transformed EEG data in this manner on a trial-by-trial basis for each separate frequency band, EEG reference, condition, and participant. After this transformation, we statistically assessed the univariate and multivariate normality of the channels again for each trial, condition, reference scheme, and participant. All tests were non-significant ($p > 0.05$, non-corrected) indicating that this Gaussian transformation process was successful. Inspection of the EEG waveforms and data histograms both before and after transformation showed that the transformation merely reduced the spread of outliers while simultaneously distributing the data more symmetrically around the mean. Importantly, we statistically-checked that this procedure did not did not distort the distributions of key EEG features of the eyes open and closed resting states (see Supplementary Material).

Statistical Analysis of EEG Measures

We performed two kinds of statistical analysis of the EEG data, a parametric approach that assessed potential differences between EEG reference and resting state conditions and a non-parametric surrogate data testing approach that assessed the degree to which EEG complexity and integration may arise from random or spurious coincident activity among the EEG signals.

Parametric Statistical Approach

All parametric statistical analyses reported in this paper were performed using the SPSS software package (IBM Corporation, Armonk, NY, USA). Resting state EEG PSD, complexity, and integration were analyzed via repeated-measures ANOVA with within-participants factors of EEG Reference (LMR, AVG, INF, LAP) and Resting State Condition (Eyes Closed, Eyes Open). These analyses were performed separately for each frequency band. Given that the EEG Reference factor involved more than two levels, the *p*-values of all omnibus tests involving this factor were adjusted using the Greenhouse–Geisser correction for nonsphericity (Geisser and Greenhouse, 1958). For ease of interpretation, reports of all significant behavior *F* tests subject to Greenhouse-Geisser correction include uncorrected degrees of freedom, corrected *p*-values, and the Greenhouse-Geisser epsilon value ε. All *post-hoc* comparisons were corrected according to the Holm-Bonferroni procedure (Holm, 1979) and all corrected *p*-values are indicated as such in the text.

We also conducted regression analyses relating PSD to $C_I(X)$ and I(X) in order to quantify the relationship between these EEG metrics across individual participants. These regressions were conducted via generalized estimating equations (GEEs; Gardiner et al., 2009; Ma et al., 2012). GEEs are a generalized regression procedure that can account for the correlation structure across repeated measure levels while robustly estimating unbiased parameter standard errors. In the present study, the GEE analysis assumed a normal distribution with identity link, a robust covariance estimate, a maximum likelihood-estimate scale parameter, and an exchangeable correlation matrix. We conducted two regressions for each frequency band. The first regression was performed after collapsing across resting state conditions in order to assess the relationship between PSD and $C_I(X)$ and I(X) across EEG references. The second regression was performed after collapsing across EEG reference conditions in order to assess the relationship between the EEG metrics across resting state condition (eyes open, eyes closed). The reports of GEE analyses in this paper include standardized regression coefficients and tests of model effects (Wald $\chi 2$ statistic values, associated degrees of freedom, *p*-values).

Surrogate Data Testing

It is well-known that random or spuriously-coincident EEG activity may produce apparent statistical dependencies among otherwise independent EEG sources, with this effect exacerbated by volume conduction (Nunez et al., 1997; Lachaux et al., 1999, 2000). In order to estimate the level of spurious complexity and integration in our EEG data that may arise from volume conduction, we created surrogate EEG data with similar statistical characteristics and spectral power distributions as the observed data, but that arise from a superposition of statistically independent sources with randomly-shifted EEG signal phases. This was achieved using a modification of the method of Shahbazi et al. (2010). In this method, each observed data set is first decomposed via Independent Components Analysis (ICA; Lee et al., 1999) to create signals that are independent as possible (ICA creates decompositions of nearly, but not perfectly, independent signals). In a second step, any remaining statistical dependencies are destroyed by randomly shifting the nth ICA component activation time course by a time $(n–1)^*$ T, where T is larger than any autocorrelation time (practically, T must be a least one trial length). In a third step, the shifted ICA activations are then transformed back into EEG sensor space via the ICA inverse mixing matrix. In the present study, we implemented the second step for each surrogate trial by randomly sampling from the remaining trials for each ICA activation time course. This sampling was performed without replacement to ensure that

none of the ICA activation signals came from the same trial; this yielded effective values for T ranging from one to several hundred trial lengths, depending on the number of trials for a given data set.

We computed distributions of complexity and integration values from 100 surrogate data sets created for each subject, condition, and EEG frequency band. We then computed the mean and two-tailed 95% confidence intervals (CIs) of these distributions. Observed mean complexity or integration values that were found to lie outside of these confidence intervals were interpreted as being significantly different from any complexity/integration that may arise purely from random or spuriously coincident volume-conducted EEG activity. Surrogate data testing was performed via in-house MATLAB scripts. ICA decompositions were implemented using the extended infomax runica algorithm (with data whitening and default stopping weight change = 1e-07) implemented within the EEGLAB toolbox for MATLAB (Delorme and Makeig, 2004).

Dipole Modeling

In order to assist interpretation of the observed EEG complexity and integration, we simulated oscillatory EEG data at the scalp from oscillating, fixed-location intracranial dipole sources with pre-determined complexity and integration. The dipole sources were positioned within a concentric 4-shell spherical head forward volume-conduction model (Cuffin and Cohen, 1979; Mosher et al., 1993; Tenke and Kayser, 2015) implemented via in-house MATLAB scripts. The model's outer shell had an 85 mm radius, with a scalp thickness = 3 mm (σ_{scalp} = 0.33 υ/m), bone thickness = 4 mm (σ_{bone} = 0.0042 υ/m), CSF layer = 2 mm (σ_{CSF} = 1 υ/m), and a brain surface at a 76 mm radius (σ_{brain} = 0.33 υ/m); shell thickness and conductivity values were taken from Cuffin and Cohen (1979) and Mosher et al. (1993). Simulated scalp electrode locations were the same as for the EEG recordings (see **Figure 2**). We created two clusters of 20 radially-oriented dipole generators (40 dipoles total) at posterior, roughly extrastriate cortical locations (**Figure 3**), one cluster in each hemisphere with the anterior-posterior location of both clusters centered on the equatorial (FPZ-T7-T8-OZ) plane. These *extrastriate dipoles* were used to simulate posterior cortical processes known to be active during EEG resting tasks (Feige et al., 2005). The remainder of the spherical surface was filled with 148 equally spaced dipoles to simulate background cortical processes (termed here *background dipoles*). All dipoles were placed at superficial cortical locations (2 mm subdural, following Tenke and Kayser, 2015).

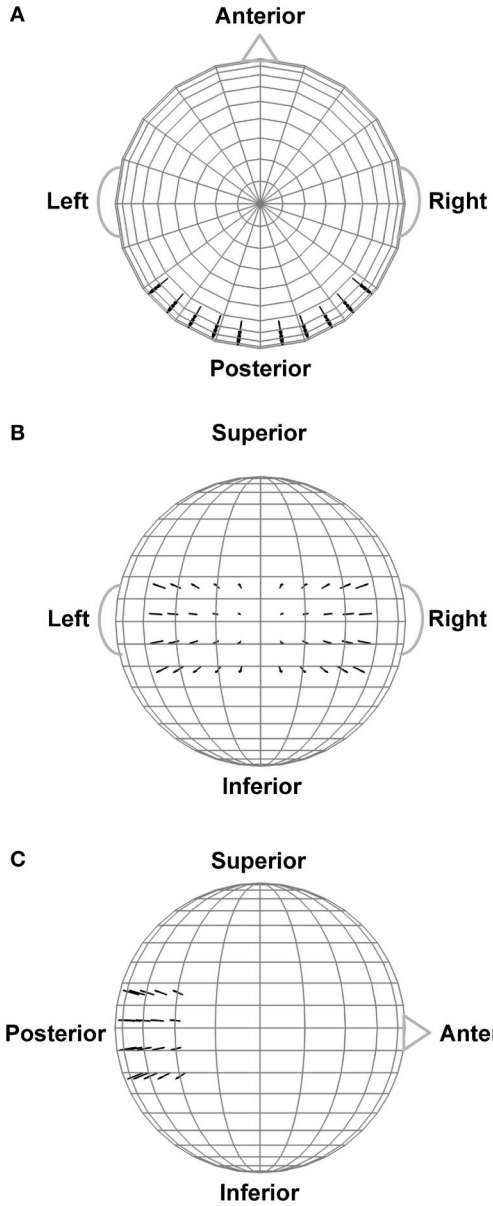

FIGURE 3 | Extrastriate dipole sources (black arrows) positioned within a 4-shell spherical head forward volume-conduction model (only the outer shell surface is represented in the figure). The remainder of the spherical surface was filled with 148 equally-spaced background activity dipoles (not shown). All dipoles were placed at a superficial (2 mm subdural) cortical locations. **(A)** Top head view. **(B)** Rear head view. **(C)** Side head view.

The magnitude of each dipole source moment varied sinusoidally over time characterized by an amplitude, frequency, and phase chosen according to a particular simulated resting state EEG condition (see below). We set the frequency ranges of these oscillations to be those analyzed for the empirical data (theta-alpha range: 4–13 Hz; beta range: 14–30 Hz); phases were uniformly distributed from 0 to 2π. The frequency and phase of each sinusoid waveform were randomly drawn with replacement (1 Hz frequency resolution) from these ranges for each simulated trial, subject to specific interdipole dependency relationships (see below). Background dipoles had a dipole source moment of 1 μA-cm for the theta-alpha range simulations and 0.50 μA-cm for the beta range simulations. For the extrastriate dipoles, we simulated potential amplitude differences between eyes closed and open resting state conditions by performing one set of simulations where the maximum magnitude of each dipole source moment was high (theta-alpha range: 1.25 μA-cm; beta-range: 0.625 μA-cm) and a second set of simulations where the maximum

magnitude of each source was low (theta-alpha range: 1.00 μA-cm; beta-range: 0.50 μA-cm). Moreover, fluctuations in ongoing EEG amplitudes were modeled by multiplying simulated dipole moment time courses by a Gaussian window ($\sigma_t = 250$ ms) whose temporal center randomly varied along the time dimension of each epoch. The Gaussian window multiplication reproduced amplitude modulations in the observed data. Window locations were different on each trial, and were different for independent sources, but the same for dependent sources (see interdipole dependencies, below). Window locations and spread were the same for all interdipole dependency and dipole amplitude conditions. These amplitude modulations introduced an extra degree of randomness into the simulations that affected the overall magnitude of complexity and integration, but did not affect the general pattern of results observed here. One hundred trials were created in each simulation; each trial was 1 s long.

Scalp potential topographies and time courses were simulated for each dipole generator separately. In order to assess the complexity and integration of the dipole moment time series, the dipole moment waveforms underwent the same Gaussian transformation procedure as the empirical EEG data; the transformed dipole moments were also used to create the forward volume-conductions to the scalp. The linearity of volume conduction allowed the final simulated EEG scalp record to be constructed from the sum of the individual dipole topographies at each time point (Tenke and Kayser, 2015). We then re-referenced the simulated scalp EEG signals according to the four EEG references investigated in this study. The scalp level time series for each reference also underwent Gaussian transformation before computation of EEG complexity, integration, and spectral power.

We created several different models that differed in terms of the temporal dependencies—and thus the complexity and integration—among the extrastriate dipole moment waveforms. These models were created by manipulating the shared frequencies and phases of each dipole waveform on any given trial

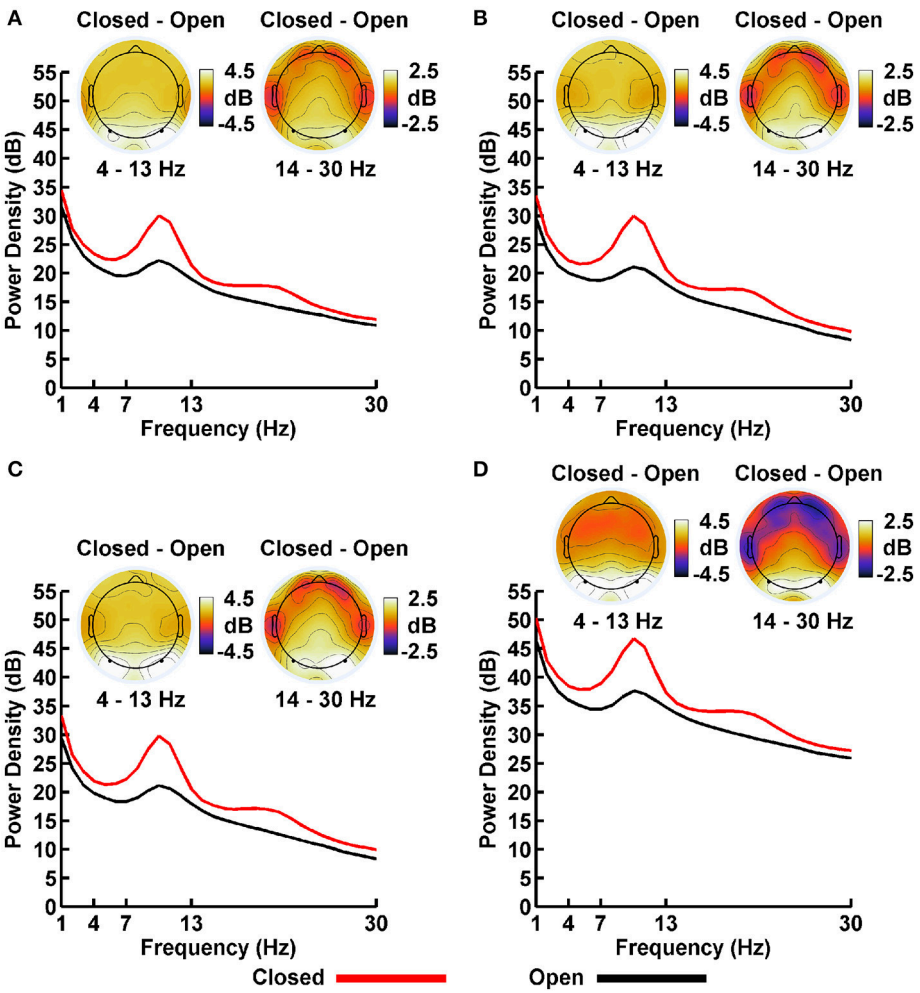

FIGURE 4 | Resting EEG spectral power density (PSD, in decibels) for eyes closed (red line) and eyes open (black line) conditions for **(A)** LM, **(B)** AVG, **(C)** INF, and **(D)** LAP reference schemes. Power spectra are collapsed across a priori electrodes of interest indicated by black/white circles on the head maps (see Methods). Head maps display power difference topographies averaged over the stated frequency intervals; light/dark colors indicate ± values.

as follows: (1) all dipoles shared the same frequency, phase, and amplitude fluctuation patterns on any given trial (*full dependency model*); (2) shared frequency/phase/amplitude fluctuations for 75% of the dipoles, independent frequencies/phases/amplitude fluctuations for the remaining dipoles (*interdependent model—level 1*); (3) shared frequency/phase/amplitude fluctuations for 50% of the dipoles, independent frequencies/phases/amplitude fluctuations for the remaining dipoles (*interdependent model—level 2*); (4) shared frequency/phase/amplitude fluctuations for 25% of the dipoles, independent frequencies/phases/amplitude fluctuations for the remaining dipoles (*interdependent model—level 3*); (5) all dipole waveforms independent in frequency/phase and amplitude fluctuations, but with the same phase for each time point (*independent model—level 1*); (6) all dipole waveforms initially created with independent frequencies/phases/amplitude fluctuations, but then phases randomized further via a FFT-based procedure (Theiler et al., 1992) that reduces the autocorrelation of a signal (*independent model—level 2*); and (7) dipole waveforms composed of multivariate Gaussian noise with an identity covariance matrix (*full independency model*). Although the additional phase randomization step used for the level-2 independent model may seem redundant, we found that it further increased the independence of the dipole moment waveforms (see Results, below), most likely due to a reduction of signal autocorrelation. In contrast to the extrastriate dipoles, all background dipole waveforms were given level-2 independent model temporal dependencies in order to simulate random background noise within a frequency range of interest.

RESULTS

All empirical data and MATLAB data analysis and dipole simulation scripts are available online at the Texas State University Data Repository (Trujillo et al., 2017; https://dataverse.tdl.org/dataverse/rsed2017).

Power Spectral Density (PSD)

Plots of non-Gaussian-transformed resting state EEG PSD are shown in **Figure 4**; mean power values are listed in **Table 1** (mean PSD values for Gaussian-transformed data are listed in Table S1). Preliminary analysis (not shown) indicated that the posterior topographical distributions of resting-state theta- and alpha-PSD differences were nearly identical, thus justifying the collapse across these two frequency bands for statistical analysis and data presentation. In contrast, beta-range PSD had a slightly more anterior topographical distribution relative to the theta-alpha range.

For both frequency ranges, EEG PSD was largest for the LAP transformation, followed by the LM reference, AVG reference, and INF reference [Theta/Alpha: $F_{(3,\ 63)} = 7{,}046.32$, $p_{\_GG-corrected} < 0.001$, $\varepsilon = 0.57$, $\eta^2_P = 0.99$; Beta: $F_{(3,\ 63)} = 4{,}551.63$, $p_{\_GG-corrected} < 0.001$, $\varepsilon = 0.63$, $\eta^2_P = 0.99$; all *post-hoc* $ps_{\_HB-corrected} < 0.048$]. Furthermore, EEG PSD was larger for the eyes closed vs. eyes open resting state condition across both frequency ranges [Theta/Alpha: $F_{(1,\ 21)} = 204.18$, $p_{\_GG-corrected} < 0.001$, $\eta^2_P = 0.91$; Beta: $F_{(1,\ 21)} = 85.29$, $p_{\_GG-corrected} < 0.001$, $\eta^2_P = 0.80$]. However, EEG Reference × Resting State Condition interactions were significant for both frequency bands [Theta/Alpha: $F_{(3,\ 63)} = 28.77$, $p_{\_GG-corrected} < 0.001$, $\varepsilon = 0.68$, $\eta^2_P = 0.58$; Beta: $F_{(3,\ 63)} = 12.51$, $p_{\_GG-corrected} < 0.001$, $\varepsilon = 0.70$, $\eta^2_P = 0.37$; all *post-hoc* $ps_{\_HB-corrected} < 0.004$]. Decomposition of the interaction for the theta/alpha frequency band indicated that the resting state eyes closed vs. eyes open PSD differences were largest for the LM reference (4.45 ± 0.30 dB), followed by the LAP transformation (5.17 ± 0.38 dB), and then the AVG (4.80 ± 0.33 dB) and INF (4.82 ± 0.35 dB) references, $ps_{\_corrected} < 0.006$, although the resting state condition PSD relative to the AVG and INF references did not significantly differ from each other in this frequency band, $p_{\_corrected} > 0.525$. Decomposition of the interaction for the beta frequency band indicated that the resting state eyes closed vs. eyes open PSD difference was larger for the LM reference (2.38 ± 0.27 dB) vs. the other reference schemes (LAP: 2.92 ± 0.33 dB; AVG: 2.74 ± 0.30 dB; INF: 2.78 ± 0.29 dB), $ps_{\_corrected} < 0.006$, whereas beta-range PSD differences were not significantly different among the LAP, AVG, and INF schemes, $ps_{\_corrected} > 0.215$; see **Table 1**.

TABLE 1 | Mean EEG power spectral density by EEG frequency band, resting state condition, and EEG reference.

EEG band	EEG reference	Eyes closed	Eyes open
Theta/Alpha	*LM*	24.95 (0.60)	20.50 (0.53)
	AVG	24.35 (0.63)	19.55 (0.54)
	INF	24.16 (0.64)	19.34 (0.55)
	LAP	40.91 (0.68)	35.74 (0.62)
Beta	*LM*	16.95 (0.53)	14.57 (0.44)
	AVG	16.00 (0.55)	13.26 (0.42)
	INF	15.91 (0.54)	13.13 (0.41)
	LAP	32.95 (0.61)	30.03 (0.50)

All values are in dB; SE in parentheses.

EEG Complexity and Integration

Mean observed resting EEG interaction complexity $C_I(X)$ and integration $I(X)$ values are given in the left columns of **Tables 2, 3**; ANOVA results are given in **Table 4**.

In the theta/alpha frequency range, $C_I(X)$ was significantly largest for the LAP transformation (79.68 ± 0.32 bits), smallest for the LM reference (69.03 ± 0.45 bits), with the AVG reference (72.06 ± 0.59 bits) and INF reference (71.86 ± 0.57 bits) taking intermediate values (see **Figure 3A**); all between-reference $C_I(X)$ differences were significant, *post-hoc* $ps_{\_corrected} < 0.006$. A main effect of resting state condition indicated that $C_I(X)$ was larger for eyes open (75.01 ± 0.46 bits) than the eyes closed condition (71.30 ± 0.53 bits) collapsed across EEG references in this frequency range (**Table 2** and **Figure 3A**). Decomposition of the

TABLE 2 | Mean resting EEG complexity by EEG frequency band, resting state condition, and EEG reference.

EEG band	EEG reference	Observed data		Surrogate data	
		Eyes closed	Eyes open	Eyes closed	Eyes open
Theta/Alpha	*LM*	67.15 (0.52)	70.90 (0.43)	69.23 (67.41,71.05)	72.33 (70.61,74.05)
	AVG	69.84 (0.65)	74.19 (0.59)	73.38 (71.18,75.58)	77.88 (75.64,80.12)
	INF	69.62 (0.63)	74.10 (0.58)	73.34 (71.14,75.54)	77.53 (75.38,79.68)
	LAP	78.60 (0.37)	80.76 (0.31)	100.58 (99.53,101.63)	103.17 (102.28,104.06)
Beta	*LM*	78.12 (0.78)	81.59 (0.69)	77.64 (75.32,79.95)	80.04 (77.49,82.59)
	AVG	84.77 (0.94)	89.30 (0.92)	85.68 (83.05,88.30)	89.57 (86.97,92.17)
	INF	84.27 (0.89)	88.71 (0.84)	84.85 (82.39,87.31)	88.21 (85.87,90.54)
	LAP	92.57 (0.47)	93.29 (0.57)	109.56 (108.36,110.75)	109.82 (108.25,111.40)

All values are in bits; SE in parentheses for observed data, 95% CIs in parentheses for surrogate data.

TABLE 3 | Mean resting EEG integration by EEG frequency band, resting state condition, and EEG reference.

EEG band	EEG reference	Observed data		Surrogate data	
		Eyes closed	Eyes open	Eyes closed	Eyes open
Theta/Alpha	*LM*	197.75 (2.15)	184.77 (1.42)	189.37 (183.24,195.51)	175.51 (171.04,179.99)
	AVG	179.16 (1.79)	167.71 (1.41)	169.84 (164.48,175.19)	157.95 (153.02,162.88)
	INF	180.95 (1.75)	168.94 (1.38)	171.77 (166.57,176.97)	159.18 (154.40,163.95)
	LAP	156.53 (0.66)	152.70 (0.55)	138.33 (135.61,141.04)	133.33 (130.66,136.01)
Beta	*LM*	173.50 (2.01)	165.66 (1.84)	167.32 (162.28,172.36)	158.58 (153.90,163.26)
	AVG	152.84 (1.57)	145.10 (1.40)	146.08 (141.47,150.68)	137.57 (133.51,141.64)
	INF	154.31 (1.52)	146.23 (1.30)	147.17 (142.78,151.55)	138.17 (134.52,141.82)
	LAP	142.27 (0.74)	141.39 (1.08)	129.85 (127.35,132.34)	128.60 (125.24,131.96)

All values are in bits; SE in parentheses for observed data, 95% CIs in parentheses for surrogate data.

significant EEG Reference × Resting State Condition interaction (**Table 2**) indicated that the theta/alpha-range eyes open vs. eyes closed $C_I(X)$ differences were larger for the INF (4.48 ± 0.38 bits) and AVG (4.45 ± 0.37 bits) references vs. the LAP transformation (2.16 ± 0.24 bits) and LM reference (3.75 ± 0.33 bits), $ps_{\_corrected} < 0.006$. Eyes closed vs. eyes open complexity was also significantly different between the LAP transformation and LM reference, $p_{\_corrected} < 0.006$, but not between the INF and AVG references, $p_{\_corrected} = 0.432$; see **Table 2**.

Theta/alpha range I(X) followed an opposite pattern than complexity, being significantly smallest for the LAP transformation (154.61 ± 0.57 bits), largest for the LM reference (191.26 ± 1.66 bits), with the INF reference (174.95 ± 1.47 bits) and AVG reference (173.43 ± 1.52 bits) taking intermediate values (see **Figure 3A**); all between-reference $C_I(X)$ differences were significant, *post-hoc* $ps_{\_corrected} < 0.006$. A main effect of resting state condition indicated that I(X) was larger for eyes closed (178.60 ± 1.52 bits) than the eyes open (168.53 ± 1.11 bits) condition across EEG references in this frequency range (**Table 2** and **Figure 3A**). However, decomposition of the significant EEG Reference x Resting State Condition interaction (**Table 2**) indicated that the magnitude of the resting state eyes closed vs. eyes open integration differences were smallest for the LAP transformation (3.83 ± 0.4 bits) vs. the other references (LM: 12.98 ± 1.50 bits; AVG: 11.46 ± 1.07 bits; INF: 12.01 ± 1.12 bits), $ps_{\_corrected} < 0.006$, whereas these integration differences were not significantly different among the LM, AVG, and INF references, $ps_{\_corrected} > 0.09$; see **Table 3**.

In the beta frequency range, $C_I(X)$ was significantly largest for the LAP transformation (92.93 ± 0.50 bits), followed by the AVG reference (87.03 ± 0.91 bits), INF reference (86.49 ± 0.84 bits), and LM reference (79.85 ± 0.72 bits), *post-hoc* $ps_{\_corrected} < 0.006$; see **Figure 3B**. Additionally, $C_I(X)$ was larger in the eyes open (88.22 ± 0.63 bits) vs. eyes closed

TABLE 4 | Analysis of variance (ANOVA) results for EEG complexity and integration for each frequency band (see Material and Methods—Computation of EEG Complexity and Integration).

EEG band	EEG measure	Effect	F	p	ε	η^2_P
Theta/Alpha	C_I(X)	*REF*	662.80	†0.001	0.55	0.97
		RS	133.19	0.001	–	0.86
		REF × *RS*	96.12	†0.001	0.53	0.82
	I(X)	*REF*	468.32	†0.001	0.65	0.96
		RS	100.86	0.001	–	0.83
		REF × *RS*	64.25	†0.001	0.51	0.75
Beta	C_I(X)	*REF*	39.59	†0.001	0.68	0.87
		RS	96.85	0.105	–	0.82
		REF × *RS*	92.64	†0.041	0.63	0.82
	I(X)	*REF*	114.96	†0.001	0.52	0.85
		RS	67.18	0.001	–	0.76
		REF × *RS*	91.01	†0.001	0.58	0.81

ANOVA factor labels: REF, EEG Reference; RS, EEG Resting State. REF factor effects dfs = 3, 63; RS main effect df = 1, 21. The †symbol indicates p-values subject to Greenhouse-Geisser correction (see Materials and Methods—Statistical Analysis of EEG/ERP Measures section).

(84.93 ± 0.71 bits) resting state conditions for $C_I(X)$ collapsed across EEG references (see **Table 2**). Decomposition of the significant EEG Reference x Resting State Condition interaction (**Table 2**) indicated that the beta resting state eyes open vs. eyes closed $C_I(X)$ differences were larger for the INF (4.44 ± 0.40 bits) and AVG (4.53 ± 0.42 bits) references vs. the LAP transformation (3.48 ± 0.35 bits) and LM reference (0.72 ± 0.30 bits), $ps_{\_corrected}$ <0.006. Eyes closed vs. eyes open complexity was also significantly different between the LAP transformation and LM reference, $p_{\_corrected} < 0.006$, but not between the INF and AVG references, $p_{\_corrected} = 0.203$; see **Table 2**.

Beta-range I(X) followed an opposite across-reference pattern than complexity, being significantly smallest for the LAP transformation (141.83 ± 0.87 bits), largest for the LM reference (169.58 ± 1.87 bits), with the INF reference (150.26 ± 1.34 bits) and AVG reference (148.97 ± 1.43 bits) taking intermediate values (see **Figure 3B**); all between-reference $C_I(X)$ differences were significant, *post-hoc* $ps_{\_corrected} < 0.006$. A main effect of resting state condition indicated that I(X) was larger for eyes closed (155.73 ± 1.22 bits) than the eyes open (149.59 ± 1.01 bits) condition across EEG references in this frequency range (**Table 2** and **Figure 3B**). However, decomposition of the significant EEG Reference x Resting State Condition interaction (**Table 2**) indicated that the magnitude of the resting state eyes closed vs. eyes open integration differences were smaller for the LAP transformation (0.88 ± 0.61 bits) vs. the other references (LM: 7.84 ± 0.92 bits; AVG: 7.73 ± 0.83 bits; INF: 8.08 ± 0.86 bits), $ps_{\_corrected} < 0.006$, and smaller for the AVG vs. INF reference, $p_{\_corrected} < 0.006$. The integration differences between the LM and AVG/INF references were not significant different, $ps_{\_corrected} > 0.589$; see **Table 3**.

Finally, the GEE-based regression analysis examining the relationship between PSD and $C_I(X)$ and I(X) across EEG references (collapsed across resting state condition) showed that theta-alpha PSD was positively associated with $C_I(X)$, $\beta = 0.94 \pm 0.02$, Wald $\chi^2_{(1, 22)} = 1{,}481.87$, $p < 0.001$, but negatively associated with I(X), $\beta = -0.72 \pm 0.03$, Wald $\chi^2_{(1, 22)} = 579.93$, $p < 0.001$. Similarly, beta PSD was positively associated with $C_I(X)$, $\beta = 0.55 \pm 0.07$, Wald $\chi^2_{(1, 22)} = 64.03$, $p < 0.001$, but negatively associated with I(X), $\beta = -0.31 \pm 0.07$, Wald $\chi^2_{(1, 22)} = 19.32$, $p < 0.001$. Thus, the increase in EEG power across EEG reference schemes corresponded to an increase in EEG complexity and decrease in EEG integration. The regression analysis examining the relationship between PSD and $C_I(X)$ and I(X) across resting state conditions (collapsed across EEG reference) showed that theta-alpha PSD was negatively associated with $C_I(X)$, $\beta = -0.95 \pm 0.04$, Wald $\chi^2_{(1, 22)} = 477.46$, $p < 0.001$, but positively associated with I(X), $\beta = 0.96 \pm 0.05$, Wald $\chi^2_{(1, 22)} = 390.93$, $p < 0.001$. Similarly, beta PSD was negatively associated with $C_I(X)$, $\beta = -0.86 \pm 0.05$, Wald $\chi^2_{(1, 22)} = 346.63$, $p < 0.001$, but positively associated with I(X), $\beta = 0.94 \pm 0.04$, Wald $\chi^2_{(1, 22)} = 516.04$, $p < 0.001$. Thus, the increase in EEG power across resting state conditions corresponded to a decrease in EEG complexity and an increase in EEG integration.

Surrogate Data Tests

Mean surrogate resting EEG interaction complexity $C_I(X)$ and integration I(X) values are given in the right columns of **Tables 2**, **3**. It is clear from the tables that, in the theta-alpha frequency range, all observed mean complexity values lay outside the surrogate 95% two-tailed confidence intervals for all four EEG references in the eyes closed condition, and for the AVG, INF, and LAP references in the eyes open condition. In the beta range, only the LAP reference yielded complexity values outside the surrogate confidence intervals for either resting state condition. All EEG references yielded mean integration values outside the surrogate confidence intervals for both resting state conditions and frequency ranges. It is unlikely that the observed complexity and integration values outside the surrogate confidence intervals are attributable to spurious interactions.

The observed mean integration values tended to be larger than the surrogate values, whereas the observed mean complexity values tended to be lower than the surrogate values. This pattern in integration and complexity is consistent with the theoretical prediction (Tononi et al., 1994; see **Figure 1**) that as system elements in the high integration regime become more independent (in this case, artificially via the surrogate data creation procedure), $C_I(X)$ should increase and I(X) should decrease. Indeed, this predicted relationship becomes apparent when the eyes closed and eyes open observed and surrogate EEG data are ordered in terms of monotonically increasing integration values (**Figure 5**).

Dipole Modeling

In order to match the number of participants in the observed data and to ensure that our modeling results did not depend on one specific set of randomly determined parameters, we created 22 separate simulations for each specific model and then averaged across each set of simulations and trials within a simulation for a given model. **Figure 6** displays mean simulated resting state EEG PSD differences between the high vs. low amplitude simulations for the theta-alpha and beta frequency ranges. The qualitative features of the simulated topography differences are in good agreement with the difference topographies of the observed data, although this agreement is reduced somewhat for the full interdipole dependency simulations. **Figure 7** shows mean $C_I(X)$ as a function of mean I(X) for simulated extrastriate dipole moment sources only (not including the background sources). The simulated relationship between complexity and integration is in agreement with theoretical predictions (e.g., **Figure 1**). $C_I(X)$ and I(X) are low for the full independency model when the extrastriate dipoles are statistically independent. $C_I(X)$ and I(X) increase for level-2 independence, with $C_I(X)$ achieving a maximum for level-1 independence of the extrastriate dipoles at intermediate values of I(X). As integration continues to increase, $C_I(X)$ decreases through the three increasing levels of interdependency among the extrastriate dipoles, reaching a local minimum for the fully dependent extrastriate dipoles. In addition, **Figure 7** also shows that $C_I(X)$ and I(X) tended to be greater for the high amplitude dipole moments vs. the low amplitude moments at higher levels of statistical dependence among the extrastriate dipoles.

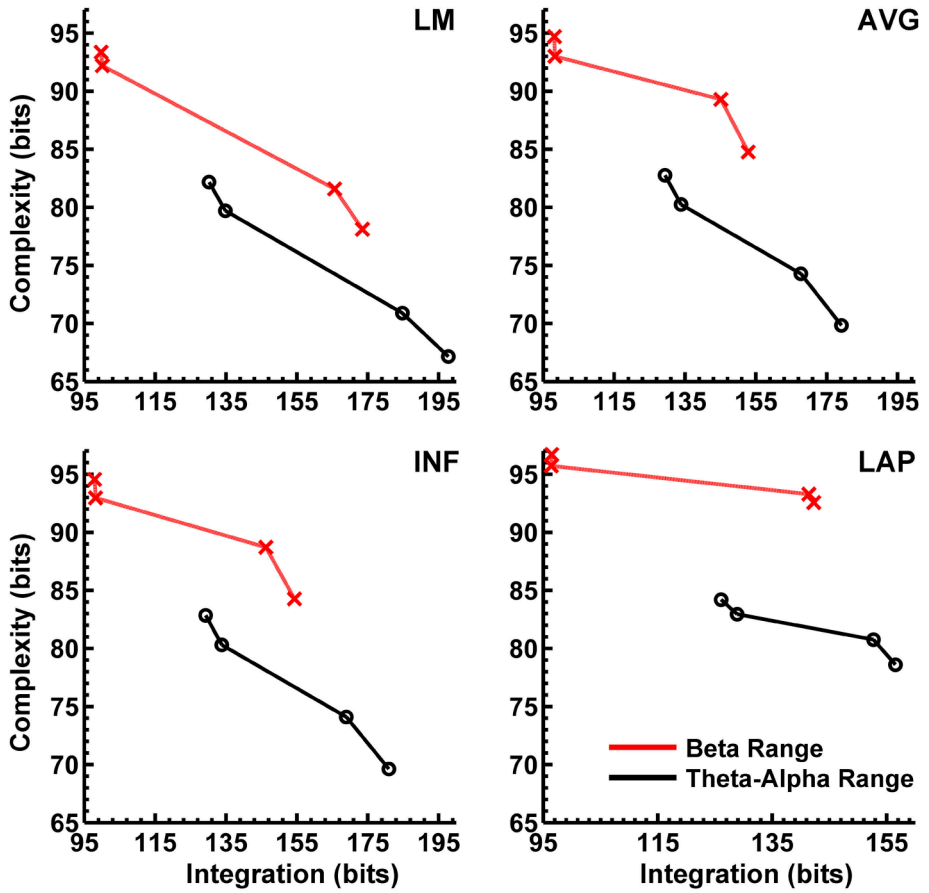

FIGURE 5 | Empirical interaction complexity $C_I(X)$ as a function of integration I(X) for observed and surrogate scalp EEG. Data points are ordered in increasing dependency from left to right (eyes open surrogate, eyes closed surrogate, eyes open observed, eyes closed observed). Red lines, beta-range data; black lines, theta-alpha-range data. Data points reflect averages across 22 participants; standard errors of data points (not shown) are given in **Tables 2**, **3**.

Figures 8, **9** display mean $C_I(X)$ as a function of mean I(X) for the theta-alpha-range and beta-range simulated scalp EEG resulting from volume-conduction of all simulated dipole source activity (extrastriate and background dipoles). The figures show results for the simulated data reference with respect to all four EEG references. In the high integration range where theoretically $C_I(X)$ is a monotonically decreasing function of I(X) (see **Figure 1**), all four EEG references were able to correctly reproduce the gradient of the complexity-integration relationship among the visual dipole moments. However, in the low integration range, where theoretically $C_I(X)$ is a monotonically increasing function of I(X), the functional $C_I(X)$ vs. I(X) pattern is distorted from that seen for the dipole moment sources for all four EEG references. Although the same basic inverted-U pattern is present at the scalp level, $C_I(X)$ reaches a maximum for the level-2 independent model, rather than the level-1 independent model in the low integration range. This distortion was also present when the background sources were removed from the simulation and scalp level signals were generated from the extrastriate sources only (see Figures S1, S2). In addition, scalp-level $C_I(X)$ was smaller for the high amplitude vs. the low amplitude extrastriate dipole moments in the context of the background noise sources[1]. This $C_I(X)$ pattern is similar to that seen for the observed eyes closed vs. open EEG resting states, but opposite that seen for $C_I(X)$ computed from the simulated dipole sources directly. However, this distortion was absent when the background sources were removed from the simulations (Figures S1, S2); then $C_I(X)$ was larger for high vs. low amplitude simulations, in agreement with the $C_I(X)$ pattern computed from the dipole source moments directly. Possible reasons for these differences between the full dipole model (extrastriate +

[1]We also performed simulations with a 400% amplitude difference in order to investigate the effects of amplitude on EEG complexity and integration (although such an amplitude difference is unlikely to be biologically typical of the two resting state conditions). This increased scalp-level integration in the full dependency condition by about 35–40 bits depending on EEG reference, with the other dependency conditions unaffected. We believe this pattern obtains because complexity and integration are differential entropies (i.e., they involve the subtraction of two entropy terms; see Methods, Computation of EEG Complexity and Integration section) that are independent of scale (except for signal dispersion effects due to volume conduction, which are likely greatest in the full dependency condition).

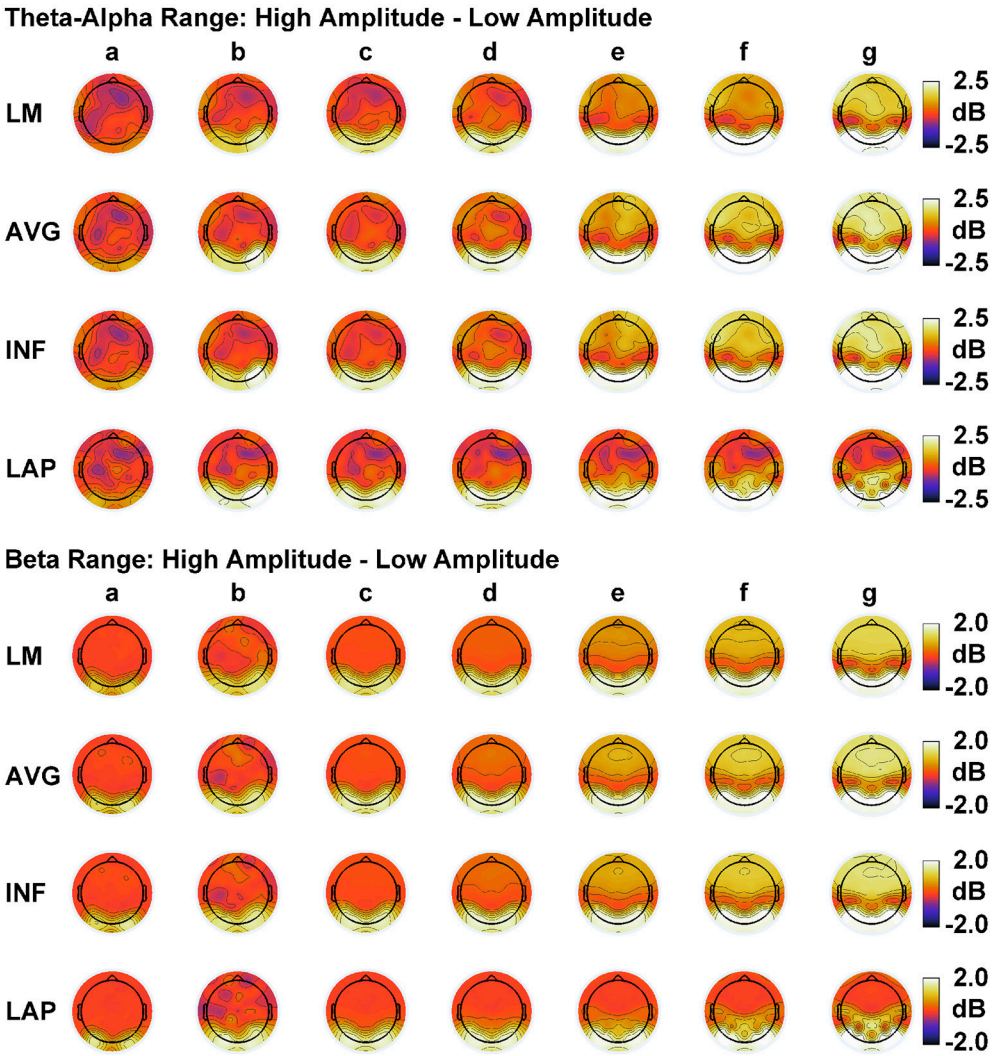

FIGURE 6 | Simulated resting state EEG. Scalp topographies show high amplitude—low amplitude PSD differences over the theta-alpha frequency range **(top)** and beta frequency range **(bottom)**. PSD topographies are generated from seven different interdipole dependency models (in increasing dependency from left to right): **(a)** full independency model, **(b)** independent model—level 2, **(c)** independent model—level 1, **(d)** interdependent model—level 3, **(e)** interdependent model—level 2, **(f)** interdependent model—level 1, and **(g)** full dependency model. Head maps display PSD topographies averaged over the stated frequency ranges; light/dark colors indicate ± values. Scalp maps reflect averages across 22 separate simulations.

background dipoles) and the extrastriate dipole only models are taken up in the Discussion section, below.

Finally, **Figures 8**, **9** show that scalp-level complexity was largest, and scalp-level integration was smallest, for the simulated LAP-referenced data. This is the same pattern observed for the LAP-referenced empirical data. In addition, comparison of **Figures 8**, **9** with **Figure 7** indicate that the absolute complexity and integration values at the scalp are much higher than those observed for the dipole sources, an inflation most likely due to volume conduction (see also Tables S3, S4).

DISCUSSION

The present study investigated the effect of four EEG reference schemes on the quantification of EEG complexity $C_I(X)$ and integration I(X) during a resting state task. In the context of a simple measurement of resting state EEG, we found that EEG reference influenced both the magnitude and sensitivity to volume-conduction artifacts of scalp EEG $C_I(X)$ and/or I(X) collapsed across eyes open and eyes closed resting state conditions, as well as the magnitude of scalp EEG $C_I(X)$ and I(X) differences between resting state conditions. For all EEG references, these effects were observed in the context of theta/alpha-range and beta-range PSD differences previously reported for resting state EEG recordings (i.e., greater PSD for eyes closed vs. eyes open resting states; Kornguth et al., 2013; Witkowski et al., 2015). However, consistent with previous reports (e.g., Yao et al., 2005), the magnitude of these spectral power differences also varied according to EEG reference. In addition, we performed dipole source modeling in order to

assess the accuracy of scalp-level estimates of complexity and integration of neural sources and how these estimates are affected by EEG reference choice. The dipole source modeling showed that simulated scalp EEG-level $C_I(X)$ and I(X) accurately reflect changes in underlying neural source dependencies when using all four EEG references, but only in the high integration range.

Effects of EEG Reference on Scalp EEG Complexity

Our first main finding was that scalp EEG interaction complexity $C_I(X)$ was largest for the LAP transformation, smallest for the LM reference, and at intermediate values for INF and AVG references for both theta-alpha and beta frequency ranges. However, the surrogate data analysis indicated a differential across-reference pattern of non-random or non-spuriously coincident complexity arising due to volume conduction. In the theta-alpha frequency range, the $C_I(X)$ values of both resting states lay outside the surrogate confidence intervals for the LAP, INF, and AVG EEG references, whereas LM-referenced data were outside the surrogate confidence intervals only for the eyes closed data. In the beta frequency range, only the $C_I(X)$ values of both resting states for the LAP reference lay outside the surrogate confidence intervals. Thus, of all the EEG references, the LAP reference was the most "robust" in the sense that it returned large-magnitude $C_I(X)$ values that were less sensitive to volume-conduction artifacts across both EEG frequency ranges and resting state conditions. We suggest that this pattern reflects two characteristics of an EEG reference: (1) its impact on neuroelectric signal quality and statistics, and (2) the accuracy with which neuroelectric signals measured with respect to a particular reference can represent the activity of the cortical sources underlying EEG topographies. LAP-transformed EEG signals possess higher levels of both characteristics relative to the other reference schemes. First, these signals are "reference free" estimates of radial (transcranial) current flow entering and leaving the scalp, and thus are not prone to across-electrode contamination of activity from a single physical scalp location, such as a monopolar recording reference site. Second, the LAP-transformed signals provide an enhanced representation of superficial EEG current generators that are (mostly) radially-oriented, at the expense of less sensitivity to deep sources and/or spatially-broad activities arising from distributed sources (Pernier et al., 1988; Law et al., 1993; Dien, 1998; Kayser and Tenke, 2006a,b). However, we argue that the last characteristic may actually be beneficial for the assessment of EEG complexity because some information about those distributed sources is likely lost in the constructive summation of their activity that produces the spatially-broad EEG response across the scalp. Instead, the LAP transformation distinguishes the local activity of those distributed sources from each other in a manner that is highly informative. Evidence that the LAP data provided a more robust measurement of EEG source activity than the other references is given by the present observation that LAP-transformed signals had the highest PSD values of the four different EEG reference schemes. This finding was not due to the fact that the LAP-transformed PSD values are measured in different units ($\mu V^2/m^4/Hz$) than the other references ($\mu V^2/Hz$), because all PSD values were converted to decibel units before statistical comparison (see Computation of Resting EEG Power Spectral Density section, above). Moreover, the GEE-based regression analysis indicated that $C_I(X)$ level was positively associated with PSD magnitude across EEG references schemes, again suggesting that the EEG reference scheme that provides a more accurate assessment of EEG source activity also provides a robust estimate of EEG complexity.

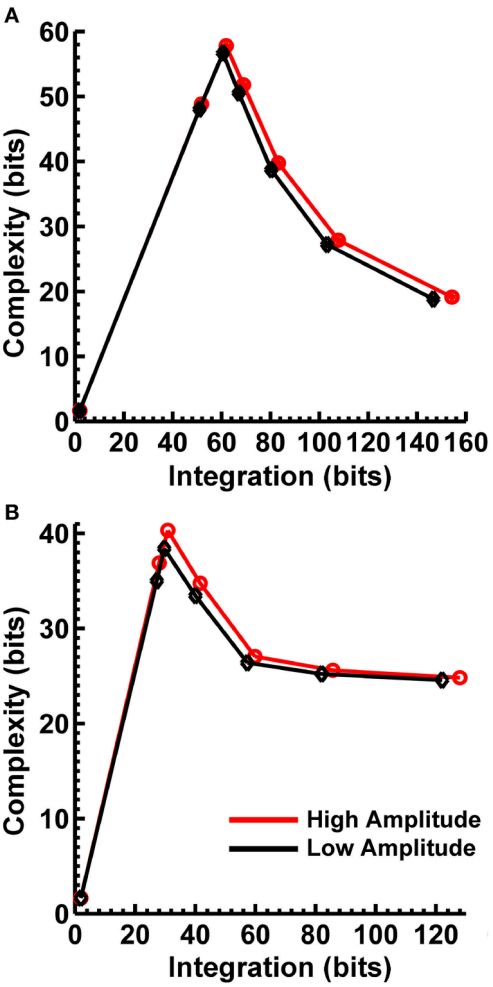

FIGURE 7 | Interaction complexity $C_I(X)$ as a function of integration I(X) for simulated **(A)** theta-alpha range and **(B)** beta-range visual dipole moment sources (excluding background sources). Data points are generated from the seven different interdipole dependency models and are ordered from left to right in terms of increasing dependency/integration (full independency model, independent model—level 2, independent model—level 1, interdependent model—level 3, interdependent model—level 2, interdependent model—level 1, full dependency model). Red lines, high amplitude simulations; black lines, low amplitude simulations. Data points reflect averages across 22 separate simulations; standard errors of simulated $C_I(X)$ and I(X) are too small to be displayed but range from 0.01 to 0.21 bits.

Taken together, the above findings support the conclusion that the LAP-transformed EEG data provides the most robust

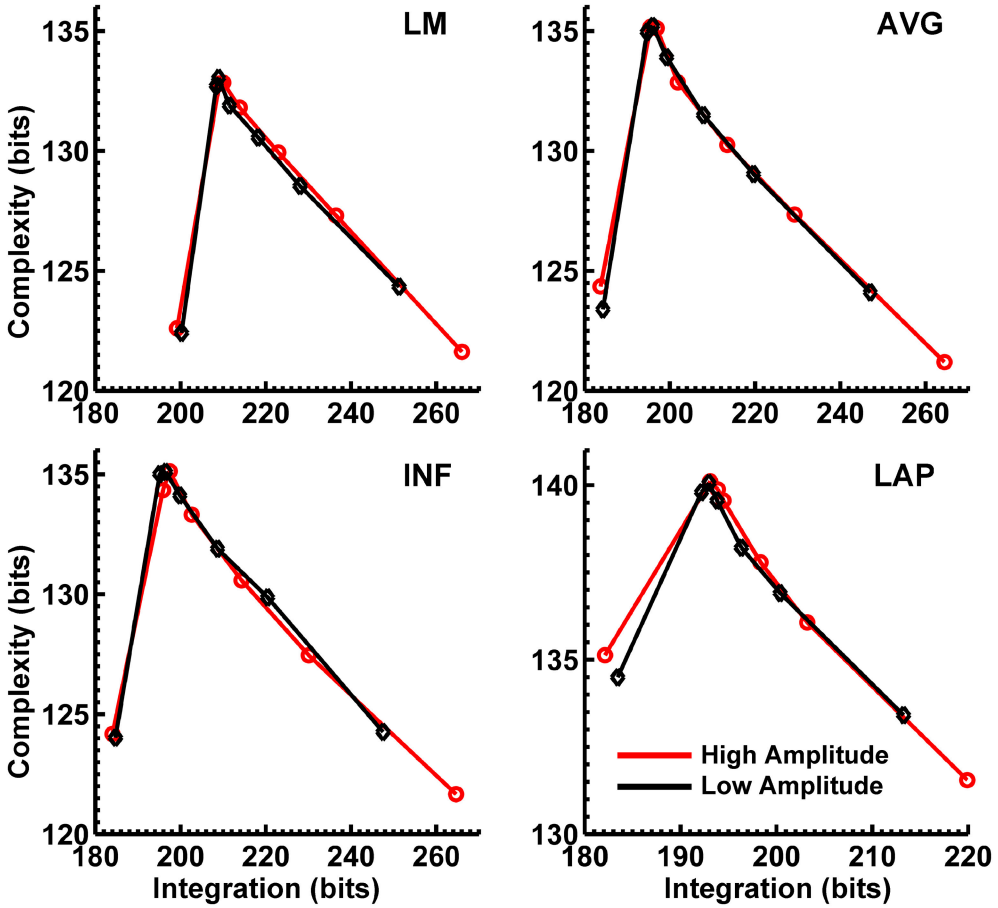

FIGURE 8 | Interaction complexity $C_I(X)$ as a function of integration I(X) for theta-alpha-range simulated scalp EEG resulting from all dipole source activity (visual and background dipoles). Data points are generated from the seven different interdipole dependency models and are ordered form left to right in terms of increasing dependency/integration (full independency model, independent model—level 2, independent model—level 1, interdependent model—level 3, interdependent model—level 2, interdependent model—level 1, full dependency model). Red lines, high amplitude simulations; black lines, low amplitude simulations. Data points reflect averages across 22 separate simulations; standard errors of simulated $C_I(X)$ and I(X) are too small to be displayed but range from 0.04 to 0.15 bits.

estimates of EEG complexity relative to the other EEG reference schemes. In contrast to the LAP transformation, the LM reference, being close to the jaw and neck, is fairly noisy and highly sensitive to subtle head/neck movements and muscle activity. Moreover, LM-referenced EEG signals express changes in transverse scalp electric potential rather than radial current, and thus provide a spatially-limited representation of the underlying cortical sources. Hence, as we observed, the LM reference should provide the least robust estimate of EEG complexity. The AVG and INF references also provide spatially-limited representations of cortical EEG sources. However, given that these references approximate a noiseless zero potential with sufficient spread and density of electrode coverage across the scalp (Bertrand et al., 1985; Yao, 2001), they should produce more informative, and thus complex, EEG signals than the LM reference, again as we observed.

We note that the present observation of larger complexity for the LAP transformation is in apparent contrast to the observation of van Putten and Stam (2001), who found the magnitude of a related measure of EEG complexity [neural complexity $C_N(X)$] to be larger for an average reference vs. a source reference consisting of the voltage difference between a given recording site and the mean voltage of 3–4 neighboring recording sites. As described, this source reference appears to be a multi-channel version of a bipolar montage with the EEG signals still expressed in terms of transverse scalp electric potentials rather than radial scalp current flow. Thus, it is unclear to what degree this reference can spatially represent cortical EEG sources, how susceptible it is to local noise, and the effects this would have on the computation of EEG complexity relative to the LAP-transformation. This should be a subject of further research.

Effects of EEG Reference on Scalp EEG Integration

The second main finding of the present study is that EEG integration I(X) was smallest for the LAP transformation, largest for the LM reference, and at intermediate values for the INF and AVG references for both theta-alpha and beta frequency

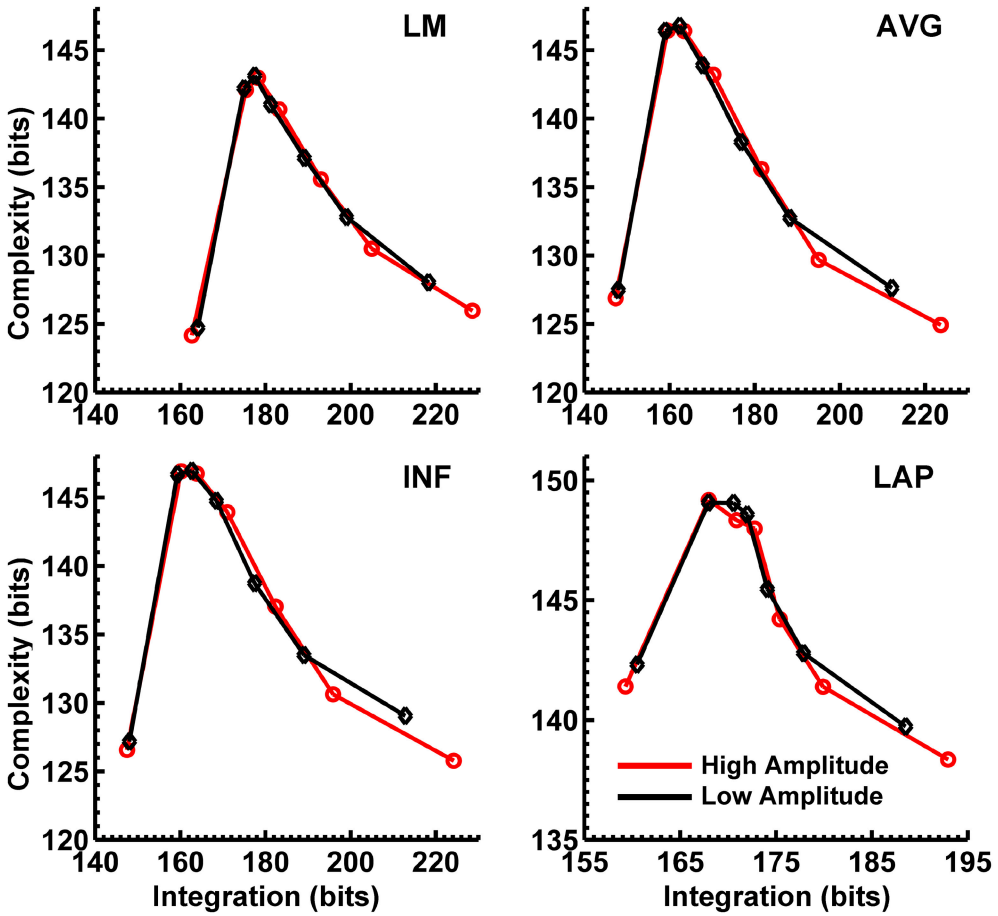

FIGURE 9 | Interaction complexity $C_I(X)$ as a function of integration I(X) for beta-range simulated scalp EEG resulting from all dipole source activity (visual and background dipoles). Data points are generated from the seven different interdipole dependency models and are ordered from left to right in terms of increasing dependency/integration (full independency model, independent model—level 2, independent model—level 1, interdependent model—level 3, interdependent model—level 2, interdependent model—level 1, full dependency model). Red lines, high amplitude simulations; black lines, low amplitude simulations. Data points reflect averages across 22 separate simulations; standard errors of simulated $C_I(X)$ and I(X) are too small to be displayed but range from 0.04 to 0.40 bits.

ranges. Surrogate data analysis showed that computed I(X) values were unlikely to be due to random or spuriously coincident volume-conducted EEG activity for any of the EEG references. The GEE-based regression analyses indicated that this change in I(X) was accompanied by an opposing change in PSD across EEG reference schemes, with larger EEG integration values associated with lower EEG power and vice versa. Integration is a measure of the overall deviation from statistical independence of the individual elements of a multivariate system. Thus, I(X) should be affected by factors that influence the measured independence of a set of signals. Volume conduction is one such factor because volume-conducted signals may be detected at neighboring scalp channels and thus can introduce a non-physiological source of correlation between their measured signals. Given that the LAP transformation reduces the effects of volume conduction and is reference free (Law et al., 1993; Kayser and Tenke, 2006a,b; Nunez and Srinivasan, 2006), integration should be smallest for this reference, as we observed. This observation is consistent with the report of van Putten and Stam (2001) of a lower overall level of integration for the source reference vs. the average reference. On the other hand, derivation of the EEG signals relative to LM, AVG, and INF references should have no effect on volume conduction. Moreover, these monopolar references may cause activity at reference sites to be shared across the other EEG channels and thus introduce a form of artifactual correlation between them. These effects should be greatest for the LM reference given its proximity to the neck, jaw, and lower head muscles. The AVG and INF references are less prone to the correlating effects of common reference activity because most of the idiosyncratic activity of individual EEG channels is averaged out in the construction of the AVG reference (unless a large number of channels show high-amplitude, synchronous activity), whereas the INF reference estimates a neutral (noiseless) reference at infinity. Hence, though all four EEG references will express true and artifactual integration among EEG signals, the LM reference should produce

larger integration values than the AVG and INF references, which in turn should be larger than the LAP transformation, as we observed.

The Interaction of EEG Statistics and EEG Reference on EEG Complexity and Integration

Although the present EEG integration findings are consistent with previous reports (van Putten and Stam, 2001; van Cappellen van Walsum et al., 2003; Rapp et al., 2005), we note that the direction of between-resting state condition differences in complexity is not. These previous studies found a reduction in complexity during the eyes open vs. eyes closed resting state conditions (van Putten and Stam, 2001; van Cappellen van Walsum et al., 2003; Rapp et al., 2005), in contrast to the present observations for $C_I(X)$. What might account for this discrepancy between past studies and ours? van Putten and Stam (2001) suggested their observations may be due to use of a low-spatial resolution scalp montage (21 channels) and that the mixture of different signal frequencies in the electroencephalogram decrease interelectrode correlations in wideband data even though the electrodes are mostly synchronized within a single frequency range. We bandpass-filtered our data in narrow ranges and used a high-density scalp montage (72 channels) to rule out these concerns. However, other studies have observed the same resting state condition differences as van Putten and Stam (2001) in filtered data with a high-density MEG montage (van Cappellen van Walsum et al., 2003).

Instead, we suggest this discrepancy between our study and previous reports may arise from the fact that the analytic expressions for the complexity and integration measures utilized in all of these studies assume the EEG signals to be approximately Gaussian distributed (Norwich, 1993; Tononi et al., 1994; van Putten and Stam, 2001; Ince et al., 2017). It is well known that this assumption is often partially or completely violated for physiological signals (Dumermuth, 1968; Elul, 1969; Dumermuth et al., 1972; Pollock et al., 1990). In the present study, our EEG data exhibited a substantial deviation from normality (see Methods—Computation of EEG Complexity and Integration section). Thus, we applied a method to transform non-normal distributions to Gaussian that has been successfully used before with EEG data (van Albada and Robinson, 2007). We then verified that the transformed data met univariate and multivariate Gaussian assumptions before computing $C_I(X)$ and $I(X)$ (see Methods—Computation of EEG Complexity and Integration section). Additionally, we carefully verified that the Gaussian transformation did not distort key resting state EEG features (see Supplementary Materials). However, to our knowledge, the previous studies observing greater complexity for eyes closed than eyes open resting state conditions assumed a Gaussian distribution for their data, but did not report any assessment of how well this assumption fit their data sets. Hence, if the physiological data of these previous studies either partially or completely failed to meet Gaussian statistical assumptions, then this might explain the discrepancy between past studies and ours regarding resting state complexity differences. It is entirely possible that the character of EEG or MEG statistics departs from normality to a greater degree or lesser degree in one resting state condition relative to the other, which would produce inaccurate estimations of $C_I(X)$ and $I(X)$.

To test this hypothesis, we computed $C_I(X)$ and $I(X)$ on the original non-Gaussian-transformed data (see Supplementary Material) and found resting state $C_I(X)$ to be greater for the eyes closed than eyes open resting state condition, which was the pattern reported by previous reports (van Putten and Stam, 2001; van Cappellen van Walsum et al., 2003; Rapp et al., 2005). The overall resting state integration pattern was unchanged by the Gaussian transformation, however, and was also consistent with previous results. Importantly, these earlier studies used several seconds' worth of data to compute $C_I(X)$ and $I(X)$, whereas here we used 1-s (256-sample) trials (see Methods—EEG Recording and Pre-Processing). The similarity between previous observations and the present non-Gaussian-transformed results rule out the possibility that our use of short trials may have biased the statistical distribution of the data toward non-normality, or were otherwise too short to provide a correct estimate of the statistical properties of the data, in a manner that affected the computation of EEG complexity. Moreover, our statistical testing indicated that, at the very least, the Gaussian-transformed data better met the required statistical assumptions of the entropy formulas then the non-transformed data (see Methods—Computation of EEG Complexity and Integration).

Hence, we conclude that the computation of $C_I(X)$ via the analytical expressions used in the present and past studies is highly dependent on the degree to which the data meet the Gaussian statistical assumptions. One should always employ a verification and/or correction procedure such as the one we utilized in this study. Alternatively, one may utilize discrete methods of computing EEG entropy that do not require data to be distributed in a particular way (Misra et al., 2005; Magri et al., 2009). This matter is relevant to the main issue of EEG reference choice explored in this paper, because different reference transformations may change the statistics of the EEG signals in various ways, which in turn may affect the computation of $C_I(X)$ and $I(X)$ across references. In fact, we did find different across-reference patterns of $C_I(X)$ and $I(X)$ for the non-Gaussian-transformed data relative to the transformed data (see Supplementary Material).

Scalp-Level Estimation of Neural Source Complexity and Integration

We performed dipole source modeling-based simulations in order to assess the accuracy of scalp-level estimates of complexity and integration of neural sources and how these estimates are affected by EEG reference choice. Our simulations were based on a 4-shell spherical model (Cuffin and Cohen, 1979; Mosher et al., 1993; Tenke and Kayser, 2015) with 40 oscillating dipole sources spread over posterior extrastriate cortical shell regions, and 148 oscillating background "noise" dipoles equally spread over the remainder of the cortical shell. We created different statistical dependencies among the extrastriate dipoles in order to recreate different points of the theoretical "inverted-U"

non-monotonic complexity-integration function (Tononi et al., 1994; see **Figure 1**) at the neural source level. We then computed the forward solutions of these source configurations, referenced the simulated scalp EEG with respect to all four EEG references examined here, and computed complexity and integration.

Our simulations reproduced the basic scalp topography of between-resting state condition differences in PSD (**Figure 6**). We also found that the dipole sources followed the theoretical complexity-integration curve (**Figure 7**), with fully independent sources yielding low complexity and integration values, fully dependent sources yielding low complexity and high integration, and heterogeneously dependent sources yielding high complexity and intermediate integration values. At the level of simulated scalp EEG (**Figures 8**, **9**), $C_I(X)$ and I(X) correctly reproduced the gradient of the complexity-integration relationship among the extrastriate dipole sources in the high integration range where $C_I(X)$ is a monotonically decreasing function of I(X). This was the case for all four EEG references. However, in the low integration range—where dipole $C_I(X)$ is a monotonically increasing function of I(X)—the scalp-level pattern of $C_I(X)$ and I(X) was distorted from that seen for the dipole moment sources for all four EEG references. Here, scalp-level $C_I(X)$ reached a maximum at the level-2 stage of independence among the dipoles, rather than the level-1 independence stage as observed for $C_I(X)$ computed from the dipole sources directly. Interestingly, this distortion was also present if the background sources were removed from the simulation (see Figures S1, S2), suggesting that it results from the mixing effects of the extrastriate source signals due to volume conduction. This scalp-level distortion of the complexity-integration function of the neural sources may represent a fundamental limitation of the use of scalp-recorded EEG to estimate neural source complexity in the low integration range. However, this limit may not pose a problem for most EEG studies, as the neural processes detectable by EEG are oscillatory in nature and thus likely operate at higher levels of integration. This is because oscillating signals, even those with random phases, have an intrinsic non-random autocorrelative structure that cannot be broken down further without changing the periodicity of the signals. In the absolute limit, full randomization would cause these signals to either become non-oscillatory or turn into white noise with equal spectral power across frequencies. In this case, scalp signals would either no longer be detectable as rapidly alternating voltage fluctuations (although they may be present as slow DC potentials) or if detectable, would manifest as very low levels of complexity and integration resolvable at the scalp (for example, as seen for the fully independent dipole source model).

Our simulations also yielded smaller scalp-level $C_I(X)$ for the high vs. low amplitude extrastriate dipole sources at intermediate and high levels of integration (**Figures 7**, **8**). This is a pattern similar to that observed for the empirical eyes closed vs. open EEG resting state data. However, this scalp-level $C_I(X)$ difference pattern was reversed when the background sources were removed from the simulations (Figures S1, S2). Here, $C_I(X)$ was larger for high vs. low amplitude simulations, in agreement with the $C_I(X)$ pattern computed from the dipole source moments directly. This was the case for all four EEG references. We suggest that the reversed scalp-level $C_I(X)$ differences seen in the full dipole model results from the volume conduction of the background noise sources in the model. The high level of scalp complexity that arises from the large number of randomly oscillating background sources likely dominated the output of the $C_I(X)$ estimator, with this dominance modulated by the presence of the partially- or fully-dependent extrastriate sources. As the latter increased in amplitude, they contributed more to the scalp signal, thus reducing scalp-level complexity and increasing scalp-level integration.

We note that the absolute values of $C_I(X)$ and I(X) were considerably higher than the corresponding values for the dipole sources; this is likely due in part to the added complexity of the additional background dipole sources. However, volume conduction also played a role in the inflation of $C_I(X)$ and I(X) values at the scalp because this inflation was also observed when the background sources were removed from the simulation and scalp level signals were generated from the extrastriate sources only (see Figure S1 and Tables S3, S4). Nevertheless, regardless of whether the background sources were present or not in the simulation, scalp-level $C_I(X)$ values were highest, and I(X) values were lowest, for the simulated Laplacian-transformed data, as observed for the empirical EEG data. These observations suggest that the LAP reference produces the closest approximation to the true absolute dipole source integration values, but the worst approximation to the true absolute source complexity values. However, researchers are more often interested in between-source dependency level differences across different EEG references and experimental conditions. In this case, a better criterion for EEG reference performance is a source- vs. scalp-level comparison between complexity and integration gradients across source dependency levels. We compared these gradients for the case when the background sources were removed from the simulation and scalp level signals were generated from the extrastriate sources only (see Table S5). This analysis showed that, with the exception of theta-alpha-range integration, the Laplacian-referenced data was better able to reproduce the gradients of complexity and integration changes across source dependency levels than the other EEG references.

Finally, we note that the observed $C_I(X)$ was larger, and observed I(X) was smaller, for the eyes open vs. eyes closed resting state conditions, regardless of choice of EEG reference scheme. The GEE-based regressions showed that $C_I(X)$ was negatively related, and I(X) was positively-related, to PSD magnitude across resting state conditions. It is unclear from our simulations if these PSD, $C_I(X)$, and I(X) differences reflect passive volume-conducted differences in neural source amplitudes between resting state conditions and the resultant differences in interelectrode correlations at the scalp, or if they reflect between-condition differences in the dependency relationships among the neural sources (irrespective of differences in neural source amplitude). The latter case could produce between-condition differences in EEG power without an increase in the amplitude of individual EEG sources. This is illustrated in **Figure 10**, which shows example mean PSD differences between successive interdipole-dependency levels for the high amplitude simulations. (Other interdipole dependency levels contrasts are

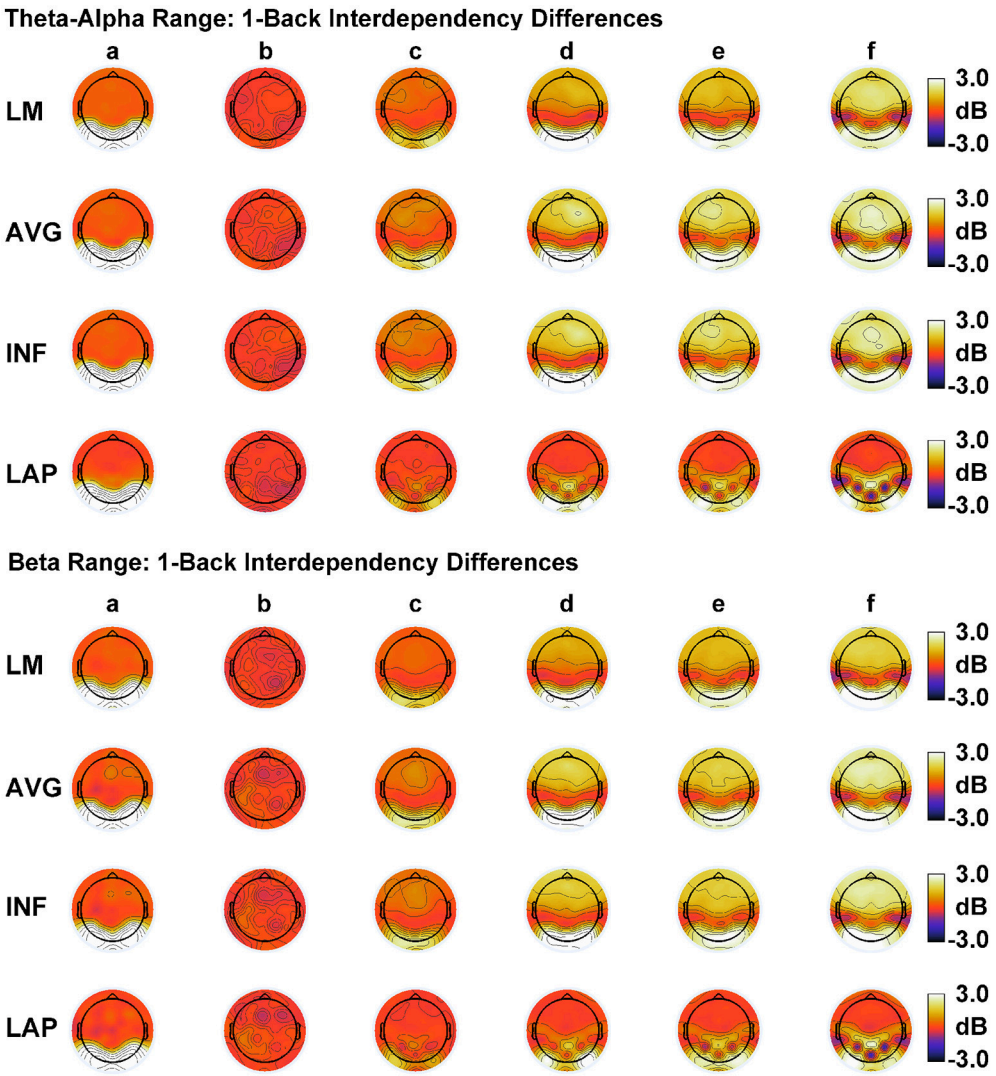

FIGURE 10 | Resting state EEG PSD differences may result from differences in dipole source dependencies. Representative pairwise interdependency level *n* + *1*—level *n* ("1-back") scalp PSD topography differences for simulated theta-alpha range **(top)** and beta-range **(bottom)** EEG data. **(a)** independent model-level 2—full independency model, **(b)** independent model-level 1—independent model-level 2, **(c)** interdependent model-level 3—independent model-level 1, **(d)** interdependent model-level 2—interdependent model-level 3, **(e)** interdependent model-level 1—interdependent model-level 2, **(f)** full dependency model—interdependent model-level 1. Head maps display PSD topographies averaged over the stated frequency ranges; light/dark colors indicate ± values. Scalp maps reflect averages across 22 separate simulations.

possible, such as the differences between *n*+*2* and *n* dependency levels.) The figure shows that simulations with high I(X) and low C_I(X) produced higher PSD levels than simulations with lower I(X) and C_I(X) levels. This explanation would be consistent with evidence that during the eyes closed resting state the visual cortex is driven by endogenous pacemakers in the thalamus which synchronize much of the visual cortex in the alpha, theta and beta ranges (Adrian and Yamagiwa, 1935; Buzáki, 1992). This explanation would also be consistent with the hypothesis that in order to perform specialized information-processing during rich neurocognitive conditions (such as the eyes open resting state), the brain organizes itself into distributed neuronal groups that interact more strongly with themselves than with the rest of the brain (Tononi et al., 1994, 1996, 1998a). Determining which neural source model best explains the observed resting state data could be achieved by either (1) fitting the empirical data to a dipole model with free parameters (dipole source frequency, phase, amplitude, and interdipole dependencies) that minimize an objective error function, or (2) conducting a source localization analysis (e.g., beamformer, minimum norm estimation, LORETA) and quantifying the complexity and integration of the localized sources. These analyses are beyond the scope of the present study and are a subject for future research.

Study Limitations

We performed dipole simulations that provided a benchmark to compare the ability of scalp-level $C_I(X)$ and I(X) measures to resolve the complexity and integration of neural sources and how these estimates are affected by choice of EEG reference. Nevertheless, our models specifically described resting state conditions that involved ongoing non-phase-locked EEG oscillations with varying statistical dependencies among posterior cortical sources. Our models also did not examine situations in which the number and location of dependent sources varied between conditions. Moreover, our models were phenomenological in the sense that they did not directly simulate the interactions through which neural groups form interdependent relationships. That said, we believe our findings will generalize to other tasks that engage similar ongoing non-phase-locked EEG activity (such as mental arithmetic, motor grasping, or vigilant attention tasks). However, they may not generalize to tasks that engage different kinds of neural dynamics, such as evoked potentials time-locked to specific events, or conditions that engage vastly different mental states (e.g., sleep, anesthesia). Moreover, our study utilized a 72-channel sensor montage; it is unclear how the number of channels affects the computation of $C_I(X)$ and I(X). Future research is needed to determine how these factors affect the quantification of $C_I(X)$ and I(X), and how this interacts with the choice of EEG reference. One guiding principle that should assist such endeavors is the theoretical complexity-integration function (**Figure 1**), which is a general relationship that should apply across all experimental situations.

CONCLUSION

In conclusion, we have shown that information-theoretic measures of integration I(X) are relatively robust to volume-conduction artifacts across all four EEG references when comparing resting state condition differences, whereas complexity $C_I(X)$ is the most robust to volume-conduction artifacts when computed with respect to the LAP reference. In addition, dipole simulations showed that of the four EEG references, the LAP reference produced the closest approximation to the true absolute dipole source integration values, and more accurately estimated the gradients of complexity and integration changes across source dependency levels. Moreover, the magnitude of the resting state $C_I(X)$ and I(X) differences were generally lowest for the LAP transformation, suggesting that LAP-transformed data provides a conservative estimate of between-condition complexity and integration differences. Thus, when measuring EEG complexity and integration during resting states (or similar tasks that involve ongoing, relatively stationary EEG signals), we recommend use of the Laplacian-transformation due to its positive impact on EEG signal quality, sharpening of source topography, reduction of volume-conduction effects, and the resultant positive effect these have on the measurement of complexity and integration. Although average or infinity references do not reduce volume conduction, their use for the computation of EEG complexity and integration is acceptable in situations when the Laplacian-transformation is precluded (i.e., the expectation of deep cortical sources) and when they can approximate a neutral reference (i.e., when there is sufficient spread and density of electrode coverage across the scalp; Junghöfer et al., 1999; Liu et al., 2015). Furthermore, although we found the average and infinity references to display roughly equivalent performance for the computation of complexity and integration, the infinity reference is to be favored due to its greater accuracy in representing resting state EEG activity (Qin et al., 2010). Finally, we do not recommend use of a linked-mastoid reference for the computation of EEG complexity and integration due to its greater noise levels and tendency to induce artifactual correlations among scalp electrodes.

AUTHOR CONTRIBUTIONS

LT contributed to the experimental design, data collection and analysis, and manuscript preparation. CS and RV contributed to the data collection and analysis, and manuscript preparation.

ACKNOWLEDGMENTS

We thank the manuscript reviewers for their constructive suggestions and comments on earlier drafts of this manuscript.

SUPPLEMENTARY MATERIAL

The Supplementary Material for this article can be found online at: http://journal.frontiersin.org/article/10.3389/fnins.2017.00425/full#supplementary-material

REFERENCES

Adrian, E., and Yamagiwa, K. (1935). The origin of the Berger rhythm. *Brain* 58, 323–351. doi: 10.1093/brain/58.3.323

Bertrand, O., Perrin, F., and Pernier, J. (1985). A theoretical justification of the average reference in topographic evoked potential studies. *Electroencephalogr. Clin. Neurophysiol.* 62, 462–464. doi: 10.1016/0168-5597(85)90058-9

Branston, N. M., El-Deredy, W., and McGlone, F. P. (2005). Changes in neural complexity of the EEG during a visual oddball task. *Clin. Neurophysiol.* 116, 151–159. doi: 10.1016/j.clinph.2004.07.015

Bullmore, E., and Sporns, O. (2009). Complex brain networks: graph theoretical analysis of structural and functional systems. *Nat. Rev. Neurosci.* 10, 186–198. doi: 10.1038/nrn2575

Buzáki, G. (1992). "Network properties of the thalamic clock: role of oscillatory behavior in mood disorders," in *Induced Rhythms in the Brain*, eds E. Başar and T. H. Bullock (New York, NY: Springer Science+Business Media), 235–250

Cuffin, B. N., and Cohen, D. (1979). Comparison of the magnetoencephalogram and electroencephalogram. *Electroencephalogr. Clin. Neurophysiol.* 47, 132–146. doi: 10.1016/0013-4694(79)90215-3

Delorme, A., and Makeig, S. (2004). EEGLAB: an open source toolbox for analysis of single-trial EEG dynamics including independent component analysis. *J. Neurosci. Methods* 134, 9–21. doi: 10.1016/j.jneumeth.2003.10.009

Desmedt, J. E., Chalklin, V., and Tomberg, C. (1990). Emulation of somatosensory evoked potential (SEP) components with the 3-shell head model and the problem of 'ghost potential fields' when using an average reference in brain mapping. *Electroencephalogr. Clin. Neurophysiol.* 77, 243–258. doi: 10.1016/0168-5597(90)90063-j

Dien, J. (1998). Issues in the application of the average reference: review, critiques, and recommendations. *Behav. Res. Methods Instrum. Comput.* 30, 34–43. doi: 10.3758/BF03209414

Dumermuth, G. (1968). "Variance spectra of electroencephalogram in twins. A contribution to the problem of quantification of EEG background activity in childhood," in *Clinical Electroencephalography in Childhood*, eds P. Kellaway and I. Petersén (Stockholm: Almqvist and Wiksell), 119–154.

Dumermuth, G., Walz, W., ScolloLavizzari, G., and Kleiner, B. (1972). Spectral analysis of EEG activity during sleep stages in normal adults. *Eur. Neurol.* 7, 265–296. doi: 10.1159/000114432

Elul, R. (1969). Gaussian behavior of the electroencephalogram: changes during performance of mental task. *Science* 164, 328–331. doi: 10.1126/science.164.3877.328

Fair, D. A., Cohen, A. L., Power, J. D., Dosenbach, N. U. F., Church, J. A., Miezin, F. M., et al. (2009). Functional brain networks develop from a "local to distributed" organization. *PLoS Comput. Biol.* 5:e1000381. doi: 10.1371/journal.pcbi.1000381

Feige, B., Scheffler, K., Esposito, F., Di Salle, F., Hennig, J., and Seifritz, E. (2005). Cortical and subcortical correlates of electroencephalographic alpha rhythm modulation. *J. Neurophysiol.* 93, 2864–2872. doi: 10.1152/jn.00721.2004

Gardiner, J. C., Luo, Z., and Roman, L. A. (2009). Fixed effects, random effects and GEE: what are the differences? *Stat. Med.* 28, 221–239. doi: 10.1002/sim.3478

Geisser, S., and Greenhouse, S. W. (1958). An extension of Box's results on the use of the F distribution in multivariate analysis. *Ann. Math. Stat.* 29, 885–889. doi: 10.1214/aoms/1177706545

Gencer, N. G., Williamson, S. J., Gueziec, R., and Hummel, R. (1996). Optimal reference electrode selection for electric source imaging. *Electroencephalogr. Clin. Neurophysiol.* 99, 163–173. doi: 10.1016/0013-4694(96)95139-1

Holm, S. (1979). A simple sequentially rejective multiple test procedure. *Scand. J. Stat.* 6, 65–70.

Ince, R. A. A., Giordano, B. L., Kayser, C., Rousselet, G. A., Gross, J., and Schyns, P. G. (2017). A statistical framework for neuroimaging data analysis based on mutual information estimated via a gaussian copula. *Hum. Brain Mapp.* 38, 1541–1573. doi: 10.1002/hbm.23471

Jarque, C. M., and Bera, A. K. (1987). A test for normality of observations and regression residuals. *Int. Stat. Rev.* 55, 163–172. doi: 10.2307/1403192

Junghöfer, M., Elbert, T., Tucker, D. M., and Braun, C. (1999). The polar average reference effect: a bias in estimating the head surface integral in EEG recording. *Clin. Neurophysiol.* 110, 1149–1155. doi: 10.1016/S1388-2457(99)00044-9

Jurcak, V., Tsuzuki, D., and Dan, I. (2007). 10/20, 10/10, and 10/5 systems revisited: Their validity as relative head-surface-based positioning systems. *Neuroimage* 34, 1600–1611. doi: 10.1016/j.neuroimage.2006.09.024

Kayser, J. (2009). *Current Source Density (CSD) Interpolation Using Spherical Splines - CSD Toolbox (Version 1.1)*. New York State Psychiatric Institute: Division of Cognitive Neuroscience. Available online at: http://psychophysiology.cpmc.columbia.edu/Software/CSDtoolbox

Kayser, J., and Tenke, C. E. (2006a). Principal components analysis of Laplacian waveforms as a generic method for identifying ERP generator patterns: I. Evaluation with auditory oddball tasks. *Clin. Neurophysiol.* 117, 348–368. doi: 10.1016/j.clinph.2005.08.034

Kayser, J., and Tenke, C. E. (2006b). Principal components analysis of Laplacian waveforms as a generic method for identifying ERP generator patterns: II. Adequacy of low-density estimates. *Clin. Neurophysiol.* 117, 369–380. doi: 10.1016/j.clinph.2005.08.033

Kornguth, S., Steinberg, R., Schnyer, D. M., and Trujillo, L. T. (2013). Integrating the human into the total system: degradation of performance under stress. *Nav. Eng. J.* 125, 85–90.

Lachaux, J.-P., Rodriguez, E., Le Van Quyen, M., Lutz, A., Martinerie, J., and Varela, F. J. (2000). Studying single-trials of phase synchronous activity in the brain. *Int. J. Bifurcat. Chaos* 10, 2429–2439. doi: 10.1142/S0218127400001560

Lachaux, J.-P., Rodriguez, E., Martinerie, J., and Varela, F. J. (1999). Measuring phase synchrony in brain signals. *Hum. Brain Mapp. 8*, 194–208.

Law, S. K., Nunez, P. L., and Wijesinghe, R. S. (1993). High resolution EEG using spline generated surface laplacians on spherical and ellipsoidal surfaces. *IEEE Trans. Biomed. Eng.* 40, 145–153. doi: 10.1109/10.212068

Lay, D. C. (2005). *Linear Algebra and Its Applications, 3rd Edn.* Lebanon: Addison Wesley.

Lee, T.-W., Girolami, M., and Sejnowski, T. J. (1999). Independent component analysis using an extended infomax algorithm for mixed sub-gaussian and super-gaussian sources. *Neural Comput.* 11, 417–441. doi: 10.1162/089976699300016719

Liu, Q., Balsters, J. H., Baechinger, M., van der Groen, O., Wenderoth, N., and Mantini, D. (2015). Estimating a neutral reference for electroencephalographic recordings: the importance of using a high-density montage and a realistic head model. *J. Neural Eng.* 12:056012. doi: 10.1088/1741-2560/12/5/056012

Ma, Y., Mazumdar, M., and Memtsoudis, S. G. (2012). Beyond repeated measures ANOVA: advanced statistical methods for the analysis of longitudinal data in anesthesia research. *Reg. Anesth. Pain Med.* 37, 99–105. doi: 10.1097/AAP.0b013e31823ebc74

Magri, C., Whittinstall, K., Singh, V., Logothetis, N. K., and Panzeri, S. (2009). A toolbox for the fast information analysis of multiple-site LFP, EEG and spike train recordings. *BMC Neurosci.* 10:81. doi: 10.1186/1471-2202-10-81

Misra, N., Singh, H., and Demchuk, E. (2005). Estimation of the entropy of a multivariate normal distribution. *J. Multivar. Anal.* 92, 324–342. doi: 10.1016/j.jmva.2003.10.003

Mosher, J. C., Spencer, M. E., Leahy, R. M., and Lewis, P. S. (1993). Error bounds for EEG and MEG source localization. *Electroencephalogr. Clin. Neurophysiol.* 86, 303–321 doi: 10.1016/0013-4694(93)90043-U

Norwich, K. H. (1993). *Information, Sensation, and Perception.* San Diego, CA: Academic Press, Inc.

Nunez, P. L., Silberstein, R. B., Shi, Z., Carpenter, M. R., Srinivasan, R., Tucker, D. M.,., et al. (1999). EEG coherency II: experimental comparisons of multiple measures. *Clin. Neurophysiol.* 110, 469–486. doi: 10.1016/S1388-2457(98)00043-1

Nunez, P. L., and Srinivasan, R. (2006). *Electric Fields of the Brain: The Neurophysics of EEG, 2nd Edn*. New York, NY: Oxford University Press, Inc.

Nunez, P. L., Srinivasan, R., Westdorp, A. F., Wijesinghe, R. S., Tucker, D. M., Silberstein, R. B., et al. (1997). EEG coherency I: statistics, reference electrode, volume conduction, Laplacians, cortical imaging, and interpretation at multiple scales. *Electroencephalogr. Clin. Neurophysiol.* 103, 499–515. doi: 10.1016/S0013-4694(97)00066-7

Pernier, J., Perrin, F., and Bertrand, O. (1988). Scalp current density fields: concept and properties. *Electroencephalogr. Clin. Neurophysiol.* 69, 385–389. doi: 10.1016/0013-4694(88)90009-0

Perrin, F., Pernier, J., Bertrand, O., and Echallier, J. F. (1989). Spherical splines for scalp potential and current density mapping. *Electroencephalogr. Clin. Neurophysiol.* 72, 184–187. doi: 10.1016/0013-4694(89)90180-6

Perrin, F., Pernier, J., Bertrand, O., and Echallier, J. F. (1990). Corrigenda EEG 02274. *Electroencephalogr. Clin. Neurophysiol.* 76:565. doi: 10.1016/0013-4694(90)90009-9

Perrin, F., Pernier, J., Bertrand, O., Giard, M. H., and Echallier, J. F. (1987). Mapping of scalp potentials by surface spline interpolation. *Electroencephalogr. Clin. Neurophysiol.* 66, 75–81. doi: 10.1016/0013-4694(87)90141-6

Pola, G., Schultz, S. R., Petersen, R. S., and Panzeri, S. (2003). "A practical guide to information analysis of spike trains," in *Neuroscience Databases: A Practical Guide*, ed R. Kötter (New York, NY: Springer Science+Business Media), 139–154.

Pollock, V. E., Schneider, L. S., and Lyness, S. A. (1990). EEG amplitudes in healthy, late-middle-aged and elderly adults: normality of the distributions and correlations with age. *Electroencephalogr. Clin. Neurophysiol.* 75, 276–288. doi: 10.1016/0013-4694(90)90106-T

Qin, Y., Xu, P., and Yao, D. (2010). A comparative study of different references for EEG default mode network: the use of the infinity reference. *Clin. Neurophysiol.* 121, 1981–1991. doi: 10.1016/j.clinph.2010.03.056

Rapp, P. E., Cellucci, C. J., Watanabe, T. A. A., and Albano, A. M. (2005). Quantitative characterization of the complexity of multichannel human EEGs. *Int. J. Bifurcat. Chaos* 15, 1737–1744. doi: 10.1142/S0218127405012764

Royston, J. P. (1983). Some techniques for assessing multivarate normality based on the Shapiro-Wilk W. *J. R. Stat. Soc. Ser. C. Appl. Stat.* 32, 121–133. doi: 10.2307/2347291

Rubinov, M., and Sporns, O. (2010). Complex network measures of brain connectivity: uses and interpretations. *Neuroimage* 52, 1059–1069. doi: 10.1016/j.neuroimage.2009.10.003

Shahbazi, F., Ewald, A., Ziehe, A., and Nolte, G. (2010). "Constructing surrogate data to control for artifacts of volume conduction for functional connectivity measures," in *17th International Conference on Biomagnetism Advances in Biomagnetism—Biomag2010. IFMBE Proceedings*, Vol. 28. eds S. Supek and A. Sušac (Berlin, Heidelberg: Springer), 207–210.

Tenke, C. E., and Kayser, J. (2015). Surface Laplacians (SL) and phase properties of EEG rhythms: simulated generators in a volume-conduction model. *Int. J. Psychophysiol.* 97, 285–298. doi: 10.1016/j.ijpsycho.2015.05.008

Theiler, J., Eubank, S., Longtin, A., Galdrikian, B., and Farmer, J. D. (1992). Testing for nonlinearity in time series: the method of surrogate data. *Physica D* 58, 77–94. doi: 10.1016/0167-2789(92)90102-S

Tian, Y., and Yao, D. (2013). Why do we need to use a zero reference? Reference influences on the ERPs of audiovisual effects. *Psychophysiology* 50, 1282–1290. doi: 10.1111/psyp.12130

Tononi, G. (2004). An information integration theory of consciousness. *BMC Neurosci.* 5:42. doi: 10.1186/1471-2202-5-42

Tononi, G., Edelman, G. M., and Sporns, O. (1998a). Complexity and coherency: integrating information in the brain. *Trends Cogn. Sci.* 2, 474—484. doi: 10.1016/S1364-6613(98)01259-5

Tononi, G., and Koch, C. (2016). Consciousness: here, there and everywhere? *Philos. Trans. R. Soc. Lond. B Biol. Sci.* 370:20140167. doi: 10.1098/rstb.2014.0167

Tononi, G., McIntosh, A. R., Russell, D. P., and Edelman, G. M. (1998b). Functional clustering: identifying strongly interactive brain regions in neuroimaging data. *Neuroimage* 7, 133–149. doi: 10.1006/nimg.1997.0313

Tononi, G., Sporns, O., and Edelman, G. M. (1994). A measure for brain complexity: relating functional segregation and integration in the nervous system. *Proc. Natl. Acad. Sci. U.S.A.* 91, 5033–5037. doi: 10.1073/pnas.91.11.5033

Tononi, G., Sporns, O., and Edelman, G. M. (1996). A complexity measure for selective matching of signals by the brain. *Proc. Natl. Acad. Sci. U.S.A.* 93, 3422–3427. doi: 10.1073/pnas.93.8.3422

Trujillo, L. T., Peterson, M. A., Kaszniak, A. W., and Allen, J. J. B. (2005). EEG phase synchrony differences across visual perception conditions may depend on recording and analysis methods. *Clin. Neurophysiol.* 116, 171–189. doi: 10.1016/j.clinph.2004.07.025

Trujillo, L. T., Stanfield, C. T., and Vela, R. D. (2017). *Resting State EEG Data: EEG Reference/Complexity/Integration Analysis*. Available online at: https://dataverse.tdl.org/dataverse/rsed2017

Trujillo-Ortiz, A., Hernandez-Walls, R., Barba-Rojo, K., and Cupul-Magana, L. (2007). *Roystest: Royston's Multivariate Normality Test. A MATLAB File*. Available online at: http://www.mathworks.com/matlabcentral/fileexchange/loadFile.do?objectId=17811

van Albada, S. J., and Robinson, P. A. (2007). Transformation of arbitrary distributions to the normal distribution with application to EEG test–retest reliability. *J. Neurosci. Methods* 161, 205–211. doi: 10.1016/j.jneumeth.2006.11.004

van Cappellen van Walsum, A.-M., Pijnenburg, Y. A. L., Berendse, H. W., van Dijk, B. W., Knol, D. L., Scheltens, P., et al. (2003). A neural complexity measure applied to MEG data in Alzheimer's disease. *Clin. Neurophysiol.* 114, 1034–1040. doi: 10.1016/S1388-2457(03)00072-5

van Putten, M. J. A. M., and Stam, C. J. (2001). Application of a neural complexity measure to multichannel EEG. *Phys. Lett. A* 281, 131–141. doi: 10.1016/S0375-9601(01)00121-9

Witkowski, S., Trujillo, L. T., Sherman, S. M., Carter, P., Matthews, M. D., and Schnyer, D. M. (2015). An examination of the association between chronic sleep restriction and electrocortical arousal in college students. *Clin. Neurophysiol.* 126, 549–557. doi: 10.1016/j.clinph.2014.06.026

Wolpaw, J. R., and Wood, C. C. (1982). Scalp distribution of human auditory evoked potentials. I. Evaluation of reference electrode sites. *Electroencephalogr. Clin. Neurophysiol.* 54, 15–24. doi: 10.1016/0013-4694(82)90227-9

Yao, D. (2001). A method to standardize a reference of scalp EEG recordings to a point at infinity. *Physiol. Meas.* 22, 693–711. doi: 10.1088/0967-3334/22/4/305

Yao, D. (2002). The theoretical relation of scalp Laplacian and scalp current density of a spherical shell head model. *Phys. Med. Biol.* 47, 2179–2185. doi: 10.1088/0031-9155/47/12/312

Yao, D., Wang, L., Arendt-Nielsen, L., and Chen, A. C. N. (2007). The effect of reference choices on the spatio-temporal analysis of brain evoked potentials: the use of infinite reference. *Comput. Biol. Med.* 37, 1529–1538. doi: 10.1016/j.compbiomed.2007.02.002

Yao, D., Wang, L., Oostenveld, R., Nielsen, K. D., Arendt-Nielsen, L., and Chen, A. C. N. (2005). A comparative study of different references for EEG spectral mapping: the issue of the neutral reference and the use of the infinity reference. *Physiol. Meas.* 26, 173–184. doi: 10.1088/0967-3334/26/3/003

Conflict of Interest Statement: The authors declare that the research was conducted in the absence of any commercial or financial relationships that could be construed as a potential conflict of interest.

frontiers in Neuroscience

ORIGINAL RESEARCH
published: 12 September 2017
doi: 10.3389/fnins.2017.00506

The EEG Split Alpha Peak: Phenomenological Origins and Methodological Aspects of Detection and Evaluation

Elzbieta Olejarczyk[1], Piotr Bogucki[2] and Aleksander Sobieszek[2]*

[1] Nalecz Institute of Biocybernetics and Biomedical Engineering, Polish Academy of Sciences, Warsaw, Poland, [2] Department of Neurology and Epileptology, Medical Center for Postgraduate Education, Warsaw, Poland

Electroencephalographic (EEG) patterns were analyzed in a group of ambulatory patients who ranged in age and sex using spectral analysis as well as Directed Transfer Function, a method used to evaluate functional brain connectivity. We tested the impact of window size and choice of reference electrode on the identification of two or more peaks with close frequencies in the spectral power distribution, so called "split alpha." Together with the connectivity analysis, examination of spatiotemporal maps showing the distribution of amplitudes of EEG patterns allowed for better explanation of the mechanisms underlying the generation of split alpha peaks. It was demonstrated that the split alpha spectrum can be generated by two or more independent and interconnected alpha wave generators located in different regions of the cerebral cortex, but not necessarily in the occipital cortex. We also demonstrated the importance of appropriate reference electrode choice during signal recording. In addition, results obtained using the original data were compared with results obtained using re-referenced data, using average reference electrode and reference electrode standardization techniques.

Keywords: split EEG alpha peaks, functional brain connectivity, directed transfer function, spectral analysis, average reference, reference electrode standardization technique (REST)

OPEN ACCESS

Edited by:
Jorge J. Riera, Florida International University, United States

Reviewed by:
Guido Nolte, Fraunhofer FIRST, Germany
Dezhong Yao, University of Electronic Science and Technology of China, China

****Correspondence:***
Elzbieta Olejarczyk
eolejarczyk@ibib.waw.pl

Specialty section:
This article was submitted to Brain Imaging Methods, a section of the journal Frontiers in Neuroscience

Received: *23 February 2017*
Accepted: *28 August 2017*
Published: *12 September 2017*

Citation:
Olejarczyk E, Bogucki P and Sobieszek A (2017) The EEG Split Alpha Peak: Phenomenological Origins and Methodological Aspects of Detection and Evaluation. Front. Neurosci. 11:506. doi: 10.3389/fnins.2017.00506

INTRODUCTION

There has been increased interest in understanding the mechanisms of generation of one of the basic patterns of electroencephalographic (EEG) activity—alpha waves. An individual alpha frequency depends on many factors, including age, gender, level of sleepiness, or presence of neurological disorder. All these factors can have an impact on the separation of theta and alpha bands (Klimesch, 1999; Garn et al., 2012; Grandy et al., 2013a; Bazanova and Vernon, 2014). Research shows that alpha power is lower in early childhood and in the elderly than in adulthood (Chiang et al., 2011; Cottone et al., 2013; Grandy et al., 2013b; Ponomareva et al., 2013; Soroko et al., 2014; Vysata et al., 2014; Miskovic et al., 2015; Zappasodi et al., 2015), and that alpha peak frequency is higher in females than in males in posterior parts of the brain (Langrova et al., 2012; Garces et al., 2013). Moreover, alpha power decreases and theta power increases during the transition from wakefulness to sleep (Klimesch, 1999). Change in spectral characteristics of EEG patterns has also been observed in various neurological disorders (Garces et al., 2013; Ponomareva et al., 2013; Zappasodi et al., 2014; Vollebregt et al., 2015).

It is well-known that the amplitude of alpha is higher at occipital relative to frontal derivations, and that alpha peak frequency is higher at occipital relative to frontal electrodes. The frequency difference in alpha peaks between frontal and occipital lobes can result in overlapping double peaks, so called "split alpha." The split alpha effect was predicted by a model of alpha rhythm generation (Robinson et al., 2001, 2003; O'Connor and Robinson, 2004; Xiong and Yao, 2005; Gray and Robinson, 2013), and was previously observed in a study of healthy volunteers (Chiang et al., 2011). Chiang et al. developed a method for the automatic identification of multiple alpha peaks in EEG data (Chiang et al., 2008).

Robinson et al. (2003) studied a modified model of the corticothalamic system and demonstrated that splitting of the spectral alpha peak can result from spatial brain heterogeneity. Alpha frequency and power are greater in occipital part of the brain compared to the frontal ones. Dominance of the occipital alpha power seems to be driven by a decrease in cortical and an increase in thalamic activity, while the frequency shift may be driven by a decrease in the corticothalamic propagation delay (O'Connor and Robinson, 2004). Spatial heterogeneity may be associated with the diversity of functions associated with lower (8–11 Hz) and higher (11–13 Hz) frequency alpha. Specifically, upper alpha is implicated in cortical processes related to semantic memory, whereas low alpha is implicated in processes related to attention (Klimesch, 1999). Increased upper alpha and decreased lower alpha power have been observed in patients with mild cognitive impairment and Alzheimer's disease, relative to normal elderly subjects (Moretti et al., 2012; Ponomareva et al., 2013).

The aim of this paper was to explain the mechanism of split alpha generation. EEG signals were analyzed using spatiotemporal maps of EEG amplitude and spectral analysis. In addition, Directed Transfer Function (DTF), a method used to evaluate functional brain connectivity, was used to determine the sources of alpha activity with different peak frequencies. We have demonstrated that the mechanism of split alpha generation is much more complicated than was predicted by the Robinson et al. model. In particular, we found that choice of reference electrode and the window size were important factors in the identification of split alpha.

MATERIALS AND METHODS

Subjects

EEG was performed in a group of 27 patients who varied in age and sex (23 females, 4 males; mean age: 29.9 ± 11.5 years), and consisted primarily of ambulatory patients with headache, fainting, loss of consciousness, or epilepsy. Patient EEG data were included in analyses if they demonstrated adequate expression of alpha waves.

EEG Registration and Preprocessing

EEG data were acquired with the sampling frequency of 250 Hz in a standard 10–20 system of electrode placement using ELMIKO EEG DigiTrack™ Recording System with 19 EEG channels: Fp1, Fp2, F7, F3, Fz, F4, F8, T7, C3, Cz, C4, T8, P7, P3, Pz, P4, P8, O1, O2. Depending on the specified recording conditions, the original EEG signal was recorded using four different reference electrodes: linked earlobes (A1–A2), neck (NK), chin (S1), and frontal (AFz).

Then, the data were re-referenced using average reference electrode (AVERAGE) (Nunez and Srinivasan, 2006) and reference electrode standardization techniques (REST) (Yao, 2001; Zhai and Yao, 2004; Yao et al., 2005). REST is a method that allows for the transformation of original EEG data—with the reference electrode placed at an arbitrary point on the head—to a new dataset with the reference at infinity and the potential at zero or a constant. This transformation was performed using the freely available REST Toolbox (http://www.neuro.uestc.edu.cn/rest/). The procedure is based on the calculation of the leadfield matrix for the canonical concentric-three-spheres head model.

Next, the current source density (CSD) or scalp surface Laplacian was estimated from the transformed EEG data to reduce the impact of volume conduction (Kayser and Tenke, 2006a,b, 2015; Kayser, 2009). These calculations were performed using a spherical spline algorithm (Perrin et al., 1989, 1990; Jurcak et al., 2007) in the CSD Toolbox (http://psychophysiology.cpmc.columbia.edu/Software/CSDtoolbox/).

Spatiotemporal and Spectral Analysis

Spatiotemporal maps of EEG patterns were analyzed using the EEG Time-Potential Mapping Module of ELMIKO EEG DigiTrack™ Recording System, which is widely used in clinical practice (Sobieszek, 2009, 2013, 2015).

The power spectrum density (PSD) of EEG signal for each channel was calculated in the range of alpha band from 8 to 13 Hz. Maps of relative spectral power were estimated for different frequency ranges (theta: 4–7 Hz; alpha: 7–8, 8–10, 10–13 Hz; beta: 13–25 Hz).

Directed Transfer Function (DTF)

DTF is a measure based on Granger Causality, but is defined in the frequency domain (Kaminski and Blinowska, 1991).

For a multivariate k-channel process, $\mathbf{X}(t) = [X_1(t), X_2(t),..., X_k(t)]^T$, the multivariate autoregressive model takes the form:

$$\mathbf{X}(t) = \sum_{m=1}^{p} \widehat{\mathbf{A}}(m) \cdot \mathbf{X}(t-m) + \mathbf{E}(t) \tag{1}$$

where $\mathbf{E}(t)$ is a k–dimensional vector, $\widehat{\mathbf{A}}$ is a square k × k matrix.

We can rewrite (Equation 1) in the form;

$$\begin{aligned} \mathbf{E}(t) &= \sum_{m=0}^{p} \widehat{\mathbf{A}}(m) \cdot \mathbf{X}(t-m) \\ \mathbf{A}(0) &= \mathbf{I}, \mathbf{A}(m) = \widehat{\mathbf{A}}(m) \; for \; m = 1, ..., p \end{aligned} \tag{2}$$

Transforming the multivariate autoregressive model to the frequency domain, we obtain:

$$\begin{aligned} &\mathbf{E}(f) = \mathbf{A}(f)\mathbf{X}(f), \; where \; \mathbf{A}(f) = -\sum_{m=1}^{k} \mathbf{A}(m) \cdot e^{-i \cdot 2\pi \cdot f \cdot m} \\ &\rightarrow \mathbf{X}(f) = \mathbf{A}^{-1}(f)\mathbf{E}(f) = \mathbf{H}(f)\mathbf{E}(f) \end{aligned} \tag{3}$$

The matrix of coefficients $\mathbf{H}(f)$ is called the transfer matrix.

The DTF is defined as a normalized version of the transfer matrix:

$$DTF^2_{j\to i}(f) = \frac{\left|H_{ij}(f)\right|^2}{\sum_{j=1}^{k}\left|H_{ij}(f)\right|^2} \quad (4)$$

In the calculation of DTF, the product of the model order and the number of EEG channels must be several times smaller than the number of the samples in the analyzed signal (Blinowska and Kaminski, 2006). In this study, the model order was equal to 10 and the number of EEG channels was 19. The DTF was calculated for 2-, 4-, and 8-s segments sampled with frequency of 250 Hz, and the rule was found to be satisfied.

Relation between Power Spectrum and DTF

The power spectrum and DTF have the following relationship (Blinowska et al., 2004):

$$\mathbf{S}(f) = \mathbf{X}(f)\mathbf{X}^{+}(f) = \mathbf{H}(f)\mathbf{E}(f)\mathbf{E}^{+}(f)\mathbf{H}^{+}(f) = \mathbf{H}(f)\mathbf{V}\mathbf{H}^{+}(f) \quad (5)$$

where $\mathbf{V} = \mathbf{E}(f)\mathbf{E}^{+}(f)$ is the spectral matrix of input white noise processes that does not depend on frequency; + refers to the Hermitean transpose, i.e., the composition of transposition and complex conjugation of a matrix.

The power spectrum, $\mathbf{S}(f)$, depends only on the EEG amplitude. The power spectrum does not depend on the phase of the signal, which gives information about the time relations between signals, and therefore enables the estimation of directionality of the EEG activity propagation. Moreover, the source of EEG activity does not necessarily have to be located at the power spectrum maximum (Kaminski et al., 1997). Thus, the DTF provides additional information to the spectral analysis regarding the localization of generators and the directionality of signal propagation.

The multivariate model used in the DTF calculation already includes all EEG signals and their relations. Thus, the method provides the whole spectral matrix at once, with auto-spectra on the diagonal and cross-spectra on the off-diagonal. The power spectra presented in this paper correspond to the auto-spectra derived from the DTF method.

Indices Based on Graph Theory

In graph theory, the brain is modeled as a graph composed of nodes, representing brain regions (i.e., the EEG channels, here), and links between the nodes, representing functional connections (i.e., the magnitude and directionality of DTF, here).

For each of the obtained graphs, three indices were calculated: density, degree, and strength (Rubinov and Sporns, 2010). The *degree* of an individual node is equal to the number of links connected to that node, and reflects the relative importance of a node in the network. The mean network degree is commonly used as a measure of the graph *density*, or the total "wiring cost" of the network. The directed variant of the degree distinguishes the number of inward links from the number of outward links, while the weighted variant of the degree, termed the *strength*, is defined as the sum of all neighboring link weights.

RESULTS

The spectral analysis allows for the identification of split alpha effect, i.e., the presence of two or more peaks with close frequencies in the power spectrum. However, the observed power spectrum depends strongly on choice of reference electrode (Yao et al., 2005), and may therefore influence the split alpha effect. In our data, several patients illustrate the impact of choice of reference electrode, in addition to window size and volume conduction.

The Impact of Window Size on the Identification of Split Alpha

Figures 1A,B illustrates that patterns of spectral power distribution (SPD) depend on choice of window size. EEG was recorded in three window durations: 2-, 4-, and 8-s. **Figures 1A,B** shows the relative SPD in the first patient, a 27-year-old woman. The split in higher alpha (10–13 Hz) is clearly visible in the shorter, 2-s window. In the longer, 8-s window however, two peaks were observed in the SPD with maximum at electrodes O2 and T4 in theta and low alpha bands, and a broad SPD in the higher alpha range (see **Figure 1B**). Maps of the relative power spectra are shown separately in five frequency bands (theta: 4–7 Hz; alpha: 7–8, 8–10, 10–13 Hz; beta: 13–25 Hz) in **Figure 1C**. Increased level of relative power spectrum can be seen clearly at electrodes T4 and O2 in theta (4–7 Hz) and low alpha (7–8 Hz) ranges (areas marked with yellow and red color in **Figure 1C**). Moreover, high level of relative power spectrum is observed in the posterior part of the brain, with dominance in the right hemisphere at electrode O2 in the higher alpha band (10–13 Hz).

Comparison of Bipolar Montage with Monopolar Montage

Next, we tested the importance of the location of the reference electrode. **Figure 2** shows a comparison of EEG patterns recorded from a second patient (28-year-old woman) using two montages: bipolar (BIP) and monopolar. Four different reference electrodes were evaluated in the examined patients: linked earlobes (A1–A2), neck (nk), chin (S1), and frontal (AFz). Only the monopolar montages allowed for the correct localization of alpha waves' generators. The effect of split alpha is clearly observed in the PSD for both montages. However, comparing the PSD obtained with the bipolar montage (see **Figure 2A**) with that obtained with the monopolar one (c.f. **Figure 2B**) revealed the existence of hemispheric asymmetry with dominance of lower frequency alpha in the left hemisphere, and higher frequency alpha in the right hemisphere. The highest relative power spectrum was observed in the posterior part of brain (O1, O2) in higher alpha band (10–13 Hz). A dominance of lower alpha band (8–10 Hz) in the left hemisphere is also evident (see **Figure 2C**).

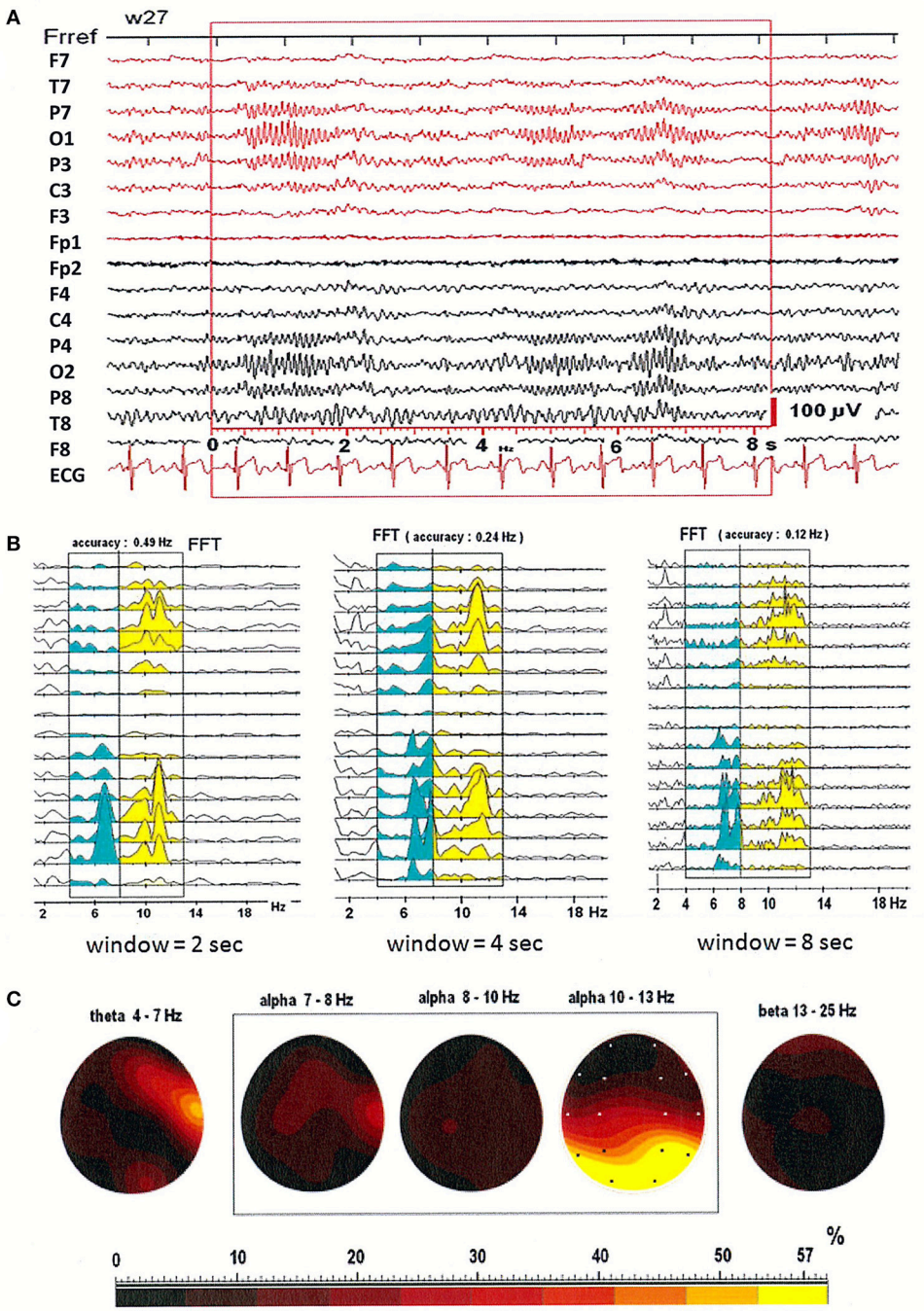

FIGURE 1 | (A) EEG recording in the first patient, a 27-year-old woman; **(B)** The power spectral density calculated for 2-, 4-, and 8-s windowed segments of the EEG record; **(C)** The relative power spectra for five frequency bands (theta: 4–7 Hz; alpha: 7–8, 8–10, 10–13 Hz; beta: 13–25 Hz) for a segment of data.

Usefulness of Spatiotemporal Maps of EEG Patterns in Daily Clinical Practice

Inspection of the spatiotemporal map of the EEG pattern in one patient revealed the existence of two sources of alpha waves, localized mainly in the occipital derivations (O1 or O2; see **Figure 3**). Slightly different oscillation frequencies suggest that the right hemisphere is more likely to generate the alpha rhythm. The segment was divided into six parts (see a–f in **Figure 3C**). The first cycle (designated with the numbers from 1 to 4 in **Figure 3A**) started with the minimum EEG amplitude at O2 (marked as a blue spot) and ended with the maximum amplitude at O1 (marked as a red spot). The next cycle (marked with the numbers from 5 to 7) ended with the maximal amplitude at the second generator, localized

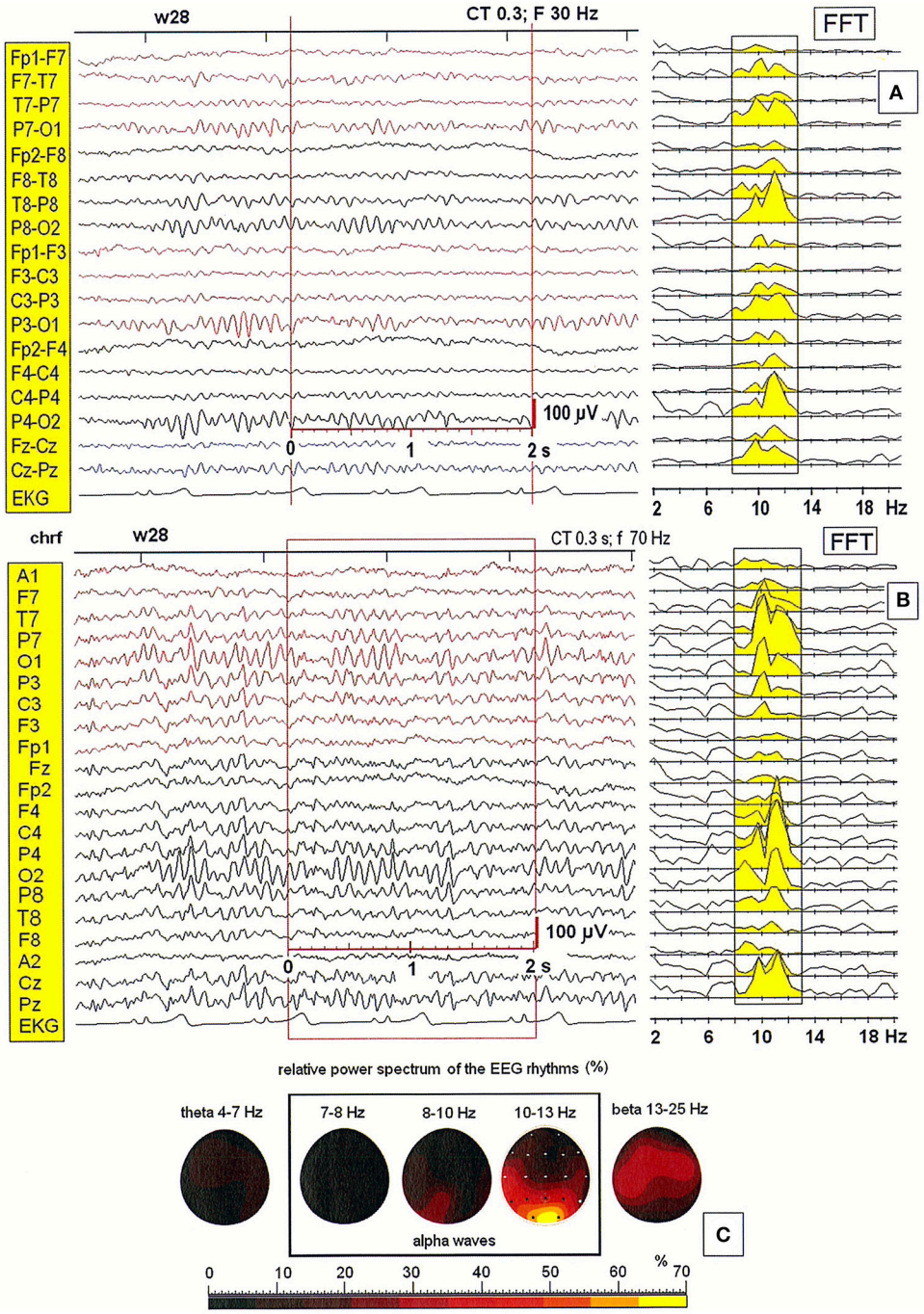

FIGURE 2 | (A,B) EEG recording and the power spectral density calculated for the 2-s segment of the EEG record in the second patient (28-year-old woman), recorded using two different montages: bipolar and monopolar (S1); **(C)** The relative power spectra for five frequency bands (theta: 4–7 Hz; alpha: 7–8, 8–10, 10–13 Hz; beta: 13–25 Hz) for a segment of data.

at O2. The synchronization of both sources subsequently occurred (at points 8 and 9). Of note, this system is not stable due to slowing of activity in the left hemisphere, which is clearly visible in the amplitude changes marked with the numbers from 16 to 21 (cf. **Figure 3B**). The activity at O2 (at point 16, 18, and 20) occurs before activity at O1 (at point 17, 19, and 21), suggesting that the source located at this electrode acts as a driver of the process. This was verified by analyzing the connectivity pattern using the DTF (data not shown).

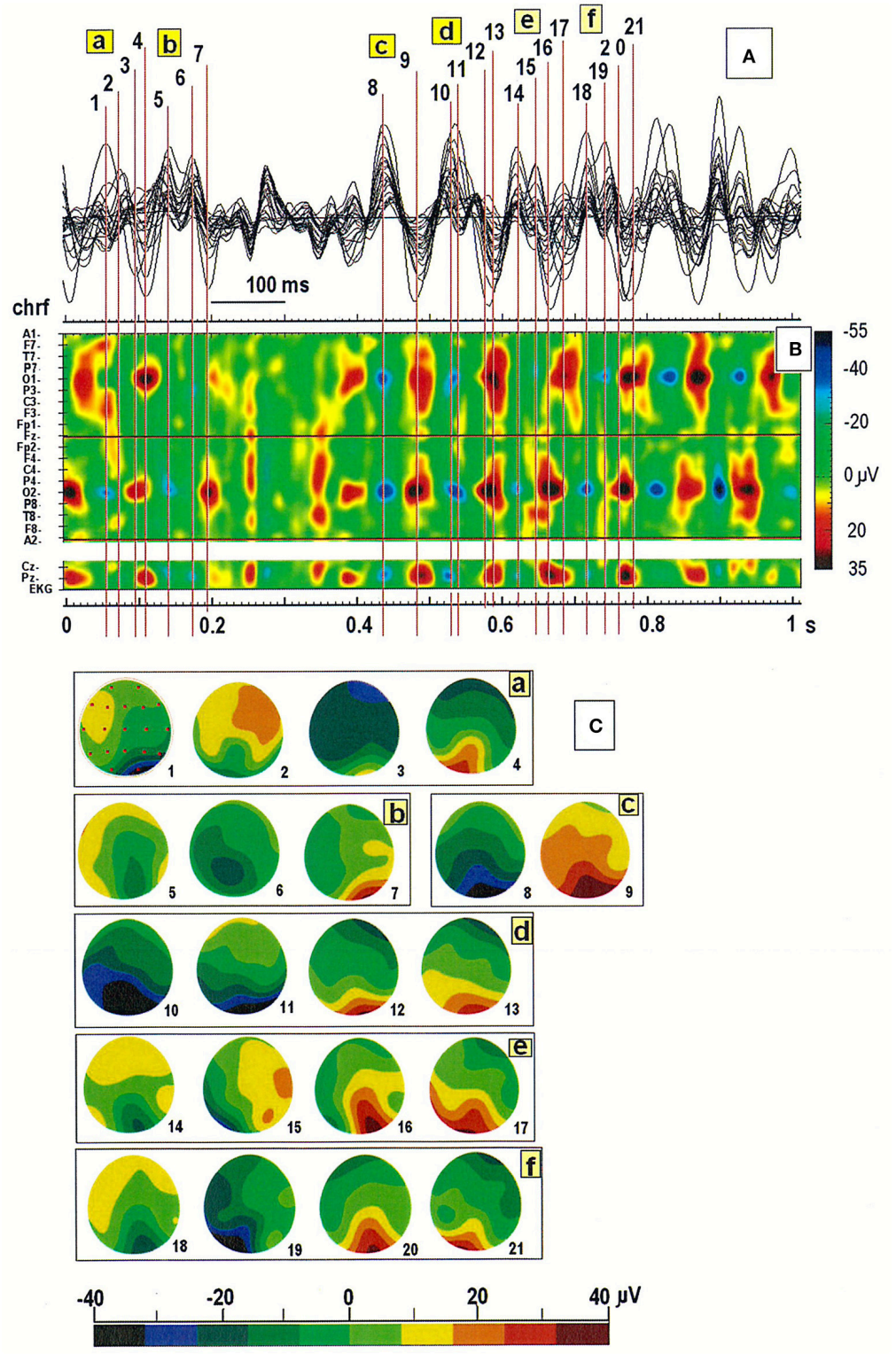

FIGURE 3 | (A) Superimposition of a 1-s segment of the EEG record in the same patient as in **Figure 2**; **(B)** Spatiotemporal map of this segment; **(C)** Six cycles in the EEG recording marked with the letters a-f in **(A,B)**. Individual map corresponds to the relative numbers from 1 to 21 in **(A,B)**.

The Importance of Appropriate Choice of Reference Electrode during EEG Recording: Existence of Alpha Rhythm Generators Outside the Occipital Lobe

Both cases discussed above illustrate the existence of generators localized in posterior areas, particularly at derivations O1 and O2. Alpha rhythms can be also generated in other parts of the brain. The coexistence of several generators was demonstrated in the third patient, a 54-year-old woman (see **Figure 4**). The localization of generators depends on the choice of the reference electrode. The EEG signal was first registered to a reference electrode placed on the neck. This registration showed a maximum of the relative power spectrum of alpha band (8–10 Hz) in frontal and left occipital regions of the brain (see **Figure 4**). The same signal was then re-referenced to the linked earlobes reference (A1–A2). Here, the maximum of the relative power spectrum was localized to the posterior part of brain in left and right hemispheres, which was accompanied by a decrease of the relative power spectrum in frontal cortex. Next, the DTF was calculated to localize the generators and identify the directionality of EEG activity propagation and DTF strength (c.f. **Figures 6A,B**). The DTF was presented in each 1 Hz-frequency interval in the range of alpha bands. The dominance of the generator at O1 for both montages was verified (see graphs in **Figures 6A,B**). In addition, other generators were identified when the reference was placed on the neck, with one at P8 (with maximum strength at 9–10 Hz) and another at O2 (with maximum strength at 11–12 Hz). These DTF results changed dramatically when the signal was re-referenced to the linked earlobes (cf. **Figure 6B**). A second generator was identified at electrode Pz, which dominated for frequency of 10 Hz. Therefore, our data show that generators do not necessarily need to be localized in occipital or frontal parts of the brain, as was predicted by the Robinson et al. model (Robinson et al., 2001, 2003).

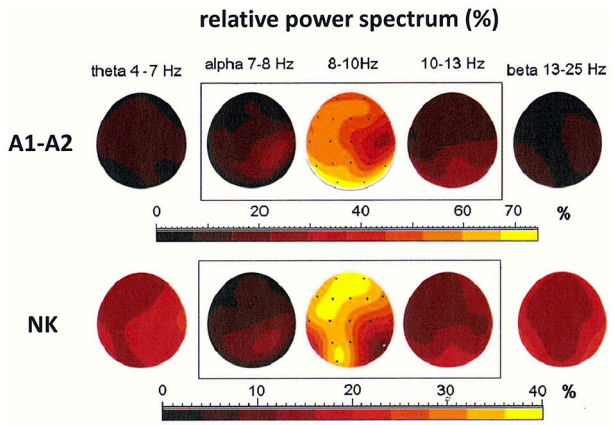

FIGURE 4 | Relative power spectrum calculated for a 2-s segment of the EEG record in the third patient (54-year-old woman), recorded using two reference electrodes: linked earlobes (A1–A2) and neck (NK). The relative power spectrum is presented in five frequency bands (theta: 4–7 Hz; alpha: 7–8, 8–10, 10–13 Hz; beta: 13–25 Hz).

Effect of Data Re-Referencing (AVERAGE and REST)

The effect of data re-referencing is illustrated in **Figures 5**, **6**. The power spectral density (PSD) of the 4-s segment of original EEG recorded in the third patient (54-year-old woman) is shown separately for each of four reference electrodes (NK, A1-A2, AVERAGE, and REST) in **Figure 5**. The frequency of split alpha peaks and the spatial distribution over the scalp surface are influenced strongly by choice of reference electrode.

The original data were re-referenced from the neck (NK) to the linked earlobes (A1–A2). The data referenced to the linked earlobes revealed two split alpha patterns: one in the occipital-parietal regions of brain and the second in frontal-central regions of brain. These patterns demonstrated a common dominant frequency of 9.5 Hz, but differed in the frequency of the second peak (8.5 Hz in the frontal-central lobe and 10 Hz in the occipital-parietal lobe; see **Figures 5A,B**).

The application of other reference electrodes (AVERAGE and REST) resulted in the reduction of low-frequency peak in frontal channels, and a sharpening of the peak at 9.5 Hz frequency (see **Figures 5C,D**). For the REST, the low-frequency alpha peak at the left and right temporal-parietal derivations (T7, T8, P7, P8) was appeared (see **Figure 5D**). Thus, it is likely that split alpha may result from an interaction between the occipital and temporo-parietal areas, rather than between left and right occipital hemispheres. However, this hypothesis can only be verified by applying REST to a high-density EEG dataset.

The strength of outward connections calculated from the adjacency matrices of DTF is presented for each of the four reference electrodes in **Figure 6**. Re-referencing the original EEG data to the linked earlobes reference (A1–A2) caused a reduction in strength at right parieto-occipital derivations (P4, P8, and O2), and an increase in strength at the central derivations (see Fz and Pz in **Figures 6A,B**). The results for the average reference also highlight the role of right frontal and parietal derivations (see F4, F8, and P8 in **Figure 6C**). The most outstanding results were obtained using the REST (cf. **Figure 6D**). The strength at electrode P8 was much higher than strength observed at other derivations. Interestingly, strength at occipital derivations was significantly reduced, reaching levels in both hemispheres that were comparable to levels observed in other channels in posterior brain regions.

The spatial distribution of the strongest 60% of connections between EEG channels are presented in graphs in **Figure 6**, for three frequencies (7, 8, and 10 Hz).

The Impact of Volume Conduction on the Identification of Split Alpha

The impact of volume conduction on the identification of split alpha is illustrated in **Figure 7**. The PSD of transformed data using the CSD transformation of the original EEG with the reference electrode placed at NK is showed in **Figure 7B**. The characteristic pattern of split alpha was completely abolished by the application of the CSD transform. In addition, although a few peak frequencies were still visible, their spatial distribution became disjointed. Comparing the PSD of the original EEG

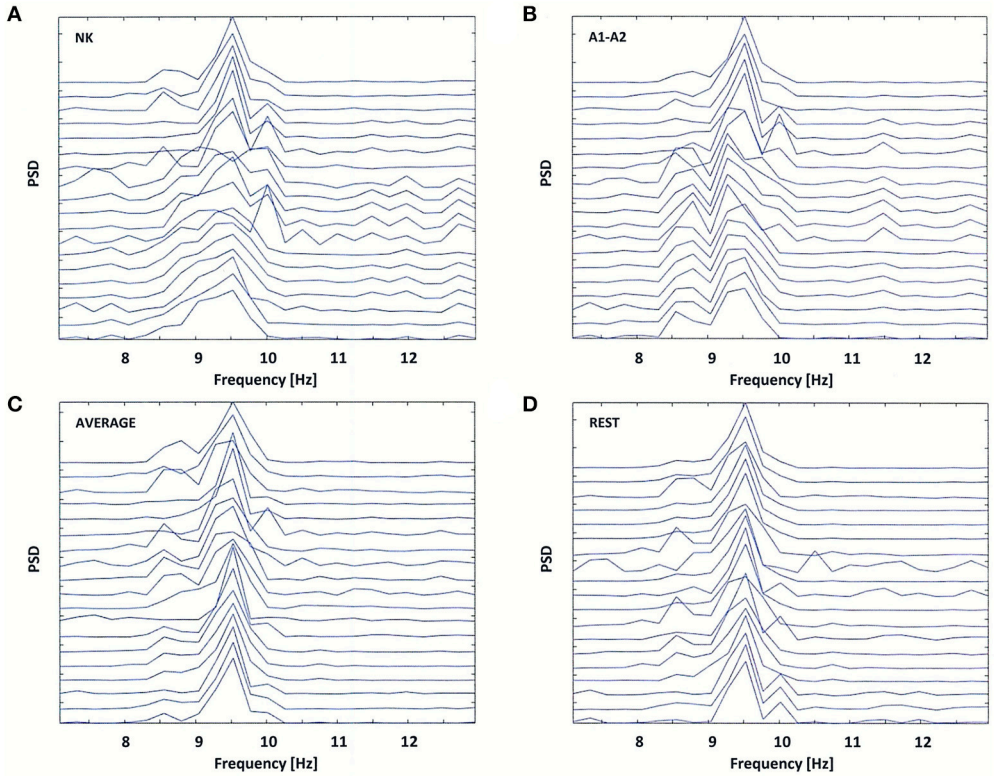

FIGURE 5 | Power Spectral Density (PSD) for the same EEG segment as in **Figure 4 (A)**, and for the re-referenced data to: **(B)** linked earlobes reference (A1–A2), **(C)** average reference electrode (AVERAGE), and **(D)** reference electrode standardization techniques (REST).

(see **Figure 5A**) with that of the transformed data (cf. **Figure 7B**), there was a shift in the dominant frequency of 9.5 Hz from the occipital lobe (the last seven channels: P7, P3, Pz, P4, P8, O1, O2) to the frontal lobe. In addition, the high-frequency alpha (10 Hz) was replaced by the low-frequency alpha (8.5–9 Hz).

Pearson correlation coefficients (R) between the PSD calculated for the CSD and the PSD for the four reference electrodes (NK, A1-A2, AVERAGE, REST) are presented in **Figure 7C**. The highest R values were between CSD and AVERAGE at almost all EEG derivations, and only at a few electrode locations did REST correlated with the CSD better than the AVERAGE (F3, Fz, T7, P3).

Figure 7D shows the average strength of outward links calculated with the transformed data using the CSD transform and with the four reference electrodes. These graphs were created by averaging the strength of outward links over all frequencies in the alpha band (from 7 to 13 Hz) shown in **Figure 7A**. Evaluating the results presented in **Figure 7**, reduction of volume conduction by applying the CSD transform resulted in an increase in strength of connections, particularly at the frontal derivations (Fp1, Fp2, F7), and a decrease in strength at central posterior derivation (Pz). Statistically significant differences ($p < 0.05$) between the CSD and each of the four reference electrodes were found for almost all EEG derivations, excluding C4, P4, and O1 for NK, T7, and C3 for A1–A2, T7, C3, O1, and O2 for AVERAGE.

DISCUSSION

Careful examination of the spatiotemporal maps of the EEG recordings, together with spectral analysis and analysis of connectivity using DTF, allowed for better explanation of the mechanism of split alpha effect generation. The SPD analysis allowed for the identification of at least two peaks with close frequencies in the alpha frequency range, consistent with the so called "split alpha" effect. The impact of window size on split alpha identification was tested, and a window size of 2 s was found to be optimal for this purpose. Next, the localization of split alpha peaks was examined using maps of the relative power spectra. These maps allowed us to compare the spatial distribution of power spectra in separate frequency bands (theta: 4–7 Hz; alpha: 7–8, 8–10, 10–13 Hz; beta: 13–25 Hz). We also calculated DTF, which allowed us to localize the generators and identify the directionality of EEG activity propagation. The index strength was calculated at every EEG channel to examine the importance of individual nodes in the network. Finally, spatiotemporal analysis of EEG amplitude evidenced several sources of alpha waves that underwent a dynamical process. One of the hemispheres was more likely to generate an alpha rhythm, which may be due to the slightly different oscillation frequencies of the two interconnected generators (i.e., O1 and O2).

Robinson et al. predicted the split alpha effect by analyzing a modified model of alpha rhythm generator (Robinson et al., 2001,

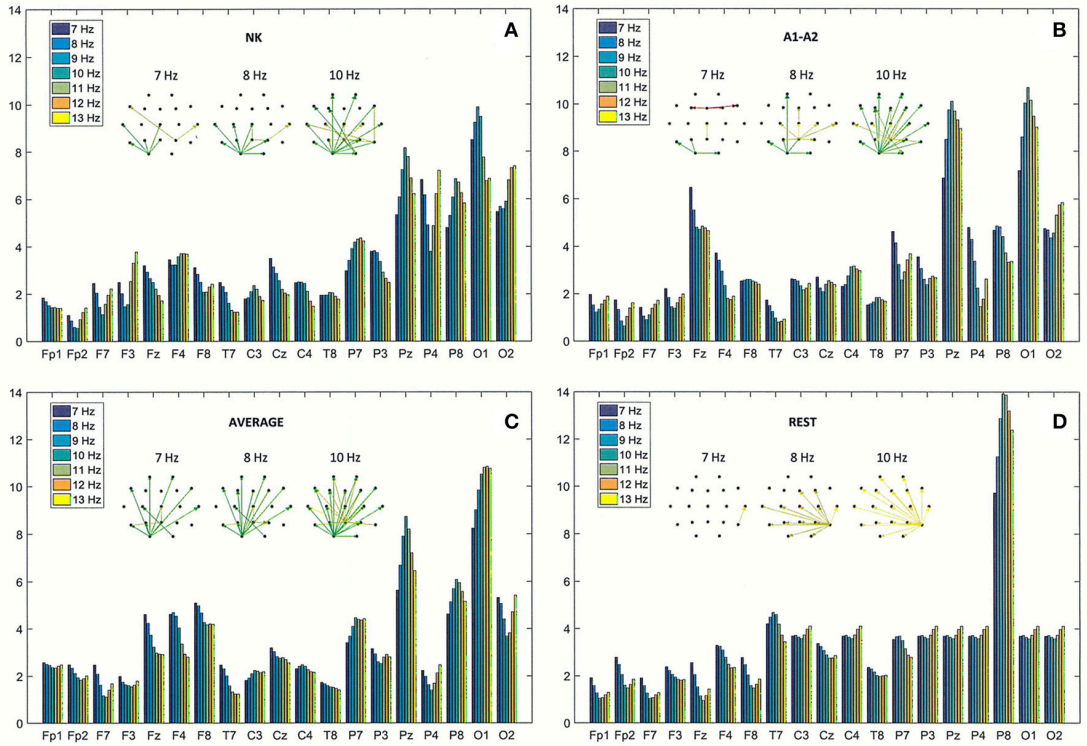

FIGURE 6 | Directed Transfer Function (DTF) strength of outward links for the same EEG segment as in **Figure 4 (A)**, and for the re-referenced data to: **(B)** linked earlobes reference (A1–A2), **(C)** average reference electrode (AVERAGE), and **(D)** reference electrode standardization techniques (REST). Each chart contains graphs that represent the strongest 60% of connections between EEG channels, determined by the magnitudes and directions of the DTF calculated for three frequencies (7, 8, and 10 Hz).

2003). They concluded that the frequency difference between two generators localized in frontal and occipital lobes could result in overlapping double peaks. In this study, we demonstrated that split alpha can be generated from the interaction between at least two distant alpha generators located in different brain regions that are not necessarily in occipital or frontal lobes. Moreover, the mechanism of split alpha generation may differ by individual, and hemispheric and fronto-posterior asymmetry may impact this variability. A decrease in cortico-cortical and cortico-thalamic propagation delay may also contribute to the frequency shift.

In this study, we evaluated, for the first time, the impact of reference electrode placement on the split alpha effect. Our data demonstrate the importance of reference electrode placement at the level of signal recording. Indeed, our results suggest that the monopolar montage with a reference electrode placed in an appropriate head position allows for better localization of alpha waves generators. Results obtained with the original data were also compared with results of re-referenced data, using the average reference electrode (AVERAGE) (Nunez and Srinivasan, 2006) and reference electrode standardization techniques (REST) (Yao, 2001, 2017; Zhai and Yao, 2004; Yao et al., 2005). The AVERAGE and REST techniques may be more appropriate, however, for application in high-density EEG recordings, which yield low re-referencing reconstruction errors (Liu et al., 2015). For low-density EEG recordings (e.g., 21-channel montage), the average global relative error of AVERAGE and REST from a three-layer spherical model was estimated to be ∼21 and ∼13%, respectively (Liu et al., 2015). However, in clinical practice the standard 10–20 system with 19 electrodes is more frequently used to evaluate EEG data in ambulatory patients. In such circumstances, more conventional references such as linked earlobes (A1–A2), neck (NK), or chin (S1), are still useful. It is important to note, however, which reference is used in each specific case. As a general rule, the reference electrode should be placed as far as possible from the source of brain activity. Further work is needed to better understand the mechanisms of split alpha generation using high-density EEG data with AVERAGE and REST techniques. Future work should also evaluate the impact of age on mechanisms of split alpha generation, particularly in healthy subjects who range widely in age.

Of note, the problem of volume conduction should be considered when the DTF method is applied (Kaminski and and Blinowska, 2017). CSD (Kayser and Tenke, 2006a,b, 2015; Kayser, 2009) may be one solution. However, also in this case a high-density EEG data should be analyzed.

CONCLUSIONS

We found that the split alpha peak was a common phenomenon observed in EEG data. However, identification of this phenomenon depended on several methodological choices.

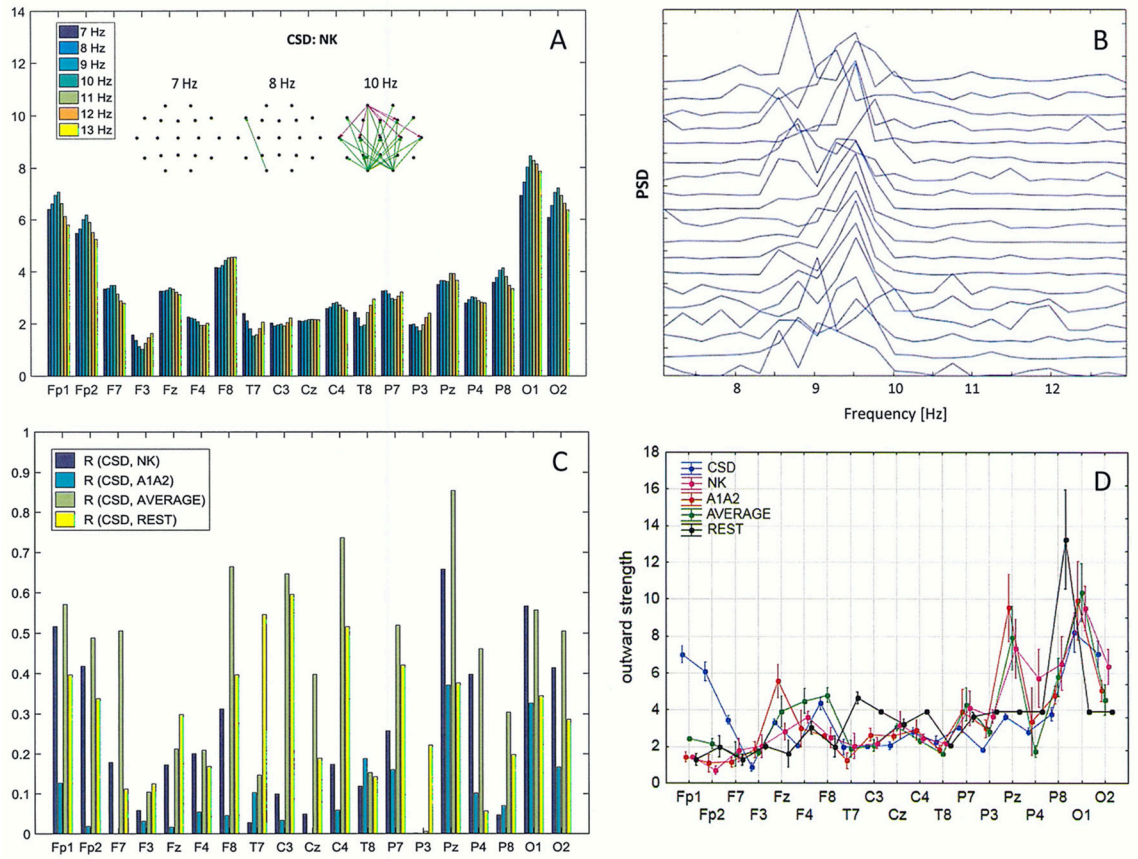

FIGURE 7 | Impact of volume conduction on the identification of split alpha. **(A)** Directed Transfer Function (DTF) strength of outward links for the transformed data using the CSD transformation of the original EEG with the reference electrode placed at NK. Graphs represent the strongest 60% of connections between EEG channels, determined by the magnitudes and directions of the DTF calculated for three frequencies (7, 8, and 10 Hz). **(B)** Power Spectral Density (PSD) for the same data as in **(A)**. **(C)** Pearson correlation coefficients between CSD and four reference electrodes (NK, A1A2, AVERAGE, REST) at every EEG derivation. **(D)** Comparison of the average strength of outward links calculated for the transformed data using the CSD transform and for each of the four reference electrodes (NK, A1–A2, AVERAGE, REST).

For occipital alpha wave generators, the presence of occipital split alpha peaks may be associated with variation in interhemispheic connectivity, which leads to relatively independent activity of occipital alpha wave generators in left and right hemispheres.

The example re-referenced data using the REST technique suggested that the split alpha effect may be driven by an interaction between the occipital and temporo-parietal areas, rather than between left and right occipital lobes. This hypothesis should be confirmed by applying the REST technique to high-density EEG data.

CSD is frequently used to reduce the effect of volume conduction. Another feature of the CSD transform is it is free from reference effects, so the highest correlation between CSD and REST should be expected. However, our data showed that CSD correlated better with AVERAGE than with REST, which may be due to the use of low-density EEG data.

In sum, our data suggest that recording montage, duration of the analytical window, and EEG activity dynamics should be considered when collecting and analyzing EEG data. Our results demonstrate an association between the composition of the SPD within alpha wave frequencies and connectivity patterns between different alpha rhythm generators.

ETHICS STATEMENT

This study was carried out in accordance with the recommendations of Ethics Committee of the Medical Centre for Postgraduate Education in Warsaw, Poland with written informed consent from all subjects.

AUTHOR CONTRIBUTIONS

EO: Conception of the work, EEG analysis, wrote the manuscript; PB: Conception of the work, acquisition of EEG data; wrote the manuscript; AS: Conception of the work, interpretation of EEG data, wrote the manuscript.

REFERENCES

Bazanova, O. M., and Vernon, D. (2014). Interpreting EEG alpha activity. *Neurosci. Biobehav. Rev.* 44, 94–110. doi: 10.1016/j.neubiorev.2013.05.007

Blinowska, K. J., and Kaminski, M. J. (2006). "Multivariate signal analysis by parametric models," in *Handbook of time Series Analysis. Recent Theoretical Developments and Applications*, eds B. Schelter, M. Winterhalder, and J. Timmer (Wernheim: Wiley – VCH), 373–411. doi: 10.1002/9783527609970.ch15

Blinowska, K. J., Kus, R., and Kaminski, M. J. (2004). Granger causality and information flow in multivariate processes. *Phys. Rev. E Stat. Nonlin. Soft Matter. Phys.* 70(5 Pt 1):050902. doi: 10.1103/PhysRevE.70.050902

Chiang, A. K. I., Rennie, C. J., Robinson, P. A., Roberts, J. A., Rigozzi, M. K., Whitehouse, R. W., et al. (2008). Automated characterization of multiple alpha peaks in multi-site electroencephalograms. *J. Neurosci. Methods* 168, 396–411. doi: 10.1016/j.jneumeth.2007.11.001

Chiang, A. K. I., Rennie, C. J., Robinson, P. A., van Albada, S. J., and Kerr, C. C. (2011). Age trends and sex differences of alpha rhythms including split alpha peaks. *Clin. Neurophysiol.* 122, 1505–1517. doi: 10.1016/j.clinph.2011.01.040

Cottone, C., Tomasevic, L., Porcaro, C., Filligoi, G., and Tecchio, F. (2013). Physiological aging impacts the hemispheric balances of resting state primary somatosensory activities. *Brain Topogr.* 26, 186–199. doi: 10.1007/s10548-012-0240-3

Garces, P., Vicente, R., Wibral, M., Pineda-Pardo, J. A., Lopez, M. E., Aurtenetxe, S., et al. (2013). Brain-wide slowing of spontaneous alpha rhythms in mild cognitive impairment. *Front. Aging Neurosci.* 5:100. doi: 10.3389/fnagi.2013.00100

Garn, H., Waser, M., Lechner, M., Dorfer, M., and Grossegger, D. (2012). "Robust, automatic real-time monitoring of the time course of the individual alpha frequency in the time and frequency domain," in *Proceedings of the Engineering in Medicine and Biology Society (EMBC), 34th Annual International Conference of the IEEE*, (San Diego, CA: IEEE, 2012), 2227–2231. doi: 10.1109/EMBC.2012.6346405

Grandy, T. H., Werkle-Bergner, M., Chicherio, C., Lovden, M., Schmiedek, F., and Lindenberger, U. (2013a). Individual alpha peak frequency is related to latent factors of general cognitive abilities. *Neuroimage* 79, 10–18. doi: 10.1016/j.neuroimage.2013.04.059

Grandy, T. H., Werkle-Bergner, M., Chicherio, C., Schmiedek, F., Lovden, M., and Lindenberger, U. (2013b). Peak individual alpha frequency qualifies as a stable neurophysiological trait marker in healthy younger and older adults. *Psychophysiology* 50, 570–582. doi: 10.1111/psyp.12043

Gray, R. T., and Robinson, P. A. (2013). Stability constraints on large-scale structural brain networks. *Front. Comput. Neurosci.* 7:31. doi: 10.3389/fncom.2013.00031

Jurcak, V., Tsuzuki, D., and Dan, I. (2007). 10/20, 10/10, and 10/5 systems revisited: their validity as relative head-surface-based positioning systems. *Neuroimage* 34, 1600–1611. doi: 10.1016/j.neuroimage.2006.09.024

Kaminski, M., and Blinowska, K. J. (2017). The influence of volume conduction on DTF estimate and the problem of its mitigation. *Front. Comput. Neurosci.* 11:26. doi: 10.3389/fncom.2017.00036

Kaminski, M. J., and Blinowska, K. J. (1991). A new method of the description of the information flow in the brain structures. *Biol. Cybern.* 65, 203–210. doi: 10.1007/BF00198091

Kaminski, M. J., Blinowska, K. J., and Szelenberger, W. (1997). Topographic analysis of coherence and propagation of EEG activity Turing Steep and wakefulness. *Electroenceph. Clin. Neurophysiol.* 102, 216–277. doi: 10.1016/S0013-4694(96)95721-5

Kayser, J. (2009). *Current Source Density (CSD) Interpolation using Spherical Splines - CSD Toolbox (Version 1.1)*. New York, NY State Psychiatric Institute: Division of Cognitive Neuroscience. Available online at: http://psychophysiology.cpmc.columbia.edu/Software/CSDtoolbox

Kayser, J., and Tenke, C. E. (2006a). Principal components analysis of Laplacian waveforms as a generic method for identifying ERP generator patterns: I. Evaluation with auditory oddball tasks. *Clin. Neurophysiol.* 117, 348–368. doi: 10.1016/j.clinph.2005.08.034

Kayser, J., and Tenke, C. E. (2006b). Principal components analysis of Laplacian waveforms as a generic method for identifying ERP generator patterns: II. Adequacy of low-density estimates. *Clin. Neurophysiol.* 117, 369–380. doi: 10.1016/j.clinph.2005.08.033

Kayser, J., and Tenke, C. E. (2015). On the benefits of using surface Laplacian (current source density) methodology in electrophysiology. *Int. J. Psychophysiol.* 97, 171–173. doi: 10.1016/j.ijpsycho.2015.06.001

Klimesch, W. (1999). EEG alpha and theta oscillations reflect cognitive and memory performance: a review and analysis. *Brain Res. Brain Res. Rev.* 29, 169–195. doi: 10.1016/S0165-0173(98)00056-3

Langrova, J., Kremlacek, J., Kuba, M., Kubova, Z., and Szanyi, J. (2012). Gender impact on electrophysiological activity of the brain. *Physiol. Res.* 61(Suppl. 2), S119–S127.

Liu, Q., Balsters, J. H., Baechinger, M., van der Groen, O., Wenderoth, N., and Mantini, D. (2015). Estimating a neutral reference for electroencephalographic recordings: the importance of using a high-density montage and a realistic head model. *J. Neural Eng.* 12:056012. doi: 10.1088/1741-2560/12/5/056012

Miskovic, V., Ma, X. P., Chou, C. A., Fan, M. L., Owens, M., Sayama, H., et al. (2015). Developmental changes in spontaneous electrocortical activity and network organization from early to late childhood. *Neuroimage* 118, 237–247. doi: 10.1016/j.neuroimage.2015.06.013

Moretti, D. V., Prestia, A., Fracassi, C., Binetti, G., Zanetti, O., and Frisoni, G. B. (2012). Specific EEG changes associated with atrophy of hippocampus in subjects with mild cognitive impairment and Alzheimer's disease. *Int. J. Alzheimers Dis.* 2012:253153. doi: 10.1155/2012/253153

Nunez, P. L., and Srinivasan, R. (2006). *Electric Fields of the Brain: The Neurophysics of EEG, 2nd Edn*. New York, NY: Oxford University Press.

O'Connor, S. C., and Robinson, P. A. (2004). Spatially uniform and nonuniform analyses of electroencephalographic dynamics, with application to the topography of the alpha rhythm. *Phys. Rev. E Stat. Nonlin. Soft Matter. Phys.* 70(1 Pt 1):011911. doi: 10.1103/PhysRevE.70.011911

Perrin, F., Pernier, J., Bertrand, O., and Echallier, J. F. (1989). Spherical splines for scalp potential and current density mapping. *Electroencephalogr. Clin. Neurophysiol.* 72, 184–187. doi: 10.1016/0013-4694(89)90180-6

Perrin, F., Pernier, J., Bertrand, O., and Echallier, J. F. (1990). Corrigenda EEG 02274. *Electroencephalogr. Clin. Neurophysiol.* 76, 565. doi: 10.1016/0013-4694(90)90009-9

Ponomareva, N., Andreeva, T., Protasova, M., Shagam, L., Malina, D., Goltsov, A., et al. (2013). Age-dependent effect of Alzheimer's risk variant of CLU on EEG alpha rhythm in non-demented adults. *Front. Aging Neurosci.* 5:86. doi: 10.3389/fnagi.2013.00086

Robinson, P. A., Loxley, P. N., O'Connor, S. C., and Rennie, C. J. (2001). Modal analysis of corticothalamic dynamics, electroencephalographic spectra, and evoked potentials. *Phys. Rev. E Stat. Nonlin. Soft Matter. Phys.* 63(4 Pt 1):041909. doi: 10.1103/PhysRevE.63.041909

Robinson, P. A., Whitehouse, R. W., and Rennie, C. J. (2003). Nonuniform corticothalamic continuum model of electroencephalographic spectra with application to split-alpha peaks. *Phys. Rev. E Stat. Nonlin. Soft Matter. Phys.* 68(2 Pt 1):021922. doi: 10.1103/PhysRevE.68.021922

Rubinov, M., and Sporns, O. (2010). Complex network measures of brain connectivity: uses and interpretations. *Neuroimage* 52, 1059–1069. doi: 10.1016/j.neuroimage.2009.10.003

Sobieszek, A. (2009). Imaging methods of the central nervous system function: electroencephalography (in Polish; summary in English). *Postępy Nauk Medycznych* XXII, 864–868.

Sobieszek, A. (2013). EEG paroxysmal patterns. (in Polish; summary in English). *Postępy Nauk Medycznych* XXVI, 683–690.

Sobieszek, A. (2015). In search of the sharp wave of epileptic nature (in Polish; summary in English). *Przegląd Lekarski* 72, 690–693.

Soroko, S. I., Shemyakina, N. V., Nagornova, Z. V., and Bekshaev, S. S. (2014). Longitudinal study of EEG frequency maturation and power changes in children on the Russian North. *Int. J. Dev. Neurosci.* 38, 127–137. doi: 10.1016/j.ijdevneu.2014.08.012

Vollebregt, M. A., van Dongen-Boomsma, M., Slaats-Willemse, D., Buitelaar, J. K., and Oostenveld, R. (2015). How the individual alpha peak frequency helps unravel the neurophysiologic underpinnings of behavioral functioning in children with attention-deficit/hyperactivity disorder. *Clin. EEG Neurosci.* 46, 285–291. doi: 10.1177/1550059414537257

Vysata, O., Kukal, J., Prochazka, A., Pazdera, L., Simko, J., and Valis, M. (2014). Age-related changes in EEG coherence. *Neurol. Neurochir. Pol.* 48, 35–38. doi: 10.1016/j.pjnns.2013.09.001

Xiong, H. C., and Yao, D. Z. (2005). "The study of the split of alpha rhythm spectra," in *Proceedings of the International Conference on Neural Networks and Brain* (Beijing), 1–3.

Yao, D. (2001). A method to standardize a reference of scalp EEG recordings to a point at infinity. *Physiol. Meas.* 22, 693–711. doi: 10.1088/0967-3334/22/4/305

Yao, D. (2017). Is the surface potential integral of a dipole in a volume conductor always zero? A Cloud Over the Average Reference of EEG and ERP. *Brain Topogr.* 30, 161–171. doi: 10.1007/s10548-016-0543-x

Yao, D., Wang, L., Oostenveld, R., Nielsen, K. D., Arendt-Nielsen, L., and Chen, A. C. N. (2005). A comparative study of different references for EEG spectral mapping: the issue of the neutral reference and the use of the infinity reference. *Physiol. Meas.* 26, 173–184. doi: 10.1088/0967-3334/26/3/003

Zappasodi, F., Marzetti, L., Olejarczyk, E., Tecchio, F., and Pizzella, V., (2015). Age-related changes in electroencephalographic signal complexity. *PLoS ONE* 10:e0141995. doi: 10.1371/journal.pone.0141995

Zappasodi, F., Olejarczyk, E., Marzetti, L., Assenza, G., Pizzella, V., and Tecchio, F. (2014). Fractal dimension of EEG activity senses neuronal impairment in acute stroke. *PLoS ONE* 9:e100199. doi: 10.1371/journal.pone.0100199

Zhai, Y., and Yao, D. (2004). A study on the reference electrode standardization technique for a realistic head model. *Comput. Methods Programs Biomed.* 76, 229–238. doi: 10.1016/j.cmpb.2004.07.002

Conflict of Interest Statement: The authors declare that the research was conducted in the absence of any commercial or financial relationships that could be construed as a potential conflict of interest.

frontiers in Neuroscience

ORIGINAL RESEARCH
published: 12 September 2017
doi: 10.3389/fnins.2017.00509

A Comparative Study on the Dynamic EEG Center of Mass with Different References

Yun Qin[1,2], Xiuwei Xin[2], Hao Zhu[2], Fali Li[1], Hongchuan Xiong[1], Tao Zhang[1,2] and Yongxiu Lai[1]**

[1] Key Laboratory for NeuroInformation of Ministry of Education, Center for Information in Medicine, University of Electronic Science and Technology of China, Chengdu, China, [2] High-Field Magnetic Resonance Brain Imaging Key Laboratory of Sichuan Province, School of Life Science and Technology, University of Electronic Science and Technology of China, Chengdu, China

One of the most fundamental issues during an EEG study is choosing an available neutral reference. The infinity zero reference obtained by the reference electrode standardization technique (REST) has been recommended and used for its higher accuracy. This paper examined three traditional references, the average reference (AR), the linked mastoids reference (LM), and REST, in the study of the EEG center of mass (CM) using simulated and real ERPs. In the simulation, the relative error of REST was the smallest among the references. As for the ERP data with the visual oddball paradigm, the dynamic CM trajectory and its traveling velocity obtained by REST characterized three typical stages in spatial domain and temporal speed metrics, which provided useful information in addition to the distinct ERP waveform in the temporal domain. The results showed that the CM traveling from the frontal to parietal areas corresponding to the earlier positive components (i.e., P200 and P250), stays temporarily at the parietal area corresponding to P300 and then returns to the frontal area during the recovery stage. Compared with REST, AR, and LM not only changed the amplitude of P300 significantly but distorted the CM trajectory and its instantaneous velocity. As REST continues to provide objective results, we recommend that REST be used in future EEG/ERP CM studies.

Keywords: neutral reference, center of mass, ERPs, trajectory, traveling velocity

OPEN ACCESS

Edited by:
Rui Zhang,
Zhengzhou University, China

Reviewed by:
Ling Zou,
Changzhou University, China
Jin Xu,
Xi'an Jiaotong University, China

****Correspondence:***
Tao Zhang
tao.zhang@alltechmed.com
Yongxiu Lai
laiyx@uestc.edu.cn

Specialty section:
This article was submitted to Brain Imaging Methods, a section of the journal Frontiers in Neuroscience

Received: *19 May 2017*
Accepted: *28 August 2017*
Published: *12 September 2017*

Citation:
Qin Y, Xin X, Zhu H, Li F, Xiong H, Zhang T and Lai Y (2017) A Comparative Study on the Dynamic EEG Center of Mass with Different References. Front. Neurosci. 11:509. doi: 10.3389/fnins.2017.00509

INTRODUCTION

Electroencephalogram (EEG) denotes the spatiotemporal dynamic process of the encephalic neural activities. The choice of reference influences both the spatial and temporal aspects of the EEG, which is one of the most fundamental issues in EEG analysis and interpretation. For the scalp distribution of the EEG at a set time point, different reference choice will introduce a constant value at all locations, similar to raising or lowering the water level of a landscape, without changing the shape (Pascualmarqui and Lehmann, 1993; Geselowitz, 1998). When the reference site on the body surface is active, the EEG dynamic process may be distorted due to the temporal bias of the reference signal. Thus, research teams are searching for the best available reference option for cross-study comparison (Kayser and Tenke, 2010; Nunez, 2010).

Abbreviations: REST, Reference electrode standardization technique; AR, Average reference; LM, Linked mastoids reference; CZ, Vertex reference; CM, Center of mass.

Different reference methods, such as, the average reference (AR), the linked mastoids reference (LM), and the vertex reference (CZ), are commonly used under certain assumptions (Yao, 2001; Nunez and Srinivasan, 2006a; Marzetti et al., 2007) while ignoring that they are not zero references. Previous studies have found that these references can introduce false voltage waveform fluctuation, spectrum scalp distribution shifts, and EEG network distortion (Yao, 2001; Kayser and Tenke, 2010; Nunez, 2010; Qin et al., 2010; Tian and Yao, 2013; Liu et al., 2015; Chella et al., 2016). AR is limited by an insufficient spatial sampling of the scalp field, as well as by the source distribution, which brings potential variance and network distortion (Yao, 2001; Zhai and Yao, 2005; Qin et al., 2010; Tian and Yao, 2013). The LM reference, obtained by combining the two mastoid electrodes, is independent of the electrode montage; however, the LM reference is challenged by its effect on the bilateral and posterior electrodes resulting in the power shift to the frontal and superficial positions (Yao et al., 2005). Although the Cz electrode is located farther from the sources, but the information-contained potential of the Cz electrode introduces large error to the vertex areas (Liu et al., 2015).

The reference electrode standardization technique (REST) proposed by Yao has been increasingly used in EEG studies (Yao, 2001). REST provides a standardized technique for approximately transforming multi-channel recordings with a scalp point into real EEG data using an infinity neutral reference. Studies on spectra imaging, EEG coherence, and connectivity using spontaneous EEG showed that REST tends to obtain more accurate and objective results (Yao et al., 2005; Marzetti et al., 2007; Qin et al., 2010). ERP components, cognitive psychology (Yao et al., 2007; Tian and Yao, 2013; Liu et al., 2015), and clinical EEG analysis (Xu et al., 2014) have shown that REST is also valuable in cognition and disease recognition.

Center of mass (CM) has been used as a metric to investigate the systematic integration and variability of the EEG (Wackermann et al., 1993; Manjarrez et al., 2007). In physics, CM is the point in an object or system that can describe the system's response to external forces and torques. Computationally, CM is the average of the masses factored by their distances from a reference point. For EEG study, CM is usually calculated by averaging the scalp potentials weighted by the spatial coordinates of all channels. Thus, spatial information from the entire scalp is used to calculate the CM rather than choosing only certain electrodes. The micro-states of the EEG time series can be distinguished by analyzing the positive and negative CM of the EEG (Wackermann et al., 1993). By applying the CM method, Manjarrez et al. found that the alpha wave trajectory starts and ends in specific brain regions (Manjarrez et al., 2007). Compared to the traditional focal electrodes and topographical analysis, CM trajectory is useful for presenting global temporal and spatial properties. In addition, varying the CM's instantaneous velocity may provide quantitative information on EEG patterns with certain cognitive characteristics.

In this study, we comparatively investigated the dynamic CM of the EEG to evaluate the performance of different reference strategies. Simulation was conducted to test the accuracy of EEG references. ERP data from the visual oddball paradigm were then used to show the dynamic CM trajectory with different references. In addition, the CM's traveling velocity was computed to helpfully reveal the P300 cognitive mechanism.

MATERIALS AND METHODS

Reference Electrode Standardization Technique (REST)

REST is derived from the theoretical relationship between the scalp recordings with a body reference point and a distributed source model S (Yao, 2001; Yao et al., 2005). For a neutral reference at infinity, we have:

$$V = GS \tag{1}$$

where the lead field matrix G depends on the head model, source configuration and electrode montage and has a reference at infinity. Similarly, the scalp EEG recordings V_{cz} referenced to CZ can be generated by:

$$V_{CZ} = G_{CZ}S \tag{2}$$

where G_{cz} is the EEG lead-field matrix with the CZ reference. A minimum norm solution (MNS) for the source distribution S is given by:

$$S = G_{CZ}{}^{-}V_{CZ} \tag{3}$$

where $G_{CZ}{}^{-}$ denotes the Moore-Penrose generalized inverse of the matrix $G_{cz.}$

From Equations (2) and (3), we can see that the source S is the same, which indicates that the source localization and activity will not be influenced by the references. Thus, the potential with a reference at infinity can be reconstructed as the following:

$$V_{IR} = G(G_{CZ}{}^{-}V_{CZ}) = UV_{CZ}, U = GG_{CZ}- \tag{4}$$

where U is the final transfer matrix determined by the lead-field matrices G and G_{cz}, both of which can be easily derived. Details of the REST algorithm can be found in Yao (2001), and the free software can be downloaded at www.neuro.uestc.edu.cn. Similarly, recordings with linked mastoids and average references (Dien, 1998; Hagemann et al., 2001) can be transformed to the neutral infinite reference using the formula in Equation (4) and different lead field matrix is used for the chosen reference.

In this study, the head model for all cases was a three-concentric-sphere model, and the normalized radii of the three concentric spheres were 0.87 (inner radius of the skull), 0.92 (outer radius of the skull), and 1.0 (radius of the scalp). The conductivities were 1.0, 0.0125, and 1.0 for the brain, skull and scalp, respectively. The center of the spheres was defined as the coordinate origin. The x-axis was oriented from the origin to the right ear, and the y-axis was oriented from the origin to the nasion. The z-axis was oriented from the origin to the vertex.

The Center of Mass (CM)

In this study, we used the positive CM to evaluate the performance of different references. Positive CM at time point t is the position weighted average of the EEG data with positive

amplitude, and it is calculated with the following equations (Manjarrez et al., 2007):

$$X(t) = \frac{\sum_{a_i m_i}(t)}{\sum_{m_i}(t)}, \qquad m_i(t) > 0, i = 1 \ldots N$$
$$Y(t) = \frac{\sum_{b_i m_i}(t)}{\sum_{m_i}(t)}, \qquad m_i(t) > 0, i = 1 \ldots N \quad (5)$$
$$Z(t) = \frac{\sum_{c_i m_i}(t)}{\sum_{m_i}(t)}, \qquad m_i(t) > 0, i = 1 \ldots N$$

where $X(t)$, $Y(t)$, and $Z(t)$ are the orthogonal coordinates of CM; a_i, b_i and c_i are the coordinates of the electrode channel i; and $m_i(t)$ is the positive voltage of channel i at time point t; and N is the electrode number. At any time point, a definite spatial CM point can be achieved.

CM Traveling Velocity

The traveling velocity of CM at one time point was computed according to the Euclidean distance between the orthogonal coordinate of CM at one time point t and that at the prior time point *t-1*. These differential values characterize the propagation velocity of the ERP waveforms. The CM traveling velocity in a two-dimensional scalp field was calculated by

$$V(CM(t)) = \sqrt{(X(t) - X(t-1))^2 + (Y(t) - Y(t-1))^2}/dt \quad (6)$$

During the ERP data analysis, we normalized the electrode and CM coordinates to the head model with the sphere radius $r =$ 10 cm. The sampling rate of the CM trajectory (i.e., 250 Hz in the real data analysis) was used in formula (6). Thus, we obtained the quantified CM traveling velocity with the metric (i.e., m/s).

Simulation

A dipole source model was used for the EEG forward calculation (Yao, 2003; Yao and He, 2003). Simulation was conducted for each voxel with a discrete cubic as a dipole source. The discrete cubic grid, consisting of 1994 dipoles, was constructed and confined within radius $r \leq 0.86$ with an inter-grid distance of 0.0905. That is, the Cartesian coordinates of the grid cubic (x, y, z) satisfy the conditions $x^2 + y^2 + z^2 \leq 0.86^2$ and $z \geq 0$. Considering that dipoles with any direction can be decomposed into three components along the X, Y, and Z directions, we studied the sensitivities of different references when dipoles were directed to the X, Y, or Z axis, respectively. The temporal process of a dipole source was simulated using a damped Gaussian function,

$$h(t_i) = \exp\left(-\left(2\pi f \frac{t_i - t_0}{\gamma}\right)^2\right) \cos\left(2\pi f\,(t_i - t_0) + \alpha\right)$$
$$i = 1, \cdots, k \quad (7)$$

with parameters$t_0 = 35^* dt, f = 10Hz, \gamma = 5, \alpha = \pi/2$. Forward calculation was conducted for each dipole with one direction, and then, the scalp EEG was re-referenced to the average reference (AR), linked mastoid reference (LM), CZ reference, and the neutral reference with REST. Based on the scalp distribution, CM was calculated with different references. As the forward result was the true recordings with the reference at infinity, the CM was also calculated from the original EEG distribution without any reference transformation, and regarded as the standard to evaluate the other four reference methods. The CM error between the infinity reference and any one of the four references is defined as:

$$Err = \left\| CM_{ref} - CM_{ir} \right\| / \left\| CM_{ir} \right\| \quad (8)$$

where CM_{ir} and CM_{ref} are the Euclidean norm of the CM coordinates with the reference at infinity and the other four transformed references.

ERP Application

Participants

Twelve healthy postgraduate students (males, right-handed, 22–27 years) participated in this experiment. All subjects gave written informed consent in accordance with the Declaration of Helsinki. The study was performed according to the guidelines approved by the Ethics Committee of the University of Electronic Science and Technology of China (UESTC). No subject reported using medication or having a personal or family history of psychiatric or neurological disease.

Experimental Procedures and EEG Recording

The traditional visual oddball paradigm was implemented in this experiment. The stimulus type consisted of target stimulus and standard stimulus. The target stimulus was a downward-oriented triangle with a thin cross in the center, and the standard stimulus was an upward-oriented triangle with a thin cross in the center. Three sessions were performed, each consisting of 150 trials, occurring at probability of 80% for standard stimuli and 20% for target stimuli. The detailed procedure is illustrated in **Figure 1**. A 4-min resting-state EEG was initially recorded, and after a 1-min break, the P300 task was performed. During the tasks, subjects were asked to fixate on the center of the monitor. A bold cross served as a cue that appeared at the start of the task to ensure that the subjects concentrated on the monitor. After 250 ms, a thin cross lasting for 500 ms informed subjects of the stimulus onset. The stimulus was presented for 500 ms. The subjects were asked to pay attention to and count the number of target stimuli, and once the experiment was complete, they stated the number of target stimuli they counted.

EEG data were recorded by Brain Vision Recorder using a 64-channel EEG system and digitized with a sampling rate of 500 Hz (Brain Products GmbH). The EEG cap (BrainCap, EasyCap GmbH) consisted of 63 scalp electrodes distributed according to the extended 10/20 system. Electrodes Fpz, Fz, Cz, CPz, Pz, Oz were arranged along the midline of the skull, and the other electrodes were located symmetrically on both sides of the midline. The online filter band was 0.01–100 Hz and the impedance of all electrodes was maintained below 5 KΩ. The FCz and AFz electrodes served as the reference and ground, respectively. Vertical and horizontal

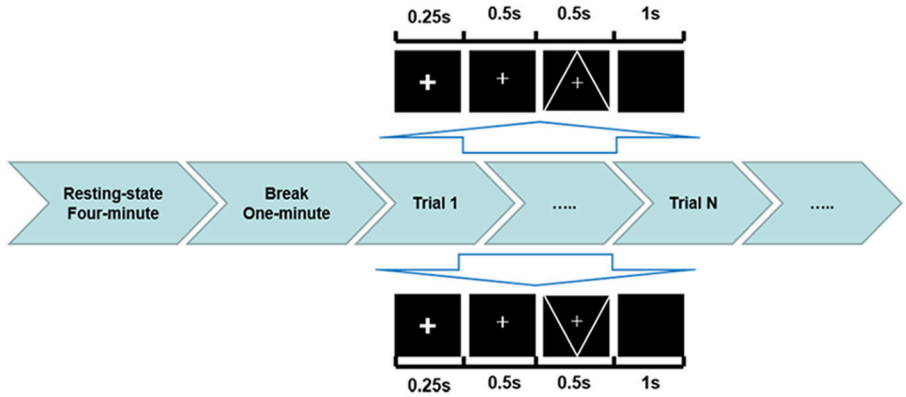

FIGURE 1 | ERP experimental protocol used in the current study. Before the visual oddball task presentation, a 4-min resting state and a 1-min break were performed. In each trial, the down-oriented triangle with a thin cross in the center represented the target stimulus with an occurring probability of 20%, while the upward-oriented triangle with a thin cross in the center indicated the standard stimulus with an occurring probability of 80%.

electrooculogram (EOG) data were recorded to monitor eye movements.

ERP Data Analysis

After the EEG data has been successfully recorded, we performed the necessary pre-processing procedures using Matlab R2013a (The MathWorks Inc.). The recorded EEG data were first re-referenced to REST, AR, and LM references, respectively. CZ reference was excluded in the real data analysis because of its serious distortion to the vertex electrodes. Then, filtering (6 Hz low-pass filter; Portin et al., 2000; Li et al., 2015) was performed, and the EEG was divided into epochs with 1,000 ms (200 ms pre-stimulus and 800 ms post-stimulus). A baseline correction for the period 200 ms before stimulus onset was performed for each epoch. To discern the ocular and other artifacts, a rejection criterion of ±75 μV was used at all of the electrode sites. On average, 90% of all epochs were retained after the artifact rejection. After pre-processing, averaging of ERP epochs for the two types of stimulus was performed.

CM of the averaged ERP was then carried out with three references, REST, AR, and LM. To keep the EEG CM trajectory on the scalp, two-dimensional CM with orthogonal coordinates $[X(t), Y(t)]$ was applied (Manjarrez et al., 2007). **Figure 2** showed the montage of 59 electrodes used in ERP CM calculation, and the EOG electrodes (VEOG, HEOG) and bilateral mastoid electrodes (TP9, TP10) have been excluded.

Statistical Analysis

One-way repeated-measures analyses of variance (ANOVAs) were performed on the values (i.e., ERP amplitude, latency, CM location, and CM traveling velocity) to evaluate the reference effects. Significant differences revealed by ANOVA were further analyzed for multiple comparisons using Tukey's *post-hoc* test. The value of epsilon (ε) of Greenhouse–Geisser would be denoted when the Greenhouse–Geisser correction was necessary. A significance level of $P < 0.05$ was used in all comparisons.

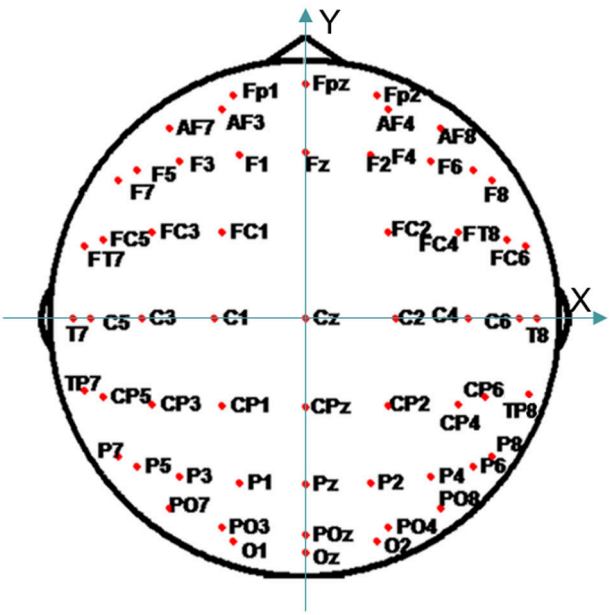

FIGURE 2 | The montage of 59 electrodes used for CM analysis.

RESULTS

Simulation Results

Figure 3 shows the CM error distribution in the form of slice display, and two slices, i.e., angle with the XY plane, 0 and 40 degrees, are illustrated. The distinct CM error distribution for the different conditions is shown in the subplots. REST had the smallest error compared to the other three references. A Tukey's test revealed significant differences ($P < 0.001$) for all pair-wise comparisons among these references in any dipole direction. Furthermore, the REST reference was hardly influenced by the dipole location or direction, while the other three references had a markedly varied error distribution map as the dipole location

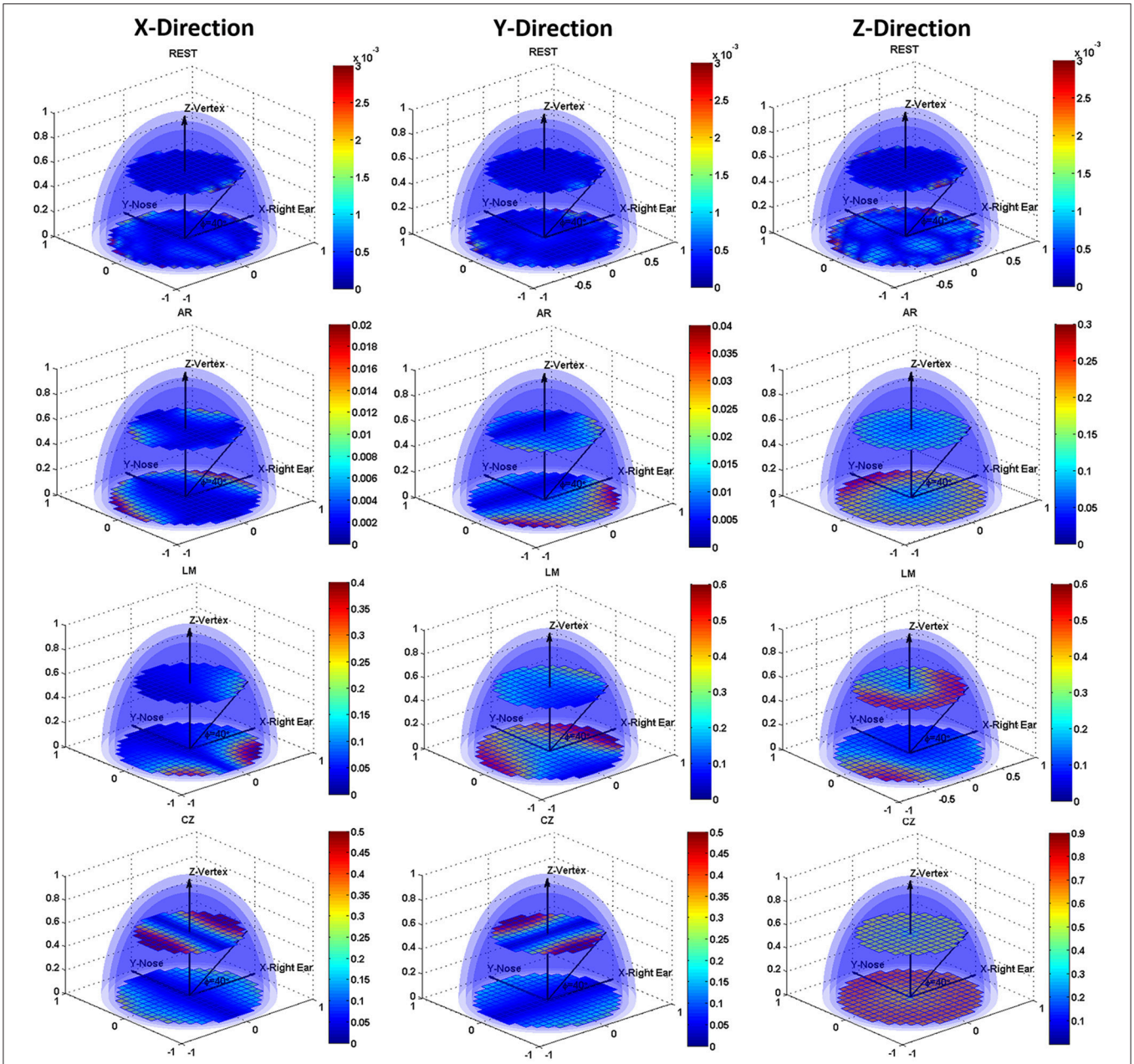

FIGURE 3 | Slice display of the volume distribution for the CM errors. Errors for REST, AR, LM, and CZ references are listed in the four rows from top to bottom, respectively. The three columns from left to right represent the error maps with dipoles orientating along X-axis, Y-axis, and Z-axis.

and direction changed. When the dipoles were directed along the positive X-axis, the error focused on the edge of the positive and negative X-axis, and all references showed some degree of symmetry along the Y-axis. The AR had a larger error in the anterior areas, while the LM reference had a larger error in the posterior areas. With dipoles orientated along the Y-axis, there was still an error distribution with the symmetry along the Y-axis. For the AR, dipoles in the posterior areas had a larger error, and for the LM reference, the largest error was near the two mastoid areas. As for CZ reference, the error was aggravated in the superficial areas. When the dipoles were directed to the Z-axis, there was a larger error than in the other two directions. The AR and CZ references showed gross error in the bottom areas, and the LM reference still had the largest error in the posterior areas.

ERP Application Results

ERP Waveforms

ERPs were obtained after the data pre-processing for the three references, REST, AR, and LM. Electrodes Cz, CPz, Pz in the

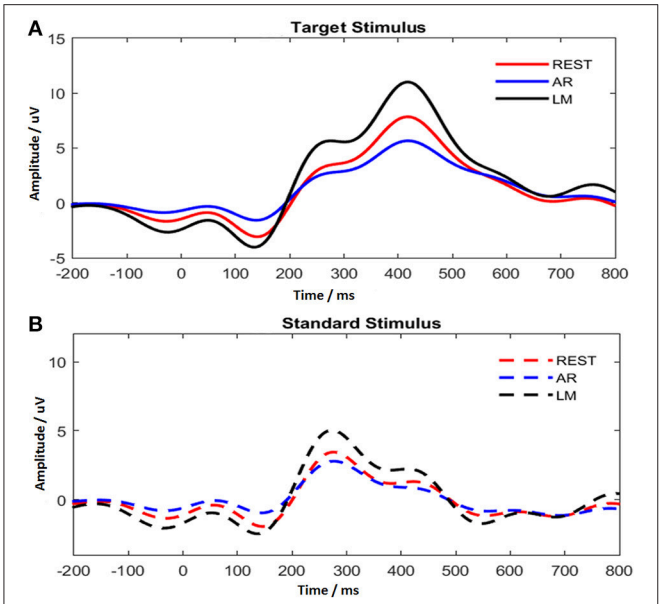

FIGURE 4 | P300 time course with different references for target stimulus **(A)** and standard stimulus **(B)**.

posterior midline of the scalp were found having the maximum P300 amplitude. To obtain a reliable estimate of P300 amplitude and latency, the averaged values across the three electrodes (Cz, CPz, and Pz) were treated as the P300 amplitude and latency for each individual subject. In **Figure 4**, the average ERP time course was demonstrated for two different stimuli. The target stimulus showed a prominent P300 component with long latency. The P250 enhancement was evoked by the standard stimulus, and no distinct positive component appeared after that.

In addition, ERP waveforms were altered by using different references. As shown in **Figure 4**, AR reduced the P300 amplitude, while LM increased the P300 amplitude. The difference for P300 amplitude with target stimulus among references was significant [$F_{(2, 22)} = 68.251$, $\varepsilon = 0.541$, $P < 0.001$], and pair-wise comparisons using Tukey's *post-hoc* test revealed significant differences for all comparisons ($P < 0.001$). In addition, no difference was found for P300 latency among references.

CM Trajectory, Traveling Velocity, and ERP Stages

The ERP CM from 200 to 800 ms after stimulus onset was computed with one time point interval (i.e., 250 Hz sampling rate). The CM trajectory constituted 150 points. As shown in **Figure 5A**, the CM trajectory traveled from the frontal to parietal areas and then back. However, the characteristic CM trajectory stemmed from different stimuli. For the target stimulus, the ERP CM shifted from the frontal area to the vertex near the Cz electrode at approximately 350 ms and then extended a short distance along the middle line. After a short period, the CM of the target stimulus returned to the frontal area. For standard stimuli, the ERP CM originated from a similar frontal area and expanded its range to the parietal and occipital areas at 310 ms. After spanning a wider coverage area and circuity, the ERP CM of the standard stimulus then traveled back to the frontal areas.

Figure 5B shows the CM traveling velocity through the whole CM trajectory from 200 to 800 ms. The CM traveling velocity ranged from 0.2 to 2 m/s during the whole time course. To more intuitively show the temporal-spatial and speed change information, the normalized CM traveling velocity was mapped in the CM trajectory using different colors, with a bright color indicating the high velocity and a dark color indicating the low value (**Figure 5A**). For the CM traveling properties, we labeled a small number of inflection time points and divided the ERP processing into three stages: S1 (210–350 ms), S2 (350–480 ms), and S3 (480–740 ms). S1 reflected the CM traveling course from the anterior to posterior areas, corresponding to when the CM velocity dropped to the minimum. S2 was the circuitous process with lower a CM traveling velocity at the P300 stage. S3 was the return process with relatively oscillating CM velocity.

In terms of different references, distinct CM trajectory and traveling velocity were illustrated. The CM trajectory was similar between REST and AR, particularly for the S1 and S3 stages, and AR had a slight posterior shift in the S2 stage. LM expressed a distinguished trajectory. The reference effect was evaluated on the CM locations and traveling velocity with target stimulus. As for CM trajectory, one-way repeated-measures analysis of variance (ANOVAs) revealed significant differences among references for both S1 and S2 stages [S1: $F_{(2, 22)} = 11.933$, $P < 0.001$; S2: $F_{(2, 22)} = 17.427$, $\varepsilon = 0.543$, $P < 0.001$], and pair-wise multiple comparisons revealed significant differences (Tukey's test, $P < 0.01$) for all comparison pairs, except between REST and AR in S1 stage. Furthermore, ANOVAs and Tukey's *post-hoc* test were performed to CM traveling velocity, and similar results were obtained. Significant differences were found among references for both S1 and S2 stages [S1: $F_{(2, 22)} = 6.840$, $\varepsilon = 0.667$, $P < 0.05$; S2: $F_{(2, 22)} = 9.765$, $\varepsilon = 0.632$, $P < 0.01$], and pair-wise multiple comparisons revealed significant differences ($P < 0.05$) for all comparison pairs, except between REST and AR in S1 stage.

The Relationships for CM Traveling Velocity between Stimuli

The average of the CM traveling velocity across all subjects was used to investigate the correlation between the two stimulus conditions, which denoted the consistency of cognitive patterns during ERP processing. In **Figure 6**, the scatter points indicate time points when the CM traveling velocity was presented for the two stimulus conditions. In the S1 stage, a significant positive time-lagged correlation was shown for the target stimulus at 250–350 ms and the standard stimulus at 210–310 ms. All references shared this consistency. In the S2 stage, a significant positive correlation was revealed at 350–480 ms for REST, while the correlation was not significant for AR and LM references. Additionally, a significant negative correlation was revealed at the S3 stage for the REST and AR references. The relationship of the CM traveling velocity between the two stimuli can be better fitted linearly by REST with a higher correlation coefficient, while the other two references were more varied at certain time points.

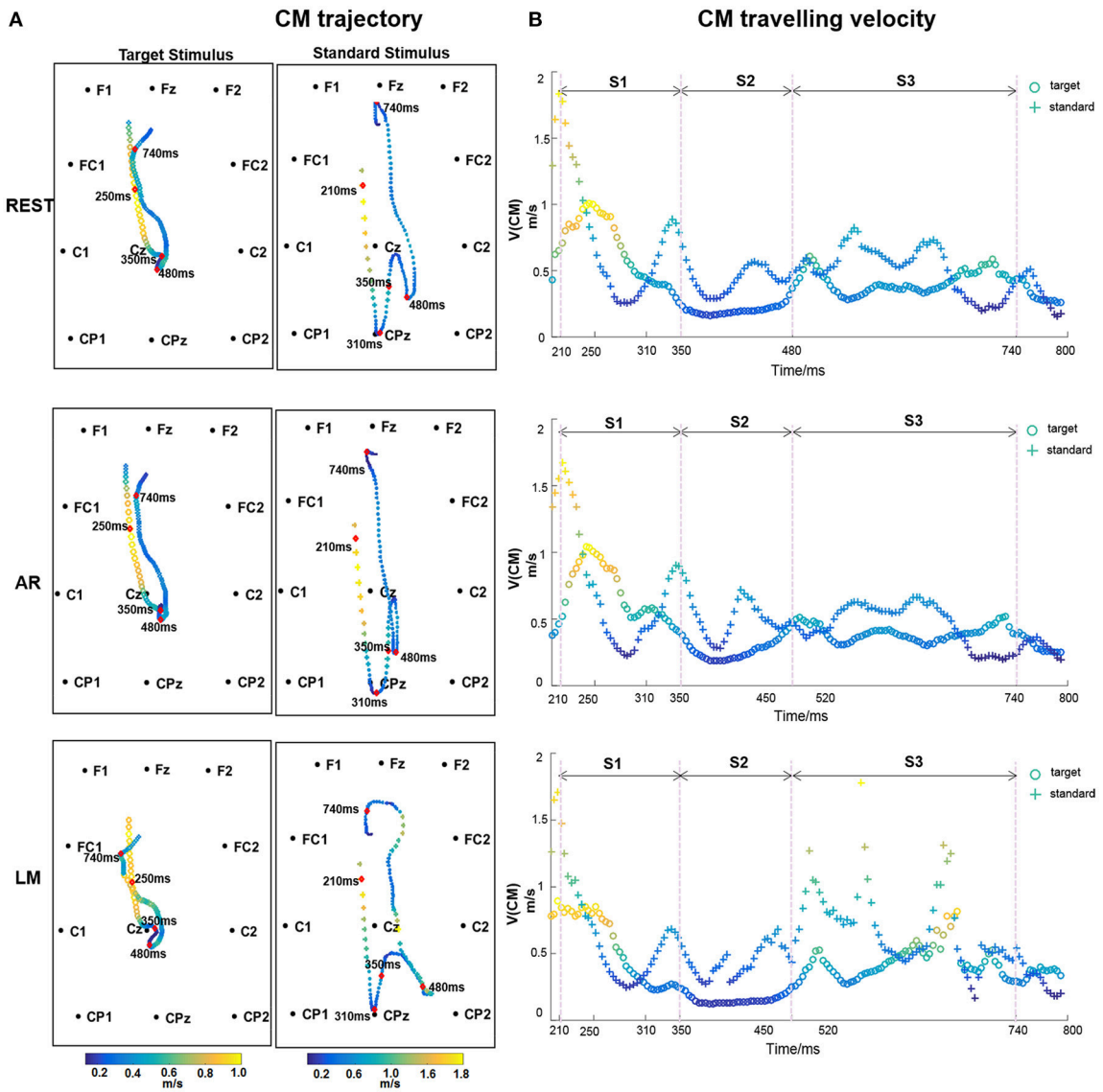

FIGURE 5 | (A) CM trajectory of ERP with different references for target stimulus and standard stimulus. CM traveling velocity in each time point is depicted using different color, with bright color indicating the high speed and dark color indicating the low values. The time points, 210, 310, 350, 480, 740 ms after stimulus onset were labeled. **(B)** CM traveling velocity curve of ERP time course. Three stages S1 (210–350 ms), S2 (350–480 ms), and S3 (480–740 ms) are divided.

DISCUSSION

Simulation Analysis

Conventional simulation verified the reference effects and takes priority over the subsequent EEG CM analysis. Errors introduced by references were influenced by the dipole location and orientation. The simulation results demonstrated that REST introduced the smallest error, while the other three references consistently distorted certain areas. The symmetrical error distribution along Y-axis of AR indicated that the effectiveness of AR depends on both the true source distribution and the assumed head surface electrode montage (Yao, 2001; Liu et al., 2015). LM reference had a profound impact on the bilateral mastoids and posterior areas which was determined by its non-zero characteristic (Tian and Yao, 2013). For CZ, the vertex areas were dramatically influenced, and this effect was aggravated in the superficial areas. Therefore, in a real ERP study, the CZ reference is always excluded because of this defect, but it can still be used as the recording reference electrode before reference transformation. This simulation may provide evidence and choice for EEG reference strategy in cases specific sources and interesting scalp areas.

ERP Processing and CM Application

A majority of ERP studies used the oddball paradigm in which P300 is evoked by the infrequent target stimulus, and P300 does not appear or exhibits a smaller amplitude from the frequent

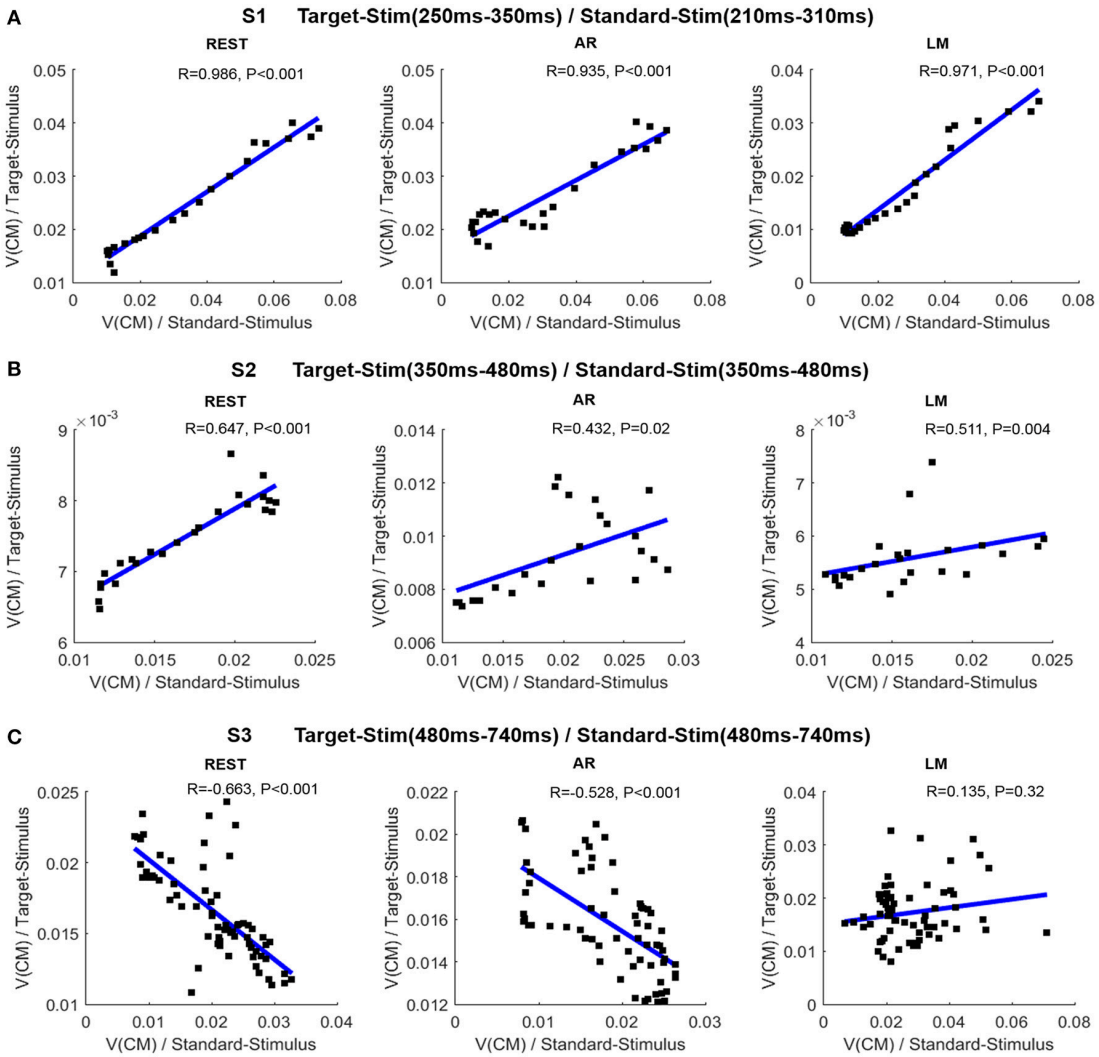

FIGURE 6 | Relationship of CM traveling velocity between target stimulus and standard stimulus in different stages. **(A)** Correlations between the two conditions for S1 stage (target stimulus: 250–350 ms; standard stimulus: 210–310 ms). **(B)** Correlations between the two conditions for S2 stage (350–480 ms). **(C)** Correlations between the two conditions for S3 stage (480–740 ms). In each sub-figure, the line is the fitted line; R is the correlation coefficient, and P is the statistical significance.

standard stimulus (Kok, 1997). **Figure 4** shows the classic P300 component in target stimulus and the P250 component in standard stimulus. The standard stimulus is commonly used as the background, however, intervening events related to the standard stimulus engage attention to modify the current neural representation and the additive information may be beneficial in assessing the cognitive process during the oddball task (Garcíalarrea et al., 1992; Polich, 2007). Cognitive processing in a two-stimulus oddball task is attributed to composite stages, such as, stimulus-driven attention, decision processing, and the neuronal response (Desmedt, 1980; Picton, 1992; Li et al., 2016), and P300 is thought to be a post-decision event (Desmedt, 1980). It is necessary to integrate the ERP stages to investigate the dynamic temporal-spatial patterns.

CM traveling trajectory describes the dynamic pattern of the EEG, and it is a sensitive indicator for exploring entire neural pathways in large scale cortical signals (Chao et al., 2007; Manjarrez et al., 2007) which can be extended to the positive potential, the negative potential and the power spectra application (Wackermann et al., 1993; Manjarrez et al., 2007; Qin et al., 2010). In this experiment, a two-dimensional positive CM trajectory map described the propagation of ERP waves switching from the frontal to the parietal and occipital areas and then back. This dynamic circuitous pathway produced multiple cognitive processes including attention, decision, response and post-response, probably stemming from cortico-cortical coupling. The initial CM propagation from anterior to posterior areas covered the fronto-parietal attention dominant brain regions including the frontal lobe, the center area, and part of the parietal areas (Kirino et al., 2000; Daffner et al., 2003; Li et al., 2010). The standard stimulus traveled a similar trajectory but with a wider coverage area in the parietal areas, which may indicate the

more thorough cognitive processing (Garcíalarrea et al., 1992). In addition, the combination of trajectory and traveling velocity extended the observation of ERP cognitive processing. The CM traveling velocity dropped to a slower flat process with the presence of P300 comparing to other time periods. During the whole time course, the CM velocity ranged from 0.2 to 2 m/s, which was within the range of previous measurements of wave propagation velocity on the human scalp (Massimini et al., 2004; Nunez and Srinivasan, 2006b; Manjarrez et al., 2007), and it provided a quantified metric to describe wave propagation.

Three stages were divided according to the CM trajectory and velocity changes. In the earlier S1 stage, CM shifted from the frontal to the parietal area with a minimum CM speed. The time-lagged consistency of CM velocity between the two stimuli may be related with the widely appeared P250 component and the overlap of the typical positive components in both stimulus conditions, i.e., P200, P250, and earlier P3a (Garcíalarrea et al., 1992; Polich, 2007). Therefore, the cognitive treatment to different stimulus in this stage may belong to the same modality, indicating stimulus-driven process stemming from the frontal attention mechanism, involving the simulation identification, attention orienting, and cognitive evaluation (Polich, 2007). Then, CM trajectory turned back at 310 ms for the standard stimulus, and consistent cognitive modality between two stimulus conditions appeared at S2 stage starting from 350 ms. This phenomenon may suggest an additive evaluation process existing at the end of S1 due to the standard stimulus engagement. That is, after the earlier process at 310 ms, if no target stimulus was recognized, small or no P300 would appear. The following S2 indicating the P300 stage with lower CM traveling velocity may be associated with the top-down guided control and memory operation, and the positive correlation between the two stimuli showed a consistent cognitive pattern (Polich, 2007; Salmela et al., 2016). In the post-response stage at about 480–740 ms, the CM trajectory turned back to the frontal area, and the negative correlation indicated the late divergence of a cognitive pattern between two stimuli, which may be caused by the response control and mental state, i.e., mental counting and the relaxed state after responding (Strüber and Polich, 2002). An intracerebral electrode recording showed the existence of identical ERPs between the target and standard stimulus from 300 to 470 ms in most intra-cerebral sites, while a divergence was found in the late phase of the ERPs in most intra-cerebral sites after 570 ms (Kukleta et al., 2003; Damborská et al., 2012). Thus, with the help of the CM dynamic pattern, three stages were suggested for oddball visual processing: stimulus-driven orienting, top-down control and memory operation, and the post-response mental state, with the stimulus-independent and mental-dependent neural operation being dominant during the oddball tasks.

Reference Effect

The reference effect was obviously embodied on the ERP analysis, and many studies have reported that this impact varied with the temporal course and channel locations (Yao, 2001; Liu et al., 2015). In addition to the prominent waveform deflections, peak polarity reversal, and topographic shift may dramatically affect the identification, qualification and interpretation in EEG studies (Kayser and Tenke, 2010). LM, CZ, and other scalp site references that contain large potential values are undesirable in ERP studies (Kayser and Tenke, 2010; Tian and Yao, 2013). For the P300 peak, subtracting a positive average value will result in a reduction or polarity reversal for the positive potential and an increase in the negative potential, which was the cause of the topography distribution distortion and CM shift. Moreover, the distortion varied in different scalp areas. As the mastoids are located at the bilateral occipital regions, LM tends to have a greater effect on the bilateral posterior electrodes. Similarly, CZ would mess extensive areas around the vertex due to electrode location. Hence, using the non-neutral references will lead to information loss and hide the physiological nature of the condition. AR is recommended in many papers because it seems to be independent on any particular electrodes (Ferree, 2006; Nunez and Srinivasan, 2006a). However, the average of all recording channels also leads to a varying degree of effect on special locations. Comparing AR, LM, and CZ references revealed that AR produced results that were much closer to those of REST, when applied to both simulated and real ERP data. These findings indicated that AR is a better choice than LM and CZ, which have been adopted in many neurocognitive EEG studies.

REST provides a true electrically neutral reference based on the physical essence of EEG generation (Yao, 2001). It is recommended and widely used in neural cognitive and clinical applications (Yao et al., 2005; Kayser and Tenke, 2010; Qin et al., 2010; Tian and Yao, 2013; Xu et al., 2014; Liu et al., 2015). It was shown in the simulation that the error is greatly reduced with REST compared with other commonly used references. Although a realistic head model constructed for each individual subject would likely improve the accuracy of REST for each subject, previous reports (Yao, 2001; Zhai and Yao, 2005) have showed that REST is effective even when the volume conductor differs from the true head model. Comparing with other reference-free methods such as, scalp Laplacian, the cortical imaging technique (Tenke and Kayser, 2005; Nunez and Srinivasan, 2006a), the operation involved in REST is from "scalp to scalp," therefore, the noise in data and error in head model will not be enlarged. In the current study, in terms of CM trajectory and traveling velocity, REST best represented the three stages corresponding to cognitive mechanisms. CM traveling velocity could be better linearly fitted with REST and had a higher correlation coefficient for two stimuli. This indicates that REST recovers the lost information and provides the optimal approximation for the neutral reference.

CONCLUSIONS

In this study, the reference effect on simulated data as well as on ERP data measured by CM trajectory and CM traveling velocity was examined. The simulation results indicated that REST introduced less error than the AR, LM, and CZ references and was less affected by dipole location and orientation. As a metric to measure the dynamic pattern of EEG spatiotemporal

activity, CM and the traveling velocity extend the exploration of these cognitive mechanisms. Distinct CM trajectory and CM traveling velocity for the alternative references were represented by visual oddball task processing. As REST better represented the cognitive stages, we recommend REST as a beneficial technique for pursuing the ideal zero reference.

AUTHOR CONTRIBUTIONS

Conceived and designed the work: YQ, XX, HZ, HX, and YL. Acquired the data: FL and XX. Analyzed the data: YQ, XX, and FL. Wrote the paper: YQ and TZ. All authors revised the work for important intellectual content. All of the authors have read and approved the manuscript.

ACKNOWLEDGMENTS

This work was supported by grants from the National Nature Science Foundation of China (grant number NSFC81571759); Special-Funded Program on National Key Scientific Instruments and Equipment Development of China (grant number 2013YQ490859).

REFERENCES

Chao, Z. C., Bakkum, D. J., and Potter, S. M. (2007). Region-specific network plasticity in simulated and living cortical networks: comparison of the center of activity trajectory (CAT) with other statistics. *J. Neural Eng.* 4, 294–308. doi: 10.1088/1741-2560/4/3/015

Chella, F., Pizzella, V., Zappasodi, F., and Marzetti, L. (2016). Impact of the reference choice on scalp EEG connectivity estimation. *J. Neural Eng.* 13:036016. doi: 10.1088/1741-2560/13/3/036016

Daffner, K. R., Scinto, L. F. M., Weitzman, A. M., Faust, R., Rentz, D. M., Budson, A. E., et al. (2003). Frontal and parietal components of a cerebral network mediating voluntary attention to novel events. *J. Cogn. Neurosci.* 15, 294–313. doi: 10.1162/089892903321208213

Damborská, A., Brázdil, M., Rektor, I., Janoušová, E., Chládek, J., and Kukleta, M. (2012). Late divergence of target and nontarget ERPs in a visual oddball task. *Physiol. Res.* 61, 307–318.

Desmedt, J. E. (1980). P300 in serial tasks: an essential post-decision closure mechanism. *Prog. Brain Res.* 54, 682–686. doi: 10.1016/S0079-6123(08)61690-8

Dien, J. (1998). Issues in the application of the average reference: review, critiques, and recommendations. *Behav. Res. Methods* 30, 34–43. doi: 10.3758/BF03209414

Ferree, T. C. (2006). Spherical splines and average referencing in scalp electroencephalography. *Brain Topogr.* 19:43. doi: 10.1007/s10548-006-0011-0

Garcíalarrea, L., Lukaszewicz, A. C., and Mauguière, F. (1992). Revisiting the oddball paradigm, non-target vs neutral stimuli and the evaluation of ERP attentional deficits. *Neuropsychologia* 30:723. doi: 10.1016/0028-3932(92)90042-K

Geselowitz, D. B. (1998). The zero of potential. *IEEE Eng. Med. Biol. Mag.* 17, 128–132. doi: 10.1109/51.646230

Hagemann, D., Naumann, E., and Thayer, J. F. (2001). The quest for the EEG reference revisited: a glance from brain asymmetry research. *Psychophysiology* 38, 847–857. doi: 10.1111/1469-8986.3850847

Kayser, J., and Tenke, C. E. (2010). In search of the rosetta stone for scalp EEG: converging on reference-free techniques. *Clin. Neurophysiol.* 121, 1973–1975. doi: 10.1016/j.clinph.2010.04.030

Kirino, E., Belger, A., Goldmanrakic, P., and McCarthy, G. (2000). Prefrontal activation evoked by infrequent target and novel stimuli in a visual target detection task: an event-related functional magnetic resonance imaging study. *J. Neurosci.* 20, 6612–6618.

Kok, A. (1997). Event-related-potential (ERP) reflections of mental resources: a review and synthesis. *Biol. Psychol.* 45, 19–56. doi: 10.1016/S0301-0511(96)05221-0

Kukleta, M., Brázdil, M., Roman, R., and Jurák, P. (2003). Identical event-related potentials to target and frequent stimuli of visual oddball task recorded by intracerebral electrodes. *Clin. Neurophysiol.* 114, 1292–1297. doi: 10.1016/S1388-2457(03)00108-1

Li, F., Chen, B., Li, H., Zhang, T., Wang, F., Jiang, Y., et al. (2016). The time-varying networks in P300: a task-evoked EEG study. *IEEE Trans. Neural Syst. Rehabil. Eng.* 24, 725–733. doi: 10.1109/TNSRE.2016.2523678

Li, F., Liu, T., Wang, F., Li, H., Gong, D., Zhang, R., et al. (2015). Relationships between the resting-state network and the P3: evidence from a scalp EEG study. *Sci. Rep.* 5:15129. doi: 10.1038/srep15129

Li, L., Gratton, C., Yao, D., and Knight, R. T. (2010). Role of frontal and parietal cortices in the control of bottom-up and top-down attention in humans. *Brain Res.* 1344, 173–184. doi: 10.1016/j.brainres.2010.05.016

Liu, Q., Balsters, J. H., Baechinger, M., van der Groen, O., Wenderoth, N., and Mantini, D. (2015). Estimating a neutral reference for electroencephalographic recordings: the importance of using a high-density montage and a realistic head model. *J. Neural Eng.* 12:056012. doi: 10.1088/1741-2560/12/5/056012

Manjarrez, E., Vazquez, M., and Flores, A. (2007). Computing the center of mass for traveling alpha waves in the human brain. *Brain Res.* 1145, 239–247. doi: 10.1016/j.brainres.2007.01.114

Marzetti, L., Nolte, G., Perrucci, M. G., Romani, G. L., and Del Gratta, C. (2007). The use of standardized infinity reference in EEG coherency studies. *Neuroimage* 36, 48–63. doi: 10.1016/j.neuroimage.2007.02.034

Massimini, M., Huber, R., Ferrarelli, F., Hill, S., and Tononi, G. (2004). The sleep slow oscillation as a traveling wave. *J. Neurosci.* 24, 6862–6870. doi: 10.1523/JNEUROSCI.1318-04.2004

Nunez, P. L. (2010). REST: a good idea but not the gold standard. *Clin. Neurophysiol.* 121, 2177–2180. doi: 10.1016/j.clinph.2010.04.029

Nunez, P. L., and Srinivasan, R. (2006a). *Electric Fields of the Brain: the Neurophysics of EEG. 2nd Edn.* New York, NY: Oxford University Press.

Nunez, P. L., and Srinivasan, R. (2006b). A theoretical basis for standing and traveling brain waves measured with human EEG with implications for an integrated consciousness. *Clin. Neurophysiol.* 117, 2424–2435. doi: 10.1016/j.clinph.2006.06.754

Pascualmarqui, R. D., and Lehmann, D. (1993). Topographic maps, source localization inference, and the reference electrode: comments on a paper by Desmedt et al. *Electroencephalogr. Clin. Neurophysiol.* 88, 532–536. doi: 10.1016/0168-5597(93)90043-O

Picton, T. W. (1992). The P300 wave of the human event-related potential. *J. Clin. Neurophysiol.* 9, 456–479. doi: 10.1097/00004691-199210000-00002

Polich, J. (2007). Updating P300: an integrative theory of P3a and P3b. *Clin. Neurophysiol.* 118, 2128–2148. doi: 10.1016/j.clinph.2007.04.019

Portin, R., Kovala, T., Polo-Kantola, P., Revonsuo, A., Müller, K., and Matikainen, E. (2000). Does P3 reflect attentional or memory performances, or cognition more generally? *Scand. J. Psychol.* 41, 31–40. doi: 10.1111/1467-9450.00168

Qin, Y., Xu, P., and Yao, D. (2010). A comparative study of different references for EEG default mode network: the use of the infinity reference. *Clin. Neurophysiol.* 121, 1981–1991. doi: 10.1016/j.clinph.2010.03.056

Salmela, V., Salo, E., Salmi, J., and Alho, K. (2016). Spatiotemporal dynamics of attention networks revealed by representational similarity analysis of EEG and fMRI. *Cereb. Cortex* 26, 1–12. doi: 10.1093/cercor/bhw389

Strüber, D., and Polich, J. (2002). P300 and slow wave from oddball and single-stimulus visual tasks: inter-stimulus interval effects. *Int. J. Psychophysiol.* 45, 187–196. doi: 10.1016/S0167-8760(02)00071-5

Tenke, C. E., and Kayser, J. (2005). Reference-free quantification of EEG spectra: combining current source density (CSD) and frequency principal components analysis (fPCA). *Clin. Neurophysiol.* 116, 2826–2846. doi: 10.1016/j.clinph.2005.08.007

Tian, Y., and Yao, D. (2013). Why do we need to use a zero reference? Reference influences on the ERPs of audiovisual effects. *Psychophysiology* 50, 1282–1290. doi: 10.1111/psyp.12130

Wackermann, J., Lehmann, D., Michel, C. M., and Strik, W. K. (1993). Adaptive segmentation of spontaneous EEG map series into spatially defined microstates. *Int. J. Psychophysiol.* 14, 269–283. doi: 10.1016/0167-8760(93)90041-M

Xu, P., Xiong, X. C., Xue, Q., Tian, Y., Peng, Y., Zhang, R., et al. (2014). Recognizing mild cognitive impairment based on network connectivity analysis of resting EEG with zero reference. *Physiol. Meas.* 35:1279. doi: 10.1088/0967-3334/35/7/1279

Yao, D. (2001). A method to standardize a reference of scalp EEG recordings to a point at infinity. *Physiol. Meas.* 22, 693–711. doi: 10.1088/0967-3334/22/4/305

Yao, D. (2003). High-resolution EEG mapping: an equivalent charge-layer approach. *Phys. Med. Biol.* 48, 1997–2011. doi: 10.1088/0031-9155/48/13/311

Yao, D., and He, B. (2003). Equivalent physical models and formulation of equivalent source layer in high-resolution EEG imaging. *Phys. Med. Biol.* 48:3475. doi: 10.1088/0031-9155/48/21/002

Yao, D., Wang, L., Arendt-Nielsen, L., and Chen, A. C. (2007). The effect of reference choices on the spatio-temporal analysis of brain evoked potentials: the use of infinite reference. *Comput. Biol. Med.* 37:1529. doi: 10.1016/j.compbiomed.2007.02.002

Yao, D., Wang, L., Oostenveld, R., Nielsen, K. D., Arendtnielsen, L., and Chen, A. C. (2005). A comparative study of different references for EEG spectral mapping: the issue of the neutral reference and the use of the infinity reference. *Physiol. Meas.* 26:173. doi: 10.1088/0967-3334/26/3/003

Zhai, Y., and Yao, D. (2005). A study on the reference electrode standardization technique for a realistic head model. *Comput. Methods Prog. Biomed.* 76, 229–238. doi: 10.1016/j.cmpb.2004.07.002

Conflict of Interest Statement: The authors declare that the research was conducted in the absence of any commercial or financial relationships that could be construed as a potential conflict of interest.

frontiers in Neuroscience

ORIGINAL RESEARCH
published: 26 September 2017
doi: 10.3389/fnins.2017.00527

Electrophysiological Correlates of Change Detection during Delayed Matching Task: A Comparison of Different References

Tengfei Liang[1], Zhonghua Hu[1], Yuchen Li[1], Chaoxiong Ye[1,2,3] and Qiang Liu[1]*

[1] Research Center of Brain and Cognitive Neuroscience, Liaoning Normal University, Dalian, China, [2] Department of Psychology, University of Jyväskylä, Jyväskylä, Finland, [3] Faculty of Information Technology, University of Jyväskylä, Jyväskylä, Finland

Detecting the changed information between memory representation and incoming sensory inputs is a fundamental cognitive ability. By offering the promise of excellent temporal resolution, event-related potential (ERP) technique has served as a primary tool for studying this process with reference of the linked mastoid (LM). However, given that LM may distort the ERP signals, it is still undetermined whether LM is the best reference choice. The goal of the current study was to systematically compare LM, reference electrode standardization technique (REST) and average reference (AR) for assessing the ERP correlates of change detection during a delayed matching task. Colored shapes were adopted as materials while both the task-relevant shape feature and -irrelevant color feature could be changed. The results of the ERP amplitude showed that both of the task-relevant and -conjunction feature changes elicited significantly more positive posterior P2 in REST and AR, but not in LM. Besides, significantly increased N270 was observed in task-relevant and -conjunction feature changes in both the REST and LM, but in the conjunction feature change in AR. Only the REST-obtained N270 revealed a significant increment in task-irrelevant feature change, which was compatible with the delayed behavioral performance. Statistical parametric scalp mapping (SPSM) results showed a left posterior distribution for AR, an anterior distribution for LM, and both the anterior and left posterior distributions for REST. These results indicate that different types of references may provide distinct cognitive interpretations. Interestingly, only the SPSM of REST was consistent with previous fMRI findings. Combined with the evidence of simulation studies and the current observations, we take the REST-based results as the objective one, and recommend using REST technology in the future ERP data analysis.

Keywords: REST reference, average reference, linked mastoid, change detection, N270, P2, delayed matching task

OPEN ACCESS

Edited by:
Pedro Antonio Valdes-Sosa, Joint China-Cuba Laboratory for Frontier Research in Translational Neurotechnology, China

Reviewed by:
Dezhong Yao, University of Electronic Science and Technology of China, China
Laura Marzetti, Università degli Studi "G. d'Annunzio" Chieti - Pescara, Italy

***Correspondence:**
Zhonghua Hu
huzhonghua2000@163.com

Specialty section:
This article was submitted to Brain Imaging Methods, a section of the journal Frontiers in Neuroscience

Received: *30 July 2017*
Accepted: *11 September 2017*
Published: *26 September 2017*

Citation:
Liang T, Hu Z, Li Y, Ye C and Liu Q (2017) Electrophysiological Correlates of Change Detection during Delayed Matching Task: A Comparison of Different References. Front. Neurosci. 11:527. doi: 10.3389/fnins.2017.00527

INTRODUCTION

The detection of changed information between memory representation and perceptual inputs is of considerable importance to our cognitive process. It helps adjust the current cognitive operation to promote appropriate behaviors in keeping with the ever-changing environments (Hollingworth et al., 2008; Richard et al., 2008). Previous studies of this field generally adopt the delayed matching

paradigm. In this task, a memory item is displayed and followed by a test item some 100 ms later that is either change or no change from the foregoing memory item. By exploiting this paradigm, Cui et al. (2000) found that the change detection processing could be tracked by a frontal distributed N270 component. After them, this component was confirmed by the delayed matching task with various stimulus materials, like the number amplitude (Li et al., 2003), cross-modal gender mismatch (Wang et al., 2002) and the arithmetic conflicts (Newman and Connolly, 2004). N270 was also used in clinical studies to assess the patient's cognitive function (Wang et al., 2002; Sun et al., 2008). Cortical source localization evidences showed that N270 may generate from the anterior cingulate cortex (ACC) (Yin et al., 2012). In consideration of a strong connectivity existing between ACC and the dorsolateral prefrontal cortex (DLPFC) (Wang et al., 2010), it was proposed that N270 reflects the downstream process (Zhang et al., 2008; Scannella et al., 2016). This mechanism is based upon the afferent ACC signals and takes place within the DLPFC to generate an appropriate behavior response (Scannella et al., 2016).

Not only the anterior region, the posterior area was also found to be involved in the processing of change detection in delayed matching task, especially the left occipito-temporal cortex (Zhang et al., 2008). However, no corresponding electrophysiological signal was found from this brain area. What needs to be pointed out is that previous studies focused on this process mainly used the linked mastoid (LM) as the reference (Cui et al., 2000; Wang et al., 2002; Li et al., 2003; Sun et al., 2008; Scannella et al., 2016), which is the average of the left and right mastoids. While Yao et al. (2005) found that LM-obtained EEG power was markedly shifted to the frontal and superficial positions in an unreasonable way. Based on such observation, it is reasonable to speculate that the improper use of the LM reference may weaken the strength of posterior electrophysiological signals, thus makes the posterior task related ERP effects disappeared. In fact, not just the scalp distribution of power spectra, the wave amplitude of the scalp potentials, large-scale networks and non-linear features of EEG were also shown to be distorted by the use of LM (Kayser et al., 2007; Marzetti et al., 2007; Yao et al., 2007; Qin et al., 2010; Tian and Yao, 2013; Chella et al., 2017; Lei and Liao, 2017; Yang et al., 2017). Besides, taking into account the fact that there is no neutral location exists on the human body surface (Nunez et al., 1997), the average reference (AR) that relying on human upper scalp electrodes also faces similar theoretical defect (Yao, 2017). Fortunately, a newly reference electrode standardization technique (REST) was provided to compensate for this problem (Yao, 2001). Unlike the channel-based reference methods, such as AR and LM, the REST technique can avoid the use of the human body surface positions as reference by establishing a point at infinity to constitute a neutral reference. The superiority of the REST has also been confirmed by several lines of evidences. For instance, by investigating the effects of reference choice on the analysis of the non-linear features of the EEG signals, Chella et al. (2017) found that compared with all other types of references (with vertex electrode, LM AR and REST in their study), the REST technology can do a better job in approximating the zero value. With less error, Lei and Liao (2017) also observed that REST could be adopted as the preferable reference for all large-scale networks, regardless of the EEG signal-to-noise ratios and the electrodes number. Based on these findings, it is reasonable to predict that some new insights would also be got in the electrophysiological correlates of change detection if the REST technology is adopted.

To test this hypothesis, EEG data in delayed matching task were referenced to LM, AR, and REST methods with the ERP amplitude, voltage scalp distribution and the signals statistical parametric scalp mapping (SPSM) were measured. In order to create a change circumstance between memory representation and perceptual input, interval in delayed matching task was set to 1,000 ms. Given that the iconic memory trace of one item could only be last about 250 ms (Gegenfurtner and Sperling, 1993), it is sufficient to ensure that the first item was stored into visual working memory. We were also concerned with whether the REST is a more sensitive reference technique than the other two types of methods. To this end, colored shapes were adopted and its change types were manipulated by equally changing the task-relevant shape feature and -irrelevant color feature. Based on this operation, we aimed at investigating the sensitivity of different types of references to the N270 component elicited by the task-irrelevant feature change.

MATERIALS AND METHODS

Participants

All participants were recruited from the Liaoning Normal University community and reported normal or corrected-to-normal vision and none had a history of neurological disorders. Fourteen right-handed students (10 males) with a mean age of 22.5 years (range 20–26) participated in this study. This experiment was carried out in accordance with the recommendations of procedures and protocols approved by the human subjects review committee of Liaoning Normal University with written informed consent from all participants.

Stimuli

Stimuli were colored shape ($2.38^\circ \times 2.38^\circ$ images, 70 cm in front of the participants). The color of stimuli was randomly selected from a set of five colors: green (0, 255, 0), red (255, 0, 0), yellow (255, 255, 0), blue (0, 0, 255), and violet (255, 0, 255), and their shapes were randomly selected from a set of five shapes (crisscross, round, triangle, square and heart). Stimuli were presented on a 17-inch CRT monitor (1,024 × 768 pixels, 85 Hz refresh-rate), with a gray background (128, 128, 128).

Experimental Procedures

Participants performed a delayed matching task in which they had to detect the change between two successively presented figures. On each trial, memory item was presented for 300 ms, followed by a 1,000 ms blank display, and then by a probe display, which remained until participants responded using the keyboard (**Figure 1**). Participants were required to remember the shape feature of the memory item while ignoring its color feature, and judge whether the shape of the probe item was as same as that of the memory item. Participants were informed of pressing "F"

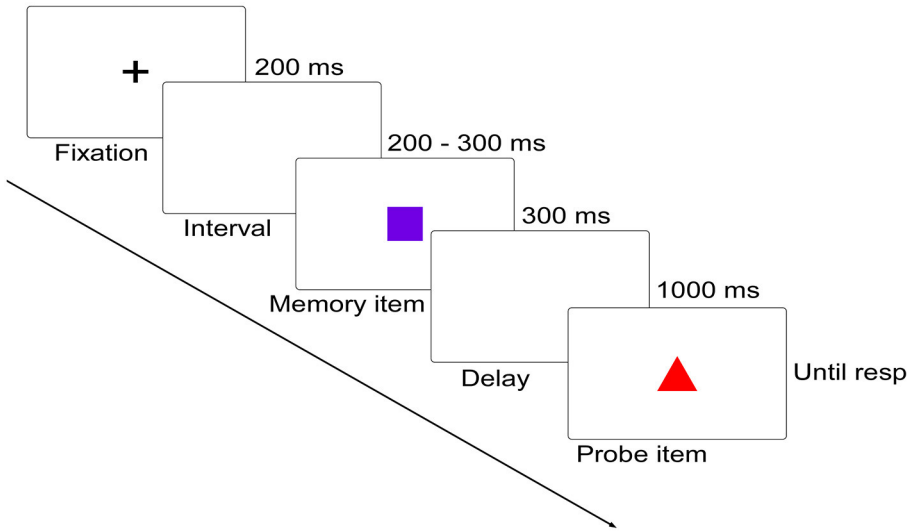

FIGURE 1 | Schematic diagram (not to scale) of the delayed matching task. In this diagram, both of the shape (relevant) and color (irrelevant) features were changed. Below are the five distinct shapes and colors used in the current study.

on the keyboard for shape feature changed trials and "J" for no shape feature changed trials as quickly and accurately as possible. Once the responses were initiated, a 1,000–1,400 ms blank display would be presented before the start of the next trial.

Four interested conditions were included: (1) memory item and probe item were complete same (No change, NC); (2) probe item was different from the memory item in the task-irrelevant color feature (Irrelevant-change, IC); (3) probe item was different from the memory item in the task-relevant shape feature (Relevant-change, RC); (4) both of the items were different in their color feature and shape feature (Conjunction-change, CC). There were 10 practice trials and 400 experimental trials, with 100 trials for each condition. Besides, another visual task was also invited to complete. Since this task has nothing to do with the current study, the data were not included in the current report.

EEG Recording

The EEG signals were recorded by using a 64-channel amplifier ANT Neuro EEGO mounted in a cap using 10/20 montage. Horizontal and vertical EOG were recorded bipolar from the outer canthi of the eyes and from above and below the observer's left eye. The GND electrode served as the ground electrode and CPz served as the on-line reference. Electrode impedances were kept below 10 kV with a sampling rate at 500 Hz for off-line analysis.

EEG Data Preprocess and Re-reference

EEGLAB (Makeig et al., 2004) and Letswave (Mouraux and Iannetti, 2008) were used for off-line processing. Original EEG signals were digitally filtered with the band-pass of 0.1 and 30 Hz. EEG epochs were then extracted with a time window of 2,000 ms (−500 ms pre-stimulus and 1,500 ms post-stimulus) for independent component decomposition. Before independent component analysis algorithm (Makeig et al., 2004) was adopted to correct EOG artifacts, trials corresponding to error or contaminated by gross movements were removed manually. After the independent component analysis, epochs were re-segmented into a time window of 1,200 ms (−200 ms before the probe item and 1,000 ms after the probe item) for ERP analysis. Baseline correction was performed using the pre-stimulus interval (−200 to 0 ms before the probe item).

After that, the remaining EEG trials were referenced to AR, LM, and REST references. LM used the average of the bilateral mastoids as reference. AR reference used the average of all channels as reference. Whereas REST (Yao, 2001) was conducted by the REST software from www.neuro.uestc.edu.cn/rest. Notably, re-reference was done after all the preprocessing had been completed. This measure could effectively avoid the impact of distinctive artifact removal standards on the reference effects.

For all the data in the present study, only the correct-response trials were analyzed. We adopted an exploratory data-driven analysis to identify the time regions of interest and their corresponding spatial regions of interest, which were the most significantly modulated by the factor of change type. Before proceeding the exploratory data-driven analysis, it is necessary to point out that we were only interested in the time window of 600 ms after probe item onset, for the reason that participants tended to finish their responses within about 600 ms after the memory item onset (see **Figure 2A**). To do the exploratory data-driven analysis, each time point of the waveforms was compared using a point-by-point one-way repeated-measure ANOVA, with change types (IC. RC, NC and CC) as the factor, combined with a non-parametric cluster-based permutation test (Maris and Oostenveld, 2007). This procedure was repeated 5,000 times. It yielded a data-driven distribution of a time map of F-value and p-value. Time points with a p-value ≤ 0.01 were selected

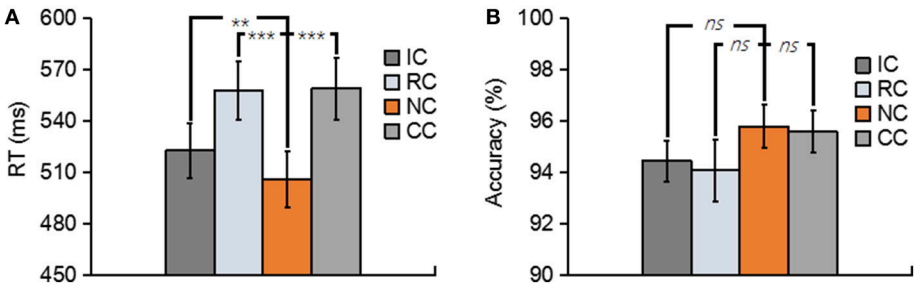

FIGURE 2 | (A) Depicts the mean reaction time (RT) for No change (NC), Irrelevant-change (IC), Relevant-change (RC), and Conjunction-change (CC) conditions. **(B)** Depicts the mean accuracy for four conditions. Error bars represent the standard errors. ns, non-significant; $^{**}p < 0.01$; $^{***}p < 0.001$.

to identify the time regions of interest and their corresponding spatial regions of interest. Scalp distributions of the *p*-value were used to form the statistical parametric scalp mapping (SPSM), which was used as the experimental effects of each reference.

Then, the mean amplitudes within the time regions of interest of the N270 and posterior P2 at the corresponding spatial regions of interest for each experimental condition were calculated. These mean amplitude values were then entered into a one-way repeated-measure ANOVA with the factor of change type. Greenhouse Geisser Epsilon was carried out to adjust the degrees of freedom if necessary. Significant main effect was followed by *post-hoc* contrasts with the Bonferroni correction.

RESULTS

Behavioral Results

Trials with a response time (RT) of less than 200 ms or greater than two standard deviations from the mean RT were removed. both the RT and the accuracy for each type of experimental condition are shown in **Figure 2**. In terms of RT, a one-way repeated-measures ANOVA with the factor of change type revealed a significant main effect [$F_{(3, 39)} = 29.76$, $p < 0.01$, $\eta_p^2 = 0.70$] (**Figure 2A**). Planned comparison contrast showed that the RC ($p < 0.01$), IC ($p < 0.01$) and CC ($p < 0.01$) significantly lengthened the response time, compared with NC. RC ($p < 0.01$) and CC ($p < 0.01$) also significantly lengthened the response time when compared with IC. The other ones were non-significant [all $p > 0.5$]. The above results suggested that whether the changed features were task relevant or not, they all considerably influenced the performance of the participants, thus generated a robust change conflict.

An identical ANOVA on the accuracy data was conducted. As shown in **Figure 2B**, accuracies were near ceiling at all conditions with all the accuracy data were greater than 94%, and no significant difference was found among four conditions [$F_{(3, 39)} = 1.44$, $p = 0.25$].

ERP Results

For the consideration of simplicity, ERP waveforms of four conditions in frontal electrodes (F7, FZ, and F8) and posterior electrodes (PO7, POz, and PO8) were displayed in **Figure 3** for the three types of reference (LM, REST, and AR). Based on previous studies and the results of the data-driven analysis, mean amplitudes were averaged at N270 latency (210–270 ms) and posterior P2 latency (210–290 ms) at the frontal electrode clusters (N270 [F1, FZ, F2]) and the left posterior electrode clusters (P2 [PO5, PO7, P7]) for three references separately. The use of the mean value of ROI and multiple adjacent electrodes was to improve the signal-to-noise ratio (Keil et al., 2014) of ERP data. **Figure 4** shows the scalp distributions of N270 and posterior P2 within the time window of 210–290 ms in all conditions and for three references separately. Besides, to clearly show the change detection-related ERP effects based on each reference at the time range of 210–290 ms, the scalp distributions of the difference waves were shown in **Figure 5A**. As can be seen, N270 culminating at the central frontal sites and posterior P2 culminating at the left posterior sites in all types of references. Then, for each type of reference, a one-way repeated-measure ANOVA with the factor of change type was conducted.

For N270, the results revealed a significant main effect in LM [$F_{(3, 39)} = 17.86$, $p < 0.01$, $\eta_p^2 = 0.58$], REST [$F_{(3, 39)} = 23.89$, $p < 0.01$, $\eta_p^2 = 0.65$] and AR [$F_{(3, 39)} = 6.79$, $p < 0.05$, $\eta_p^2 = 0.34$] (see **Figure 6**). *Post-hoc* contrast showed that in LM, the N270 amplitude of NC was significantly lower than that of RC ($p < 0.01$) and CC ($p < 0.01$), no significant difference was found between IC and NC ($p = 0.07$); in REST, the N270 amplitude of NC was significantly lower than that of RC ($p < 0.01$), CC ($p < 0.01$) and IC ($p = 0.02$); while in AR, only CC elicited a significantly more negative N270 ($p < 0.05$), but not RC ($p = 0.13$) and IC ($p = 1$).

For posterior P2, the results revealed a significant main effect in REST [$F_{(3, 39)} = 16.62$, $p < 0.01$, $\eta_p^2 = 0.56$] and AR [$F_{(3, 39)} = 28.77$, $p < 0.01$, $\eta_p^2 = 0.69$], but not in LM [$F_{(3, 39)} = 1.76$, $p = 0.19$] (see **Figure 7**). *Post-hoc* contrast showed that in REST, the posterior P2 amplitude of NC was significantly lower than that of RC ($p < 0.05$) and CC ($p < 0.01$), no significant difference was found between IC and NC ($p = 1$). In AR, the same pattern of results was obtained. Concretely, the posterior P2 amplitude of NC was significantly lower than that of RC ($p < 0.01$) and CC ($p < 0.01$), no significant difference was found between IC and NC ($p = 0.20$).

SPSM Results

Scalp distributions of *p*-value for the main effect of change type were used to form the statistical parametric scalp mappings

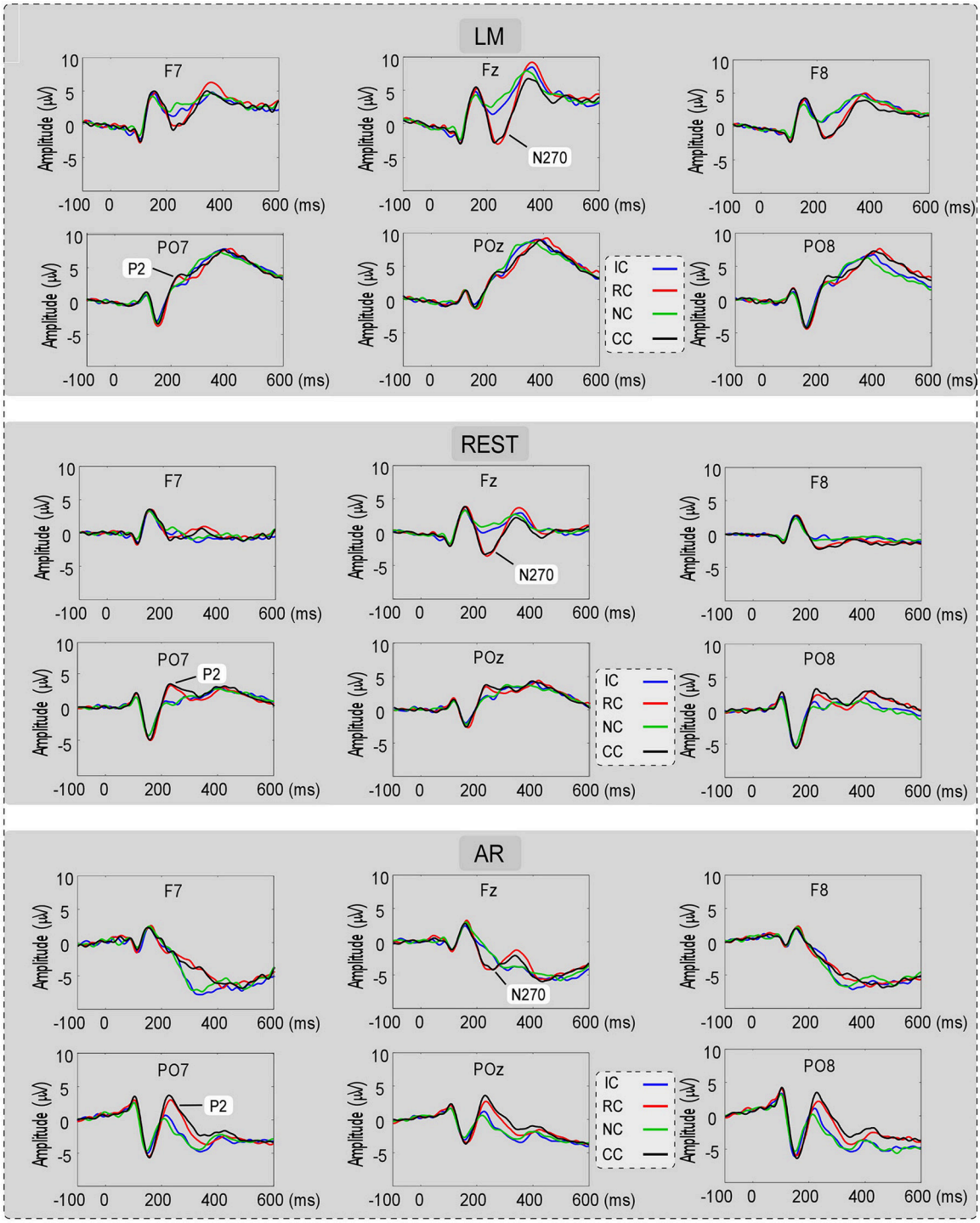

FIGURE 3 | The ERP waveforms for No change (NC), Irrelevant-change (IC), Relevant-change (RC), and Conjunction-change (CC) conditions in six electrodes (F7, FZ, F8, PO7, POz, and PO8), for three references separately.

(SPSM), which was used to represent the experimental effect of each type of reference. As can be seen from **Figure 5B**, the SPSM of each reference was different from each other, with AR mainly indicated a left posterior distribution, REST indicated center to right anterior and left posterior distributions, and LM indicated a center to right anterior distribution. Obviously, each type of reference yielded a distinct distribution pattern of the task-related ERP effect.

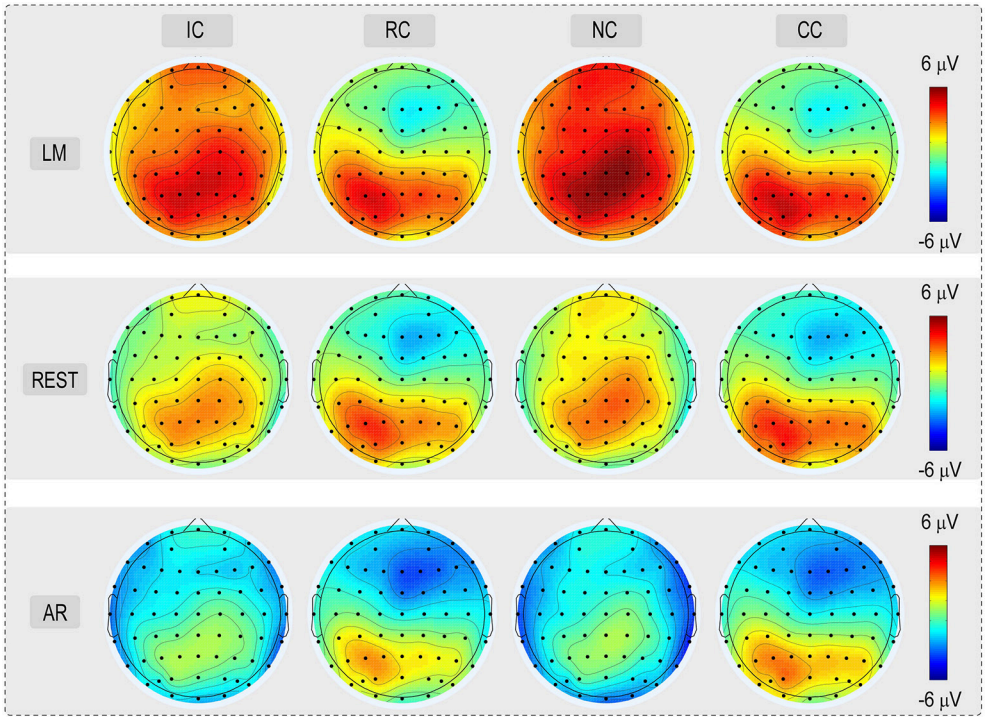

FIGURE 4 | Voltage topographies (210–290 ms) of posterior P2 and N270 for No change (NC), Irrelevant-change (IC), Relevant-change (RC), and Conjunction-change (CC) conditions, for three references separately.

DISCUSSION

In current study, the change detection-related ERP effects were systematically investigated by comparing the LM, REST, and AR references in a delayed matching task. To avoid the contamination of distinctive artifact removal standards on the reference effects, re-reference was done after all preprocessing had been completed. As predicted, both of the SPSM and the change detection-related ERP effects were changed by the adopted references. Specifically, the ERP results showed that in LM, both the relevant change and the conjunction change elicited significantly more negative N270, but not the irrelevant change. Notably, the change detection-related posterior P2 effect disappeared under LM. In AR, only the irrelevant feature change elicited a significantly more negative N270, while both the relevant change and the conjunction change elicited significantly more positive posterior P2. In REST, however, all the three types of change conditions elicited significantly more negative N270. Besides, both the relevant change and the conjunction change elicited significantly more positive posterior P2. Consistent with these findings, the SPSM showed a left posterior distribution of task-related ERP effects for AR, an anterior distribution for LM, and both anterior and left posterior distributions for REST.

Reference Effect on the ERP Amplitude

An objective fact is that the inverse problem of EEG is reference-free. It means that the spatial distribution pattern of the scalp voltages is not affected by the references used (Geselowitz, 1998; Yao, 2001; Yao et al., 2007). In the current data, we also observed that identical spatial distribution patterns of the scalp voltages of each condition were observed across all three types of references (**Figure 4**). However, consistent with previous findings (Kayser et al., 2007; Yao et al., 2007; Tian and Yao, 2013; Liu et al., 2015; She et al., 2017), ERP effects in current study also vary depending on the adopted references. In this case, each type of reference could provide distinct results from the same data. Therefore, three distinct possible explanations were suggested: (1) based on LM, the frontal conflict control system was mainly involved in detecting changed information, and the conflicting effect caused by the task irrelevant feature change was effectively ignored; (2) based on AR, it could be the case that the change detection process mainly involved the posterior attention mechanism, and only the detection of conjunction feature change requisitioned the frontal control system; (3) based on REST, both the posterior attention mechanism and frontal conflict control system were involved in the change detection processing, and therefore more in line with the multi-stage theory of percept-memory comparison (Hyun et al., 2009; Yin et al., 2012). Besides, only the REST-obtained N270 showed a significant increment in the task-irrelevant feature change. This finding was compatible with the delayed behavioral performance, and therefore is consistent with the view that frontal conflict control mechanism characterized by N270 is responsible for regulating external behavioral conflicts (Zhang et al., 2008; Yin et al., 2012; Scannella et al., 2016). Obviously, the interpretation of the ERP results

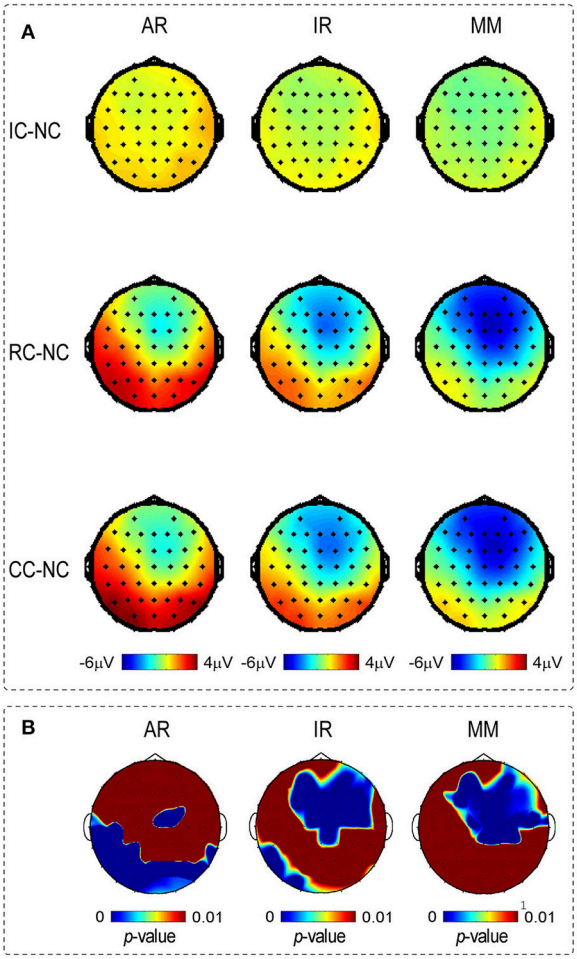

FIGURE 5 | (A) Depicts the voltage topographies (210–290 ms) of the different waveforms of posterior P2 and N270, for three references separately. Different waveforms were calculated by subtracting the Irrelevant-change (IC), Relevant-change (RC) and Conjunction-change (CC) from No change (NC). **(B)** Depicts the SPSM of the LM, REST, and AR references at the time range of 210–290 ms.

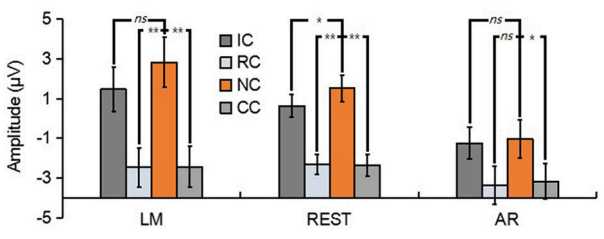

FIGURE 6 | Mean amplitude of the N270 (210–270 ms) of each condition for three types of references by averaging the electrodes at frontal electrode cluster [(F1 + Fz + F2)/3]. ns, non-significant; $^{*}p < 0.05$; $^{**}p < 0.01$.

varied with the references used, and only the REST provided the closest approximation to the relevant literatures and the delayed behavior performance.

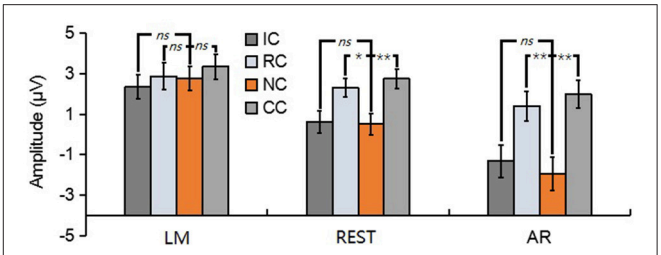

FIGURE 7 | Mean amplitude of the posterior P2 (210–290 ms) of each condition for three types of references by averaging the electrodes at left posterior electrode cluster [(PO5 + PO7 + P7)/3]. ns, non-significant; $^{*}p < 0.05$; $^{**}p < 0.01$.

Reference Effect on the SPSM

Previous studies found that SPSM varies depending on the adopted references (Tian and Yao, 2013; Yang et al., 2017). Consistent with these findings, we also observed that SPSM in current study varied with the references used (see **Figure 5B**). However, only one result is the most reasonable. The distribution of SPSM closest to the real case should correspond to the brain regions activated in the change detection processing. By using a delayed matching task as the current study, Zhang et al. (2008) found that the detection of changed information mainly activated the left occipito-temporal cortex, together with the right ACC and the right DLPFC. Notably, only the SPSM obtained by the REST was consistent with the scalp distribution of activated brain regions of Zhang et al. (2008), but not the other two types of references, thus confirming the superiority of the REST technology.

Why Is Rest More Reasonable?

In the ERP study, cognitive neuroscientists tend to pay more attention to the ERP amplitude differences induced by different experimental conditions. Tian and Yao (2013) have been pointed out that the effect of references choice on the wave amplitude of each experimental condition is a constant at the same time point of each electrode, while the constant at different time points is variable. This view explains why the task-related ERP effects in previous studies (Tian and Yao, 2013; She et al., 2017) and the current data varied with the references used, and indicates that the effects of the references choice to EEG data are unavoidable. In this case, if the adopted reference is non-neutral, task-induced electric potentials would be mixed into the calculation of the reference value of each experimental condition. If these mixed neural electric potentials vary depending on the experimental conditions, then the reference value of each experimental condition would not be a constant. This will inevitably distort the true amplitude differences between different experimental conditions. When one try to calculate the significant difference between the ERP amplitude of two experimental conditions at a certain time point, this kind of distortion induced by the use of the non-neutral reference would be manifested in three forms: (1) if the original electric potentials of two experimental conditions have the same changing trend with their respective reference values, then their amplitude difference

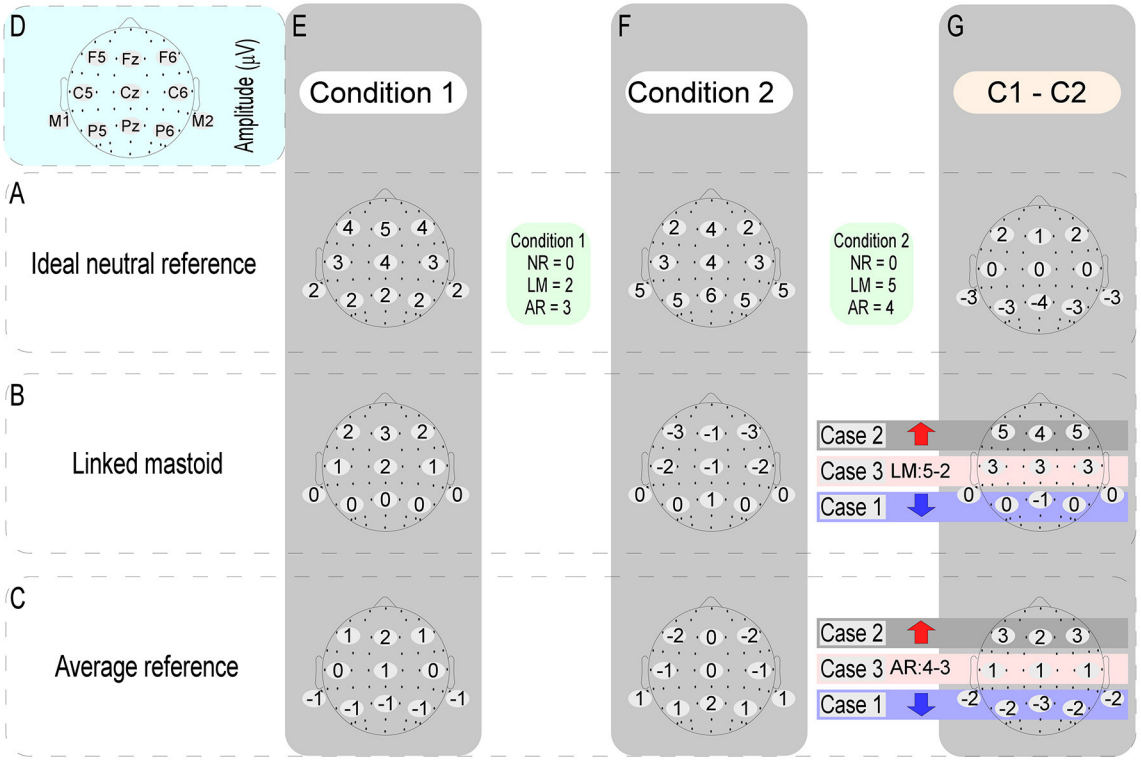

FIGURE 8 | The above figure shows when one try to calculate the significant difference between the ERP amplitudes of two experimental conditions (C1 - C2) at a certain time point, the distortion of the data induced by using of the non-neutral reference [i.e., average reference (AR) and linked mastoid (LM)] might be conveyed in three forms. We took the ERP data obtained by the ideal neutral reference (row A) as the true data. The other two types of references were referenced based on this data. As can be seen from above, compared with the true difference values (the difference map of row A and column G): (case 1) if the voltage values of any one of the electrodes (here, take F5, FZ, and F6 electrodes as examples) between two different experimental conditions have the same changing trend with their respective reference values, then their amplitude difference would be falsely reduced (as indicated by the blue arrows); (case 2) if the voltage values of any one of the electrodes (here, take P5, PZ, and P6 electrodes as examples) between two different experimental conditions have an opposite changing trend with their respective reference values, then their amplitude difference will be falsely increased (as indicated by the red arrow); (case 3) if the voltage values of any one of the electrodes (here, take C5, CZ, and C6 electrodes as examples) between two different experimental conditions are the same, however, the amplitude differences between them will depend entirely on the difference of their respective reference values.

would be decreased; (2) if the original electric potentials of two experimental conditions have an opposite changing trend with their respective reference values, then their amplitude difference would be increased; (3) however, when the original electric potentials of two experimental conditions are the same, the amplitude difference between them will depend entirely on the difference of their respective reference values (in detail, **Figure 8** illustrates a specific case). Take the LM reference as an example. This method assumes that there is no electrical activity at the electrode sites of the bilateral mastoids. However, this assumption does not hold, since there is no genuine electrically inactive reference site on the head (Katznelson, 1981; Nunez et al., 1997). Considering that bilateral mastoids adjoin the temporal occipital regions, the task-related electrical activities in these areas would inevitably be mixed into the calculation of the reference value of LM. This will weaken the electrical signals of the bilateral temporal occipital regions, while the signals away from the bilateral mastoid sites (i.e., the central frontal region) might be falsely increased. This reasoning is consistent with the current results and previous findings (Tian and Yao, 2013), which showed that the ERP power of LM was markedly shifted to the frontal region. Besides, this view can also explain why the change detection-related ERP effects in the left posterior area of current study was erased when the LM was used.

Unlike the LM, AR uses the average of all the scalp electrodes, and thus is regarded as unbiased to any electrode sites. The basic assumption of AR is that the surface potential integral of a volume conductor is zero at any given time point (Geselowitz, 1998). This means that when the whole brain is densely covered by electrodes and close to the sphere in its shape, the average of the potentials recorded at these electrode sites will be infinitely close to the theoretically desired zero value (Geselowitz, 1998). However, this kind of electrode setting is almost impossible to achieve in the real operations, in consideration of the spatial distribution of electrodes being limited to the upper part of the head (i.e., the electrode caps used in the current study). In this case, similar to LM, the reference values of AR for different experimental conditions would not be a constant. Supposing that the amplitude difference between two experimental conditions occurs in a portion of the brain region (i.e., the frontal area

of current study and the posterior region of Tian and Yao), in the light of the above logic, the task-related ERP effects in this areas might be attenuated and erroneously transferred to other brain regions (i.e., the frontal region of Tian and Yao and the posterior area of current study) when AR was adopted. Recently, the theoretical shortcomings of AR were also confirmed by Yao (2017). By showing three counter-examples, Yao pointed out that AR is not good in theory in general.

Compared with the other two types of references, REST is not a channel-based reference. More importantly, REST has a solid theoretical support from the mathematical physics (Yao, 2001; Yao et al., 2007). Approximately reconstructing a point far away from all brain sources and scalp electrode sites, REST was proved to be closer to the neutral reference (Yao, 2001; Zhai and Yao, 2004; Liu et al., 2015; Chella et al., 2016). Therefore, REST is considered the most realistic way to restore the EEG signals. The rationality of the REST was also confirmed by a series of simulation studies. These studies all suggested that the reference values provided by the REST technology are closer to the ideal zero or neutral point (Yao, 2001; Zhai and Yao, 2004; Marzetti et al., 2007; Qin et al., 2010; Liu et al., 2015; Chella et al., 2016; Huang et al., 2017; Lei and Liao, 2017). This means that the results provided by the REST are closest to the actual case. Consistent with this view, REST-based ERP results proved to be the most reasonable in the current data and previous studies (Tian and Yao, 2013; She et al., 2017; Yang et al., 2017).

CONCLUSION

In summary, the choice of reference is critical to ERP research. Although the spatial distributions of the scalp voltages were consistent between the adopted references, the task-related ERP effects might be changed. Most importantly, the current data and previous studies have consistently confirmed that REST can provide the most reasonable results. On the physical level, we point out the effects of non-neutral references on the significant differences of wave amplitudes between different experimental conditions. Coupled with the support of many theoretical evidences, we recommend future researchers use the REST technique extensively to better understand our brain.

AUTHOR CONTRIBUTIONS

TL and ZH designed the research, TL collected the data, TL, YL, and QL analyzed the data, and all authors interpreted the data and wrote the manuscript.

ACKNOWLEDGMENTS

This research was supported by grants from the National Natural Science Foundation of China (NSFC 31571123) to QL (NSFC 31600883) to ZH.

REFERENCES

Chella, F., D'Andrea, A., Basti, A., Pizzella, V., and Marzetti, L. (2017). Non-linear analysis of scalp EEG by using bispectra: the effect of the reference choice. *Front. Neurosci.* 11:262. doi: 10.3389/fnins.2017.00262

Chella, F., Pizzella, V., Zappasodi, F., and Marzetti, L. (2016). Impact of the reference choice on scalp EEG connectivity estimation. *J. Neural Eng.* 13:036016. doi: 10.1088/1741-2560/13/3/036016

Cui, L., Wang, Y., Wang, H., Tian, S., and Kong, J. (2000). Human brain sub-systems for discrimination of visual shapes. *Neuroreport* 11, 2415–2418. doi: 10.1097/00001756-200008030-00015

Gegenfurtner, K. R., and Sperling, G. (1993). Information transfer in iconic memory experiments. *J. Exp. Psychol. Hum. Percept. Perform.* 19, 845–866. doi: 10.1037/0096-1523.19.4.845

Geselowitz, D. B. (1998). The zero of potential. *IEEE Eng. Med. Biol. Mag.* 17, 128–132. doi: 10.1109/51.646230

Hollingworth, A., Richard, A. M., and Luck, S. J. (2008). Understanding the function of visual short-term memory: transsaccadic memory, object correspondence, and gaze correction. *J. Exp. Psychol. Gen.* 137, 163–181. doi: 10.1037/0096-3445.137.1.163

Huang, Y., Zhang, J., Cui, Y., Yang, G., He, L., Liu, Q., et al. (2017). How different EEG references influence sensor level functional connectivity graphs. *Front. Neurosci.* 11:368. doi: 10.3389/fnins.2017.00368

Hyun, J. S., Woodman, G. F., Vogel, E. K., Hollingworth, A., and Luck, S. J. (2009). The comparison of visual working memory representations with perceptual inputs. *J. Exp. Psychol. Hum. Percept. Perform.* 35, 1140–1160. doi: 10.1037/a0015019

Katznelson, R. D. (1981). "EEG recording, electrode placement, and aspects of generator localization," in *Electric Fields of the Brain: The Neurophysics of EEG*, ed P. L. Nunez (New York, NY: Oxford University Press), 176–213.

Kayser, J., Tenke, C. E., Gates, N. A., and Bruder, G. E. (2007). Referenceindependent ERP old/new effects of auditory and visual word recognition memory: joint extraction of stimulus- and response-locked neuronal generator patterns. *Psychophysiology* 44, 949–967. doi: 10.1111/j.1469-8986.2007.00562.x

Keil, A., Debener, S., Gratton, G., Junghöfer, M., Kappenman, E. S., Luck, S. J., et al. (2014). Committee report: publication guidelines and recommendations for studies using electroencephalography and magnetoencephalography. *Psychophysiology* 51, 1–21. doi: 10.1111/psyp.12147

Lei, X., and Liao, K. (2017). Understanding the influences of EEG reference: a large-scale brain network perspective. *Front. Neurosci.* 11:205. doi: 10.3389/fnins.2017.00205

Li, L., Wang, Y., Wang, H., Cui, L., and Tian, S. (2003). Event-related potential N270 and its distribution in adults and school-age children. *Brain Dev.* 25, 507–513. doi: 10.1016/S0387-7604(03)00059-7

Liu, Q., Balsters, J. H., Baechinger, M., van der Groen, O., Wenderoth, N., and Mantini, D. (2015). Estimating a neutral reference for electroencephalographic recordings: the importance of using a high-density montage and a realistic head model. *J. Neural Eng.* 12:056012. doi: 10.1088/1741-2560/12/5/056012

Makeig, S., Debener, S., Onton, J., and Delorme, A. (2004). Mining event-related brain dynamics. *Trends Cogn. Sci.* 8, 204–210. doi: 10.1016/j.tics.2004.03.008

Maris, E., and Oostenveld, R. (2007). Nonparametric statistical testing of EEG-and MEG-data. *J. Neurosci. Methods* 164, 177–190. doi: 10.1016/j.jneumeth.2007.03.024

Marzetti, L., Nolte, G., Perrucci, M. G., Romani, G. L., and Del Gratta, C. (2007). The use of standardized infinity reference in EEG coherency studies. *Neuroimage* 36, 48–63. doi: 10.1016/j.neuroimage.2007.02.034

Mouraux, A., and Iannetti, G. D. (2008). Across-trial averaging of event-related EEG responses and beyond. *Magn. Reson. Imaging* 26, 1041–1054. doi: 10.1016/j.mri.2008.01.011

Newman, R. L., and Connolly, J. F. (2004). Determining the role of phonology in silent reading using event-related brain potentials. *Brain Res. Cogn. Brain Res.* 21, 94–105. doi: 10.1016/j.cogbrainres.2004.05.006

Nunez, P. L., Srinivasan, R., Westdorp, A. F., Wijesinghe, R. S., Tucker, D. M., Silberstein, R. B., et al. (1997). EEG coherency. I: statistics, reference electrode, volume conduction, laplacians, cortical imaging, and

interpretation at multiple scales. electroencephal. *Clin. Neurophysiol.* 103, 499–515. doi: 10.1016/S0013-4694(97)00066-7

Qin, Y., Xu, P., and Yao, D. (2010). A comparative study of different references for EEG default mode network: the use of the infinity reference. *Clin. Neurophysiol.* 121, 1981–1991. doi: 10.1016/j.clinph.2010.03.056

Richard, A. M., Luck, S. J., and Hollingworth, A. (2008). Establishing object correspondence across eye movements: flexible use of spatiotemporal and surface feature information. *Cognition* 109, 66–88. doi: 10.1016/j.cognition.2008.07.004

Scannella, S., Pariente, J., De Boissezon, X., Castel-Lacanal, E., Chauveau, N., Causse, M., et al. (2016). N270 sensitivity to conflict strength and working memory: a combined ERP and sLORETA study. *Behav. Brain Res.* 297, 231–240. doi: 10.1016/j.bbr.2015.10.014

She, S., Li, H., Ning, Y., Ren, J., Wu, Z., Huang, R., et al. (2017). Revealing the dysfunction of schematic facial-expression processing in schizophrenia: a comparative study of different references. *Front. Neurosci.* 11:314. doi: 10.3389/fnins.2017.00314

Sun, W., Wang, Y., Wang, W., and Wu, X. (2008). Attention changes in epilepsy patients following 3-month topiramate or valproate treatment revealed by event-related potential. *Int. J. Psychophysiol.* 68, 235–241. doi: 10.1016/j.ijpsycho.2008.02.003

Tian, Y., and Yao, D. (2013). Why do we need to use a zero reference? Reference influences on the ERPs of audiovisual effects. *Psychophysiology* 50, 1282–1290. doi: 10.1111/psyp.12130

Wang, H., Wang, Y., Wang, D., Cui, L., Tian, S., and Zhang, Y. (2002). Cognitive impairment in Parkinson's disease revealed by event-related potential N270. *J. Neurol. Sci.* 194, 49–53. doi: 10.1016/S0022-510X(01)00674-8

Wang, L., Liu, X., Guise, K. G., Knight, R. T., Ghajar, J., and Fan, J. (2010). Effective connectivity of the fronto-parietal network during attentional control. *J. Cogn. Neurosci.* 22, 543–553. doi: 10.1162/jocn.2009.21210

Yang, P., Fan, C., Wang, M., and Li, L. (2017). A Comparative study of average, linked mastoid, and rest references for ERP components acquired during fMRI. *Front. Neurosci.* 11:247. doi: 10.3389/fnins.2017.00247

Yao, D. (2001). A method to standardize a reference of scalp EEG recordings to a point at infinity. *Physiol. Meas.* 22:693. doi: 10.1088/0967-3334/22/4/305

Yao, D. (2017). Is the surface potential integral of a dipole in a volume conductor always zero? a cloud over the average reference of EEG and ERP. *Brain Topogr.* 30, 161–171. doi: 10.1007/s10548-016-0543-x

Yao, D., Wang, L., Arendt-Nielsen, L., and Chen, A. C. (2007). The effect of reference choices on the spatio-temporal analysis of brain evoked potentials: the use of infinite reference. *Comput. Biol. Med.* 37, 1529–1538. doi: 10.1016/j.compbiomed.2007.02.002

Yao, D., Wang, L., Oostenveld, R., Nielsen, K. D., Arendt-Nielsen, L., and Chen, A. C. (2005). A comparative study of different references for EEG spectral mapping: the issue of the neutral reference and the use of the infinity reference. *Physiol. Meas.* 26, 173–184. doi: 10.1088/0967-3334/26/3/003

Yin, J., Gao, Z., Jin, X., Ding, X., Liang, J., and Shen, M. (2012). The neural mechanisms of percept-memory comparison in visual working memory. *Biol. Psychol.* 90, 71–79. doi: 10.1016/j.biopsycho.2012.02.023

Zhai, Y., and Yao, D. (2004). A study on the reference electrode standardization technique for a realistic head model. *Comput. Methods Programs Biomed.* 76, 229–238. doi: 10.1016/j.cmpb.2004.07.002

Zhang, X., Ma, L., Li, S., Wang, Y., Weng, X., and Wang, L. (2008). A mismatch process in brief delayed matching-to-sample task: an fMRI study. *Exp. Brain Res.* 186, 335–341. doi: 10.1007/s00221-008-1285-0

Conflict of Interest Statement: The authors declare that the research was conducted in the absence of any commercial or financial relationships that could be construed as a potential conflict of interest.

frontiers in Neuroscience

ORIGINAL RESEARCH
published: 10 October 2017
doi: 10.3389/fnins.2017.00560

Effect of EEG Referencing Methods on Auditory Mismatch Negativity

Yatin Mahajan[1,2]*, *Varghese Peter*[1] *and Mridula Sharma*[2,3]

[1] *The MARCS Institute for Brain, Behaviour and Development, Western Sydney University, Penrith, NSW, Australia,* [2] *The HEARing CRC, Melbourne, VIC, Australia,* [3] *Department of Linguistics, Australian Hearing Hub, Macquarie University, Sydney, NSW, Australia*

Auditory event-related potentials (ERPs) have consistently been used in the investigation of auditory and cognitive processing in the research and clinical laboratories. There is currently no consensus on the choice of appropriate reference for auditory ERPs. The most commonly used references in auditory ERP research are the mathematically linked-mastoids (LM) and average referencing (AVG). Since LM and AVG referencing procedures do not solve the issue of electrically-neutral reference, Reference Electrode Standardization Technique (REST) was developed to create a neutral reference for EEG recordings. The aim of the current research is to compare the influence of the reference on amplitude and latency of auditory mismatch negativity (MMN) as a function of magnitude of frequency deviance across three commonly used electrode montages (16, 32, and 64-channel) using REST, LM, and AVG reference procedures. The current study was designed to determine if the three reference methods capture the variation in amplitude and latency of MMN with the deviance magnitude. We recorded MMN from 12 normal hearing young adults in an auditory oddball paradigm with 1,000 Hz pure tone as standard and 1,030, 1,100, and 1,200 Hz as small, medium and large frequency deviants, respectively. The EEG data recorded to these sounds was re-referenced using REST, LM, and AVG methods across 16-, 32-, and 64-channel EEG electrode montages. Results revealed that while the latency of MMN decreased with increment in frequency of deviant sounds, no effect of frequency deviance was present for amplitude of MMN. There was no effect of referencing procedure on the experimental effect tested. The amplitude of MMN was largest when the ERP was computed using LM referencing and the REST referencing produced the largest amplitude of MMN for 64-channel montage. There was no effect of electrode-montage on AVG referencing induced ERPs. Contrary to our predictions, the results suggest that the auditory MMN elicited as a function of increments in frequency deviance does not depend on the choice of referencing procedure. The results also suggest that auditory ERPs generated using REST referencing is contingent on the electrode arrays more than the AVG referencing.

Keywords: mismatch negativity, event related potential, reference, REST

OPEN ACCESS

Edited by:
Rui Zhang,
Zhengzhou University, China

Reviewed by:
Dezhong Yao,
University of Electronic Science and Technology of China, China
Camillo Porcaro,
Istituto di Scienze e Tecnologie della Cognizione (ISTC)-CNR, Italy

***Correspondence:**
Yatin Mahajan
y.mahajan@westernsydney.edu.au

Specialty section:
This article was submitted to Brain Imaging Methods, a section of the journal Frontiers in Neuroscience

Received: *22 July 2017*
Accepted: *25 September 2017*
Published: *10 October 2017*

Citation:
Mahajan Y, Peter V and Sharma M (2017) Effect of EEG Referencing Methods on Auditory Mismatch Negativity. Front. Neurosci. 11:560. doi: 10.3389/fnins.2017.00560

INTRODUCTION

Event-related potentials (ERPs) are readily used to assess the brain function in response to sensory events. Excellent temporal resolution (in the order of milliseconds) and cost-effectiveness are two major advantages of the ERPs compared to other neuroimaging procedures. The high temporal resolution ability of the ERPs have been utilized to investigate, low-level cognitive functions such as encoding of sounds (Ponton et al., 2000; Mahajan and McArthur, 2012; Gilley et al., 2016), high-level functions such as attention, working memory, and language (Hillyard et al., 1973; SanMiguel et al., 2008; Peter et al., 2014; Mandikal Vasuki et al., 2017) and the functions that fall in between low and high cognitive functions such as auditory memory, sound discrimination, involuntary attention (Escera et al., 2000; Schröger et al., 2000; Winkler, 2007). Researchers have also been using basic auditory ERPs to assess and to identify auditory perceptual processing abilities and disabilities in children, adolescents, and older adults (Wible et al., 2002; Bishop et al., 2007; McArthur et al., 2009). Auditory ERPs are used to validate and document changes in auditory processing ability after intervention, and to assess auditory plasticity of the brain after hearing rehabilitation (Sharma et al., 2002, 2005, 2014; McArthur et al., 2009).

Despite its usefulness in various fields and populations, the recording of reliable EEG is dependent heavily on technical EEG recording-related factors. The technical issue of "choice of EEG referencing" has been a matter of debate for years (Kayser and Tenke, 2010). There has been no common consensus yet on the choice of appropriate referencing procedure in the ERP research laboratories across the world (Kayser and Tenke, 2010; Luck, 2014; Chella et al., 2016). The process of referencing in ERP recordings is essential as the electric potential measured at a particular electrode on the scalp is relative to the activity of a reference electrode placed elsewhere either on the scalp or non-cephalic placements; i.e., the electrical activity measured at a particular electrode is actually the potential difference between EEG signal measured at electrode and the reference cite. Selecting an appropriate reference for EEG recording becomes a crucial process as the choice of reference can induce changes in the EEG recording and subsequently the ERP analyses i.e., latency, magnitude, and spatial changes in the ERPs (Kayser and Tenke, 2010; Tian and Yao, 2013). For a more detailed technical description of referencing procedure, see Luck (2014).

Theoretically, the choice of reference location for EEG recordings should be electrically neutral or in other words, the referencing procedure should result in a neutral potential (Yao, 2001; Kayser and Tenke, 2010; Qin et al., 2010). However, a neutral position on the human body doesn't exist (Yao, 2001; Nunez and Srinivasan, 2006) and any reference position on the body would introduce an electric potential of its own. This may result in compromised quality of the recorded EEG and in turn the final ERPs. Many referencing positions that are subjectively considered relatively neutral such as the vertex (Pang and Taylor, 2000; Tonnquist-Uhlen et al., 2003), the nose (Alho and Sinervo, 1997; Sussman et al., 2008), the ear lobes (Takeshita et al., 2002), nape of the neck (Katznelson, 1981), and the linked mastoids (Peter et al., 2010; Mahajan and McArthur, 2013, 2015) have been used to quantify auditory ERPs. Widely used linked mastoid (LM) referencing procedure (especially when using auditory ERPs) that represent offline mathematically linking the right and left mastoids and subtracting the average mastoids activity from the active electrode is preferred due to its easy applicability and low impedance characteristics (Yao et al., 2005). LM also has an advantage that it can be used in low density ERP recordings as it is independent of the number of electrodes. Since, there is no electrically neutral point on the scalp or the body, referencing to mastoids may affect the characteristics of the ERPs i.e., amplitude and latencies (Yao et al., 2005, 2007) and influence the interpretability of the ERPs.

Another popular referencing procedure used widely across research laboratories is the average referencing (AVG; Offner, 1950; Nunez et al., 2001). The assumption underlying AVG is that the common average of all the recorded EEG channels will approximate zero and, hence AVG can be considered a neutral reference. This assumption is contingent on extensive spatial sampling which is achieved by using a dense electrode montages covering the full head surface for recording (Yao et al., 2005; Kayser and Tenke, 2010; Luck, 2014). However, commonly used electrode montages 32-channel, 64-channel and even the high density 128-channel electrode montages are not enough to cover the whole head surface as these montages will cover only the upper part of the head. The average activity from the channel cannot approximate zero or neutral potential inducing bias in the EEG recordings (Dien, 1998). Since, ERP laboratories across the world use various scalp-electrode montages (16, 32, 64, or 128-channel), and given the dependence of AVG on the montage, the results of various investigations may not be comparable. Nevertheless, AVG remains a popular alternative referencing procedure similar to LM in the investigation of auditory ERPs (Ponton et al., 2000; Bishop et al., 2007).

Another referencing technique which has been gaining popularity among EEG researchers is reference electrode standardization technique (REST) developed by Yao (2001). The premise behind the REST approach is the concept of infinity reference referring to a point far away from the brain sources and having an ideal neutral reference (Yao, 2001; Yao et al., 2005; Qin et al., 2010). In this approach, the recorded EEG (referenced to any scalp point) is transformed to the potentials referenced to a point located in the infinity, i.e., the neutral reference (Yao, 2001; Chella et al., 2016). The REST approach suffers from same limitations as that of average reference emitting from insufficient electrode density, head surface coverage, and inaccurate knowledge of head model (Yao, 2001; Zhai and Yao, 2004; Liu et al., 2015). However, in simulation studies REST approach has been observed to offset the disadvantages of LM and AVG referencing procedures. It recovers the spatio-temporal characteristics and the power information of the recorded EEG at the scalp level (Yao, 2001; Qin et al., 2010). There have been a few studies comparing the effects of REST technique with other commonly used referencing approaches on EEG power, functional connectivity and default mode network analysis (Yao et al., 2005; Qin et al., 2010; Chella et al., 2016). These investigations have reported that different referencing

procedures result in changes in the EEG power, functional connectivity, and default network measures but all recommended using REST for referencing to offset the variability in these EEG domains.

There is limited research examining the effect of referencing procedures on ERPs. Joyce and Rossion (2005) compared AVG, LM, averaged earlobes, non-cephalic, and nose referencing sites on face-sensitive N170 and vertex positive potential (VPP). They found that while referencing procedures did not affect the latencies of these potentials, the amplitude varied drastically with reference sites for both VPP and N170. They concluded that the discrepancy of the N170/VPP effects across studies could be explained by the difference in reference methodology. Similarly, Yao et al. (2007) compared unilateral mastoids, LM, AVG, vertex reference, and the infinity reference (REST) for temporal and spatial characteristics of four peaks of somatosensory evoked potentials (P30, P40, N90, and P230). The results revealed that referencing procedures influenced the amplitude of all the four peaks across many electrodes but did not change the relative scalp distribution of the potentials. They recommended the use of a common referencing approach across the laboratories. In an another study, Tian and Yao (2013) investigated the influence of average reference, linked mastoids and infinity reference on experimental effects on ERPs elicited using audiovisual stimuli. They found that the scalp distribution of N1 potential was similar (posterior) when REST referenced validated by two spatial analyses methods (SPSM and LORETA). AVG and LM referencing produced different results with these methods. It was suggested that using REST in ERP analyses will increase the accuracy of ERP results. Recently, Chella et al. (2017) reported effectiveness of REST procedures for the analyses of non-linear features of EEG such as frequency analyses for both simulation and real EEG experiments for a less dense 21-channel montage as well. Substantial evidence exist comparing different referencing procedures including REST, LM, and AVG in simulation studies (Liu et al., 2015; Chella et al., 2016, 2017), functional connectivity analyses (Qin et al., 2010), source analyses (Tian and Yao, 2013), with results proving the validity and effectiveness of REST in these EEG measures. Following this promising evidence, a comparative assessment of commonly used referencing procedures such as LM and AVG needs to be conducted against REST to extend the validity of the infinity referencing procedures in the ERP domain as well.

To our knowledge there is no report that has examined the effect of different referencing techniques on auditory ERPs. It is essential to compare different referencing procedures because research on auditory processing using auditory ERPs in basic and clinical audiological and psychological research has used myriad referencing procedures across the research laboratories. Using different referencing procedures for a same research question can result in different inferences and cross-study comparisons across research laboratories may not be comparable. In these cases, it would be constructive to know the effect different referencing procedures (commonly used) may have on auditory ERPs to facilitate uniform comparisons and using a common referencing procedure across the research and clinical laboratories.

In the current experiment, the influence of three commonly used referencing approaches, LM, AVG, and REST was measured on amplitude and latencies of the mismatch negativity (MMN), the auditory ERP. The MMN is a low level cognitive potential and is thought to represent pre-attentive sensory memory (Näätänen, 1992), auditory discrimination (Naatanen et al., 2005; Sharma et al., 2006; Mahajan and McArthur, 2015), and redirection of focussed attention (Naatanen et al., 2005). The auditory MMN can be measured by subtracting an ERP elicited by a frequently occuring "standard" sound from an ERP elicited by an infrequent "deviant" sound of certain physical attribute (frequency, duration, or intensity). In adults, the MMN typically presents as a negative response found 100–250 ms after the onset of a sound. It is established that large frequency differences between standard and the deviant sounds elicit large amplitude and shorter latency of MMN, where as a small difference results in smaller and prolonged latencies of MMN (Tiitinen et al., 1994; Novitski et al., 2004; Kujala et al., 2007). This experimental effect was investigated in the current study. Following Tian and Yao (2013), we investigated the effect of referencing on the experimental effect (increasing difference in deviant and standard frequency) rather than the absolute auditory ERPs. The effect of referencing will be more pronounced on the experimental effects than the absolute ERPs (Tian and Yao, 2013) resulting in varied inferences about the investigated research questions depending upon the reference used.

Given that there are no direct comparisons on the effect of referencing procedures on auditory MMN and the importance of MMN in clinical and basic auditory processing research, the aim of the current experiment was to examine how the choice of ERP referencing procedure will influence the latency and amplitude of the MMN as a function of the magnitude of frequency deviance between the standard and the deviant sounds. Also, given the dependence of AVG and REST referencing procedures on the electrode montage we examined the influence of AVG and REST referencing on the MMN amplitude and latency as function of three commonly used electrode montages (16-, 32-, and 64-channel). Less dense montages are usually recommended for recording auditory MMN for clinical use (Duncan et al., 2009). Since, the LM and AVG are considered non-neutral references as compare to REST, it would be reasonable to predict that an increment in MMN amplitude and decrement in MMN latency as a function of increasing deviant frequency magnitude will be better exhibited in the REST condition.

METHOD

Ethics

Methods were approved by the Human Research Ethics Committee at the Western Sydney University. Written informed consents were obtained from all the participants prior to the experiment.

Participants

Twelve participants (7 females), aged 22–35 years participated in the experiment. All the participants were right handed

as assessed by Edinburgh handedness inventory and reported no significant neurological and psychological history. Routine hearing screening audiometry conducted revealed normal hearing bilaterally with hearing thresholds of $\leq$ 15 dB HL at 500, 1,000, and 2,000 Hz for all the participants.

Experimental Stimuli

The experimental stimuli consisted of four pure tones (175, 10 ms rise and fall time) with the frequency of, 1,000, 1,030, 1,100, and 1,200 Hz. The 1,000 Hz pure tone served as the "standard stimulus" in all three blocks and was presented at 85% of the trials. In each block the standard stimulus were replaced in 15% of the trials either by 1,030, 1,100, or 1,200 Hz pure tone termed the "small-deviant," "medium-deviant," and "large-deviant." Each block contained 666 stimuli (566 standards; 100 deviants) that were presented binaurally via headphones at 80 dB SPL. Each block started by 10 repetitions of the standard stimulus after which the standards and deviants were presented in a pseudo-random order with the constraint that a minimum of three standards and a maximum of eight standards were presented between the deviants. The stimuli were separated by a jittered stimulus-onset synchrony (SOA) of 0.7–0.9 s to minimize the confounding effect of ERP artifacts related to anticipation of a stimulus and overt attention (P3a and P3b; Lang et al., 1995). An increasing magnitude in frequency was used as deviants, as MMN generated by increase in frequency in the deviant stimulus produce larger amplitude than MMN generated by decrease in frequency of deviant (Peter et al., 2010). The participants were instructed to ignore the sounds and they watched a subtitled muted movie of their choice to divert their attention. The soundtrack of the movies was switched off to avoid any inhibitory effects on the MMN component (Pettigrew et al., 2004; Mahajan and McArthur, 2011). The order of the blocks was counter-balanced between the participants.

Electrophysiological Recording

The participants were seated on a comfortable chair while the electrode cap was fitted. Prior to the electrode cap placement, the scalp of each participant was combed in a pre-set procedure to reduce the time taken to achieve the optimal scalp electrode impedance (Mahajan and McArthur, 2010). A BioSemi Active-Two amplifier system (BioSemi, Amsterdam, Netherlands) was used to record raw electroencephalograph (EEG). The 64 Ag-AgCl electrodes were mounted on a nylon electrode cap according to the international standard 10–10 system (Oostenveld and Praamstra, 2001). There were two electrodes on the electrode cap (CMS and DRL) which served as online references. Six additional electrodes were also placed on the participants. Four of them were bipolar electrodes placed above and below the left eye and outer canthi of both the eyes to monitor vertical and horizontal eye movements (EOG channel) respectively and two electrodes were placed on two mastoids which were used for re-referencing later. The raw EEG recording was sampled at 256 Hz with online band-pass filtering of 0.05–200 Hz. This raw EEG data was stored for later offline analysis for each participant.

EEG Data Analysis

The pre-processing and analysis of the stored raw EEG data from each participant was carried out using EEGLAB version 13.2 (Delorme and Makeig, 2004), ERPLAB toolbox version 5.0 (Lopez-Calderon and Luck, 2014) and custom written functions in MATLAB 2014b (Mathworks, Natick, MA, USA). Initially, any obvious artifact was removed after visually inspecting the continuous raw data. Then this data was band-pass filtered (0.1 Hz high pass and 30 Hz low pass; 12 dB per octave roll-off) using finite FIR filters. The filtered data then was subjected to *runica,* an ICA (Independent component analysis) algorithm incorporated in EEGLAB to detect and remove eye blinks, horizontal eye movements, and other artifacts (muscle noise and line noise artifacts). The ICA algorithm resulted in 64 components and based on the scalp topography, activity power spectrum, and activity over trials, the artifactual components were identified and removed from the EEG data. The ICA-corrected resultant EEG activity was then divided into three scalp-electrode montages namely, 64-, 32-, and 16-channel, according to the international standard 10–10 system (see **Figure 1**). At this stage of the data processing, a three-way re-referencing of the continuous data was performed to create three different experimental referencing conditions for each electrode montage separately.

In the first method, the ICA-corrected data was re-referenced to the average of two mastoids that were mathematically linked for each of the three electrode montages and formed the first referencing condition termed as "linked-mastoid referencing" (LM). For the second method, the data was averaged referenced to all the channels with in each electrode montage i.e., averaged reference to 64-, 32-, and 16-channel. This condition was termed as "AVG." Third, the ICA-corrected data in each electrode montage was subjected to REST referencing procedure using the REST EEGLAB plugin resulting "REST referencing." A three-concentric-sphere model was used as the head model for REST. The radii of the three concentric spheres are 0.87 (inner radius of the skull), 0.92 (outer radius of the skull) and 1.0 (radius of the head), and the conductivities are 1.0 (brain and scalp) and 0.0125 (skull). The lead field matrix was calculated for all the montages separately by the forward theory proposed in Yao (2000), following which the data was referenced to the REST.

The resulting re-referenced data in each of the referencing condition and electrode montage was divided into 800 ms epochs with a pre-stimulus period of 100 ms, which was used for the baseline correction. All the epochs with a voltage change exceeding $\pm$ 100 μV in any channel were removed from the analyses. All the participants had at least 80 accepted trials for each deviant. All epochs generated for each referencing condition and electrode montage by the 1,000 Hz standard tone were averaged (excluding the first 10 standards and the standards that immediately follow a deviant) together to produce a "standard" ERP. All epochs generated by 1,030, 1,100, and

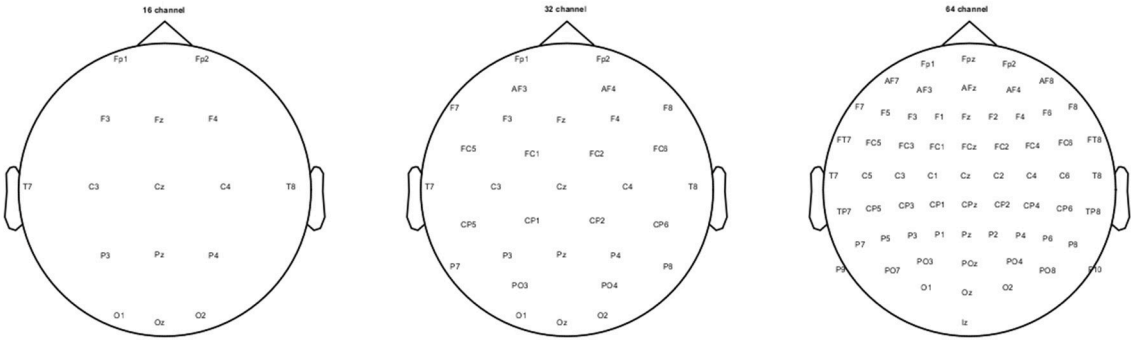

FIGURE 1 | 16-, 32-, and 64-channel electrode montages used in the current study.

1,200 Hz tones were averaged to produce the "small," "medium," and "large" deviant ERPs, respectively. To create the MMN, the standard ERP were subtracted from each of the small, medium, and large deviant ERP (i.e., a difference waveform) which produced three difference waveforms for each referencing condition.

The MMN was identified from the difference waveforms for each condition and each electrode montage. We focused on the frontal channel Fz to measure the amplitude and the latency of the MMN, as Fz is the site most commonly used to represent the MMN (Näätänen, 1992; Jacobsen and Schröger, 2003; Naatanen et al., 2005; Kujala et al., 2007). Also at Fz, comparable auditory ERPs and reliable group differences can be found (Ponton et al., 2000; Naatanen et al., 2005; Bishop et al., 2007; Mahajan and McArthur, 2012, 2015). The largest negative deflection between 100 and 250 ms was identified as MMN for each condition and MMN mean latency was measured at this point. The MMN amplitude was indexed as the mean amplitude of the MMN waveform over a 50 ms window (Peter et al., 2010, 2012; Mahajan and McArthur, 2011, 2015), centered on the peak latency for each participant.

Statistical Analyses

The MMN amplitude and latency measurements (54 datasets) were subjected to the Shapiro-Wilk test of normality. The results revealed that the MMN amplitude and latency data across the electrode montages and referencing procedures were normally distributed ($p < 0.05$). To determine the effect of referencing procedures on the magnitude of auditory MMN as a function of deviance magnitude across three electrode montages, the data on the mean amplitude and peak latency was subjected to two separate analyses. (1) To see the effect of referencing procedure on MMN amplitude and latency across the deviant magnitudes, a 3 ("deviant magnitude"; small, medium, and large) × 3("referencing procedure"; LM, AVG, and REST) within participant repeated measures analysis of variance (ANOVA) was conducted for each electrode montage separately. (2) To see the effect of referencing procedure, electrode montage, and the deviance magnitude on MMN, a 2 ("referencing procedure"; average reference and REST) × 3 ("montage"; 16-, 32-, and 64-channel) × 3 ("deviant magnitude"; small, medium, and large) was performed. LM referencing was not included in this analysis as MMN at Fz for LM condition is independent of the electrode montage. For all the above ANOVA analyses, wherever the assumption of sphericity was violated the Greenhouse-Geisser correction was applied. The results obtained are reported in the section below.

RESULTS

Figure 2 shows the grand averaged standard and deviant ERP waveforms re-referenced using LM, AVG and REST procedures across 16-, 32- and 64-channel montages. **Figure 3** shows the grand average deviant-standard difference waveforms across different referencing procedures and montages. The topographic maps show the distribution of MMN amplitude at its peak across the scalp.

Amplitude of MMN

The results of the 2-way repeated measures of ANOVA with factors magnitude (small, medium, large) and referencing procedure (LM, AVG, REST) revealed that there was no main effect of magnitude of deviance on MMN amplitude for all the montages [64-channel; $F_{(2, 22)} = 0.09$, $p = 0.91$, $\eta_p^2 = 0.008$; 32-channel $F_{(2, 22)} = 0.09$, $p = 0.91$, $\eta_p^2 = 0.008$; 16-channel $F_{(2, 22)} = 0.09$, $p = 0.91$, $\eta_p^2 = 0.008$], However, there was a significant main effect of the referencing procedure for all the montages [64 channel $F_{(2, 22)} = 88.61$, $p < 0.001$, $\eta_p^2 = 0.90$; 32-channel $F_{(2, 22)} = 94.90$, $p < 0.001$, $\eta_p^2 = 0.90$; a16-channel $F_{(2, 22)} = 93.58$, $p < 0.001$, $\eta_p^2 = 0.90$]. These results indicate that for all the three electrode montages, the change in the magnitude of frequency deviance did not alter the mean MMN amplitude across the three referencing procedures but the choice of referencing procedure influenced the MMN amplitude significantly. Bonferroni corrected pairwise comparisons revealed that, for 64-channel montage when the EEG data was re-referenced to mastoids, largest MMN amplitude was obtained (M = −3.39 μV, SE = 0.41) followed by the REST

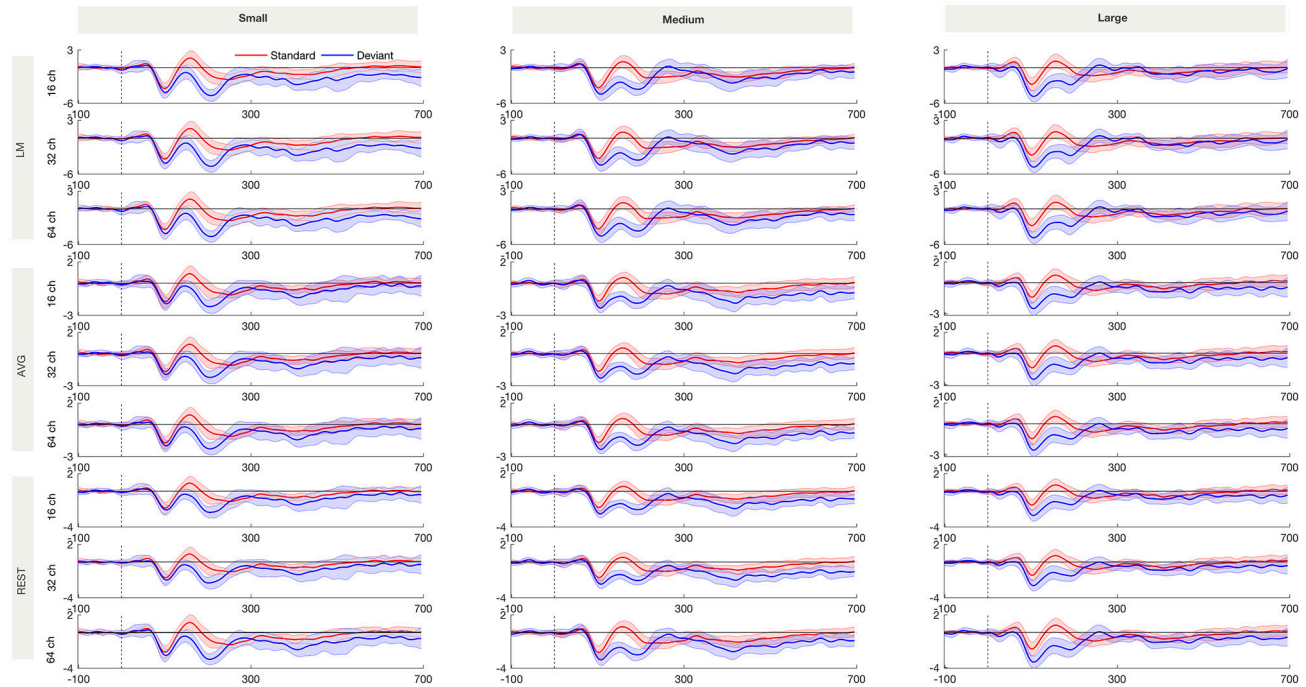

FIGURE 2 | Standard and deviant waveforms referenced with LM, AVG, and REST procedures recorded from Fz for small, medium and large frequency deviance across 16, 32, and 64-channel montages. The shading encompasses 95% Cousineau- Morey confidence intervals (Morey, 2008).

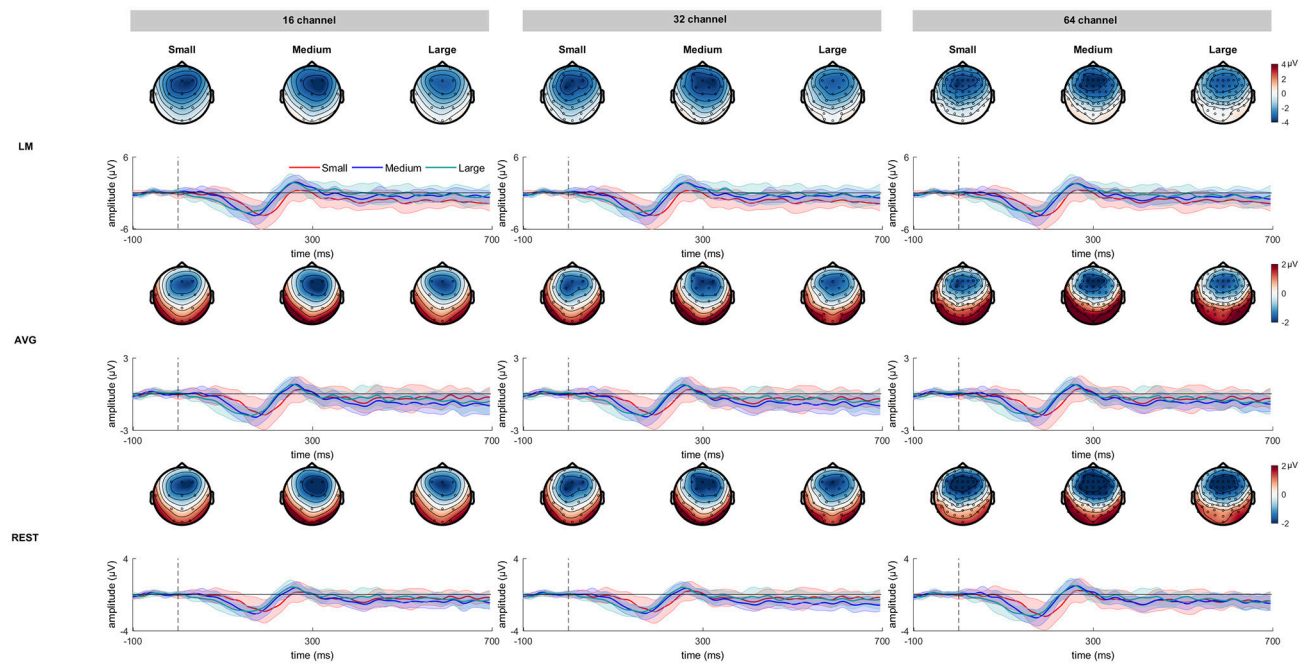

FIGURE 3 | The deviant minus standard difference waveforms as a function of frequency deviance across three channel montages referenced at LM, AVG, and REST procedures. The corresponding topographical maps for small, medium, and large frequency deviance representing a strong fronto-central distribution are also shown. The shading encompasses 95% Cousineau- Morey confidence intervals (Morey, 2008).

referencing (M = −2.25 μV, SE = 0.31) which was significantly larger than the AVG (M = −1.67, SE = 0.26). Similar results were obtained for MMN amplitude for 32-channel, LM (M = −3.36 μV, SE = 0.40), REST (M = −1.80 μV, SE = 0.29) AVG (M = −1.66 μV, SE = 0.25) and 16-channel LM (M = −3.34 μV, SE = 0.40), REST (M = −1.80 μV, SE = 0.26) AVG (M

$= -1.67$ μV, SE = 0.26). There were no significant interactions between the variables "referencing procedures" and "magnitude of deviance" for all the electrode montages. It is expected that the amplitude of MMN at Fz should be identical for all the three montages for LM. The small change in MMN amplitude across the montages in the present study could be due to the small difference in the number of artifact free trials across montages. Since the artifact rejection (± 100 μV criterion) was applied on all the channels in the montage, there are slight differences in the number of artifact free trials across 16-, 32-, and 64-channel montages. This made the ERPs slightly different across montages.

The three-way ANOVAs with factors magnitude (small, medium, large), montage (16-, 32-, 64- channel) and referencing procedure (AVG, REST) revealed that while there was no main effect of magnitude of deviance on MMN amplitude [$F_{(2, 22)} = 0.14$, $p = 0.91$, $\eta_p^2 = 0.01$], there were significant main effects of electrode montage [$F_{(2, 22)} = 30.86$, $p < 0.001$, $\eta_p^2 = 0.73$], and referencing procedures [$F_{(2, 22)} = 53.11$, $p < 0.001$, $\eta_p^2 = 0.83$] on the mean amplitude of MMN. These results suggest that AVG and REST procedures influenced the MMN amplitude across the electrode montages and change in deviance did not alter the MMN amplitude across these two procedures and montages. Among the three different scalp electrode montages across both these referencing procedures, Bonferroni corrected pairwise comparisons showed that the largest MMN was obtained when 64-channel were used (M = −1.96 μV, SE = 0.28) as compared to 32-channel (M = −1.73 μV, SE = 0.27) and 16-channel montage (M = −1.73 μV, SE = 0.26). Similar to previous findings MMN generated through REST referencing elicited larger amplitude (M = −1.95 μV, SE = 0.28) than the AVG referencing (M = −1.67 μV, SE = 0.26) across all the montages. "Referencing procedures" and "montage" significantly interacted with each other [$F_{(2, 22)} = 40.72$, $p < 0.001$, $\eta_p^2 = 0.79$]. There were no other significant interactions between the independent variables.

To investigate the significant interaction between referencing procedure and montage, subsequent one-way ANOVAs were conducted for each referencing procedure separately. The results revealed that when the EEG data was re-referenced using REST procedure, the mean MMN amplitude was largest for 64-channel montage (M = −2.25 μV, SE = 0.31; $F_{(2, 10)} = 25.09$, $p < 0.001$, $\eta_p^2 = 0.83$] which was significantly different from MMN amplitude using 32-channel montage (M = −1.79 μV, SE = 0.29) and 16-channel montage (M = −1.80 μV, SE = 0.27). There was no difference in mean MMN amplitude between 32 and 16-channel montages when re-referenced using REST. Also, the mean MMN amplitude did not differ across the montages when the EEG data was referenced to AVG procedure [$F_{(2, 10)} = 0.20$, $p = 0.81$, $\eta_p^2 = 0.03$].

In summary, the magnitude of deviance did not have an effect on MMN amplitude. LM had largest MMN amplitude followed by REST and AVG referencing had MMN with smallest amplitude. REST referencing depended on the montage with 64-channel montage generating larger MMN response compared to 32 and 16 channel.

Latency of MMN

The results of two way ANOVAs revealed that for 64-channel there was a significant main effect of magnitude of frequency deviance on the latency of MMN [$F_{(2,22)} = 4.99$, $p = 0.01$, $\eta_p^2 = 0.31$]. Bonferroni corrected pairwise comparisons revealed that large difference between standards and deviants (1,200 Hz; M = 153 ms, SE = 5.28) had significantly shorter latency of MMN than medium difference (M = 175 ms, SE = 7.44) or small difference (M = 184 ms, SE = 7.09). No difference was found between medium and small magnitude of frequency deviance. The referencing procedures did not have any main effects on the latency of MMN [$F_{(2, 22)} = 0.13$, $p = 0.87$, $\eta_p^2 = 0.01$]. Similar significant main effect of magnitude of frequency deviance was found on MMN latency for both 32-channel [$F_{(2, 22)} = 4.96$, $p = 0.01$, $\eta_p^2 = 0.31$] and 16-channel [$F_{(2, 22)} = 6.22$, $p = 0.007$, $\eta_p^2 = 0.36$] scalp electrode montages. For these electrode montages as well, large deviance elicited the shortest MMN latency (M = 154 ms, SE = 5.45, 32-channel; M = 153 ms, SE = 5.29, 16-channel) than medium (M = 172 ms, SE = 7.47, 32-channel; M = 174 ms, SE = 7.37, 16-channel) and small deviances (M = 187 ms, SE = 7.88, 32-channel; M = 185 ms, SE = 6.66, 16-channel). There was no main effect of referencing procedures for these channel montages as well and none of these independent variables significantly interacted with each other.

The results of the three way repeated measures of ANOVA analyses also revealed a significant main effect of the magnitude of frequency deviance across three electrode montages and sAVG and REST referencing procedures [$F_{(2, 22)} = 5.39$, $p = 0.01$, $\eta_p^2 = 0.33$]. This suggests that increasing the frequency deviance shortened the MMN latency for both the referencing procedures and all the three scalp-electrode montages (M = 151 ms, SE = 6.96, large; M = 174 ms, SE = 7.29, medium; M = 185 ms, SE = 7.56, small). The MMN latency for large deviance significantly differed from medium and small deviance, with no difference between the latter two.

DISCUSSION

The primary aim of the current study was to determine the extent to which choice of referencing procedure influence the amplitude and latency of the auditory ERP, the MMN as a function of magnitude of frequency deviance across three different electrode montages. To this end, we compared the effects of LM, AVG, and REST referencing procedure on the MMN as a function of increase in deviance magnitude and 64, 32, and 16-channel scalp-electrode montages. The results revealed that the referencing procedure did not alter the MMN amplitude and latency as a function of frequency deviance across the three montages. While the magnitude of frequency deviance did not change the amplitude of the MMN, the latency of the MMN decreased with increase in the frequency deviance. For all the three scalp-electrode montages, the LM referencing procedure elicited the largest MMN amplitude across the magnitude of deviance. After applying REST referencing on the EEG data, the MMN amplitude was found to be largest for the EEG data recorded from 64-channel than other two electrode montages.

The experimental effect used in the current study (increasing the frequency deviance) was validated with the findings of reduction in the latency of the MMN with an increase in the difference between the standard and the deviant frequencies used in oddball presentation. This finding is in agreement with previous results (Sams et al., 1985; Tiitinen et al., 1994; Novitski et al., 2004; Kujala et al., 2007). These results reinforce the established fact that the MMN accurately reflects auditory discrimination ability and the speed of neural conduction underlying auditory discrimination is faster when the difference between the standards and the deviants is large. No effect of an increment of the frequency deviance was found on the amplitude of the MMN. This result was contrary to the common prediction of large amplitude with increase in the frequecy difference between the sounds (Kujala et al., 2007) but in agreement with a previous finding (Horvath et al., 2008). Horvath et al. (2008) suggested that the MMN amplitude reflects the neural representation of percentage of deviants detected rather than the neural representation of the index of magnitude of deviance. This means that if the difference between the standards and deviants is large enough (greater than the threhsold frequency discrimination level), index of deviance detection will be high irrespective of the deviance difference resulting in no change in the amplitude of MMN across deviance.

Although the MMN latency changes as a function of magnitude of frequency deviance, there was no effect of three referencing procedures (LM, AVG, and REST) on this experimental effect. This result suggests that the experimental effect of change in MMN latency as a function of frequency deviance is not contingnent on choice of referencing procedure for the three commonly used electrode montages. These results are not in agreement with previous research that investigated effect of referencing procedures on the experimental effects in sensory perception (Joyce and Rossion, 2005; Tian and Yao, 2013) and found that choice of referencing alters the evoked potentials. Lower electrode density, incomplete head coverage and inaccurate head model are some known disadvantages of the AVG and REST referencing procedures (Yao, 2001; Zhai and Yao, 2004; Liu et al., 2015). These limitations can results in contamination of the resultant electrical potential, (auditory MMN in this case) with non-zero potentials. It is possible that due to these limitations, there was no effect of AVG or REST procedures on the desired experimental changes in MMN amplitude and latencies. It should be noted however, that recent simulation and real EEG studies have reported the effectiveness of REST for the analysis of non-linear features of EEG data for montages with 21 channels (Chella et al., 2017). To our knowledge, this is the first empirical investigation of comparing the effects of three commonly used referencing procedures on experimental effects on auditory MMN. Further research is required to identify the effect of referencing procedure on the experimental manipulations using other auditory contrasts (duration, speech discrimination etc.), more complex paradigms (abstract MMN) and denser electrode montages such as 128 and 256 channels.

The results of the current study revealed that when the EEG data was re-referenced to the linked mastoids, the MMN amplitude was the largest for all three scalp-electrode montages used. LM referencing has been recommended when the amplitude of MMN is small (Picton et al., 2000; Kujala et al., 2007). For frequency deviance, enhanced MMN is reported at Fz scalp location due to the source orientation of the MMN generators (Deouell et al., 1998; Kujala et al., 2007). In the LM referencing, the distance from the reference sites is equidistant to Fz leading to a strong representation of the underlying MMN generating dipole at Fz, which will result in enhanced MMN amplitude. The synchronous activity of the neurons underlying the generation of MMN is coordinated by a neural dipole which has a negative and a positive end. The LM referencing enables addition of negative and positive components of the MMN response (dipole), resulting in a higher signal-to-noise ratio (SNR) of the MMN and hence a larger amplitude.

Recent research in search of a gold standard referencing procedure for EEG/ERP research have determined that the potential at mastoid electrode sites used for referencing is non-zero (Yao, 2001, 2017; Chella et al., 2017). When the EEG data is re-referenced to LM, the non-zero potentials at mastoids may get added or subtracted to the potential at the active electrode in effect increasing or decreasing its amplitude. In the current study, the non-zero components may have got added up to the true potential resulting in larger MMN amplitude. This result may also suggest that when sparse electrode montages are used (e.g., 16-channel) such as in case of young children or clinical participants, linked mastoid referencing may be used that will elicit large MMN amplitude and can facilitate experimental comparisons. However, at the same time caution must be exercised while interpreting these results as the resultant ERP may constitute both true experimental and non-zero potential from the mastoids.

The amplitude of ERPs generated from AVG and REST referencing procedures, is generally found to be smaller than LM reference. The potential calculated using REST and AVG referencing can be non-zero in case of less electrode density, non-whole brain coverage and non-spherical head shape (Chella et al., 2017; Yao, 2017). In such cases, the non-zero component from the channels contributes to the resultant potential at active electrode sites. The scalp electrode montages employed in the current study also did not cover the whole scalp and it is plausible that the non-zero potentials across the channels were subtracted from true potential leading to a reduction in the MMN amplitude for AVG and REST referencing procedures across the three channel montages compared to LM reference. Given that we used a three-layered spherical model for the REST approach, the EEG data referenced with REST may show a better MMN reconstruction than AVE referencing for low density electrode montages such as used in the current study (Chella et al., 2017). This could be a possible explanation for larger MMN amplitude when computed after REST referencing than AVG referencing.

Another crucial set of results obtained from the current study revealed the level of dependence of two reference-free procedures (AVG and REST) on the electrode montages. The MMN amplitude when computed using AVG referencing was not contingent on the number of electrodes of the electrode montage with no difference in MMN amplitude across the three

montages. This result is contrary to the common consensus that denser the electrode array better will be the effectiveness of the AVG referencing to have a neutral potential that would result in reconstruction of the true potential from an electrode site. The MMN amplitude resulting from application of AVG referencing was the smallest across three electrode montages when compared to LM or REST referencing. The smaller size of the MMN here might have impeded any interaction between the AVG referencing and the electrode montages. Also, recent EEG simulation experiment have shown that electrode density may not be a critical factor when using AVG referencing as compared to the montage coverage of the scalp (Chella et al., 2016, 2017; Yao, 2017). The non-dependence of AVG referencing on montage density may have led to no differences in MMN amplitude across 16, 32, and 64-channel montages in the current study.

On the other hand, when infinity reference technique i.e., REST was applied to compute MMN amplitude, it was revealed that, the size of MMN amplitude is dependent on the number of electrodes used in the reconstruction of the potential. The MMN amplitude was the greatest when REST procedure was applied on a 64-channel montage as compared less dense arrays of 32 and 16-channel. This result is related to the previous findings of simulation studies using REST that reported, denser the electrodes (in a montage) better the reconstruction of the target potential (Yao, 2001; Zhai and Yao, 2004). The results of these simulation studies established that when the electrode montage had more than 32 electrodes, the quality of the reconstructed potential was better than when constructed from AVG and LM referencing. Larger MMN amplitude computed with REST referencing with 64-channel montage when compared to AVG referencing suggests that REST referencing is more dependent on the denser electrode montage used for recording auditory ERPs than AVG referencing.

CONCLUSION

The results of the current study indicate that (1) experimental effect of magnitude of frequency deviance on MMN amplitude and latency do not depend on the choice of referencing procedure (LM, AVG, or REST). (2) Auditory MMN will be largest if the EEG data is referenced with LM followed by REST and then AVG referencing. (3) MMN amplitude computed using REST referencing depends on the number of electrodes used in the montage with 64-channel montage producing largest MMN amplitude. (4) The MMN amplitude elicited using average AVG referencing did not depend on the electrode montage.

The results of the present study contribute to the increasing empirical investigations regarding the use of infinity referencing procedures in various electrophysiological domains. This is the first study investigating the effects of two commonly used referencing procedures (LM and AVG) and REST referencing on auditory ERP the MMN as a function of frequency deviance. While the results revealed no effect of referencing procedures on auditory MMN amplitude and latency as a function of frequency deviance, it is possible that the AVG and REST may have suffered from limited scalp electrode coverage and the sparse scalp electrode density in the current study. Though the utility of REST in less dense montages have been proved recently, there is a probability that 16, 32, and 64-channel montages used in the current study might have altered the final MMN waveforms across the experimental conditions. Hence, to confirm and extend these findings, replication studies using dense montages such as 128 and 256-channels and different experimental manipulations such as change in duration deviance to elicit MMN should be employed in future.

AUTHOR CONTRIBUTIONS

YM, VP, and MS designed the study. YM conducted the experiment. YM and VP analyzed and interpreted the data. YM, VP, and MS wrote the paper. All authors approved the final version of the manuscript.

ACKNOWLEDGMENTS

The authors acknowledge the financial support of the HEARing CRC, established under the Cooperative Research Centres (CRC) Programme. The CRC Programme supports industry-led end-user driven research collaborations to address the major challenges facing Australia. This research was also supported by MARCS Institute research fund. We would also like to thank reviewers for their helpful comments on earlier versions of the manuscript.

REFERENCES

Alho, K., and Sinervo, N. (1997). Preattentive processing of complex sounds in the human brain. *Neurosci. Lett.* 233, 33–36. doi: 10.1016/S0304-3940(97)00620-4

Bishop, D. V., Hardiman, M., Uwer, R., and von Suchodoletz, W. (2007). Atypical long-latency auditory event-related potentials in a subset of children with specific language impairment. *Dev. Sci.* 10, 576–587. doi: 10.1111/j.1467-7687.2007.00620.x

Chella, F., D'Andrea, A., Basti, A., Pizzella, V., and Marzetti, L. (2017). Non-linear analysis of scalp EEG by using bispectra: the effect of the reference choice. *Front. Neurosci.* 11:262. doi: 10.3389/fnins.2017.00262

Chella, F., Pizzella, V., Zappasodi, F., and Marzetti, L. (2016). Impact of the reference choice on scalp EEG connectivity estimation. *J. Neural. Eng.* 13:036016. doi: 10.1088/1741-2560/13/3/036016

Delorme, A., and Makeig, S. (2004). EEGLAB: an open source toolbox for analysis of single-trial EEG dynamics including independent component analysis. *J. Neurosci. Methods* 134, 9–21. doi: 10.1016/j.jneumeth.2003.10.009

Deouell, L. Y., Bentin, S., and Giard, M. H. (1998). Mismatch negativity in dichotic listening: evidence for interhemispheric differences and multiple generators. *Psychophysiology* 35, 355–365. doi: 10.1111/1469-8986.3540355

Dien, J. (1998). Issues in the application of the average reference: review, critiques, and recommendations. *Behav. Res. Methods. Instrum. Comput.* 30, 34–43. doi: 10.3758/BF03209414

Duncan, C. C., Barry, R. J., Connolly, J. F., Fischer, C., Michie, P. T., Näätänen, R., et al. (2009). Event-related potentials in clinical research: guidelines for eliciting, recording, and quantifying mismatch negativity, P300, and N400. *Clin. Neurophysiol.* 120, 1883–1908. doi: 10.1016/j.clinph.2009.07.045

Escera, C., Alho, K., Schroger, E., and Winkler, I. (2000). Involuntary attention and distractibility as evaluated with event-related brain potentials. *Audiol. Neurootol.* 5, 151–166. doi: 10.1159/000013877

Gilley, P. M., Sharma, M., and Purdy, S. C. (2016). Oscillatory decoupling differentiates auditory encoding deficits in children with listening problems. *Clin. Neurophysiol.* 127, 1618–1628. doi: 10.1016/j.clinph.2015.11.003

Hillyard, S. A., Hink, R. F., Schwent, V. L., and Picton, T. W. (1973). Electrical signs of selective attention in the human brain. *Science* 182, 177–180. doi: 10.1126/science.182.4108.177

Horvath, J., Czigler, I., Jacobsen, T., Maess, B., Schroger, E., and Winkler, I. (2008). MMN or no MMN: no magnitude of deviance effect on the MMN amplitude. *Psychophysiology* 45, 60–69. doi: 10.1111/j.1469-8986.2007.00599.x

Jacobsen, T., and Schröger, E. (2003). Measuring duration mismatch negativity. *Clin. Neurophysiol.* 114, 1133–1143. doi: 10.1016/S1388-2457(03)00043-9

Joyce, C., and Rossion, B. (2005). The face-sensitive N170 and VPP components manifest the same brain processes: the effect of reference electrode site. *Clin. Neurophysiol.* 116, 2613–2631. doi: 10.1016/j.clinph.2005.07.005

Katznelson, R. D. (1981). "EEG recording, electrode placement, and aspects of generator localization," in *Electric Fields of the Brain,* eds P. Nunez and R. D. Katznelson (London: Oxford University Press), 176–213.

Kayser, J., and Tenke, C. E. (2010). In search of the Rosetta Stone for scalp EEG: converging on reference-free techniques. *Clin. Neurophysiol.* 121, 1973–1975. doi: 10.1016/j.clinph.2010.04.030

Kujala, T., Tervaniemi, M., and Schroger, E. (2007). The mismatch negativity in cognitive and clinical neuroscience: theoretical and methodological considerations. *Biol. Psychol.* 74, 1–19. doi: 10.1016/j.biopsycho.2006.06.001

Lang, A. H., Eerola, O., Korpilahti, P., Holopainen, I., Salo, S., and Aaltonen, O. (1995). Practical issues in the clinical application of mismatch negativity. *Ear. Hear.* 16, 118–130. doi: 10.1097/00003446-199502000-00009

Liu, Q., Balsters, J. H., Baechinger, M., van der Groen, O., Wenderoth, N., and Mantini, D. (2015). Estimating a neutral reference for electroencephalographic recordings: the importance of using a high-density montage and a realistic head model. *J. Neural. Eng.* 12:056012. doi: 10.1088/1741-2560/12/5/056012

Lopez-Calderon, J., and Luck, S. J. (2014). ERPLAB: an open-source toolbox for the analysis of event-related potentials. *Front. Hum. Neurosci.* 8:213. doi: 10.3389/fnhum.2014.00213

Luck, S. J. (2014). *An Introduction to Event Related Potential Technique*. Cambridge, MA: MIT Press.

Mahajan, Y., and McArthur, G. (2010). Does combing the scalp reduce scalp electrode impedances? *J. Neurosci. Methods* 188, 287–289. doi: 10.1016/j.jneumeth.2010.02.024

Mahajan, Y., and McArthur, G. (2011). The effect of a movie soundtrack on auditory event-related potentials in children, adolescents, and adults. *Clin. Neurophysiol.* 122, 934–941. doi: 10.1016/j.clinph.2010.08.014

Mahajan, Y., and McArthur, G. (2012). Maturation of auditory event-related potentials across adolescence *Hear. Res.* 294, 82–94. doi: 10.1016/j.heares.2012.10.005

Mahajan, Y., and McArthur, G. (2013). Maturation of auditory t-complex brain response across adolescence. *Int. J. Dev. Neurosci.* 31, 1–10. doi: 10.1016/j.ijdevneu.2012.10.002

Mahajan, Y., and McArthur, G. (2015). Maturation of mismatch negativity and P3a response across adolescence. *Neurosci. Lett.* 587, 102–106. doi: 10.1016/j.neulet.2014.12.041

Mandikal Vasuki, P. R., Sharma, M., Ibrahim, R. K., and Arciuli, J. (2017). Musicians' online performance during auditory and visual statistical learning tasks. *Front. Hum. Neurosci.* 11:114. doi: 10.3389/fnhum.2017.00114

McArthur, G., Atkinson, C., and Ellis, D. (2009). Atypical brain responses to sounds in children with specific language and reading impairments. *Dev. Sci.* 12, 768–783. doi: 10.1111/j.1467-7687.2008.00804.x

Morey, R. D. (2008). Confidence intervals from normalized data: a correction to Cousineau (2005). *Tutor. Quant. Methods. Psychol.* 4, 61–64. doi: 10.20982/tqmp.04.2.p061

Näätänen, R. (1992). *Attention and Brain Function.* Hillsdale, NJ: Lawrence Erlbaum.

Naatanen, R., Jacobsen, T., and Winkler, I. (2005). Memory-based or afferent processes in mismatch negativity (MMN): a review of the evidence. *Psychophysiology* 42, 25–32. doi: 10.1111/j.1469-8986.2005.00256.x

Novitski, N., Tervaniemi, M., Huotilainen, M., and Näätänen, R. (2004). Frequency discrimination at different frequency levels as indexed by electrophysiological and behavioral measures. *Brain. Res. Cogn. Brain. Res.* 20, 26–36. doi: 10.1016/j.cogbrainres.2003.12.011

Nunez, P. L., and Srinivasan, R. (2006). A theoretical basis for standing and traveling brain waves measured with human EEG with implications for an integrated consciousness. *Clin. Neurophysiol.* 117, 2424–2435. doi: 10.1016/j.clinph.2006.06.754

Nunez, P. L., Wingeier, B. M., and Silberstein, R. B. (2001). Spatial-temporal structures of human alpha rhythms: theory, microcurrent sources, multiscale measurements, and global binding of local networks. *Hum. Brain. Mapp.* 13, 125–164. doi: 10.1002/hbm.1030

Offner, F. F. (1950). The EEG as potential mapping: the value of the average monopolar reference. *Electroencephalogr. Clin. Neurophysiol.* 2, 213–214. doi: 10.1016/0013-4694(50)90040-X

Oostenveld, R., and Praamstra, P. (2001). The five percent electrode system for high-resolution EEG and ERP measurements. *Clin. Neurophysiol.* 112, 713–719. doi: 10.1016/S1388-2457(00)00527-7

Pang, E. W., and Taylor, M. J. (2000). Tracking the development of the N1 from age 3 to adulthood: an examination of speech and non-speech stimuli. *Clin. Neurophysiol.* 111, 388–397. doi: 10.1016/S1388-2457(99)00259-X

Peter, V., McArthur, G., and Crain, S. (2014). Using event-related potentials to measure phrase boundary perception in English. *BMC. Neurosci.* 15:129. doi: 10.1186/s12868-014-0129-z

Peter, V., McArthur, G., and Thompson, W. F. (2010). Effect of deviance direction and calculation method on duration and frequency mismatch negativity (MMN). *Neurosci. Lett.* 482, 71–75. doi: 10.1016/j.neulet.2010.07.010

Peter, V., McArthur, G., and Thompson, W. F. (2012). Discrimination of stress in speech and music: a mismatch negativity (MMN) study. *Psychophysiology* 49, 1590–1600. doi: 10.1111/j.1469-8986.2012.01472.x

Pettigrew, C. M., Murdoch, B. E., Ponton, C. W., Kei, J., Chenery, H. J., and Alku, P. (2004). Subtitled videos and mismatch negativity (MMN) investigations of spoken word processing. *J. Am. Acad. Audiol.* 15, 469–485. doi: 10.3766/jaaa.15.7.2

Picton, T. W., Bentin, S., Berg, P., Donchin, E., Hillyard, S. A., Johnson, R. Jr., et al. (2000). Guidelines for using human event-related potentials to study cognition: recording standards and publication criteria. *Psychophysiology* 37, 127–152. doi: 10.1111/1469-8986.3720127

Ponton, C. W., Eggermont, J. J., Kwong, B., and Don, M. (2000). Maturation of human central auditory system activity: evidence from multi-channel evoked potentials. *Clin. Neurophysiol.* 111, 220–236. doi: 10.1016/S1388-2457(99)00236-9

Qin, Y., Xu, P., and Yao, D. (2010). A comparative study of different references for EEG default mode network: the use of the infinity reference. *Clin. Neurophysiol.* 121, 1981–1991. doi: 10.1016/j.clinph.2010.03.056

Sams, M., Paavilainen, P., Alho, K., and Naatanen, R. (1985). Auditory frequency discrimination and event-related potentials. *Electroencephalogr. Clin. Neurophysiol.* 62, 437–448. doi: 10.1016/0168-5597(85)90054-1

SanMiguel, I., Corral, M. J., and Escera, C. (2008). When loading working memory reduces distraction: behavioral and electrophysiological evidence from an auditory-visual distraction paradigm. *J. Cogn. Neurosci.* 20, 1131–1145. doi: 10.1162/jocn.2008.20078

Schröger, E., Giard, M. H., and Wolff, C. (2000). Auditory distraction: event-related potential and behavioral indices. *Clin. Neurophysiol.* 111, 1450–1460. doi: 10.1016/S1388-2457(00)00337-0

Sharma, A., Dorman, M. F., and Kral, A. (2005). The influence of a sensitive period on central auditory development in children with unilateral and bilateral cochlear implants. *Hear. Res.* 203, 134–143. doi: 10.1016/j.heares.2004.12.010

Sharma, A., Dorman, M. F., and Spahr, A. J. (2002). Rapid development of cortical auditory evoked potentials after early cochlear implantation. *Neuroreport* 13, 1365–1368. doi: 10.1097/00001756-200207190-00030

Sharma, M., Purdy, S. C., and Kelly, A. S. (2014). The contribution of speech-evoked cortical auditory evoked potentials to the diagnosis and measurement of intervention outcomes in children with auditory processing disorder. *Semin. Hear.* 35, 051–064. doi: 10.1055/s-0033-1363524

Sharma, M., Purdy, S. C., Newall, P., Wheldall, K., Beaman, R., and Dillon, H. (2006). Electrophysiological and behavioral evidence of auditory processing

deficits in children with reading disorder. *Clin. Neurophysiol.* 117, 1130–1144. doi: 10.1016/j.clinph.2006.02.001

Sussman, E., Steinschneider, M., Gumenyuk, V., Grushko, J., and Lawson, K. (2008). The maturation of human evoked brain potentials to sounds presented at different stimulus rates. *Hear. Res.* 236, 61–79. doi: 10.1016/j.heares.2007.12.001

Takeshita, K., Nagamine, T., Thuy, D. H. D., Satow, T., Matsuhashi, M., Yamamoto, J., et al. (2002). Maturational change of parallel auditory processing in school-aged children revealed by simultaneous recording of magnetic and electric cortical responses. *Clin. Neurophysiol.* 113, 1470–1484. doi: 10.1016/S1388-2457(02)00202-X

Tian, Y., and Yao, D. (2013). Why do we need to use a zero reference? Reference influences on the ERPs of audiovisual effects. *Psychophysiology* 50, 1282–1290. doi: 10.1111/psyp.12130

Tiitinen, H., May, P., Reinikainen, K., and Naatanen, R. (1994). Attentive novelty detection in humans is governed by pre-attentive sensory memory. *Nature* 372, 90–92. doi: 10.1038/372090a0

Tonnquist-Uhlen, I., Ponton, C. W., Eggermont, J. J., Kwong, B., and Don, M. (2003). Maturation of human central auditory system activity: the T-complex. *Clin. Neurophysiol.* 114, 685–701. doi: 10.1016/S1388-2457(03)00005-1

Wible, B., Nicol, T., and Kraus, N. (2002). Abnormal neural encoding of repeated speech stimuli in noise in children with learning problems. *Clin. Neurophysiol.* 113, 485–494. doi: 10.1016/S1388-2457(02)00017-2

Winkler, I. (2007). Interpreting the mismatch negativity. *J. Psychophysiol.* 21, 147–163. doi: 10.1027/0269-8803.21.34.147

Yao, D. (2000). Electric potential produced by a dipole in a homogeneous conducting sphere. *IEEE Trans. Biomed. Eng.* 47, 964–966. doi: 10.1109/10.846691

Yao, D. (2001). A method to standardize a reference of scalp EEG recordings to a point at infinity. *Physiol. Meas.* 22, 693–711. doi: 10.1088/0967-3334/22/4/305

Yao, D. (2017). Is the surface potential integral of a dipole in a volume conductor always zero? A cloud over the average reference of EEG and ERP. *Brain Topgr.* 30, 161–171. doi: 10.1007/s10548-016-0543-x

Yao, D., Wang, L., Arendt-Nielsen, L., and Chen, A. C. N. (2007). The effect of reference choices on the spatio-temporal analysis of brain evoked potentials: the use of infinite reference. *Comput. Biol. Med.* 37, 1529–1538. doi: 10.1016/j.compbiomed.2007.02.002

Yao, D., Wang, L., Oostenveld, R., Nielsen, K. D., Arendt-Nielsen, L., and Chen, A. C. (2005). A comparative study of different references for EEG spectral mapping: the issue of the neutral reference and the use of the infinity reference. *Physiol. Meas.* 26, 173–184. doi: 10.1088/0967-3334/26/3/003

Zhai, Y., and Yao, D. (2004). A study on the reference electrode standardization technique for a realistic head model. *Comput. Methods. Programs. Biomed.* 76, 229–238. doi: 10.1016/j.cmpb.2004.07.002

Conflict of Interest Statement: The authors declare that the research was conducted in the absence of any commercial or financial relationships that could be construed as a potential conflict of interest.

frontiers in Neuroscience

TECHNOLOGY REPORT
published: 30 October 2017
doi: 10.3389/fnins.2017.00601

MATLAB Toolboxes for Reference Electrode Standardization Technique (REST) of Scalp EEG

Li Dong[1], Fali Li[1], Qiang Liu[2], Xin Wen[1], Yongxiu Lai[1], Peng Xu[1] and Dezhong Yao[1]**

[1] Key Laboratory for NeuroInformation of Ministry of Education, Center for Information in Medicine, High-Field Magnetic Resonance Brain Imaging Key Laboratory of Sichuan Province, School of Life Science and Technology, University of Electronic Science and Technology of China, Chengdu, China, [2] Research Center of Brain and Cognitive Neuroscience, Liaoning Normal University, Dalian, China

Reference electrode standardization technique (REST) has been increasingly acknowledged and applied as a re-reference technique to transform an actual multi-channels recordings to approximately zero reference ones in electroencephalography/event-related potentials (EEG/ERPs) community around the world in recent years. However, a more easy-to-use toolbox for re-referencing scalp EEG data to zero reference is still lacking. Here, we have therefore developed two open-source MATLAB toolboxes for REST of scalp EEG. One version of REST is closely integrated into EEGLAB, which is a popular MATLAB toolbox for processing the EEG data; and another is a batch version to make it more convenient and efficient for experienced users. Both of them are designed to provide an easy-to-use for novice researchers and flexibility for experienced researchers. All versions of the REST toolboxes can be freely downloaded at http://www.neuro.uestc.edu.cn/rest/Down.html, and the detailed information including publications, comments and documents on REST can also be found from this website. An example of usage is given with comparative results of REST and average reference. We hope these user-friendly REST toolboxes could make the relatively novel technique of REST easier to study, especially for applications in various EEG studies.

Keywords: electroencephalography, EEG reference, reference electrode standardization technique (REST), MATLAB toolbox, open source

OPEN ACCESS

Edited by:
Silvina Horovitz,
National Institute of Neurological Disorders and Stroke (NIH), United States

Reviewed by:
Erwei Yin,
China Astronaut Research and Training Center, China
Federico Chella,
Università degli Studi "G. d'Annunzio" Chieti—Pescara, Italy
Ling Zou,
Changzhou University, China

****Correspondence:***
Li Dong
lidong@uestc.edu.cn
Dezhong Yao
dyao@uestc.edu.cn

Specialty section:
This article was submitted to Brain Imaging Methods, a section of the journal Frontiers in Neuroscience

Received: *19 June 2017*
Accepted: *13 October 2017*
Published: *30 October 2017*

Citation:
Dong L, Li F, Liu Q, Wen X, Lai Y, Xu P and Yao D (2017) MATLAB Toolboxes for Reference Electrode Standardization Technique (REST) of Scalp EEG. Front. Neurosci. 11:601. doi: 10.3389/fnins.2017.00601

INTRODUCTION

Since human electroencephalography (EEG) was first reported by Berger (1929), due to its high temporal resolution and non-invasive direct measure of neuronal activity, EEG has been widely utilized as a cost-effective technique for the study of brain function and dysfunction in a wide range of clinical and cognitive research applications (Niedermeyer and Da Silva, 2005; Antonenko et al., 2010; Xu et al., 2014; Li et al., 2015). Currently, EEG has been further developed by using high-density montage systems to increase topographic resolution, updating hardware to improve data quality and using dry electrodes to reduce preparation time of experiment (Kleffner-Canucci et al., 2012; Mullen et al., 2015). Additionally, the opportunities of combining scalp EEG with other neuroimaging modalities have made EEG more valuable for many other fields, including EEG and functional magnetic resonance imaging (fMRI) fusion due to their complementarity of the

spatiotemporal resolution (Laufs, 2012; Dong et al., 2014, 2015), brain-computer interfaces (BCIs; He et al., 2013) and neurostimulation (Bestmann and Feredoes, 2013) etc.

However, there is a long-term debate of the EEG reference issue that it is essential to have a reference during the scalp EEG recording; unfortunately, there is no such a point on the body or scalp surface where the ideal potential of the reference is zero or constant (Dien, 1998; Yao, 2017). In order to minimize potential effects of the EEG reference on signals, a number of different references have been proposed, including the tip of the nose (Andrew and Pfurtscheller, 1996), the vertex (Lehmann et al., 1998), unimastoid or ear (Başar et al., 1998), neck ring (Katznelson, 1981), linked mastoids or ears (Gevins and Smith, 2000), and average reference (Offner, 1950). These references have been used by many research groups or institutes around the world; however, there may be a non-negligible bias to the EEG signals because none of them is neutral. Therefore, a method, named reference electrode standardization technique (REST) and first proposed in 2001, is developed to approximately transform average or any scalp points to a reference point at infinity (i.e., theoretically desired zero reference), and thus acting as an ideal neutral reference (Yao, 2001; Yao et al., 2005). Noting that, although the fundamental assumption of average reference is reasonable to some degree (i.e., the surface potential integral of a volume conductor is zero), in a current communication (Yao, 2017), three particular examples are given to display that the potential integral over the surface of a dipole in a volume conductor maybe not zero. So far, the merit of REST reference has been proved in many studies including EEG spectrum (Yao et al., 2005; Chella et al., 2014, 2017), event-related potentials (ERPs; Tian and Yao, 2013; Liu et al., 2015; Yang et al., 2017), EEG coherence (Marzetti et al., 2007), and brain network analyses (Qin et al., 2010; Chella et al., 2016; Lei and Liao, 2017). The proposed EEG zero reference technique (i.e., REST) has also been applied in EEG studies of brain functions and dysfunctions such as schizophrenia (She et al., 2017), consciousness (Bonfiglio et al., 2013) and depressive disorder (Khodayari-Rostamabad et al., 2013). Currently, REST is increasingly acknowledged by EEG/ERPs community around the world (to our knowledge, at least 12 countries/areas), and more than 50 studies have actually adopted REST to get zero reference as the foundation of their novel findings. Meanwhile, the REST has been regarded as the Rosetta Stone for scalp EEG (Kayser and Tenke, 2010) and listed in the new guidelines of International Federation of Clinical Neurophysiology (IFCN) for EEG analysis.

Here, we have therefore developed two open-source versions of MATLAB (The Mathworks, Inc., Natick, MA, USA) toolboxes for reference electrode standardization technique of scalp EEG. The REST toolboxes utilize functions (e.g., functions for loading EEG data) in EEGLAB and run on major computer operating systems such as Windows (Win7/8/10) and Linux (Ubuntu). Both of them are designed to provide a convenient for inexperienced researchers and flexibility for experienced researchers. All versions of the REST toolbox can be downloaded for free at http://www.neuro.uestc.edu.cn/rest/Down.html, and the detailed information can also be found from this website. The main purpose of current technology report is to summarize the theory, framework and usage of REST toolboxes.

REFERENCE ELECTRODE STANDARDIZATION TECHNIQUE

Theory of Rest

REST is a mathematical technique that aims at building a bridge between the traditional references (e.g., a scalp point or average reference) and the theoretical zero reference (Yao, 2001; Yao et al., 2005). A reference point at infinity, which is far from all the possible neural sources and has a theoretically neutral potential, is used as an approximate zero of potential and realized by REST. Considering a scalp EEG recording with m electrodes and n samples, the scalp potentials with an infinity reference (V_{REST}) can be modeled as:

$$V_{REST} = G \cdot S \tag{1}$$

where V_{REST} is the scalp EEG signals with an infinity reference (m electrodes $\times$ n samples), S is the neural source (k sources $\times$ n samples) in the head model and G (m electrodes $\times$ k sources) is the leadfield matrix determined by the head model, electrode montage and source configuration. For a scalp point (V_e) or average (V_{AR}) referenced recordings, we similarly have

$$V_e = V_{REST} - lv_e = G \cdot S - lg_e \cdot S = (G - lg_e) \cdot S = G_e \cdot S \tag{2}$$

$$\begin{aligned} V_{AR} &= V_{REST} - lv_{AR} = G \cdot S - \frac{1}{m} ll^T G \cdot S = (G - \frac{1}{m} ll^T G) \cdot S \\ &= G_{AR} \cdot S \end{aligned} \tag{3}$$

where l is a column vector ($m \times 1$), g_e is the row vector ($1 \times k$) in G corresponding to the reference electrode, v_e and v_{AR} are the row vector in V_{REST} corresponding to a scalp point and average references, respectively, G_e and G_{AR} are the leadfield matrices with a scalp point and average references, respectively and m is the total number of electrodes. Equations (1–3) represent the scalp EEG recordings with the infinity reference, a scalp point and average, respectively.

Based on the equivalent source technique, the choice of the reference does not influence the source localization (Pascualmarqui and Lehmann, 1993; Geselowitz, 1998); that is, the neural source S in the brain is the same. Because, the dipole layer on a closed surface theoretically encloses all the actual sources inside, and the layer equivalently generates the same potentials outside the closed surface as that produced by the actual sources. Then, we have

$$\hat{S} = G_e^+ \cdot V_e = G_{AR}^+ \cdot V_{AR} \tag{4}$$

where G_e^+ and G_{AR}^+ are the Moore-Penrose generalized inverses of matrices G_e and G_{AR}, respectively; $\hat{S}$ is the estimate of

reconstructed equivalent sources. And the potential with the infinity reference (V_{REST}) can thus be obtained as follows:

$$V_{REST} = G \cdot S \approx G \cdot \hat{S} = G \cdot (G_e^+ \cdot V_e) = (G \cdot G_e^+) \cdot V_e = R_e \cdot V_e$$
$$V_{REST} = G \cdot S \approx G \cdot \hat{S} = G \cdot (G_{AR}^+ \cdot V_{AR}) = (G \cdot G_{AR}^+) \cdot V_{AR} = R_{AR} \cdot V_{AR} \quad (5)$$

where $\hat{S}$ is the estimate of reconstructed equivalent sources, R_e and R_{AR} are the reference electrode standardization matrices and the sign "+" denotes the general inverse.

Algorithm and Configuration

In this work, REST contains the following 4 steps.

1. As an example, the real electrode coordinates and the scalp EEG recordings (V_{AR}) with average reference are given first.
2. A head model (three-concentric-sphere) shown in **Figure 1** is implemented in the REST. The radii (normalized by the radius of the head) of the concentric spheres are set as 1.0 (the head), 0.92 (outer radius of the skull), and 0.87 (inner radius of the skull), and the conductivities of brain and scalp are set as 1.0 and the conductivity of skull is 0.0125 (normalized by the brain's conductivity; Rush and Driscoll, 1969). Meanwhile, an equivalent source model of the discrete dipole layer sources is used. A spherical cap surface (radius is 0.869, normalized by the radius of the head) and a transverse plane at $z = -0.076$ are implemented in the equivalent source model, which included 3,000 equivalent sources (including 2,600 dipoles on the spherical cap surface and 400 dipoles on the transverse plane).
3. Based on the electrode distribution (normalized and uniformly distributed on the upper spherical cap of head model), head model (the three-concentric-sphere model) and equivalent source model, the forward theory of the spherical harmonic spectra (Yao, 2000) is used to calculate the leadfield matrix G in Equation (1) and G_{AR} in Equation (3). Then, the general inverse G_{AR}^+ of the matrix G_{AR} can be calculated.
4. The standardization matrix R_{AR} in Equation (5) can be calculated from the known G and G_{AR}^+. As

$$V_{REST} = V_{AR} + lv_{AR}$$
$$\hat{V}_{REST} = R_{AR} \cdot V_{AR} = \hat{V}_{AR} + l \cdot average(\hat{V}_{REST}) = \hat{V}_{AR} + l\hat{v}_{AR} \quad (6)$$

and the V_{AR} is known, the finial reconstructed EEG recordings $\hat{V}_{REST}$ can be further obtained by $\hat{V}_{REST} = V_{AR} + l\hat{v}_{AR} = V_{AR} + l \cdot average(R_{AR} \cdot V_{AR})$.

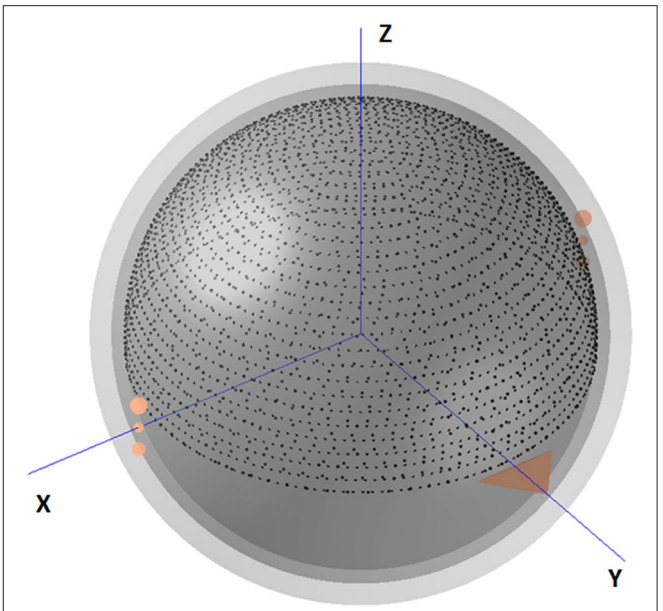

FIGURE 1 | The three-concentric-sphere model and equivalent source model in REST. The triangle shows the nose. The center of the spheres is defined as the coordinate origin. The axis directed away from the origin toward the right ear is defined as the +X axis, and that from the origin to the nasion is the +Y axis. The +Z axis is defined as the axis that is perpendicular to both these axes and directed from the origin to the vertex. The radii of the three concentric spheres (normalized by the radius of the head) are 0.87 (inner radius of the skull), 0.92 (outer radius of the skull) and 1.0 (radius of the head), while the conductivities (normalized by the brain's conductivity) are 1.0 (brain and scalp) and 0.0125 (skull). A spherical cap surface (2,600 dipoles) with radius $r = 0.869$ (normalized) and a transverse plane (400 dipoles) at $z = -0.076$ are implemented in the equivalent source model.

USAGE OF TOOLBOX

EEGLAB Plugin Version

EEGLAB (Delorme and Makeig, 2004) is a popular MATLAB toolbox for processing the scalp EEGs, and has built in facilities for the addition of plugins. In this work, a plugin version of REST toolbox is tightly integrated into EEGLAB toolbox, making it to be added on to EEGLAB in a modular fashion. The installation of REST toolbox is quite easy: 1) download the zip file "EEGLAB Plugin Version (V1.0)" from http://www.neuro.uestc.edu.cn/rest/Down.html, unzip and place the folder in the "plugins" folder of your existing EEGLAB installation (so something like ~/eeglab/plugins/REST_reference_v1.0/eegplugin_rest.m exists); 2) when the correct EEGLAB folder is in your current MATLAB path, enter "eeglab" as a command into the MATLAB command window; 3) then, load data using EEGLAB, and click "REST" → "Re-referencing to REST." In **Figure 2**, a REST menu is contained in the EEGLAB graphical user interface (GUI), which implies that REST has been successfully installed in the folder "plugins" of EEGLAB. The main interface of REST toolbox is also showed in **Figure 2**. REST toolbox relies on EEGLAB's functions for (1) importing EEG data from many major EEG recording systems (e.g., NeuroScan "*.CNT" data etc.,); (2) plotting EEG wave forms; and (3) saving the re-referenced EEG dataset.

In EEGLAB, EEG data from a single subject is stored in a set of EEG data and associated information in the MATLAB workspace, while in most commercial EEG recording systems it

corresponds to an EEG file. Therefore, REST will load data from the current dataset in EEGLAB (i.e., structure array "EEG" in the workspace). Ordinarily, each new dataset created by REST is stored in memory (i.e., structure array "ALLEEG" in the workspace) and not saved in a file. And, the final re-referenced dataset is recommended to be saved as "*.set" file. This makes it more convenient for the customer to backup and/or repeat re-referencing (by selecting a previous dataset from EEGLAB datasets menu), without frequently reading and writing the hard drive with large numbers of files.

The use of REST toolbox (v1.0) is quite easy, which consists of the following steps (see **Figure 2**):

1. Select original reference of your EEG data (default is average). In REST toolbox, the EEG reference will be transformed to average first, then re-referenced to REST.
2. Select channels you want to re-reference. Check the box ("Retain remaining channels") if you want to retain unselected channels (e.g., electrocardiogram (ECG), electro-oculogram (EOG) etc.) in the results. Labels of all selected channels will be displayed in the list of re-referencing channels. Noting that, it is suggested to reconstitute bad channels (e.g., average of the N channels neighboring it) before re-referencing to REST;
3. Select a leadfield file, which has been calculated and saved as "*.txt/*.xls/*.xlsx/*.dat." To calculate a new leadfield matrix, press the button "Calculate Lead Field" (additional steps are listed in section Leadfield Calculation);
4. Press the button "Run," and relative information will be printed in the command window;
5. Press the button "OK" to save the re-referenced EEG data to workspace (ALLEEG). Then, click "Datasets" → "*_REST" in EEGLAB.

The "Help" button in REST is designed to guide users to the REST website (http://www.neuro.uestc.edu.cn/rest/#) for detailed information.

Batch Version

To make it more convenient and efficient for users, a batch version of REST toolbox is further developed based on MATLAB.

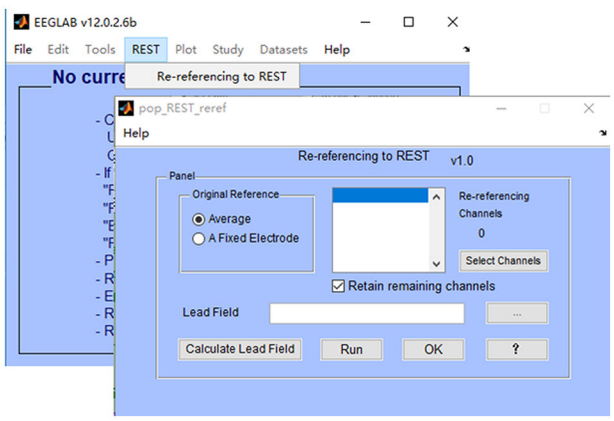

FIGURE 2 | The main interface of EEGLAB plugin version of REST.

The installation of batch version of REST toolbox is easy: (1) download the zip file "MATLAB version 1.1" from http://www.neuro.uestc.edu.cn/rest/Down.html, unzip and add path in MATLAB; (2) enter "REST" as a command into the MATLAB command window, and enjoy it. The batch version supports EEG data with formats Neuroscan "*.cnt," Brain Product "*.vhdr" and MATLAB "*.mat." For "*.cnt" and "*.vhdr" data, EEGLAB functions were integrated to load the EEG data and corresponding electrode information. For each "*.mat" data file, make sure that the structure array "data" with size m channels × n time points is imported in MATLAB workspace only.

Use of batch version toolbox is convenient, which consists of the following steps (**Figure 3**):

1. Click "File → Import data" to import EEG data files with format "*.cnt," "*.vhdr," or "*.mat;"

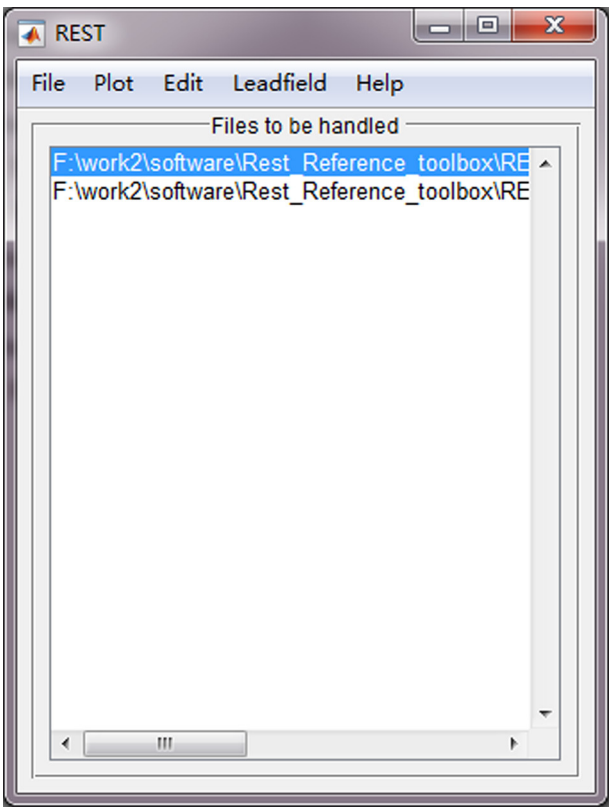

FIGURE 3 | The main interface of batch version of REST.

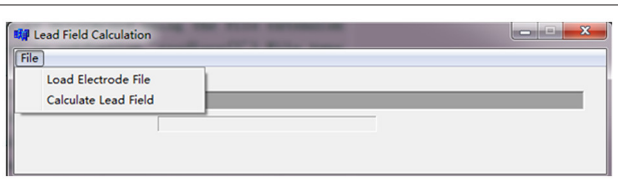

FIGURE 4 | The interface of leadfield calculation.

2. Click "Leadfield→ Import leadfield" to select a leadfield file, which has been calculated and saved as "*.dat." To calculate a new leadfield matrix file, press the button "Calculate leadfield" (additional steps are listed in section Leadfield Calculation);
3. Click "Edit → Exclude channel" to exclude non-EEG channels (e.g., ECG and EOG etc.). These channels will be removed from the subsequent REST transformation processing. Noting that, it is suggested to reconstitute bad channels (e.g., average of the N channels neighboring it) before re-referencing to REST;
4. Click "File → Run&Export" to perform the REST transformation processing. The re-referenced data files will be postfixed with "*_REST_Ref" and saved in the same folder of the original data.

The "Plot" button in REST is utilized to plot the original EEG data, and the "Help" button is used to guide users to the REST website (http://www.neuro.uestc.edu.cn/rest/#) for more detailed information.

Leadfield Calculation

For a new electrode system, the leadfield matrix is required to be re-calculated. In REST toolboxes, users can press the button "Calculate Lead Field" to calculate a new leadfield matrix (**Figure 4**). It calculates the leadfield matrix from the 3,000 cortical dipoles (spherical equivalent dipoles) and the newly given electrode array for the canonical concentric-three-spheres head model. The array of real electrode coordinates (coordinates of fiducial points are not required) is suggested to be saved in a "*.txt" ASCII file with their Cartesian x (the left ear is defined as -x axis), y (the nasion is the +y axis), z coordinates in three columns, while the coordinates will be auto-normalized and -matched to the upper spherical cap of head model inside the program. In addition, noting that the executable file "Leadfield.exe" in REST software is compiled using C language on Windows system to calculate the leadfield matrix; if you want to run it on Linux system (Ubuntu), a simple solution is to install the "Wine" software first (i.e., enter the command "sudo apt-get install wine" in a terminal). The leadfield calculation consists of the following 2 steps.

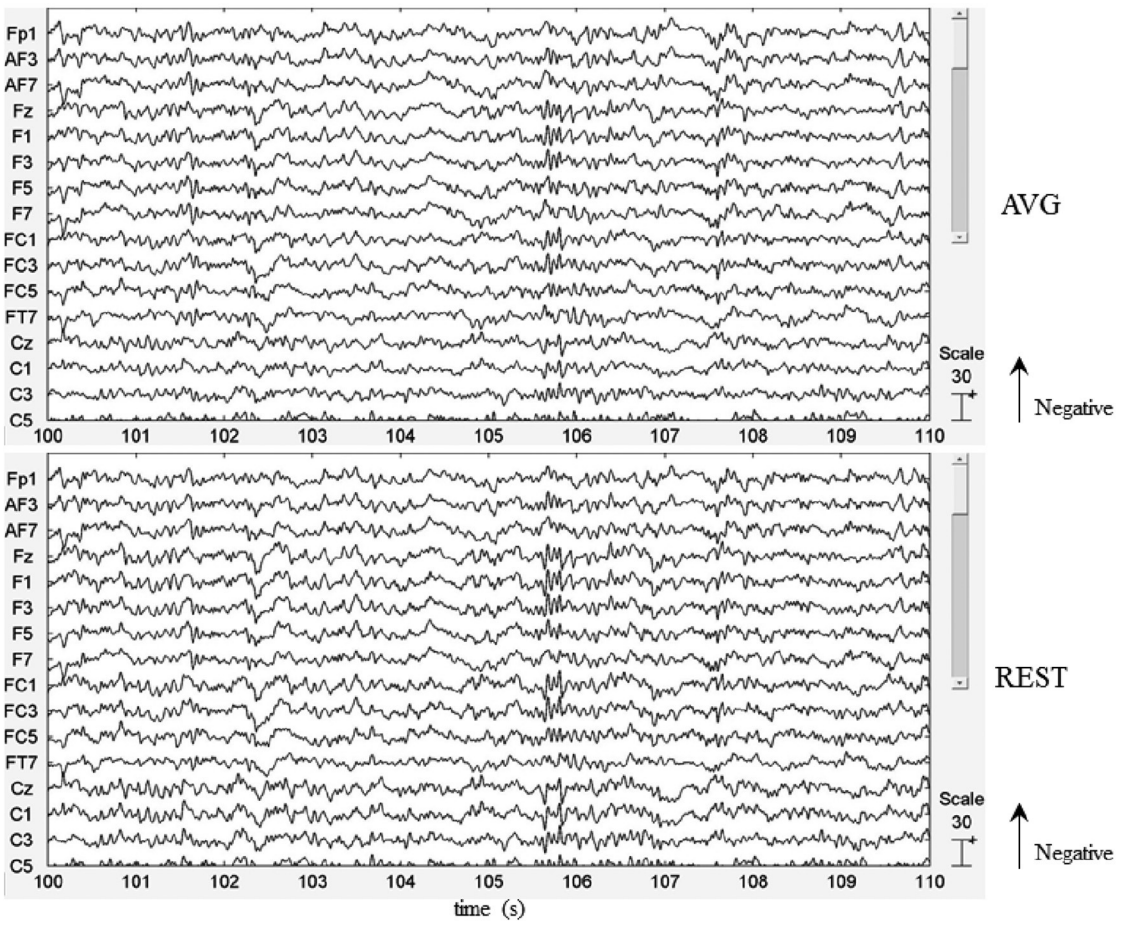

FIGURE 5 | EEG figures of average (AVG) and REST references.

1. File → Load Electrode File: "*.txt" ASCII file; x, y, z positions in three columns only;
2. File → Calculate Lead Field. It may take a few minutes that depends on the size of the matrix and the computer. When the calculation is completed, the leadfield matrix is saved as "Lead_Field.dat" (sources × channels) in the directory of electrode file.

ILLUSTRATIONS

To illustrate the usage of REST toolboxes based on MATLAB, an example of EEG data was used.

Participant and Experiment

A right-handed healthy adult (male, age = 26 years) participated in the experiment after providing the written informed consent in line with the Declaration of Helsinki. A visual oddball P300 task was designed, which consisted of 4 min of resting-state (eye-closed), followed by a 1-min break and 337.5 s task (150 trials × 2.25 s). For each trial, a bold cross was first presented 250 ms to note the subject to concentrate their attention on the computer monitor, and a thin cross was subsequently presented 500 ms to inform the subject a target or standard stimulus would appear, then a stimulus was presented for 500 ms and ended by a 1,000 ms break. The target stimulus (a total of 30 trials) is a downward-oriented triangle with a thin cross in its centers, and the standard one (a total of 120 trials) is an upward-oriented triangle with a thin cross in its centers. The subject was instructed to count the number of target stimuli and to omit the standard ones. More details of the experimental task can also be found in relative article (Li et al., 2015). The experiment was approved by the local Ethics Committee of University of Electronic Science and Technology of China.

EEG Acquisition

The EEG signals were recorded using a 64-channel EEG system (Brain Products GmbH, Gilching, Germany). Sixty-two EEG electrodes were distributed using international extended 10–20 cap system, and 2 additional channels were used to record the vertical and horizontal EOG data. The sampling rate was set at 500 Hz, and the FCz served as the reference. The impedance of all channels was maintained <5 KΩ, and EEG data were online band-pass filtered between 0.01 and 100 Hz.

Data Analysis

The task-related EEG dataset was first preprocessed including the exclusion of bad channels (no bad channel was found in the example data), average (AVG) re-referencing, 1–30 Hz bandpass filtering, data segmentation (−200 ~ 800 ms), baseline correction (−200 ~ 0 ms), and the exclusion of artifact-containing trials (exceeding ± 75 μv). Then, the preprocessed EEG data were re-referenced to REST reference using EEGLAB plugin version of REST, and ERPs (P300) according to average and REST references were obtained by averaging epochs of target trials. In addition, paired *t*-test was used to reveal differences between amplitudes of P300 for REST and AVG across trials.

RESULTS AND DISCUSSION

In this work, the EEG data of a healthy subject were used to illustrate the use of REST. **Figure 5** showed that by visually inspecting the EEG figures of AVG and REST references, the similar EEG waves were observed, roughly. The peaking times of P300 with AVG and REST were 450 and 448 ms, respectively. However, the analysis of the time-courses revealed significantly (across 28 trials, paired *t*-test, $P < 0.05$) larger signal intensity of P300 for REST than AVG (see **Figure 6**). The current ERP results of P300 were consistent with the previous studies (Gong et al., 2013; Dong et al., 2014; Li et al., 2015; Liu et al., 2015). Illustrations of ERP analyses by using REST reference validated its correctness and demonstrated its effectiveness.

As it approximately reconstructed a point far from all the possible neural sources, REST provided a theoretically neutral reference of scalp EEG (Yao, 2001; Yao et al., 2005). So far, superior performance of REST reference has been proved in various studies such as ERPs (Tian and Yao, 2013; Liu et al., 2015; Yang et al., 2017) and EEG network analyses (Qin et al., 2010; Chella et al., 2016; Lei and Liao, 2017). The REST is likely to represent a promising EEG standardization technique for various areas of research, such as epilepsy (Li et al., 2009; Kugiumtzis and Kimiskidis, 2015; Dong et al., 2016; Kimiskidis et al., 2017), depressive disorder (Khodayari-Rostamabad et al., 2013) and BCIs (He et al., 2013; Yin et al., 2016) etc. In addition, it has been argued that the performance of REST reference may be influenced by the electrode density and head model; however, several studies have showed that REST can reduce the potential bias introduced by other references for many of EEG channels ranging from

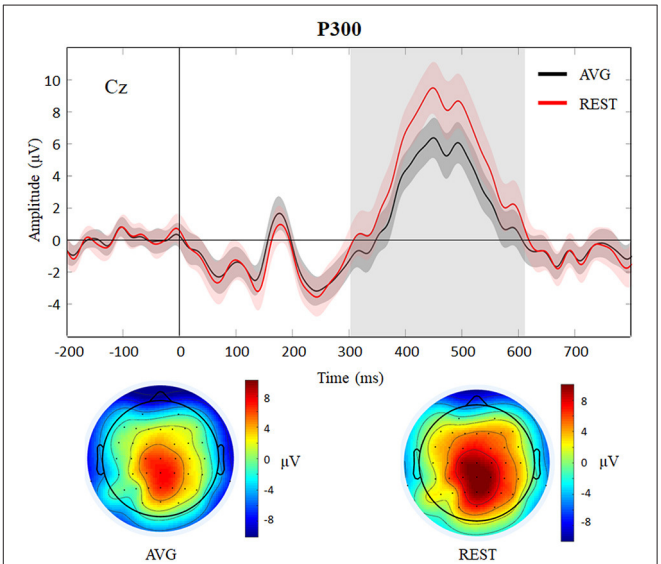

FIGURE 6 | Results of P300 (target) with AVG and REST references. P300 waves (with standard error) of AVG and REST references for Cz are showed and topographies of AVG (peaking at 450 ms) and REST (peaking at 448 ms) references are displayed below. The gray region represents significantly (paired *t*-test, $P < 0.05$) larger signal intensity of P300 for REST than AVG.

16 to 128 and for different accuracy levels of the head model (Zhai and Yao, 2004; Liu et al., 2015; Chella et al., 2016). And the REST performance can be improved by the high-density EEG recording systems and/or an accurate head model.

REST toolboxes still largely need to be improved in the future. For example, first, a potential development of REST is to integrate it into neuroscience computing platforms such as the Canadian brain imaging research platform (CBRAIN; Sherif et al., 2014). Second, the application programming interface in script of REST toolboxes could be fully checked, and GUI scripts in REST could be regarded as calling samples. Thirdly, noting that the MATLAB version of REST is able to run on Linux (Ubuntu), except the function "Calculate leadfield" (the file "Leadfield.exe" cannot be run on Linux directly). To calculate the leadfield matrix on Linux system (Ubuntu), a solution is to install the "Wine" software first (i.e., enter the command "sudo apt-get install wine" in the terminal). Therefore, the recommended operating system is "Windows 7/8/10 64 bit," and the leadfield calculation module on Linux will be further compiled in the future. Meanwhile, it is recommended to reconstitute bad channels (e.g., the average of the N channels neighboring it) before re-referencing to REST, and the updated version of REST software will contain this function. Fourthly, because it is a matter of fact that REST relies on the accuracy of the head model, a realistically shaped head model is suggested to be used to calculate leadfield matrix and will be considered in the new version of REST toolboxes. All updates of REST software will be announced at the same website. In addition, debugging and updating is an inevitable work of any software. Any users are encouraged to report bugs, constructive suggestions and/or problems about REST toolboxes via email to the authors (Lidong@uestc.edu.cn) or leave a message in the REST community (http://www.neuro.uestc.edu.cn/rest/#).

CONCLUSION

Based on MATLAB, REST toolboxes provide an easy-to-use and transparent packages for re-referencing EEG data to zero reference. REST's GUI reduces the time required for novice users to learn the usage of toolboxes. We hope these two user-friendly toolboxes could make the relatively novel technique of REST easier to study, especially for applications in various EEG studies.

AUTHOR CONTRIBUTIONS

Conceived and designed the work: LD, FL, YL, PX, and DY. Acquired the data: FL and PX. Analyzed the data and tested the software: LD, FL, QL, and XW. Wrote the paper: LD and FL. All authors revised the paper for important intellectual content. All of the authors have read and approved the manuscript.

FUNDING

The present study was financially supported with the National Natural Science Foundation of China (No. 81571759).

REFERENCES

Andrew, C., and Pfurtscheller, G. (1996). Dependence of coherence measurements on EEG derivation type. *Med. Biol. Eng. Comput.* 34, 232–238. doi: 10.1007/BF02520079

Antonenko, P., Paas, F., Grabner, R., and van Gog, T. (2010). Using electroencephalography to measure cognitive load. *Educ. Psychol. Rev.* 22, 425–438. doi: 10.1007/s10648-010-9130-y

Başar, E., Rahn, E., Demiralp, T., and Schürmann, M. (1998). Spontaneous EEG theta activity controls frontal visual evoked potential amplitudes. *Electroencephalogr. Clin. Neurophysiol.* 108, 101–109. doi: 10.1016/S0168-5597(97)00039-7

Berger, H. (1929). Über das elektrenkephalogramm des menschen. *Euro. Arch. Psychiat. Clin. Neurosci.* 87, 527–570. doi: 10.1007/BF01797193

Bestmann, S., and Feredoes, E. (2013). Combined neurostimulation and neuroimaging in cognitive neuroscience: past, present, and future. *Ann. N. Y. Acad. Sci.* 1296, 11–30. doi: 10.1111/nyas.12110

Bonfiglio, L., Olcese, U., Rossi, B., Frisoli, A., Arrighi, P., Greco, G., et al. (2013). Cortical source of blink-related delta oscillations and their correlation with levels of consciousness. *Hum. Brain Mapp.* 34, 2178–2189. doi: 10.1002/hbm.22056

Chella, F., D'Andrea, A., Basti, A., Pizzella, V., and Marzetti, L. (2017). Non-linear analysis of scalp EEG by using bispectra: the effect of the reference choice. *Front. Neurosci.* 11:262. doi: 10.3389/fnins.2017.00262

Chella, F., Marzetti, L., Pizzella, V., Zappasodi, F., and Nolte, G. (2014). Third order spectral analysis robust to mixing artifacts for mapping cross-frequency interactions in EEG/MEG. *Neuroimage* 91, 146–161. doi: 10.1016/j.neuroimage.2013.12.064

Chella, F., Pizzella, V., Zappasodi, F., and Marzetti, L. (2016). Impact of the reference choice on scalp EEG connectivity estimation. *J. Neural. Eng.* 13:036016. doi: 10.1088/1741-2560/13/3/036016

Delorme, A., and Makeig, S. (2004). EEGLAB: an open source toolbox for analysis of single-trial EEG dynamics including independent component analysis. *J. Neurosci. Methods* 134, 9–21. doi: 10.1016/j.jneumeth.2003.10.009

Dien, J. (1998). Issues in the application of the average reference: review, critiques, and recommendations. *Behav. Res. Methods* 30, 34–43. doi: 10.3758/BF03209414

Dong, L., Gong, D., Valdes-Sosa, P. A., Xia, Y., Luo, C., Xu, P., et al. (2014). Simultaneous EEG-fMRI: trial level spatio-temporal fusion for hierarchically reliable information discovery. *Neuroimage* 99, 28–41. doi: 10.1016/j.neuroimage.2014.05.029

Dong, L., Luo, C., Zhu, Y., Hou, C., Jiang, S., Wang, P., et al. (2016). Complex discharge-affecting networks in juvenile myoclonic epilepsy: a simultaneous EEG-fMRI study. *Hum. Brain Mapp.* 37, 3515–3529. doi: 10.1002/hbm.23256

Dong, L., Wang, P., Bin, Y., Deng, J., Li, Y., Chen, L., et al. (2015). Local multimodal serial analysis for fusing EEG-fMRI: a new method to study familial cortical myoclonic tremor and epilepsy. *IEEE Trans. Auton. Ment. Dev.* 7, 311–319. doi: 10.1109/TAMD.2015.2411740

Geselowitz, D. B. (1998). The zero of potential. *IEEE Eng. Med. Biol. Mag.* 17, 128–136. doi: 10.1109/51.646230

Gevins, A., and Smith, M. E. (2000). Neurophysiological measures of working memory and individual differences in cognitive ability and cognitive style. *Cereb. Cortex* 10, 829–839. doi: 10.1093/cercor/10.9.829

Gong, D. K., Ma, W., Kendrick, K. M., Hu, Q., and Yao, D. (2013). How cognitive plasticity resolves the brain's information processing dilemma. *Sci. Rep.* 3:2860. doi: 10.1038/srep02860

He, B., Gao, S., Yuan, H., and Wolpaw, J. R. (2013). "Brain–computer interfaces," in *Neural Engineering*, ed B. He (Boston, MA: Springer), 87–151.

Katznelson, R. D. (1981). "EEG recording, electrode placement, and aspects of generator localization," in *Electric Fields of the Brain*, ed P. L. Nunez (New York, NY: Oxford University Press), 176–213.

Kayser, J., and Tenke, C. E. (2010). In search of the Rosetta Stone for scalp EEG: converging on reference-free techniques. *Clin. Neurophysiol.* 121, 1973–1975. doi: 10.1016/j.clinph.2010.04.030

Khodayari-Rostamabad, A., Reilly, J. P., Hasey, G. M., de Bruin, H., and Maccrimmon, D. J. (2013). A machine learning approach using EEG data to predict response to SSRI treatment for major depressive disorder. *Clin. Neurophysiol.* 124, 1975–1985. doi: 10.1016/j.clinph.2013.04.010

Kimiskidis, V. K., Tsimpiris, A., Ryvlin, P., Kalviainen, R., Koutroumanidis, M., Valentin, A., et al. (2017). TMS combined with EEG in genetic generalized epilepsy: a phase II diagnostic accuracy study. *Clin. Neurophysiol.* 128, 367–381. doi: 10.1016/j.clinph.2016.11.013

Kleffner-Canucci, K., Luu, P., Naleway, J., and Tucker, D. M. (2012). A novel hydrogel electrolyte extender for rapid application of EEG sensors and extended recordings. *J. Neurosci. Methods* 206, 83–87. doi: 10.1016/j.jneumeth.2011.11.021

Kugiumtzis, D., and Kimiskidis, V. K. (2015). Direct causal networks for the study of transcranial magnetic stimulation effects on focal epileptiform discharges. *Int. J. Neural Syst.* 25:1550006. doi: 10.1142/S0129065715500069

Laufs, H. (2012). A personalized history of EEG-fMRI integration. *Neuroimage* 62, 1056–1067. doi: 10.1016/j.neuroimage.2012.01.039

Lehmann, D., Strik, W. K., Henggeler, B., Koenig, T., and Koukkou, M. (1998). Brain electric microstates and momentary conscious mind states as building blocks of spontaneous thinking: I. Visual imagery and abstract thoughts. *Int. J. Psychophysiol.* 29, 1–11.

Lei, X., and Liao, K. (2017). Understanding the Influences of EEG reference: a large-scale brain network perspective. *Front. Neurosci.* 11:205. doi: 10.3389/fnins.2017.00205

Li, F., Liu, T., Wang, F., Li, H., Gong, D., Zhang, R., et al. (2015). Relationships between the resting-state network and the P3: evidence from a scalp EEG study. *Sci. Rep.* 5:15129 doi: 10.1038/srep15129

Li, Q., Luo, C., Yang, T., Yao, Z., He, L., Liu, L., et al. (2009). EEG-fMRI study on the interictal and ictal generalized spike-wave discharges in patients with childhood absence epilepsy. *Epilepsy Res.* 87, 160–168. doi: 10.1016/j.eplepsyres.2009.08.018

Liu, Q., Balsters, J. H., Baechinger, M., van der Groen, O., Wenderoth, N., and Mantini, D. (2015). Estimating a neutral reference for electroencephalographic recordings: the importance of using a high-density montage and a realistic head model. *J. Neural. Eng.* 12:056012. doi: 10.1088/1741-2560/12/5/056012

Marzetti, L., Nolte, G., Perrucci, M. G., Romani, G. L., and Del Gratta, C. (2007). The use of standardized infinity reference in EEG coherency studies. *Neuroimage* 36, 48–63. doi: 10.1016/j.neuroimage.2007.02.034

Mullen, T. R., Kothe, C. A., Chi, Y. M., Ojeda, A., Kerth, T., Makeig, S., et al. (2015). Real-time neuroimaging and cognitive monitoring using wearable dry EEG. *IEEE Trans. Biomed. Eng.* 62, 2553–2567. doi: 10.1109/TBME.2015.2481482

Niedermeyer, E., and Da Silva, F. H. L. (2005). *Electroencephalography: Basic Principles, Clinical Applications, and Related Fields*. London, UK: Lippincott Williams and Wilkins.

Offner, F. F. (1950). The EEG as potential mapping: the value of the average monopolar reference. *Electroencephalogr. Clin. Neurophysiol.* 2, 213–214. doi: 10.1016/0013-4694(50)90040-X

Pascualmarqui, R. D., and Lehmann, D. (1993). Topographic maps, source localization inference, and the reference electrode - comments. *Electroencephalogr. Clin. Neurophysiol.* 88, 532–533. doi: 10.1016/0168-5597(93)90043-O

Qin, Y., Xu, P., and Yao, D. (2010). A comparative study of different references for EEG default mode network: the use of the infinity reference. *Clin. Neurophysiol.* 121, 1981–1991. doi: 10.1016/j.clinph.2010.03.056

Rush, S., and Driscoll, D. A. (1969). EEG electrode sensitivity-an application of reciprocity. *IEEE Trans. Biomed. Eng.* 16, 15–22. doi: 10.1109/TBME.1969.4502598

She, S., Li, H., Ning, Y., Ren, J., Wu, Z., Huang, R., et al. (2017). Revealing the dysfunction of schematic facial-expression processing in schizophrenia: a comparative study of different references. *Front. Neurosci.* 11:314. doi: 10.3389/fnins.2017.00314

Sherif, T., Rioux, P., Rousseau, M. E., Kassis, N., Beck, N., Adalat, R., et al. (2014). CBRAIN: a web-based, distributed computing platform for collaborative neuroimaging research. *Front. Neuroinform.* 8:54. doi: 10.3389/fninf.2014.00054

Tian, Y., and Yao, D. (2013). Why do we need to use a zero reference? Reference influences on the ERPs of audiovisual effects. *Psychophysiology* 50, 1282–1290. doi: 10.1111/psyp.12130

Xu, P., Xiong, X., Xue, Q., Li, P., Zhang, R., Wang, Z., et al. (2014). Differentiating between psychogenic nonepileptic seizures and epilepsy based on common spatial pattern of weighted EEG resting networks. *IEEE Trans. Biomed. Eng.* 61, 1747–1755. doi: 10.1109/TBME.2014.2305159

Yang, P., Fan, C., Wang, M., and Li, L. (2017). A comparative study of average, linked mastoid, and REST references for ERP components acquired during fMRI. *Front. Neurosci.* 11:247. doi: 10.3389/fnins.2017.00247

Yao, D. (2000). High-resolution EEG mappings: a spherical harmonic spectra theory and simulation results. *Clin. Neurophysiol.* 111, 81–92. doi: 10.1016/S1388-2457(99)00205-9

Yao, D. (2001). A method to standardize a reference of scalp EEG recordings to a point at infinity. *Physiol. Meas.* 22, 693–711. doi: 10.1088/0967-3334/22/4/305

Yao, D. (2017). Is the surface potential integral of a dipole in a volume conductor always zero? a cloud over the average reference of EEG and ERP. *Brain Topogr.* 30, 161–171. doi: 10.1007/s10548-016-0543-x

Yao, D., Wang, L., Oostenveld, R., Nielsen, K. D., Arendt-Nielsen, L., and Chen, A. C. (2005). A comparative study of different references for EEG spectral mapping: the issue of the neutral reference and the use of the infinity reference. *Physiol. Meas.* 26, 173–184. doi: 10.1088/0967-3334/26/3/003

Yin, E., Zeyl, T., Saab, R., Hu, D., Zhou, Z., and Chau, T. (2016). An auditory-tactile visual saccade-independent P300 brain-computer interface. *Int. J. Neural. Syst.* 26:1650001. doi: 10.1142/S0129065716500015

Zhai, Y., and Yao, D. (2004). A study on the reference electrode standardization technique for a realistic head model. *Comput. Methods Programs Biomed.* 76, 229–238. doi: 10.1016/j.cmpb.2004.07.002

Conflict of Interest Statement: The authors declare that the research was conducted in the absence of any commercial or financial relationships that could be construed as a potential conflict of interest.

frontiers in Neuroscience

ORIGINAL RESEARCH
published: 04 December 2017
doi: 10.3389/fnins.2017.00670

Effect of Different References on Auditory-Evoked Potentials in Children with Cochlear Implants

Maojin Liang[1,2,3†], *Jiahao Liu*[1,2,3†], *Junpeng Zhang*[4†], *Junbo Wang*[5], *Yuebo Chen*[1,2,3], *Yuexin Cai*[1,2,3], *Ling Chen*[1,2,3] *and Yiqing Zheng*[1,2,3*]

[1] Department of Otolaryngology, Sun Yat-Sen Memorial Hospital, Sun Yat-Sen University, Guangzhou, China, [2] Department of Otolaryngology, Sun Yat-Sen Memorial Hospital, Institute of Hearing and Speech-Language Science, Sun Yat-Sen University, Guangzhou, China, [3] Department of Hearing and Speech Science, Xin Hua College of Sun Yat-Sen University, Guangzhou, China, [4] Department of Medical Information and Engineering, Sichuan University, Chengdu, China, [5] Department of Clinical Medicine, Sun Yat-Sen University, Guangzhou, China

Background: Nose reference (NR), mastoid reference (MR), and montage average reference (MAR) are usually used in auditory event-related potential (AEP) studies with a recently developed reference electrode standardization technique (REST), which may reduce the reference effect. For children with cochlear implants (CIs), auditory deprivation may hinder normal development of the auditory cortex, and the reference effect may be different between CIs and a normal developing group.

Methods: Thirteen right-side-CI children were recruited, comprising 7 males and 6 females, ages 2–5 years, with CI usage of ∼1 year. Eleven sex- and age-matched healthy children were recruited for normal controls; 1,000 Hz pure tone evoked AEPs were recorded, and the data were re-referenced to NR, left mastoid reference (LMR, which is the opposite side of the implanted cochlear), MAR, and REST. CI artifact and P1–N1 complex (latency, amplitudes) at Fz were analyzed.

Results: Confirmed P1–N1 complex could be found in Fz using NR, LMR, MAR, and REST with a 128-electrode scalp. P1 amplitude was larger using LMR than MAR and NR, while no statistically significant difference was found between NR and MAR in the CI group; REST had no significant difference with the three other references. In the control group, no statistically significant difference was found with different references. Group difference of P1 amplitude could be found when using MR, MAR, and REST. For P1 latency, no significant difference among the four references was shown, whether in the CI or control group. Group difference in P1 latency could be found in MR and MAR. N1 amplitude in LMR was significantly lower than NR and MAR in the control group. LMR, MAR, and REST could distinguish the difference in the N1 amplitude between the CI and control group. Contralateral MR or MAR was found to be better in differentiating CI children versus controls. No group difference was found for the artifact component.

Conclusions: Different references for AEP studies do not affect the CI artifact. In addition, contralateral MR is preferable for P1–N1 component studies involving CI children, as well as methodology-like studies.

Keywords: cochlear implant, nose reference, mastoid reference, montage average reference, reference electrode standardization technique, event related potential

OPEN ACCESS

Edited by:
Rui Zhang,
Zhengzhou University, China

Reviewed by:
Diankun Gong,
University of Electronic Science and Technology of China, China
Gaoxiang Ouyang,
Beijing Normal University, China
Hong-Jin Sun,
McMaster University, Canada

***Correspondence:**
Yiqing Zheng
yiqingzheng@hotmail.com

[†] *These authors have contributed equally to this work.*

Specialty section:
This article was submitted to Brain Imaging Methods, a section of the journal Frontiers in Neuroscience

Received: *22 March 2017*
Accepted: *20 November 2017*
Published: *04 December 2017*

Citation:
Liang M, Liu J, Zhang J, Wang J, Chen Y, Cai Y, Chen L and Zheng Y (2017) Effect of Different References on Auditory-Evoked Potentials in Children with Cochlear Implants. Front. Neurosci. 11:670. doi: 10.3389/fnins.2017.00670

INTRODUCTION

Event-related potentials (ERPs), with excellent temporal resolution, are one of the most informative and noninvasive methods of monitoring and studying the cognitive processes in the living brain. ERPs are linked in time with a physical or mental event and are typically extracted from scalp-recorded electroencephalogram (EEG) by means of signal averaging (Duncan et al., 2009).

In the auditory field, the latency and morphology of auditory evoked potentials (AEPs) can provide information about the maturation of the auditory system. There are several studies that reported that compared to children, adults show smaller amplitudes and latency in the P1 component (Ponton et al., 2000; Wunderlich and Cone-Wesson, 2006; Wunderlich et al., 2006; Shafer et al., 2015). P1 is described as a result of synaptic activity in the primary auditory cortex, thalamo-cortical projections, and intercortical recurrent activity (Ponton et al., 2000; Eggermont and Ponton, 2003). The latency of P1, as well as N1, AEPs decrease with age systematically in normal hearing children (Ponton et al., 2002). In cochlear implanted children, AEPs are also used to study auditory system plasticity and rehabilitation efficacy after regaining auditory information (Kral and Sharma, 2012; Sharma et al., 2015a). It is reported that compared to age-matched normal hearing children, CI individuals have larger P1 amplitudes and longer P1 latency (Kral and Sharma, 2012; Sharma et al., 2015a).

EEG is measured against a specific reference electrode. The reference electrode is the electrode keeping a relatively steady potential in ERP studies. The underlying assumption is that the reference should be electrically quiet; however, there is no such point on the human body surface (Yao, 2001; Nunez and Srinivasan, 2006). Fluctuation of the voltage at the reference electrode will lead to changes of the potential at the active electrode, even if the voltage at that point is actually stable. Thus, with different references, the voltage waveforms extracted from the same measuring electrode often show different results. Therefore, the choice of reference is a critical issue for obtaining reliable ERPs when investigating cognitive processing.

To minimize the possible effect of different references in ERP studies, different reference sites have been used, as lab personnel have historically used them, or as is widely used in most research, which we found from literature in this field (Wolpaw and Wood, 1982). The average reference is widely considered to be superior to all other known reference schemes because it is independent of any particular recording sites included in the EEG montage (Kayser and Tenke, 2015).

In cochlear implant (CI) users, CI stimulation creates electrical artifacts on the scalp that corrupt the EEG signal, which interfere with identification of the ERP components. The strength, morphology, and spatial distribution of the CI artifact are influenced by the type and location of the CI devices and the mode of stimulation. For example, devices running with bipolar electrodes in the CI show smaller artifacts on the scalp compared to the now commonly used monopolar-coupled electrodes (Gilley et al., 2006). Thus, the reference electrode location chosen may be of great importance.

Although there are several studies that showed that the AEP component, P1, can reflect the auditory cortex ability in processing auditory information (Wunderlich et al., 2006; Sharma et al., 2015b), unfortunately, we have not found sufficient recent articles discussing which reference is the most suitable one in an auditory P1 study. With respect to the reference site, our study aimed at comparing three commonly used references [nose reference (NR), mastoid reference (MR), and montage average reference (MAR)] and one technique, reference electrode standardization technique (REST) (Yao, 2001), to determine whether different references impact the AEP characteristics in CIs. A secondary purpose of this study was to evaluate which reference is preferable for AEP studies in CIs.

METHODS

Participants

Thirteen patients (aged 4.37 ± 0.73 years) who had undergone surgical implantation of a multichannel CI device on their right side were recruited after ∼1 year of cochlear device usage. In these patients who were diagnosed with congenital bilateral profound sensorineural deafness, the average age of cochlear implantation was 1.21 ± 0.09 years. **Table 1** shows the demographic profiles of the CI participants. The etiology of deafness was unclear in all participants. None of the participants had any record of neurological or psychiatric illnesses. In addition, no inner ear or auditory nerve malformation was found during pre-operative CT and MRI evaluations. The peripheral hearing investigations revealed pure tone thresholds to 500, 1,000, 2,000, and 4,000 Hz stimuli in the 30–40 dB range in all participants. After surgery, all of the participants received standard speech rehabilitation from speech rehabilitation centers. Eleven children (aged 4.58 ± 0.52 years, matched with the age of cochlear implanted children) with congenital left external and middle ear malformation but normal hearing in the right ear were put in the control group. Ethical approval was obtained from the Institutional Review Board at Sun Yat-sen Memorial Hospital of Sun Yat-sen University before the study began. Written consent was obtained from the parents of all participants before any of the study procedures were conducted.

AEP Measurement

Participants were comfortably seated in front of a high-resolution VGA computer monitor at a viewing distance of ∼1 m in a soundproof and electromagnetically shielded room. The participants watched silent movies throughout the entire experiment. Parents and participants were asked to avoid/minimize body movements. A DELL computer running the E-prime® 2.0 program-generated 1,000 Hz pure tone stimulus elicited the AEPs. The pure tone was 60 ms in duration (5 ms rising and 5 ms descending) and was followed by inter-stimulus intervals (ISI) ranging from 600 to 800 ms. A total of 100 stimuli were delivered through loudspeakers in the booth, placed at a 45° angle on either side of the participants, ∼1 m from the participants (75 dB SPL).

TABLE 1 | Demographic characteristics of CI children.

Participant code (gender)	Age at experiment (years)	Implant device	Age at implantation (years)	Duration of CI experiment (years)
CI1 (M)	4.45	MEDEL SONATAti100	3.39	1.06
CI2 (M)	3.25	MEDEL SONATAti100	2.05	1.20
CI3 (F)	5.3	MEDEL SONATAti100	4.05	1.25
CI4 (M)	5.23	AB	4.15	1.08
CI5 (F)	2.79	COCHLEAR	1.52	1.27
CI6 (M)	4.6	COCHLEAR CI24RE	3.40	1.20
CI7 (F)	4.5	MEDEL SONATAti100	3.07	1.43
CI8 (F)	4.34	COCHLEAR CI24RE	3.19	1.15
CI9 (M)	5.09	MEDEL SONATAti100	3.90	1.19
CI10 (F)	4.22	MEDEL SONATAti100	2.93	1.29
CI11 (F)	4.79	AB	3.59	1.20
CI12 (M)	3.94	MEDEL SONATAti100	2.76	1.18
CI13 (M)	4.34	MEDEL SONATAti100	3.13	1.21

Participants in the cochlear group all had undergone surgical implantation of a multichannel cochlear implant device on their right side.

EEG Recording and Analysis

A 128-channel electroencephalography (EEG) electrode recording system (Electrical Geodesics, Inc.) physically referenced to the vertex was used to record the AEPs. CI children with the external coil protected used plastic wrap during testing. The sampling rate for the EEG recording was 1 kHz, and all electrode impedances remained below 40 kΩ (Liang et al., 2014). The EEG recordings of each child were bandpass filtered offline at 0.1–30 Hz and segmented with 100 ms pre-stimulus and 600 ms post-stimulus time. Artifact rejection set at 200 μV was applied to EEG, and epochs were rejected if they contained any eye blinking (eye channel exceeded 140 μV) or eye movement (eye channel exceeded 55 μV). Bad channels were removed from the recording. The response waveforms evoked by the stimuli were obtained by averaging all valid segments. To test the effects of reference electrode difference, the original CZ-referenced EEG signals were re-referenced offline to (1) nose reference (NR), (2) left mastoid reference (LMR), (3) montage average reference (MAR), and (4) REST (Wolpaw and Wood, 1982), which was transformed from MAR. Reference-free or reference-independent potential could not be measured, which is why such all kinds of reference schemes were used in various research groups and institutes. Among all of the reference schemes, REST could reduce the effect of the reference and could improve analysis of temporal characteristics of ERP for some cases. The data were finally baseline corrected to the pre-stimulus period of −100 to 0 ms. The artifact rejection was conducted by the EGI program automatically.

CI artifact and P1–N1 complex (latency, amplitude) at Fz electrode for individual participants were analyzed. The highest positive amplitude between 90 and 180 ms was selected as P1. The N1 component was defined as the highest negative amplitude between 110 and 320 ms. In addition, the artifact was observed as the highest negative amplitude between 0 and 80 ms. Amplitudes of the P1, N1, and artifact peaks were measured from baseline to the peak value. Latencies were chosen at the highest amplitude of the peak.

RESULTS

Data and Explanation

The reference, whose AEP result of P1 could better distinguish the difference between the CI and control group, would be considered as a more preferable one in our study. The reason behind our consideration is that P1 is the biomarker of assessing cortical maturation in pediatric hearing loss (Liang et al., 2014); thus, the CI group would show differences with the control group on the P1 component, which is supported by the main effect of group in our study. In addition, the simple effect test result of the ideal reference should be consistent with it.

We also performed similar experiments in other components, such as N1 and artifact. Since researchers cannot reach an agreement to change these components in their study, we used them in second place of our study.

To compare results of different groups on the level of the reference, and only if the significant main effect of the group exists, we would perform a simple effect test whether the reference* group interaction was significant or not.

The grand average AEPs re-referenced offline to NR, LMR, MAR, and REST of the cochlear and control group at the vertex (Fz) electrode site are shown in **Figure 1.**

The latencies and amplitudes of P1, N1, and artifact recorded at the Fz electrode re-referenced offline to NR, LMR, and MAR, respectively, in the cochlear and control group are presented in **Table 2**. The latencies and amplitudes of the P1, N1, and artifact components were analyzed by two-way repeated-measures analysis of variance (ANOVA) with one between-group factor (group) and one within-group factor (NR, LMR, and MAR reference). The results of the simple effect test are shown in **Tables 3**, **4**.

P1 COMPONENT

P1 Amplitude

Significant main effects of reference ($F = 8.926$, $p = 0.001$, adjusted by Greenhouse-Geisser) and group ($F = 10.102$, $p = 0.004$) with no reference* group interaction ($F = 3.139$, $p = 0.059$, adjusted by Greenhouse-Geisser) were found on the P1 amplitude.

Further simple effect analysis showed that in the cochlear group, the amplitudes (mean = 12.99 μV, std = 9.33) using LMR were found to be significantly larger than that using NR (mean = 5.88 μV, std = 4.88) and MAR (mean = 6.87 μV, std = 3.26) (LMR&NR: $p = 0.009$; LMR&MAR: $p = 0.037$). No significant difference was found in amplitudes using these four references in the control group.

Using NR as a reference probe, no significant difference was found between the cochlear and control group for P1 amplitude ($p = 0.135$). While using LMR, REST or MAR as a reference, the difference among these groups reached a significant level (LMR: $p = 0.000$; MAR: $p = 0.021$; REST: $p = 0.011$) and using LMR led

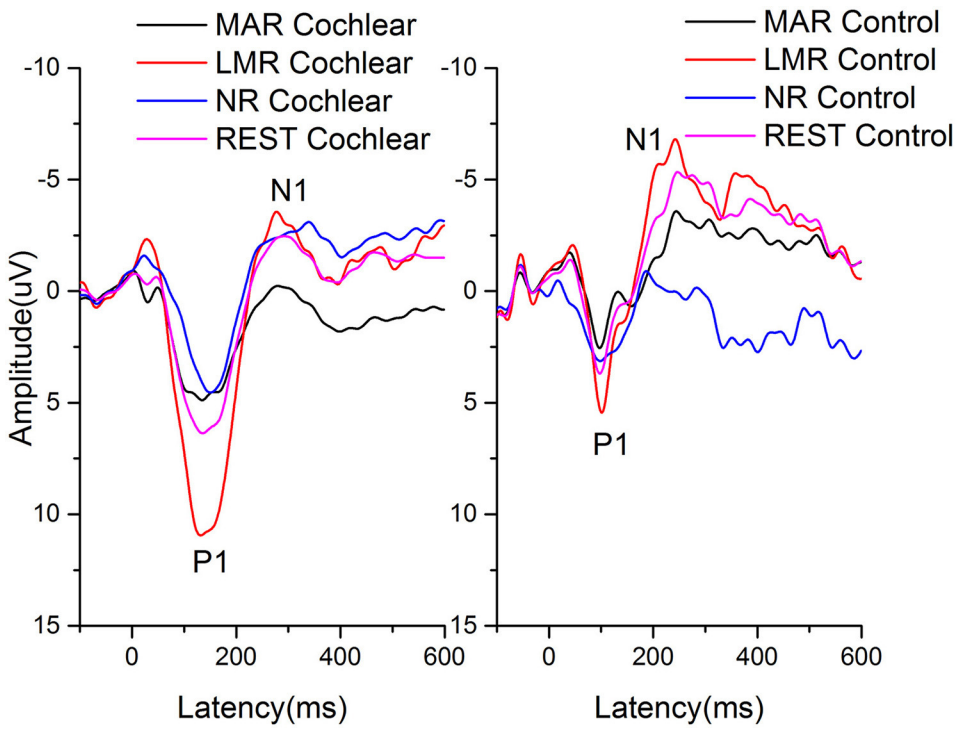

FIGURE 1 | The grand average AEPs re-referenced offline to NR, LMR, MAR, and REST of the cochlear and control group at the vertex (Fz) electrode site are shown. Amplitudes are in microvolts on the vertical axis and time, in ms, is on the horizontal axis.

TABLE 2 | P1, N1, and artifact latencies and amplitudes recorded at the Fz location.

		Amplitude (ms)			Latency (uv)		
		P1	**N1**	**Artifact**	**P1**	**N1**	**Artifact**
CI	NR	5.88 ± 4.88	−4.39 ± 3.64	−2.90 ± 2.43	154.00 ± 21.47	282.15 ± 36.32	38.08 ± 25.68
	LMR	12.99 ± 9.33	−5.60 ± 10.31	−3.76 ± 3.46	138.62 ± 23.38	267.54 ± 58.74	33.69 ± 21.82
	MAR	6.87 ± 3.26	−1.84 ± 4.09	−2.03 ± 2.63	138.08 ± 35.74	255.77 ± 72.23	25.77 ± 26.93
	REST	8.05 ± 4.82	−3.62 ± 5.48	−2.52 ± 3.21	133.38 ± 33.84	266.23 ± 56.95	25.0 ± 27.08
Control	NR	2.69 ± 3.43	−5.90 ± 5.74	−1.57 ± 2.31	132.80 ± 36.45	244.20 ± 71.96	23.93 ± 23.83
	LMR	4.12 ± 7.83	−12.72 ± 5.28	−2.95 ± 3.49	110.73 ± 22.67	270.73 ± 43.30	37.73 ± 29.10
	MAR	1.90 ± 3.54	−6.03 ± 2.76	−1.67 ± 1.57	108.40 ± 24.01	258.53 ± 57.08	32.27 ± 30.62
	REST	2.55 ± 4.74	−8.03 ± 3.50	−1.78 ± 2.24	113.00 ± 26.16	258.40 ± 56.84	33.67 ± 30.32

to less of a chance to make a type I error (LMR: $p = 0.000$; MAR: $p = 0.021$; REST: $p = 0.011$). REST had the least chance to make a type I error, besides LMR.

P1 Latency

For P1 latency, significant main effects of reference ($F = 7.830$, $p = 0.002$, adjusted by Greenhouse-Geisser) and group ($F = 7.731$, $p = 0.010$) were found with no significant reference* group interaction ($F = 0.440$, $p = 0.628$, adjusted by Greenhouse-Geisser).

After the simple effect test, we found that whether in the CI or control group, no significant difference existed among the four references.

A difference in the CI and control group can be observed in LMR and MAR. In addition, MAR had less of a chance to make a type I error (LMR, $p = 0.011$; MAR, $p = 0.007$) in distinguishing the difference between the CI and control group.

N1 COMPONENT

N1 Amplitude

For N1 amplitude, significant main effects of reference ($F = 7.999$, $p = 0.002$, adjusted by Greenhouse-Geisser) and group ($F = 7.604$, $p = 0.011$) were found with no significant reference* group interaction ($F = 2.103$, $p = 0.139$, adjusted by Greenhouse-Geisser).

TABLE 3 | Comparison of the CI group and control group on the level of different references.

AEP component	Reference	Ability to distinguish the difference between CI and control group
P1 A	NR	N, $p = 0.135$
	MR	Y, $p = 0.000$
	MAR	Y, $p = 0.021$
	REST	Y, $p = 0.011$
P1 L	NR	N, $p = 0.052$
	MR	Y, $p = 0.011$
	MAR	Y, $p = 0.007$
	REST	N, $p = 0.062$
N1 A	NR	N, $p = 0.470$
	MR	Y, $p = 0.001$
	MAR	Y, $p = 0.046$
	REST	Y, $p = 0.036$

With the result of the simple effect test, we acknowledged that in the CI group, there was no significant difference among the N1 amplitude the 4 references. However, in the control group, LMR (Mean = −12.72 μV, std = 5.28) showed a difference with NR (Mean = −5.90 μV, std = 5.74) and MAR (Mean = −6.03 μV, std = 2.76) (LMR&NR: $p = 0.006$; LMR&MAR: $p = 0.007$).

LMR, MAR, and REST could distinguish the difference of N1 amplitude between the CI and control group (LMR: $p = 0.001$; MAR: $p = 0.046$; REST: $p = 0.036$), while NR could not. In addition, LMR had the least chance to make a type I error.

N1 Latency

No significant main effects of reference ($F = 0.412$, $p = 0.653$, adjusted by Greenhouse-Geisser) or group ($F = 0.325$, $p = 0.574$) with no reference* group interaction ($F = 1.351$, $p = 0.213$, adjusted by Greenhouse-Geisser) were found on N1 latency.

ARTIFACT

Artifact Amplitude

For artifact amplitude, no significant main effects in reference ($F = 5.956$, $p = 0.007$, adjusted by Greenhouse-Geisser) and group ($F = 0.769$, $p = 0.389$) were found. No reference* group interaction ($F = 0.549$, $p = 0.561$, adjusted by Greenhouse-Geisser) existed.

Artifact Latency

For artifact latency, no significant main effects in reference ($F = 1.095$, $p = 0.338$, adjusted by Greenhouse-Geisser) or group ($F = 0.020$, $p = 0.889$) were found.

COMPARISON OF DIFFERENT DIFFERENCES

Contralateral MR has a greater ability in distinguishing CI children from the control group with less of a chance to make a type I error on P1 amplitude, while MAR did better on P1 latency. Further comparison can be found in the discussion.

TABLE 4 | Comparison of different references in different groups.

	CI			Control		
AEP component	Reference (I)	Reference (II)	Sig	Reference (I)	Reference (II)	Sig
P1 A	NR	LMR	0.009*	NR	LMR	0.981
	NR	MAR	0.998	NR	MAR	0.999
	NR	REST	0.905	NR	REST	1.000
	LMR	MAR	0.037*	LMR	MAR	0.861
	LMR	REST	0.147	LMR	REST	0.971
	MAR	REST	0.995	MAR	REST	1.000
P1 L	NR	LMR	0.678	NR	LMR	0.200
	NR	MAR	0.643	NR	MAR	0.120
	NR	REST	0.346	NR	REST	0.310
	LMR	MAR	1.000	LMR	MAR	1.000
	LMR	REST	0.998	LMR	REST	1.000
	MAR	REST	0.999	MAR	REST	0.998
N1 A	NR	LMR	0.994	NR	LMR	0.006*
	NR	MAR	0.803	NR	MAR	1.000
	NR	REST	1.000	NR	REST	0.872
	LMR	MAR	0.406	LMR	MAR	0.007*
	LMR	REST	0.931	LMR	REST	0.120
	MAR	REST	0.957	MAR	REST	0.902

*Significant difference exists ($p < 0.05$).

NR and REST are not ideal for a P1 study, as they cannot distinguish two groups on P1 latency, which contrasts the present study.

DISCUSSION

In this study, the characteristics of the AEPs in three typical references were analyzed between the right-side-CI children and age-matched congenital left external and middle ear malformation children. Children used their implants for a similar time period (∼1 year) on average. For P1, our results demonstrated that in the CI group, the amplitudes using LMR were found significantly larger than that using NR or MAR. However, no significant difference was found between amplitudes using NR and MAR. In addition, the REST result had no significant difference with the three other references. However, our results showed that different references for the AEP study did not affect the CI artifact. This might be due to that a 128 channel setup can help detect and reject CI artifacts (e.g., Artifact rejection) and replace the bad channels (e.g., bad channels replacement) (Luu et al., 2011).

Methodological differences between studies indicate that the chosen reference electrode location may determine which component is more prevalent in a given study. It is important to note and to insist on the fact that the topography of the potential field is completely independent of the choice of the reference (Geselowitz, 1998). Different references have been recommended for studies of different components (Wolpaw and Wood, 1982; Shih et al., 1988; Hagemann et al., 2001; Joyce and Rossion, 2005;

Kulaichev, 2016). There has been some research adopting the nose as a reference because it is a long distance from the regions of interest, such as visual- and auditory-related regions (Banerjee et al., 2011; Tian and Yao, 2013). Duncan et al. (2009) reported that the preferred reference is the nose, as this method allows both frontal negative and mastoid positive aspects of the signal to be visualized and measured. In addition, Shafer et al. (2015) reported that studies using a mastoid or NR will show a relatively prominent Tb peak (compared to Na). The underlying principle of average reference is that the electrical events produce both positive and negative poles. The integral part of these potential fields in a conducting sphere sums to exactly zero (Bertrand et al., 1985; Dien, 1998). It is important to note that for CI users, implant devices create electrical artifacts on the scalp; these artifacts might lead to outlier potentials, which affect the average. For this reason, the average reference may not be suitable for all components of the AEP study. To reduce electrical artifacts, it is well accepted that contralateral mastoid as the reference electrode is one of the best references for AEPs of CI users (He et al., 2012; Mc Laughlin et al., 2012, 2013; Miller and Zhang, 2014). Meanwhile, our results showed that different references for the AEP study do not affect the CI artifact.

The P1 component originating from the primary auditory cortex and thalamus reflects the summed synaptic transmission along the ascending auditory pathway (Sharma et al., 2015b), which can assess the maturation of the central auditory system via changes in latency and amplitude (Ponton et al., 2000; Wunderlich and Cone-Wesson, 2006; Wunderlich et al., 2006; Shafer et al., 2015). In CI children who received an implant before age 3.5 years, the latency and amplitude of the P1 component of the AEPs decrease rapidly and finally reach the normal age range (Sharma et al., 2002; Kral and Sharma, 2012). Our findings suggest that latencies of the P1 peak were significantly longer, and amplitudes were significantly larger in the CI than in the control group, which are consistent with previous studies (Eggermont and Ponton, 2003). Cortical ERPs mainly reflect the postsynaptic activity in pyramidal neurons, which is subject to the largest spatial and temporal summation, with each pyramidal cell neuronal column behaving as an electrical dipole (Steinschneider et al., 2011). Thus, our studies indicate immaturity of the primary auditory cortex in CI children; the transmission and synaptic delays along peripheral and central auditory pathways became longer, and the synchronization of neurons became poor after periods of auditory deprivation. The AEPs of CI children exhibited broader neural firing and formed broader positive potentials and higher P1 amplitudes over the cortex.

Although the midline electrodes (e.g., Fz, Cz, Pz) were usually used in the ERP studies, it had been reported that the early components (i.e., P1–N1) of AEP had a significant higher distribution in fronto-central areas, and Fz electrode site is most frequently used in studying P1–N1 components for its obvious observation (Brandwein et al., 2011; He et al., 2012; Cooper et al., 2013). In addition, in our previous studies, we also found that the Fz was a suitable electrode site (easy to distinguish P1–N1) in an auditory ERP study in normal and CI children (Zheng et al., 2011; Liang et al., 2014). Furthermore, a 128 channel setup can help minimize the error during the EEG data analysis (e.g., Artifact rejection, Bad channels) (Luu et al., 2011). Therefore, only the Fz was chosen for the present study, though the 128-channel setup was used. However, for the reference electrode in our study, we found that the amplitudes using LMR were significantly larger than other references in the CI group. The positive potential on the Fz electrode may be neutralized while using NR and MAR reference, which leads to the decline of the P1 amplitude. As the ERP components suggest to be determined by subjective visual observation (Zheng et al., 2011), a more apparent P1 should be preferable for the clinical ERP test. Therefore, the selection of the contralateral MR can be suitable for the test of the P1 response on Fz.

The positive potential on the Fz electrode may be neutralized while using NR and MAR, which leads to the decline of the P1 amplitude. With a relatively inactive contralateral mastoid as the reference electrode, the spatial distance between the recording electrode and reference electrode increases; then, the P1 amplitude should be more prominent. In the control group whose children had moderate-severe conductive hearing loss in the left ear and normal hearing in the right ear, the auditory cortex would be much more mature, and the positive potential would then be more concentrated, which results in shorter latency and a smaller amplitude of the P1 component. The choice of reference makes little difference in the control group. However, our present study found that it was easier to enhance the amplitude differences between the CI and control group with a smaller variation while using LMR. Furthermore, the use of LMR achieved the minimal type I error. Therefore, we assumed that contralateral MR should be a more preferable reference in AEP studies, as it has a greater ability to distinguish CI children from children with ear malformation, while studying P1 amplitudes. In addition, we recommend contralateral MR as the reference to assess the mature degree of the P1 component in the CI group. In addition, we used a one side MR to reduce the interference of the implanted cochlear, which is contrary to the traditional two side MRs. MAR and MR are acceptable for the P1 and N1 study. In addition, REST is acceptable only for N1 studies. Generally, taking the more obvious P1 amplitude into consideration, contralateral MR is more ideal for the N1–P1 component study.

CONCLUSION

P1 amplitude is significantly larger with contralateral MR than with NR and MAR and has a greater ability to distinguish CI children from children with ear malformation, with less of a chance to make a type I error. MAR and MR can distinguish the difference of two groups on P1 latency, and MAR is less likely to make type I errors. We recommend contralateral MR or MAR as an acceptable reference in the AEP P1 component study in CI patients. Considering that MR also showed greater P1 amplitude, contralateral MR is a more ideal choice for a general AEP study. REST is acceptable to study the N1 component.

NR is not acceptable for P1 or N1 studies. Different references for AEP studies do not affect the CI artifact.

AUTHOR CONTRIBUTIONS

ML: Designed the experiment, interpreted the results, and wrote the manuscript; JL: Performed the experiment, analyzed the data, and wrote the manuscript; JZ: Interpreted the results and revised the manuscript; JW: Analyzed the data; YCh: Helped to improve the experiment and the paper; YCa: Did some work on discussion; LC: Helped to collect patient; YZ: Supervised the work. All authors read and approved the final manuscript.

FUNDING

This work was supported by the National Natural Science Foundation of China (to YZ, Grant no. 81570935; to YCa, Grant no. 81600808; to JZ, Grant no. 81470085, 31271204), Project from Chengdu Science and Technology Bureau (Grant no. 2016-HM01-00462-SF), and the National University Student Innovation Training Scheme (Grant no. 201610558112).

REFERENCES

Banerjee, S., Snyder, A. C., Molholm, S., and Foxe, J. J. (2011). Oscillatory alpha-band mechanisms and the deployment of spatial attention to anticipated auditory and visual target locations: supramodal or sensory-specific control mechanisms? *J. Neurosci.* 31, 9923–9932. doi: 10.1523/JNEUROSCI.4660-10.2011

Bertrand, O., Perrin, F., and Pernier, J. (1985). A theoretical justification of the average reference in topographic evoked potential studies. *Electroencephalogr. Clin. Neurophysiol.* 62, 462–464. doi: 10.1016/0168-5597(85)90058-9

Brandwein, A. B., Foxe, J. J., Russo, N. N., Altschuler, T. S., Gomes, H., and Molholm, S. (2011). The development of audiovisual multisensory integration across childhood and early adolescence: a high-density electrical mapping study. *Cereb. Cortex.* 21, 1042–1055. doi: 10.1093/cercor/bhq170

Cooper, R. J., Atkinson, R. J., Clark, R. A., and Michie, P. T. (2013). Event-related potentials reveal modelling of auditory repetition in the brain. *Int. J. Psychophysiol.* 88, 74–81. doi: 10.1016/j.ijpsycho.2013.02.003

Dien, J. (1998). Issues in the application of the average reference: review, critiques, and recommendations. *Behav. Res. Methods Instrum. Comput.* 30, 34–43. doi: 10.3758/BF03209414

Duncan, C. C., Barry, R. J., Connolly, J. F., Fischer, C., Michie, P. T., Näätänen, R., et al. (2009). Event-related potentials in clinical research: guidelines for eliciting, recording, and quantifying mismatch negativity, P300, and N400. *Clin. Neurophysiol.* 120, 1883–1908. doi: 10.1016/j.clinph.2009.07.045

Eggermont, J. J., and Ponton, C. W. (2003). Auditory-evoked potential studies of cortical maturation in normal hearing and implanted children: correlations with changes in structure and speech perception. *Acta Otolaryngol.* 123, 249–252. doi: 10.1080/0036554021000028098

Geselowitz, D. B. (1998). The zero of potential. *IEEE Eng. Med. Biol. Mag.* 17, 128–132. doi: 10.1109/51.646230

Gilley, P. M., Sharma, A., Dorman, M., Finley, C. C., Panch, A. S., and Martin, K. (2006). Minimization of cochlear implant stimulus artifact in cortical auditory evoked potentials. *Clin. Neurophysiol.* 117, 1772–1782. doi: 10.1016/j.clinph.2006.04.018

Hagemann, D., Naumann, E., and Thayer, J. F. (2001). The quest for the EEG reference revisited: a glance from brain asymmetry research. *Psychophysiology* 38, 847–857. doi: 10.1111/1469-8986.3850847

He, S., Grose, J., Hang, A. X., and Buchman, C. A. (2012). Cochlear implant-evoked cortical activation in children with cochlear nerve deficiency. *Otol. Neurotol.* 33, 1188–1196. doi: 10.1097/MAO.0b013e31826426d2

Joyce, C., and Rossion, B. (2005). The face-sensitive N170 and VPP components manifest the same brain processes: the effect of reference electrode site. *Clin. Neurophysiol.* 116, 2613–2631. doi: 10.1016/j.clinph.2005.07.005

Kayser, J., and Tenke, C. E. (2015). Hemifield-dependent N1 and event-related theta/delta oscillations: an unbiased comparison of surface Laplacian and common EEG reference choices. *Int. J. Psychophysiol.* 97, 258–270. doi: 10.1016/j.ijpsycho.2014.12.011

Kral, A., and Sharma, A. (2012). Developmental neuroplasticity after cochlear implantation. *Trends Neurosci.* 35, 111–122. doi: 10.1016/j.tins.2011.09.004

Kulaichev, A. P. (2016). Optimal choice of a reference electrode for EEG recording. *Moscow Univ. Biol. Sci. Bull.* 71, 145–150. doi: 10.3103/s0096392516030068

Liang, M., Zhang, X., Chen, T., Zheng, Y., Zhao, F., Yang, H., et al. (2014). Evaluation of auditory cortical development in the early stages of post cochlear implantation using mismatch negativity measurement. *Otol. Neurotol.* 35, e7–e14. doi: 10.1097/MAO.0000000000000181

Luu, P., Jiang, Z., Poulsen, C., Mattson, C., Smith, A., Tucker, D. M., et al. (2011). Learning and the development of contexts for action. *Front. Hum. Neurosci.* 5:159. doi: 10.3389/fnhum.2011.00159

Mc Laughlin, M., Lopez Valdes, A., Reilly, R. B., and Zeng, F. G. (2013). Cochlear implant artifact attenuation in late auditory evoked potentials: a single channel approach. *Hear. Res.* 302, 84–95. doi: 10.1016/j.heares.2013.05.006

Mc Laughlin, M., Lu, T., Dimitrijevic, A., and Zeng, F. G. (2012). Towards a closed-loop cochlear implant system: application of embedded monitoring of peripheral and central neural activity. *IEEE Trans. Neural. Syst. Rehabil. Eng.* 20, 443–454. doi: 10.1109/TNSRE.2012.2186982

Miller, S., and Zhang, Y. (2014). Validation of the cochlear implant artifact correction tool for auditory electrophysiology. *Neurosci. Lett.* 577, 51–55. doi: 10.1016/j.neulet.2014.06.007

Nunez, P. L., and Srinivasan, R. (2006). A theoretical basis for standing and traveling brain waves measured with human EEG with implications for an integrated consciousness. *Clin. Neurophysiol.* 117, 2424–2435. doi: 10.1016/j.clinph.2006.06.754

Ponton, C. W., Eggermont, J. J., Kwong, B., and Don, M. (2000). Maturation of human central auditory system activity: evidence from multi-channel evoked potentials. *Clin. Neurophysiol.* 111, 220–236. doi: 10.1016/S1388-2457(99)00236-9

Ponton, C., Eggermont, J. J., Khosla, D., Kwong, B., and Don, M. (2002). Maturation of human central auditory system activity: separating auditory evoked potentials by dipole source modeling. *Clin. Neurophysiol.* 113, 407–420. doi: 10.1016/S1388-2457(01)00733-7

Shafer, V. L., Yu, Y. H., and Wagner, M. (2015). Maturation of cortical auditory evoked potentials (CAEPs) to speech recorded from frontocentral and temporal sites: three months to eight years of age. *Int. J. Psychophysiol.* 95, 77–93. doi: 10.1016/j.ijpsycho.2014.08.1390

Sharma, A., Campbell, J., and Cardon, G. (2015a). Developmental and cross-modal plasticity in deafness: evidence from the P1 and N1 event related potentials in cochlear implanted children. *Int. J. Psychophysiol.* 95, 135–144. doi: 10.1016/j.ijpsycho.2014.04.007

Sharma, A., Dorman, M. F., and Spahr, A. J. (2002). A sensitive period for the development of the central auditory system in children with cochlear implants: implications for age of implantation. *Ear Hear.* 23, 532–539. doi: 10.1097/00003446-200212000-00004

Sharma, A., Glick, H., Deeves, E., and Duncan, E. (2015b). The P1 biomarker for assessing cortical maturation in pediatric hearing loss: a review. *Otorinolaringologia* 65, 103–114.

Shih, P. Y., Aminoff, M. J., Goodin, D. S., and Mantle, M. M. (1988). Effect of reference point on visual evoked potentials: clinical relevance. *Electroencephalogr. Clin. Neurophysiol.* 71, 319–322. doi: 10.1016/0168-5597(88)90033-0

Steinschneider, M., Liegeois-Chauvel, C., and Brugge, J. (2011). "Auditory evoked potentials and their utility in the assessment of complex sound processing, Chapter 25," in *The Auditory Cortex,* eds J. A. Winer and C. Schreiner (New York, NY: Springer), 535–559.

Tian, Y., and Yao, D. (2013). Why do we need to use a zero reference? Reference influences on the ERPs of audiovisual effects. *Psychophysiology* 50, 1282–1290. doi: 10.1111/psyp.12130

Wolpaw, J. R., and Wood, C. C. (1982). Scalp distribution of human auditory evoked potentials. I. Evaluation of reference electrode sites. *Electroencephalogr. Clin. Neurophysiol.* 54, 15–24. doi: 10.1016/0013-4694(82)90227-9

Wunderlich, J. L., and Cone-Wesson, B. K. (2006). Maturation of CAEP in infants and children: a review. *Hear. Res.* 212, 212–223. doi: 10.1016/j.heares.2005.11.008

Wunderlich, J. L., Cone-Wesson, B. K., and Shepherd, R. (2006). Maturation of the cortical auditory evoked potential in infants and young children. *Hear. Res.* 212, 185–202. doi: 10.1016/j.heares.2005.11.010

Yao, D. (2001). A method to standardize a reference of scalp EEG recordings to a point at infinity. *Physiol. Meas.* 22, 693–711. doi: 10.1088/0967-3334/22/4/305

Zheng, Y., Zhao, F., Liang, M., Bardsley, B., Yang, H., and Zhang, Z., et al. (2011). Toward an understanding of auditory evoked cortical event-related potentials: characteristics and classification. *Audiol. Med.* 9, 16–25. doi: 10.3109/1651386X.2010.537910

Conflict of Interest Statement: The authors declare that the research was conducted in the absence of any commercial or financial relationships that could be construed as a potential conflict of interest.

frontiers in Neuroscience

METHODS
published: 11 December 2017
doi: 10.3389/fnins.2017.00683

How Electroencephalogram Reference Influences the Movement Readiness Potential?

Yuxia Hu[1†], *Lipeng Zhang*[1†], *Mingming Chen*[1], *Xiaoyuan Li*[1] *and Li Shi*[2*]

[1] Henan Key Laboratory of Brain Science and Brain-Computer Interface Technology, Department of Automation, School of Electric Engineering, Zhengzhou University, Zhengzhou, China, [2] Department of Automation, Tsinghua University, Beijing, China

Readiness potential (RP) based on electroencephalograms (EEG) has been studied extensively in recent years, but no studies have investigated the influence of the reference electrode on RP. In order to investigate the reference effect, 10 subjects were recruited and the original vertex reference (Cz) was used to record the raw EEG signal when the subjects performed a motor preparation task. The EEG was then transformed to the common average reference (CAR) and reference electrode standardization technique (REST) reference, and we analyzed the RP waveform and voltage topographies and calculated the classification accuracy of idle and RP EEG segments. Our results showed that the RP waveform and voltage topographies were greatly influenced by the reference, but the classification accuracy was less affected if proper channels were selected as features. Since the Cz channel is near the primary motor cortex, where the source of RP is located, using the REST and CAR references is recommended to get accurate RP waveforms and voltage topographies.

Keywords: EEG, re-reference, readiness potential (RP), reference electrode standardization technique (REST), common average reference (CAR)

OPEN ACCESS

Edited by:
Maria L. Bringas, University of Electronic Science and Technology, China

Reviewed by:
Guido Nolte, Fraunhofer FIRST, Germany
Jing Jin, East China University of Science and Technology, China

***Correspondence:**
Li Shi
shilits@mail.tsinghua.edu.cn

[†] *These authors have contributed equally to this work and co-first authors.*

Specialty section:
This article was submitted to Brain Imaging Methods, a section of the journal Frontiers in Neuroscience

Received: *29 August 2017*
Accepted: *22 November 2017*
Published: *11 December 2017*

Citation:
Hu Y, Zhang L, Chen M, Li X and Shi L (2017) How Electroencephalogram Reference Influences the Movement Readiness Potential? Front. Neurosci. 11:683. doi: 10.3389/fnins.2017.00683

INTRODUCTION

The idea of motor task prediction was first proposed by von Helmholtz (1867), who attempted to explain how humans localize objects (Ahmadian et al., 2013). With the discovery of the brain's electrical activity and the improvement of acquisition equipment performance, predicting motor task became a real possibility. Without a doubt, the interpretation of readiness potential (RP) is meaningful and challenging (Wolpert and Flanagan, 2001; Baker et al., 2012).

The readiness potential is a slow negative potential that can begin as early as 1.5 s before voluntary movement. It features a steeper slope and larger amplitude over the contralateral primary motor cortex (Shibasaki and Hallett, 2006). As a slow cortical potential close to direct-current, the RP is typically not visible in single trial. However, it can be observed clearly using average technology. When the signals are filtered in the 0.1–1 Hz range, the results are better (Garipelli et al., 2011). To date, most of the research on RP has focused on the accuracy of single-trial signal extraction, which can be used in a brain–computer interface. A recent study utilizing a 0.1–1 Hz filter and down-sampling methods to detect self-paced reaching movement intention from EEG signals achieved an average sensitivity of 76 ± 0.07% (Lew et al., 2012). A subsequent study of single-trial RP analysis combing a spatial smoothing filter and common average reference (CAR) reported an average accuracy of 88 ± 0.05% in a contingent cue variation paradigm (Garipelli et al., 2013). In addition, some studies have investigated the use of lateralized RP in combination with imagined movement rhythms to improve the speed and accuracy of brain–computer interfaces (Blankertz et al., 2003, 2006).

Some of the above authors mentioned the effects of the reference; however, none of them discussed how the reference influences RP. Despite the enormous technological advances in the field, an accepted EEG reference is yet still to be settled upon. Ideally, the reference site should be an electrically neutral location, where there are no potential changes; however, there are no truly neutral locations in the human body. In order to reduce the influence of the reference electrode, a number of different reference schemes have been proposed, such as the Cz (Lehmann et al., 1998; Hesse et al., 2004), nose (Andrew and Pfurtscheller, 1996; Essl and Rappelsberger, 1998), linked mastoids or ears (Gevins and Smith, 2000; Croft et al., 2002; Jin et al., 2015), and CAR (Offner, 1950; Nunez et al., 2001). Related studies have indicated that the CAR reference has obtained a large consensus because it is least biased (Srinivasan et al., 1998; Ferree, 2006). Since the surface integral of the electric potential over a volume conductor containing all the current sources is zero, a virtual zero-potential point is provided by the average potential of all the electrodes (Bertrand et al., 1985).

A groundbreaking study of the reference electrode standardization technique (REST) used scalp potentials to determine neural electrical activity and approximately reconstructed the equivalent sources from scalp EEG recordings with a scalp point or average reference, with the potentials referenced at infinity approximately reconstructed from the equivalent sources (Yao, 2001). Although the REST has been shown to be advantageous (Ferree, 2006; Marzetti et al., 2007; Yao et al., 2007; Kayser and Tenke, 2010; Qin et al., 2010; Chella et al., 2016), most recent EEG studies have not used this method, especially for RP, which is sensitive to the reference.

The present study examined the impact of different references (Cz, CAR, and REST) on RP. First, we analyzed the waveform of RP across the three reference electrodes. Next, the reference effect on the activation of brain regions was investigated by drawing the voltage topographies of RP. Finally, the recognition accuracies of the idle and RP states were calculated and compared across the three references.

MATERIALS AND METHODS

Participants

Ten healthy subjects (S1–S10, age 26.5 ± 2.1 years, one female, all right-handed) recruited from Zhengzhou University participated in the experiment. All of the participants had normal or corrected-to-normal vision. Prior to the experiment, they were informed of the experimental procedure and signed a letter of consent. The study was approved by the local ethics committee for the Protection of Human Subjects for the Zhengzhou University.

Experiment Paradigm

Each participant was seated in a comfortable chair in a room with normal lighting and temperature. The participant sat facing a screen and was asked to watch the center of the screen. During the recording, the participant was asked to try to avoid eye movement, swallowing, and unnecessary limb movements.

At the beginning of each trial, a white cross was presented in the center of the screen (**Figure 1**). For the next 3 s, participants remained idle, with their hands, forearms, and elbows resting on the armrest of the chair. Next, a green arrow pointing either left or right appeared in the center of the screen for 0.5 s. After the cue disappeared, the participants prepared to perform the corresponding task instructed by the visual cue (left hand movement for left-pointing arrow, right hand movement for right-pointing arrow). After a preparation time of about 2 s, the participants performed the hand movement. Then, five seconds after the visual cue, an auditory cue was presented to inform the participant to return to the idle state. Six sessions were conducted for each participant, with 40 trials per session (20 trials each for left and right).

Two bipolar electrodes were attached to the participant's left and right arm to record electromyograms (EMG) during arm movement.

EEG Recording

EEG data was recorded using a Neuroscan NuAmps digital amplifier system with 58 electrodes arranged in the standard 10–20 EEG configuration. All of the brain regions were covered by these electrodes. Two extended bipolar channels (BP3 and BP4) were used to acquire the left and right arms' EMG signals. The EEG signals were acquired at a sampling rate of 1,000 Hz with the Cz-REF as a reference, and the impedance of all electrodes was less than 5 KΩ. The Cz-REF was located between the Cz and CPZ electrodes. The selected electrodes and the Cz-REF are shown in **Figure 2**.

Data Preprocessing and Re-Reference

Data analysis consisted of two parts: EMG analysis and EEG data analysis. We acquired the onset time of hand movement for each trial by processing the EMG data, as shown in **Figure 3**. The event-related potential, brain voltage topographies, and classification accuracy of the RP state and idle state under different references were acquired by processing the EEG data.

The EMG data were filtered by a basic finite impulse response filter with respective cutoff frequencies of 6 and 50 Hz. We then calculated the energy of the filtered data and set the proper threshold to detect the onset time of motion. We recorded the onset times in a TXT file for EEGLAB toolbox analysis (Delorme and Makeig, 2004).

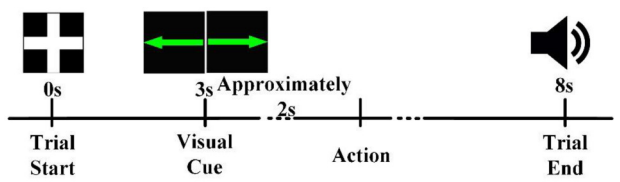

FIGURE 1 | The timeline of a trial. Each trial began in the idle state, in which the participant rested his or her hands, forearms, and elbows on the armrest of a chair and relaxed his or her hands. A visual cue informed the participant that a task should be performed about 2 s later. After completion of the task, an auditory cue instructed the participant to return to the idle state.

For the EEG data, EOG artifacts were first removed by Scan 4.5 software (the threshold was set at 60 μV). Then the processed data was exported to EEGLAB for further analysis.

Both the CAR and REST (Yao, 2001, 2017) were conducted offline to generate the re-referenced EEG. The CAR was conducted using the *reref* function from the EEGLAB toolbox (Delorme and Makeig, 2004), and the REST was conducted using the *rest_refer* function (http://www.neuro.uestc.edu.cn/REST/).

RP Analysis

The original and re-referenced EEG were filtered by a band-pass filter (basic FIR filter, 0.1–1 Hz) and segmented into epochs from −3.5 to −3.4 s with respect to the onset time of motor execution (0 s). The data in the interval [−3.5, −3.4 s] was considered the baseline, and baseline correction was conducted for the segmented EEG epoch.

In order to examine the influence of different reference electrodes on the latency, amplitude, and waveform of RP, the RPs were plotted for the three reference methods. Then, we measured the RP's peak amplitude and latency on channels Cz, C1, C2, FC1, FC2, FCz, F1, F2, and Fz under different reference conditions.

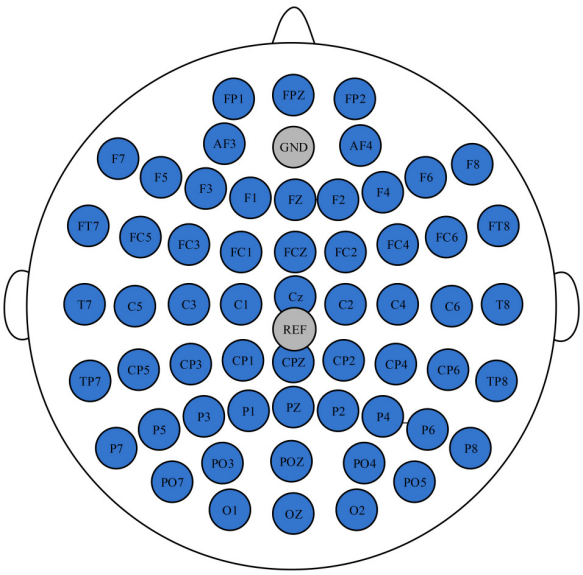

FIGURE 2 | The position of the selected electrodes and the Cz-REF.

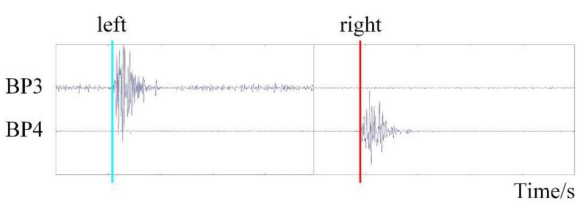

FIGURE 3 | The time of movement onset detection based on EMG.

RP Topography Analysis

Brain voltage topographies can reflect the topological structure of brain activation. It was important for us to analyze the activation areas of the brain and their change over time. However, previous studies usually drew the RP topographies under only one reference method (such as Cz-REF, CAR, or REST) and ignored the influence of different references. In our study, the 0.5 s averaged EEG segments before motion onset were extracted and voltage topographies were drawn every 0.1 s under the three reference methods.

Feature Extraction

Since RP has obvious time-domain features, we performed classification by the time-domain features. First, the preprocessed data (re-referenced, filtered, segmented, and baseline corrected) were resampled to 10 Hz. Then, the data were divided into two datasets: an idle dataset (i.e., no hand movement) and an RP dataset (i.e., left or right hand movement preparation). We extracted [−2.8 s, −2.2 s] and [−0.6 s, 0 s] of the signals above as idle and RP datasets, respectively (**Figure 4**).

According to the activated brain regions of RP, the channels (including F3, FZ, F4, FC1, FC2, C3, C4, Cz, CP1, and CP2) were selected for feature extraction in order to ensure the classification accuracy of different subjects. Finally, 60 features were acquired for each trial.

Classification

The LIBSVM 3.11 toolbox was used for classification (Chih-Chung and Chih-Jen, 2011). The radial basis function kernel was utilized, and the penalty factor (C) and gamma (Γ) parameters were optimized by the grid method. The classification accuracy of the RP and idle state was obtained using 5-fold cross-validation.

RESULTS

Reference Effects on RP

Figure 5 shows S7's grand average of the RP interval in three references. When using Cz-REF as a reference, both the left and right RP followed a straight line at the Cz channel, and it was difficult to discern when movement preparation occurred. However, the RP was clear at the Cz channel when the EEG data was adjusted to a CAR or REST reference. For channels C1 and C2, which are near Cz, we can see that the amplitude of RP was smaller from the Cz-REF reference than from the CAR and REST references. The left RP amplitude was higher on channel C2, while the right RP amplitude was higher on channel C1. On channels FC1, FC2, and FCZ, which are located far from Cz-REF, although a clear RP could be seen in all three references,

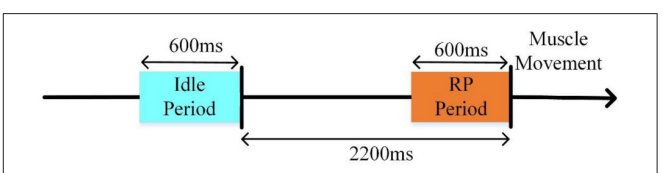

FIGURE 4 | The selected EEG datasets for the RP classifier.

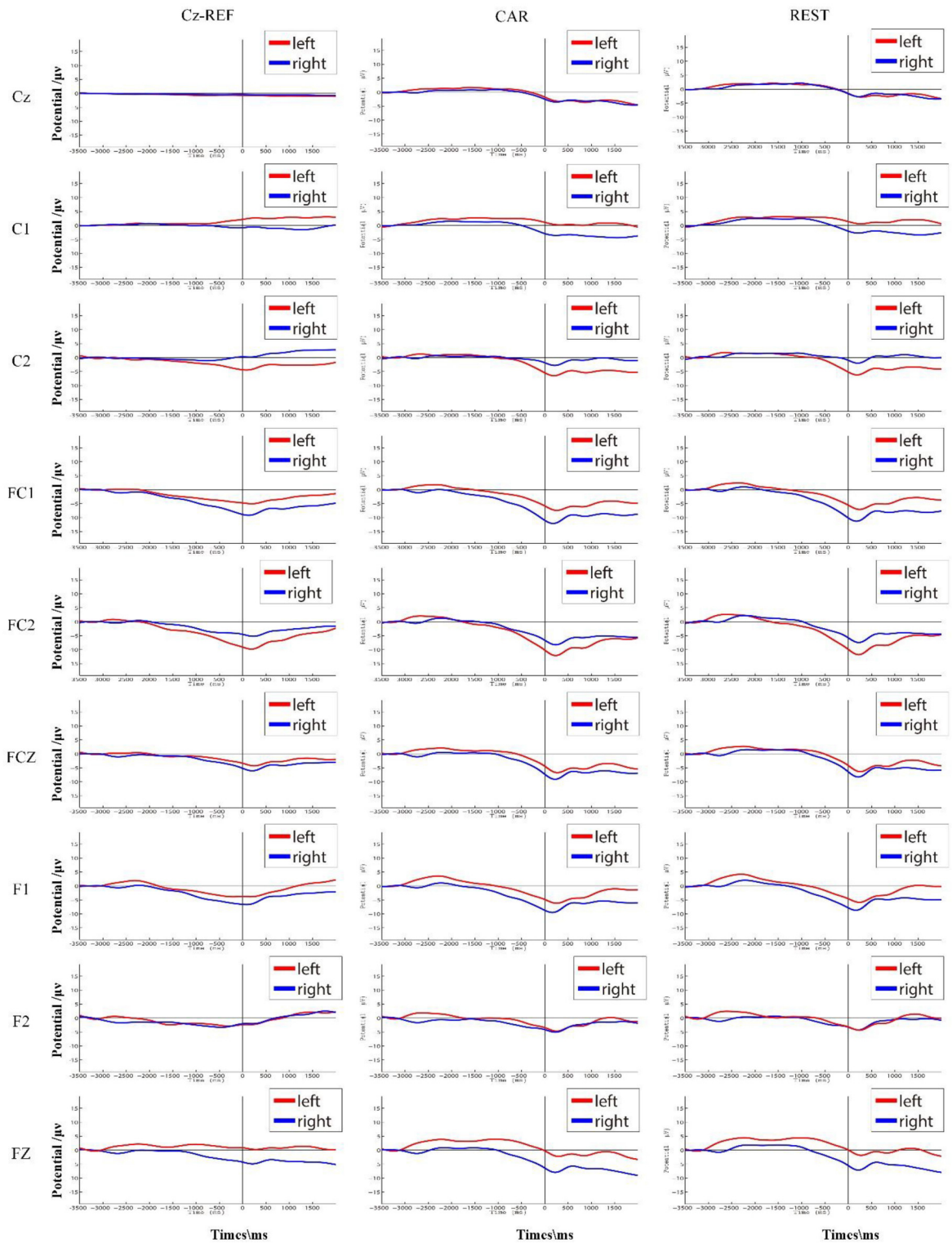

FIGURE 5 | S7's average RP interval (corresponding to [−3.5 s, 2 s] with respect to muscle movement) in three references. The RPs of the left and right hand movements are shown in red and blue, respectively.

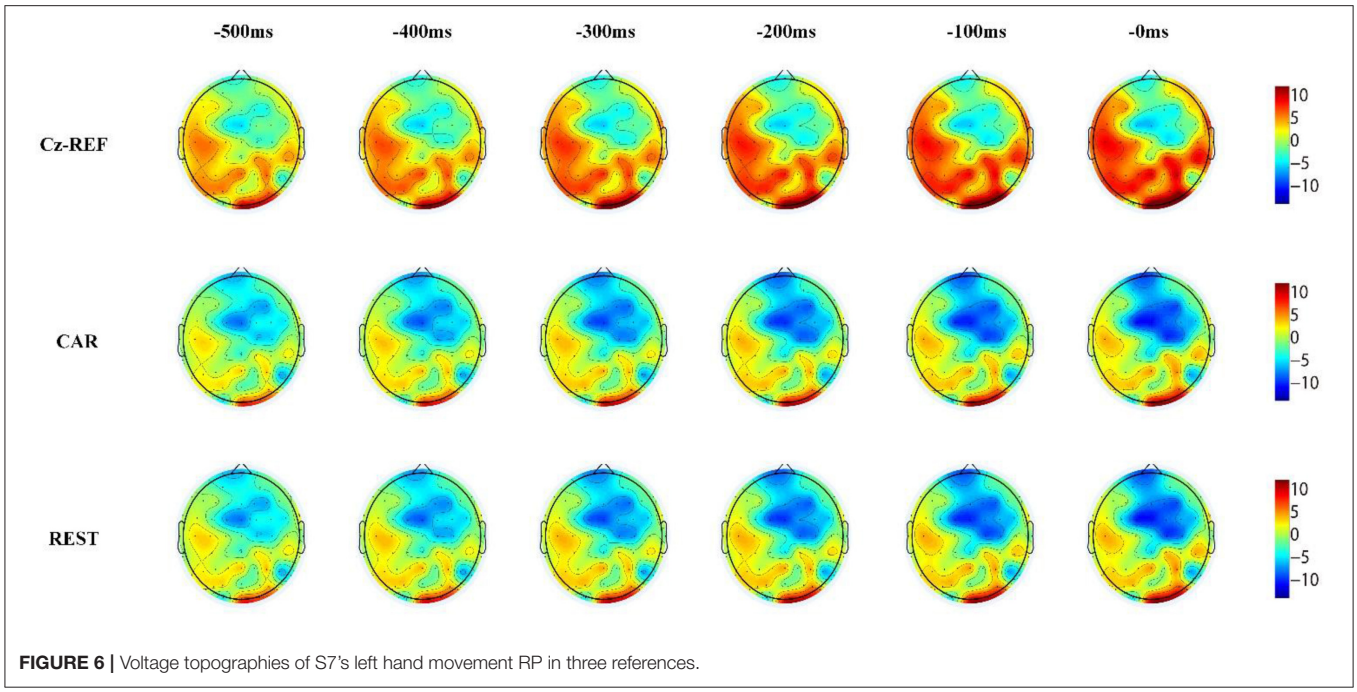

FIGURE 6 | Voltage topographies of S7's left hand movement RP in three references.

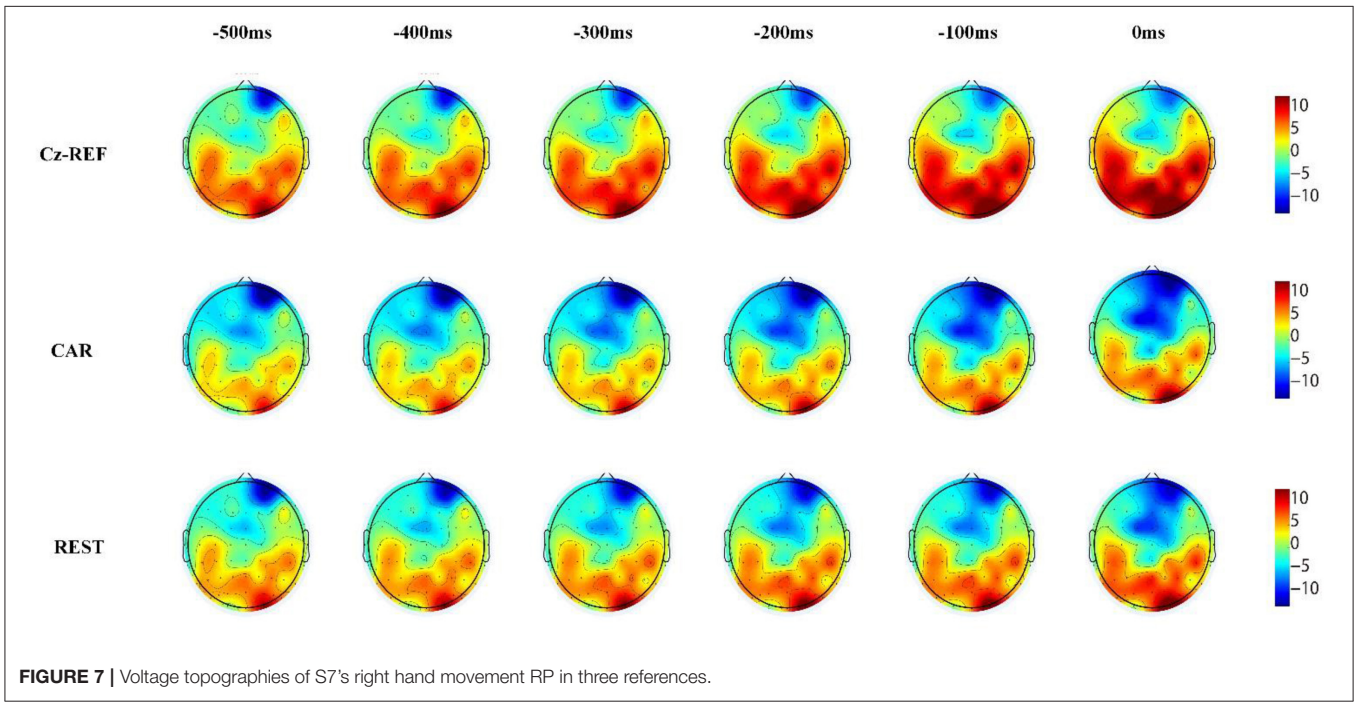

FIGURE 7 | Voltage topographies of S7's right hand movement RP in three references.

TABLE 1 | Accuracy of classification accuracy between idle and RP periods in three references over all 10 participants.

	S1 (%)	S2 (%)	S3 (%)	S4 (%)	S5 (%)	S6 (%)	S7 (%)	S8 (%)	S9 (%)	S10 (%)	Average (%)
Cz	98.52	83.10	89.66	89.03	86.12	96.01	88.42	70.88	85.23	86.52	87.35
CAR	98.06	87.84	92.67	88.28	91.72	96.08	89.98	67.67	84.00	87.80	88.41
REST	99.07	91.46	91.28	92.83	92.87	96.73	90.01	69.11	82.78	82.78	88.91

the RP amplitude of Cz-REF was still smaller than those of CAR and REST. On channels F1, F2, and Fz, which are the farthest from Cz-REF, the RP became unclear compared with channels FC1, FC2, and FCZ, and the RP amplitude also became small in the CAR and REST references. The waveforms of CAR and REST were similar for all nine channels, but the amplitude of the REST reference was slightly higher than that of the CAR reference.

Reference Effects on RP Voltage Topographies

Figures 6, **7** show the same subject's RP voltage topographies for the left and right hand movements in the three references. From these two figures, the following three observations can be made. First, the activation areas of the RP were similar. Second, compared with the other two references, the RP voltage topographies of the Cz-REF reference did not show obvious activation, especially for the primary motor cortex. Finally, the REST reference was as good as the CAR reference for drawing the voltage topographies of the RP. The same results were obtained for the other subjects in the experiment.

Reference Effects on Classification

Table 1 shows the classification accuracy of the idle and RP periods from 10 participants in three references. High classification accuracy was achieved for all participants except S8, for whom the accuracy was around 70%. The average classification accuracies from the three references were 88.41% (CAR), 87.35% (Cz-REF), and 88.91% (REST), respectively. The REST reference achieved the highest classification accuracy, and the Cz-REF reference achieved the lowest classification accuracy, but the differences among the three references were not statistically significant ($p < 0.05$).

DISCUSSION

The aim of this study was to explore the effects of the reference on RP analysis, including waveforms, voltage topographies, and recognition. As far as we know, this is the first work to compare three commonly used reference schemes—the Cz-REF, CAR, and REST references—in a study of RP. Specifically, we evaluated the amplitude and latency of the RP, then plotted the voltage topographies of the RP and investigated the reference effects on the active area. Finally, the recognition accuracy for the idle and RP periods was calculated over the 10 participants.

We found that the waveform of the RP was influenced by Cz-REF, particularly on the channels near the reference electrode. The main reason for this is that the activation area of motor preparation is close to the Cz-REF reference, and the electrical activity could be conducted to the reference channel. Thus, we could not observe the RP waveform at the Cz channel or even at the C1 and C2 channels near Cz. The RP appeared clearly at the FC1, FC2, and FCz channels due to the longer distance between these channels and the Cz-REF reference. For the F1, F2, and Fz channels, the RP was not better than it was for the FC1, FC2, and FCz channels even though they were the farthest from the reference electrode. We think a plausible explanation is that those channels are not located over the central activation area of the RP (Soon et al., 2008; Andersen and Cui, 2009). There was no significant difference between the CAR and REST references, both of which achieved better results than the Cz-REF reference. Therefore, the CAR and REST references are better choices than the Cz-REF reference when investigating RP.

The RP voltage topographies were also influenced by the reference. With the Cz-REF reference, due to the electrical activity change on the reference electrode, the RP-associated activation brain area could not be observed clearly. However, the activation area could be observed clearly by the CAR and REST references. The RP voltage topographies were almost the same in the CAR and REST references. These results confirmed that the REST reference was as good as the CAR reference for RP voltage topography analysis.

Unlike the RP waveform and voltage topographies, the results of classification accuracy in the three references were similar. The reason may be that although the channels near Cz have disadvantageous features, there are some channels with useful features, such as FC1, FC2, and FCz. High classification accuracy was achieved for all participants except one (S8), for whom the correct rate was around 70%. This could be due to inter-subject differences. Although the REST reference had a slight advantage (0.5% higher than CAR and 1.56% higher than Cz-REF), the difference was not statistically significant. These results indicate that the choice of reference channel does not significantly influence the classification accuracy of the RP and idle EEG segments.

CONCLUSION

In conclusion, the results of our research revealed that the RP waveform and voltage topographies were greatly influenced by the reference, but the classification accuracy was less affected if proper channels were selected as features. Since the Cz-REF reference is near the primary motor cortex, where the source of RP is located, the REST and CAR references are better choices for obtaining accurate RP waveforms and voltage topographies.

AUTHOR CONTRIBUTIONS

YH, LZ, MC, XL, and LS conceived and designed the experiments. YH, LZ, and XL performed the experiments and analyzed the data. YH and LZ wrote the main manuscript text. All authors reviewed the manuscript.

ACKNOWLEDGMENTS

This research was supported by grants from the National Natural Science Foundation of China projects (NSFC, No. 61603344) and the Key Research Projects of Henan Higher Education Institutions (Project Number: 16A120008).

REFERENCES

Ahmadian, P., Cagnoni, S., and Ascari, L. (2013). How capable is non-invasive EEG data of predicting the next movement? A mini review. *Front. Hum. Neurosci.* 7:124. doi: 10.3389/fnhum.2013.00124

Andersen, R. A., and Cui, H. (2009). Intention, action planning, and decision making in parietal-frontal circuits. *Neuron* 63, 568–583. doi: 10.1016/j.neuron.2009.08.028

Andrew, C., and Pfurtscheller, G. (1996). Dependence of coherence measurements on EEG derivation type. *Med. Biol. Eng. Comput.* 34, 232–238. doi: 10.1007/BF02520079

Baker, K. S., Piriyapunyaporn, T., and Cunnington, R. (2012). Neural activity in readiness for incidental and explicitly timed actions. *Neuropsychologia* 50, 715–722. doi: 10.1016/j.neuropsychologia.2011.12.026

Bertrand, O., Perrin, F., and Pernier, J. (1985). A theoretical justification of the average reference in topographic evoked potential studies. *Electroencephalogr. Clin. Neurophysiol.* 62, 462–464. doi: 10.1016/0168-5597(85)90058-9

Blankertz, B., Dornhege, G., Krauledat, M., Müller, K. R., Kunzmann, V., Losch, F., et al. (2006). The Berlin brain-computer interface: EEG-based communication without subject training. *IEEE Trans. Neural Syst. Rehabil. Eng.* 14, 147–152. doi: 10.1109/TNSRE.2006.875557

Blankertz, B., Dornhege, G., Schäfer, C., Krepki, R., Kohlmorgen, J., Müller, K. R., et al. (2003). Boosting bit rates and error detection for the classification of fast-paced motor commands based on single-trial EEG analysis. *IEEE Trans. Neural Syst. Rehabil. Eng.* 11, 127–131. doi: 10.1109/TNSRE.2003.814456

Chella, F., Pizzella, V., Zappasodi, F., and Marzetti, L. (2016). Impact of the reference choice on scalp EEG connectivity estimation. *J. Neural Eng.* 13:036016. doi: 10.1088/1741-2560/13/3/036016

Chih-Chung, C., and Chih-Jen, L. (2011). LIBSVM: a library for support vector machines. *ACM Trans. Intell. Syst. Technol.* 2:27. doi: 10.1145/1961189.1961199

Croft, R. J., Chandler, J. S., Burgess, A. P., Barry, R. J., Williams, J. D., and Clarke, A. R. (2002). Acute mobile phone operation affects neural function in humans. *Clin. Neurophysiol.* 113, 1623–1632. doi: 10.1016/S1388-2457(02)00215-8

Delorme, A., and Makeig, S. (2004). EEGLAB: an open source toolbox for analysis of single-trial EEG dynamics including independent component analysis. *J. Neurosci. Methods* 134, 9–21. doi: 10.1016/j.jneumeth.2003.10.009

Essl, M., and Rappelsberger, P. (1998). EEG coherence and reference signals: experimental results and mathematical explanations. *Med. Biol. Eng. Comput.* 36, 399–406. doi: 10.1007/BF02523206

Ferree, T. C. (2006). Spherical splines and average referencing in scalp electroencephalography. *Brain Topogr.* 19, 43–52. doi: 10.1007/s10548-006-0011-0

Garipelli, G., Chavarriaga, R., and Millán Jdel R. (2013). Single trial analysis of slow cortical potentials: a study on anticipation related potentials. *J. Neural Eng.* 10:036014. doi: 10.1088/1741-2560/10/3/036014

Garipelli, G., Chavarriaga, R., Millan, J. D. R., and IEEE (2011). "Single trial recognition of anticipatory slow cortical potentials: the role of spatio-spectral filtering," in *5th International IEEE Engineering-in-Medicine-and-Biology-Society (EMBS) Conference on Neural Engineering* (Cancun: NER), 408–411.

Gevins, A., and Smith, M. E. (2000). Neurophysiological measures of working memory and individual differences in cognitive ability and cognitive style. *Cereb. Cortex* 10, 829–839. doi: 10.1093/cercor/10.9.829

Hesse, C. W., Seiss, E., Bracewell, R. M., and Praamstra, P. (2004). Absence of gaze direction effects on EEG measures of sensorimotor function. *Clin. Neurophysiol.* 115, 29–38. doi: 10.1016/S1388-2457(03)00302-X

Jin, J., Sellers, E. W., Zhou, S., Zhang, Y., Wang, X., and Cichocki, A. (2015). A P300 brain-computer interface based on a modification of the mismatch negativity paradigm. *Int. J. Neural Syst.* 25:1550011. doi: 10.1142/S0129065715500112

Kayser, J., and Tenke, C. E. (2010). In search of the Rosetta Stone for scalp EEG: converging on reference-free techniques. *Clin. Neurophysiol.* 121, 1973–1975. doi: 10.1016/j.clinph.2010.04.030

Lehmann, D., Strik, W. K., Henggeler, B., Koenig, T., and Koukkou, M. (1998). Brain electric microstates and momentary conscious mind states as building blocks of spontaneous thinking: I. Visual imagery and abstract thoughts. *Int. J. Psychophysiol.* 29, 1–11.

Lew, E., Chavarriaga, R., Silvoni, S., and Millán Jdel R. (2012). Detection of self-paced reaching movement intention from EEG signals. *Front. Neuroeng.* 5:13. doi: 10.3389/fneng.2012.00013

Marzetti, L., Nolte, G., Perrucci, M. G., Romani, G. L., and Del Gratta, C. (2007). The use of standardized infinity reference in EEG coherency studies. *Neuroimage* 36, 48–63. doi: 10.1016/j.neuroimage.2007.02.034

Nunez, P. L., Wingeier, B. M., and Silberstein, R. B. (2001). Spatial-temporal structures of human alpha rhythms: theory, microcurrent sources, multiscale measurements, and global binding of local networks. *Hum. Brain Mapp.* 13, 125–164. doi: 10.1002/hbm.1030

Offner, F. F. (1950). The EEG as potential mapping: the value of the average monopolar reference. *Electroencephalogr. Clin. Neurophysiol.* 2, 213–214. doi: 10.1016/0013-4694(50)90040-X

Qin, Y., Xu, P., and Yao, D. (2010). A comparative study of different references for EEG default mode network: the use of the infinity reference. *Clin. Neurophysiol.* 121, 1981–1991. doi: 10.1016/j.clinph.2010.03.056

Shibasaki, H., and Hallett, M. (2006). What is the Bereltschaftspotential? *Clin. Neurophysiol.* 117, 2341–2356. doi: 10.1016/j.clinph.2006.04.025

Soon, C. S., Brass, M., Heinze, H.-J., and Haynes, J.-D. (2008). Unconscious determinants of free decisions in the human brain. *Int. J. Psychol.* 43, 238–238. doi: 10.1038/nn.2112

Srinivasan, R., Nunez, P. L., and Silberstein, R. B. (1998). Spatial filtering and neocortical dynamics: estimates of EEG coherence. *IEEE Trans. Biomed. Eng.* 45, 814–826. doi: 10.1109/10.686789

von Helmholtz, H. (1867). *Handbuch der Physiologischen Optik,* Hamburg: Voss.

Wolpert, D. M., and Flanagan, J. R. (2001). Motor prediction. *Curr. Biol.* 11, R729–R732. doi: 10.1016/S0960-9822(01)00432-8

Yao, D. (2017). Is the surface potential integral of a dipole in a volume conductor always zero? A cloud over the average reference of EEG and ERP. *Brain Topogr.* 30, 161–171. doi: 10.1007/s10548-016-0543-x

Yao, D., Wang, L., Arendt-Nielsen, L., and Chen, A. C. (2007). The effect of reference choices on the spatio-temporal analysis of brain evoked potentials: the use of infinite reference. *Comput. Biol. Med.* 37, 1529–1538. doi: 10.1016/j.compbiomed.2007.02.002

Yao, D. (2001). A method to standardize a reference of scalp EEG recordings to a point at infinity. *Physiol. Meas.* 22, 693–711. doi: 10.1088/0967-3334/22/4/305

Conflict of Interest Statement: The authors declare that the research was conducted in the absence of any commercial or financial relationships that could be construed as a potential conflict of interest.

frontiers in Neuroscience

ORIGINAL RESEARCH
published: 08 March 2018
doi: 10.3389/fnins.2018.00143

Event-Related Potential Responses to Task Switching Are Sensitive to Choice of Spatial Filter

Aaron S. W. Wong[1,2†], *Patrick S. Cooper*[1,2,3†], *Alexander C. Conley*[1,2,4], *Montana McKewen*[1,3], *W. Ross Fulham*[1,3], *Patricia T. Michie*[1,3] *and Frini Karayanidis*[1,2,3*]

[1] *Functional Neuroimaging Laboratory, School of Psychology, University of Newcastle, Callaghan, NSW, Australia,* [2] *Priority Research Centre for Stroke and Brain Injury, University of Newcastle, Callaghan, NSW, Australia,* [3] *Priority Research Centre for Brain and Mental Health, University of Newcastle, Callaghan, NSW, Australia,* [4] *Department of Psychiatry, Center for Cognitive Medicine, Vanderbilt University Medical Center, Nashville, TN, United States*

Event-related potential (ERP) studies using the task-switching paradigm show that multiple ERP components are modulated by activation of proactive control processes involved in preparing to repeat or switch task and reactive control processes involved in implementation of the current or new task. Our understanding of the functional significance of these ERP components has been hampered by variability in their robustness, as well as their temporal and scalp distribution across studies. The aim of this study is to examine the effect of choice of reference electrode or spatial filter on the number, timing and scalp distribution of ERP elicited during task-switching. We compared four configurations, including the two most common (i.e., average mastoid reference and common average reference) and two novel ones that aim to reduce volume conduction (i.e., reference electrode standardization technique (REST) and surface Laplacian) on mixing cost and switch cost effects in cue-locked and target-locked ERP waveforms in 201 healthy participants. All four spatial filters showed the same well-characterized ERP components that are typically seen in task-switching paradigms: the cue-locked switch positivity and target-locked N2/P3 effect. However, both the number of ERP effects associated with mixing and switch cost, and their temporal and spatial resolution were greater with the surface Laplacian transformation which revealed rapid temporal adjustments that were not identifiable with other spatial filters. We conclude that the surface Laplacian transformation may be more suited to characterize EEG signatures of complex spatiotemporal networks involved in cognitive control.

Keywords: Laplacian, REST, common average, average mastoids, cognitive control, ERP, switch cost, mixing cost

OPEN ACCESS

Edited by:
Pedro Antonio Valdes-Sosa, Clinical Hospital of Chengdu Brain Science Institute, China

Reviewed by:
Dezhong Yao, University of Electronic Science and Technology of China, China
Juliana Yordanova, Institute of Neurobiology (BAS), Bulgaria

***Correspondence:**
Frini Karayanidis
frini.karayanidis@newcastle.edu.au

[†]*Equal first authorship.*

Specialty section:
This article was submitted to Brain Imaging Methods, a section of the journal Frontiers in Neuroscience

Received: *13 October 2017*
Accepted: *22 February 2018*
Published: *08 March 2018*

Citation:
Wong ASW, Cooper PS, Conley AC, McKewen M, Fulham WR, Michie PT and Karayanidis F (2018) Event-Related Potential Responses to Task Switching Are Sensitive to Choice of Spatial Filter. Front. Neurosci. 12:143. doi: 10.3389/fnins.2018.00143

INTRODUCTION

Cognitive control processes support the ability to flexibly adapt to changing contextual demands by coordinating the integration of goal-appropriate neural and cognitive resources (Diamond, 2013). The task-switching paradigm is used to experimentally manipulate proactive and reactive cognitive control processes (Monsell, 2003; for a review see, Jamadar et al., 2015). In cued-trials task-switching paradigms, participants alternate between two or more 2-choice

decision tasks using cues that on each trial reliably signal the need to change or repeat task. Performance is characterized by a switch cost, i.e., poorer performance on trials where the task changes as compared to trials where the task repeats and a mixing cost, i.e., poorer performance on repeat trials that are interspersed with switch trials (mixed-task block) compared to a block of repeat trials alone (single-task block). These performance costs are believed to arise from different contextual demands on the cognitive control system. For instance, switch cost is often attributed to the need to proactively or reactively adjust to changing task demands by resetting, whereas mixing cost to the need to maintain the relevant task goals in working memory. When the cue-target interval (CTI) is sufficiently long, performance costs reduce, indicating the engagement of proactive cognitive control processes (Braver, 2012) that prepare the system to update the new task-set or maintain the same task-set. However, a substantial residual switch cost remains even with long CTIs, indicating that reactive cognitive control processes are required for interference control even under highly prepared conditions. The excellent time resolution of event-related potentials (ERP) makes them a highly sensitive tool in characterizing proactive and reactive control processes involved in switching between tasks. Long CTI conditions can temporally dissociate cue-locked ERPs associated with preparation to switch or repeat from target-locked ERPs associated with implementation of the relevant task set.

When examining switching costs, cue-locked ERP waveforms show a robust differential *switch positivity* that manifests as a larger positivity for switch than repeat cues in mixed-task blocks extending around 200–600 ms after cue onset (e.g., Nicholson et al., 2006a; Lavric et al., 2008; Karayanidis et al., 2009; Barceló and Cooper, 2018). This switch positivity is most often maximal over parietal electrodes, although it typically spreads across the scalp (for review see Karayanidis et al., 2010) and has occasionally also been reported at frontal sites (Rushworth et al., 2002; Barceló et al., 2006; Astle et al., 2008; Barceló and Cooper, 2018). A number of other ERP differences between switch and repeat trials have also been reported during the CTI, including early and late frontal negativities and late centrally maximal negative shifts (see Karayanidis et al., 2010). Target-locked ERPs are also modulated by task-switching, with the most robust effect being a larger posterior P3b for repeat compared to switch trials (e.g., Astle et al., 2006, 2008; Nicholson et al., 2006b; Jamadar et al., 2010b).

Electrophysiological indices of the mixing cost have also been reported. In cue-locked ERPs, repeat trials in mixed-task blocks show larger frontal negativity (Goffaux et al., 2006; Manzi et al., 2011; Czernochowski, 2015) and centroparietal positivity (Jost et al., 2008; Manzi et al., 2011; Whitson et al., 2014) compared to repeat trials in single-task blocks. Following target onset, ERPs show smaller parietal P3b amplitude for repeat trials in mixed-task blocks than in single-task blocks (Goffaux et al., 2006; Whitson et al., 2014). Taken together, ERPs in task-switching paradigms have shown modulation of a number of anterior and posterior positivities as well as frontal negativities associated with task-switching costs.

These electrophysiological indices of task-switching costs are consistent with evidence from functional magnetic resonance imaging (fMRI) studies that frontoparietal brain networks are involved in implementation of cognitive control (Ruge et al., 2013). However, the lack of consistency in the number and spatial distribution of both cue-locked and target-locked ERP components across different studies and paradigms, makes it difficult to map the process-specificity of these ERP effects.

The Influence of Spatial Transformations

Even with modern EEG systems that record from 64 to 256 electrode sites, the spatial resolution of the EEG signal is inherently low. Moreover, the distribution of the EEG signal recorded at the scalp is highly sensitive to the type of spatial transformations that is applied to the EEG data, including the choice of reference configuration. Most commonly, ERP studies use a reference derived from the average of the signal recorded at the left and right mastoid processes or earlobes, a nasal electrode or a common average reference (e.g., the average signal across all electrode sites). Kayser and Tenke (2015) demonstrated that common average, average mastoids and nasal reference schemes produced subtle but complex differences in the timing, amplitude, polarity and distribution of ERP components.

The majority of ERP studies on task-switching use either common average or average mastoid reference while linked-ear (Goffaux et al., 2006) and nasal-weighted reference montages are less frequently employed (e.g., Jost et al., 2008; Kieffaber et al., 2013). In an early review of the ERP task-switching literature, Karayanidis et al. (2010) noted that the choice of a common average or an average mastoid reference configuration may contribute to discrepancies in the occurrence of early and late frontal switch effects. Despite the dramatic impact that the choice of reference configuration may have on the morphology of the ERP waveform, the effect of reference montage on ERPs elicited in task-switching paradigms has not been systematically investigated.

The cue-locked centroparietal switch positivity has been reported with both common average reference (Astle et al., 2006, 2008; Swainson et al., 2006; Lavric et al., 2008; Travers and West, 2008; Li et al., 2012; Capizzi et al., 2015; Lange et al., 2015) and average mastoids reference (Rushworth et al., 2002, 2005; Barceló, 2003; Miniussi et al., 2005; Barceló et al., 2006, 2008; Nicholson et al., 2006a,b; Karayanidis et al., 2009, 2011; Periáñez and Barceló, 2009; Jamadar et al., 2010a; Gajewski and Falkenstein, 2011; Hsieh and Wu, 2011; Manzi et al., 2011; Cunillera et al., 2012; Nessler et al., 2012; Tarantino et al., 2016; Barceló and Cooper, 2018). However, in cue-locked ERPs, a frontal switch positivity (Astle et al., 2008) and a frontal switch negativity (Poulsen et al., 2005; Astle et al., 2006; Lavric et al., 2008; Travers and West, 2008; Li et al., 2012; Capizzi et al., 2015) have been reported most consistently when using a common average reference (but see Rushworth et al., 2002; Barceló et al., 2006; Barceló and Cooper, 2018; for average mastoid effects using the intermittent instructions cued-trials design).

Discrepancies in the pattern of ERP findings as a function of reference montage have also been reported in mixing costs. For example, mixing cost effects are found at frontal, frontocentral and centroparietal electrodes when using average mastoids (Manzi et al., 2011; Czernochowski, 2015; Tarantino

et al., 2016) and linked-ear references (Goffaux et al., 2006), but only centroparietally with a nasal reference (Jost et al., 2008). As cognitive control processes involved in task switching are thought to rely on extensive frontoparietal networks (e.g., Sauseng et al., 2006; Cooper et al., 2015; see also Kim et al., 2012), the choice of reference montage may impact on whether ERP waveforms capture the network dynamics underpinning cognitive control.

Use of "Reference Free" Spatial Transformations

While a reference electrode is *sine qua non* for *recording* voltage potentials with EEG, when analyzing ERPs this reference can be changed arbitrarily. Ideally, entirely removing the confounding influence of a reference choice should improve the specificity (spatial, temporal or otherwise) of scalp-recorded neural activity. In recent years, two such *reference-free* transformation schemes have gained popularity: The reference electrode standardization technique (REST) or infinity reference scheme (Yao, 2001) and the surface Laplacian transformation (or current source density, Kayser and Tenke, 2006, 2015; Nunez and Srinivasan, 2006).

REST approximates a reference-free transformation for scalp-recorded electrical activity by computing a "reference at infinity." This is derived using a distributed source model of cortical activity within a head model. In effect, the source model is fit to the observed data and then the model is used to compute the scalp-recorded EEG referenced to a neutral point at infinity. The rationale behind this approach is that the source-level EEG activity is independent of the choice of reference at the scalp: i.e., the generators of EEG signals within cerebral tissue are not dependent on the arrangement of recording electrodes placed on the head. Only the recorded signal depends on the reference choice and the REST procedure is intended to correct for this (for a technical review, see Yao, 2001).

Scalp-recorded EEG potentials are assumed to be associated with cortically generated electric current that flows radially outwards through the cranium and dissipates across the scalp. The radial outflow of cortical current is referred to as current source density, CSD (or alternatively, scalp current density; see Yao, 2002 for further explanation) and can be estimated using a surface Laplacian transformation (Hjorth, 1975). Most current implementations of this approach begin by interpolating the EEG scalp topography across electrodes using a surface spline. The Laplacian of a surface spline can be computed efficiently. Importantly, CSD is independent of the original choice of reference electrode. The surface Laplacian also acts as a high pass spatial filter, attenuating the effects of volume conduction such that it enhances sensitivity to focal activity in the cortical mantel, while suppressing widespread EEG signals originating from deeper layers (Kayser and Tenke, 2006). As such, the surface Laplacian is insensitive to broad changes in signal, resulting from volume conduction and reference choice, and more sensitive to activity from cortical generators. This results in improved spatial and temporal information (for a technical review, see Hjorth, 1975; Yao, 2002; Kayser and Tenke, 2015).

Present Study

Some task-switching ERP components show a similar spatial distribution across different reference schemes (e.g., cue-locked centroparietal switch positivity) whereas others vary as a function of reference choice (e.g., cue-locked frontocentral switch negativities), an observation previously made by Karayanidis et al. (2010). Despite concerns that the ERP components elicited during task-switching may vary with reference configuration, the effect of different references on ERPs related to task-switching has not been systematically examined. Moreover, *reference-free* spatial transformations that can improve the spatial localization of neural activity recorded at the scalp have not been widely used. No task-switching ERP study has used the REST transformation. A few studies have applied the surface Laplacian transformation only to ascertain that the switch effects found in average mastoid referenced data were not the result of volume conduction (Gajewski et al., 2010; Gajewski and Falkenstein, 2011; Barceló and Cooper, 2018). In this study, we directly compare the effect of four reference transformations on cue-locked and target-locked ERP data recorded using a cued-trials task-switching paradigm. We use two conventional references commonly used in task-switching studies that have produced some discrepant results: average mastoids and common average reference. We compare these to the two more recent approaches that are designed to reduce the impact of choice of reference electrode and volume conduction: REST and surface Laplacian. We aim to demonstrate that reference-free spatial transformations may help identify and differentiate between distinct ERP components associated with task switching.

Given that the posterior cue-locked switch positivity is robust across different standard referencing schemes, we expect that a large switch positivity will be evident in all four spatial transformations, and will show a strong midline parietal-occipital focus with surface Laplacian. Cue-locked frontal switch positivity and negativity effects have typically been reported only when using a common average referencing scheme, suggesting that this frontal component is sensitive to spatial transformation. If these frontal switch effects are an artifact of volume conduction in the common average transformation, they will be absent in the surface Laplacian transformation. Alternatively, if these switch effects represent distinct cognitive processes generated in frontal sources, they will be evident in both REST and surface Laplacian transformations.

Cue-locked mixing cost effects are also strongly linked to the choice of spatial transformation. Thus, this centroparietal component is unlikely to be due to volume conduction and should therefore be evident in all spatial transformations, including REST and surface Laplacian. In contrast, frontal and frontocentral effects are only seen for mastoid (or linked-ear) transformations. As before, if these frontal/frontocentral effects are the result of volume conduction, we expect to see no frontal mixing costs in the surface Laplacian transformation. If they represent activity originating from the frontal lobe, they will be present for both REST and surface Laplacian transformations.

With averaged mastoids, target-locked ERPs typically produce a sustained parietal negative shift in the ERP waveform for switch compared to repeat trials overlapping the N2 and P3b period.

Reduced volume conduction with surface Laplacian may indicate whether this represents a broadly distributed component that overlaps the target-locked ERP or differential modulation of N2 and P3b components.

METHODOLOGY

Participants

Two hundred and thirty eight community participants took part in the current study as part of the larger Age-ility project (Karayanidis et al., 2016; http://www.age-ility.org.au/). Written, informed consent was obtained from all participants prior to testing, with parental consent also given for persons under 18 years of age. All participants were reimbursed $20 per hour for their time and were directed to abstain from caffeine and alcohol for at least 2 h prior to the experimental session. The protocol was approved by the University of Newcastle Human Research Ethics Committee (HREC: H-2012-0157).

In order to ensure strong signal-to-noise for ERP analyses, participants who had fewer than 50 trials on any trial type after EEG preprocessing were removed ($n = 37$). This resulted in a final sample of 201 participants (mean age 21.32 ± 4.91 years, 91 male, 91.5% right handed).

Task and Stimuli

On each trial, participants performed a cued two-choice response task involving either the letter, digit or color features of the stimuli. Throughout each block of trials, a gray circle (5° of visual angle) was continuously displayed. The circle was divided into six segments with pairs of adjacent segments allocated to one of the three tasks: letter, digit, and color (see **Figure 1A**). The target was a pair of characters consisting of combinations of a letter, a digit, or a non-alphanumeric symbol and was presented either in gray or in color. Each target (e.g., gray A4) consisted of three dimensions: one relevant to the currently cued task (e.g., the letter A mapped to a left-hand response), one selected randomly from the two alternative tasks and incongruently mapped with the relevant task (e.g., the digit 4 mapped to a right-hand response) and one that was neutral, i.e., not mapped to any response (e.g., letter and digit presented in gray). The same target could not appear on consecutive trials and targets remained onscreen until a response was emitted or for 5,000 ms.

Each trial consisted of a cue-target sequence (see **Figure 1B**). Different cue locations resulted in four cue types that varied in information regarding the task to be performed on the target. In this paper, we restricted analyses to the fully informative cue types in order to focus on switch cost and mixing cost effects. All-repeat trials refer to trials derived from single-task blocks (i.e., where the same task was repeated on all trials in a block). Switch and repeat trials were derived from mixed-task blocks (i.e., trials on which the location of the cue fully identified the task to be performed on the next target). Thus, in both single-task and mixed-task blocks, repeat cues highlighted the same two segments as on the preceding trial (see **Figure 1C**), thereby indicating the task would be repeated. Switch cues highlighted two segments associated with one of the two tasks not completed on the previous trial. Contrasts were derived for switch cost (switch—repeat trials) and mixing cost (repeat—all-repeat trials).

Participants responded using their left and right index fingers. The hand assigned to each response was counterbalanced across participants. Participants were instructed to respond as quickly and as accurately as possible. A feedback tone was presented only when responses were incorrect. At the end of each block, average accuracy and RT were displayed and a short, humorous video (5–10 s) was presented to encourage inter-block rests. Participants were offered a longer rest halfway through the experiment to minimize fatigue.

Procedure

Participants completed two training sessions (circa 14 days apart) to establish strong cue-stimulus-response links. Within each training session, participants first learned each task alone

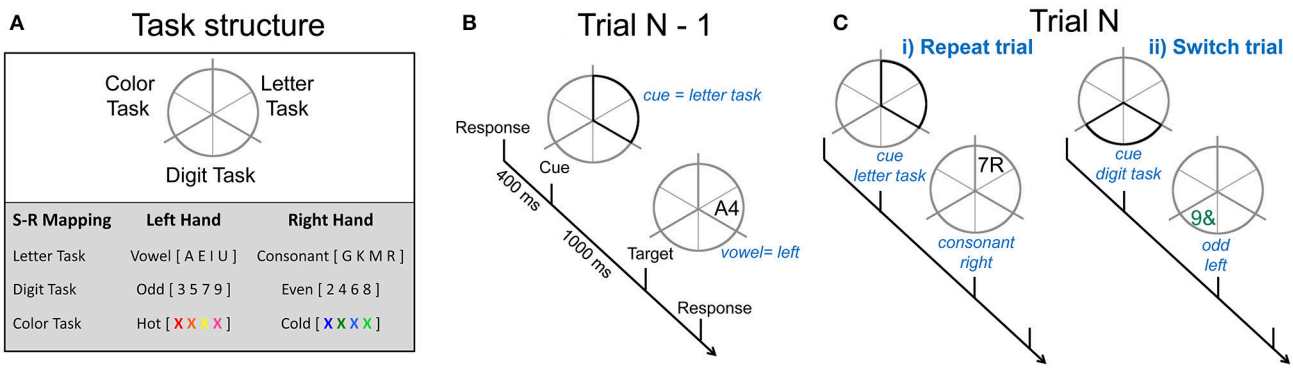

FIGURE 1 | Cued-trials task-switching paradigm. **(A)** Adjoining segments were associated with different 2-choice classification tasks. An example of stimulus-response mappings is shown. **(B)** Example of one trial. A cue occurs 400 ms after the response to the preceding trial and highlights two segments, in this instance, related to the letter task, indicating that the next target will occur in one of these segments and will require a vowel vs. consonant decision. A target replaced the cue after 1,000 ms. Participants respond to the task-appropriate feature of this target. **(C)** The sequence of N-1 to N trials determines whether the current trial is a (i) repeat trial. i.e., the same two segments are highlighted and the same task is performed, or (ii) switch trial, i.e., the cue highlights segments associated with one of the other two tasks and validly indicates which task to perform on the target.

(single-task blocks) and then practiced switching between these tasks (mixed-task blocks, total of 1,320 practice trials). Following the second training session, the EEG was recording while participants performed 10 mixed-task blocks (72 trials/block) and three single-task blocks (48 trials/block, one block per task). Each block included an additional five warm-up trials.

EEG was recorded continuously using an ActiveTwo Biosemi EEG system (2,048 Hz, bandpass filter of DC-400Hz) from 64 scalp electrodes plus external electrodes at left and right mastoids and outer canthi, as well as supraorbital, and infraorbital ocular sites. Common mode sense (CMS) and driven right leg (DRL) electrodes were positioned inferior to P1 and P2, respectively. EEG data were recorded relative to an amplifier reference voltage, and then re-referenced offline to Cz in order to remove common-mode signals.

Data Analysis

Trials were removed from behavioral and EEG analyses if the trial (i) had an RT faster than 200 ms or slower than three SD above the individual's mean RT, (ii) was associated with an incorrect response or followed an incorrect response, or iii) was one of the warm-up trials at the beginning of each block. On average, 18% ± 7.6% of trials were removed. Trials with high EEG noise levels (see below, EEG Analysis, for more details) were also excluded from behavioral and EEG analyses.

Behavioral Analysis

Mean RT and accuracy were assessed using separate one-way ANOVAs on the *trial type* factor (i.e., *all-repeat*, *repeat* and *switch*). Planned comparisons were performed to assess *switch cost*, (*switch—repeat*) and *mix cost* (*repeat—all-repeat*). Family-wise error Bonferroni correction was applied to RT and accuracy comparisons separately (i.e., $\alpha < 0.05/2$) with Greenhouse-Geisser corrections for the assumption of sphericity.

EEG Analysis

EEG data were processed using MATLAB (MATLAB, 2015) through a pipeline utilizing Fieldtrip (Oostenveld et al., 2011), REST software (from http://www.neuro.uestc.edu.cn/rest/; Yao, 2001) and CSD Toolbox (Kayser and Tenke, 2006) and in-house functions (A. Wong and P. Cooper). Preprocessing was performed using Fieldtrip as follows. EEG data were re-referenced off-line to electrode Cz, down-sampled from 2,048 to 512 Hz using a zero-phase anti-aliasing filter with a low-pass cut off frequency of 245 Hz and then had high pass and notch filtering applied to remove line noise and low-frequency drift (high pass: 0.1 Hz, forward phase; 50 Hz notch: zero phase). Excessively noisy channels were identified with visual inspection and excluded (on average 0.84 ± 1.59 electrode channels were removed per participant). For each cue type (*switch, repeat, all-repeat*) epochs were extracted from −1,000 to 3,500 ms with respect to cue onset. To remove blink and vertical eye-movement artifact, independent components analysis (ICA) was performed using the fastICA algorithm, (Hyvärinen and Oja, 2000). This produces a set of components, one less than the amount of available electrodes. Based on visual inspection by a trained observer, 1.40 ± 0.80 components were removed because they corresponded to ocular artifact (i.e., a deflection consistent with the time course of an eyeblink coupled with a frontal topographical distribution) The remaining components were projected back into sensor (electrode) space. The data were low pass filtered (30 Hz, zero-phase) to remove high frequency noise including muscular artifacts. Trials that contained residual artifact larger than ±120 μV were deleted, resulting in an average of 111.62 (±22.32 SD) *all-repeat*, 132.65 (±26.75 SD) *repeat*, and 127.29 (±28.66 SD) *switch* trials per participant for further analysis.

After preprocessing, EEG data were re-referenced using two commonly employed referencing schemes: *average mastoids* (i.e., the algebraic average of the mastoids) and *common average* (i.e., the average of all scalp electrodes). In addition, the *infinity referencing* transformation was applied using the REST software to obtain a reference-free EEG dataset. Finally, the *surface Laplacian* transformation was computed. For the *surface Laplacian*, a spherical spline function was applied across all scalp electrode locations, with the spline flexibility parameter, $m = 4$, for increased rigidness (Kayser and Tenke, 2015). An iterative process was used to solve a Legendre differential equation to obtain the surface Laplacian and surface potential matrices (Kayser and Tenke, 2006). As the EEG signal is transformed based on the second partial derivate of the signal (μV) over a spatial area (cm^2–i.e., the scalp), the measurement scale is μV/cm2 (Kayser and Tenke, 2006, 2015)

ERP Analysis

For each participant, epochs spanning from 200 ms before to 1,200 ms after event onset were extracted around the cue and the target, using a ±50 ms peri-event baseline. ERP waveforms were extracted by averaging across all trials for each cue type, and grand average ERPs were obtained by averaging across all participants for each cue type, separately for cue-locked and target-locked epochs.

As ERP activity related to task-switching is commonly larger at midline electrodes, we analyzed switch cost and mixing cost contrasts at frontal (Fz), central (Cz), and parietal (Pz) electrodes using paired sample *t*-tests using false discovery rate for type 1 errors (FDR, Benjamini and Yekutieli, 2001; $\alpha < 0.001$). Intervals of significant activity were defined, if this level of significance was held for 25 ms or 13 consecutive time points, sampled at 512 Hz. These analyses were conducted on waveforms derived from each spatial transformation separately.

The intersection of these significant time points across all spatial transformations was derived to identify effects that were common across all transformations. For each common interval, the effect size, Hedges' g, of the cost at each spatial filter were also obtained and reported. These common intervals were used to examine the scalp distribution map of switch cost and mixing cost effects across different spatial transformations. For each scalp distribution map, we examined the spatial distribution of significant switch and mixing effects using a paired sample *t*-test (FDR, $\alpha < 0.001$) at each electrode site.

RESULTS

Behavioral Results

Figure 2 shows mean RT and accuracy for each cue type [$F_{(2, 400)} = 263.9$, $p < 0.001$, $\eta^2 = 0.569$, $F_{(2, 400)} = 75.0$, $p < 0.001$, $\eta^2 = 0.273$, respectively]. There was a significant mixing cost effect for RT [$t_{(200)} = 14.9$, $p < 0.001$] and a significant switch cost for both RT [$t_{(200)} = 14.0$, $p < 0.001$] and accuracy [$t_{(200)} = 10.0$, $p < 0.001$].

Cue-Locked ERP Analyses

Figure 3 depicts cue-locked ERP waveforms for *all-repeat, repeat* and *switch* at three midline electrodes for each reference type. At first glance, there are substantial differences in global morphology across different transformations. However, as discussed below, there are many commonalities in both switch cost and mixing cost effects.

Switch Costs

Both average mastoid and common average references produced a pattern of result very consistent with prior studies using these reference configurations. For average mastoids, the most prominent effect was a large parietally maximal switch positivity over roughly 120–600 ms that extended across all midline sites. This switch positivity was also evident with the common average reference, but was more restricted parietally, evident in Pz but not Cz nor Fz, whereas frontally there emerged a small sustained late switch negativity over 600–1,000 ms. This switch negativity was smaller and more brief with the average mastoid reference, however, it still reached statistical significance in this very large sample. REST showed a pattern remarkably similar to common average reference. The surface Laplacian showed the same effects but much more temporally and spatially defined. Specifically, the switch positivity was differentiated into an early brief centroparietal effect superimposed on the P2 and later parietally-restricted effect over 250–600 ms. The frontal switch negativity first emerged around 400 ms and then extended to the end of the epoch.

We identified intervals that produced significant switch effects across all transformations (see thick significance intervals in **Figure 3**), in order to compare their scalp distribution. This resulted in five intervals: a very early switch positivity over the parietal P2 (A1: 165–215 ms), a second effect most clearly evident at tail end of P2 centroparietally (A2: 215–275 ms), early and late windows to define the parietal switch positivity "proper" (A3: 270–350 ms, A4: 350–550 ms), and the frontal switch negativity (A5: 700–800 ms). **Table 1** shows effect sizes for these of common cue-locked switch intervals for each transformation. With the exception of the frontal switch negativity, most intervals showed large effect sizes.

As shown in **Figure 4A**, the average mastoids reference shows a switch positivity that spread across the first four intervals A1-A4 (i.e., 165–550 ms) and had a very broad scalp distribution with a centroparietal focus. Common average and REST references produced a similar centroparietally maximal switch positivity, however REST reference was less spatially distributed when compared to average mastoids and was accompanied by a concurrent frontal switch negativity. In contrast, the scalp distribution of the switch positivity varied over A1 to A4 in the surface Laplacian reference. There was an early bilateral parietal effect (A1) that shifted posteriorly and anteriorly (A2, A3) before developing a tight parietoccipital focus (A4). The late frontal switch negativity was present across all referencing schemes (A5), but was much more localized over the frontal midline for surface Laplacian. Thus, average mastoids, common average and REST indicate the presence of two temporally widespread components: a broadly distributed switch positivity and a later frontal switch negativity. However, the surface Laplacian is suggestive of a much more complex pattern of temporal and spatial dynamics associated with preparation to switch vs. preparation to repeat a task-set.

Mixing Costs

The averaged mastoids reference showed the typical pattern of mixing effects consisting of an early mixing positivity followed by a late pretarget mixing negativity spread across midline electrodes (**Figure 3**). These effects were also significant with common average and REST references, albeit smaller and more variable (e.g., note the early mixing negativity at Pz). Once again, while the same pattern of effects was evident with surface

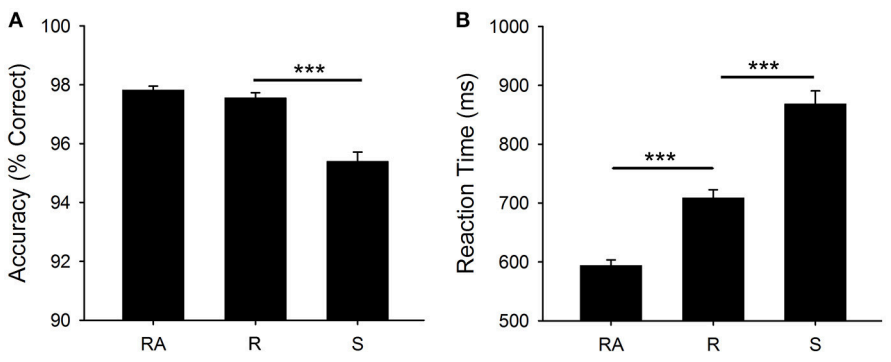

FIGURE 2 | Behavioral Results: **(A)** Mean accuracy (percentage correct) and **(B)** Mean RT (ms). Significant differences are shown at ***$p < 0.001$. RA, *all-repeat*; R, *repeat*; and S, *switch*.

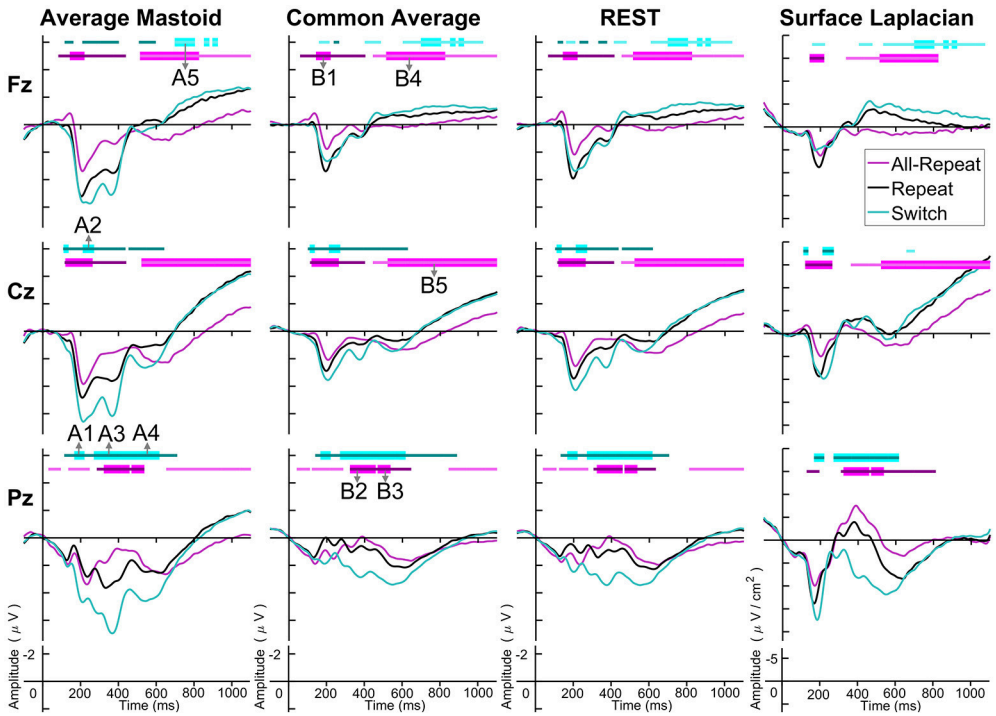

FIGURE 3 | Cue-locked grand average ERPs for each spatial transformation at the three midline electrodes. All-repeat = magenta; repeat = black; switch = cyan. Significant intervals of switch or mix cost (FDR $\alpha < 0.001$) are shown as thin cyan and magenta bars, respectively, with darker bars indicating positive costs (i.e., switch > repeat, repeat > all-repeat) and lighter bars indicating negative costs (i.e., reverse contrasts). Thick bars represent intervals over which the effect was significant for all spatial transformations. The scalp distribution of common effects for switch cost (A1-A5) and mixing cost (B1-B5) are shown in **Figure 4**. Note that average mastoid, common average and REST use the same amplitude scale in microvolts, whereas surface Laplacian uses microvolts/cm^2. Gray line at 1,000 ms denotes target stimulus onset.

Laplacian, the mixing effects were better defined both temporally and spatially.

The intersection of significant effects in **Figure 3** across different spatial configurations was used to define five intervals: an early frontocentral mixing positivity (B1: 150–220 ms), a later parietal mixing positivity that was split into two windows (B2: 330–450 ms, B3: 470–530 ms), a slow frontal mixing negativity (B4: 540–800 ms) and a central ramp-like mixing negativity (B5: 800–1,000 ms). **Table 1**, show mostly medium size effects, with no clear indication of a superior reference choice across all time intervals.

Figure 4B shows that, as with switch cost effects, the average mastoids reference produce broadly distributed effects that were more spatially confined with common average and REST references and even further with surface Laplacian. Specifically, average mastoids suggest two temporally separable components: a frontocentral mixing positivity (B1) that spread across the scalp (B2) and dissipated mostly by 450 ms, and a centrally maximal mixing negativity that emerged around 500 ms and extended to the end of epoch. The surface Laplacian suggests a somewhat more complex pattern, differentiating more clearly between the early mixing effect that was characterized by a midline frontal positivity and bilateral posterior negativities (B1), a sustained parietoccipital mixing positivity spreading to the end of the epoch (B2–B5), and a frontocentral midline mixing negativity that emerged as early as 330 ms and increased in strength across the remainder of the epoch, as it overlapped the pretarget negativity (B2–B5). Scalp maps showed a frontal to central negative focus, accompanied by an occipital midline positivity, possibly suggesting of a parietal dipole.

Target-Locked ERP Analyses

Target-locked ERP waveforms depicted in **Figure 5** are characterized by a large parietally maximal P3b that partially overlapped a centrally maximal N2 for all spatial transformations.

Switch Costs

Averaged mastoid and common average references show a pattern consistent with previous work, including a broad parietal negative shift for switch as compared to repeat cues extending over 200–600 ms. This is typically interpreted as either a broad negativity superimposed on the N2-P3b complex or a reduced P3b. REST showed a very similar pattern to the common average reference. However, the morphology of the ERP waveform was very different for surface Laplacian. Parietally, there was a very well defined N1, P2, N2, P3 sequence and a switch negativity that clearly spread from early P2 to late P3b. This switch negativity was also evident at Cz where it overlapped a broad N2-P3b complex. However, both the waveform morphology and the switch effect were very different at Fz. Here, the waveform shows

TABLE 1 | Hedge's g effect size for common intervals of significant switch cost and mixing cost effects in cue-locked ERP waveforms shown in **Figure 3**.

	Cue-locked ERPs				
Figure 3 label (electrode)	**A1 (Pz)**	**A2 (Cz)**	**A3 (Pz)**	**A4 (Pz)**	**A5 (Fz)**
SWITCH COST					
Interval (ms)	165–215	215–270	270–350	350–550	700–800
Average mastoids	0.69675	**0.61711**	**0.78378**	0.7158	−0.14975
Common average	**0.71151**	0.54026	0.68418	**0.79799**	−0.25344
REST	0.68465	0.566	0.72001	0.7826	**−0.29526**
Surface laplacian	0.43806	0.40959	0.40991	0.78949	−0.21915
Figure 3 label (electrode)	**B1 (Fz)**	**B2 (Pz)**	**B3 (Pz)**	**B4 (Fz)**	**B5 (Cz)**
MIXING COST					
Interval (ms)	150–220	330–450	470–530	540–800	800–1000
Average mastoids	0.59228	**0.65469**	0.22783	**−0.40918**	−0.58697
Common average	**0.84222**	0.28965	0.26836	−0.39057	−0.62036
REST	0.80191	0.38942	0.23567	−0.40876	**−0.63154**
Surface laplacian	0.32606	0.34368	**0.38611**	−0.34382	−0.4957

Bold effect sizes denotes the largest of the four reference transformations.

a large sustained negative wave from 200 ms and that is smaller for switch trials. Careful inspection of Fz shows that the reversed switch effect was evident for all other references (though less temporally widespread with average mastoids), but the effect was much smaller.

Four intervals were defined for topographical analyses: An early centrally maximal switch negativity (A1: 160–220 ms), a frontally maximal switch positivity (A2: 220–290 ms), a long centroparietal switch negativity (A3: 290–640 ms) and a late slow frontal switch negativity (A4: 640–900 ms). **Table 2** shows small to medium effect sizes that were largest for common average and surface Laplacian transformations at different time intervals. In **Figure 6**, all four reference schemes show a very consistent centroparietal switch negativity spanning across A1-A3 (160–640 ms), but becoming increasingly spatially localized in common average, REST and surface Laplacian, compared to averaged mastoids. All four reference schemes also show a frontal switch positivity spreading across A2–A4, with a midline focus in surface Laplacian.

Mixing Costs

Mixing cost effects were also widespread for the averaged mastoids (**Figure 5**). A mixing positivity first emerged frontally around 200 ms, extending across to the end of the epoch. The effect emerged later centroparietally (~600 ms). The common average reference emphasized the late centroparietal mixing positivity, whereas the REST more closely resembled average mastoids. Surface Laplacian also showed the late centroparietal mixing positivity, but this was preceded by a centroparietal mixing negativity with little frontal differential activity. Intersection analyses defined three mixing positivities for topographical analyses: an early frontal (B1: 330–400 ms), a parietal (B2: 550–750 ms) and a late centroparietal (B3: 750–900 ms). The effect size of these effects were largest with average mastoids reference for three intervals (**Table 2**). Scalp maps for average mastoids show a temporally and spatially extended mixing positivity across all windows (**Figure 6B**). The effect was similar for common average and REST, but more centrally localized. However, the surface Laplacian showed a pattern of effects that varied with time and spatial location. The early frontal midline mixing positivity was accompanied centroparietally by bilateral positive and midline negative mixing effects (B1) that morphed into a late centroparietal mixing positivity, spreading bilaterally more frontally.

Surface Laplacian

Across both cue-locked and target-locked ERPs, the surface Laplacian reference scheme was sensitive to the temporal and spatial dynamics of task-switching effects that were not readily evident in other montages. Furthermore, effects that were common to all reference schemes showed a more spatially localized distribution with the surface Laplacian reference. The scalp distribution maps in **Figures 4**, **6** were optimized to areas of significant differences that were common across all montages. In order to focus further discussion on effects that emerge with surface Laplacian, **Figures 7**, **8** display these waveforms together with difference waveforms for switch cost and mixing cost at midline electrodes for cue-locked and target-locked waveforms, respectively, with shaded 95% confidence intervals calculated for a within-subjects design (c.f., Loftus and Masson, 1994), respectively. Scalp distribution maps show activity averaged across 50 ms intervals over 150–300 ms and across 100 ms intervals thereafter to examine the relative scalp distribution and time-course of switch and mixing effects.

Cue-locked mixing effects (**Figure 7**) represent processes required to repeat the same task within a context where task can randomly change on a trial-by-trial basis (mixed-task block) as compared to a context where the task remains the same across all trials (single-task block). Compared to all-repeat trials, repeat trials produced an increased frontocentral P2 (150–250 ms), that was accompanied by reduced activity at bilateral temporal-occipital sites (**Figure 7C**). A centroparietal N2-like component and a parietoccipital P3b-like component emerged for both all-repeat and repeat trials. However, the repeat cues showed a positive shift, resulting in a smaller N2 and a larger P3b, especially parietoccipitally, where it extended to the end of the CTI. From around 400 ms, repeat cues showed a slow frontal negativity and a ramp-like central negativity compared to all-repeat trials. These effects first emerged at midline sites (400–500 ms), but spread across the frontocentral scalp as CTI progressed. With one early exception, the switch cues showed a similar pattern of deviation from the all-repeat cues as the repeat cues, but the deviation was larger resulting in significant switch effects.

As seen **Figure 7B**, differential switch effects are characterized by a number of early rapid modulations beginning from

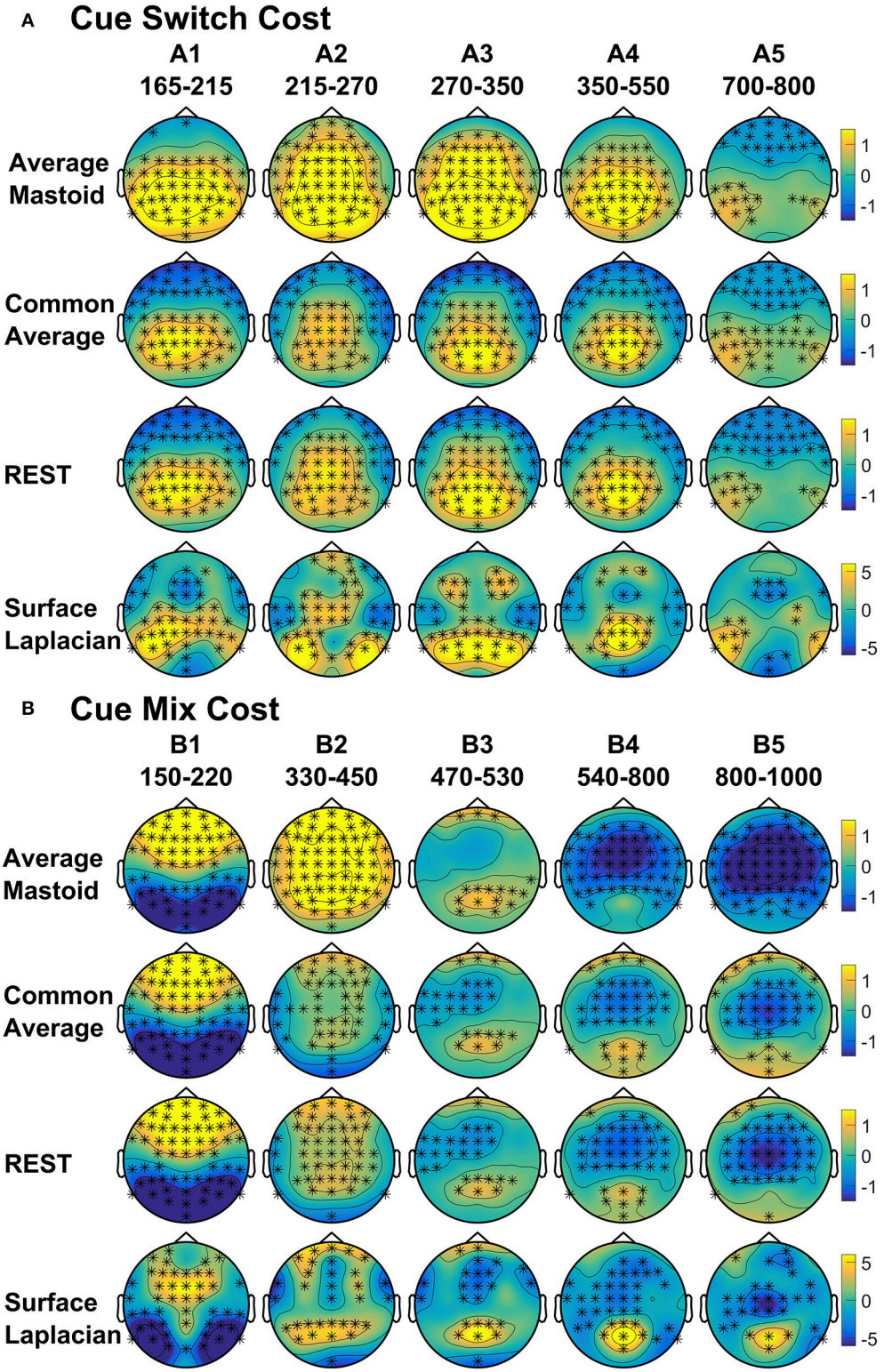

FIGURE 4 | Scalp topography of cue-locked **(A)** Switch costs and **(B)** Mix costs for each spatial transformation depicted for the intersection of significant time intervals across all spatial transformations. Electrodes with significant differences (FDR $\alpha < 0.001$) are marked with an asterisk. Note that average mastoid, common average and REST use the same amplitude scale in microvolts, whereas surface Laplacian uses microvolts/cm^2.

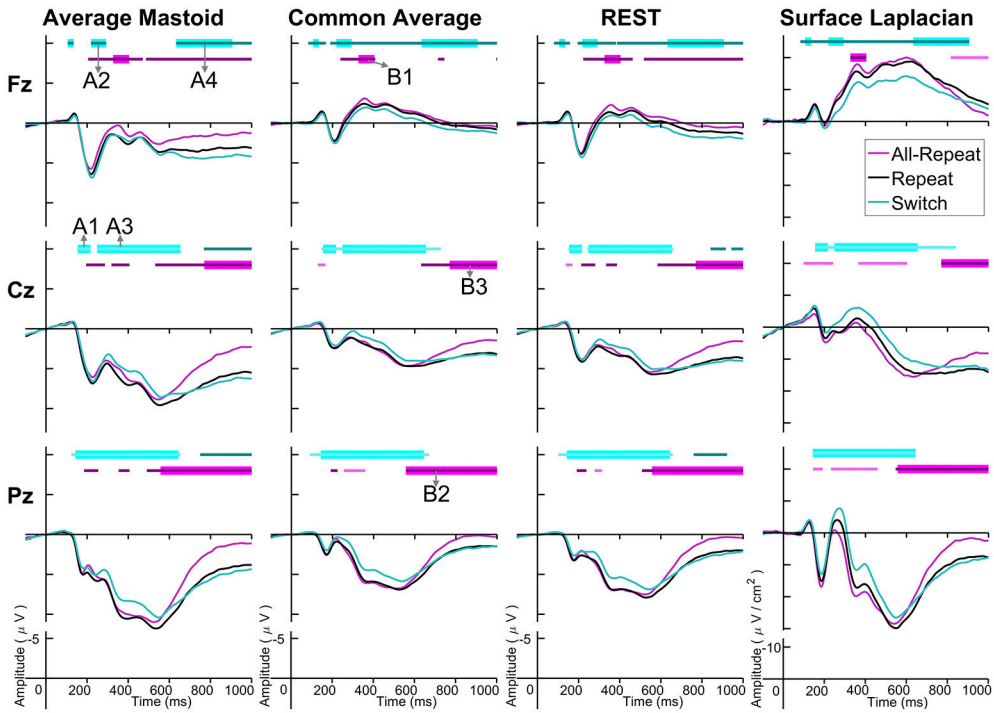

FIGURE 5 | Target-locked grand average ERPs for each spatial transformation at three electrodes. All-repeat = magenta; repeat = black; switch = cyan. Significant intervals of switch or mix cost (FDR $\alpha < 0.001$) are shown as thin cyan and magenta bars, respectively, with darker bars indicating positive costs (i.e., switch > repeat, repeat > all-repeat) and lighter bars indicating negative costs (i.e., reverse contrasts). Thick bars represent intervals over which the effect was significant for all spatial transformations. The scalp distribution of common effects for switch cost (A1-A4) and mixing cost (B1-B3) are shown in **Figure 6**. Note that average mastoid, common average and REST use the same amplitude scale in microvolts, whereas surface Laplacian uses microvolts/cm^2.

TABLE 2 | Hedge's g effect size for common intervals of significant switch cost and mixing cost effects in target-locked ERP waveforms shown in **Figure 5**.

	Target-locked ERPs			
Figure 5 label (electrode)	**A1 (Cz)**	**A2 (Fz)**	**A3 (Cz)**	**A4 (Fz)**
SWITCH COST				
Interval (ms)	160–220	220–290	290–640	640–900
Average mastoids	−0.17474	0.17268	−0.28326	0.24711
Common average	**−0.23927**	0.34019	**−0.32397**	0.27201
REST	−0.18199	0.29828	−0.27831	0.31543
Surface laplacian	−0.22777	**0.45722**	−0.30336	**0.32762**
Figure 5 label (electrode)	**B1 (Fz)**	**B2 (Pz)**	**B3 (Cz)**	
MIXING COST				
Interval (ms)	330–400	550–750	750–900	
Average mastoids	0.59228	**0.65469**	0.22783	
Common average	**0.84222**	0.28965	0.26836	
REST	0.80191	0.38942	0.23567	
Surface laplacian	0.32606	0.34368	**0.38611**	

Bold effect sizes denotes the largest of the four reference transformations.

the parietally maximal P2 and extending to circa 300 ms. Compared to repeat cues, switch cues show a larger and more prolonged parietoccipital P2 extending over time to central and bilateral frontal sources (**Figure 7D**). This is followed by a sharp parietal positivity with a very tight parietoccipital focus that is superimposed on a parietal N2-like component for repeat trials and that sharply dissipates by 600 ms. The sustained midline frontocentral negativity emerges around 500 ms, showing partial temporal overlap with the parietal switch positivity and extending beyond target onset. Note also the sustained bilateral parietotemporal and central positivities that are not evident at midline sites from where ERP measurements are usually derived.

Figure 8 shows the midline distribution of different trial types (**Figure 8A**) and difference waveforms (**Figure 8B**), as well as scalp distribution of mixing cost (**Figure 8C**) and switch cost (**Figure 8D**) effects after target onset. Mixing effects revealed early and transient parietal and frontal components in the first 400 ms after target, followed by a sustained, central negativity emerged from ∼350–700 ms at central sites. Following this, two mixing effects emerged simultaneously: a late (∼800+ ms) frontal negativity and a longer-lasting centroparietal positivity (∼600+ ms). Interestingly, the scalp maps show a number of bilateral effects that are not captured at midline electrodes.

Two simultaneous signatures of the switch cost were present: A frontal switch positivity that emerged almost immediately after target onset (∼80 ms) and a centroparietal switch negativity (P3b) emerging ∼180 ms post-target. Interestingly, both of these switch effects were long-lasting, likely remaining until response

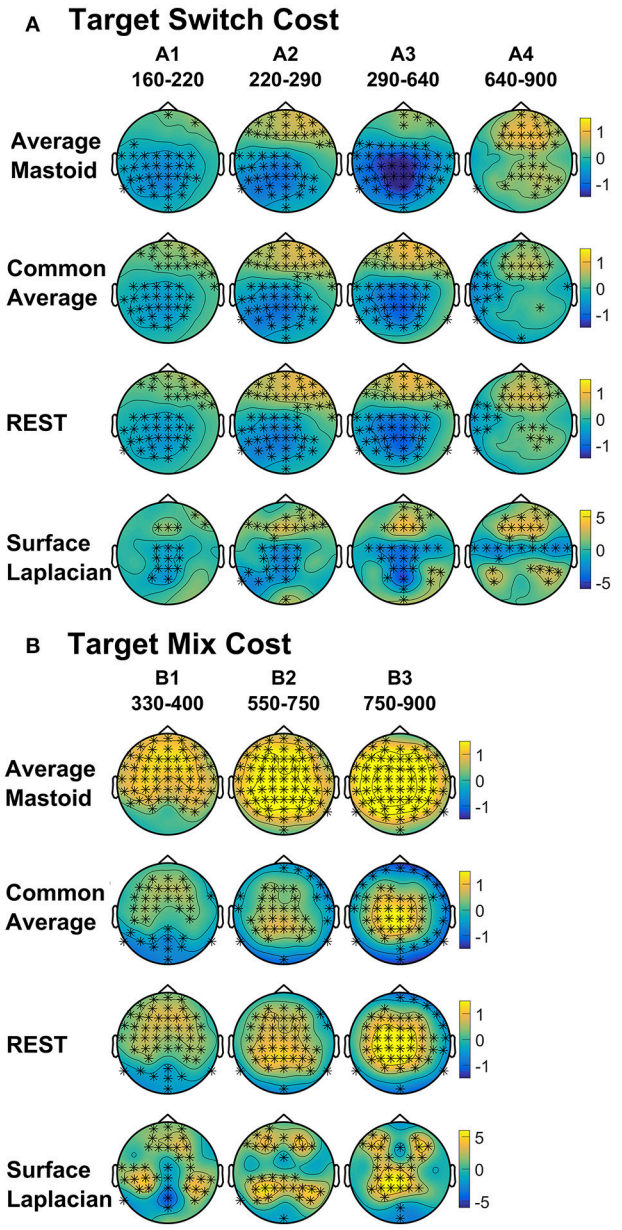

FIGURE 6 | Scalp topography of target-locked **(A)** Switch costs and **(B)** Mix costs for each spatial transformation depicted for the intersection of significant time intervals across all spatial transformations. Electrodes with significant differences (FDR $\alpha < 0.001$) are marked with an asterisk. Note that average mastoids, common average and REST use the same amplitude scale in microvolts, whereas surface Laplacian uses microvolts/cm^2.

(i.e., reliable differences were still observed as late as 900 ms after target appearance).

DISCUSSION

The present study compared the effects of four different spatial filters: two commonly used montages (common average and average mastoids) and two reference-free transformations (REST and surface Laplacian) on cue-locked and target-locked ERPs in a cued trials task-switching paradigm. We report three major findings. Firstly, that the commonly reported cue-locked posterior switch positivity and centroparietal mixing effects, as well as the target-locked centroparietal switch negativity were present in all four spatial transformations. However, the surface Laplacian transformation brought out a more fine-grained spatial and temporal distribution of these effects—for example, the cue-locked switch positivity was shown to have a focal, midline parietal topography compared to the broadly distributed component seen with common reference choices such as the average mastoids (**Figure 4**). This suggests that these commonly reported ERP effects are robust to the choice of spatial reference but that the topography (and therefore the neural generators) of these components may be misattributed when using average mastoid or common average transformations.

Secondly, the cue-locked frontal/frontocentral switch and mixing effects seen in particular reference schemes cannot be attributed to volume conduction effects. Both the frontal switch positivity and the frontocentral mixing negativity were clearly evident in the REST and surface Laplacian transformations that minimize volume conduction effects (**Figure 3**). This is consistent with a potential frontal generator associated with both switch and mixing costs, that has previously only been reported sporadically (e.g., Astle et al., 2008; Manzi et al., 2011; Czernochowski, 2015; Tarantino et al., 2016).

Finally, the surface Laplacian transformation revealed a rich spatiotemporal landscape associated with task-switching that was absent in all other reference choices. For example, cue-locked surface Laplacian ERPs uncovered an early emerging, transient frontal mixing positivity that resolved prior to the later canonical mixing component found in other referencing schemes. Likewise, in the first 250 ms post-cue, rapid frontal negativities and bilateral posterior positivities were associated with the switch cost—prior again to the classic parietal switch positivity. These transient effects provide new evidence of early, frontal and parietal dynamics associated with task switching. It is important to note that, given the aim of this paper, we restricted our focus on common time windows that were significant across all four transformations at three midline electrodes only. Future work focussing on a broader array of sites may reveal an even richer landscape.

Further work will be needed to identify the functional significance of these components within a task switching context. For example, both an early, cue-locked frontal N2-like and centroparietal P2-like component was seen in the surface Laplacian transformation (**Figure 7**). These N2-like features are typically observed in conflict paradigms relying on reactive control processes to resolve interference (see Folstein and Van Petten, 2008). An N2-like feature in a cue-locked ERP suggests that a similar action-monitoring system may be engaged early after cue onset when participants are cued to switch tasks. Perhaps such monitoring serves as a critical, stimulus-driven prerequisite step for further goal-updating processes (associated with later switch positivity).

To date, few studies have applied surface Laplacian transformations to task-switching electrophysiological data

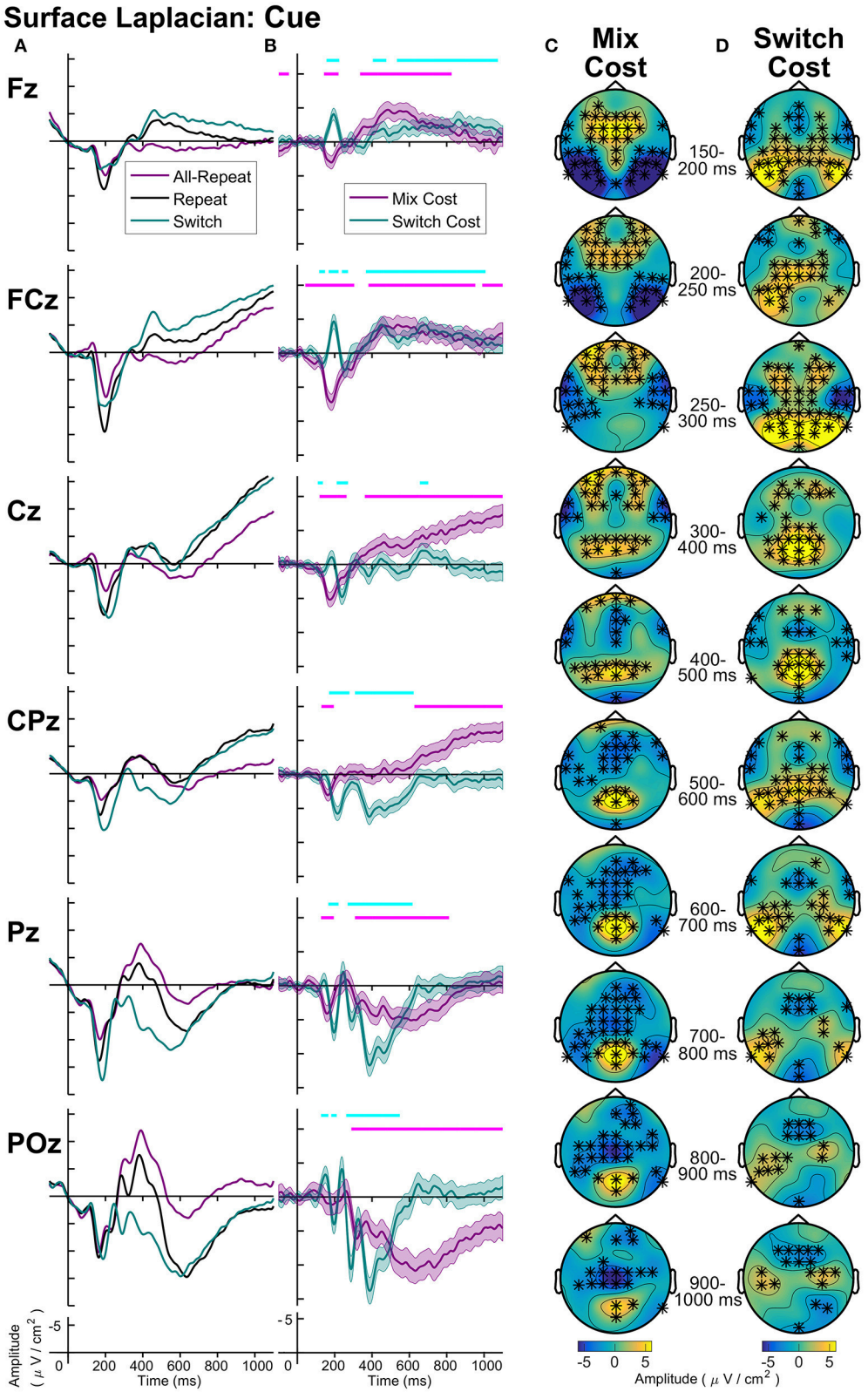

FIGURE 7 | Surface laplacian cue-locked: **(A)** Grand average ERPs, **(B)** Difference waveforms (Costs), Shaded 95% confidence intervals calculated for a within-subjects design (c.f., Loftus and Masson, 1994), Significant intervals of switch or mix cost (FDR $\alpha < 0.001$) are shown as thin cyan and magenta bars, respectively, **(C)** Mix Cost Topographies and **(D)** Switch Cost Topographies.

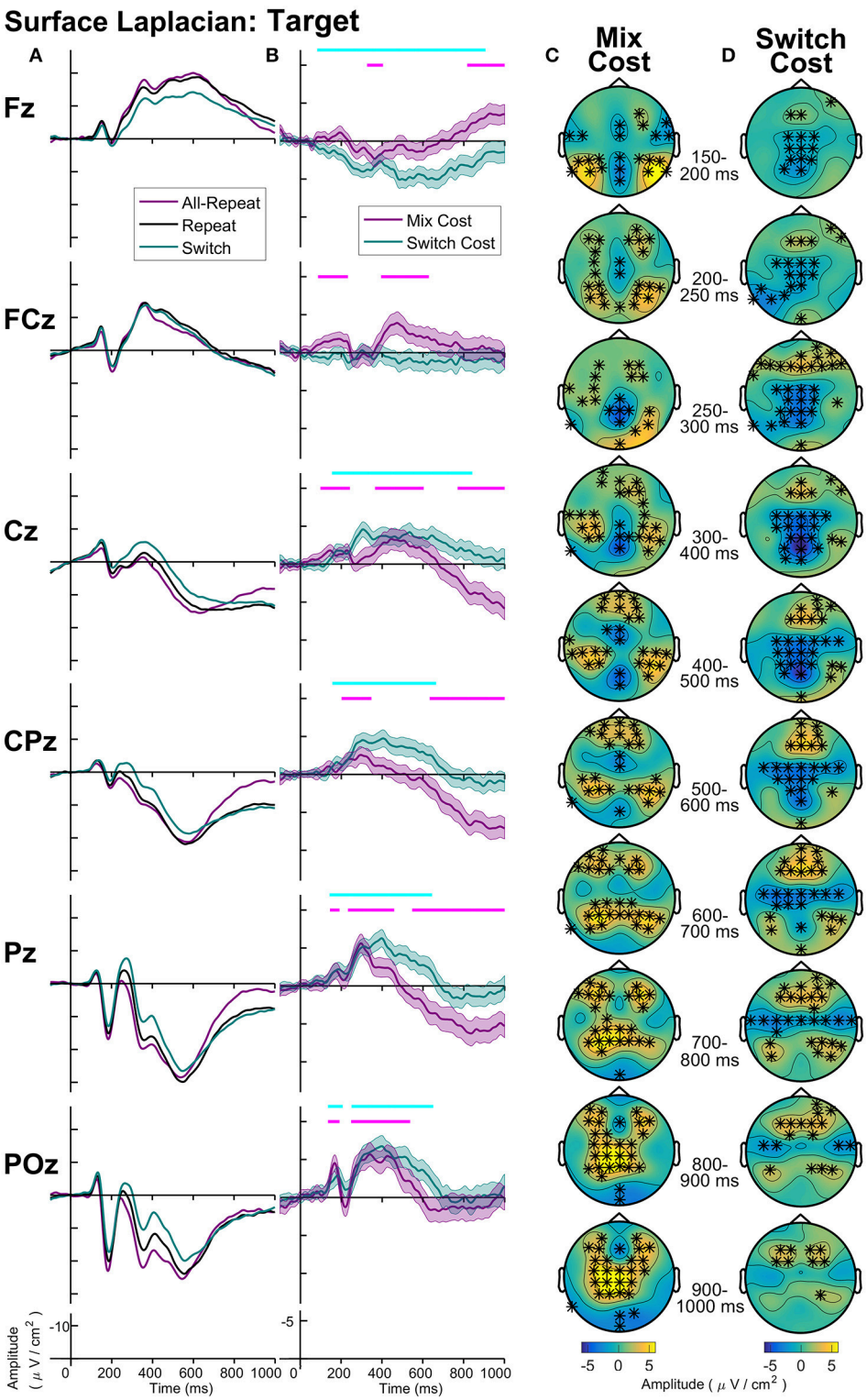

FIGURE 8 | Surface laplacian target-locked: **(A)** Grand average ERPs, **(B)** Difference waveforms (Costs), Shaded 95% confidence intervals calculated for a within-subjects design (c.f., Loftus and Masson, 1994), Significant intervals of switch or mix cost (FDR $\alpha < 0.001$) are shown as thin cyan and magenta bars, respectively, **(C)** Mix Cost Topographies and **(D)** Switch Cost Topographies.

(e.g., Barceló and Cooper, 2018). When used, they are typically implemented to minimize volume conduction effects in time-frequency decompositions (e.g., Mansfield et al., 2012; Cooper et al., 2015). However, the complex pattern of spatiotemporal features seen here with the surface Laplacian transformation, suggests that these spatial filters may provide novel insights into frontoparietal network dynamics necessary for effective task switching.

For instance, it is interesting to note that the fast and slow frontal and parietal switch effects during the cue-target interval as well as the slow switch effects that emerge post-target are consistent with functional MRI evidence of frontal and parietal network involvement in task-switching. For instance, a recent ALE showed posterior parietal cortex, precuneus, inferior frontal gyrus and presupplementary motor area activations associated with switch as compared to repeat trials (Jamadar et al., 2015).

In fact, the complex temporal and spatial activation network that emerges with surface Laplacian transformations is highly consistent with evidence from time-frequency analyses showing simultaneous or partially temporally overlapping patterns of activation in different frequency bands across different scalp locations (Cooper et al., 2016) It is also consistent with evidence of distinct frontoparietal networks operating at different timepoints both in cue-target and post-target intervals (Cooper et al., 2015) and temporal shifts of theta activation across parietal and frontal regions (Cooper et al., 2017). This evidence invites future work to map out the complex frontoparietal dynamics of cognitive control processes (for recent review, see Gratton et al., 2017, 2018).

The increased spatial and temporal information provided by the surface Laplacian transformation also provides a way to examine common and distinct aspects of the neural dynamics of processes contributing to mixing and switch effects. With conventional reference montages, cue-locked mixing and switch costs appear to have common broadly distributed effects (**Figure 4**). Surface Laplacian shows some common components (e.g., an early parietal positivity that emerges for both mixing and switch effects, as well as distinct components (e.g., this positivity has additional later parietal components for switch costs only). Both costs again share a similar topography prior to target onset (**Figure 7**).

CONCLUSION

The choice of spatial filter can have a strong impact on the pattern of ERPs recorded at the scalp during task-switching paradigms. All four transformations used here showed the same well-characterized ERP components that are typically seen in task-switching paradigms. However, the surface Laplacian transformation produced a much richer component landscape than conventional reference montages. The use of surface Laplacian transformation in both ERP and time-frequency analyses is recommended to increase the integration of information across these two analyses approaches of the EEG signal and to characterize EEG signatures of complex spatiotemporal networks involved in cognitive control. However, as a final cautionary note, all spatial transformations of EEG data come with their own weaknesses. As surface Laplacian is limited in its ability to model edge electrodes in the array, effects at edge electrodes need to be considered with caution.

AUTHOR CONTRIBUTIONS

AW, PC are equal first authors; AW, methodology implementation, data analysis, idea conceptualization, over all manuscript drafting, manuscript review; PC, idea conceptualization, over all manuscript drafting, manuscript review; AC, manuscript drafting, introduction, results and discussion; MM, data analysis, manuscript drafting, manuscript review; WF, idea conceptualization, manuscript review; PM, idea conceptualization, manuscript review; FK, idea conceptualization, manuscript drafting, manuscript review.

FUNDING

This research was supported by The Australian Research Council Discovery Projects (DP120100340, DP170100756) to FK.

REFERENCES

Astle, D. E., Jackson, G. M., and Swainson, R. (2006). Dissociating neural indices of dynamic cognitive control in advance task-set preparation: an erp study of task switching. *Brain Res.* 1125, 94–103. doi: 10.1016/j.brainres.2006.09.092

Astle, D. E., Jackson, G. M., and Swainson, R. (2008). The role of spatial information in advance task-set control: an event-related potential study. *Eur. J. Neurosci.* 28, 1404–1418. doi: 10.1111/j.1460-9568.2008.06439.x

Barceló, F., and Cooper, P. S. (2018). An information theory account of late frontoparietal ERP positivities in cognitive control. *Psychophysiology* 55. doi: 10.1111/psyp.12814

Barceló, F. (2003). The Madrid card sorting test (MCST): a task switching paradigm to study executive attention with event-related potentials. *Brain Res. Protoc.* 11, 27–37. doi: 10.1016/S1385-299X(03)00013-8

Barceló, F., Escera, C., Corral, M. J., and Periáñez, J. A. (2006). Task switching and novelty processing activate a common neural network for cognitive control. *J. Cogn. Neurosci.* 18, 1734–1748. doi: 10.1162/jocn.2006.18.10.1734

Barceló, F., Periáñez, J. A., and Nyhus, E. (2008). An information theoretical approach to task-switching: evidence from cognitive brain potentials in humans. *Front. Hum. Neurosci.* 1:13. doi: 10.3389/neuro.09.013.2007

Benjamini, Y., and Yekutieli, D. (2001). The control of the false discovery rate in multiple testing under dependency. *Annals Stat.* 29, 1165–1188. doi: 10.1214/aos/1013699998

Braver, T. S. (2012). The variable nature of cognitive control: a dual mechanisms framework. *Trends Cogn. Sci.* 16, 106–113. doi: 10.1016/j.tics.2011.12.010

Capizzi, M., Fehér, K., Penolazzi, B., and Vallesi, A. (2015). Task-switching preparation across semantic and spatial domains: an event-related potential study. *Biol. Psychol.* 110, 148–158. doi: 10.1016/j.biopsycho.2015.06.011

Cooper, P. S., Darriba Á, A., Karayanidis, F., and Barceló, F. (2016). Contextually sensitive power changes across multiple frequency bands underpin cognitive control. *Neuroimage* 132, 499-511. doi: 10.1016/j.neuroimage.2016.03.010.

Cooper, P. S., Wong, A. S., Fulham, W., Thienel, R., Mansfield, E., Michie, P. T., et al. (2015). Theta frontoparietal connectivity associated with proactive and reactive cognitive control processes. *Neuroimage* 108, 354–363. doi: 10.1016/j.neuroimage.2014.12.028

Cooper, P. S., Wong, A. S. W., McKewen, M., Michie, P. T., and Karayanidis, F. (2017). Variability in task-switching behavioral performance is associated with lower frequency oscillatory activity. *Biol. Psychol.* 129, 253–264. doi: 10.1016/j.biopsycho.2017.09.008

Cunillera, T., Fuentemilla, L., Periañez, J., Marco-Pallarès, J., Krämer, U. M., Ca'mara, E., et al. (2012). Brain oscillatory activity associated with task switching and feedback processing. *Cogn. Affect. Behav. Neurosci.* 12, 16–33. doi: 10.3758/s13415-011-0075-5.

Czernochowski, D. (2015). Erps dissociate proactive and reactive control: evidence from a task-switching paradigm with informative and uninformative cues. *Cogn. Affect. Behav. Neurosci.* 15, 117–131. doi: 10.3758/s13415-014-0302-y

Diamond, A. (2013). Executive functions. *Annu. Rev. Psychol.* 64, 135–168. doi: 10.1146/annurev-psych-113011-143750

Folstein, J. R., and Van Petten, C. (2008). Influence of cognitive control and mismatch on the N2 component of the ERP: a review. *Psychophysiology* 45, 152–170. doi: 10.1111/j.1469-8986.2007.00602.x

Gajewski, P. D., and Falkenstein, M. (2011). Diversity of the p3 in the task-switching paradigm. *Brain Res.* 1411, 87–97. doi: 10.1016/j.brainres.2011.07.010

Gajewski, P. D., Kleinsorge, T., and Falkenstein, M. (2010). Electrophysiological correlates of residual switch costs. *Cortex* 46, 1138–1148. doi: 10.1016/j.cortex.2009.07.014

Goffaux, P., Phillips, N. A., Sinai, M., and Pushkar, D. (2006). Behavioural and electrophysiological measures of task switching during single and mixed-task conditions. *Biol. Psychol.* 72, 278–290. doi: 10.1016/j.biopsycho.2005.11.009

Gratton, C., Sun, H., and Petersen, S. (2017). Control networks and hubs. *Psychophysiology* 55:e13032. doi: 10.1111/psyp.13032

Gratton, G., Cooper, P. S., Fabiani, M., Carter, C. S., and Karayanidis, F. (2018). Dynamics of cognitive control: Theoretical bases, paradigms, and a view for the future. *Psychophysiology* 55:e13016. doi: 10.1111/psyp.13016

Hjorth, B. (1975). An on-line transformation of EEG scalp potentials into orthogonal source derivations. *Electroencephalogr. Clin. Neurophysiol.* 39, 526–530. doi: 10.1016/0013-4694(75)90056-5

Hsieh, S., and Wu, M. (2011). Electrophysiological correlates of preparation and implementation for different types of task shifts. *Brain Res.* 1423, 41–52. doi: 10.1016/j.brainres.2011.09.018

Hyvärinen, A., and Oja, E. (2000). Independent component analysis: algorithms and applications. *Neural Netw.* 13, 411–430. doi: 10.1016/S0893-6080(00)00026-5

Jamadar, S., Hughes, M., Fulham, W., Michie, P., and Karayanidis, F. (2010a). The spatial and temporal dynamics of anticipatory preparation and response inhibition in task-switching. *Neuroimage* 51, 432–449. doi: 10.1016/j.neuroimage.2010.01.090

Jamadar, S., Michie, P. T., and Karayanidis, F. (2010b). Sequence effects in cued task switching modulate response preparedness and repetition priming processes. *Psychophysiology* 47, 365–386. doi: 10.1111/j.1469-8986.2009.00932.x

Jamadar, S., Thienel, R., and Karayanidis, F. (2015). "Task switching processes," in *Brain Mapping: An Encyclopedic Reference*, 1 Edn., ed A. W. Toga (Academic Press), 327–335.

Jost, K., Mayr, U., and Rösler, F. (2008). Is task switching nothing but cue priming? evidence from erps. *Cogn. Affect. Behav. Neurosci.* 8, 74–84. doi: 10.3758/CABN.8.1.74

Karayanidis, F., Jamadar, S., Ruge, H., Phillips, N., Heathcote, A., and Forstmann, B. (2010). Advance preparation in task-switching: converging evidence from behavioral, brain activation, and model-based approaches. *Front. Psychol.* 1:25. doi: 10.3389/fpsyg.2010.00025

Karayanidis, F., Keuken, M. C., Wong, A., Rennie, J. L., de Hollander, G., Cooper, P. S., et al. (2016). The age-ility project (phase 1): structural and functional imaging and electrophysiological data repository. *Neuroimage* 124, 1137–1142. doi: 10.1016/j.neuroimage.2015.04.047

Karayanidis, F., Mansfield, E. L., Galloway, K. L., Smith, J. L., Provost, A., and Heathcote, A. (2009). Anticipatory reconfiguration elicited by fully and partially informative cues that validly predict a switch in task. *Cogn. Affect. Behav. Neurosci.* 9, 202–215. doi: 10.3758/CABN.9.2.202

Karayanidis, F., Provost, A., Brown, S., Paton, B., and Heathcote, A. (2011). Switch-specific and general preparation map onto different erp components in a task-switching paradigm. *Psychophysiology* 48, 559–568. doi: 10.1111/j.1469-8986.2010.01115.x

Kayser, J., and Tenke, C. (2006). Principal components analysis of laplacian waveforms as a generic method for identifying erp generator patterns: I. evaluation with auditory oddball tasks. *Clin. Neurophysiol.* 117, 348–368. doi: 10.1016/j.clinph.2005.08.034

Kayser, J., and Tenke, C. E. (2015). Issues and considerations for using the scalp surface laplacian in eeg/erp research: a tutorial review. *Int. J. Psychophysiol.* 97, 189–209. doi: 10.1016/j.ijpsycho.2015.04.012

Kieffaber, P. D., Kruschke, J. K., Cho, R. Y., Walker, P. M., and Hetrick, W. P. (2013). Dissociating stimulus-set and response-set in the context of task-set switching. *J. Exp. Psychol. Hum. Percept. Perform.* 39, 700-719. doi: 10.1037/a0029545

Kim, C., Cilles, S. E., Johnson, N. F., and Gold, B. T. (2012). Domain general and domain preferential brain regions associated with different types of task switching: a meta-analysis. *Hum. Brain Mapp.* 33, 130–142. doi: 10.1002/hbm.21199

Lange, F., Seer, C., Müller, D., and Kopp, B. (2015). Cognitive caching promotes flexibility in task switching: evidence from event-related potentials. *Sci. Rep.* 5:17502. doi: 10.1038/srep17502

Lavric, A., Mizon, G. A., and Monsell, S. (2008). Neurophysiological signature of effective anticipatory task-set control: a task-switching investigation. *Eur. J. Neurosci.* 28, 1016–1029. doi: 10.1111/j.1460-9568.2008.06372.x

Li, L., Wang, M., Zhao, Q.-J., and Fogelson, N. (2012). Neural mechanisms underlying the cost of task switching: an erp study. *PLoS ONE* 7:e42233. doi: 10.1371/journal.pone.0042233

Loftus, G. R., and Masson, M. E. (1994). Using confidence intervals in within-subject designs. *Psychon. Bull. Rev.* 1, 476–490. doi: 10.3758/BF03210951

Mansfield, E., Karayanidis, F., and Cohen, M. X. (2012). Switch-related and general preparation processes in task-switching: evidence from multivariate pattern classification of EEG data. *J. Neurosci.* 32, 18253–18258. doi: 10.1523/JNEUROSCI.0737-12.2012

MATLAB (2015). *version 8.6.0.267246 (R2015b)*. Natick, MA: The MathWorks Inc.

Manzi, A., Nessler, D., Czernochowski, D., and Friedman, D. (2011). The development of anticipatory cognitive control processes in task-switching: an erp study in children, adolescents, and young adults. *Psychophysiology* 48, 1258–1275. doi: 10.1111/j.1469-8986.2011.01192.x

Miniussi, C., Marzi, C., and Nobre, A. (2005). Modulation of brain activity by selective task sets observed using event-related potentials. *Neuropsychologia* 43, 1514–1528. doi: 10.1016/j.neuropsychologia.2004.12.014

Monsell, S. (2003). Task switching. *Trends Cogn. Sci. (Regul. Ed).* 7, 134–140. doi: 10.1016/S1364-6613(03)00028-7

Nessler, D., Friedman, D., and Johnson, R. (2012). A new account of the effect of probability on task switching: erp evidence following the manipulation of switch probability, cue informativeness and predictability. *Biol. Psychol.* 91, 245–262. doi: 10.1016/j.biopsycho.2012.07.005

Nicholson, R., Karayanidis, F., Bumak, E., Poboka, D., and Michie, P. T. (2006a). Erps dissociate the effects of switching task sets and task cues. *Brain Res.* 1095, 107–123. doi: 10.1016/j.brainres.2006.04.016

Nicholson, R., Karayanidis, F., Davies, A., and Michie, P. T. (2006b). Components of task-set reconfiguration: differential effects of switch-toand switch-awaycues. *Brain Res.* 1121, 160–176. doi: 10.1016/j.brainres.2006.08.101

Nunez, P. L., and Srinivasan, R. (2006). *Electric Fields of the Brain: the Neurophysics of EEG*. New York, NY: Oxford University Press.

Oostenveld, R., Fries, P., Maris, E., and Schoffelen, J.-M. (2011). Fieldtrip: open source software for advanced analysis of meg, eeg, and invasive electrophysiological data. *Comput. Intell. Neurosci.* 2011:156869. doi: 10.1155/2011/156869

Periáñez, J. A., and Barceló, F. (2009). Updating sensory versus task representations during task-switching: insights from cognitive brain potentials in humans. *Neuropsychologia* 47, 1160–1172. doi: 10.1016/j.neuropsychologia.2009.01.014

Poulsen, C., Luu, P., Davey, C., and Tucker, D. M. (2005). Dynamics of task sets: evidence from dense-array event-related potentials. *Cogn. Brain Res.* 24, 133–154. doi: 10.1016/j.cogbrainres.2005.01.008

Ruge, H., Jamadar, S., Zimmermann, U., and Karayanidis, F. (2013). The many faces of preparatory control in task switching: reviewing a decade of fmri research. *Hum. Brain Mapp.* 34, 12–35. doi: 10.1002/hbm.21420

Rushworth, M. F., Passingham, R. E., and Nobre, A. (2002). Components of switching intentional set. *J. Cogn. Neurosci.* 14, 1139–1150. doi: 10.1162/089892902760807159

Rushworth, M. F., Passingham, R. E., and Nobre, A. C. (2005). Components of attentional set-switching. *Exp. Psychol.* 52, 83–98. doi: 10.1027/1618-3169.52.2.83

Sauseng, P., Klimesch, W., Freunberger, R., Pecherstorfer, T., Hanslmayr, S., and Doppelmayr, M. (2006). Relevance of eeg alpha and theta oscillations during task switching. *Exp. Brain Res.* 170, 295–301. doi: 10.1007/s00221-005-0211-y

Swainson, R., Jackson, S. R., and Jackson, G. M. (2006). Using advance information in dynamic cognitive control: an erp study of task-switching. *Brain Res.* 1105, 61–72. doi: 10.1016/j.brainres.2006.02.027

Tarantino, V., Mazzonetto, I., and Vallesi, A. (2016). Electrophysiological correlates of the cognitive control processes underpinning mixing and switching costs. *Brain Res.* 1646, 160–173. doi: 10.1016/j.brainres.2016.05.048

Travers, S., and West, R. (2008). Neural correlates of cue retrieval, task set reconfiguration, and rule mapping in the explicit cue task switching paradigm. *Psychophysiology* 45, 588–601. doi: 10.1111/j.1469-8986.2008.00658.x

Whitson, L. R., Karayanidis, F., Fulham, R., Provost, A., Michie, P. T., Heathcote, A., et al. (2014). Reactive control processes contributing to residual switch cost and mixing cost across the adult lifespan. *Front. Psychol.* 5:383. doi: 10.3389/fpsyg.2014.00383

Yao, D. (2001). A method to standardize a reference of scalp eeg recordings to a point at infinity. *Physiol. Meas.* 22, 693-711. doi: 10.1088/0967-3334/22/4/305

Yao, D. (2002). The theoretical relation of scalp Laplacian and scalp current density of a spherical shell head model. *Phys. Med. Biol.* 47, 2179–2185 doi: 10.1088/0031-9155/47/12/312

Conflict of Interest Statement: The authors declare that the research was conducted in the absence of any commercial or financial relationships that could be construed as a potential conflict of interest.

frontiers in Neuroscience

ORIGINAL RESEARCH
published: 13 March 2018
doi: 10.3389/fnins.2018.00148

Hearing the Sound in the Brain: Influences of Different EEG References

Dan Wu [1,2]*

[1] School of Computer and Information Technology, Beijing Jiaotong University, Beijing, China, [2] The Key Laboratory for NeuroInformation of Ministry of Education, University of Electronic Science and Technology of China, Chengdu, China

If the scalp potential signals, the electroencephalogram (EEG), are due to neural "singers" in the brain, how could we listen to them with less distortion? One crucial point is that the data recording on the scalp should be faithful and accurate, thus the choice of reference electrode is a vital factor determining the faithfulness of the data. In this study, music on the scalp derived from data in the brain using three different reference electrodes were compared, including approximate zero reference—reference electrode standardization technique (REST), average reference (AR), and linked mastoids reference (LM). The classic music pieces in waveform format were used as simulated sources inside a head model, and they were forward calculated to scalp as standard potential recordings, i.e., waveform format music from the brain with true zero reference. Then these scalp music was re-referenced into REST, AR, and LM based data, and compared with the original forward data (true zero reference). For real data, the EEG recorded in an orthodontic pain control experiment were utilized for music generation with the three references, and the scale free index (SFI) of these music pieces were compared. The results showed that in the simulation for only one source, different references do not change the music/waveform; for two sources or more, REST provide the most faithful music/waveform to the original ones inside the brain, and the distortions caused by AR and LM were spatial locations of both source and scalp electrode dependent. The brainwave music from the real EEG data showed that REST and AR make the differences of SFI between two states more recognized and found the frontal is the main region that producing the music. In conclusion, REST can reconstruct the true signals approximately, and it can be used to help to listen to the true voice of the neural singers in the brain.

Keywords: brainwave music, EEG, reference electrode, reference electrode standardization technique (REST), scale-free

OPEN ACCESS

Edited by:
Rui Zhang,
Zhengzhou University, China

Reviewed by:
Laura Marzetti,
Università degli Studi G. d'Annunzio Chieti e Pescara, Italy
Yin Tian,
Chongqing University of Posts and Telecommunications, China

***Correspondence:**
Dan Wu
wudan@bjtu.edu.cn

Specialty section:
This article was submitted to Brain Imaging Methods, a section of the journal Frontiers in Neuroscience

Received: *27 July 2017*
Accepted: *23 February 2018*
Published: *13 March 2018*

Citation:
Wu D (2018) Hearing the Sound in the Brain: Influences of Different EEG References. Front. Neurosci. 12:148. doi: 10.3389/fnins.2018.00148

INTRODUCTION

The electroencephalogram (EEG), one of the most useful technologies for brain research, has been recommended for its non- invasiveness and high time resolution. However, the obtained EEG information is almost always presented as complicated visual images or waveforms. If brain waves could be heard after translation by a proper sonification rule, we may be able to directly "perceive" brain activity and its variations using our auditory system. Some studies investigate that the rhythm

of human breathing, movements, and even synchronization follow the scale free law (Torre and Wagenmakers, 2009; Hennig, 2014), which is shared with music (Manaris et al., 2005; Levitin et al., 2012; Liu et al., 2013). In that way, the brain activities recorded from the scalp may be due to neural singers in the brain.

To hear sound of the brain, many strategies are adopted by researchers in different fields, from neuroscience to music composition. Because the main frequency of EEG is so low that it cannot be hear directly, the most basic method is parameter mapping, which translates a few parameters of EEG to the characteristic parameters of music. In some early works, for example, the earliest attempt to hear brainwaves as music (Adrian and Matthews, 1934) and a concert called "Music for Solo Performer" (Rosenboom, 1976), the amplitude of the alpha waves from EEG signals were utilized as the driving sources of the musical sound. In the 1990s, various new music generating rules were created from digital filtering or coherent analysis of EEG (Rosenboom, 1997). To date, parameter mapping is the most popular method and widely used (Rosenboom, 1976; Hinterberger and Baier, 2005), because it not only provides a sensitive way to detect the small variations in the amplitude and frequency of brain waves that are ignored by conventional EEG technique in real time (Väljamäe et al., 2013), but also can indicate some essential features, i.e., the scale free law, followed by both EEG and music (Wu et al., 2009). Another typical method was the event triggering, which utilizes specific events such as interictal epileptic discharges as triggers for the beginning of supposed music tones or other sound events (Baier et al., 2007).

In fact, more than one strategy is used for the music generation in real systems. The musical application of Brain Computer Interface (BCI) can represent the connections between mental states and music (Miranda and Brouse, 2005; Miranda, 2010; Wu et al., 2010), and detect users' current affective states significantly (Daly et al., 2016). To express the activities of different brain regions, several instruments were used to represent different brain regions and that just make the brain like an orchestra (Hinterberger and Baier, 2005); the voice or music for the left and right channels were deduced by the activities of the respective spheres (Wu et al., 2014). Deriving a quartet from multi-channel EEGs with artistic beat and tonality filtering, we can harmonically distinguish the different states of the brain activities (Wu et al., 2013). The combination of EEG and fMRI provided more information of the brain which can be heard (Lu et al., 2012). Listen to the music or sound of the brain is a good way for investigating the brain activities, but a crucial factor is that the reality and accuracy of the sound we heard.

During EEG scalp recording, one of the most fundamental points which influences the accuracy of data, is the reference choosing, and that is a very attractive question in brain electrophysiology research. Using an appropriate reference is essential for data collecting and analyzing, because the potential difference only can be measured between two points, the objective electrodes and the reference (Geselowitz, 1998). Several different types of reference, including the vertex reference (CZ), the linked mastoids reference (LM), the average reference (AR), and the left mastoid reference (L), are currently used for EEG measurement. However, all of these references may lead to an undesired temporal bias since no neutral point exists on the body surface. Thus, the reference signal itself may involve physiological dynamic processes that will inevitably influence the data. Previous studies have examined the effects of reference choice on EEG data using several methods, including the estimation of the effect of head surface on recordings using AR (Junghöfer et al., 1999; Yao, 2017), the examination of coherence and reference signals (Nunez et al., 1997; Essl and Rappelsberger, 1998). To entirely resolve the problems involved in using body surface points for referencing, a reference with neutral potential is required. Theoretically, a point at infinity is far from brain sources, and has an ideally neutral potential. In 2001, Yao proposed a "reference electrode standardization technique (REST)" to approximately transform EEG data recorded with a scalp point reference to recordings using an infinity reference (the software for REST transformation can be downloaded at http://www.neuro.uestc.edu.cn/rest). In recent years, the REST has been quantitatively validated through simulation studies with assumed neural sources in both a concentric three-sphere head model (Yao, 2001) and a realistic head model (Zhai and Yao, 2004). These studies have shown that data referenced with REST are more consistent with physiology than data referenced using traditional scalp references. This has been shown using a variety of techniques, including EEG spectral imaging (Yao et al., 2005), EEG coherence (Marzetti et al., 2007), brain evoked potentials (EP) and spatiotemporal analysis (Yao et al., 2007), default network (Qin et al., 2010).

However, if we believe that brain activities are musical, the influence of reference to scalp EEG recordings definitely will affect the music of EEG. Especially, our scale free music is supposed to be an objective reflection of the physiological signal, we need to have the true objective EEG signal without non-zero reference effect etc. In this work, we assume that the neural activities are musical, for the EEG shows 1/f fluctuation (Leistedt et al., 2007; Tomasi et al., 2017) the same as the pitch, rhythm and consonance of the music (Manaris et al., 2005; Levitin et al., 2012; Wu et al., 2015). Then we primarily use classical music as the source of EEG, and forward calculate the scalp "potential" of them, and to see what's the effect of the reference on the scalp potential, the music of the brain. In this study, the tested reference are REST, average reference (AR), and linked mastoids (LM), and the evaluation metrics is the relative error between the true scalp potential/music and the re-reference potential/music. Finally, a real data music was comparatively investigated.

MATERIALS AND METHODS

Music Materials for Simulation

Since the neural activities in the brain may be musical, we use some classical music pieces as the EEG source to test the scalp potential. The music piece *Two Part Inventions* (*BWV 772*), which wrote by composer Johann Sebastian Bach (1685–1750), was used as one-source and two-source signals for simulation. The music was firstly translated from MIDI format to waveform before using as the one source signal in the brain.

The next, the original MIDI file was separated into two parts according to the polyphonic principle, translating into two

series of audio waves, and then used as two source signals for simulation. BWV772 was a typical polyphonic music style, which contained two related independent melody and the two parts or two voices were skillfully interweaving in the work according to the polyphonic principle.

Another classical music piece used in the simulation was one of the famous works of Wolfgang Amadeus Mozart (1756–1791), *Quartet No.14 in G for strings (K387)*, which was used as four-source signals. A quartet was wrote for four instruments, thus we can easily divide the work into four simultaneous parts in the MIDI sequences, and then translate them into four channel waveforms, finally put these signals in the head modal as four sources. **Figure 1** has shown 10 s of the MIDI and waveform format files of these music pieces.

Simulation Process

Before the simulation, all the music pieces were prepared in waveform format (the file name was *.wav) with sampling rate 44,100 Hz, and it can be read into MATLAB as matrixes. The music data were represented as M, which was a 1^*N, 2^*N or 4^*N matrix for the three cases in **Figure 1**. Here N was the time point length of the music and 1, 2, or 4 represented the number of the music parts, also of the sources. For simulation, the forward EEG calculation is given by

$$V = GS \tag{1}$$

where G is the transfer matrix referenced at infinity, only dependent on the head model, source configuration and electrode montage; S is the distributed source; and V is the scalp EEG recording with a reference at infinity generated by S. Scalp noise is not considered in this model and is assumed to be zero. To simulate a source in a brain model, the transfer matrix (G) must be established by using the location information of an electrode cap system. In this work, with known electrode location, source locations, and a three-layer spherical head model, the transfer matrix G can be obtained. With known source temporal processes, matrix S, it can be further assumed that the sources are all radial dipoles (Yao, 2000). Therefore, the signals on the scalp (V) were obtained by forward modeling Equation (1), and V was the standard signals with reference at infinity in the simulation.

In this study, the head model for all cases was a three-concentric-sphere model. The normalized radii of the three concentric spheres were 0.87 (inner radius of the skull), 0.92 (outer radius of the skull) and 1.0 (radius of the scalp). The normalized conductivities were 1.0, 0.0125, and 1.0 for the brain, skull and scalp, respectively. The center of the spheres was defined as the coordinate origin. The x-axis was oriented from the origin to the direction of the right ear, and the y-axis was oriented in the posterior–anterior direction. The z-axis was oriented from the origin to the vertex.

With known simulated V with zero reference, or actual scalp recordings V with one point such as Cz or left ear, etc. as reference, it is easy to translate them to data with any one of the three references: REST, average reference (AR), and linked mastoids reference (LM) (Yao, 2001). Here, we adopt the free software REST to do it (www.neuro.uestc.edu.cn/rest). And we chose a classical 10-20 system with 32 electrodes.

The Comparison of Three References

To compare the influences of the REST, AR, and LM, we should first calculate the standard scalp signals at different electrodes according to the sources, and then translate into the three references occasions. For the simulation, signals on the scalp were the music with distortion by the references, so that we can listen to these music pieces for further investigation. In order to quantify the differences, relative error and correlation coefficients between the standard signal and the three re-referenced signals were calculated. Relative error demonstrated the relative value difference between the estimated signals and the standard at every time point, while the correlation coefficients can explain the variations in a holistic view. For all the simulations in this study, the head model was a three-concentric-sphere model mentioned in section Simulation Process. The locations of sources were used as another factor in the comparison. For one source situation, we tested 300 locations, which picked up from the 3,000 locations according to the positions of the head modal proposed in transfer matrix calculating (Yao, 2000). And for two sources situation, we tested 380 pairs of locations that means each source was put in 20 locations, respectively. At last, 360 pairs of location for four sources were performed.

Real EEG to Brainwave Music With Different References

We also used real EEG data with different references to generate brainwave music. The data was recorded in an orthodontic pain control experiment (Huang et al., 2016). This study was approved by the Ethics Committee of the West China Hospital of Stomatology. All subjects gave written informed consent in accordance with the Declaration of Helsinki. In the experiment, 24 subjects (23 $\pm$ 5 years old) were right-handed, had mild dental crowding. There were two groups (each group 12 subjects): subjects group 1 (brain music group) were just listening the brainwave music of their own; those in group 2 (control group) without any interfering. The brainwave music used in group 1 was generated from the EEG before the subjects been treatment, in that time they did not suffer the pain. The EEG data adopted in this study were recorded on the second day after the initial archwire placement for the subjects.

EEG signals were recorded by the SymTop EEG system (SymTop Instrument, Beijing, China) with 16 Ag/AgCl surface electrodes fixed in a cap at the standard positions according to the 10–20 system. The EEG was referenced to the mean of the signals recorded at the participants' mastoids (LM). Impedances were kept below 5 kΩ. EEG signals were sampled at 1000 Hz, 0.3–45 Hz band-pass filter. These parameters were used for all the EEG recordings in this study. The data, recording in the second day after the pain beginning, were chosen for translating into music pieces to compare the differences of the three references.

The method for brainwave music generation in this paper was proposed in 2013 (Wu et al., 2013), which deriving a quartet from multi-channel EEGs with artistic beat and tonality filtering. EEG data from multiple electrodes were first translated into MIDI

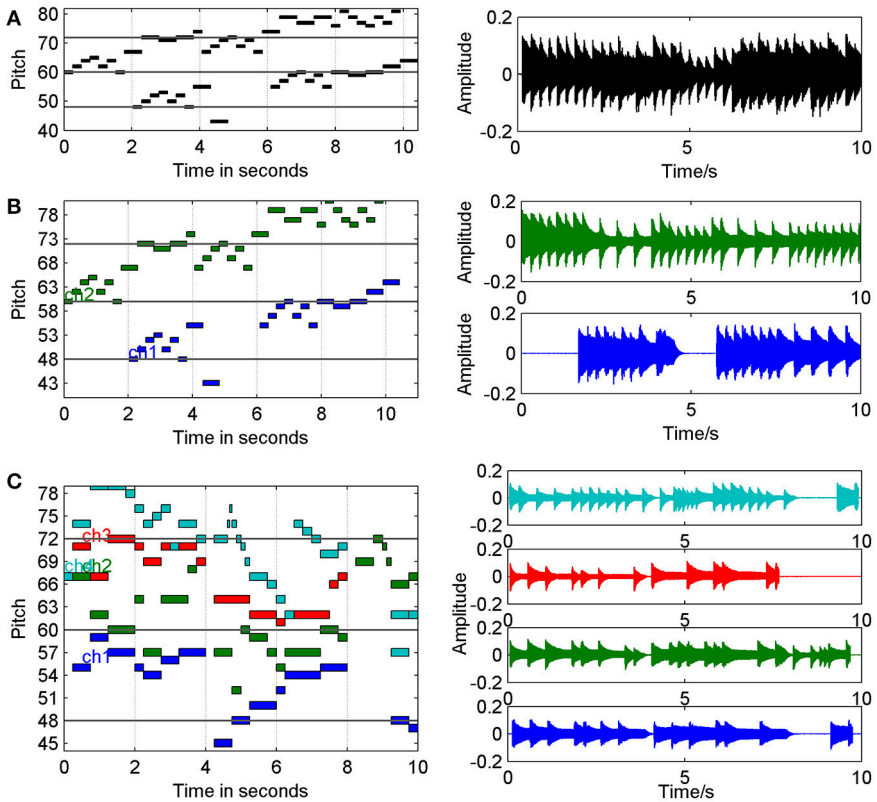

FIGURE 1 | Music materials for simulation in MIDI and waveform format (10 s for example). **(A)** MIDI and waveform of Bach, BWV 772, with one voice. **(B)** MIDI and waveform of Bach, BWV 772, with two voices. **(C)** MIDI and waveform of Mozart, K387, with four instruments.

sequences by scale free brainwave music method (SFBM) (Wu et al., 2009), respectively. Then, these sequences were processed by a beat filter which adjusted the duration of notes in terms of the characteristic frequency. And the sequences were further filtered from atonal to tonal according to a key defined by the analysis of the original music pieces. The note which lasted for the longest time in the music was determined as the main note of a certain key, and after that the musical filter would chose the notes which supported the key from the original sequences produced by the EEG.

The original reference of the recorded EEG data was the LM reference, and we changed it to the AR and REST reference for comparison. The EEG of three different references were translated into music pieces, respectively. The features of music, such as pitch, tempo, note duration, scale free exponent of pitch, and the weight of every electrode in the music generation were calculated.

RESULTS

Single Source Simulation

The signal used as a single source in the simulation was *BWV 772* (**Figure 1A**) that composed by Bach. The source was put in 300 different locations of the head modal, and I calculated the relative errors between the standard signals and the re-reference. The average relative errors of the 300 locations were 0.72 ± 2.88 (REST), 4.93 ± 16.69 (AR), and 4.39 ± 7.79 (LM). The one way ANOVA were used to test the differences between the three groups ($p < 0.01$). And the results of *post-hoc* test showed significant differences between REST and AR, REST, and LM (Tukey's honestly significant difference criterion).

As an example, the coordinate of one source location was (0.087, 0.859, 0.097), and marked by a red dot in **Figure 2A**. Relative errors of the three different electrode references were calculated compared to the standard signals and showed in **Figure 2B**. In this location, the REST method showed a significant smallest relative errors, about 0.049 ± 0.006; next was the AR, 0.41 ± 0.05; and the LM was the highest, 1.52 ± 0.20, averagely. **Figure 2C** showed correlation coefficients between the standard signals and the three references, respectively. It was obvious that all the three re-referenced methods highly correlated to the standard signal, especially the REST, the coefficients of all the 32 electrodes were 1. For AR and LM, coefficient values for several electrodes were −1, which means just a phase shift during the process. For AR, its overbearing assumption, that the average of the whole recordings would be zero, definitely result part of the scalp positive and other part negative, for LM, the electrodes with signals smaller than the average of the two ears will be negative, and the larger one will be positive if the actual value of LM is positive relative to infinity. Four music

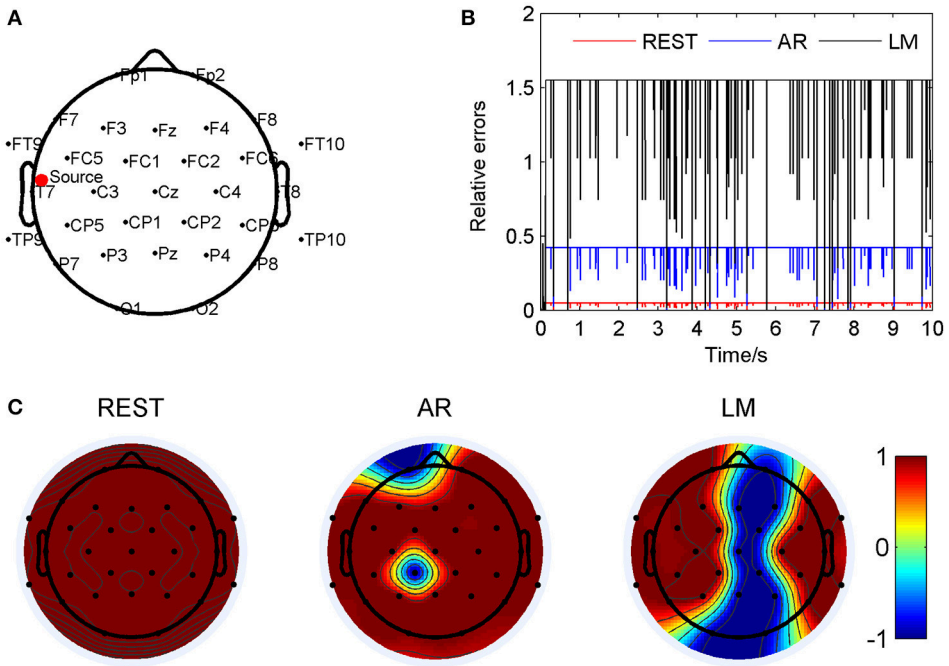

FIGURE 2 | Comparison of the three reference electrode methods for the one source of BWV772 shown in **Figure 1A**. **(A)** The location of the source is (−0.65674, −0.06352, 0.56552). The red dot indicates the projected position of the source on the scalp surface. **(B)** Relative errors of the music signals with three references compared to the standard signals. **(C)** Correlation coefficients of three references with the standard signals.

pieces, including the standard signal, the signal from electrode CP1 on the scalp of REST, AR, and LM, were provided in the Supplementary Material. It was easy to find that the standard signal and REST music sounded the same, while the AR and LM music had small volume compared to the formers.

Two Sources Simulation

Testing 20*19 pairs of sources, which were chosen from all the 3,000 locations according to the head modal, I found that the waveform/music showed distinct differences in the three references. The average relative errors of the 380 pairs were 0.17 ± 0.26 (REST), 2.29 ± 1.71 (AR), and 4.12 ± 3.18 (LM). The one way ANOVA were used to test the differences between the three groups ($p < 0.01$). And the results of *post-hoc* test showed significant differences between REST and AR, REST, and LM, AR and LM (Tukey's honestly significant difference criterion). Here two location pairs were shown because of their typical distributions for the AR and LM references, respectively.

Figure 3 has shown the situation with source locations at (-0.264, 0.352, 0.750) and (0.278, 0.457, 0.689), so that AR reference was deflected from the standard signal mostly. The two sources were marked as Source 1 and Source 2 in **Figure 3A**. The relative errors of the three different electrodes were calculated compared to the standard signals and showed in **Figure 3B**. For the location pair, the REST method showed a significant smallest relative errors, about 0.053 ± 0.060; next was the AR, 1.38 ± 0.96; and the LM was the highest, 2.74 ± 2.14, averagely. **Figure 3C** showed correlation coefficients between the standard signals and the three references, respectively. In this situation of source pair, it was obvious that REST was almost the same with the standard signals; the coefficient of every electrode was 1. For AR reference, most regions were accordant with the standard, but at electrode T7 was 0.05, and P7 was 0.35. For LM reference, the electrodes, T7 was 0.99, but P7 was 0.33, CP5 was −0.97, also showed a low correlation to the standard signal. Four music pieces, lasting 30 s, from the electrode T7 on the scalp, including the standard signal, REST, AR, and LM, were provided in the Supplementary Material. To listen to these music, it can be found that in the standard signal and REST music, the volume of channel two was larger than channel one, while in AR music, channel one was larger. LM music sounded a little larger volume than the standard.

Figure 4 has shown the situation when the two source were at (0.254, 0.124, 0.822) and (−0.678, −0.267, 0.473) so that LM reference was deflected from the standard signal mostly. The two sources were marked as Source 1 and Source 2 in **Figure 4A**. For such location pair, the REST method showed a significant smallest relative errors, about 0.036 ± 0.017; next was the AR, 0.90 ± 0.67; and the LM was the highest, 4.13 ± 2.24, averagely. These results have shown in **Figure 4B**. The correlation coefficients between the standard signals and the three references were shown in **Figure 4C**, which demonstrated that the REST reference was the same as standard signal. The LM reference dedicated low correlation coefficients in many electrodes, especially in the occipital of the cap. For example, P8 was −0.89 and O1 was −0.87. Compared to LM, the AR reference was the almost high correlated with the standard, P8 of AR was 0.95, O1 was 0.93, but in FC5 and FC6, the correlation was down

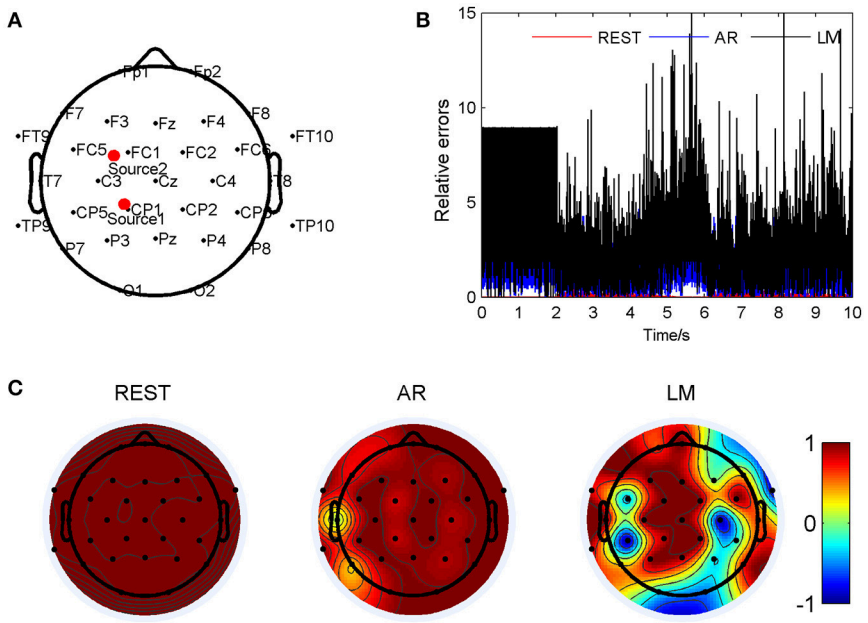

FIGURE 3 | Comparison of three reference electrode methods for the two sources of BWV 772 shown in **Figure 1B**. **(A)** The location of the sources are (−0.264, 0.352, 0.750) and (0.278, 0.457, 0.689). The red dots indicate the projected positions of the source on the scalp surface. **(B)** Relative errors of the music signals with three references compared to the standard signals. **(C)** Correlation coefficients of three references with the standard signals.

to 0.85 and 0.71. By listening the music from the electrode P8 on the scalp, it was observed that channel one in LM music was hardly been heard compared to the other three pieces.

Four Sources Simulation

Three hundred and sixty pairs of electrodes which were chosen from all the 3,000 locations of the head modal were tested in the four source simulation, and the average relative errors were 0.07 ± 0.03 (REST), 0.77 ± 0.13 (AR), and 2.28 ± 0.75 (LM), respectively. The one way ANOVA were used to test the differences between the three groups ($p < 0.01$). And the results of *post-hoc* test showed significant differences between REST and AR, REST, and LM, AR, and LM (Tukey's honestly significant difference criterion).

Figure 5 have shown an example of four source simulation with the locations were (0.087, 0.859, 0.097), (0, 0, −0.076), (0.342, 0.643, 0.473) and (0.495, −0.638, 0.320). These sources were marked in **Figure 5A**. Relative errors were calculated and the results were showed in **Figure 5B**: these of REST method were lower (0.10 ± 0.10) than the others during all the music pieces; while the AR method was 0.95 ± 0.81; the LM method demonstrated highest variance (1.28 ± 1.04) among the three in such source locations. In such situation, AR method demonstrated a quite low coefficient (0.29) to the standard signal in FP1. And REST method was also almost the same with the standard signals; the coefficient of every electrode was 1. For LM reference, the electrodes, O1 and O2, showed low correlations (0.28 and 0.26) to the standard signal, while in FP1 it was 0.89. Four music pieces from the electrode FP1 on the scalp, including the standard signal, REST, AR and LM, were provided as the Supplementary Materials. Listening to these music, it can be found that in standard and REST music at FP1, the four parts of the melody were not the same as the original music, for channel three had been emphasized. However, in music of AR, this channel was not so prominent.

Another situation of four sources, including (0.087, 0.859, 0.097), (−0.865, −0.030, −0.076), (0.495, −0.638, 0.320) and (0.342, 0.643, 0.473) were represented in **Figure 6**. The four sources were marked in **Figure 6A** as red dots. Relative errors were calculated and the results were showed in **Figure 6B**, we can find that these of REST method were lower (0.05 ± 0.04) than the others during all the music pieces; while the AR method was 0.52 ± 0.41; the LM method demonstrated highest variance (3.34 ± 2.48) among the three in such source locations. In such situation, LM reference demonstrated a quite low coefficient −0.85 and −0.68 to the standard signal in PZ and P4, respectively. And REST method was also almost the same with the standard signals; the coefficient of every electrode was 1. For AR reference, in all the electrodes, showed high correlations (>0.8) to the standard signal, while in PZ it was 0.98. In LM music from the electrode PZ on the scalp, melody of channel four was decreased, and that made the music sounded different from the others.

Brainwave Music From Real EEG

The brainwave music generated from real EEG recorded in the pain control experiment was analyzed for the comparison of the references. After EEG segments were translated into quartet music pieces (Wu et al., 2013), there were totally 24 × 3 music sequences from two group's subjects with three references. The music features, note pitch, note duration, tempo, scale free

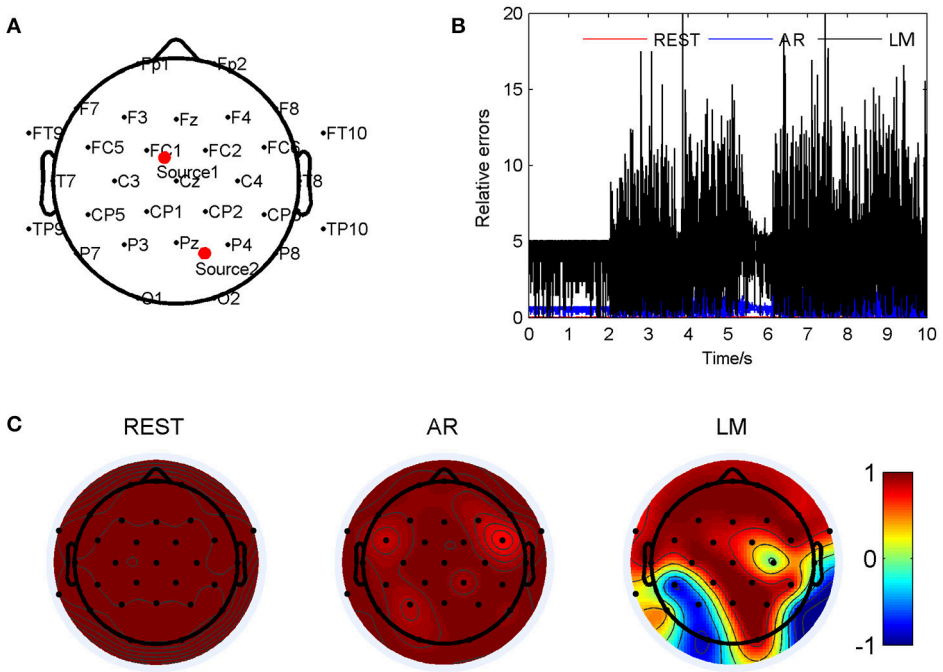

FIGURE 4 | Comparison of the three reference electrode methods for the two sources of BWV 772 shown in **Figure 1B**. **(A)** The location of the sources are (0.254, 0.124, 0.822) and (−0.678, −0.267, 0.473). The red dots indicate the projected positions of the source on the scalp surface. **(B)** Relative errors of the music signals with three references compared to the standard signals. **(C)** Correlation coefficients of three references with the standard signals.

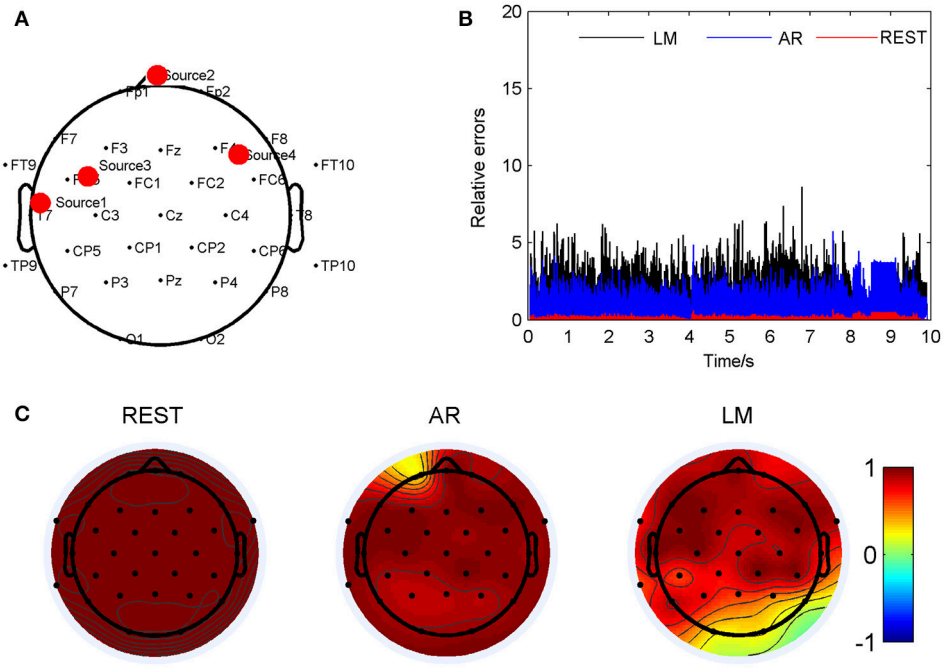

FIGURE 5 | Comparison of the three reference electrode methods for the four sources of K387 shown in **Figure 1C**. **(A)** The location of the sources are (0.087, 0.859, 0.097), (0, 0, −0.076), (0.342, 0.643, 0.473) and (0.495, −0.638, 0.320). The red dots indicate the projected positions of the source on the scalp surface. **(B)** Relative errors of the music signals with three references compared to the standard signals. **(C)** Correlation coefficients of three references with the standard signals.

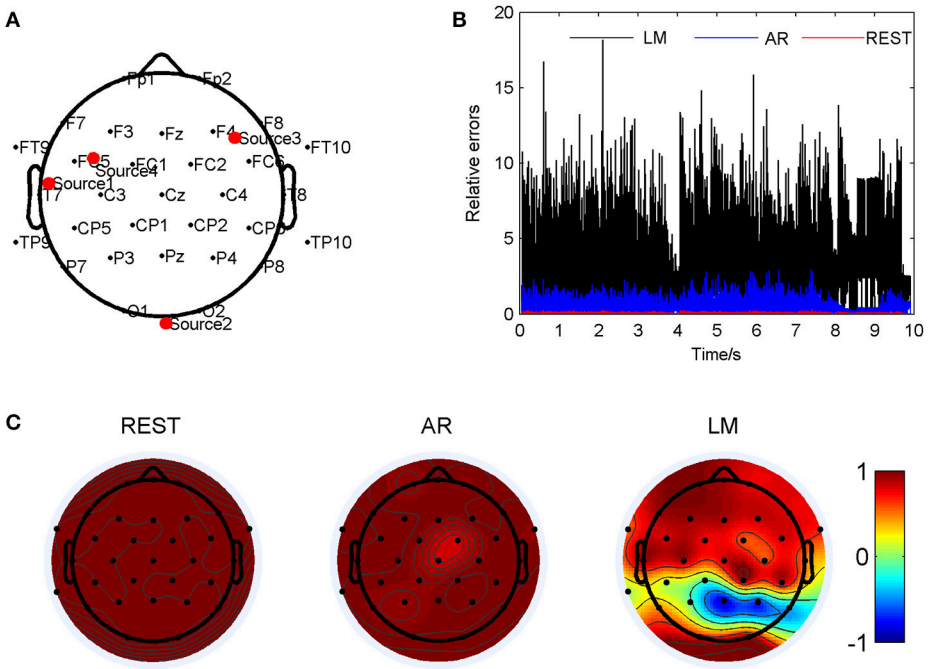

FIGURE 6 | Comparison of the three reference electrode methods for the four sources of K387 shown in **Figure 1C**. **(A)** The location of the sources are (0.087, 0.859, 0.097), (−0.865, −0.030, −0.076), (0.495, −0.638, 0.320) and (0.342, 0.643, 0.473). The red dots indicate the projected positions of the source on the scalp surface. **(B)** Relative errors of the music signals with three references compared to the standard signals. **(C)** Correlation coefficients of three references with the standard signals.

exponent of pitch, and consonance fluctuation were calculated. In MIDI file, the pitch range is from 1 to 127, and 60 represent the middle C. The average pitch of REST was 49.6 ± 10.9; AR was 49.5 ± 11.2; LM was 43.36 ± 10.7. And the differences were significant between REST and LM (*t*-test, $p < 0.01$), AR and LM (*t*-test, $p < 0.01$). However, the REST and AR were not significant different. For all the three references, the differences of music pitch between the two groups were not significant different. The average note duration of REST was 0.71 ± 0.17 s; AR was 0.70 ± 0.15; LM was 0.79 ± 0.18. The REST was significant different from LM (*t*-test, $p < 0.01$), while AR was significant different from LM (*t*-test, $p < 0.01$). The note duration of REST and AR seem to be similar.

The scale free exponents of the music pitch are important in our study. The results were showed in **Figure 7**. The exponents of Group 1 were 1.25 ± 0.16 for REST, 1.28 ± 0.10 for AR, 1.32 ± 0.18 for LM. And for Group 2, REST was 1.38 ± 0.18, AR was 1.45 ± 0.19, and LM was 1.46 ± 0.25. The trend for both two groups was the same: REST < AR < LM. The REST was near 1, which means a more "aesthetic" music, similar with the EEG activities. A two way ANOVA showed significant differences between Group 1 and 2, but no differences between the three references and no interaction of the references and groups. Furthermore, between the two groups, the differences were significant with REST (*t*-test, $p < 0.05$) and AR (*t*-test, $p < 0.05$); while the differences were not significant with LM reference. By listening to the music pieces, it might be easier for distinguishing the two groups when the REST was used.

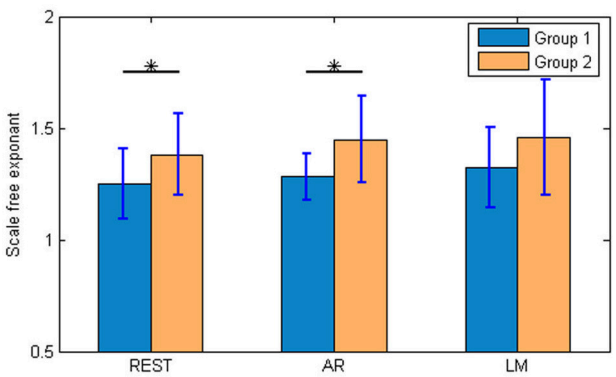

FIGURE 7 | The scale-free exponents of the brainwave music pitch. The scale free exponents of the music pitch were calculated by the Zipf's law. Group 1 was the brainwave music group, while group 2 was the control group. For REST and AR, there were significant differences between the groups. (*t*-test, $^*p < 0.05$).

The consonance fluctuation of these brain music pieces were compared. To calculated the consonance fluctuation, the consonance, which was quantified in terms of the pitch frequency's numerical proportions, at every time point were calculated at first, then the curve of consonance can be obtained, at last, the DFA(detrended fluctuation analysis) were used to analyze the scale exponents of the consonance fluctuation. The

more details can be found in my paper of 2015 (Wu et al., 2015). The scale exponents of consonance fluctuation of REST was 0.85 $\pm$ 0.05, AR was 0.86 $\pm$ 0.04, and LM was 0.88 $\pm$ 0.04. The results of REST was significantly different from LM (*t*-test, $p < 0.05$), however the differences between REST and AR, AR, and LM, were not significant.

Furthermore, the weight of every electrode in the music generation was analyzed. In the translating process of EEG to music, after the data from all the electrodes were changed into music respectively, the notes were selected by a musical filter from the original sequences, so I analyzed the electrodes or regions which were provided more notes in the music generation, which was the weight of electrodes. At last, dividing the number of notes originated from an electrode (weight of electrode) by the total number of notes, I can obtain the probability of electrodes. **Figure 8** demonstrated the topographic map of the probability of electrodes being represented for REST, AR, and LM references. The main region of the music generation was the frontal of head in both two groups, though the group 2 (control group) was more concentrated to the frontal. For the distribution of probability, the REST was significant different from AR at electrode P3, and from LM at FP1, FP2, C4, P3, and P4 (*t*-test, $p < 0.05$). These results mean that the frontal region may play an important role in music generation.

The differences of electrodes' probability between the two groups for the three references were also tested respectively. The results showed that for REST, there were significant differences between Group 1 and Group 2 in electrodes FP1, FP2, and T6. And for AR, FP1, FP2, and T6 were also different. Furthermore, FP1, FP2, T6, C4, P3, P4, and O1 were significantly different for LM reference.

DISCUSSIONS

We can listen to the brain activities through the brainwave methods proposed previously; whether the music is real reflection of the mental, it depends on whether the data is a true represent of the soul. In the proposed work, I inspect the distortion caused by non-zero reference in the scalp recordings and the corresponding music by simulation and real data. This study draws a picture for us that the "musical" dipoles in the brain generating a piece of music sequence, and then how the different references influence the music we can hear outside the brain. The results of the simulation have shown that the music on the scalp is varied accompanying with the number of the source and distorted by different non-zero reference. When there was more than one source, the scalp music distribution is based on the sources' locations. Therefore, it is important to use a proper reference technology to minimum the errors between real values and the scalp recording values when we plan to preserve the musical information of the EEG.

From the View of Brain Signal

Some previous studies compared the three different references method by using simulated dipoles and real EEG data. And the results of simulated data showed that through all the EEG frequency bands including theta, delta, alpha, beta, the features, like power spectra (Trujillo et al., 2017), non-linear features (Chella et al., 2017), the different network connectivity structures, such as default mode network (Qin et al., 2010), the EEG center of mass (Qin et al., 2017), sensor level functional connectivity graphs (Huang et al., 2017), the large-scale brain network (Lei and Liao, 2017), obtained from the REST were more accurate than other references. For real EEG data, there were significant differences existing in the statistics for REST and other references, for example, the ERPs in the audiovisual stimulus, REST changed in the experimental effect (Tian and Yao, 2013). In this study, music is used as the signal source to provide a new view of EEG analysis. Although there are many differences between music waveforms and real EEG data, certain common rhythm exists in the both, i.e., the scale free law (Levitin et al., 2012; Tomasi et al., 2017).

The electrode density and head model are important factors in the reference methods. The previous studies found that the relative error values for Cz and LM references are not noticeably affected by the EEG electrode density. And when electrode density was increasing, the distortion induced by the AR reference may increase (Chella et al., 2017). For the tested montage with 21-channel or 71-channel, REST shows a more reliable reconstruction than AR and LM either with a realistic or a three-layer spherical head model (Liu et al., 2015). Head model is crucial to REST, the more accurate the head model is, the performance of REST is better, so realistic head model usually show better results than the spherical model. However, even in the case of a spherical head model, the REST performance was better than the ones of AR and LM. In this study, 32-channel and the three-concentric-sphere head model were used for simulation, and they are the typical choices in current practices.

The previous studies found that AR reference produced results that were much closer to those of REST, when applied REST, AR and LM references to both simulated and real resting-state EEG data. In the proposed study, the application of the music through the different reference methods demonstrated the same tendency. For most location pairs, REST shows the best, then AR showed high correlation coefficients with the standard signals, and LM is the last one. It means to get the true signal wave, we need to use REST.

From the View of Brain Music

It is interesting when some music concepts and analysis are introduced in the study. After the simulation, the music pieces of three references were compared. There were no significant differences between the music on the scalp when there is one singer in the brain (the single source case). Two parts of the music would be restructured on the scalp when there are two singers in the brain, and the variations of the scalp music compared to the inner actual music depend on the position of the two singers and the reference adopted. However, REST is always much better than LM and AR. For four singers in the brain, the phenomena is similar as two singers. Based on simulation, we can recognize the melody because every voice has its own regular. That means the musical conception may be an inspiration of the neuroscience data analysis.

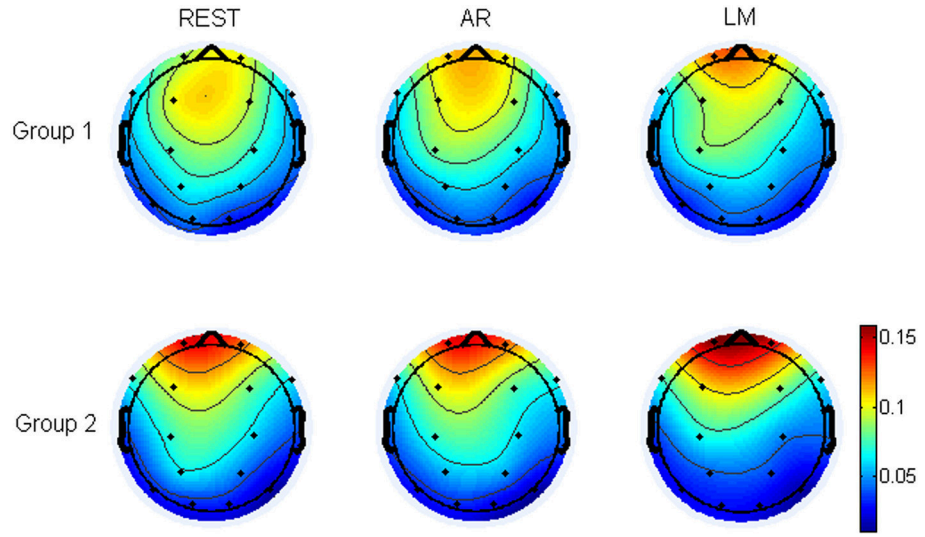

FIGURE 8 | The topographic map of the probability of electrodes being represented for REST, AR and LM references. The topographic map was the average probability for 24 subjects, group 1 (12 subjects) was the brainwave music group, group 2 (12 subjects) was the control group.

Using music as the source signal have two main advantages. First, it can be recognized very easily through our auditory way when there are some varieties of the original signals. Compared with other generated signals, such as random signal, for simulation, music can be heard when it is analyzed. The distorted music parameters, pitch, volume, tempo, melody, and harmony can be preserved. Second, for two or more sources, it is reasonable that using signals of different music parts as sources. Because each part or voice in the music has its own melody line, but when all of the parts are gathered, they become an integrated work. That is similar to the brain. There may be several active centers or network hubs working separately, and all of them constructing the brain. In the simulation, the comparison of the music parts reveals that the influence of the reference choice when the brain having two or more active sources in a novel perspective.

However, music waveform signals are quite different from real EEG in both frequency and amplitude. To investigate the influence, music pieces may be translated to signals which have the same range of frequency and amplitude of EEG, according to the method proposed in my 2009's paper (Wu et al., 2009). Using these generated EEG as sources for simulation, the comparisons are performed with the three references by calculating the relative errors and coefficients. The details of results are shown in Supplementary Materials. The results indicate that the REST causes the least distortion of the sources, then is AR, and the last is LM. When the EEG sources are put in the same location with the music waveform sources, the coefficients' distributions in the two situations are quite similar (see the figures in Supplementary Materials). However, when using EEG or EEG-like signals as sources, we can't identify the differences between the references by just listening, because the method in Wu's paper (Wu et al., 2009) is mainly for EEG to monophonic music, how to translate EEG into two or four channels is still an open problem.

For Real Data Exploration

The real EEG data were used as the materials for generating brain music pieces, and the references have caused some differences in some musical parameters. In the exploration, EEG data from two groups were translated into four voices music which is called quartet, according to two main principles: the first is the scale free law that obeyed by both EEG and music (Wu et al., 2009), and the second is a music tone filter method that finding important note and obtaining a sequence with certain tonality (Wu et al., 2013). The references have influenced the musical melodies, for parameters of music represents the features of EEG data. During music generation, EEG amplitude can be indicated by note pitch and EEG period are related to note duration, therefore the data accuracy was one of the most important factors for the data sonified expressing and analyzing. Furthermore, the brain quartet are consisting of notes which picked up by the music tone filter from certain electrodes. The references have also influenced the effects of music filter, making a various note distribution for the quartet. All of these can result in the differences of pitch and duration among the three references.

The scale free exponents of the music are the crucial property of data analyzing, for that is the bridge and connection between EEG and music according to the translation. First, it is interesting that music of REST's exponents are the most close to 1, the next is AR and the last is LM. Previous studies revealed that scale free, of say the 1/f distribution, is a natural feature of human, from the body movement (Torre and Wagenmakers, 2009) to ion channel (Lowen et al., 1999), and brain activity is no exception (Freeman and Breakspear, 2007; Palva et al., 2013). In music, scale free law exists in pitch, tempo, rhythm, and even harmony. The brain music obtained in the experiment maintains such property during the translation from EEG to music note. If it is believed that the brain music indicates the intrinsic rhythm of brain, REST has provided the most faithful

signals on the scalp because of its most standard exponents. Second, the exponents of scale free are sometimes regarded as an index for states identification, for example, the sleep stages. In our experiment, the difference between two groups are identified by REST and AR, not the LM. Such results reflect the effects of references on comparing data. Consequently, more accurate data can turn out more useful and meaningful results in data analysis.

The weight of every electrode which were showed in **Figure 8** demonstrate the proportion of information provided by each electrode in the music. The filtering criterions, determining which electrodes to be expressed, are derived from the music theory. These criterions make the most stable rhythm and important activities to be represented in the melody. The electrode's weight of three references are different. Although both the brain music group and control group are focused on the frontal region, the distribution of REST can be found with more expressing of the central and occipital region especially in group 1. Such variability makes the identification of the two group more easily.

CONCLUSION

The simulation of music as signal sources in the brain indicates that the references deduce the different scalp music which has been heard. The REST showed the smallest relative errors compared to the AR and LM references, and the highest correlation coefficients with the standard sources. The results of real EEG data proved that REST can provide more accurate and natural topographies on the scalp to represent the inner activities. As an inspiration of the neuroscience data analysis, hearing sound in the brain reveals some essential properties with the help of REST.

AUTHOR CONTRIBUTIONS

DW conceived and designed the study, acquired the data, performed the analysis, interpreted the results, wrote the manuscript and critically reviewed the manuscript.

FUNDING

This research was supported by the Fundamental Research Funds for the Central Universities (2015JBM038, 2016RC022), the National Natural Science Foundation of China projects (NSFC, 81201159, 61773048, 61671049).

ACKNOWLEDGMENTS

The author thanks Dezhong Yao and Peng Xu for discussions of the concept designing and analysis performing, thanks Fali Li for his help of using the REST software.

SUPPLEMENTARY MATERIAL

The Supplementary Material for this article can be found online at: https://www.frontiersin.org/articles/10.3389/fnins.2018.00148/full#supplementary-material

The two original MIDI music and 20 pieces of music (*.wav) were provided as Supplementary Material.

REFERENCES

Adrian, E. D., and Matthews, B. H. C. (1934). The Berger rhythm: potential changes from the occipital lobes in man. *Brain* 57, 355–385. doi: 10.1093/brain/57.4.355

Baier, G., Hermann, T., and Stephani, U. (2007). Event-based sonification of EEG rhythms in real time. *Clin. Neurophysiol.* 118, 1377–1386. doi: 10.1016/j.clinph.2007.01.025

Chella, F., D'Andrea, A., Basti, A., Pizzella, V., and Marzetti, L. (2017). Non-linear analysis of scalp EEG by using bispectra: the effect of the reference choice. *Front. Neurosci.* 11:262. doi: 10.3389/fnins.2017.00262

Daly, I., Williams, D., Kirke, A., Weaver, J., Malik, A., Hwang, F., et al. (2016). Affective brain–computer music interfacing. *J. Neural Eng.* 13:046022. doi: 10.1088/1741-2560/13/4/046022

Essl, M., and Rappelsberger, P. (1998). EEG coherence and reference signals: experimental results and mathematical explanations. *Med. Biol. Eng. Comput.* 36, 399–406. doi: 10.1007/BF02523206

Freeman, W., and Breakspear, M. (2007). Scale-free neocortical dynamics. *Scholarpedia* 2:1357. doi: 10.4249/scholarpedia.1357

Geselowitz, D. B. (1998). The zero of potential. *IEEE Eng. Med. Biol. Mag. Q. Mag. Eng. Med. Biol. Soc.* 17:128. doi: 10.1109/51.646230

Hennig, H. (2014). Synchronization in human musical rhythms and mutually interacting complex systems. *Proc. Natl. Acad. Sci. U.S.A.* 111, 12974–12979. doi: 10.1073/pnas.1324142111

Hinterberger, T., and Baier, G. (2005). Parametric orchestral sonification of EEG in real time. *IEEE Multimedia* 12, 70–79. doi: 10.1109/MMUL.2005.36

Huang, R., Wang, J., Wu, D., Long, H., Yang, X., Liu, H., et al. (2016). The effects of customised brainwave music on orofacial pain induced by orthodontic tooth movement. *Oral Dis.* 22, 766–774. doi: 10.1111/odi.12542

Huang, Y., Zhang, J., Cui, Y., Yang, G., He, L., Liu, Q., et al. (2017). How different EEG references influence sensor level functional connectivity graphs. *Front. Neurosci.* 11:368. doi: 10.3389/fnins.2017.00368

Junghöfer, M., Elbert, T., Tucker, D. M., and Braun, C. (1999). The polar average reference effect: a bias in estimating the head surface integral in EEG recording. *Clin. Neurophysiol.* 110:1149. doi: 10.1016/S1388-2457(99)00044-9

Lei, X., and Liao, K. (2017). Understanding the influences of EEG reference: a large-scale brain network perspective. *Front. Neurosci.* 11:205. doi: 10.3389/fnins.2017.00205

Leistedt, S., Dumont, M., Lanquart, J. P., Jurysta, F., and Linkowski, P. (2007). Characterization of the sleep EEG in acutely depressed men using detrended fluctuation analysis. *Clin. Neurophysiol.* 118, 940–950. doi: 10.1016/j.clinph.2007.01.003

Levitin, D. J., Chordia, P., and Menon, V. (2012). Musical rhythm spectra from Bach to Joplin obey a 1/f power law. *Proc. Nat. Acad. Sci. U.S.A.* 109, 3716–3720. doi: 10.1073/pnas.1113828109

Liu, L., Wei, J., Zhang, H., Xin, J., and Huang, J. (2013). A statistical physics view of pitch fluctuations in the classical music from bach to chopin: evidence for scaling. *PLoS ONE* 8:e58710. doi: 10.1371/journal.pone.0058710

Liu, Q., Balsters, J. H., Baechinger, M., van der Groen, G. O., Wenderoth, N., and Mantini, D. (2015). Estimating a neutral reference for electroencephalographic recordings: the importance of using a high-density montage and a realistic head model. *J. Neural Eng.* 12:056012. doi: 10.1088/1741-2560/12/5/056012

Lowen, S. B., Liebovitch, L. S., and White, J. A. (1999). Fractal ion-channel behavior generates fractal firing patterns in neuronal models. *Phys. Rev. E* 59, 5970–5980. doi: 10.1103/PhysRevE.59.5970

Lu, J., Wu, D., Yang, H., Luo, C., Li, C., and Yao, D. (2012). Scale-free brain-wave music from simultaneously EEG and fMRI recordings. *PLoS ONE* 7:e49773. doi: 10.1371/journal.pone.0049773

Manaris, B., Romero, J., Machado, P., Krehbiel, D., Hirzel, T., Pharr, W., et al. (2005). Zipf's law, music classification, and aesthetics. *Comput. Music J.* 29, 55–69. doi: 10.1162/comj.2005.29.1.55

Marzetti, L., Nolte, G., Perrucci, M. G., Romani, G. L., and Del Gratta, C. (2007). The use of standardized infinity reference in EEG coherency studies. *Neuroimage* 36, 48–63. doi: 10.1016/j.neuroimage.2007.02.034

Miranda, E. R. (2010). Plymouth brain-computer music interfacing project: from EEG audio mixers to composition informed by cognitive neuroscience. *Int. J. Arts Technol.* 3, 154–176. doi: 10.1504/IJART.2010.032562

Miranda, E. R., and Brouse, A. (2005). Interfacing the brain directly with musical systems: on developing systems for making music with brain signals. *Leonardo* 38, 331–336. doi: 10.1162/0024094054762133

Nunez, P. L., Srinivasan, R., Westdorp, A. F., Wijesinghe, R. S., Tucker, D. M., Silberstein, R. B., et al. (1997). EEG coherency. I: statistics, reference electrode, volume conduction, Laplacians, cortical imaging, and interpretation at multiple scales. *Electroencephalogr. Clin. Neurophysiol.* 103, 499. doi: 10.1016/S0013-4694(97)00066-7

Palva, J. M., Zhigalov, A., Hirvonen, J., Korhonen, O., Linkenkaer-Hansen, K., and Palva, S. (2013). Neuronal long-range temporal correlations and avalanche dynamics are correlated with behavioral scaling laws. *Proc. Nat. Acad. Sci. U.S.A.* 110, 3585–3590. doi: 10.1073/pnas.1216855110

Qin, Y., Xin, X., Zhu, H., Li, F., Xiong, H., Zhang, T., et al. (2017). A comparative study on the dynamic EEG center of mass with different references. *Front. Neurosci.* 11:509. doi: 10.3389/fnins.2017.00509

Qin, Y., Xu, P., and Yao, D. (2010). A comparative study of different references for EEG default mode network: the use of the infinity reference. *Clin. Neurophysiol.* 121, 1981–1991. doi: 10.1016/j.clinph.2010.03.056

Rosenboom, D. (1976). *Biofeedback and the Arts, Results of Early Experiments*. Vancouver, BC: Aesthetic Research Centre of Canada.

Rosenboom, D. (1997). *Extended Musical Interface with the Human Nervous System: Assessment and Prospectus*. San Francisco, CA: Internationhal Society for the Arts, Sciences and Technology.

Tian, Y., and Yao, D. (2013). Why do we need to use a zero reference? Reference influences on the ERPs of audiovisual effects. *Psychophysiology* 50, 1282–1290. doi: 10.1111/psyp.12130

Tomasi, D. G., Shokri-Kojori, E., and Volkow, N. D. (2017). Brain network dynamics adhere to a power law. *Front. Neurosci.* 11:72. doi: 10.3389/fnins.2017.00072

Torre, K., and Wagenmakers, E. J. (2009). Theories and models for 1/f(β) noise in human movement science. *Hum. Mov. Sci.* 28, 297–318. doi: 10.1016/j.humov.2009.01.001

Trujillo, L. T., Stanfield, C. T., and Vela, R. D. (2017). The Effect of Electroencephalogram (EEG) reference choice on information-theoretic measures of the complexity and integration of EEG signals. *Front. Neurosci.* 11:425. doi: 10.3389/fnins.2017.00425

Väljamäe, A., Steffert, T., Holland, S., Marimon, X., Benitez, R., Mealla, S., et al. (2013). "A review of real-time EEG sonification research," in *International Conference on Auditory Display 2013*, (Lodz), 85–93.

Wu, D., Kendrick, K. M., Levitin, D. J., Li, C., and Yao, D. (2015). Bach is the father of harmony: revealed by a 1/f fluctuation analysis across musical genres. *PLoS ONE* 10:e0142431. doi: 10.1371/journal.pone.0142431

Wu, D., Li, C. Y., and Yao, D. Z. (2009). Scale-free music of the brain. *PLoS ONE* 4:e5915. doi: 10.1371/journal.pone.0005915

Wu, D., Li, C., and Yao, D. (2013). Scale-free brain quartet: artistic filtering of multi-channel brainwave music. *PLoS ONE* 8:e64046. doi: 10.1371/journal.pone.0064046

Wu, D., Li, C., Liu, J., Lu, J., and Yao, D. (2014). Scale-free brain ensemble modulated by phase synchronization. *J. Zhejiang Univ. Sci. C* 15, 821–831. doi: 10.1631/jzus.C1400199

Wu, D., Li, C., Yin, Y., Zhou, C., and Yao, D. (2010). Music composition from the brain signal: representing the mental state by music. *Comput. Intell. Neurosci.* 2010:267671. doi: 10.1155/2010/267671

Yao, D. (2000). High-resolution EEG mappings: a spherical harmonic spectra theory and simulation results. *Clin. Neurophysiol.* 111, 81–92. doi: 10.1016/S1388-2457(99)00205-9

Yao, D. (2001). A method to standardize a reference of scalp EEG recordings to a point at infinity. *Physiol. Meas.* 22:693. doi: 10.1088/0967-3334/22/4/305

Yao, D. (2017). Is the surface potential integral of a dipole in a volume conductor always zero? a cloud over the average reference of EEG and ERP. *Brain Topogr.* 30, 161–171. doi: 10.1007/s10548-016-0543-x

Yao, D., Wang, L., Arendt-Nielsen, L., and Chen, A. C. (2007). The effect of reference choices on the spatio-temporal analysis of brain evoked potentials: the use of infinite reference. *Comput. Biol. Med.* 37:1529. doi: 10.1016/j.compbiomed.2007.02.002

Yao, D., Wang, L., Oostenveld, R., Nielsen, K. D., Arendt-Nielsen, L., and Chen, A. C. (2005). A comparative study of different references for EEG spectral mapping: the issue of the neutral reference and the use of the infinity reference. *Physiol. Meas.* 26, 173. doi: 10.1088/0967-3334/26/3/003

Zhai, Y., and Yao, D. (2004). A study on the reference electrode standardization technique for a realistic head model. *Comput. Methods Prog. Biomed.* 76, 229–238. doi: 10.1016/j.cmpb.2004.07.002

Conflict of Interest Statement: The author declares that the research was conducted in the absence of any commercial or financial relationships that could be construed as a potential conflict of interest.

frontiers in Neuroscience

ORIGINAL RESEARCH
published: 13 March 2018
doi: 10.3389/fnins.2018.00158

A Comparative Study of Standardized Infinity Reference and Average Reference for EEG of Three Typical Brain States

*Gaoxing Zheng, Xiaoying Qi, Yuzhu Li, Wei Zhang and Yuguo Yu**

State Key Laboratory of Medical Neurobiology, School of Life Science and Institutes of Brain Science, Center for Computational Systems Biology, Fudan University, Shanghai, China

The choice of different reference electrodes plays an important role in deciphering the functional meaning of electroencephalography (EEG) signals. In recent years, the infinity zero reference using the reference electrode standard technique (REST) has been increasingly applied, while the average reference (AR) was generally advocated as the best available reference option in previous classical EEG studies. Here, we designed EEG experiments and performed a direct comparison between the influences of REST and AR on EEG-revealed brain activity features for three typical brain behavior states (eyes-closed, eyes-open and music-listening). The analysis results revealed the following observations: (1) there is no significant difference in the alpha-wave-blocking effect during the eyes-open state compared with the eyes-closed state for both REST and AR references; (2) there was clear frontal EEG asymmetry during the resting state, and the degree of lateralization under REST was higher than that under AR; (3) the global brain functional connectivity density (FCD) and local FCD have higher values for REST than for AR under different behavior states; and (4) the value of the small-world network characteristic in the eyes-closed state is significantly (in full, alpha, beta and gamma frequency bands) higher than that in the eyes-open state, and the small-world effect under the REST reference is higher than that under AR. In addition, the music-listening state has a higher small-world network effect than the eyes-closed state. The above results suggest that typical EEG features might be more clearly presented by applying the REST reference than by applying AR when using a 64-channel recording.

Keywords: brain lateralization effect, brain functional connectivity density, phase lag index, weighted small-world network, average reference (AR), reference electrode standardization technique (REST)

OPEN ACCESS

Edited by:
Maria L. Bringas, Clinical Hospital of Chengdu Brain Science Institute, China

Reviewed by:
Yury (Juri) Kropotov, N. P. Bechtereva Institute of the Human Brain (RAS), Russia
Dezhong Yao, University of Electronic Science and Technology of China, China
Peng Xu, University of Electronic Science and Technology of China, China

***Correspondence:**
Yuguo Yu
yuyuguo@fudan.edu.cn

Specialty section:
This article was submitted to Brain Imaging Methods, a section of the journal Frontiers in Neuroscience

Received: *22 December 2017*
Accepted: *27 February 2018*
Published: *13 March 2018*

Citation:
Zheng G, Qi X, Li Y, Zhang W and Yu Y (2018) A Comparative Study of Standardized Infinity Reference and Average Reference for EEG of Three Typical Brain States. Front. Neurosci. 12:158. doi: 10.3389/fnins.2018.00158

INTRODUCTION

Electroencephalography (EEG) records the mean electrical activity of the brain in different sites of the head (Berger, 1929). The signals reflect the total electronic potential projected from large pools of the extracellular current flows of tens of thousands of neurons under the electrode recording site. It is one of the most important tools in clinical neurophysiology and is also applied in human cognitive research because of its high temporal resolution and noninvasive safety feature (Cohen, 2017). However, to date, EEG analysis, especially in clinical diagnostic examinations, still relies

primarily on visual inspection, and there is a lack of standard analysis approaches and standard references (Nunez et al., 1997) to help decipher the functional meaning of the scalp-recorded EEG. To evaluate the accurate characteristics of EEG (including electrode polarity, scalp area, frequency spectrum, latency and voltage amplitude), it is usually necessary to use an inactive electrode as a reference, making the selection of a reference electrode particularly relevant and critical (Yao, 2001). Electrode reference methods commonly used in EEG studies include the average reference (AR), the linked mastoid reference (LM), the vertex reference (Cz), and the infinity zero reference. Previous studies using model simulation have revealed that non-zero references, including AR, LM and Cz, can result in distortion of scalp power spectral distribution, changes in the potential of electrodes and differences in network configurations (Yao et al., 2005, 2007). Yao et al. have developed a theoretical approach to propose an infinity zero reference to minimize errors by using the reference electrode standardization technique (REST) (Yao, 2001; Dong et al., 2017). REST is a method that approximately converts a record that uses a point or mean potential on the scalp as a reference point to a spatial infinity point as a reference position. The physical basis of this operation is that the potentials before and after conversion are all derived from the actual neural electrical activity source in the brain (Hu et al., 2018). Although different reference electrodes have been investigated in many studies (Ferree, 2006; Nunez and Srinivasan, 2006; Huang et al., 2017; Lei and Liao, 2017; Qin et al., 2017), most of them are based on model simulated data; it is still unclear what the accurate estimation of the differences is for real EEG recordings in various experimental conditions.

While different cognitive tasks involve different brain regions, more researchers are focusing on the changes of brain functional networks (Bullmore and Sporns, 2009; Van Den Heuvel and Pol, 2010). Studying the effect of reference electrodes on brain functional networks may be critically important to access functional meanings of EEG recordings.

Researchers have found that biological networks generally have the characteristics of small-world network properties, that is, the network has a large clustering coefficient and a short characteristic path length (Watts and Strogatz, 1998; Strogatz, 2001). Shi et al. found in electrophysiological recordings of primary visual cortex in mice that their coding properties have small-world structural properties (Shi et al., 2015). He et al. applied the reciprocal of global efficiency instead of the traditional characteristic path length in the study of magnetic resonance brain network characteristics, effectively avoiding the problem of isolated points of the network (Liao et al., 2017). Wu et al. found that music perception shows an enhancement of small-world network organizations in brain functional connectivity (Wu et al., 2012, 2013).

The aim of this study is to directly evaluate the choice influence of AR and REST on the properties of brain lateralization effect, brain functional connectivity density and small-world network characteristics in the analysis of recorded EEG signals during resting and music listening states.

MATERIALS AND METHODS

Participants

The experiment collected EEG data from 38 healthy subjects (mean age 21.55 years, standard deviation (SD) 3.70; right-handed; 18 females and 20 males). All participants signed an informed consent form before the experiment. This project was approved by the Ethics Committee of Fudan University. Most of the subjects had no professional music training except for one student who had previously received piano training. None of the participants took medication within the first 2 weeks of the experiment or had a history of potential mental illness.

Experimental Procedures and EEG Recording

EEG data were recorded using the actiCHamp 64-channel EEG system from Brian Products, and the sampling rate was 1,000 Hz. Using Cz as a reference, all the other electrodes were placed symmetrically on both sides of the brain. The impedance of all electrodes was maintained below 10 kΩ during the experiment. The entire experimental paradigm was completed in the E-Prime Pro 2.0 software environment. At the beginning of the experiment, the participants were asked to keep their eyes closed for 1 min, and then to keep their eyes opened and fixed on the screen for 1 min. After a short break, they listened to the selected music for approximately two and a half minutes with their eyes closed. Next, participants were asked to keep their eyes open for 1 min and then keep their eyes closed for another minute in a quiet condition. The detailed experimental procedure is shown in **Figure 1**.

In the experimental protocol, the experiment consists of 60 s eyes closed, 60 s eyes open, 150 s music, 60 s eyes closed and 60 s eyes open with EEG recordings. In the data preprocessing, the 10 s before and after each state (eyes closed, eyes open or music state) are discarded in order to reduce the error caused by the moment of state change, and the remaining EEG data were used for analysis. We choose the first period of eyes closed and eyes open because the brain activity in the second period may be influenced by the previous music listening.

Data Preprocessing

We used MATLAB R2015b to process the EEG data. EEG data were divided into different segments according to the event marker, and each segment was filtered to be in a frequency range of 0.5–100 Hz. Meanwhile, the 50 Hz frequency interference was removed by using a notch filter. Data preprocessing was performed using the EEGLAB toolbox (Delorme and Makeig, 2004) to remove artifacts based on the ICA algorithm. The plugin ADJUST toolbox identified the artifact components for removal. All preprocessing was kept equivalent except for choosing the two different reference methods. We aimed to compare the difference in the data processing when using the average reference (AR) and REST (Yao, 2001) to evaluate the influences of reference selection on the analysis. We applied the MATLAB ANOVA toolbox to examine the differences in using these references.

In traditional studies, a large amount of experimental analysis advocated for the average reference as the best available reference

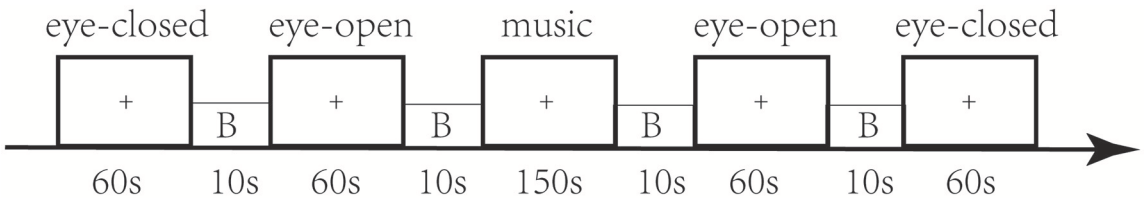

FIGURE 1 | Experimental protocol used in our study. All subjects were asked to keep their eyes closed for 1 min without thinking about anything, and after a short break (B = Break), they kept their eyes fixed on the "+" in the middle of the screen for 1 min. After 2 min in the resting state, there was two and half minutes of music playing; subjects were asked to keep their eyes closed and listen quietly without thinking about anything. Next, there was 1 min with eyes open, followed by 1 min of eyes closed, and then the experiment was complete.

option during EEG recording and analysis. As the number of electrodes is large enough to cover the whole brain, it is widely believed that the average potential of all the electrodes can be regarded as approaching the zero-potential point (Bertrand et al., 1985). However, a more recent paper (Yao, 2017) noted that such a zero integral assumption has been proven only for a spherical surface. Indeed, the potential integral over the surface of a dipole in a volume conductor may not be zero, depending on the shape variances of the head-shape conductor and the orientation changes of the head conductor with electronic signals flowing through it. Thus, the average reference might not be a theoretical "gold standard" reference. In particular, in the case of small numbers of electrodes in the EEG recording, AR may provide a large biased estimate of reference-independent potentials. To entirely resolve the problems involved in using body surface points for referencing, a reference with neutral potential is required. Theoretically, a point at infinity is far from brain sources and has an ideally neutral potential. Yao et al. (Yao, 2001; Dong et al., 2017) proposed a reference electrode standardization technique (REST) to mathematically transform the actual multi-channel EEG data recorded with a scalp point reference to recordings referenced at infinity reference (the Matlab toolbox for REST transformation can be downloaded at www.neuro.uestc.edu.cn/rest) (Dong et al., 2017). This technique transforms the EEG potentials referenced at AR into potentials referenced to an infinity point, i.e., a zero-potential point. For both the AR and REST methods, this experiment has used the same placement of the electrodes. Prior to the REST transformation, the real electrode coordinates and the scalp EEG recordings with average reference (AR) should be obtained first from the experiment method as well as EEGLAB pre-processing process. A head model and equivalent source model in the REST toolbox are then implemented to calculate the new channel data, referenced at the infinity reference.

To verify the validity of EEG data after preprocessing, the power spectrum at resting state were analyzed. In general, the alpha rhythm is the prominent EEG wave pattern of an adult who is awake but relaxed with eyes closed. Each region of the brain has a characteristic alpha rhythm, while alpha waves of larger amplitude are generally observed in the frontal and occipital regions. The amplitudes of alpha waves diminish when subjects open their eyes. This is called the alpha-blocking effect. To quantify under which reference condition the alpha-blocking effect is distinguished, we calculated the reduction of total alpha power $\overline{\Delta P_\alpha}$ in the frequency range of 8–12 Hz for each channel and then averaged over 64 channels.

$$\overline{\Delta P_\alpha} = \frac{1}{64}\sum_{i=1}^{64}\sum_{f=8}^{12}[(log_{10}(P_{close}(f)) - log_{10}(P_{open}(f))) / log_{10}(P_{close}(f))] \quad (1)$$

where $P_{close}(f)$ and $P_{open}(f)$ represent power spectrum of recorded EEG signals.

All the alpha-blocking effects of the 38 subjects were calculated to compare the difference between REST and AR.

Brain Lateralization Analysis

The human brain has specific task division in the process of information processing, and different brain regions have their own preferences in handling tasks LeMay, 1977). Studies have indicated that there is typical left brain lateralization in the language region (e.g., Broca Area and Wernicke Area) and in the default network (e.g., lateral intraparietal sulcus, anterior insula, area MT, and frontal eye fields), whereas there was significant right-lateralization of the attention control network (Stephan et al., 2003; Nielsen et al., 2013). Researchers have found that the degree of lateralization of the brain is significantly different between patients with autism spectrum disorders or schizophrenia and normal people, and the study of brain lateralization may be important for understanding the mechanism of neurological disease (Chance et al., 2008; Kleinhans et al., 2008). In this paper, we analyzed the lateralization of the prefrontal cortex brain regions under the resting states. We used the logarithm of the power spectrum in the alpha band to obtain the lateralization index (LI), calculated as LI =(Pleft-Pright)/(Pleft+Pright), to quantify the lateralization effect. Our aim was to evaluate the difference between AR and REST from the perspective of the brain lateralization effect.

Phase Lag Index

We built up networks of EEG brain functions in an attempt to determine the effect of different reference choices on analysis results under different behavior states. To construct the brain functional network, we defined the relationship between the two

electrodes as the state of connection among the networks. The phase lag index (PLI) was calculated to evaluate the connection characteristics between each pair of electrodes (Wu et al., 2013; Hardmeier et al., 2014). PLI indeed quantifies the consistency of phase synchronizations between two electrodes (Stam et al., 2007). For any segment of EEG signal $x(t)$, its phase $\phi(t)$ can be calculated by a Hilbert transform:

$$\phi(t) = \arctan \frac{x_H(t)}{x(t)} \tag{2}$$

where $x_H(t)$ is the imaginary part of the signal after the Hilbert transform. For two signals, $x_a(t)$and$x_b(t)$, the phase difference can be expressed as Equation (3):

$$\varphi_{ab}(t) = \phi_a(t) - \phi_b(t) \tag{3}$$

The PLI is then calculated as:

$$PLI_{ab} = \left| \frac{1}{N} \sum_{n=0}^{N-1} sign(\varphi_{ab}(n)) \right| \tag{4}$$

where $sign(\varphi_{ab}(n))$ returns 1 when $\varphi_{ab}(n) > 0$ and returns -1 when $\varphi_{ab}(n) < 0$. The symbol N is the number of sampling points. The stronger the nonzero phase locking is, the larger PLI and stronger phase synchronization will be. The PLI value is restricted in the range of 0∼1, and PLI = 0 means no coupling (or coupling with a relative phase that encircled 0 modπ , which is likely to result from volume conduction). PLI = 1 indicates the condition of strict phase locking at a constant nonzero phase lag.

Network Analysis

To study brain functional connectivity in different states, global brain functional connectivity density (GFCD) and local brain functional connectivity density (LFCD) (Tomasi and Volkow, 2010, 2011) were adopted. GFCD characterizes the connection between one electrode and the others among the whole brain, and LFCD can characterize the connectivity relationship between local scalp recording channel networks. To access the LFCD of the preprocessed EEG activities, there are two parameters to calculate: the threshold Tc determines the significant correlations between two channels, and the local cluster radius determines the size of the local scalp recording networks. Taking into account that a lower Tc may increase the false positive rate and become larger with lower sensitivity, we computed Tc based on the small network, and the local cluster radius was set to 5 cm. We first computed the PLI for all pairs of EEG channels. The PLI values were considered significant if they were larger than the Tc, and the number of significant PLI values per channel was computed as LFCD values. The preprocessing and post-processing steps of GFCD are similar to LFCD, except with the local cluster restrictions.

Weighted Small-World Network

This network consists of a series of points and the edges that connect these points. Above, we used the PLI to describe the functional connection strength of each pair of electrodes, and then we could construct a brain network using the PLI matrix (Stam et al., 2007; Hardmeier et al., 2014). Here, we set the thresholds (start is 0.01, step is 0.01, end is 0.99) to construct different brain functional networks using different thresholds (Liu et al., 2008; Rubinov and Sporns, 2010). We investigate the clustering coefficients and characteristic path lengths to compare the difference of network characteristics under different reference electrodes. In this paper, we choose a weighted network, as it can more truly reflect the functional connections of the brain network, and we define the PLI as the weight between the two vertexes when the value is greater than the threshold.

For a network, the clustering coefficient of the vertex i characterizes the proportion of connections among their neighbors. It can be calculated as (Onnela et al., 2005)

$$C_i = \frac{\sum_{j \neq i} \sum_{\substack{k \neq i \\ k \neq j}} w_{ij} w_{ik} w_{jk}}{\sum_{j \neq i} \sum_{\substack{k \neq i \\ k \neq j}} w_{ij} w_{ik}} \tag{5}$$

Where w_{ij} is the edge weight (i.e., PLI value) between vertex i and j, when the PLI is larger than a given threshold, otherwise, w equals 0.

The clustering coefficient of the whole network can be obtained by averaging the clustering coefficient over all vertexes.

$$C = \frac{1}{N} \sum_{i=1}^{N} C_i \tag{6}$$

where N represents the number of nodes in the network. The traditional characteristic path length is defined as the average of the distance between any two nodes; such a definition will bring outliers in the network. We applied the global efficiency to characterize the path length of a weighted network, in which the length of an edge equals the reciprocal of the edge weight when it does not equal 0, while it returns infinity if the weight equals 0. The shortest path length between node i and node j was defined asd_{ij}, and the characteristic path length of the entire network can be defined as the reciprocal of global efficiency (Latora and Marchiori, 2001).

$$L = \frac{1}{E} = \frac{1}{(1/N(N-1)) \sum_{i=1}^{N} \sum_{\substack{j=1 \\ j \neq i}}^{N} d_{ij}^{-1}} \tag{7}$$

where N represents the number of nodes in the network. We calculated the clustering coefficient divided by the characteristic path length as the small-world property (SW). SW characterizes the efficiency of network information transmission and the network connection cluster size (Bassett and Bullmore, 2017). Then, small-world effects under different states were calculated to evaluate the influences of reference choice.

$$SW = \frac{C}{L} \tag{8}$$

RESULTS

Alpha-Blocking Results

The human alpha rhythm is generally defined as neural electronic oscillations with a frequency of 8–12 Hz and is normally recorded as sinusoidal waves with larger amplitudes over posterior head regions, present in approximately 95% of healthy adults, especially during wakeful relaxation with an eyes-closed resting state (Berger, 1929). The alpha waves are temporarily blocked or largely reduced by in the influx of light input during the eyes-open state or other afferent stimuli (see **Figures 2A,B**). Pfurtscheller (Pfurtscheller and Klimesch, 1990) conceived the stimulus-induced alpha-blocking phenomenon as desynchronized neural population activities during active stimuli. Smith et al. (1998) have observed unilateral alpha rhythm to eye opening and closing, that is, right-sided alpha activity appears with the left eye closed, while left-sided alpha activity occurs with the right eye closed. Alpha-blocking occurs with the opening of both eyes. Therefore, in our study, we could use the alpha-blocking effect with eyes open compared with eyes closed to monitor the stability of experimental recording processes.

We first quantified the alpha-blocking effect of the eyes-open condition compared with the eyes-closed condition to verify the validity of the data (see **Figures 2A,B**). By calculating the difference in the logarithm of alpha wave power spectrum between eyes-closed and eyes-open as the signal-to-noise ratio (SNR), we observed that 19 out of 38 subjects had a larger alpha-blocking effect with REST as a reference than with AR (**Figure 2C**). Matlab ANOVA Toolbox was applied to test the statistical significance between AR and REST of the alpha-blocking effect, and ANOVA1 analysis showed there was no significant difference [$F_{(1, 74)} = 0.02, P = 0.8842 > 0.05$] between AR and REST in the alpha-blocking effect. The two methods were almost equivalent to each other in the analysis of the alpha-blocking effect of the eyes-open condition.

Brain Lateralization Effect

Figures 3A,B depicts the effects on the EEG data preprocessing and the power spectrum analysis under AR and REST. REST appeared to make the signal smoother than AR. Left and right lateral cerebral hemispheric effects at resting state in the prefrontal area please see **Figure 3C** (Left: Fp1, AF7, AF3, F7, F5, F3, F1; Right: FP2, AF8, AF4, F8, F6, F4, F2) showed that there was indeed more alpha wave activity in the right brain than in the left. Additionally, REST had a greater degree of lateralization than AR (**Figure 3D**). The ANOVA1 indicated that there was no significant difference between AR and REST, whether in the eyes-open state [$F_{(1, 74)} = 1.55$, $P = 0.2164 > 0.05$] or in the eyes-closed state [$F_{(1, 74)} = 3.11$, $P = 0.0819 > 0.05$]. The statistical results showed that the different references may induce a difference in brain lateralization. However, the differences are not statistically significant between AR and REST.

Brain Functional Connectivity Density Results

The result of global functional connectivity density (Global FCD) showed that brain functional connectivity is stronger in the eyes-closed state than in the eyes-open state ($p < 0.01$, ANOVA1 analysis). The distribution of FCD under the eyes-closed state was larger in the left frontal area than other regions, indicating that the strength of the brain networks was much more activated at rest, especially in the alpha band. The distinction between eyes-closed and music-listening is obvious in full bands and low frequencies (e.g., theta and delta bands), illustrating that listening to music can activate slow-wave brain rhythms in frontal lobes. The comparison between REST and AR indicated that brain functional connectivity density under the REST condition has a larger value than the AR condition in the eyes-open state in all frequency bands for both global FCD (see **Figure 4**) and local FCD (see **Figure 5**). The averaged global and local FCD values under the eyes-closed condition are significantly higher than those under the eyes-open condition in full, alpha, beta and gamma frequency bands (Matlab ANOVA1, $p < 0.01$), while the music-listening condition is almost equivalent to the eyes-closed condition (see right panels of **Figures 4A–D**, **5A–D**). The significant difference analysis is provided in the Supplementary Material for the right sub-panels in **Figures 4**, **5**. Table S2 lists the statistically significant results of **Figure 4** and Figure S2. Table S3 lists the statistically significant results of **Figure 5** and Figure S3.

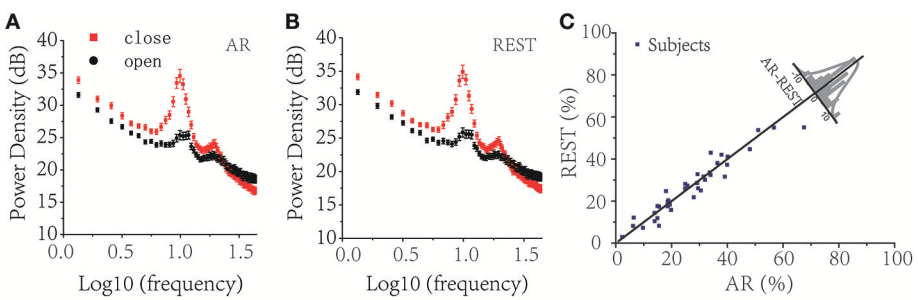

FIGURE 2 | Resting EEG Power spectrum analysis between eyes-closed (red square solid points) and eyes-open (black round solid dots) under different reference choices. **(A)** AR, **(B)** REST. **(C)** Difference of alpha-blocking rate (characterized as $\overline{\Delta P_\alpha}$ under alpha band, 8–12 Hz, Pclose is the summation of logarithm of eyes-closed power spectrum and Popen is the summation of the logarithm of the eyes-open power spectrum) of 38 subjects (average all electrodes) at different reference electrodes (AR & REST), in which 19 of 38 subjects showed that REST performed better than AR.

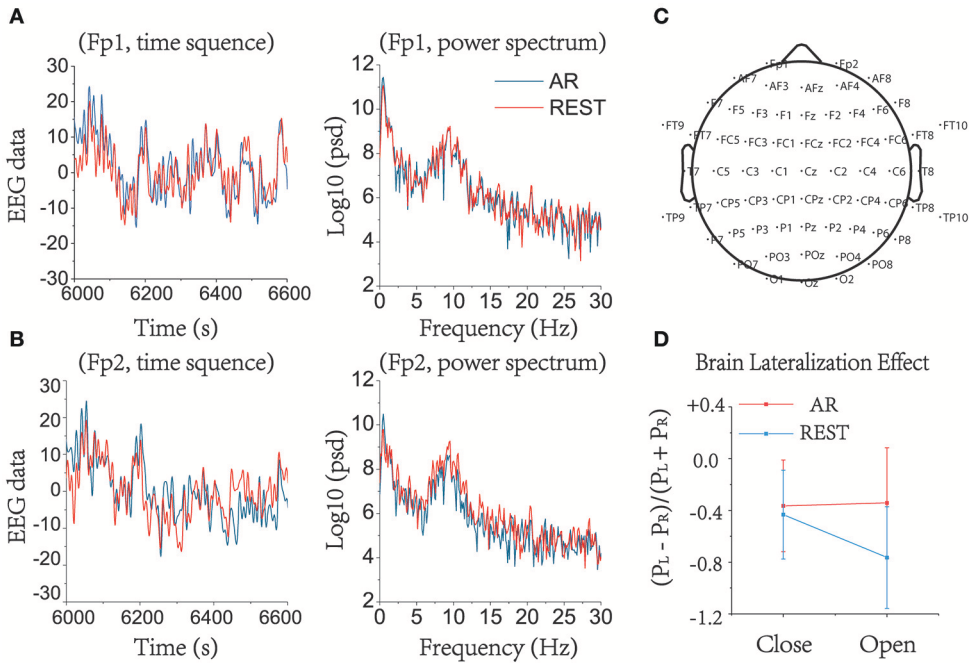

FIGURE 3 | Brain lateralization effect in prefrontal area (Left: Fp1, AF7, AF3, F7, F5, F3, F1; Right: FP2, AF8, AF4, F8, F6, F4, F2) in alpha band under resting state. EEG raw data and power spectrum under eyes-closed when using AR and REST as a reference in **(A)** Fp1. **(B)** Fp2. It can be seen that AR and REST can result in differences when preprocessing the data. **(C)** The array of 64 electrodes used in this study. **(D)** Brain lateralization effect in alpha band between left prefrontal area and right prefrontal area, characterized as (PL – PR)/(PL + PR). The degree of lateralization under REST was higher than under AR.

Brain Functional Network Results

When comparing different resting states, we found that the values of small-world characteristics in the eyes-closed condition are more significant than those of the eyes-open condition (Matlab ANOVA1 analysis, $p < 0.01$). Furthermore, the small-world values for all the different states under the REST reference are observed to be higher than those for the AR condition (**Figure 6**). In addition, the results of different frequency band analysis indicated that brain have a larger small-world network property in the eyes-closed state than in the eyes-open state (**Figure 6**). We calculated the sum of the small-world values within the significant threshold range (threshold from 0.2 to 0.5) and found that the small-world effect showed the following trend: SWmusic > SWclose > SWopen in full- and low-frequency bands (including delta, theta and alpha bands). Additionally, the difference between eyes-closed and eyes-open was significant in full, alpha, beta and gamma frequency bands ($p < 0.01$, ANOVA1), and the music-listing state and eyes-closed state have no significant difference in all bands ($p > 0.05$, ANOVA1) (see right panel of **Figures 6A–D**, and Figure S1). Please also see Table S1 and Figure S4 for the statistically significant results for **Figure 6**.

DISCUSSION

In recent years there have been an increasing number of theoretical and experimental studies suggesting the superior merits of REST. Over the years, many researchers have provided evidence and advice on the choice of different reference electrodes. Simulation and experimental ERP studies with a visual oddball paradigm indicated that AR and LM (Linked Mastoids) may change the amplitude of P300 and distort the CM trajectory and its instantaneous velocity, while REST continues to provide objective results (Qin et al., 2017). A large-scale brain network simulation analysis compared REST with Fz, Oz, LM and AR and showed that the relative errors followed the pattern REST < AR < LM < (Fz, Oz), which indicated that REST was a potentially preferable reference (Lei and Liao, 2017). In addition, high electrode density helps to lower the re-referencing reconstruction errors for both AR and REST (Liu et al., 2015). A functional connectivity graph study showed that REST not only achieved excellent performance for superficial and radial sources but also performed stable and robust variable source locations and orientations, while AR performed stably only when there was no upward component in the sources' orientation (Huang et al., 2017). With high-density electrode coverage, AR may approach the true reference method, as it averages the signals and noise of all the electrodes (Ferree, 2006; Nunez and Srinivasan, 2006).

This study aimed to evaluate the differences between AR and REST from the perspective of power spectrum density, the brain lateralization effect and brain functional network based on real recorded EEG data. During the eyes-open resting condition, the typical alpha-blocking effect could be detected from the EEG recordings. Our results show that half of the 38 subjects were observed to have larger alpha-blocking effects with the REST reference than with AR when using 64 channel recordings. This

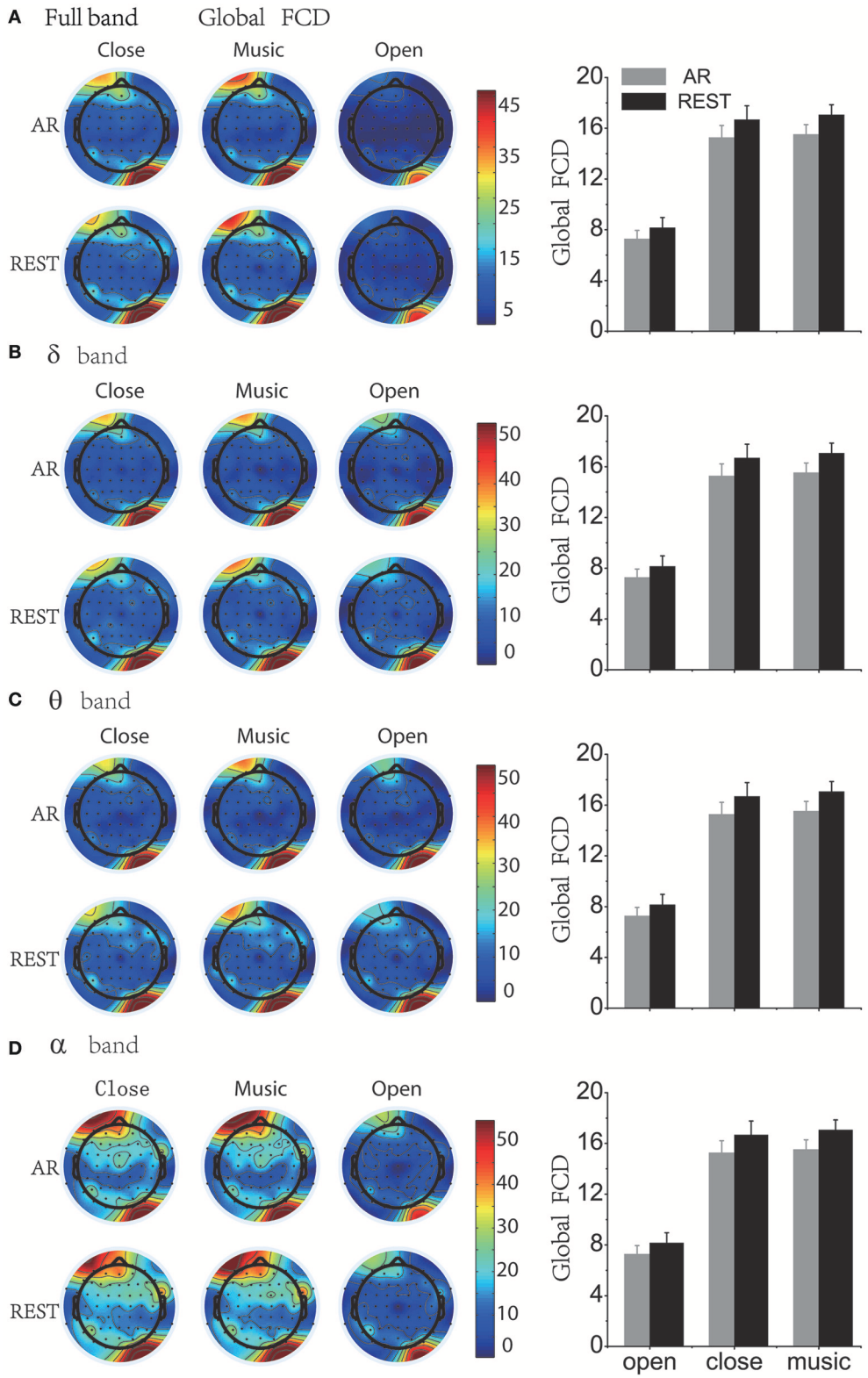

FIGURE 4 | Global brain functional connectivity density (Global FCD) topography and average of Global FCD under AR and REST reference. "AR" = average reference and "REST" = reference electrode standardization technique, that is, infinity reference. **(A)** Full band. **(B)** Delta band. **(C)** Theta band. **(D)** Alpha band. For high-frequency bands such as beta and gamma bands, please see the Supplementary Materials.

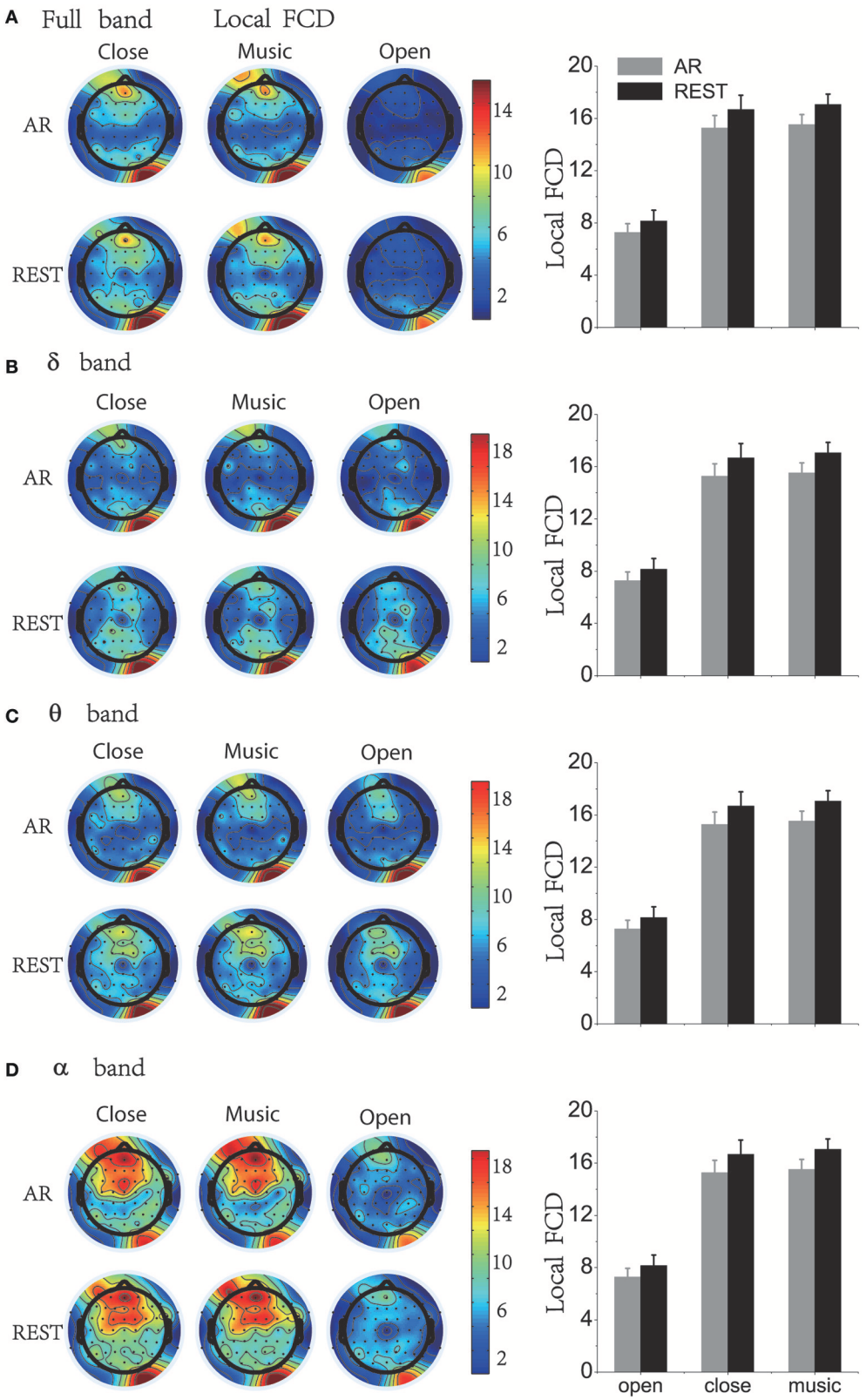

FIGURE 5 | Local brain functional connectivity density (Local FCD) topography and average of Global FCD under AR and REST reference. "AR" = average reference and "REST" = reference electrode standardization technique, that is, infinity reference. **(A)** Full band. **(B)** Delta band. **(C)** Theta band. **(D)** Alpha band. For high-frequency bands such as beta and gamma bands, please see the Supplementary Materials.

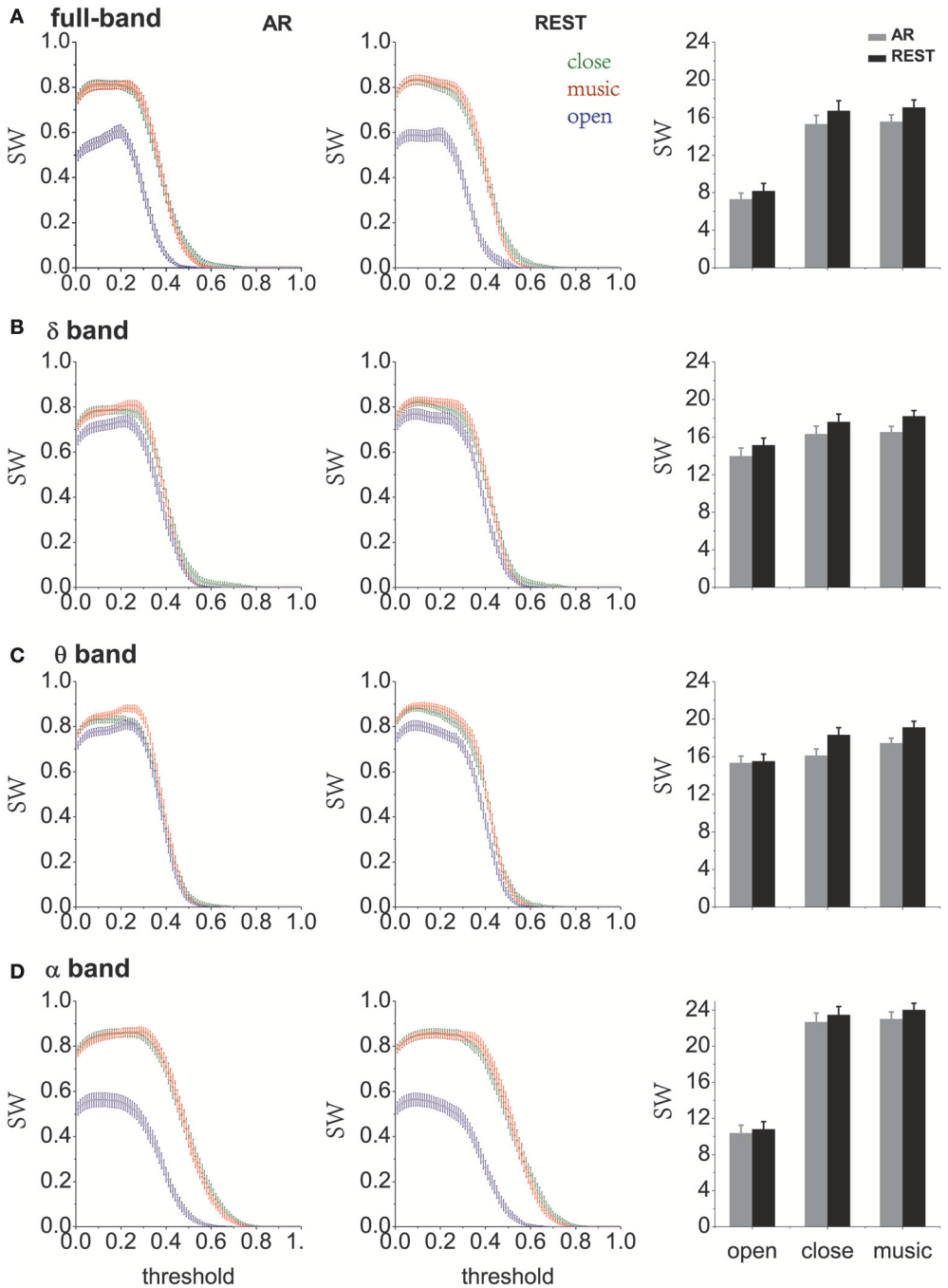

FIGURE 6 | The small-world characteristics in different states (eyes-open, eyes-closed and music) under different reference electrodes. "SW" = small-world characteristics. "AR" = average reference and "REST" = reference electrode standardization technique, that is, infinity reference. **(A)** Full band. **(B)** Delta band. **(C)** Theta band. **(D)** Alpha band. For high-frequency bands such as beta and gamma bands, please see the Supplementary Materials.

suggests that in certain situations when using a relatively large number of EEG recording channels, the differences between AR and REST analysis results might be difficult to detect. In this case, neither REST nor AR can be regarded as a "gold standard." Furthermore, we observed a clear right-lateralized phenomenon in the prefrontal area at resting state, which is consistent with previous reports (Nielsen et al., 2013). Additionally, the brain lateralization effect under REST was more significant than that under AR (**Figure 3D**). Brain functional network results indicated that small-world property values under different states showed the following tendency: music > close > open (**Figure 6**). The results of the music state may be instructive for the study

of music to improve brain function. After counting the small-world property values in the significant threshold, it was found that REST was generally more effective than AR (see right panel of **Figures 6A–D**). As indicated more recently by Yao (2017), because the shape of the human head is not a perfect spherical surface and its dipole orientation is not theoretically perfect, using the average value over all recording sites as an AR reference might be far from a zero reference. For these reasons, REST may provide better analysis results than AR to reveal brain functional network properties (Qin et al., 2010).

Reference Influence on Brain Lateralization Effect

Resting anterior EEG asymmetry in the alpha (8–12 Hz) band is known as a potential bio-marker of emotional predisposition (Tomarken et al., 1992). Generally, positive emotion has been associated with left-frontal activation (i.e., less alpha wave in left than right brain regions, as alpha activity is taken as an inverse index of brain activation), while negative emotion has been associated with higher activation of the right frontal regions (Henriques and Davidson, 1990). The 38 subjects employed here were all from Fudan University, and none had depressive or anxiety symptoms measured by subscales of the SCL-90 (Derogatis and Cleary, 1977). Our results demonstrated that most of the subjects had more distinct right-lateralized phenomenon in the prefrontal area, i.e., more alpha wave in right brain regions especially, under the REST condition than under AR. Perhaps EEG analysis under the REST condition preserves more information than that under the AR condition due to averaging. It should be noted that this study only compared the degree of lateralization under resting states and did not conduct further studies on emotion-related effects. In addition, the effects of lateralization can only reflect the differences between the left and right sides and cannot reveal the entire brain functional connectivity in different states. The brain functional network is critical for us to understand how the brain processes information efficiently.

Reference Influence on Brain Functional Network

Neuroscientists are becoming increasingly concerned with the study of the brain functional network; however, the choice of reference electrodes may lead to relatively large deviations of this network. We studied the brain functional network characteristics of subjects in different states and found that in the resting state, the average properties of weighted small-world at eyes-closed were significantly higher than those at eyes-open ($p < 0.01$, ANOVA1 analysis). The difference between eyes-closed and eyes-open in all bands shows that REST was higher than those at average reference (**Figure 6**). Although our results have indicated that in most situations the estimated measures using REST were larger than those using AR, this does not mean that REST is a better reference than AR unless further solid evidence becomes available.

In this study, the measurement of brain functional connectivity may be problematic, although using the electrodes as nodes of the network is primarily used in this study. EEG signals recorded on the scalp consist of synaptic electrical activity from neurons in the cerebral cortex. The ideal method of brain functional connectivity analysis is to locate the signal source of cognitive activity and then analyze the flow of information among different sources. However, the source analysis of EEG recordings is not completely accurate, and the source location is under dispute. First, EEG is not reliable for source localization because of its low spatial resolution. Second, due to the volume conduction effect, the cerebrospinal fluid, skull, and scalp cause the electrical current generated by ensembles of neurons deep inside the cortex to diffuse spatially before reaching the scalp electrodes. Thus, each recording from an electrode on the scalp is not necessarily generated by a source below that electrode. This is the typical volume conductor problem which produces relatively large zero-lag correlation among recording electrodes. The traditional network analysis cross-correlation and phase coherence are seriously distorted by the volume conduction effect (Christodoulakis et al., 2013). However, the volume conductor effect could be largely avoided in functional network re-construction by using the phase lag index, which uses phase information of time sequences of different channels to construct the network correlations (Peraza et al., 2012). In this way, the reconstructed brain functional network might reflect real spatio-temporal relations among different scalp recording channels. Even when this works well, each individual recording channel signal is still a mixture derived from underlying neuronal pool resources within the deep cortex. A better method would be to use magnetic resonance imaging (MRI) to locate the source and then use EEG to explore the flow of information among different sources. In the future we will combine EEG and fMRI to locate the sources of different cognitive tasks to reveal useful information.

CONCLUSIONS

In this study, we evaluated the difference between the average reference and the infinity reference from the perspective of alpha-blocking, brain lateralization effect, functional connectivity density and weighted small-world network characteristics. Alpha-blocking results indicated REST and AR had no significant difference. The brain lateralization effect results indicated that infinity reference had a greater lateralization effect than the average reference. The network results showed that small-world network parameters in the REST condition were larger than that of AR for all frequency bands. These distinct results deserve further exploration. In sum, the choice of reference electrode can introduce some bias into analysis results. Our results showed that in most cases, the typical features evaluated here were more clearly presented when EEG was referenced by REST. AR might smear these intrinsic effects slightly. However, until verified by further studies the application of both REST and AR during analysis might be a reasonable way to validate analysis-derived measurements.

ETHICS STATEMENT

This study was approved and supervised by the Ethics Committee of the School of Life Sciences at Fudan University (No.290). All participants signed written informed consent.

AUTHOR CONTRIBUTIONS

YY supervised the research; GZ, WZ, and YY designed the research; GZ, WZ, YL, and XQ performed the research, and GZ and YY wrote the paper. All authors reviewed the manuscript.

ACKNOWLEDGMENTS

YY thanks for the support from the National Natural Science Foundation of China (31571070, 81761128011), Shanghai Science and Technology Committee support (16410722600), the program for the Professor of Special Appointment (Eastern Scholar SHH1140004) at Shanghai Institutions of Higher Learning, the Research Fund for the Doctoral Program of Higher Education of China (1322051) and Omics-based precision medicine of epilepsy entrusted by the Key Research Project of the Ministry of Science and Technology of China (Grant No. 2016YFC0904400) for their support.

SUPPLEMENTARY MATERIAL

The Supplementary Material for this article can be found online at: https://www.frontiersin.org/articles/10.3389/fnins.2018.00158/full#supplementary-material

REFERENCES

Bassett, D. S., and Bullmore, E. T. (2017). Small-world brain networks revisited. *Neuroscientist* 23, 499–516. doi: 10.1177/1073858416667720

Berger, H. (1929). Electroencephalogram in humans. *Arch. Psychiatr. Nervenkr.* 87, 527–570.

Bertrand, O., Perrin, F., and Pernier, J. (1985). A theoretical justification of the average reference in topographic evoked potential studies. *Electroencephalogr. Clin. Neurophysiol.* 62, 462–464. doi: 10.1016/0168-5597(85)90058-9

Bullmore, E., and Sporns, O. (2009). Complex brain networks: graph theoretical analysis of structural and functional systems. *Nat. Rev. Neurosci.* 10, 186–198. doi: 10.1038/nrn2575

Chance, S. A., Casanova, M. F., Switala, A. E., and Crow, T. J. (2008). Auditory cortex asymmetry, altered minicolumn spacing and absence of ageing effects in schizophrenia. *Brain* 131, 3178–3192. doi: 10.1093/brain/awn211

Christodoulakis, M., Hadjipapas, A., Papathanasiou, E. S., Anastasiadou, M., Papacostas, S. S., and Mitsis, G. D. (2013). "Graph-theoretic analysis of scalp EEG brain networks in epilepsy—The influence of montage and volume conduction," in *2013 IEEE 13th International Conference on Bioinformatics and Bioengineering (BIBE)* (Chania: IEEE), 1–4.

Cohen, M. X. (2017). Where Does EEG Come From and What Does It Mean? *Trends Neurosci.* 40, 208–218. doi: 10.1016/j.tins.2017.02.004

Delorme, A., and Makeig, S. (2004). EEGLAB: an open source toolbox for analysis of single-trial EEG dynamics including independent component analysis. *J. Neurosci. Methods* 134, 9–21. doi: 10.1016/j.jneumeth.2003.10.009

Derogatis, L. R., and Cleary, P. A. (1977). Confirmation of dimensional structure of Scl-90: study in construct-validation. *J. Clin. Psychol.* 33, 981–989. doi: 10.1002/1097-4679(197710)33:4<981::AID-JCLP2270330412>3.0.CO;2-0

Dong, L., Li, F., Liu, Q., Wen, X., Lai, Y., Xu, P., et al. (2017). MATLAB toolboxes for reference electrode standardization technique (REST) of scalp EEG. *Front. Neurosci.* 11:601. doi: 10.3389/fnins.2017.00601

Ferree, T. C. (2006). Spherical splines and average referencing in scalp electroencephalography. *Brain Topogr.* 19, 43–52. doi: 10.1007/s10548-006-0011-0

Hardmeier, M., Hatz, F., Bousleiman, H., Schindler, C., Stam, C. J., and Fuhr, P. (2014). Reproducibility of functional connectivity and graph measures based on the phase lag index (PLI) and weighted phase lag index (wPLI) derived from high resolution EEG. *PLoS ONE* 9:e108648. doi: 10.1371/journal.pone.0108648

Henriques, J. B., and Davidson, R. J. (1990). Regional brain electrical asymmetries discriminate between previously depressed and healthy control subjects. *J. Abnorm. Psychol.* 99, 22–31. doi: 10.1037/0021-843X.99.1.22

Hu, S., Lai, Y., Valdés-Sosa, P. A., Brings-Vega, M. L., and Yao, D. (2018). How do the reference montage and electrodes setup affect the measured scalp EEG potentials? *J. Neural Eng.* 15:026013. doi: 10.1088/1741-2552/aaa13f

Huang, Y., Zhang, J., Cui, Y., Yang, G., He, L., Liu, Q., et al. (2017). How different EEG references influence sensor level functional connectivity graphs. *Front. Neurosci.* 11:368. doi: 10.3389/fnins.2017.00368

Kleinhans, N. M., Müller, R.-A., Cohen, D. N., and Courchesne, E. (2008). Atypical functional lateralization of language in autism spectrum disorders. *Brain Res.* 1221, 115–125. doi: 10.1016/j.brainres.2008.04.080

Latora, V., and Marchiori, M. (2001). Efficient behavior of small-world networks. *Phys. Rev. Lett.* 87:198701. doi: 10.1103/PhysRevLett.87.198701

Lei, X., and Liao, K. (2017). Understanding the influences of EEG reference: a large-scale brain network perspective. *Front. Neurosci.* 11:205. doi: 10.3389/fnins.2017.00205

LeMay, M. (1977). Asymmetries of the skull and handedness: phrenology revisited. *J. Neurol. Sci.* 32, 243–253. doi: 10.1016/0022-510X(77)90239-8

Liao, X., Vasilakos, A. V., and He, Y. (2017). Small-world human brain networks: perspectives and challenges. *Neurosci. Biobehav. Rev.* 77, 286–300. doi: 10.1016/j.neubiorev.2017.03.018

Liu, Q., Balsters, J. H., Baechinger, M., Van Der Groen, O., Wenderoth, N., and Mantini, D. (2015). Estimating a neutral reference for electroencephalographic recordings: the importance of using a high-density montage and a realistic head model. *J. Neural Eng.* 12:056012. doi: 10.1088/1741-2560/12/5/056012

Liu, Y., Liang, M., Zhou, Y., He, Y., Hao, Y., Song, M., et al. (2008). Disrupted small-world networks in schizophrenia. *Brain* 131, 945–961. doi: 10.1093/brain/awn018

Nielsen, J. A., Zielinski, B. A., Ferguson, M. A., Lainhart, J. E., and Anderson, J. S. (2013). An evaluation of the left-brain vs. right-brain hypothesis with resting state functional connectivity magnetic resonance imaging. *PLoS ONE* 8:e71275. doi: 10.1371/journal.pone.0071275

Nunez, P. L., and Srinivasan, R. (2006). *Electric Fields of the Brain: the Neurophysics of EEG*. New York, NY: Oxford University Press.

Nunez, P. L., Srinivasan, R., Westdorp, A. F., Wijesinghe, R. S., Tucker, D. M., Silberstein, R. B., et al. (1997). EEG coherency. I: statistics, reference electrode, volume conduction, Laplacians, cortical imaging, and interpretation at multiple scales. *Electroencephalogr. Clin. Neurophysiol.* 103, 499–515. doi: 10.1016/S0013-4694(97)00066-7

Onnela, J.-P., Saramäki, J., Kertész, J., and Kaski, K. (2005). Intensity and coherence of motifs in weighted complex networks. *Phys. Rev. E* 71:065103. doi: 10.1103/PhysRevE.71.065103

Peraza, L. R., Asghar, A. U., Green, G., and Halliday, D. M. (2012). Volume conduction effects in brain network inference from electroencephalographic recordings using phase lag index. *J. Neurosci. Methods* 207, 189–199. doi: 10.1016/j.jneumeth.2012.04.007

Pfurtscheller, G., and Klimesch, W. (1990). Topographical display and interpretation of event-related desynchronization during a visual-verbal task. *Brain Topogr.* 3, 85–93. doi: 10.1007/BF01128865

Qin, Y., Xin, X., Zhu, H., Li, F., Xiong, H., Zhang, T., et al. (2017). A comparative study on the dynamic EEG center of mass with different references. *Front. Neurosci.* 11:509. doi: 10.3389/fnins.2017.00509

Qin, Y., Xu, P., and Yao, D. (2010). A comparative study of different references for EEG default mode network: the use of the infinity reference. *Clin. Neurophysiol.* 121, 1981–1991. doi: 10.1016/j.clinph.2010.03.056

Rubinov, M., and Sporns, O. (2010). Complex network measures of brain connectivity: uses and interpretations. *Neuroimage* 52, 1059–1069. doi: 10.1016/j.neuroimage.2009.10.003

Shi, L., Niu, X., and Wan, H. (2015). Effect of the small-world structure on encoding performance in the primary visual cortex: an electrophysiological and modeling analysis. *J. Comp. Physiol. A Neuroethol. Sens. Neural Behav. Physiol.* 201, 471–483. doi: 10.1007/s00359-015-0996-5

Smith, S. A., Wong, P. K., and Jan, J. E. (1998). Unilateral alpha reactivity: an electroencephalographic finding in albinism. *J. Clin. Neurophysiol.* 15, 146–149. doi: 10.1097/00004691-199803000-00007

Stam, C. J., Nolte, G., and Daffertshofer, A. (2007). Phase lag index: assessment of functional connectivity from multi channel EEG and MEG with diminished bias from common sources. *Hum. Brain Mapp.* 28, 1178–1193. doi: 10.1002/hbm.20346

Stephan, K. E., Marshall, J. C., Friston, K. J., Rowe, J. B., Ritzl, A., Zilles, K., et al. (2003). Lateralized cognitive processes and lateralized task control in the human brain. *Science* 301, 384–386. doi: 10.1126/science.1086025

Strogatz, S. H. (2001). Exploring complex networks. *Nature* 410, 268–276. doi: 10.1038/35065725

Tomarken, A. J., Davidson, R. J., Wheeler, R. E., and Kinney, L. (1992). Psychometric properties of resting anterior EEG asymmetry: temporal stability and internal consistency. *Psychophysiology* 29, 576–592. doi: 10.1111/j.1469-8986.1992.tb02034.x

Tomasi, D., and Volkow, N. D. (2010). Functional connectivity density mapping. *Proc. Natl. Acad. Sci. U.S.A.* 107, 9885–9890. doi: 10.1073/pnas.1001414107

Tomasi, D., and Volkow, N. D. (2011). Aging and functional brain networks. *Mol. Psychiatry* 17, 549–558. doi: 10.1038/mp.2011.81

Van Den Heuvel, M. P., and Pol, H. E. H. (2010). Exploring the brain network: a review on resting-state fMRI functional connectivity. *Eur. Neuropsychopharmacol.* 20, 519–534. doi: 10.1016/j.euroneuro.2010.03.008

Watts, D. J., and Strogatz, S. H. (1998). Collective dynamics of 'small-world'networks. *Nature* 393, 440–442.

Wu, J., Zhang, J., Ding, X., Li, R., and Zhou, C. (2013). The effects of music on brain functional networks: a network analysis. *Neuroscience* 250, 49–59. doi: 10.1016/j.neuroscience.2013.06.021

Wu, J., Zhang, J., Liu, C., Liu, D., Ding, X., and Zhou, C. (2012). Graph theoretical analysis of EEG functional connectivity during music perception. *Brain Res.* 1483, 71–81. doi: 10.1016/j.brainres.2012.09.014

Yao, D. (2001). A method to standardize a reference of scalp EEG recordings to a point at infinity. *Physiol. Meas.* 22, 693–711. doi: 10.1088/0967-3334/22/4/305

Yao, D. (2017). Is the surface potential integral of a dipole in a volume conductor always zero? A cloud over the average reference of EEG and ERP. *Brain Topogr.* 30, 161–171. doi: 10.1007/s10548-016-0543-x

Yao, D., Wang, L., Arendt-Nielsen, L., and Chen, A. C. (2007). The effect of reference choices on the spatio-temporal analysis of brain evoked potentials: the use of infinite reference. *Comput. Biol. Med.* 37, 1529–1538. doi: 10.1016/j.compbiomed.2007.02.002

Yao, D., Wang, L., Oostenveld, R., Nielsen, K. D., Arendt-Nielsen, L., and Chen, A. C. (2005). A comparative study of different references for EEG spectral mapping: the issue of the neutral reference and the use of the infinity reference. *Physiol. Meas.* 26, 173–184. doi: 10.1088/0967-3334/26/3/003

Conflict of Interest Statement: The authors declare that the research was conducted in the absence of any commercial or financial relationships that could be construed as a potential conflict of interest.

frontiers in Neuroscience

ORIGINAL RESEARCH
published: 20 March 2018
doi: 10.3389/fnins.2018.00169

Electrophysiological Responses to Expectancy Violations in Semantic and Gambling Tasks: A Comparison of Different EEG Reference Approaches

Ya Li[1], *Yongchun Wang*[1], *Baoqiang Zhang*[1], *Yonghui Wang*[1]* *and Xiaolin Zhou*[2,3,4,5]

[1] School of Psychology, Shaanxi Normal University, Xi'an, China, [2] School of Psychological and Cognitive Sciences, Peking University, Beijing, China, [3] Beijing Key Laboratory of Behavior and Mental Health, Peking University, Beijing, China, [4] Key Laboratory of Machine Perception (Ministry of Education), Peking University, Beijing, China, [5] PKU-IDG/McGovern Institute for Brain Research, Peking University, Beijing, China

OPEN ACCESS

Edited by:
Pedro Antonio Valdes-Sosa, Clinical Hospital of Chengdu Brain Science Institute, China

Reviewed by:
Dezhong Yao, University of Electronic Science and Technology of China, China
Delin Sun, Duke University, United States

***Correspondence:**
Yonghui Wang
wyonghui@snnu.edu.cn

Specialty section:
This article was submitted to Brain Imaging Methods, a section of the journal Frontiers in Neuroscience

Received: *22 December 2017*
Accepted: *02 March 2018*
Published: *20 March 2018*

Citation:
Li Y, Wang Y, Zhang B, Wang Y and Zhou X (2018) Electrophysiological Responses to Expectancy Violations in Semantic and Gambling Tasks: A Comparison of Different EEG Reference Approaches. Front. Neurosci. 12:169. doi: 10.3389/fnins.2018.00169

Dynamically evaluating the outcomes of our actions and thoughts is a fundamental cognitive ability. Given its excellent temporal resolution, the event-related potential (ERP) technology has been used to address this issue. The feedback-related negativity (FRN) component of ERPs has been studied intensively with the averaged linked mastoid reference method (LM). However, it is unknown whether FRN can be induced by an expectancy violation in an antonym relations context and whether LM is the most suitable reference approach. To address these issues, the current research directly compared the ERP components induced by expectancy violations in antonym expectation and gambling tasks with a within-subjects design and investigated the effect of the reference approach on the experimental effects. Specifically, we systematically compared the influence of the LM, reference electrode standardization technique (REST) and average reference (AVE) approaches on the amplitude, scalp distribution and magnitude of ERP effects as a function of expectancy violation type. The expectancy deviation in the antonym expectation task elicited an N400 effect that differed from the FRN effect induced in the gambling task; this difference was confirmed by all the three reference methods. Both the amplitudes of the ERP effects (N400 and FRN) and the magnitude as the expectancy violation increased were greater under the LM approach than those under the REST approach, followed by those under the AVE approach. Based on the statistical results, the electrode sites that showed the N400 and FRN effects critically depended on the reference method, and the results of the REST analysis were consistent with previous ERP studies. Combined with evidence from simulation studies, we suggest that REST is an optional reference method to be used in future ERP data analysis.

Keywords: expectancy violation, reference electrode standardization technique (REST), average reference (AVE), linked mastoid (LM), N400, feedback-related negativity (FRN)

INTRODUCTION

To perform efficiently in a changing world, we must rapidly evaluate the outcomes of our actions or thoughts to guide future behaviors or thoughts. According to previous event-related potential (ERP) studies, feedback-related negativity (FRN) is the most important component associated with outcome evaluations. FRN is a negative-going component that is usually the largest over a fronto-central electrode site between 250 and 300 ms after the onset of a feedback stimulus (Miltner et al., 1997; Gehring and Willoughby, 2002; Holroyd and Coles, 2002; Nieuwenhuis et al., 2004; Yeung et al., 2005; Heldmann et al., 2008). FRN is typically observed in response to unexpected outcomes, such as money losses (Gehring and Willoughby, 2002), incorrect responses (Miltner et al., 1997) and unexpected negative feedback (Nieuwenhuis et al., 2004). Moreover, a previous study showed that the unexpected perceptual incompatibility between an expected color and the color that was actually presented could also elicit FRN (Jia et al., 2007). The expectancy-deviation hypothesis proposes that FRN is elicited by a mismatch between the expected feedback and the actual feedback (Oliveira et al., 2007). However, consensus regarding the role of the FRN component in outcome evaluations is lacking. It is still unknown whether FRN codes a violation of expectancies in general.

In a previous study, Roehm et al. (2007) investigated the ERP responses to the expectancy violation in an antonym relation task. Specifically, antonym word pairs were presented in the fixed context as "*The opposite of X is Y*." The participants were asked to indicate the correctness of the sentence. In this task, the second word (Y) of the antonym word pair served as the feedback to the prediction of the first word (X). The authors found that an expectancy deviation under an antonym relations context could induce a negative component with a peak at approximately 300 ms. Although the authors considered this negative component N400, the negative component in this study occurred earlier and had a more anterior distribution than the typical N400 component. The profile of this component was similar to that of the FRN component. In addition, FRN is likely elicited by expectancy deviations under the antonym relations context since an antonym relations violation is also a type of expectancy deviation. However, the profile of the so-called "N400" in the antonym study was obtained under conditions that differ from those used in FRN studies. For example, the EEG recording method, the analysis method and the participants all differed across these studies. We could not directly compare the components observed in the different research studies. Hence, additional studies using the same methods and a within-subjects experimental design are required to address this issue. These studies could extend our understanding of the nature of the FRN component.

Furthermore, the choice of reference approach could influence the observed EEG data. The "choice of EEG reference point" has been an issue for many years. The EEG reference method choice is crucial since the potential measured at each electrode on the scalp is calculated as the potential difference between the active electrode site and the reference site. This method assumes that the recorded data at the reference site cannot be contaminated by brain activity. However, this approach cannot be guaranteed when the reference site is on the scalp. Previous FRN and N400 studies have mainly utilized the linked mastoid (LM) as a reference (Gehring and Willoughby, 2002; Roehm et al., 2007), which is calculated as the average of the signals from the left and right mastoids. However, previous simulation studies have shown that the scalp distribution of LM-obtained EEG data has significant distortions (Yao, 2001; Yao et al., 2005; Qin et al., 2010) because the EEG signal of the left and right mastoids is influenced by physiologically dynamic signals from the brain. In addition, no point on the scalp or body surface always has a zero potential. Hence, the choice of the EEG reference method might influence the spatial and temporal profiles of the observed N400 and FRN components.

Fortunately, accumulating evidence suggests that the reference electrode standardization technique (REST) should be used as a neutral reference-free approach in EEG studies (Yao, 2001; Tian and Yao, 2013). The premise behind the REST approach is to re-reference the EEG or ERP data to a neutral infinite reference point that is unlikely to be influenced by brain activity through a transfer matrix (Yao, 2001; Yao et al., 2005). The transfer matrix is computed by using a non-unique equivalent dipole source model and a proposed three-concentric-sphere head model. Given these merits, the REST approach was used in this study to avoid the possible influences of the reference method and to confirm the observed results. Moreover, the AVE reference approach, which is calculated as the average of all electrode sites, is also commonly used as a reference-free approach in EEG studies. However, the influence of the AVE reference procedure on the N400 and FRN effects is still unknown.

To determine whether the expectancy violation under an antonym relations context could induce FRN, the current study directly compared the components elicited by expectancy violations in an antonym relations task and gambling task using a within-subjects experimental design. Moreover, the current study examined the influence of the choice of ERP reference approach on the amplitude and scalp distribution of the experimental effects. Hence, the current study compared the effects of the LM, REST, and AVE reference approaches on the amplitude and scalp distribution of the ERP effects as the expectancy violation increased.

METHODS

Participants

Twenty-three naïve participants (11 males, 12 females; mean age = 22; SD = 2.9) with normal or corrected-to-normal vision were recruited for this experiment. All participants were right-handed without any known neurological or visual disorders. Each participant received a basic payment of 50 yuan for his/her participation, and the participants were informed that they would receive an additional bonus based on their performance in the gambling task. The participants provided written informed consent before the experiment. The study was approved by the local research ethics committee.

Stimuli and Procedure

Gambling Task

Procedure

The stimuli were displayed on a black uniform background on a 22-inch CRT monitor with a refresh rate of 60 Hz and a resolution of 1,024 × 768 pixels. The stimuli and procedures were programmed using Presentation (Neurobehavioral System Inc., San Francisco, CA). The participants viewed the stimuli at a distance of 100 cm in a dimly lit room, and their heads were stabilized by a chin-and-head rest.

As shown in **Figure 1A**, each trial started with the presentation of two gray cards on a uniform black background (2.3° wide, 3.2° high) on the left and right sides of a fixation dot (3.6° away from the fixation dot) for 1,000 ms. Then, the number 5 and/or the number 25 was shown at the center of the gray cards. Four possible combinations (i.e., 25/25, 5/5, 5/25, and 25/5) were presented at an equal probability. The numbers remained until a response was given. After the response, the white outline of the card thickened for 550 ms (range: 500–600 ms) to confirm the selection. Finally, the chosen card became red or green to inform the participant of the outcome of the current trial. To emphasize the valence of the outcome, the "+" or "−" symbol was added before the number to indicate the gain or loss, respectively. The inter-trial interval was 1000 ms. The participants were informed that they could be rewarded or penalized the amount of money indicated by the feedback. In addition, the cumulative outcome across each trial was presented at the end of the experiment. The experiment consisted of two

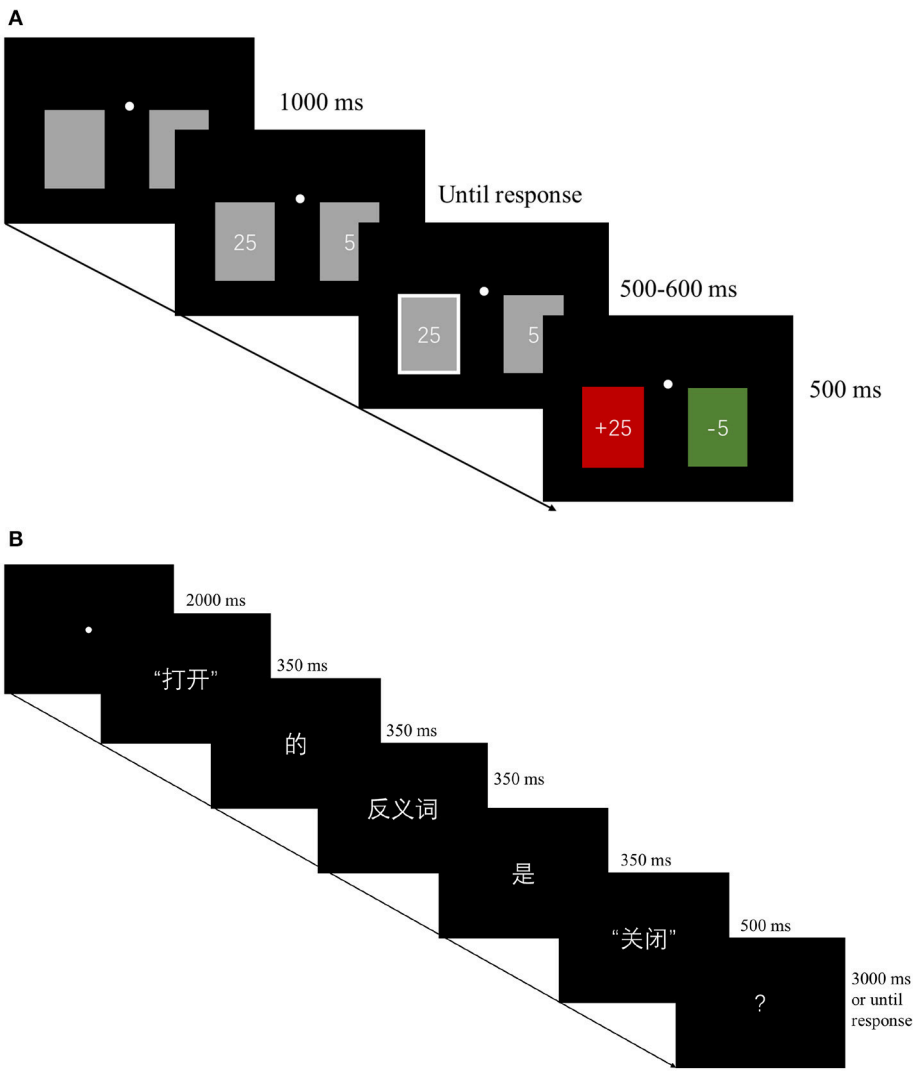

FIGURE 1 | Experimental procedures. **(A)** An example trial of the gambling task. The four possible number combinations (i.e., 25/25, 5/5, 5/25, and 25/5) was shown at the center of the gray cards until response. The inter-trial interval was 1,000 ms. **(B)** An example trial of the antonym task. The illustration shows "The opposite of *open* is *close*" in Chinese (word-by-word translation: "打开*(open)*/的(of)/反义词(opposite)/是(is)/关闭*(close)*"). The ISI between each word was 200 ms, except that the ISI between the word *is* and the critical stimuli (Y) was 200–300 ms with a 50-ms per jitter step. After a 750 ms ISI (range: 500–1,000 ms), a question mark (?) was shown until a response was given or 3 s had elapsed. The inter-trial interval was 2,250 ms.

blocks of 160 trials each. A practice block was performed before the formal test.

Unknown to the participants, the sequence of different types of trials was pseudorandomized, and no more than 4 consecutive trials were from the same condition. The gain and loss status of the participants' chosen cards was predetermined before the experiment at an equal probability. The assignment of the green/red colors to represent the gain/loss was counterbalanced between participants.

Antonym Task

Materials

One hundred and twenty sets of the three experimental conditions (i.e., antonyms, related and unrelated) were used in the main experiment, resulting in a total of 360 critical stimuli. The word frequency and strokes of the critical stimuli are shown in **Table 1**. Repeated-measures analyses of variance (ANOVAs) revealed that the differences among the three conditions were not significant [Frequency: $F_{(2, 357)} = 0.31$, $p > 0.74$; Stroke: $F_{(2, 357)} = 1.62$, $p > 0.20$]. To ensure that no single word was repeated for any particular participant, all critical stimuli were divided into three lists, and each participant was presented with stimuli on one particular list. To balance the responses, 40 additional antonym pairs serving as filter conditions were added to each list. Thus, each list contained 160 items (i.e., 80 antonym pairs, 40 related pairs and 40 unrelated pairs). The assignment of each list was counterbalanced across participants using a Latin square design.

Questionnaire Pretest

To determine whether the experiment conditions indeed differed from each other in terms of antonymy and semantic relatedness, we conducted a questionnaire pretest. Seventy-two participants (28 males, 44 females) completed the questionnaire. The participants were randomly and averagely assigned to two groups (Group A: 23 females, age: 22 ± 2.4; 13 males, age: 23 ± 2.2. Group B: 21 females, age: 22 ± 2.2; 13 males, age: 23 ± 2.6.). No significant age difference was observed between Groups A and B, F (1.36) = 0.003, $p > 0.96$.

Both groups were instructed to rate the relationship of each word pair on a 7-point scale. The only difference between these two groups was the judgment task. Group A was tasked with judging *the degree of antonymy* (i.e., the degree to which the pair could be considered an antonym pair, 1: optimal antonymy, 7: not at all an antonym), while Group B was tasked with judging *the degree of relatedness* between the two words (1: very strongly related, 7: completely unrelated). Other than the judgment task, the questionnaires were identical in both groups. Both groups completed three versions of the questionnaire including 160 word pairs (antonym pairs: 80; related word pairs: 40; and unrelated word pairs: 40). The assignment of each version was counterbalanced across the participants using a Latin square design. No single word was repeated in each version. Thus, 12 participants rated the degree of relatedness and antonymy of each word pair.

TABLE 1 | Mean rating scores in both groups.

Condition	Stroke	Frequency	Antonymy	Relatedness
	Mean (SD)	Mean (SD)	Mean (SD)	Mean (SD)
A. Antonyms	17.65 (5.47)	32.18 (43.76)	1.32 (0.26)	1.48 (0.25)
B. Related	17.42 (4.24)	28.71 (51.29)	5.16 (1.18)	2.84 (0.79)
C. Unrelated	16.63 (4.64)	27.92 (34.01)	6.55 (0.25)	6.07 (0.50)

The rating scores of both groups are shown in **Table 1**. Repeated-measures ANOVAs with two factors (experiment condition: antonym, related and unrelated; group: antonymy judgment, relatedness judgment) revealed a main effect of group, $F_{1(1, 22)} = 100.78$, $p < 0.001$, $F_{2(1, 238)} = 351.56$, $p < 0.001$, a main effect of condition, $F_{1(1, 22)} = 858.77$, $p < 0.001$, $F_{2(1, 238)} = 1{,}433.85$, $p < 0.001$, and a significant interaction between condition and group, $F_{1(1, 22)} = 194.73$, $p < 0.001$, $F_{2(1, 238)} = 324.64$, $p < 0.001$. Pairwise comparisons revealed that the differences between any two conditions (i.e., antonym vs. related, antonym vs. unrelated, and related vs. unrelated) were all significant (all $p < 0.001$) in both groups. In summary, these results confirmed that the stimuli sets of the three conditions differed along the two desired dimensions of *antonymy* and *relatedness*.

Procedure

As shown in **Figure 1B**, each trial started with a 2,000-ms fixation period, followed by a sentence that was presented word by word in the fixed sequence *The opposite of X is Y* in Chinese. Each word, except for the word Y, was presented for 350 ms, while the word Y was shown for 500 ms to reduce the off-stimulus influence on the ERP signal. The ISI between each word, except for the ISI between the word *is* and the critical stimuli (Y), was 200 ms. The mean duration of the ISI between the word *is* and the critical stimuli (Y) was 250 ms with a 50-ms per jitter step (range: 200–300 ms). After a 750 ms ISI (range: 500–1,000 ms) with a black background only, a question mark (?) was shown until a response was given or 3 s had elapsed. The inter-trial interval was 2,250 ms. The participants were asked to indicate whether the sentence was correct or incorrect as quickly and accuracy as possible.

Unknown to the participants, the sequence of the different types of trials were pseudorandomized, no more than 3 consecutive trials represented the same condition and no more than 5 trials had the same responses of "yes" or "no." The experiment consisted of two blocks of 80 trials each. A practice block of 32 trials was performed before the formal test.

Electrophysiological Recordings

The electroencephalogram (EEG) data were recorded using a 64-channel EEG cap according to the international 10/20 system (Brain Products, Munich, Germany), and the reference electrode was placed on the tip of the nose. The horizontal and vertical electrooculograms (EOG) were monitored via electrodes placed lateral to the external canthus of the left eye and above the right eye, respectively. The AFz electrode on the cap served as a ground. During the recordings, all electrode site impedances were maintained below 10 kΩ. The EEG data were recorded at

a sampling rate of 500 Hz and amplified using a 0.016–100 Hz bandpass for offline analysis.

Data Analysis

The offline data preprocessing was performed using Brain Vision Analyzer 2.0 (Brain Products, Munich, Germany). The EEG data were re-referenced using the average mastoids. The ocular artifacts were corrected using an eye-movement correction algorithm (Gratton et al., 1983). Then, the continuous EEG data were separated into epochs from −200 to 800 ms around the onset of the feedback stimuli. The baseline was defined as the epoch from 200 to 0 ms before the stimulus onset. Baseline corrections were performed by subtracting the average activity of each channel during the baseline period from each sample. All epochs in which the EEG voltages exceeded the threshold of ±70 μV were excluded from further analysis. The EEG data were low-pass filtered below 30 Hz (decay of stop band: 24 dB per octave). The remaining epochs with correct responses were then averaged across trials according to each condition. After all preprocessing steps were completed, the ERP data were re-referenced using the AVE (computed as the average of all channels) and REST methods. This step was performed to effectively maintain the same standard of artifact removal across all reference approaches.

All further analyses were performed using EEGLAB, ERPLAB and/or the REST toolbox (Yao, 2001; Dong et al., 2017; Hu et al., 2018) in a MATLAB environment. For the gambling task, the ERP experimental effect was calculated by subtracting the gain condition (expected condition) from the loss condition (unexpected condition). For the antonym relations task, the experimental effect of expectancy violation was measured by subtracting the antonym condition (expected condition) from the related and unrelated conditions (unexpected condition). All further statistical analyses were performed based on these difference waves.

The statistical analyses were conducted using both mass univariate analysis and multifactor statistical analyses. To assess the component induced in the antonym relations task and gambling task in an unbiased manner, a mass univariate approach was performed to determine exactly when and where the ERP effect appeared (Groppe et al., 2011; Luck and Gaspelin, 2017). Specifically, one-sample *t*-tests (compared with zero) were conducted for each difference wave (deviation condition–baseline condition) at each time bin and electrode site. The permutation-based strong control of the familywise error rate (FWER) was performed to correct for the multiple comparisons. Thus, the ERP effect was confirmed based on the time window and electrode sites that showed a significant effect.

To determine the influence of the reference method on the experimental effect across sites, the identified ERP effects were entered into a repeated-measures ANOVAs with experimental condition, reference method (LM, REST, and AVE) and topographical factors (Fz, FCz, Cz, CPz, and Pz) entered separately for the gambling task and the antonym relations task. The midline electrodes were chosen because the FRN effect and the N400 effect have been shown to be the greatest at these electrodes in previous studies. The Greenhouse-Geisser adjustment for non-sphericity was applied as appropriate. *Post hoc* tests and one-sample *t*-tests were also conducted, and *p*-values were corrected by performing Bonferroni adjustments to avoid multiple comparisons errors.

RESULTS

Behavioral Results

The mean accuracy is shown in **Table 2**. Regarding the accuracy, a repeated-measures ANOVA revealed a main effect of experimental condition, $F_{(2, 46)} = 55.70$, $p < 0.001$, partial $\eta^2 = 0.71$. Pairwise comparisons showed that the performance under the antonyms and unrelated conditions was better than that under the related condition (antonyms vs. related: 0.12, $SE = 0.02$, $p < 0.001$; unrelated vs. related: 0.14, $SE = 0.02$, $p < 0.001$). Regarding the reaction time (RT), a repeated-measures ANOVA revealed a main effect of experimental condition, $F_{(2, 46)} = 13.6$, $p < 0.001$, partial $\eta^2 = 0.37$. Pairwise comparisons showed that the performance under the antonyms and unrelated conditions was better than that under the related condition (antonyms vs. related: 59 ms, $SE = 16$ ms, $p < 0.01$; unrelated vs. related: 88 ms, $SE = 22$ ms, $p = 0.001$). These behavioral results showed higher accuracy and faster reaction times for the antonyms and unrelated conditions than for the related condition.

Mass Univariate Analysis

A mass univariate analysis was first conducted to analyze the differences in the waveforms in each task with the LM reference method to maintain the same reference method used in previous studies (Gehring and Willoughby, 2002; Roehm et al., 2007). Specifically, we performed *t*-tests at each time point and each electrode site to analyze the different waveforms to assess the distribution of the experimental effects over the electrode sites. As shown in **Figure 2**, a more negative component was observed under the loss condition compared with that observed under the gain condition in the gambling task. The mass univariate analysis showed that the significant difference was mainly focused at 180-330 ms and peaked at 275 ms (**Figure 3**). The experimental effect was the largest at the fronto-central recording sites. The early negative component observed in our study is consistent with the FRN effect defined by previous studies (e.g., Gehring and Willoughby, 2002; Holroyd and Coles, 2002; Heldmann et al., 2008). The observed pattern was confirmed using the REST and AVE reference methods. Thus, the current study replicated the FRN effect induced by a gambling task.

TABLE 2 | Behavioral results for the antonym task.

Condition	Accuracy	RT (ms)
	Mean (SD)	Mean (SD)
A. Antonyms	0.98 (0.29)	441 (165)
B. Related	0.86 (0.77)	498 (204)
C. Unrelated	0.99 (0.15)	412 (165)

RT, Reaction time.

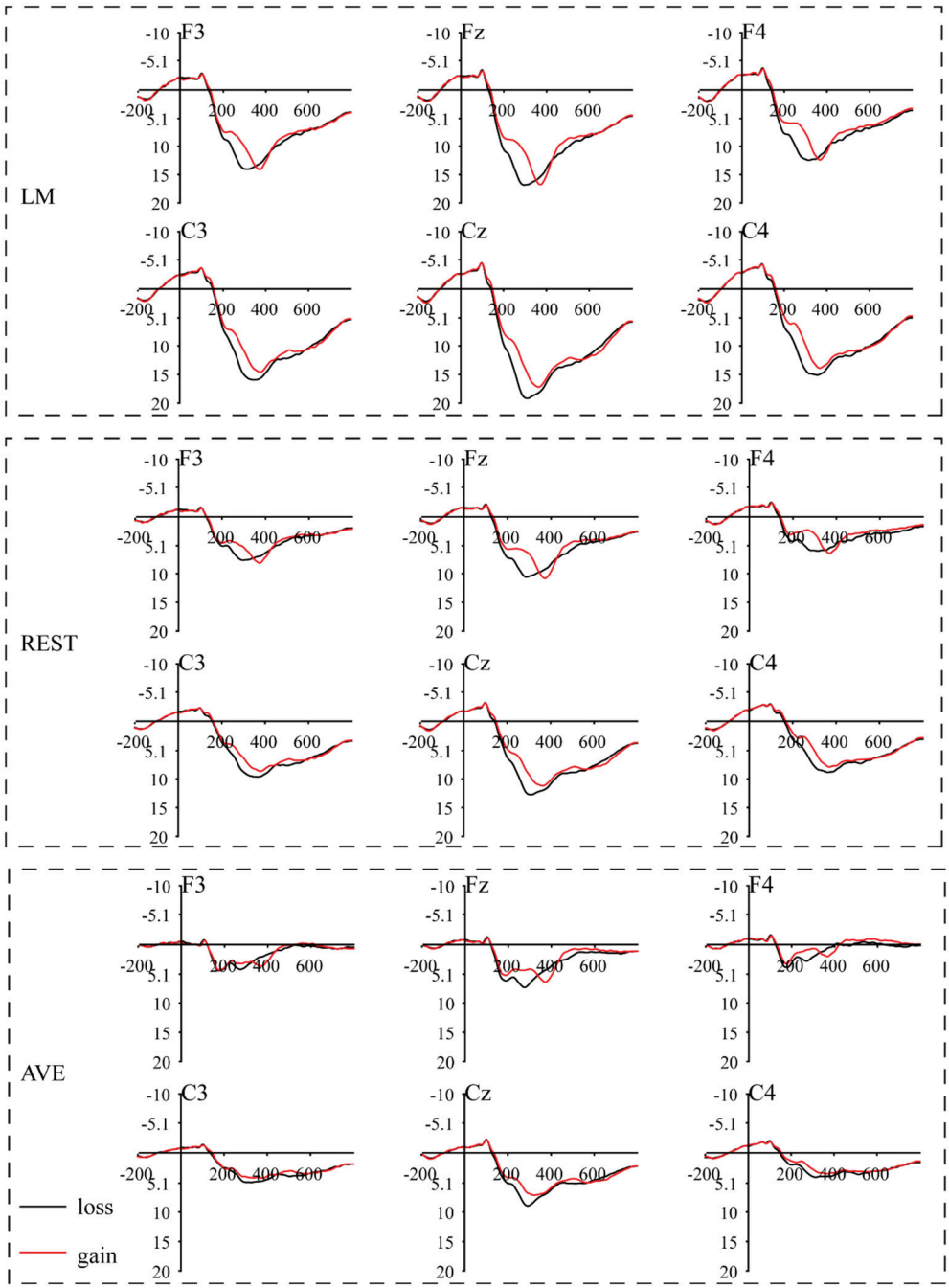

FIGURE 2 | Grand-average event-related potential (ERP) waveforms under the gain and loss conditions in a gambling task using three separate reference approaches. The feedback stimulus onset occurred at 0 ms. Negativity is plotted upward.

Figure 4 shows that the waveform under the unrelated and related conditions was more negative-going than that under the antonym condition in the antonym task. The mass univariate analysis showed that the significant difference was focused at 290–500 ms and peaked at 370 ms (**Figure 5**). The negative component observed in our study was consistent with the N400 effect defined by previous studies (e.g., Kutas and Hillyard, 1980; Luck, 2014) and was confirmed using the REST and AVE reference methods. Thus, the negative component induced by the antonym task was an N400 effect rather than an FRN effect, and the N400 effect indicates an unexpected sematic prediction violation process.

For the FRN effect, the electrode sites of the revealed significant effects were different among all three reference

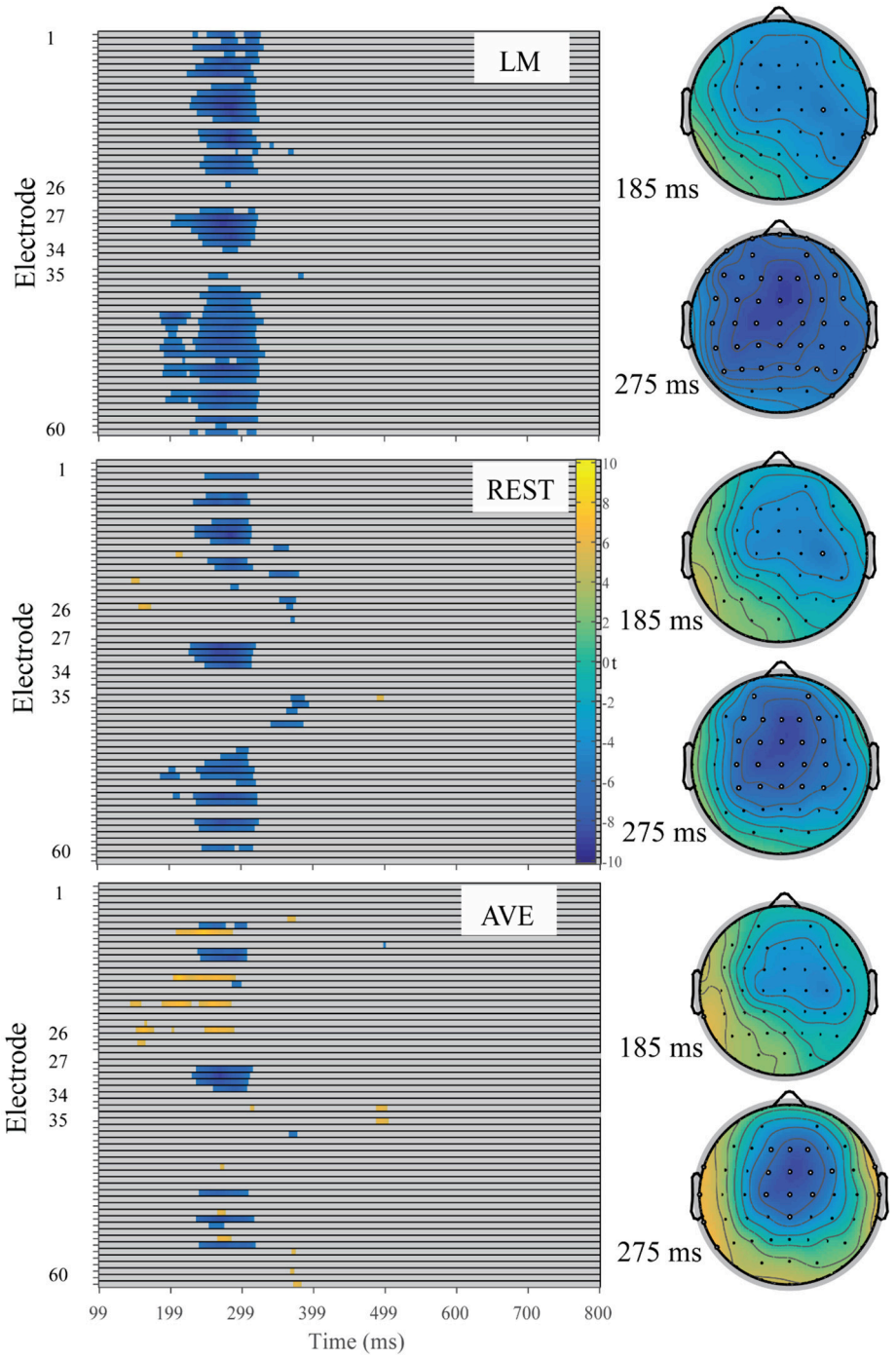

FIGURE 3 | Raster diagram illustrating the significant FRN effects according to *t*-test permutation tests using three reference approaches. Blue and yellow rectangles indicate the time points and electrode sites at which the ERP effects are significantly smaller and larger than zero, respectively. Gray rectangles indicate time points and electrode sites at which no significant differences were found. Right: the corresponding *t*-value topographical maps at 185 and 275 ms for each reference approach. The white electrode indicates the significant FRN effect at that site while the black electrode indicates no significant at that moment.

approaches. Specifically, the significant electrode sites were widely distributed using the LM reference approach and focused in the front-central electrode sites using the REST reference approach. In addition, the AVE-obtained FRN effect was reversed in polarity (positive amplitude) at certain electrode sites. For the N400 effect, the electrode sites showing significant effects were also widely distributed in the LM reference method, while the significant effects were mainly focused in the posterior

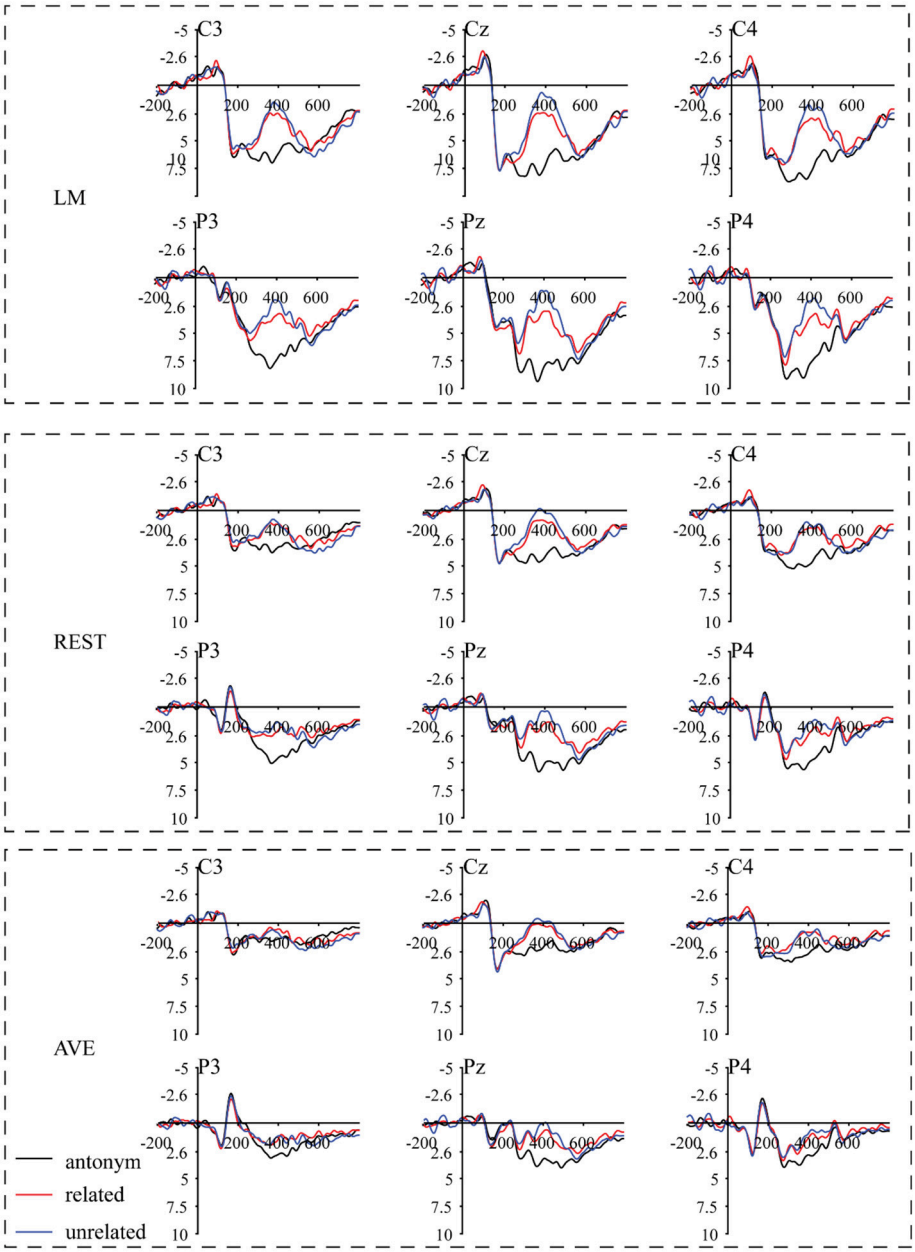

FIGURE 4 | Grand-average ERP waveforms under the antonyms, related and unrelated conditions in an antonym relations task using three separate reference approaches. The second word (Y), as the feedback stimulus onset, occurred at 0 ms. Negativity is plotted upward.

electrode sites using the REST reference approach. However, the AVE-obtained N400 effect was reversed in polarity at the right frontal electrode sites. These results suggested that the sites of the revealed significant effects were dependent on the choice of reference approach.

In summary, the time window and site of the revealed negative components suggest that the ERP effects induced by the prediction violations differed between the gambling task and the antonym task. The observed patterns were confirmed by using all three reference methods, suggesting that the ERP components induced by these two tasks differ.

Multifactor Statistical Results

FRN Effect and N400 Effect

A visual inspection of the data showed an FRN effect under the gambling task using all three reference methods. Based on visual inspection and results from the mass univariate analysis, the FRN effects were calculated as the mean amplitude of the loss-minus-gain difference wave between 220 and 320 ms (**Figure 6**). One-sample *t*-tests were performed to statistically examine the reliability of the FRN effect at each electrode site across all reference methods in both tasks. In the gambling task, using the LM reference method, the FRN effect was significant at all

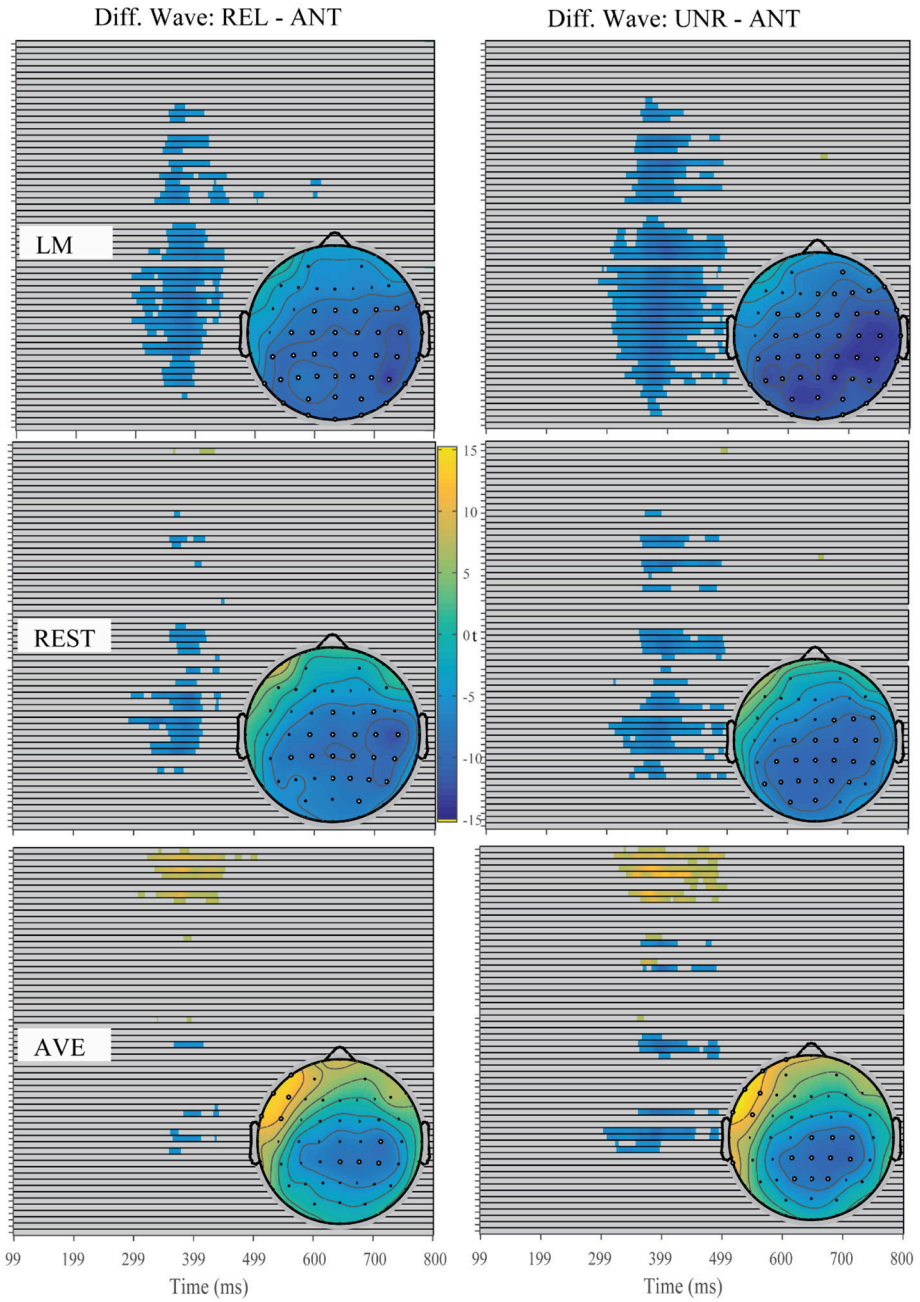

FIGURE 5 | Raster diagram illustrating the significant N400 effects according to the *t*-test permutation tests using three reference approaches. Blue and yellow rectangles indicate the time points and electrode sites at which the ERP effects are significantly smaller and larger than zero, respectively. Gray rectangles indicate the time points and electrode sites at which no significant differences were found. The inset topographical maps reveals the corresponding *t*-value maps at 370 ms for each experimental condition and each reference approach. The white electrode indicates the significant N400 effect at that site while the black electrode indicates no significance at that moment.

electrode sites except for Oz (all other Bonferroni-corrected $p < 0.05$, Cohen's $d > -0.78$). Using the REST reference method, a significant FRN effect was observed at all electrode sites, except for POz and Oz (all other Bonferroni-corrected $p < 0.01$, Cohen's $d > -0.96$). Using the AVE reference method, a significant FRN effect was observed at the fronto-central electrode sites (i.e., Fz, FCz, Cz, and CPz, all Bonferroni-corrected $p < 0.001$, Cohen's $d > -1.25$); however, a significant positive component was observed at Oz (Bonferroni-corrected $p < 0.05$, Cohen's $d > 0.93$). In contrast, in the antonym task, the FRN effect was not significant at all electrode sites across all reference methods (smallest Bonferroni-corrected p

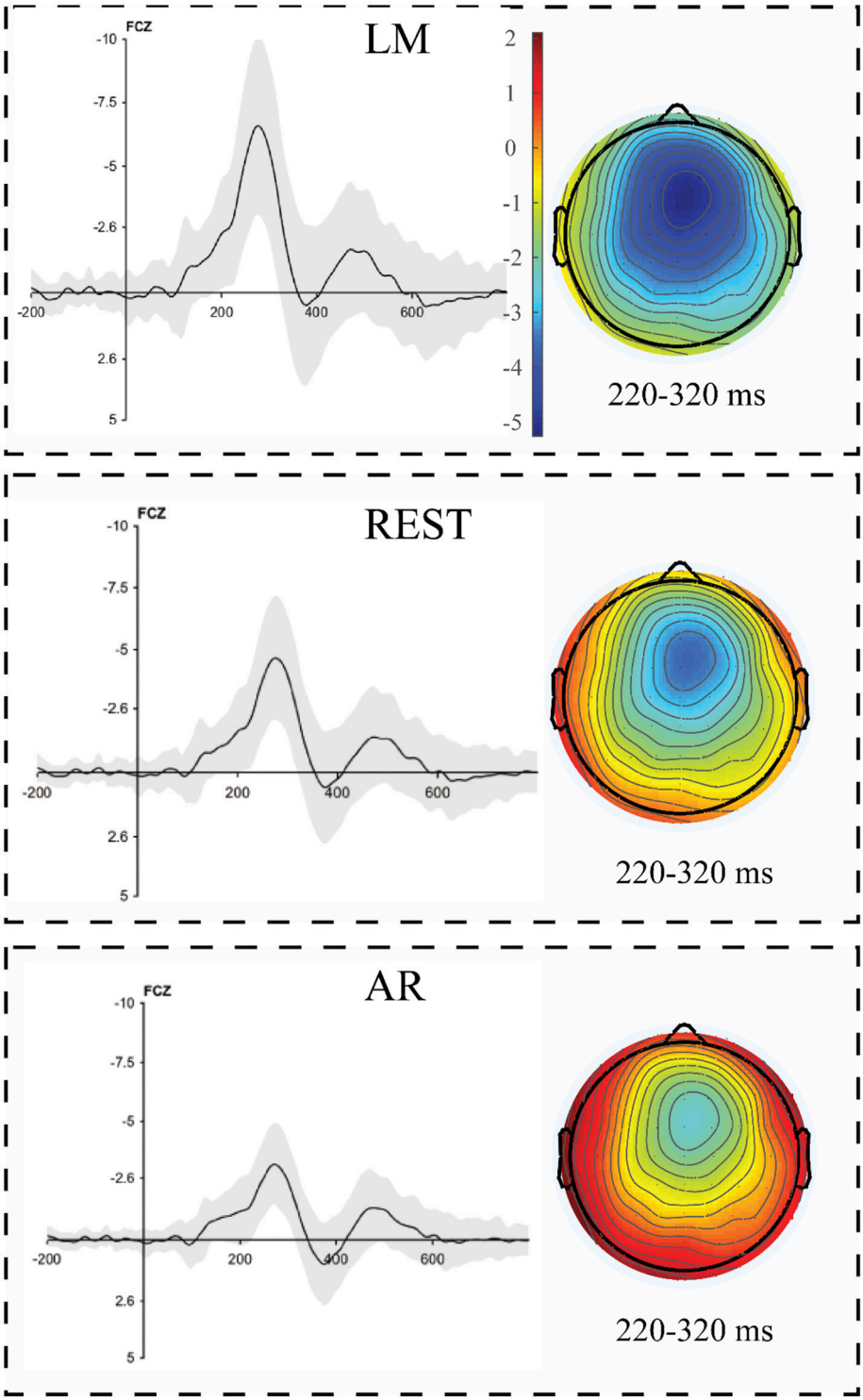

FIGURE 6 | The loss minus gain difference waveforms in a gambling task using three separate reference approaches. The corresponding topographical maps of the FRN effect (180–330 ms) revealed a strong fronto-central distribution using all three reference approaches. The shading indicates the standard error across the participants.

= 0.06; all other ps > 0.2). These results suggested that the unexpected outcomes induced the FRN effect in the gambling task and that this effect was confirmed by all reference approaches.

A visual inspection of the data showed a typical N400 effect under the related and unrelated conditions using both the LM and REST reference methods, while the AVE method revealed the opposite pattern, with a negative amplitude at the posterior electrode sites and positive amplitudes at the frontal electrode sites (**Figure 7**). One-sample *t*-tests were conducted to statistically examine whether the N400 effect was induced under each experimental condition at each electrode site using all reference methods in both tasks. According to the one-sample *t*-tests with Bonferroni corrections, the mean amplitude of the N400 effect (310–490 ms) under the related condition was significant at all sites, except for Fz, using the LM and REST reference methods (LM: all other Bonferroni-corrected ps < 0.008, Cohen's $d > -0.97$; REST: all other Bonferroni-corrected ps < 0.05, Cohen's $d > -0.82$), and the N400 effect obtained with the AVE method was significant at Cz, CPz, Pz, and POz (all Bonferroni-corrected ps < 0.05, Cohen's $d > -0.80$). Under the unrelated condition, the N400 effect was significant at most sites using all three reference methods (LM: all except for Fz, all other Bonferroni-corrected ps < 0.008, Cohen's $d > -0.96$; REST: all except for Fz and FCz, all other Bonferroni-corrected ps < 0.002, Cohen's $d > -1.09$; AVE: all except for Fz, FCz, and Oz, all other Bonferroni-corrected ps < 0.002, Cohen's $d > -1.08$). In the gambling task, however, it was not significant at all electrode sites across all reference methods (smallest Bonferroni-corrected $p > 0.7$). Thus, the typical N400 effect could be reliably observed under both the related and unrelated conditions in the antonym task, which was confirmed using both the LM and REST reference method. However, the AVE method could distort the experimental effect, which, in turn, could alter the results.

Reference Effects on the Amplitude and Scalp Distribution

To further statistically examine the influence of the reference method on the amplitude and scalp distribution of the FRN effect, we included the amplitude of the FRN effect in a two-way (electrode site × reference) repeated-measures ANOVA. The ANOVA revealed a main effect of reference method [$F_{(2, 44)} = 306.56$, $p < 0.001$, partial $\eta^2 = 0.75$], and the pairwise comparisons revealed that the FRN effect using the LM reference method was larger than that using the REST reference method, which, in turn, was larger than that using the AVE reference method. A main effect of topographical factors was also observed [$F_{(2, 44)} = 37.4$, $p < 0.001$, partial $\eta^2 = 0.63$], and pairwise comparisons revealed that the FRN effect was the largest at FCz, which was significantly larger than that at Cz, CPz, and Pz (ps < 0.001). The interaction between these two factors was not significant ($F < 0.1$). As clearly shown in **Figure 6**, the topographical pattern was similar across the LM, REST, and AVE reference approaches. The effect of the reference method on the FRN effect was mainly revealed in the amplitude differences but not in the scalp distribution.

To statistically examine the possible influence of the reference approach on the N400 effect and the magnitude of the ERP effect between the two expectancy violations, repeated-measures ANOVAs with three factors (i.e., experimental condition, reference method and ROI) were performed for the middle electrode site. A main effect of experimental condition was revealed [$F_{(1, 22)} = 12.74$, $p = 0.002$, partial $\eta^2 = 0.37$], indicating that the N400 effect under the unrelated condition was larger than that under the related condition. Furthermore, a main effect of ROI was observed [$F_{(6, 132)} = 13.08$, $p < 0.001$, partial $\eta^2 = 0.37$], with the maximal N400 effect occurring at Pz (mean: −3.51, $SE = 0.32$) and the minimal effect occurring at Fz (mean: −0.63, $SE = 0.45$). A main effect of reference method was also observed [$F_{(2, 44)} = 44.29$, $p < 0.001$, partial $\eta^2 = 0.67$], indicating that the amplitude of the N400 effect observed with the LM reference approach was larger than that observed with the REST reference approach, followed by that with the AVE reference method. More importantly, the interaction between reference method and experimental condition was significant [$F_{(2, 44)} = 6.25$, $p < 0.01$, partial $\eta^2 = 0.22$]. The *post hoc* tests and Bonferroni adjustment revealed that the N400 effect under the unrelated condition was larger than that under the related condition using all three reference methods [LM: $F_{(1, 22)} = 11.33$, $p = 0.003$, partial $\eta^2 = 0.34$; REST: $F_{(1, 22)} = 9.70$, $p = 0.005$, partial $\eta^2 = 0.31$; AVE: $F_{(1, 22)} = 8.34$, $p = 0.008$, partial $\eta^2 = 0.27$], indicating that all reference approaches could capture the experimental pattern of increasing N400 effect magnitudes with increasing expectancy violations. Moreover, the *p*-value and effect sizes using the LM method were larger than those using the REST, followed by those using the AVE reference approach. Thus, all three reference methods could capture the nature of the N400 effect.

DISCUSSION

The current study examined whether a violation of antonym relation expectancy could induce an FRN effect and to determine the extent to which the choice of reference method influences the amplitude and scalp distribution of the experimental effect. Thus, we compared the effects of the LM, REST, and AVE reference methods on the ERP components induced by expectancy deviations of antonym relations and gambling outcomes using a within-subject design. The results revealed that the expectancy violation of antonym relations elicited N400 rather than FRN components. In addition, the reference approach influenced the magnitudes of the N400 and FRN effects but did not change the N400 and FRN responses as a function of expectancy deviation. The magnitudes of the N400 and FRN effects using the LM reference method were larger than those using the REST method, followed by those using the AVE reference approach. Moreover, although the scalp distributions of the N400 and FRN effects were similar among all three reference methods, the electrode sites that revealed significant expectancy deviation effects differed among the three reference methods.

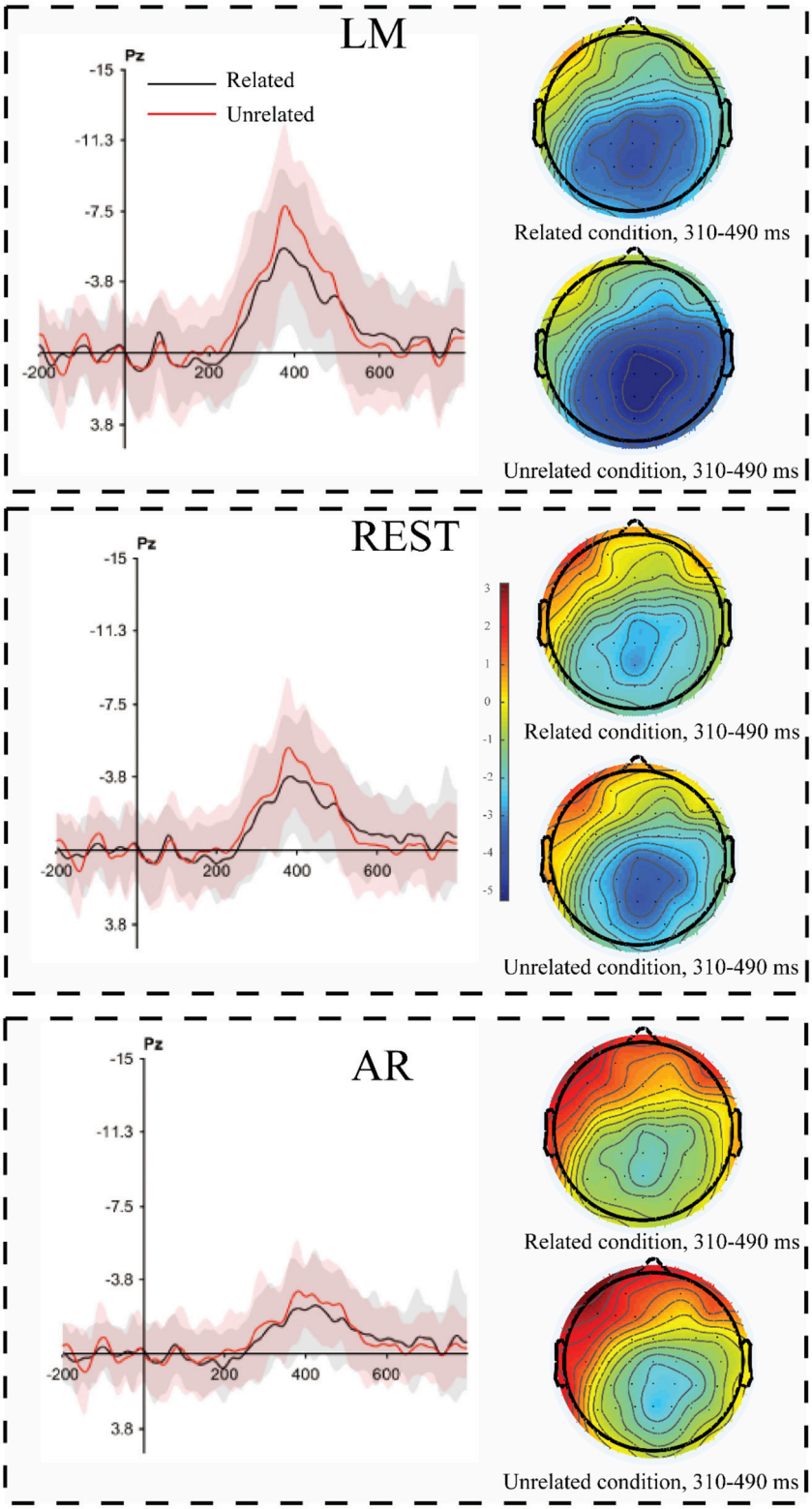

FIGURE 7 | The violation minus antonym difference waveforms as a function of the magnitude of the expectancy violation. The corresponding topographical maps of the N400 effect (310–490 ms) for large violations (unrelated condition) and small violations (related condition) revealed a strong central-parietal distribution across all three reference approaches. The shading indicates the standard error across the participants.

N400 and FRN

According to the mass univariate analysis, the statistically significant negative component in the gambling task mainly appeared at 180-330 ms and was distributed in the front-central area using all three reference methods, which reliably replicates the typical FRN effect observed in gambling tasks (Gehring and Willoughby, 2002). Thus, we reliably replicated the FRN effect. However, the negative component in the antonym task mainly appeared at 290–500 ms under both the related and unrelated conditions and had the maximum values at the more posterior electrode sites, which is consistent with the N400 component revealed in previous semantic violation tasks (Kutas and Hillyard, 1980; Kutas and Federmeier, 2000). Furthermore, the multifactor statistical analysis showed that the FRN effect was specific to the gambling task but not the antonym task, whereas the negative component at the N400 window was significant only in the antonym task but not the gambling task. These results further confirmed that the FRN effect was induced in the gambling task, but that the negative component induced in the antonym task was the N400.

N400 is a negative-going wave with a central-parietal topographic distribution that occurs at 300–600 ms and peaks at 400 ms post-stimulus onset; N400 was first observed in sematic expectancy violations in participants reading a sentence (Kutas and Hillyard, 1980). However, the temporal and spatial profiles of the N400 in the current study differed from those of Roehm et al. (2007). There were three differences between these two studies in addition to the language difference. First, the number of word pair sets was larger in our study than that in the Roehm study. The larger word sets in the current study guaranteed that each word (both X and Y) was only presented once, while word repetition of X occurred in the previous study. Second, although both studies presented the fixed sentence "*The opposite of X is Y,*" X was the first word of the fixed sentence in the Chinese sentence. The processing duration of word X was longer in this sequence, which might lead to a stable expectation about the opposite of X. Third, in our study, the ISI between the critical word Y and the previous word was 250 ms with a 50-ms per jitter step (range: 200–300 ms), while the ISI was fixed at 200 ms in the Roehm study (2007). The ISI jitter is functionally similar to high frequencies without waveform distortion (Luck, 2014). These differences might lead to the different profiles in the ERP components between these two studies. Given the observed patterns in the present study, the violation of the expected antonym relations likely induced the N400 instead of the FRN component.

Previous studies have suggested that the FRN codes violations of expectancy as feedback related to monetary loss (Gehring and Willoughby, 2002; Yu and Zhou, 2006a,b; Wu and Zhou, 2009), unexpected outcomes related to performance (Holroyd and Coles, 2002; Hajcak et al., 2007; Oliveira et al., 2007, and even stimuli of unexpected colors (Jia et al., 2007). For example, when the participants were asked to guess whether the color of the first stimulus would be the same as that of the second stimulus, the results showed that the second stimulus could induce FRN if it was an unexpected different color from the first stimulus (Jia et al., 2007). The pattern of stimulus presentation in the antonym task of our study is similar with the color guessing task in Jia et al. (2007). However, the second word in the current study induced N400 rather than FRN if it was an unexpected antonym word. Thus, an unexpected antonym word could not induce FRN, and FRN cannot codes all kinds of expectancy violations.

Reference Effect on the ERP Amplitude

Generally, in the current study, all reference methods could effectively distinguish the sematic violation-evoked N400 and gambling-evoked FRN. In addition, for all experimental effects (N400 under the related and unrelated conditions and FRN), the LM reference approach elicited larger amplitudes than the REST reference approach. In addition, the amplitudes of the AVE-obtained N400 and FRN responses were even smaller than those obtained using the REST reference method, which is consistent with previous MMN (mismatch negativity) studies (Mahajan et al., 2017). The ERP effects observed in this study varied depending on the adopted reference method, which is also consistent with previous studies (Kayser et al., 2007; Yao et al., 2007; Tian and Yao, 2013; Liu et al., 2015). The LM reference method is a non-zero reference approach in which the potential of the mastoid electrode sites is contaminated by brain activity and is not zero (i.e., a positive or negative potential) (Yao, 2001). Thus, the recorded positive or negative potential at the mastoids could lead to increases or decreases in the potential measured at the active electrode sites. According to previous simulation studies, REST has been proposed as a reference-free approach and gold standard reference method (Yao, 2001, 2017; Chella et al., 2017). In the current study, we observed that the amplitudes using the LM reference approach were larger than those observed using the REST method, which might be caused by the fact that the non-zero potentials of the mastoid electrode sites obtained using the LM reference approach increased the true potentials.

The pattern in which the N400 effect was larger under the related condition than that under the unrelated condition was observed in all reference approaches. Thus, the N400 effect is a function of deviation and is not contingent on the choice of reference method. Moreover, only a slight difference was observed among the reference approaches in the extent of the significance level (p-value) and effect size (Cohen's d). This might be benefited from the fact that the N400 amplitude is large and the signal-to-noise ratio is also high, which led to a small influence of the reference approach on the experimental effect. The experimental effect, as measured by the amplitude differences among conditions, is an important index in ERP studies. However, the experimental effects could be influenced by the reference approach (Tian and Yao, 2013; Liang et al., 2017; She et al., 2017), which might alter the results. Hence, choosing a neutral reference approach is important. Previous simulation studies suggest that the REST method is a neutral reference method since it can approximately reconstruct an infinite reference site that is not contaminated by brain activity (Yao, 2001; Zhai and Yao, 2004; Liu et al., 2015; Chella et al., 2017). Combined with previous simulation studies, the observed results in the current study suggest that REST usually achieves more objective results, which could possibly change the significance of

the ERP pattern or experimental effects compared to the other reference methods (Tian and Yao, 2013).

Reference Effect on the Scalp Distribution

According to the mass univariate analysis, the scalp distributions of the significant experimental effects differed among the three reference methods. In the antonym relations task, the distribution appeared similar between LM and REST, while REST showed more significant sites in the right hemisphere, which was consistent with the typical distribution of N400 effects (Luck, 2014). The distribution of the FRN effect also appeared similar between LM and REST, while the significant electrode sites were mainly focused in the front-central area using the REST reference approach, which is consistent with the typical distribution of FRN effects (Gehring and Willoughby, 2002). In addition, the AVE-obtained N400 effect and FRN effect were reversed in polarity (positive amplitude) at certain electrode sites, which is consistent with previous studies (Luck, 2014). The reverse pattern observed using the AVE reference method is common since the potentials of all active sites are subtracted from the sum of the voltages across all electrode sites, which is zero at each time point. This leads to positive effects along with negative effects. Thus, researchers should be cautious when using the AVE reference approach.

To statically assess the scalp distribution of N400 and FRN, repeated-measured ANOVA of the amplitude of N400 and FRN at the middle electrode site was conducted. Both the topographical distribution and statistical analysis revealed similar patterns, and only a few differences were observed among all reference approaches. This finding is consistent with previous studies (Tian and Yao, 2013; Liang et al., 2017; Yang et al., 2017). Given the results of these two analyses, the scalp distribution of the experimental effect obtained by using the REST method was more consistent with the results of previous studies, highlighting the objectivity of the REST reference approach.

CONCLUSION

The results of the current study indicate that expectancy violations in the antonym relations context induced an N400 effect instead of an FRN effect. Considering the theoretical and simulated evidence, we suggest that REST is an optional reference method to be used in future ERP data analyses. These findings contribute to other empirical investigations regarding the choice of reference approach in ERP domains.

ETHICS STATEMENT

This study was carried out in accordance with the recommendations of the Ethics Committee of the School of Psychological and Cognitive Sciences, Peking University with written informed consent from all subjects. All subjects gave written informed consent in accordance with the Declaration of Helsinki. The protocol was approved by the Ethics Committee of the School of Psychological and Cognitive Sciences, Peking University.

AUTHOR CONTRIBUTIONS

YL, YcW, and XZ designed the study. YL conducted the experiment. YL, YcW, and BZ analyzed and interpreted the data. YL, Yhw, and XZ wrote the paper. All authors contributed to and have approved the final version of the manuscript.

ACKNOWLEDGMENTS

This work was supported by The Humanity and Social Science Youth Foundation of the Ministry of Education of China (17YJC190015) and China Postdoctoral Science Foundation (2016M602754) to YL.

REFERENCES

Chella, F., D'Andrea, A., Basti, A., Pizzella, V., and Marzetti, L. (2017). Non-linear analysis of scalp EEG by using bispectra: the effect of the reference choice. *Front. Neurosci.* 11:262. doi: 10.3389/fnins.2017.00262

Dong, L., Li, F., Liu, Q., Wen, X., Lai, Y., Xu, P., et al. (2017). MATLAB toolboxes for reference electrode standardization technique (REST) of Scalp EEG. *Front. Neurosci.* 11:601. doi: 10.3389/fnins.2017.00601

Gehring, W. J., and Willoughby, A. R. (2002). The medial frontal cortex and the rapid processing of monetary gains and losses. *Science* 295, 2279–2282. doi: 10.1126/science.1066893

Gratton, G., Coles, M. G., and Donchin, E. (1983). A new method for off-line removal of ocular artifact. *Electroencephalogr. Clin. Neurophysiol.* 55, 468–484. doi: 10.1016/0013-4694(83)90135-9

Groppe, D. M., Urbach, T. P., and Kutas, M. (2011). Mass univariate analysis of event - related brain potentials/fields I: a critical tutorial review. *Psychophysiology* 48, 1711–1725. doi: 10.1111/j.1469-8986.2011.01273.x

Hajcak, G., Moser, J. S., Holroyd, C. B., and Simons, R. F. (2007). It's worse than you thought: the feedback negativity and violations of reward prediction in gambling tasks. *Psychophysiology* 44, 905–912. doi: 10.1111/j.1469-8986.2007.00567.x

Heldmann, M., Rüsseler, J., and Münte, T. F. (2008). Internal and external information in error processing. *BMC Neruosci.* 9:33. doi: 10.1186/1471-2202-9-33

Holroyd, C. B., and Coles, M. G. H. (2002). The neural basis of human error processing: reinforcement learning, dopamine, and the error-related negativity. *Psychol. Rev.* 109, 679–709. doi: 10.1037/0033-295X.109.4.679

Hu, S., Lai, Y., Valdes-Sosa, P. A., Bringas-Vega, M. L., and Yao, D. (2018). How do reference montage and electrodes setup affect the measured scalp EEG potentials? *J. Neural. Eng.* 15:026013.

Jia, S., Li, H., Luo, Y., Chen, A., Wang, B., and Zhou, X. (2007). Detecting perceptual conflict by the feedback-related negativity in brain potentials. *NeuroReport* 18, 1385–1388. doi: 10.1097/WNR.0b013e3282c48a90

Kayser, J., Tenke, C. E., Gates, N. A., and Bruder, G. E. (2007). Referenceindependent ERP old/new effects of auditory and visual word recognition memory: joint extraction of stimulus- and response-locked neuronal generator patterns. *Psychophysiology* 44, 949–967. doi: 10.1111/j.1469-8986.2007.00562.x

Kutas, M., and Federmeier, K. D. (2000). Electrophysiology reveals semantic memory use in language comprehension. *Trends Cogn. Sci. (Regul. Ed).* 4, 463–470. doi: 10.1016/S1364-6613(00)01560-6

Kutas, M., and Hillyard, S. A. (1980). Reading senseless sentences: brain potentials reflect semantic incongruity. *Science* 207, 203–205. doi: 10.1126/science.7350657

Liang, T., Hu, Z., Li, Y., Ye, C., and Liu, Q. (2017). Electrophysiological correlates of change detection during delayed matching task: a comparison of different references. *Front. Neurosci.* 11:527. doi: 10.3389/fnins.2017.00527

Liu, Q., Balsters, J. H., Baechinger, M., van der Groen, O., Wenderoth, N., and Mantini, D. (2015). Estimating a neutral reference for electroencephalographic recordings: the importance of using a high-density montage and a realistic head model. *J. Neural Eng.* 12:056012. doi: 10.1088/1741-2560/12/5/056012

Luck, S. J. (2014). *An Introduction to the Event-Related Potential Technique*. Cambridge, MA: MIT Press.

Luck, S. J., and Gaspelin, N. (2017). How to get statistically significant effects in any ERP experiment (and why you shouldn't). *Psychophysiology* 54, 146–157. doi: 10.1111/psyp.12639

Mahajan, Y., Peter, V., and Sharma, M. (2017). Effect of EEG referencing methods on auditory mismatch negativity. *Front. Neurosci.* 11:560. doi: 10.3389/fnins.2017.00560

Miltner, W. H. R., Braun, C. H., and Coles, M. G. H. (1997). Event-related brain potentials following incorrect feedback in a time-estimation task: evidence for a "generic" neural system for error detection. *J. Cogn. Neurosci.* 9, 787–796. doi: 10.1162/jocn.1997.9.6.788

Nieuwenhuis, S., Holroyd, C. B., Mol, N., and Coles, M. G. H. (2004). Reinforcement-related brain potentials from medial frontal cortex: origins and functional significance. *Neurosci. Biobehav. Rev.* 28, 441–448. doi: 10.1016/j.neubiorev.2004.05.003

Oliveira, F. T. P., McDonald, J. J., and Goodman, D. (2007). Performance monitoring in the anterior Cingulate is not all error related: expectancy deviation and the representation of action-outcome associations. *J. Cogn. Neurosci.* 19, 1994–2004. doi: 10.1162/jocn.2007.19.12.1994

Qin, Y., Xu, P., and Yao, D. (2010). A comparative study of different references for EEG default mode network: the use of the infinity reference. *Clin. Neurophysiol.* 121, 1981–1991. doi: 10.1016/j.clinph.2010.03.056

Roehm, D., Bornkessel-Schlesewsky, I., Rösler, F., and Schlesewsky, M. (2007). To predict or not to predict: influences of task and strategy on the processing of semantic relations. *J. Cogn. Neurosci.* 19, 1259–1274. doi: 10.1162/jocn.2007.19.8.1259

She, S., Li, H., Ning, Y., Ren, J., Wu, Z., Huang, R., et al. (2017). Revealing the dysfunction of schematic facial-expression processing in schizophrenia: a comparative study of different references. *Front. Neurosci.* 11:314. doi: 10.3389/fnins.2017.00314

Tian, Y., and Yao, D. (2013). Why do we need to use a zero reference? Reference influences on the ERPs of audiovisual effects. *Psychophysiology* 50, 1282–1290. doi: 10.1111/psyp.12130

Wu, Y., and Zhou, X. (2009). The P300 and reward valence, magnitude, and expectancy in outcome evaluation. *Brain Res.* 1286, 114–122. doi: 10.1016/j.brainres.2009.06.032

Yang, P., Fan, C., Wang, M., and Li, L. (2017). A Comparative study of average, linked mastoid, and rest references for ERP components acquired during fMRI. *Front. Neurosci.* 11:247. doi: 10.3389/fnins.2017.00247

Yao, D. (2001). A method to standardize a reference of scalp EEG recordings to a point at infinity. *Physiol. Meas.* 22:693. doi: 10.1088/0967-3334/22/4/305

Yao, D. (2017). Is the surface potential integral of a dipole in a volume conductor always zero? A cloud over the average reference of EEG and ERP. *Brain Topogr.* 30, 161–171. doi: 10.1007/s10548-016-0543-x

Yao, D., Wang, L., Arendt-Nielsen, L. N., and Chen, A. C. (2007). The effect of reference choices on the spatio-temporal analysis of brain evoked potentials: the use of infinite reference. *Comput. Biol. Med.* 37, 1529–1538. doi: 10.1016/j.compbiomed.2007.02.002

Yao, D., Wang, L., Oostenveld, R., Nielsen, K. D., Arendt-Nielsen, L., and Chen, A. C. (2005). A comparative study of different references for EEG spectral mapping: the issue of the neutral reference and the use of the infinity reference. *Physiol. Meas.* 26, 173–184. doi: 10.1088/0967-3334/26/3/003

Yeung, N., Holroyd, C. B., and Cohen, J. D. (2005). ERP correlates of feedback and reward processing in the presence and absence of response choice. *Cereb. Cortex* 15, 535–544. doi: 10.1093/cercor/bhh153

Yu, R., and Zhou, X. L. (2006a). Brain potentials associated with outcome expectation and outcome evaluation. *Neuroreport* 17, 1649–1653. doi: 10.1097/01.wnr.0000236866.39328.1d

Yu, R., and Zhou, X. L. (2006b). Brain responses to outcomes of one's own and other's performance in a gambling task. *Neuroreport* 17, 1747–1751. doi: 10.1097/01.wnr.0000239960.98813.50

Zhai, Y., and Yao, D. (2004). A study on the reference electrode standardization technique for a realistic head model. *Comput. Methods Programs Biomed.* 76, 229–238. doi: 10.1016/j.cmpb.2004.07.002

Conflict of Interest Statement: The authors declare that the research was conducted in the absence of any commercial or financial relationships that could be construed as a potential conflict of interest.

frontiers in Neuroscience

ORIGINAL RESEARCH
published: 18 April 2018
doi: 10.3389/fnins.2018.00250

The Scalp Time-Varying Networks of N170: Reference, Latency, and Information Flow

Yin Tian[1†], Wei Xu[1†], Huiling Zhang[1], Kin Y. Tam[2], Haiyong Zhang[1], Li Yang[1], Zhangyong Li[1] and Yu Pang[1]*

[1] Chongqing Key Laboratory of Photoelectronic Information Sensing and Transmitting Technology, Chongqing High School Innovation Team of Architecture and Core Technologies of Smart Medical System, Bio-information College, Chongqing University of Posts and Telecommunications, Chongqing, China, [2] Faculty of Health Sciences, University of Macau, Taipa, China

Using the scalp time-varying network method, the present study is the first to investigate the temporal influence of the reference on N170, a negative event-related potential component (ERP) appeared about 170 ms that is elicited by facial recognition, in the network levels. Two kinds of scalp electroencephalogram (EEG) references, namely, AR (average of all recording channels) and reference electrode standardization technique (REST), were comparatively investigated via the time-varying processing of N170. Results showed that the latency and amplitude of N170 were significantly different between REST and AR, with the former being earlier and smaller. In particular, the information flow from right temporal-parietal P8 to left P7 in the time-varying network was earlier in REST than that in AR, and this phenomenon was reproduced by simulation, in which the performance of REST was closer to the true case at source level. These findings indicate that reference plays a crucial role in ERP data interpretation, and importantly, the newly developed approximate zero-reference REST would be a superior choice for precise evaluation of the scalp spatio-temporal changes relating to various cognitive events.

Keywords: N170, time-varying network, REST, AR, latency

OPEN ACCESS

Edited by:
Pedro Antonio Valdes-Sosa, Clinical Hospital of Chengdu Brain Science Institute, China

Reviewed by:
Dezhong Yao, University of Electronic Science and Technology of China, China
Maria L. Bringas, Clinical Hospital of Chengdu Brain Science Institute, China
Xu Lei, Southwest University, China

***Correspondence:**
Yin Tian
tiany20032003@163.com

†These authors have contributed equally to this work.

Specialty section:
This article was submitted to Brain Imaging Methods, a section of the journal Frontiers in Neuroscience

Received: *26 April 2017*
Accepted: *03 April 2018*
Published: *18 April 2018*

Citation:
Tian Y, Xu W, Zhang H, Tam KY, Zhang H, Yang L, Li Z and Pang Y (2018) The Scalp Time-Varying Networks of N170: Reference, Latency, and Information Flow. Front. Neurosci. 12:250. doi: 10.3389/fnins.2018.00250

INTRODUCTION

For scalp EEG/ERP data, the choice of reference is a critical issue for not only the ERP amplitude (Yao et al., 2005), the difference between two ERPs (Tian and Yao, 2013), but also the brain network topology (Yao et al., 2005; Qin et al., 2010; Thatcher, 2012). In fact, only the voltage differences between two points can be measured (Geselowitz, 1998). However, due to the lack of a neutral (or zero) point on the human body surface, all of the current recording references, such as the mean mastoid reference (MM) and the vertex reference (Cz), might unavoidably lead to some unknown false fluctuations that destroy the genuine EEG information (Yao, 2001; Zhai and Yao, 2004; Yao et al., 2007; Kayser and Tenke, 2010; Nunez, 2010; Qin et al., 2010; Tian and Yao, 2013). For average reference (AR), though it is the most widely used re-reference in current practice, its value is not the ideal zero reference not only due to the insufficient coverage, but also due to the non-spherical shape of our human head (Yao, 2017). As a point at infinity is theoretical far from the brain sources and has an ideal zero or neutral potential, a reference electrode standardization technique (REST) was proposed to mathematically re-reference the EEG recordings to infinity to get a zero reference (Yao, 2001), and its efficiency was repeatedly confirmed by the

following studies (Marzetti et al., 2007; Tian and Yao, 2013; Chella et al., 2017). The details about REST were shown in Appendix 1. In this work, REST will be firstly used comparatively to AR to evaluate the potential effects on N170, which is an event-related potential elicited by face recognition (Bentin et al., 1996; Itier and Taylor, 2004).

Face recognition is an important ability in human daily communication. Previous electrophysiological studies found that pictures of faces elicited a larger scalp event-related potential (ERP) of negative amplitude peaking around 150–200 ms than other object categories (Bentin et al., 1996; Itier and Taylor, 2004). This early visual first negative component (N1) appeared at about 170 ms following face stimulus onset, which is termed as N170 (Bentin et al., 1996). The N170 is recorded at bilateral temporal-parietal electrode sites and is functionally associated with stages of face-specific structural encoding and/or faces detection (Bentin et al., 1996).

Though previous findings on the face-specific N170 consistency suggested that the amplitude of the N170 is largest on the posterior temporal areas, and larger on the right brain hemisphere when compared to the left brain hemisphere (Bentin et al., 1996; Webb et al., 2010; Dalrymple et al., 2011), a meta-analysis research revealed that the amplitude of N170 response to facial expressions was significantly affected by the reference electrode (Hinojosa et al., 2015). For example, the effects of facial expression on N170 amplitude were stronger based on AR than that on other references (Rellecke et al., 2013).

Unlike reaction time used in behavior studies, the latency and amplitude of ERP may definitely give us abundant information of what is happening in the brain. Except the amplitude was widely used in N170 studies (Rellecke et al., 2013; Hinojosa et al., 2015), some works also noticed the latency change. A study found that the N170 latency was delayed by inversion of faces, suggesting the extraction of the natural face gestalt was sensitive in brain (Sagiv and Bentin, 2001). A shorter N170 latency was also found in positive faces than that in negative faces, revealing the possible facial feature encoding mechanism (Batty and Taylor, 2003). These results indicated that the N170 latency plays an important role in the study of electrophysiology. However, due to the effect of non-zero reference used in current practice, it is likely that the amplitude and latency of N170 could influence the true neural effect.

The N170 generation involves multiple brain areas such as temporal-parietal regions (Bentin et al., 1996; Itier and Taylor, 2004). Therefore, network analysis may be a more appropriate approach for studying the related neural mechanisms. The time-varying networks based on the adaptive directed transfer function (ADTF) method using a multivariate adaptive autoregressive mode was developed to investigate the time-variant propagation in a simulated electrocorticogram network, which provided consistent results with the cognitive neural science (Li et al., 2016) and clinical assessments performed by neurologists. This could help fully understand the dynamic variation of N170 and uncover more detailed temporal-information processing. In the present study, the time-varying networks of N170 were the first constructed based on the AR and new REST reference (REST) to test the reference effect on the time characteristics in the network levels. Our aim was to evaluate the possible reference effect on not only the current standard ERP analysis such as amplitude and latency, but also the newly information flow from time-varying network analysis on both the real data and the simulation data. Here, simulation was designed to illustrate the reasonability of the real data. We assumed that the time characteristics of REST could be closer to the true case when compared to AR and provide a superior choice for revealing the scalp spatio-temporal changes relating to various cognitive events.

MATERIALS AND METHODS

Participants

Thirty normal right-handed male subjects aged from 18 to 25 participated in the experiment. None of them has been reported to have any history of mental or neurological problems. Informed consent was signed prior to the study, and subjects also received a monetary compensation. All experiments were approved by the ethical committee of Chongqing university of Posts and Telecommunications.

Stimuli and Design

A fixation cross ($0.5^\circ \times 0.5^\circ$) was presented at the center of the display throughout the entire block. The stimuli included human face ($3^\circ \times 3^\circ$) and letters ($3^\circ \times 3^\circ$) presented above a fixation cross. Two kinds of stimuli were presented with equal probability in random order. The stimulus onset asynchrony (SOA) varied randomly from 1,000 to 1,200 ms. Stimuli were blocked into sequences of 80 trials, and each subject completed a minimum of 2 blocks. Breaks were permitted between the blocks to maintain a high level of concentration and to prevent fatigue. Subjects were required to fixate the cross and to minimize eye blinks and body motion during all of the experimental blocks. The eye position was monitored with horizontal and vertical electrooculogram (EOG) recordings. Subjects were instructed to make a button-press response with their right index finger to key 1 if face present and key 2 if letter appear, as quickly as possible without making errors.

Data Processing

The data processing included the following four steps: EEG data preprocessing (**Figure 1A**), ERP analysis (**Figure 1B**), Time-varying network analysis (**Figure 1C**) and Stimulation design (**Figure 1D**).

EEG Recording and Preprocessing (as Shown in Figure 1A)

EEG was recorded using a 64-channel NeuroScan system (Quik-Cap, band pass: 0.05–100 Hz, sampling rate: 250 Hz, impedances$<$5 kΩ). To monitor ocular movements and eye blinks, EOG signals were simultaneously recorded from four surface electrodes, one pair placed over the higher and lower eyelid and the other pair placed 1 cm lateral to the outer corner of the left and right orbit. Cz was used as the reference during recording online. Then, the EEG was divided into epochs ($-$200 ms pre- to 1,000 ms post-stimulus onset). Trials with blinks and eye movement were rejected offline on the basis of

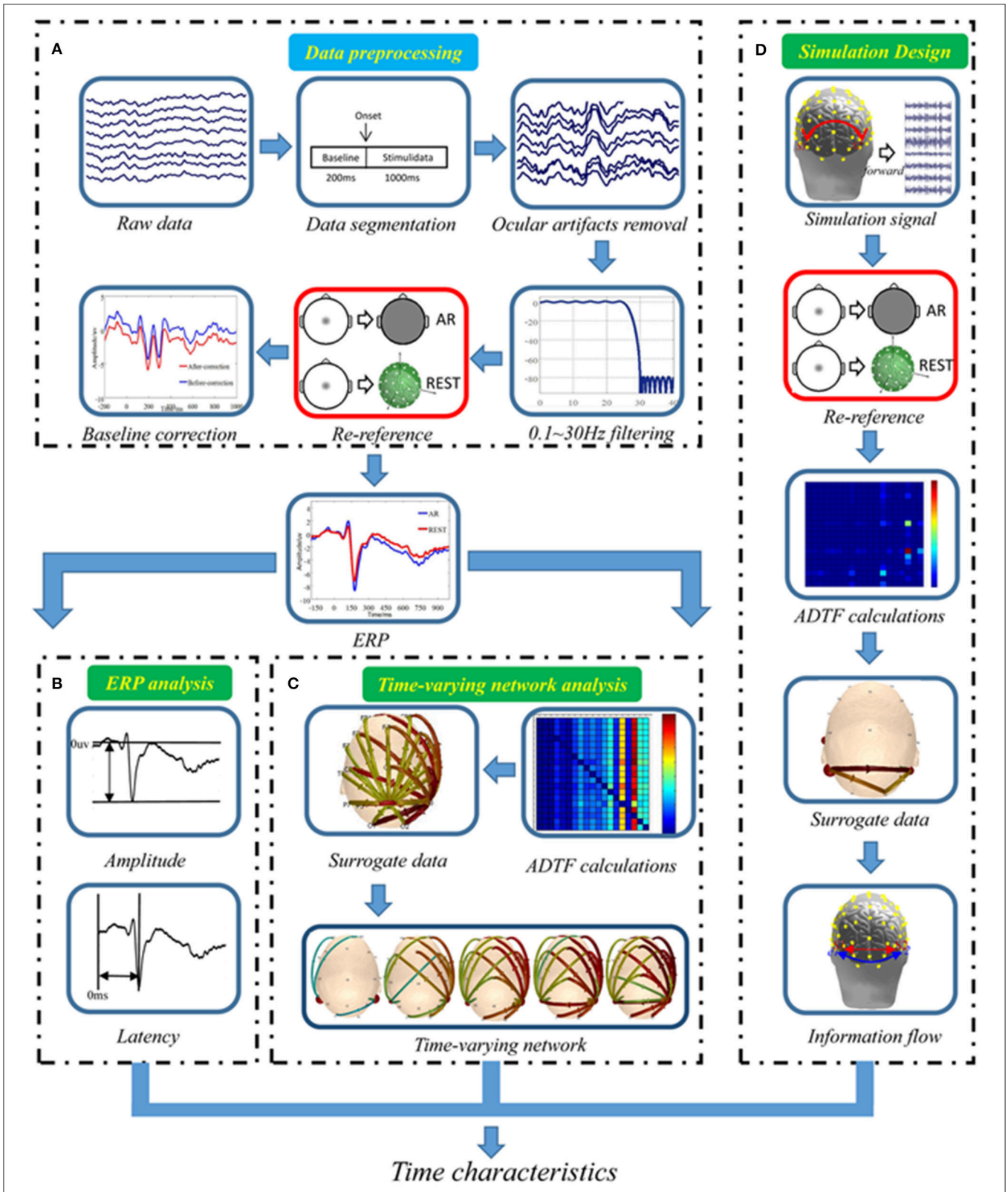

FIGURE 1 | Data analysis procedure. **(A)** Real EEG data preprocessing, **(B)** Standard ERP analysis, **(C)** Real data time-varying network analysis, **(D)** Simulation design.

the EOG. An artifact criterion of ±60 μV was used at all of the other scalp sites to reject trials with excessive electromyographs (EMGs) or other noise transients. The data were re-referenced to the AR (computed as the average of all 64 channels), and REST (the infinity zero reference reconstructed by the software REST, www.neuro.uestc.edu.cn/rest). EEG epochs were sorted according to stimulus types and were averaged from each subject to compute the ERPs. The baseline was defined as the epoch from −200 to 0 ms post-stimulus onset.

ERP Analysis (as Shown in Figure 1B)

Here, we only chose two ERPs, N170 (time window: 160–180 ms) elicited by face stimuli and N1 (time window: 160–180 ms) elicited by letter stimuli, as an example for comparing two references, with respect to amplitude and latency that were induced by the two different stimuli. The amplitudes and the latencies were separately entered into the repeated-measure ANOVAs with two factors: Reference (REST vs. AR) and Stimulus (face vs. letter). Furthermore, the latency difference of N170 between AR and REST were also tested by paired *t*-test. For ANOVA, the partial eta squared η_p^2 was used to indicate the magnitude of effect quantities.

Time-Varying Network Analysis (as Shown in Figure 1C)

To weaken the possible mixture effects such as volume conduction in the current N170 study, the 19 electrodes (i.e., Fp1, Fp2, F7, F3, Fz, F4, F8, T7, C3, Cz, C4, T8, P7, P3, Pz, P4, P8, O1, and O2) of the international 10-20 EEG system were applied in the time-varying network analysis (Xu et al., 2014; Muraja-Murro et al., 2015),which included ADTF calculation, surrogate data, stability evaluation, information flow transfer and statistical analysis (**Figure 1C**). Details were introduced in the below:

ADTF calculation

For each AR and REST related N170 data, after normalization, the multivariate adaptive autoregressive (MVAAR) model was computed by the following equation:

$$X(t) = \sum_{k=1}^{p} w(k,t)\, X(t-k) + \varepsilon(t) \tag{1}$$

where *X(t)* is the ERP data vector over the entire time window, *w(k,t)* is the coefficients matrix of the time-varying model, which can be calculated by the Kalman filter algorithm, and $\varepsilon(t)$ represents the multivariate independent white noise. The symbol p denotes the MVAAR model order selected by Schwarz Bayesian Criterion (Schwarz, 1978; Wilke et al., 2008).

After obtaining the MVAAR model coefficient, *w(k,t)*, *H(f,t)* can be obtained from *w(i,t)*, which is then transformed by Equation (2) into the frequency domain. The H_{ij} element of *H(f,t)* describes the directional information flow between the *j*th and the *i*th element at each time point *t* as:

$$w(f,t) * X(f,t) = \varepsilon(f,t) \tag{2}$$

$$X(f,t) = w^{-1}(f,t) * \varepsilon(f,t) = H(f,t) * \varepsilon(f,t) \tag{3}$$

where $w(f,t) = \sum_{k=0}^{p} w_k(t) e^{-j2\pi f \Delta t k}$ w_k is the matrix of the time-varying model coefficients. $w(f,t)$ and $\varepsilon(f,t)$ are transforming into the frequency domain as *X(t)* and $\varepsilon(t)$ respectively.

Defining the directed causal interrelation from the *j*th to the *i*th element, the normalized ADTF is described between (0, 1) as follows,

$$\iota_{ij}^2(f,t) = \frac{|H_{ij}(f,t)|^2}{\sum_k^n |H_{ik}(f,t)|^2} \tag{4}$$

To obtain the total information flow from a single node, the integrated ADTF is calculated as the ratio of summation of ADTF values divided by the interested frequency bands [*f1, f2*]:

$$\vartheta_{ij}^2(t) = \frac{\sum_{f1}^{f2} \iota_{ij}^2(k,t)}{f2 - f1} \tag{5}$$

For N170 ERP signal, the power is mainly concentrated in the 4-10 Hz frequency band (Tang et al., 2008). Hence, we choose to average ADTF values over 4–10 Hz to acquire the final directional information flow for maintaining largest information of N170.

Surrogate data

The distribution of ADTF estimator under the null hypothesis of no causal interactions is not well determined, since the ADTF function has a highly non-linear correlation with the time series where it derives. In view of this, the phases of the Fourier coefficients were independently and randomly iterated to produce a new surrogate data, which is a non-parametric statistical test (Wilke et al., 2008). The spectral structure of the time series was retained in the process of iterating the phases of the Fourier coefficients. The shuffling procedure was repeated 200 times for each model-derived time series of each subject in order to establish an empirical distribution of ADTF value under the null hypothesis of no connectivity.

Stability evaluation

In accordance with the statistical procedure (Dewan and Rao, 2005), those edges with significant differences determined by the randomly shuffled procedure were chosen by the non-parametric Wilcoxon signed rank test (details see Dewan's group study; Dewan and Rao, 2005). Three significant thresholds, i.e., $p < 0.05$, $p < 0.03$, $p < 0.01$, were set for testing stability difference between the two kinds of time-varying networks constructed via REST and AR. All thresholds were corrected by Bonferroni correction.

The present study mainly focuses on the out-degree weight at the hub electrode site to perform comparative analysis with REST- and AR-based time-varying network under distinct significance levels. Here, the out-degree weight of the *j*th node is defined as the total value of the *j*th column ADTF coefficient matrix in a time-varying network.

Information flow transfer

To measure the ability to local information transfer efficiency of the corresponding time-varying networks constructed by the ADTF based on REST and AR, the directed local efficiency based on graph theory was adopted:

$$E_{\overrightarrow{loc}} = \frac{1}{2n}\sum\nolimits_{i\,\epsilon\,N} \frac{\sum_{j,m\epsilon N, j\neq i}\left(H_{ij}+H_{ji}\right)\left(H_{im}+H_{mi}\right)\left([d_{\overrightarrow{jm}}(N_i)]^{-1}+[d_{\overrightarrow{hj}}(N_i)]^{-1}\right)}{\left(k_i^{out}+k_i^{in}\right)\left(k_i^{out}+k_i^{in}-1\right)-2\sum_{j\in N}H_{ij}H_{ji}} \tag{6}$$

where H_{ij} is the directed links from j to i and in directed networks. The H_{ij} does not necessarily equal to H_{ji}. $d_{\overrightarrow{hj}}$ denotes the directed shortest path length from h to j. n is the number of all nodes and N is the set of all nodes in the network. $k_i^{out} = \sum_{j\in N} H_{ji}$, which is the directed out-degree of node i and $k_i^{in} = \sum_{j\in N} H_{ij}$, that describes the directed in-degree of node i in the directed time-varying network.

Statistical analysis

Paired t-test was performed to measure difference between REST and AR on the out-degree of hub electrode site and the delay of information flow transfer of the time-varying network under the interested time points, respectively. The Cohen's effect size (ES) was further utilized to measure above reference difference. The detailed information about the Cohen's ES can be found in the literature (Fritz et al., 2012).

Simulation Design

In the present study, the simulation was designed to illustrate the reasonability of the real data analysis. The simulation consisted of three parts: (1) dipole selection and source waveform, (2) the realistic head model for forward computation, and (3) information flow analysis (**Figure 1D**).

Dipole selection and source waveform

In the simulation, two dipoles, S1 and S2, with fixed orientations at two specified locations with MNI coordinates (−0.57, −0.67, −0.03), and (0.61, −0.63, −0.04), respectively. One dipole was located at the left temporal-parietal region, while the other was located at right temporal-parietal region (**Figure 2A**). They were regarded as EEG sources in the cortex and had a specific interaction with each other. The forward model was constructed by the Brainstorm toolbox (http://neuroimage.usc.edu/brainstorm/), and time course of dipolar was simulated by the following time-varying casual model Equation (7):

$$\begin{cases} \mathrm{S1(t)} = 0.9 * \mathrm{S1(t-1)} - 0.9 * \mathrm{S1(t-2)} + \varepsilon_1(\mathrm{t}) \\ \mathrm{S2(t)} = 0.5 * \mathrm{S1(t-2)} + \varepsilon_2(\mathrm{t}) \end{cases} \tag{7}$$

Where $\varepsilon_1(t)$ and $\varepsilon_2(t)$ denoted uncorrelated white noise processes with identical variances. The time courses of S1 and S2 can be seen in **Figure 2B**.

The realistic head model

Here, a 3-shell realistic head model was adopted for EEG forward computation to produce scalp EEG, where conductivities for the cortex, skull, and scalp were 1.0 Ω^{-1} m^{-1}, 1/80 Ω^{-1} m^{-1}, and 1.0 Ω^{-1} m^{-1}, respectively. The solution space was restricted to the cortical gray matter, the hippocampus, and other possible source activity areas, consisting of 15002 cubic mesh voxels with 10 mm inter-distance. The lead field matrix was calculated by the boundary element method (BEM) (Fuchs et al., 1998).

Information flow analysis

Time-varying casual model was constructed by using the method of time-varying network analysis as described in the above section and the Brainstorm toolbox as mentioned above. We derived 64-channel spatiotemporally scalp EEG recordings V_{AR} and V_{REST}. 19 electrodes array of the international 10-20 system was chosen to decrease the possible effect of volume conduction (Xu et al., 2014; Muraja-Murro et al., 2015). Base on ADTF and surrogate data method, V_S, V_{AR} and V_{REST} were used to calculated the causal coefficients matrix for time-varying network analysis.

RESULTS

ERP Measures

Figure 3 showed the ERPs elicited by faces and letters based on two different effects. For the N170 amplitude, a repeated-measure ANOVA with two factors (Reference: REST vs. AR; Stimulus: face vs. letter) was performed, significant main effects of reference ($F = 17.46$, $p < 0.05$, $\eta_p^2 = 0.17$) and stimulus ($F = 24.79$, $p < 0.05$, $\eta_p^2 = 0.32$) were separately observed. The interaction effect between reference and stimulus was non-significant ($F = 0.89$, $p > 0.05$, $\eta_p^2 = 0.003$). For the N170 latency, significant main effects of reference ($F = 4.36$, $p < 0.05$, $\eta_p^2 = 0.02$) and stimulus ($F = 13.73$, $p < 0.05$, $\eta_p^2 = 0.25$) were separately observed. The interaction effect between reference and stimulus was non-significant ($F = 2.26$, $p > 0.05$, $\eta_p^2 = 0.004$). Furthermore, a paired t-test was performed to measure the reference effect on N170 elicited by human face and the result showed that the latency of N170 at the P8 based on REST was shorter than that on AR [$t = 4.37$, $p < 0.05$, $d = 0.28$; Mean latency±SD for REST: 173.01 ms ±14.69; for AR: 177.60 ms±17.96].

Time-Varying Networks in Real Data

For N170, we constructed the time-varying networks based on AR and REST. The network properties were measured to evaluate the stabilities of the out-degree on hubs and the time characteristics of local efficiency. Furthermore, paired t-test and effect size were performance to test the statistical significance of the network properties mentioned above between two references.

Stability Evaluation

The hubs and connectivity mode vary with time near 170 ms (from 164 to 180 ms) in AR- and REST-based scalp networks under three thresholds levels (**Figure 4**). For REST-based scalp time-vary networks, the hubs mainly distributed in the P8 electrode size while the out-degree weight of P8 exhibited few changes at different thresholds levels. However, for AR time-varying networks, the out-degree weight of P8 tended to be zero with the thresholds levels decreasing from 0.05 to 0.01. In contrast, the main pattern was formed earlier when REST used (same as the delay of N170 in **Figure 3**). More links survived when compared with surrogate test for the thresholds.

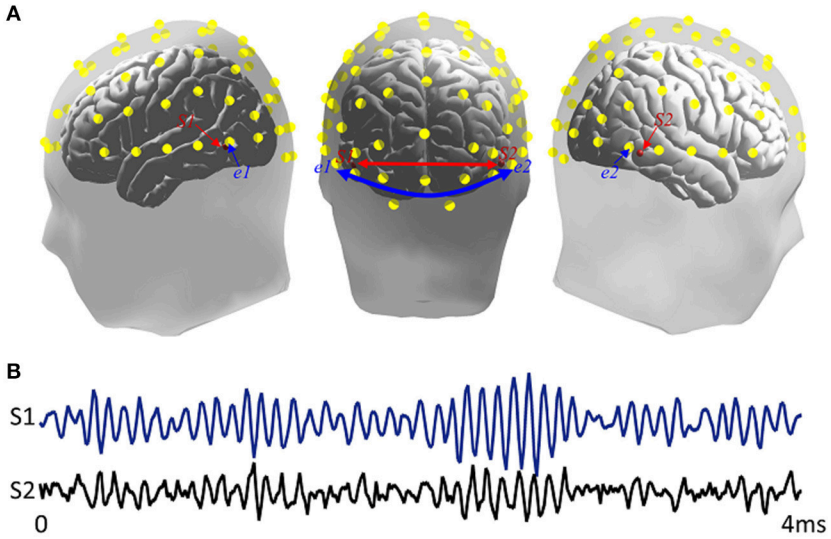

FIGURE 2 | Simulation sources. **(A)** Locations of source and scalp channels in simulation design. S1 and S2 were two dipoles separately distributed in bilateral inferior temporal areas. e1 and e2 presented two scalp electrode channels. The head model comes from Brainstorm anatomy template ICBM512, **(B)** Time series of two simulated signals.

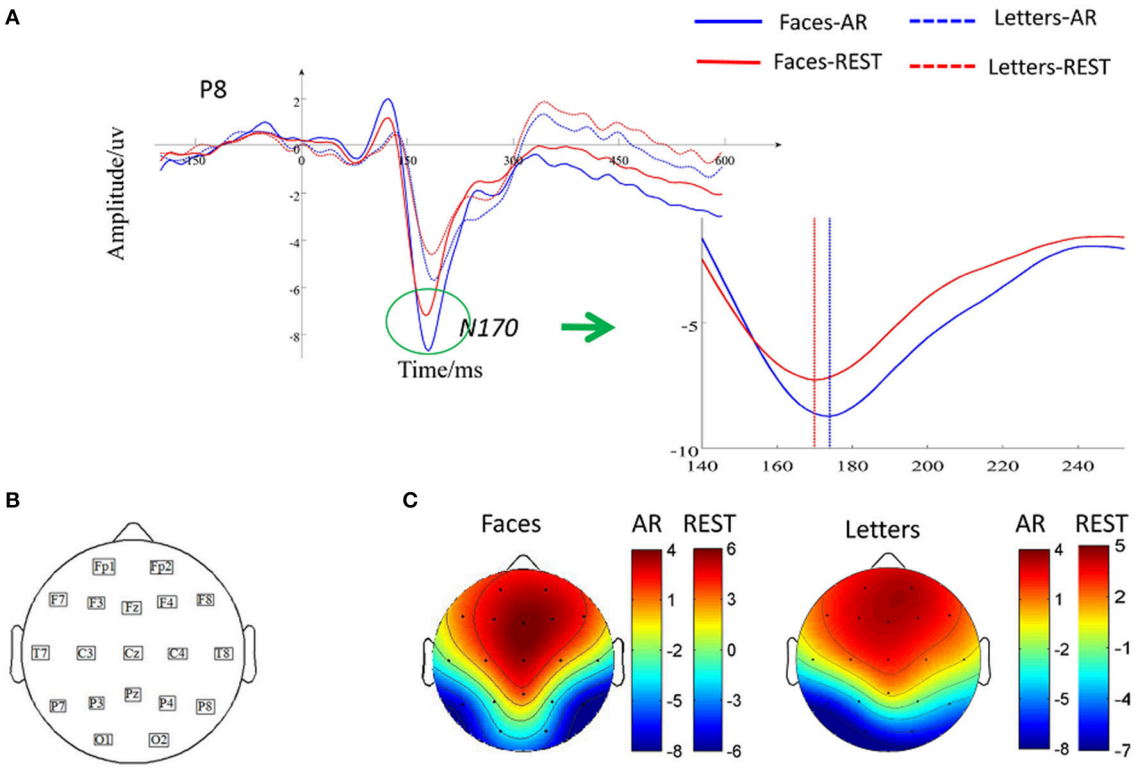

FIGURE 3 | Effects of reference during N170 peak latency and amplitude. **(A)** Grand-averaged ERP for two kinds of stimuli across all subjects at P8. Solid waveform elicited by faces and dashed waveform elicited by letters, **(B)** Distribution of 19 scalp electrodes, **(C)** Topography of ERPs induced by faces and letters in AR and REST.

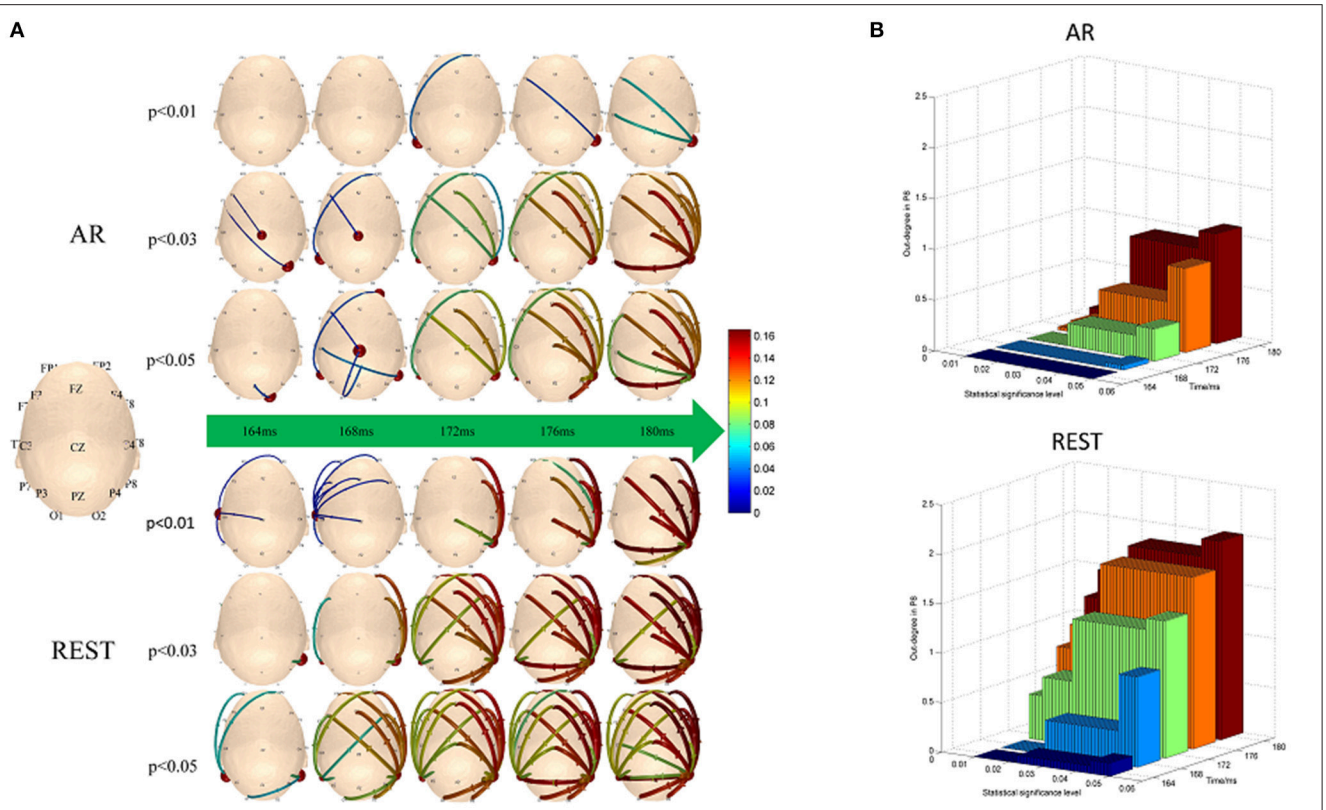

FIGURE 4 | Time-varying networks of N170. **(A)** Hubs and connection mode change over time near 170 ms under the three different significance levels, **(B)** Out-degree of P8.

Time Characteristics for Local Efficiency

According to **Figure 4**, we specially consider the local efficiency in the left temporal-parietal regions, concretely, P7, which was computed via the equation (6). The local efficiency changes over time in left temporal-parietal region (**Figure 5A**, blue bar), when information flow from right temporal-parietal region to left temporal-parietal region appears (**Figure 5A**, red asterisk). As shown from **Figure 5**, it is the appearance of links from the right to left temporal-parietal region that brings about the local efficiency of left temporal-parietal region in the REST network at 176 ms, while the similar phenomenon does not happen until 180 ms in the AR network.

Statistical Measure

The out-degree of hub node (P8) on N170 based on REST showed greater effect size than that on AR (**Table 1**). Moreover, the onset delay for information flow transfer from P8 to P7 based on REST was shown to be smaller than that on AR (**Table 2**).

Information Flow in the Simulation Case

To investigate the time characteristics of two EEG reference methods, i.e., REST and AR, as well as the theoretical possibility of the phenomenon appeared in **Figure 5**, a simulation experiment was conducted. The results from the time-varying casual model analysis were illustrated in **Figure 6**. At the given first time point (1.8 ms), there is no causal relationship from scalp electrode e2 to e1 under both AR and REST, while interconnection from S2 to S1 exists in the source space of cerebral cortex, which indicates that connection between paired scalp nodes has certain delay compared to the connection between paired sources in the cortex. At the second time point (2.0 ms), the links from e2 to e1 appear in REST network while the similar relationship does not appear until 3 ms for AR network, illustrating that the scalp information transfer in REST network is earlier than in AR network.

DISCUSSION

In the present study, two references, AR and REST, were comparatively investigated via the standard analysis of N170 and time-varying networks to reveal the potential effect of different reference on canonical analysis and newly information flow analysis. The main points found in this work were the latency change, and the temporal difference of information flow from right P8 to left P7 electrode when different references were adopted. The stability results showed that the key node distributed at temporal-parietal regions (P8). The REST-based time-varying networks represented a more robust statistical threshold than that of AR-based time-varying networks. The findings via both simulation design and real data illustrated that

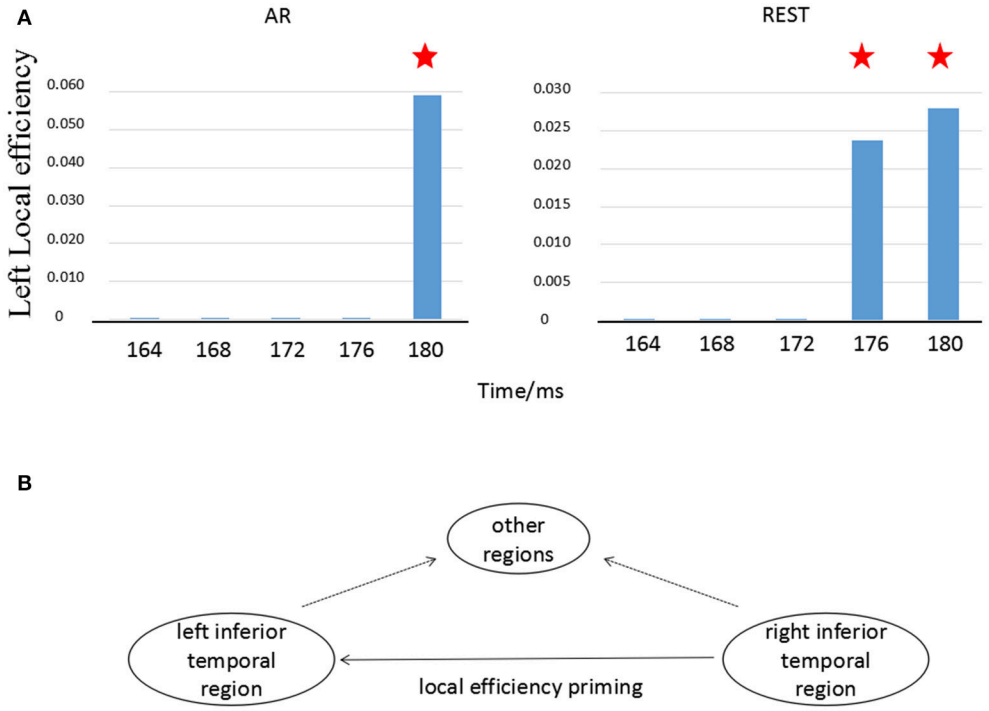

FIGURE 5 | Local efficiency in left temporal-parietal region changes with time. **(A)** Local efficiency changes in left temporal-parietal region over time, **(B)** Illustration of information transfer on local efficiency. The blue bar denotes the transformation of local efficiency in the left temporal-parietal region. The red asterisk (?) represents that there exists an information flow from right temporal-parietal region to left temporal-parietal region.

TABLE 1 | Paired *t*-test and effect size for the out-degree of P8 on N170.

Out-degree of P8	Time point (ms)	*n*	*t*	*p*	*d*
REST>AR	164	30	2.26	<0.05	0.59
REST>AR	168	30	2.18	<0.05	0.52
REST>AR	172	30	2.07	<0.05	0.43
REST>AR	176	30	2.06	<0.05	0.37
REST>AR	180	30	2.06	<0.05	0.32

n, the number of subjects. d, the effect size.

TABLE 2 | Paired *t*-test and Effect size for the onset delay for P8➔ P7 on N170.

Delay	*n*	*t*	*p*	*d*
REST<AR	24	−2.53	<0.05	−0.31

n, the number of subjects. d, the effect size Six subjects were excluded for non-information flow from P8 to P7.

REST-based networks on scalp showed the time-course closer to that on source space when compared to AR-based time-varying networks on scalp.

ERPs on Different References

In the present study, we separately observed significant main effects on stimulus types and reference as well as non-significant interaction between stimulus and reference for both the amplitude and the latency of ERPs at P8, indicating that the N170 elicited by faces was significantly bigger and earlier than that by letters regardless of REST and AR, which was consistent with the previous studies on N170 (Rellecke et al., 2013; Hinojosa et al., 2015). Moreover, the non-significant interaction illustrated that the difference of ERPs elicited by between faces and letters based on REST was similar to AR. Therefore, face-perception related N170 effects were observed based both on REST and AR through the sample analysis. However, the development of the approximate zero-reference technology would be a timely choice for precise evaluation of the scalp spatio-temporal changes related to various cognitive perceptions. Thus, the choice of correct reference will become an important issue to be addressed. In the present study, we further analyses the reference difference between REST and AR on time-varying network patterns.

Different Stability of Hub and Connectivity

In the process of establishing statistical network, choosing network statistical threshold is an inevitable step. Different significance levels may induce various network connectivity, leading to confusion in cognitive explanations. Therefore, a less-sensitive method on the aspect of scalp network connectivity threshold is highly desirable. In the present study, REST-related time-varying networks showed stronger adaptability in both hub node (P8) and connectivity strength than that of AR with various thresholds (as shown in **Figure 4**). For REST, the hubs of the bilateral temporal-parietal regions bias to the right region (P8)

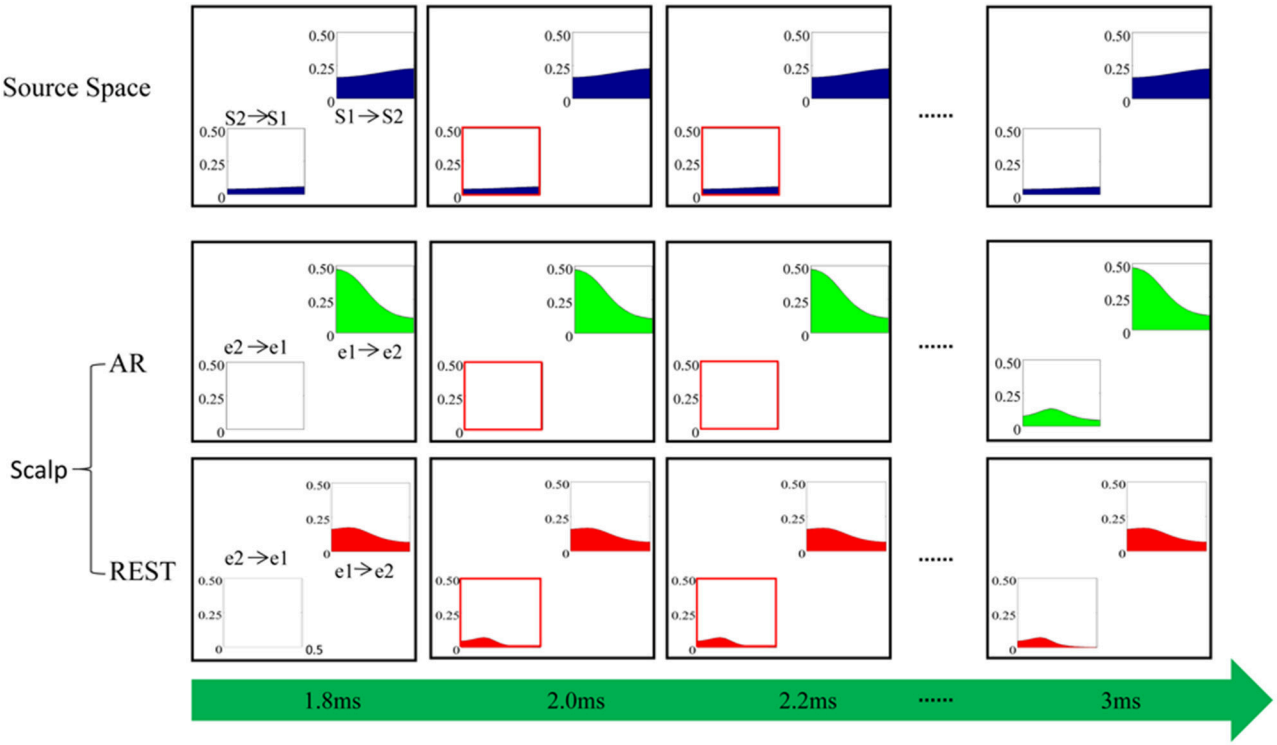

FIGURE 6 | Simulation. "S1-> S2" indicates the causal relationship from source S1 to S2 while "S2->S1" denotes the causal effect of source S2 on S1. Similarly, "e1->e2" is the causal relationship from scalp electrode e1 to e2, and "e2-> e1" denotes the causal influence of e2 on e1. The horizontal axis is normalized frequency and the ordinate represents the causal interconnection values of the corresponding frequency calculated by the ADTF algorithm.

were observed in mostly scalp networks during near 170 ms (range from 164 to 180 ms) on different thresholds, which was consistent with the previous converge evidence of N170 ERP studies (Moeller et al., 2008; Johnston and Edmonds, 2009; Dzhelyova et al., 2016). Moreover, the out-degree of P8 appeared to be relative stable regardless of the threshold levels. While for AR, the hubs mutable distributed on the posterior central region (Cz) and the bilateral temporal-parietal regions following with the changes of thresholds. The out-degree of P8 also showed a rapidly decrease when the given thresholds changed from 0.05 to 0.01 (**Figure 4B**). As shown in Figure A1 of Appendix 2 (Supplementary Material), two cortical connections of the N170 kept strong stability under different threshold levels (i.e., $p < 0.05$, $p < 0.03$, and $p < 0.01$), that is, one connection existed between the right inferior temporal area and the right occipital area in the cortical level, which is consistent with the REST connection between P8 channel and O2 channel in the scalp level. And the other connection existed between bilateral inferior temporal areas in the cortical level, which is consistent with the REST connection between P7 channel and P8 channel in the scalp level. However, AR connections did not appear these two connections observed in the cortical level. Our findings indicated that REST-based scalp varying-networks were superior to AR networks during the interval time about 170 ms which was a crucial time point for the event trigger tasks of face-related detection.

Different Time-Course of Information Flow Transfer

Cognitive processing was a multi-stage process due to the interactions of the functions of many brain regions. Previous studies have proved that face recognition resulted from synergistic effects of multiple brain regions including left and right fusiform gyrus (Devue et al., 2007; Hayes et al., 2010). Using functional magnetic resonance imaging (fMRI), researchers found that the representation of facial recognition in the left inferior temporal region depended on the support of the earlier information processing in the right inferior temporal region, suggesting that the information flow transferred from the right brain region to the left region (Verosky and Turk-browne, 2012). According to the fMRI finding, the temporal relationship between bilateral temporal-parietal regions (P7 vs. P8) was tested in the present study. We found that the priming effect of local efficiency at the left temporal-parietal region (P7) was induced by the information flow transfer originally from the right temporal-parietal region (P8) (**Figure 5A**). This phenomenon was consistent with the conception of local efficiency (Rubinov and Sporns, 2010). In other words, when the information flow from right temporal-parietal region (P8) to left temporal-parietal region (P7) existed, the connection between neighbor nodes of the hub occurred if the hub was deleted (shown in **Figure 5B**). As shown in **Figure 4A**, the different time-course on information flow was observed, i.e., the time-course separately 176 ms for

REST and 180 ms for AR. The Cohen's ES indicated that the onset delay for information flow from P8 to P7 based on REST was much less than that of AR (**Table 2**).

Temporal Difference Between Two References

Though the priming effects of local efficiency were observed in both references, the distinct time-course difference occurred between REST- and AR-based scalp time-varying networks (**Figure 5A**). The current results showed that for REST, the information transfer efficiency of synergy among multiple brain regions near the left parietal-temporal region was higher than that of AR (**Figures 4A**, **5A**). Recent research reported that the sensitivity of brain could reach sub-millisecond level responding to stimuli (Sperdin et al., 2015), indicating that the temporal difference about 4 ms between REST and AR (**Figure 5A**) was still a rather valuable time duration for the real brain response.

In the present study, the long temporal difference (4 ms) of information flow transfer between REST and AR (**Figure 5**) originated from the sampling rate (i.e., 250 Hz). In order to see the theoretical possibility of the temporal effect, a simulation study was conducted in this work. As shown by **Figure 6**, the time-course of REST-based scalp varying networks was closer to that on source space (**Figure 6**). Furthermore, the cortical time-varying networks of the N170 [Figure A1 in Appendix 2 (Supplementary Material)] also showed the appearance of the connection from the right to left inferior temporal area was found in 168 ms, which was closer to that of REST when compared to AR. Therefore, AR-based scalp varying networks could induce confusion in the explanation of N170 on temporal characteristics. This clearly suggests that the time-course of information flow for REST could be more accurate than that for AR. And the simulation further supported the time-delay between REST- and AR-based scalp time-varying networks. Further study would be required to confirm the shorter delay difference between these two references.

In general, there are two crucial factors affected scalp network analysis, they are the volume conduction and non-zero reference. For the delay problem here, the conduction from source to scalp is instantaneous, which would not be an issue. However, the mixing effect in AR with signal from all other channels mixed to each channel may change the signal dynamics, and then the latency and the information flow was possibly mislaid. This fact again emphasized the importance to have a true waveform from a zero reference as approximated by REST.

It is noted that coherence or causality has been shown to be influenced by the volume conduction (Xu et al., 2014; Zhang et al., 2015; Li et al., 2016); other techniques such as ICA and LAPLACIAN that are less influenced by the volume conduction effect may be more meaningful for this kind of EEG based network analysis. However, the implementation of them for source estimation may introduce other issues like the component selection of ICA, the effect of high frequency noise on LAPLACIAN (Yao, 2001), which needs to be carefully considered. Therefore, if the time-varying network could be realized on the scalp EEG using sparse electrode array and REST, it may provide the convenience for the corresponding researchers and also weaken the volume conduction effect.

CONCLUSION

In this work, the scalp EEG time-varying network was introduced in N170 analysis. It has been revealed that the temporal information flow occurred from right hemisphere to left hemisphere in face recognition of N170. Furthermore, the widely used AR and the newly recommended approximate zero reference (REST) was compared for both the real N170 by using experimental data and the simulation data. It has been demonstrated that AR may induce not only amplitude but also latency change in standard ERP analysis, and a change in information flow in a time-varying network analysis. In addition, our results indicated that REST would be valuable reference for precise analysis of ERP and EEG, which could become a method of choice in various cognitive studies.

AUTHOR CONTRIBUTIONS

YT: conceived, designed the experiments and Wrote the manuscipt; WX: performed the experiments, analyzed the data and Wrote the first draft; KT: wrote and re-editted the revised manuscipt; HuZ, HaZ, and LY: contributed reagents, materials, analysis tools; ZL and YP: discussed the experiment design, analyzed the data and discussed the experiment results.

ACKNOWLEDGMENTS

This research is supported by the National Natural Science Foundation of China (#61671097); the Chongqing Research Program of Basic Science and Frontier Technology (No. cstc2017jcyjBX0007; No. cstc2015jcyjA10024); the Chongqing Key Laboratory Improvement Plan (cstc2014pt-sy40001); and the University Innovation Team Construction Plan Funding Project of Chongqing (CXTDG201602009).

SUPPLEMENTARY MATERIAL

The Supplementary Material for this article can be found online at: https://www.frontiersin.org/articles/10.3389/fnins.2018.00250/full#supplementary-material

REFERENCES

Batty, M., and Taylor, M. J. (2003). Early processing of the six basic facial emotional expressions. *Brain Res. Cogn. Brain Res.* 17, 613–620. doi: 10.1016/S0926-6410(03)00174-5

Bentin, S., Allison, T., Puce, A., Perez, E., and McCarthy, G. (1996). Electrophysiological studies of face perception in humans. *J. Cogn. Neurosci.* 8, 551–565. doi: 10.1162/jocn.1996.8.6.551

Chella, F., D'Andrea, A., Basti, A., Pizzella, V., and Marzetti, L. (2017). Non-linear analysis of scalp EEG by using bispectra: the effect of the reference choice. *Front. Neurosci.* 11:262. doi: 10.3389/fnins.2017.00262

Dalrymple, K. A., Oruç, I., Duchaine, B., Pancaroglu, R., Fox, C. J., Iaria, G., et al. (2011). The anatomic basis of the right face-selective N170 IN acquired prosopagnosia: a combined ERP/fMRI study. *Neuropsychologia* 49, 2553–2563. doi: 10.1016/j.neuropsychologia.2011.05.003

Devue, C., Collette, F., Balteau, E., Degueldre, C., Luxen, A., Maquet, P., et al. (2007). Here I am: the cortical correlates of visual self-recognition. *Brain Res.* 1143, 169–182. doi: 10.1016/j.brainres.2007.01.055

Dewan, I., and Rao, B. L. S. P. (2005). Wilcoxon-signed rank test for associated sequences. *Stat. Probab. Lett.* 71, 131–142. doi: 10.1016/j.spl.2004.10.034

Dzhelyova, M., Jacques, C., and Rossion, B. (2016). At a single glance: fast periodic visual stimulation uncovers the spatio-temporal dynamics of brief facial expression changes in the human brain. *Cereb. Cortex*. 27, 4106–4123. doi: 10.1093/cercor/bhw223

Fritz, C. O., Morris, P. E., and Richler, J. J. (2012). Effect size estimates: current use, calculations, and interpretation. *J. Exp. Psychol. General* 141, 2–18. doi: 10.1037/a0024338

Fuchs, M., Drenckhahn, R., Wischmann, H. A., and Wagner, M. (1998). An improved boundary element method for realistic volume-conductor modeling. *IEEE Trans. Biomed. Eng.* 45, 980–997. doi: 10.1109/10.704867

Geselowitz, D. B. (1998). The zero of potential. *IEEE Eng. Med. Biol. Magaz.* 17, 128–132. doi: 10.1109/51.646230

Hayes, S. M., Baena, E., Truong, T. K., and Cabeza, R. (2010). Neural mechanisms of context effects on face recognition: automatic binding and context shift decrements. *J. Cogn. Neurosci.* 22, 2541–2554. doi: 10.1162/jocn.2009.21379

Hinojosa, J. A., Mercado, F., and Carreti,é, L. (2015). N170 sensitivity to facial expression: a meta-analysis. *Neurosci. Biobehav. Rev.* 55, 498–509. doi: 10.1016/j.neubiorev.2015.06.002

Itier, R. J., and Taylor, M. J. (2004). N170 or N1? Spatiotemporal differences between object and face processing using ERPs. *Cereb. Cortex* 14, 132–142. doi: 10.1093/cercor/bhg111

Johnston, R. A., and Edmonds, A. J. (2009). Familiar and unfamiliar face recognition: a review. *Memory* 17, 577–596. doi: 10.1080/09658210902976969

Kayser, J., and Tenke, C. E. (2010). In search of the rosetta stone for scalp EEG: converging on reference-free techniques. *Clin. Neurophysiol.* 121, 1973–1975. doi: 10.1016/j.clinph.2010.04.030

Li, F., Chen, B., Li, H., Zhang, T., Wang, F., Jiang, Y., et al. (2016). The time-varying networks in P300: a task-evoked EEG study. *IEEE Trans. Neural Syst. Rehabil. Eng.* 24, 725–733. doi: 10.1109/TNSRE.2016.2523678

Marzetti, L., Nolte, G., Perrucci, M. G., Romani, G. L., and Del Gratta, C. (2007). The use of standardized infinity reference in EEG coherency studies. *Neuroimage* 36, 48–63. doi: 10.1016/j.neuroimage.2007.02.034

Moeller, S., Freiwald, W. A., and Tsao, D. Y. (2008). Patches with links: a unified system for processing faces in the macaque temporal lobe. *Science* 320, 1355–1359. doi: 10.1126/science.1157436

Muraja-Murro, A., Mervaala, E., Westeren-Punnonen, S., Lepola, P., Töyräs, J., Myllymaa, S., et al. (2015). Forehead EEG electrode set versus full-head scalp EEG in 100 patients with altered mental state. *Epilepsy Behav.* 49, 245–249. doi: 10.1016/j.yebeh.2015.04.041

Nunez, P. L. (2010). REST: a good idea but not the gold standard. *Clin. Neurophysiol.* 121, 2177–2180. doi: 10.1016/j.clinph.2010.04.029

Qin, Y., Xu, P., and Yao, D. (2010). A comparative study of different references for EEG default mode network: the use of the infinity reference. *Clin. Neurophysiol.* 121, 1981–1991. doi: 10.1016/j.clinph.2010.03.056

Rellecke, J., Sommer, W., and Schacht, A. (2013). Emotion effects on the n170: a question of reference? *Brain Topogr.* 26, 62–71. doi: 10.1007/s10548-012-0261-y

Rubinov, M., and Sporns, O. (2010). Complex network measures of brain connectivity: uses and interpretations. *Neuroimage* 52, 1059–1069. doi: 10.1016/j.neuroimage.2009.10.003

Sagiv, N., and Bentin, S. (2001). Structural encoding of human and schematic faces: holistic and part-based processes. *Cogn. Neurosci. J.* 13, 937–951. doi: 10.1162/089892901753165854

Schwarz, G. (1978). Estimating the dimension of a model. *Ann. Statist.* 6, 461–464. doi: 10.1214/aos/1176344136

Sperdin, H. F., Spierer, L., Becker, R., Michel, C. M., and Landis, T. (2015). Submillisecond unmasked subliminal visual stimuli evoke electrical brain responses. *Hum. Brain Mapp.* 36, 1470–1483. doi: 10.1002/hbm.22716

Tang, Y., Liu, D., Li, Y., Qiu, Y., and Zhu, Y. (2008). The time-frequency representation of the ERPs of face processing. *Conf. Proc. IEEE Eng. Med. Biol. Soc.* 2008, 4114–4117. doi: 10.1109/IEMBS.2008.4650114

Thatcher, R. W. (2012). Coherence, phase differences, phase shift, and phase lock in EEG/ERP analyses. *Dev. Neuropsychol.* 37, 476–496. doi: 10.1080/87565641.2011.619241

Tian, Y., and Yao, D. (2013). Why do we need to use a zero reference? Reference influences on the ERPs of audiovisual effects. *Psychophysiology* 50, 1282–1290. doi: 10.1111/psyp.12130

Verosky, S. C., and Turk-browne, N. B. (2012). Representations of facial identity in the left hemisphere require right hemisphere processing. *J. Cogn. Neurosci.* 24, 1006–1017. doi: 10.1162/jocn_a_00196

Webb, S. J., Jones, E. J., Merkle, K., Murias, M., Greenson, J., Richards, T., et al. (2010). Response to familiar faces, newly familiar faces, and novel faces as assessed by ERPs is intact in adults with autism spectrum disorders. *Int. J. Psychophysiol.* 77, 106–117. doi: 10.1016/j.ijpsycho.2010.04.011

Wilke, C., Ding, L., and He, B. (2008). Estimation of time-varying connectivity patterns through the use of an adaptive directed transfer function. *IEEE Trans. Biomed. Eng.* 55, 2557–2564. doi: 10.1109/TBME.2008.919885

Xu, P., Xiong, X. C., Xue, Q., Tian, Y., Peng, Y., Zhang, R., et al. (2014). Recognizing mild cognitive impairment based on network connectivity analysis of resting EEG with zero reference. *Physiol. Meas.* 35, 1279–1298. doi: 10.1088/0967-3334/35/7/1279

Yao, D. (2001). A method to standardize a reference of scalp EEG recordings to a point at infinity. *Physiol. Meas.* 22, 693–711. doi: 10.1088/0967-3334/22/4/305

Yao, D. (2017). Is the surface potential integral of a dipole in a volume conductor always zero? a cloud over the average reference of eeg and erp. *Brain Topogr.* 30, 161–171. doi: 10.1007/s10548-016-0543-x

Yao, D., Wang, L., Arendt-Nielsen, L., and Chen, A. C. (2007). The effect of reference choices on the spatio-temporal analysis of brain evoked potentials: the use of infinite reference. *Comput. Biol. Med.* 37, 1529–1538. doi: 10.1016/j.compbiomed.2007.02.002

Yao, D., Wang, L., Oostenveld, R., Nielsen, K. D., Arendt-Nielsen, L., and Chen, A. C. (2005). A comparative study of different references for EEG spectral mapping: the issue of the neutral reference and the use of the infinity reference. *Physiol. Meas.* 26, 173–184. doi: 10.1088/0967-3334/26/3/003

Zhai, Y., and Yao, D. (2004). A study on the reference electrode standardization technique for a realistic head model. *Comput. Methods Programs Biomed.* 76, 229–238. doi: 10.1016/j.cmpb.2004.07.002

Zhang, R., Yao, D., Valdés-Sosa, P. A., Li, F., Li, P., Zhang, T., et al. (2015). Efficient resting-state EEG network facilitates motor imagery performance. *J. Neural Eng.* 12:066024. doi: 10.1088/1741-2560/12/6/066024

Conflict of Interest Statement: The authors declare that the research was conducted in the absence of any commercial or financial relationships that could be construed as a potential conflict of interest.

The reviewer MLB and handling Editor declared their shared affiliation.

frontiers in Neuroscience

ORIGINAL RESEARCH
published: 03 May 2018
doi: 10.3389/fnins.2018.00297

Unified Bayesian Estimator of EEG Reference at Infinity: rREST (Regularized Reference Electrode Standardization Technique)

Shiang Hu[1], *Dezhong Yao*[1] *and Pedro A. Valdes-Sosa*[1,2]*

[1] *The Clinical Hospital of Chengdu Brain Science Institute, MOE Key Lab for NeuroInformation, University of Electronic Science and Technology of China, Chengdu, China,* [2] *Cuban Neuroscience Center, Havana, Cuba*

OPEN ACCESS

Edited by:
Alexandre Gramfort,
Inria Saclay - Île-de-France Research Centre, France

Reviewed by:
Yury (Juri) Kropotov,
N.P.Bechtereva Institute of the Human Brain (RAS), Russia
Sara Sommariva,
Aalto University, Finland

***Correspondence:**
Pedro A. Valdes-Sosa
pedro.valdes@neuroinformatics-collaboratory.org

Specialty section:
This article was submitted to Brain Imaging Methods, a section of the journal Frontiers in Neuroscience

Received: *24 December 2017*
Accepted: *17 April 2018*
Published: *03 May 2018*

Citation:
Hu S, Yao D and Valdes-Sosa PA (2018) Unified Bayesian Estimator of EEG Reference at Infinity: rREST (Regularized Reference Electrode Standardization Technique). Front. Neurosci. 12:297. doi: 10.3389/fnins.2018.00297

The choice of reference for the electroencephalogram (EEG) is a long-lasting unsolved issue resulting in inconsistent usages and endless debates. Currently, both the average reference (AR) and the reference electrode standardization technique (REST) are two primary, apparently irreconcilable contenders. We propose a theoretical framework to resolve this reference issue by formulating both (a) estimation of potentials at infinity, and (b) determination of the reference, as a unified Bayesian linear inverse problem, which can be solved by maximum a posterior estimation. We find that AR and REST are very particular cases of this unified framework: AR results from biophysically non-informative prior; while REST utilizes the prior based on the EEG generative model. To allow for simultaneous denoising and reference estimation, we develop the regularized versions of AR and REST, named rAR and rREST, respectively. Both depend on a regularization parameter that is the noise to signal variance ratio. Traditional and new estimators are evaluated with this framework, by both simulations and analysis of real resting EEGs. Toward this end, we leverage the MRI and EEG data from 89 subjects which participated in the Cuban Human Brain Mapping Project. Generated artificial EEGs—with a known ground truth, show that relative error in estimating the EEG potentials at infinity is lowest for rREST. It also reveals that realistic volume conductor models improve the performances of REST and rREST. Importantly, for practical applications, it is shown that an average lead field gives the results comparable to the individual lead field. Finally, it is shown that the selection of the regularization parameter with Generalized Cross-Validation (GCV) is close to the "oracle" choice based on the ground truth. When evaluated with the real 89 resting state EEGs, rREST consistently yields the lowest GCV. This study provides a novel perspective to the EEG reference problem by means of a unified inverse solution framework. It may allow additional principled theoretical formulations and numerical evaluation of performance.

Keywords: EEG reference, unified estimator, regularization, inverse problem, volume conduction, relative error

INTRODUCTION

The human electroencephalogram (EEG) has been an indispensable technology for both cognitive and clinical neuroscience for almost 90 years. Ultrahigh temporal resolution, low cost, and non-invasiveness single it out as a translational tool of choice to study the brain. Nevertheless, two main drawbacks of EEG detract from its ability to localize the brain activity: (i) spatial blurring due to volume conduction; (ii) the inherent indeterminacy of potentials measurements which are always carried out with respect to a given reference (Teplan, 2002). Spatial blurring is being addressed by advanced source imaging techniques that however will not be the focus of our attention. We will rather concentrate on the vexing and still incompletely resolved "EEG reference problem." To precisely define this issue, we note that it is due to the intrinsic nature of EEG recordings that are the measurement of potential differences between two sites shown in **Figure 1**. Ideally, one would like to record the potentials of an "active electrode" that is only picking up the activities due to a few brain structures in comparison to a neutral "reference electrode" with zero activity. One might think that such a reference electrode could be placed at infinity, yielding the ideal potentials $\boldsymbol{\varphi}_\infty$. However, this would not work in practice, since this configuration would serve as an antenna, picking unwanted activity from the environment. Some researchers therefore experimented with reference electrode placed on the body so that EEG differential amplimers could eliminate environmental noise with high common mode rejection ratio. Unfortunately, because there is no neutral or inactive point upon the body, these proposals are also inadequate. A physical neutral reference seems therefore to be out of our reach.

However, the non-neutrality of the reference has consequences cascading through the following processing stages, including the final statistical result. In view of the failures of physical references, attention was turned to the construction of "virtual" estimators of the neutral references, namely, virtual estimators of $\boldsymbol{\varphi}_\infty$.

One popular virtual estimator is the "average reference" (AR, **Figure 1D**), which based on the following logic: (i) the integral of the electrical potential over a sphere, due to a current source inside it, is zero (Goldman, 1950; Offner, 1950); (ii) the head can be approximated as a sphere; (iii) therefore, a neutral reference may be obtained by summing or averaging the activities of all electrodes. Re-referencing proceeds by subtracting this average from all channels. Unfortunately, recent work (Yao, 2017) has shaken the theoretical foundation of AR: the potential integral for a realistic head surface is not zero.

A more biophysics-based virtual estimator of $\boldsymbol{\varphi}_\infty$ can be obtained by the reference electrode standardization technique (REST, **Figure 2**) which directly estimates the ideal potentials referenced to a point at infinity (Yao, 2001). REST uses a head model and equivalent sources to localize source activities, then project the source activities to electrodes—now with reference to infinity. Early work on REST was based upon a simple spherical head model. It was soon shown that EEG power maps (Yao et al., 2005), ERP peak values and latencies (Li and Yao,

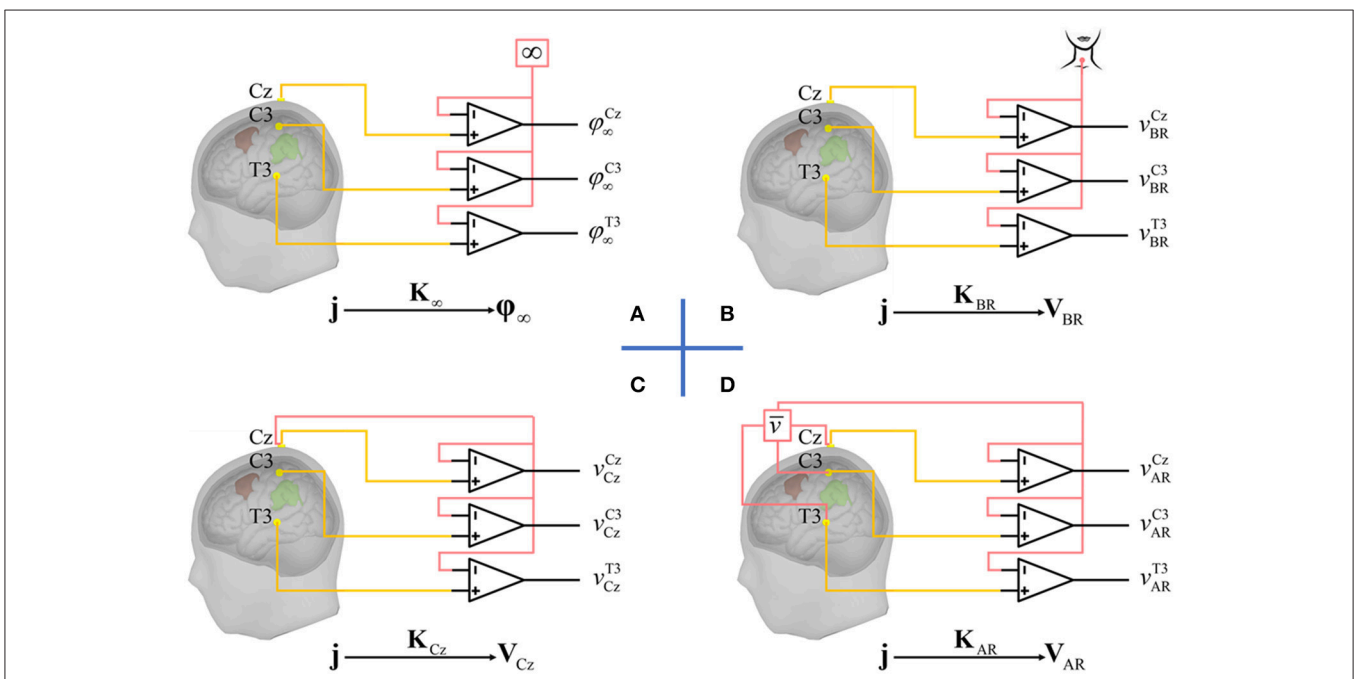

FIGURE 1 | EEG reference problem. EEG recordings measure the potential differences between active electrodes marked in yellow (only 3 for illustration) and reference marked in red which may be **(A)** a point at infinity, **(B)** an electrode placed on the body, e.g., the base of neck, **(C)** the cephalic reference (here, Cz), and **(D)** average reference: the mean of potentials over all active electrodes. All reference techniques **(B–D)** attempt to approximate infinity reference in **(A)**. The issue is that all the proposals results in different EEG waveforms originating the "EEG reference problem." It should be noted that with the identical source activities **j**, the different waveforms ($\boldsymbol{\varphi}_\infty$, $\mathbf{v}_{BR}$, $\mathbf{v}_{Cz}$,$\mathbf{v}_{AR}$) could be taken as well as the outcome of different lead fields ($\mathbf{K}_\infty$, $\mathbf{K}_{BR}$, $\mathbf{K}_{Cz}$,$\mathbf{K}_{AR}$).

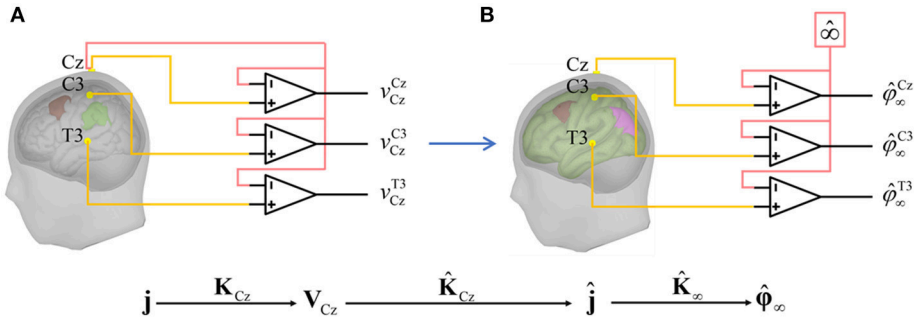

FIGURE 2 | Diagram of REST. **(A)** measured EEG potentials $\mathbf{v}_{Cz}$ with reference to Cz; $\mathbf{j}$ and $\mathbf{K}_{Cz}$ are the actual source activities and the actual lead field with reference to Cz, respectively; **(B)** for REST, one first builds the lead field $\hat{\mathbf{K}}_{\infty}$ with estimated head model and equivalent sources, then transforms the lead field with reference to Cz as $\hat{\mathbf{K}}_{Cz}$; with this lead field, one enables to estimate the equivalent source activities $\hat{\mathbf{j}}$; after, the equivalent source activities are taken the forward calculation through $\hat{\mathbf{K}}_{\infty}$ to $\hat{\boldsymbol{\varphi}}_{\infty}$ which is the approximation of EEG potentials at infinity.

2007) did, in fact, critically depend on the choice of reference. In a further study, it was shown (Tian and Yao, 2013) that scalp statistical parametric mapping with REST for audiovisual stimulus evoked potentials provided closer correspondence to the source localization by low resolution electromagnetic tomography than that with AR. These encouraging results about REST have been bolstered by several simulation experiments. Using a spherical head model for simulation, Marzetti et al. (2007) and Qin et al. (2010) indicated that REST led to better estimates of EEG spectra and coherence than AR. Several papers unsurprisingly showed that realistic head model for REST gives superior results for the reconstruction of simulated EEG scalp topographies (Liu et al., 2015), functional connectivity (Chella et al., 2016), and bispectral analysis (Chella et al., 2017).

In spite of these suggestive results in favor of REST, there is still an intense and to a certain extent unresolved debate on which reference is preferable (Nunez, 2010; Kulaichev, 2016). The lack of resolution is due to that simulation studies, while useful, are not enough to demonstrate the superiority of one reference technique over another. In addition to simulations, the evidence is needed on which reference achieves the "best fit" to actual data. The choice of the best model is a well-studied problem in modern statistics (Robert, 2007) and can be resolved by model selection criteria that approximates the Bayesian model evidence (Konishi and Kitagawa, 2008). However, to apply these techniques, an explicit Bayesian model of the "EEG reference problem" must be stated. Thus, one of the primal goals for this study is to uncover a unified estimator of EEG reference at infinity.

In the current study, we formulate, to our best knowledge for the first time, the "EEG reference problem" as a generalized Bayesian inverse problem. One surprising consequence of this approach is the insight that AR and REST share the same model and just differ in the prior distribution for the covariance of EEG potentials at infinity. On the one hand, assuming uncorrelated activities over electrodes leads to the AR estimator. On the other hand, if the correlations between electrodes are assumed to be caused by sources filtered through a volume conductor model, the resulting estimator is REST.

Our theoretical formulation will allow us to examine different reference estimators within a common statistical framework. We note that the REST estimator (Yao, 2001) was originally defined for the case of exact noise-free. In some situations, this might be unrealistic, since the scalp EEG may have quite low signal to noise ratio (Ferree et al., 2001; Lemm et al., 2006; Guruvareddy, 2013; Bigdely-Shamlo et al., 2015). Our framework allows using regularization technique as a way to accommodate noise in the data (Phillips et al., 2002, 2005). The regularized version of REST is developed which we call "rREST." It is evident that a regularized version of AR is also possible, which we term as "rAR." AR and REST are just the special cases of rAR and rREST when regularization parameter tends to zero, respectively.

We further investigate the effect of the volume conduction model on rREST. To avoid the "inverse crime" (Kaipio and Somersalo, 2007), the volume conduction model used in the simulation should be different with the one used to generate EEG potentials. We call this "volume conduction model matching problem" for REST that may produce the spurious results in simulation. Although equivalent source models are used for REST in simulation, the volume conduction model matching problem still cannot be neglected (Hu et al., 2018). Within this framework and using extensive simulations, the performances of AR, REST, rAR, and rREST are compared in terms of the relative error of estimation of $\boldsymbol{\varphi}_{\infty}$. Additionally, in these simulations, we explore the performances of the model selection criteria for selecting the regularization parameter.

Finally, we assess their performances of all the estimators using real EEG data from 89 subjects with both regularization and volume conduction matching problem tested exhaustively.

MATERIALS AND METHODS

Unified Reference Estimator

In what follows, we denote scalars with lowercase italic symbols (e.g., x), vectors with lowercase bold (e.g., $\mathbf{x}$), matrices with uppercase bold (e.g., $\mathbf{X}$); unknown parameters will be denoted by Greek letters (e.g., ξ). Furthermore, $\mathbf{1}$ is the vector of ones; $\mathbf{I}_{N_e}$ is a N_e by N_e identity matrix; $N(\mu, \Sigma)$ is the multivariable Gaussian

distribution with mean vector μ and covariance matrix Σ; $(\cdot)^{\mathbf{T}}$ is the transpose of $(\cdot)$; $\mathbf{X}^{+}$ is the pseudo-inverse of $\mathbf{X}$; $tr(\cdot)$ is the trace of $(\cdot)$; $\hat{\mathbf{X}}$ is the estimation of $\mathbf{X}$; $\|\cdot\|_2$, $\|\cdot\|_F$, and $\|\cdot\|_M$ are the Euclidean norm, the Frobenius norm, and the Mahalanobis norm, respectively.

General Reference Model

The EEG is always recorded with respect to a time-varying reference. This is usually modeled as a constant subtracted from all electrodes at each instant. In the general case, we can consider that there are two separate reference constants, one for the scalp EEG signal, and another for the sensor noise (if they come from distinctly different source). In this case, the online recorded EEG signal at a given instant is modeled as

$$\mathbf{v} = \boldsymbol{\varphi} - \mathbf{1} \times \rho + \boldsymbol{\varepsilon} - \mathbf{1} \times \zeta \tag{1}$$

where $\boldsymbol{\varphi}$ is the pure EEG signal with the neutral reference over N_e electrodes, i.e., abovementioned $\boldsymbol{\varphi}_{\infty}$, and its distribution is $N(\mathbf{0}, \Sigma_{\boldsymbol{\varphi}\boldsymbol{\varphi}})$; $\boldsymbol{\varepsilon}$ is the sensor noise with $N(\mathbf{0}, \sigma^2\mathbf{I}_{N_e})$; ρ and ζ are two reference constants of EEG signal $\boldsymbol{\varphi}$ and sensor noise $\boldsymbol{\varepsilon}$, respectively.ρ is assumed from a cephalic source, but ζ may come from either cephalic, non-cephalic or the coupled sources. Due to the uncertainty of these constants, the reference of $\mathbf{v}$ is an unknown variable. Note that other distributions for $\boldsymbol{\varphi}$ and $\boldsymbol{\varepsilon}$ may be used with our same general framework.

Applying a reference process is just a linear transformation of EEG data. Formally, it is the pre-multiplication of the reference transformation matrix with the EEG data. Thus, supposing a reference transformation matrix $\mathbf{H} = \mathbf{I} - \mathbf{1}\mathbf{f}^{\mathbf{T}}$ (Hu et al., 2018), a referential recording is

$$\mathbf{v}_r = \mathbf{H}\mathbf{v} = \mathbf{H}(\boldsymbol{\varphi} + \boldsymbol{\varepsilon}) - (\mathbf{I} - \mathbf{1}\mathbf{f}^{\mathbf{T}}) \times \mathbf{1} \times (\rho + \zeta)$$

Notably, the equation $\mathbf{f}^{\mathbf{T}}\mathbf{1} = 1$ is satisfied for all the unipolar references, such as monopolar recording references (e.g., Cz, Fz, Oz, etc.), linked mastoids and average reference.

Thus, the general EEG reference model becomes

$$\mathbf{v}_r = \mathbf{H}\boldsymbol{\varphi} + \mathbf{e}, \mathbf{e} = \mathbf{H}\boldsymbol{\varepsilon} \tag{2}$$

where r denotes a specific reference. Note that $\mathbf{H}$ is a matrix of the rank as $N_e - 1$. Thus, the estimate of $\boldsymbol{\varphi}$ is transformed into an undetermined generalized linear inverse problem.

By means of maximum a posterior estimation (Murphy, 2012), or maximum penalized likelihood estimation (LaRiccia and Eggermont, 2009), we have the objective function.

$$l = (\mathbf{v}_r - \mathbf{H}\boldsymbol{\varphi})^{\mathbf{T}}\Sigma_{\mathbf{e}\mathbf{e}}^{+}(\mathbf{v}_r - \mathbf{H}\boldsymbol{\varphi}) + \boldsymbol{\varphi}^{\mathbf{T}}\Sigma_{\boldsymbol{\varphi}\boldsymbol{\varphi}}^{+}\boldsymbol{\varphi} \tag{3}$$

After finding the partial derivative of (3) with respect to $\boldsymbol{\varphi}$, it follows that

$$\hat{\boldsymbol{\varphi}} = (\mathbf{H}^{\mathbf{T}}\Sigma_{\mathbf{e}\mathbf{e}}^{+}\mathbf{H} + \Sigma_{\boldsymbol{\varphi}\boldsymbol{\varphi}}^{+})^{+}\mathbf{H}^{\mathbf{T}}\Sigma_{\mathbf{e}\mathbf{e}}^{+}\mathbf{v}_r$$

Referring to the matrix inversion lemma (Hager, 1989; Tarantola, 2005), $\hat{\boldsymbol{\varphi}}$ is re-expressed as

$$\hat{\boldsymbol{\varphi}} = \Sigma_{\boldsymbol{\varphi}\boldsymbol{\varphi}}\mathbf{H}^{\mathbf{T}}(\mathbf{H}\Sigma_{\boldsymbol{\varphi}\boldsymbol{\varphi}}\mathbf{H}^{\mathbf{T}} + \Sigma_{\mathbf{e}\mathbf{e}})^{+}\mathbf{v}_r \tag{4}$$

which is taken as the unified Bayesian estimator in reconstructing EEG potentials at infinity.

To derive the explicit expression of (4), in addition to assuming $\Sigma_{\mathbf{e}\mathbf{e}} = \sigma^2\mathbf{H}\mathbf{H}^{\mathbf{T}}$, $\Sigma_{\boldsymbol{\varphi}\boldsymbol{\varphi}}$ is assumed to have one of the following two different forms.

Uncorrelated Prior

$$\Sigma_{\boldsymbol{\varphi}\boldsymbol{\varphi}} = \alpha^2\mathbf{I}_{N_e} \tag{5}$$

which means that the EEG potentials $\boldsymbol{\varphi}$ have independent priors across all the channels; α^2 is the mean of variances of the potentials over each electrode.

Substituting (5), $\mathbf{v}_r = \mathbf{H}\mathbf{v}$ and $\Sigma_{\mathbf{e}\mathbf{e}} = \sigma^2\mathbf{H}\mathbf{H}^{\mathbf{T}}$ into (4), it becomes

$$\hat{\boldsymbol{\varphi}} = \mathbf{H}^{+}\mathbf{H}\mathbf{v}/(1 + \sigma^2/\alpha^2\ ) \tag{6}$$

We show that $\mathbf{H}^{+}\mathbf{H} = \mathbf{I}_{N_e} - \mathbf{1}\mathbf{1}^{\mathbf{T}}/N_e$ which is the average reference transforming matrix in the Appendix. Defining the sensor noise to the scalp EEG signal ratio as $nsr_1 = \sigma^2/\alpha^2$ and $\mathbf{H}_{ar} = \mathbf{I}_{N_e} - \mathbf{1}\mathbf{1}^{\mathbf{T}}/N_e$, (6) is rewritten as

$$\hat{\boldsymbol{\varphi}} = \mathbf{H}_{ar}\mathbf{v}/(1 + nsr_1) \tag{7}$$

which we shall call the regularized average reference (rAR). It is obvious that the usual AR is the special case of rAR when $nsr_1 = 0$.

Correlated Prior

$$\Sigma_{\boldsymbol{\varphi}\boldsymbol{\varphi}} = \mathbf{K}_{\infty}\Sigma_{\mathbf{j}\mathbf{j}}\mathbf{K}_{\infty}^{\mathbf{T}} \tag{8}$$

which models the EEG potentials across all the channels as correlated due to the effect of volume conduction on neural current sources, that is, we assume that $\boldsymbol{\varphi} = \mathbf{K}_{\infty}\mathbf{j}$; $\mathbf{K}_{\infty}$ is the lead field matrix with infinity reference; $\mathbf{j}$ is the primal current density of the neural current sources with $\mathbf{j} \sim N(\mathbf{0}, \beta^2\mathbf{I}_{N_s})$; N_s is the number of neural current sources; β^2 is the variance of the multivariate Gaussian signal $\mathbf{j}$.

(4) is transformed by substituting (8) and defining $\mathbf{K}_r = \mathbf{H}\mathbf{K}_{\infty}$ as

$$\hat{\boldsymbol{\varphi}} = \mathbf{K}_{\infty} \cdot \Sigma_{\mathbf{j}\mathbf{j}}\mathbf{K}_r^{\mathbf{T}}(\mathbf{K}_r\Sigma_{\mathbf{j}\mathbf{j}}\mathbf{K}_r^{\mathbf{T}} + \Sigma_{\mathbf{e}\mathbf{e}})^{+}\mathbf{v}_r \tag{9}$$

which is the estimator for reconstructing the EEG potentials at infinity named as the regularized reference electrode standardization technique (rREST). This process can be interpreted as processing in two stages,

$$\text{Stage 1}: \quad \hat{\mathbf{j}} = \Sigma_{\mathbf{j}\mathbf{j}}\mathbf{K}_r^{\mathbf{T}}(\mathbf{K}_r\Sigma_{\mathbf{j}\mathbf{j}}\mathbf{K}_r^{\mathbf{T}} + \Sigma_{\mathbf{e}\mathbf{e}})^{+}\mathbf{v}_r$$

$$\text{Stage 2}: \quad \hat{\boldsymbol{\varphi}} = \mathbf{K}_{\infty}\hat{\mathbf{j}}$$

TABLE 1 | EEG reference model, unified estimator and schemes.

General reference model	$\mathbf{v}_r = \mathbf{H}\varphi + \mathbf{e}, \mathbf{e} = \mathbf{H}\varepsilon$				
Unified reference estimator	$\hat{\varphi} = \mathbf{\Sigma}_{\varphi\varphi}\mathbf{H}^{\mathbf{T}}(\mathbf{H}\mathbf{\Sigma}_{\varphi\varphi}\mathbf{H}^{\mathbf{T}} + \mathbf{\Sigma}_{\mathbf{ee}})^{+}\mathbf{v}_r$				
Prior of φ	$\mathbf{\Sigma}_{\varphi\varphi} = \alpha^2\mathbf{I}_{N_e}$		$\mathbf{\Sigma}_{\varphi\varphi} = \mathbf{K}_\infty\mathbf{\Sigma}_{\mathbf{jj}}\mathbf{K}_\infty^{\mathbf{T}}$		
Solutions	$\hat{\varphi} = \mathbf{H}_{ar}\mathbf{v}/(1 + nsr_1)$		$\hat{\varphi} = \mathbf{K}_\infty \cdot \mathbf{\Sigma}_{\mathbf{jj}}\mathbf{K}_r^{\mathbf{T}}(\mathbf{K}_r\mathbf{\Sigma}_{\mathbf{jj}}\mathbf{K}_r^{\mathbf{T}} + \mathbf{\Sigma}_{\mathbf{ee}})^{+}\mathbf{v}_r$		
Prior of $\mathbf{j}$			$\mathbf{\Sigma}_{\mathbf{jj}} = \beta^2\mathbf{I}_{N_s}$		$\mathbf{\Sigma}_{\mathbf{jj}} \neq \beta^2\mathbf{I}_{N_s}$
Sensor noise	zero	nonzero	zero	nonzero	nonzero
Reference schemes	AR	rAR	REST	rREST	

the first one of which is solving the inverse problem with lead field $\mathbf{K}_r$ that has the same reference as the EEG potentials $\mathbf{v}_r$ and the second one of which is taking the forward calculation to reconstruct the EEG potentials with the theoretical neutral infinity reference. In stage 1, $\hat{\mathbf{j}}$ is the standard form of solving linear inverse problems and the reference problem, simultaneously.

Defining the sensor noise to the brain source signal ratio as $nsr_2 = \sigma^2/\beta^2$ and plugging $\Sigma_{\mathbf{jj}} = \beta^2\mathbf{I}_{N_s}$, $\Sigma_{\mathbf{ee}} = \sigma^2\mathbf{H}\mathbf{H}^{\mathbf{T}}$ into (9), it becomes

$$\hat{\varphi} = \mathbf{K}_\infty \cdot \mathbf{K}_r^{\mathbf{T}}(\mathbf{K}_r\mathbf{K}_r^{\mathbf{T}} + nsr_2 \cdot \mathbf{H}\mathbf{H}^{\mathbf{T}})^{+}\mathbf{v}_r \tag{10}$$

which is the solution to reconstruct the EEG potential at infinity through solving the inverse solution by incorporating the identity diagonal structure of $\Sigma_{\mathbf{jj}}$. Apparently, REST (Yao, 2001) $\hat{\varphi} = \mathbf{K}_\infty \cdot \mathbf{K}_r^{+}\mathbf{v}_r$ is the special case of rREST when $nsr_2 = 0$ in (10).

For clarity, we summarize the general reference model and unified reference estimator in **Table 1**.

Reference Evaluation

Table 1 shows that both AR and REST are special cases of rAR and rREST if either the sensor noise is supposed to be zero or no regularization is applied. In this section, after transforming the general reference model into the standard ridge regression form, we evaluate the references via statistical model selection criteria.

Standard Regression Form

The objective function (3) of reference estimation is equivalent to the general ridge regression form (Chung et al., 2014)

$$\hat{\varphi}(\lambda) = \arg\min_{\varphi}\{\left\|\mathbf{v}_r - \mathbf{H}\varphi\right\|_M^2 + \lambda\left\|\mathbf{L}\varphi\right\|_2^2\} \tag{11}$$

where $\lambda \geq 0$ is the regularization parameter; $\mathbf{L}$ is the regularization matrix. For convenience, we call the regularization of λ and $\mathbf{L}$ as "parameter regularization" and "structure regularization," respectively.

Ridge regression is the name in statistics for Tikhonov regularization (Hoerl and Kennard, 1970). The difference between the general and the standard form of ridge regression is whether the regularization matrix $\mathbf{L}$ is identity and the misfit term is the Euclidean norm (Chung et al., 2014). Thus, we redefine $\varphi' = \mathbf{L}\varphi$ to make the regularization matrix being identity, and $\mathbf{e}' = \mathbf{D}^{\mathbf{T}}\mathbf{U}^{\mathbf{T}}\mathbf{e}$ (decompose $\mathbf{H}\mathbf{H}^{\mathbf{T}} = \mathbf{U}\mathbf{S}\mathbf{U}^{\mathbf{T}}$ and $\mathbf{S}^{+} = \mathbf{D}\mathbf{D}^{\mathbf{T}}$) to transform the Mahalanobis norm of the misfit term as the Euclidean norm. To the end, the standard ridge regression form is

$$\hat{\varphi}'(\lambda) = \arg\min_{\varphi'}\{\left\|\mathbf{v}_r{}' - \mathbf{H}'\varphi'\right\|_2^2 + \lambda\left\|\varphi'\right\|_2^2\} \tag{12}$$

with $\mathbf{v}_r{}' = \mathbf{D}^{\mathbf{T}}\mathbf{U}^{\mathbf{T}}\mathbf{v}_r$ and $\mathbf{H}' = \mathbf{D}^{\mathbf{T}}\mathbf{U}^{\mathbf{T}}\mathbf{H}\mathbf{L}^{+}$. Then, the posterior mean of φ' given $\mathbf{v}_r{}'$ is

$$\hat{\varphi}' = (\mathbf{H}'^{\mathbf{T}}\mathbf{H}' + \lambda\mathbf{I}_{N_e})^{+}\mathbf{H}'^{\mathbf{T}}\mathbf{v}_r{}' \tag{13}$$

then, the estimate of φ is $\hat{\varphi} = \mathbf{L}^{+}(\mathbf{H}'^{\mathbf{T}}\mathbf{H}' + \lambda\mathbf{I}_{N_e})^{+}\mathbf{H}'^{\mathbf{T}}\mathbf{v}_r{}'$ which is equivalent to the formula (10).

Model Selection Criteria

Since ridge regression is a linear estimator ($\hat{\mathbf{v}}_r{}' = \mathbf{P}\mathbf{v}_r{}'$) with $\mathbf{P} = \mathbf{H}'(\mathbf{H}'^{\mathbf{T}}\mathbf{H}' + \lambda\mathbf{I}_{N_e})^{+}\mathbf{H}'^{\mathbf{T}}$ where $\mathbf{P}$ is the projection ("hat") matrix. The residual sum square error (RSS) is defined as

$$\mathrm{RSS} = \sum\nolimits_{t=1}^{N_t}\left\|\mathbf{v}_{rt}{}' - \mathbf{H}'\hat{\varphi}_t{}'\right\|_2^2$$

where $\mathbf{v}_{rt}{}'$ and $\hat{\varphi}_t{}'$ with subscript t denote $\mathbf{v}_r{}'$ and $\hat{\varphi}'$at the $t^{th}(t = 1, \cdots, N_t)$ time sample, respectively; N_t is the number of time samples in the whole EEG recording.

Under the standard ridge regression form (12), we explore three information criteria for the model selection: generalized cross-validation (GCV) (Chung et al., 2014), Akaike information criteria (AIC), and Bayesian information criteria (BIC) (Konishi and Kitagawa, 2008) to compare the reference schemes in **Table 1**. To apply these, we define the degree of freedom (DF) as

$$\mathrm{DF}(\lambda) = tr(\mathbf{P}) = \sum\nolimits_{i=1}^{N_e}\frac{s_i}{s_i + \lambda}$$

where $\{s_i\}$ are the eigenvalues of $\mathbf{H}'^{\mathbf{T}}\mathbf{H}'$. Since EEG reference acts as adding or subtracting a time-varying constant over all sensors at each instant, this instantaneous effect results in the dynamical alteration in the temporal domain. To investigate the difference of references, we extend the model selection criteria from single instant to the whole recording, approximately. Predefining $N_{et} = N_e \cdot N_t$, GCV, AIC and BIC are expressed as

$$\mathrm{GCV}(\lambda) = \mathrm{RSS}/(N_{et} - \mathrm{DF})^2 \quad (14)$$

$$\mathrm{AIC}(\lambda) = N_{et}\log(\mathrm{RSS}/N_{et}) + N_t \cdot 2 \cdot \mathrm{DF} \quad (15)$$

$$\mathrm{BIC}(\lambda) = N_{et}\log(\mathrm{RSS}/N_{et}) + N_t \cdot \mathrm{DF} \cdot \log(N_{et}) \quad (16)$$

Note that GCV, AIC, and BIC at a single instant are the special cases of (14–16) with $N_t = 1$, respectively.

Regularization Parameter

The regularization parameter λ balances the goodness of fitting (i.e., likelihood) and the prior constraint on the EEG potentials at infinity. One may try to interactively estimate the hierarchal Bayesian hyperparameter via iteration (MacKay, 1992; Trujillo-Barreto et al., 2004). However, this may work for rREST but poorly for rAR because the noise term will be assimilated into the pure EEG signal in (6) due to the uncorrelated covariance prior. Namely, the objective function of AR is non-convex and it cannot converge to a global or local optimal point. Thus, we adopt a search strategy to explore how DF, GCV, AIC and BIC vary with the values of λ (Phillips et al., 2005). The idea is to plot the DF against λ, as well as GCV, AIC and BIC against DF. The theoretical solutions (7) and (10), indicate that the optimal λ is around nsr_1 for rAR, and approximates to nsr_2 for rREST, respectively. Since volume conduction acts as a lowpass spatiotemporal filter, it results in $nsr_2 \ll nsr_1$ (Srinivasan et al., 1998; Stinstra and Peters, 1998; Srinivasan, 1999; Nunez and Srinivasan, 2006). Supposing the intervals of SNR are [35, 10] dB for rREST, and [30, −10] dB for rAR, we generate 1,000 values of λ from 1e-3.5 to 1e-1 for rREST, and from 1e-3 to 10 for rAR, by using sampled logarithm, respectively.

In the simulation, we can evaluate the reference estimators with an "oracle" regularization parameter, namely, one for which the smallest relative error regarding the ground truth. Additionally, the efficacy of the model selection criteria (GCV, AIC, and BIC) for selecting the regularization parameter is evaluated. It will be trickier to find a proper λ with actual EEG data where the ground truth is unknown. The value with which one model selection criteria reaches to a global or local minimum is regarded as the optimal λ chosen by the model selection criteria for actual EEG data.

It has been suggested to avoid regularization when applying REST so as not to lose high-frequency information (Yao, 2001). Instead, a truncation of singular value decomposition (TSVD) was proposed to suppress the effect of sensor noise for REST (Zhai and Yao, 2004). Therefore, we empirically adopt the recommended truncation parameter 0.05 for REST but use the model selection criteria for rREST.

Regularization Matrix

The choice of regularization matrix **L** depends on the prior covariance structure of the potentials at infinity. **Table 1** shows that the prior covariance structure of $\boldsymbol{\varphi}$ as $\Sigma_{\boldsymbol{\varphi\varphi}} = \alpha^2\mathbf{I}_{N_e}$ for AR and rAR, and $\Sigma_{\boldsymbol{\varphi\varphi}} = \mathbf{K}_\infty\Sigma_{\mathbf{jj}}\mathbf{K}_\infty^{\mathbf{T}}$, for REST and rREST, respectively. Therefore, the choices of **L** are:

$$\text{for AR and rAR,} \quad \mathbf{L}_{ar} = \mathbf{I}_{N_e}$$

$$\text{for REST and rREST,} \quad \mathbf{L}_{rt} = [(\mathbf{K}_\infty\mathbf{K}_\infty^{\mathrm{T}})^+]^{1/2} \quad (17)$$

Several cases of $\mathbf{K}_\infty$ are detailed in the next section. The degree of faithful biophysical regularization by $\mathbf{L}_{rt}$ increases from the less realistic approximation of volume conductor to the more realistic one.

Volume Conduction Model

For rREST, we study the volume conduction model matching problem, that is, to what extent, the lead field for rREST may be different from the actual one that generated the simulated EEG data or the real EEG recordings. Here, we evaluate several types of lead fields. The well-known spherical lead field (SLF) is a frequently adopted standard lead field. The most precise volume conduction model is the individual lead field (ILF) matched to the structural Magnetic Resonance Image (sMRI) of each subject. We also evaluate the average lead field (ALF) as a substitute for the individual lead field. Finally, we evaluate the "sparse individual lead field" (sILF) for which we switch off the voxels not used in the simulations. We will use suffixes to distinguish between types of lead fields.

Spherical lead field (SLF)

$\mathbf{K}_\infty^{\mathrm{s}}$, is estimated based on the standard 3-layers concentric spherical head model comprising of brain, skull, and scalp with the conductivities being 1, 0.0125, and 1, respectively. For the spherical head shape, the radii are 1.0, 0.92, and 0.87 for the scalp surface, outer and inner skull surface, separately. The source space consists of 2600 discrete dipole sources evenly and radially distributed on the cortical surface with radius $r = 0.86$ and 400 discrete dipole sources uniformly located perpendicularly to the transverse plane with $Z = -0.076$. Here, the values of conductivities, radii, and coordinates are not the actual measurements but the relative ratios of conductivities and radii between the head layers, and the relative coordinates in the unit sphere space (Yao, 2001; Hu et al., 2018).

Individual lead field (ILF)

$\mathbf{K}_\infty^{\mathrm{i}}$, is defined by normalization as

$$\mathbf{K}_\infty^{\mathrm{i}} = \mathbf{K}_\infty^{\mathrm{iraw}}/[tr(\mathbf{K}_\infty^{\mathrm{iraw}}\mathbf{K}_\infty^{\mathrm{iraw}\mathbf{T}})]^{1/2}$$

where $\mathbf{K}_\infty^{\mathrm{iraw}}$ is the raw individual lead field matched to the $i^{th}(i = 1, \cdots, N_b)$ subject who underwent the EEG recording in Cuban Human Brain Mapping Project (CHBMP) (Uludag et al., 2009; Valdés-Hernández et al., 2010; Hernandez-Gonzalez et al., 2011; Bosch-Bayard et al., 2012). It is estimated by the finite element method based on the segmented cortical surface through CIVET pipeline (Yasser Ad-Dab'bagh, 2006) with sMRI. The cortical surface is formed by 6003 vertices and 11998*3 faces. In total, 6003 dipole sources are located at the vertices and activated perpendicularly to the cortical surface, individually. The normalization allows for comparison across subjects.

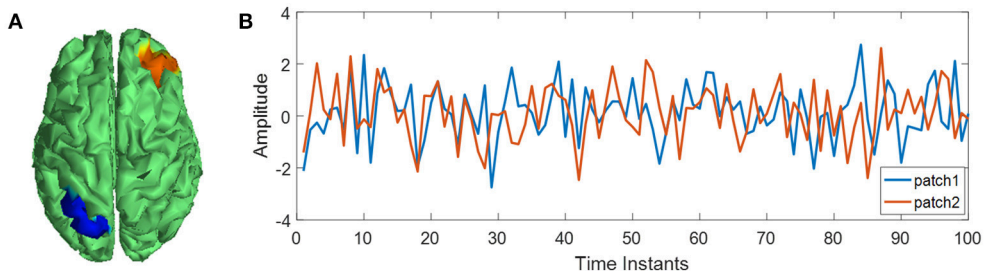

FIGURE 3 | Source activities for EEG simulation. **(A)** Location of two source patches; **(B)** activities of two source patches.

Average lead field (ALF)
$\mathbf{K}_{\infty}^{a}$, is the average of all the normalized ILFs of N_b subjects as

$$\mathbf{K}_{\infty}^{a} = \frac{1}{N_b}\sum_{\mathbf{i}=1}^{N_b}\mathbf{K}_{\infty}^{\mathbf{i}}$$

Sparse individual lead field (sILF)
$\mathbf{K}_{\infty}^{\mathrm{si}}$, (for use in simulation) is obtained after transforming ILF as follows

$$\mathbf{K}_{\infty}^{\mathrm{si}} = [\mathbf{K}_{\infty}^{\mathrm{iraw}} \circ \mathbf{W_i}]/[tr(\mathbf{K}_{\infty}^{\mathrm{iraw}} \circ \mathbf{W_i}\mathbf{W_i^T} \circ \mathbf{K}_{\infty}^{\mathrm{iraw}^{\mathbf{T}}})]^{1/2}$$

where $\circ$ means the matrix elementwise multiplication operation (i.e., Hadamard product); $\mathbf{W_i}$ is a matrix that consists of binary weights and has the same size with $\mathbf{K}_{\infty}^{\mathrm{iraw}}$; the entries at the columns of un-activated brain sources are zeros and the other columns are full of ones. In the simulation, the position of two patches of sources is incorporated into the covariance of the EEG potentials at infinity for rREST. In place of adopting l_0 norm or l_1 norm to sparse the brain electrical source signal $\mathbf{j}$, we set the entries corresponded to non-activated sources of ILF being zeros to constrain the brain source signal indirectly.

RESULTS

Simulation

EEG Generation

The simulation scheme is based on the forward equation below,

$$\begin{cases} \mathbf{v}_r = \mathbf{H}\boldsymbol{\varphi} + \mathbf{H}\boldsymbol{\varepsilon}, \boldsymbol{\varphi} = \mathbf{K}_{\infty}^{\mathrm{iraw}}\mathbf{j} \\ \mathrm{SNR} = 10\log_{10}(\alpha^2/\sigma^2) \end{cases} \quad (18)$$

where $\mathbf{v}_r$ is the simulated EEG potentials with unipolar reference; without loss of generality, the linear combination vector $\mathbf{f} = [0, \cdots, 0, 1]^{\mathbf{T}}$ with the last entry being one and the others being zeros; two patches consisting of 150 dipole sources in $\mathbf{j}$ are activated, meeting 4-order bivariate autoregressive model (**Figure 3**); SNR is the scalp EEG signal to the sensor noise variance ratio in dB unit.

With the $\mathbf{K}_{\infty}^{\mathrm{iraw}}$ of 89 subjects from the CHBMP database, the simulated EEG data of one group is 89 samples *58 channels *5120 instants. Totally, we generated the dataset A: 4 groups where the SNR values are different between groups but the same for all the samples in each group, and the dataset B: one group where the SNR values are different for all the samples. The simulation provides the ground truth of EEG potentials with the neutral reference, thus making it possible to intuitively compare the performances of references in terms of the relative error of potentials. For each data sample, the relative error (RE) of potentials is defined as

$$\mathrm{RE} = \left\|\hat{\boldsymbol{\varphi}} - \boldsymbol{\varphi}\right\|_F^2 / \left\|\boldsymbol{\varphi}\right\|_F^2 \quad (19)$$

where $\boldsymbol{\varphi}$ denotes the ground truth; $\hat{\boldsymbol{\varphi}}$ is the EEG potentials estimated by the references in **Table 1**.

Relative Error of Reference Estimators

The relative error (RE) is calculated using the simulated dataset A of 4 groups where the SNR values are 20dB, 8dB, 4dB, and 2dB for each group, respectively. **Figures 4A–D** show the REs of the reference estimators, including the lead fields variants (SLF, ILF, ALF, and sILF) for REST and rREST. Boxplots in black, green, red, and blue, show the REs of AR, rAR, REST and rREST, separately. It is evident from the boxplots (**Figures 4A–D**), that the REs of regularized references (rAR, rREST) are always less than that of unregularized references (AR, REST). Unpaired t-tests were applied to check the differences between unregularized references (AR, REST) and regularized references (rAR, rREST). **Figure 4E** lists the statistical significance levels (p-values) between AR and rAR, as well as between REST and rREST with various lead fields tested, separately. Except for the case between AR and rAR with SNR = 20dB, the p-values all reach very small values (<1e-7).

With regularization, the decreases of REs from REST to rREST are more obvious than the decreases of REs from AR to rAR. Especially, regularization with sILF is much more effective than SLF, ILF, and ALF. This is not surprising since the sparse prior information was incorporated into the covariance structure. By contrast, by the simplest volume conduction model, i.e., SLF, the REs of rREST seems to be even larger than that of AR, and REST performs worst among all the references, when SNR = 20 and 8 dB. Comparing the REs by sILF and that of rREST by SLF with the REs of REST by SLF, we found that structure regularization by precise covariance seems to be more effective than the parameter regularization by selecting the optimal λ which led the least RE among all the tested values of λ . And the REs of rREST with sILF are the least among all the REs of other references.

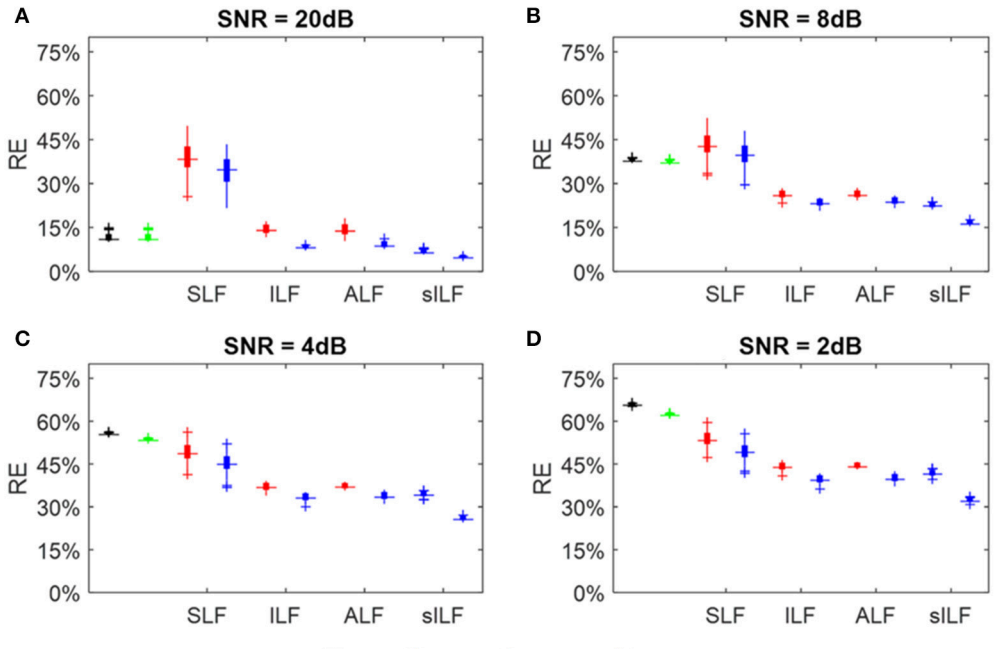

E

SNR (dB)	AR vs. rAR	REST vs. rREST			
		SLF	ILF	ALF	sILF
20	0.47	<1e-7			
8, 4, 2	<1e-20				

FIGURE 4 | Relative error (RE) of reference estimators. **(A–D)** The boxplots of REs with SNR = 20, 8, 4, and 2 dB, respectively. Volume conduction model tested for REST and rREST are spherical lead field (SLF), individual lead field (ILF), average lead field (ALF), and sparse individual lead field (sILF). **(E)** The *p*-values of REs between ordinary references (AR, REST) and regularized references (rAR, rREST) under different SNR and various lead fields, separately.

This means that structure regularization in combination with parameter regularization will have the best effect. In addition, injecting higher sensor noise with SNR being from 20 to 2 dB, the REs of rAR increase from less than 15% to higher than 60% accordingly, while the REs of rREST with SLF excluded rise from 4.1 to 40%.

These results indicate that: (1) except for the case of AR and rAR with SNR = 20 dB, AR, rAR, REST, and rREST by using SLF that roughly approximated the actual volume conduction model may be not able to reconstruct the EEG signal at infinity due to the quite large REs; (2) the effects of REST and rREST are volume conduction model dependent; (3) stronger regularization applied, better effect of rREST obtained; (4) for REST and rREST, the REs by using ALF seems to be almost same with the REs by ILF; (5) rAR may not have the effect of denoising. Over all, AR and rAR may be the alternative option when SNR is very large ($\geq$20 dB), while rREST with precise volume conduction model should be the first option to estimate the EEG signal at infinity.

Model Selection for Estimators With Simulated Data

The model selection is analyzed using the simulated dataset B where SNR values uniformly distributed in the interval of [5 20] dB are set for the 89 samples to mimic the different SNRs of subjects in the real EEG recordings. The results summarized in **Figure 5** allow determining the optimal reference via the model selection criteria. The plotted DF (degree of freedom), RSS (residual sum square), and the model selection criteria (GCV, AIC, BIC) are the average of them explored individually over the 89 data samples with all the regularization parameters λ (i.e., LMD) tested. The curves in **Figure 5A** show how the DF and GCV vary with the LMDs as well as how the RSS changes with DF. It is easy to see that the DF of rREST are always smaller than the DF of rAR. This means that rREST adopts the simpler model to reconstruct the EEG signal at infinity but employ the more realistic prior information for regularization than rAR. The lower RSS of rREST than rAR indicate that the EEG signal reconstructed by rREST is closer to the truth compared with the EEG signal restored by rAR. The curves in **Figure 5B** display how the model selection criteria (GCV, AIC, BIC) vary with the DF. Apparently, the model selection criteria values of rREST are always smaller than them of rAR. The prevalent lower values of model selection criteria provide the evidence to prefer rREST over rAR.

Regularization Parameter

For rREST, it is crucial to pick the best regularization parameter, i.e., the value of λ . **Figure 6** displays that, to what extent, the

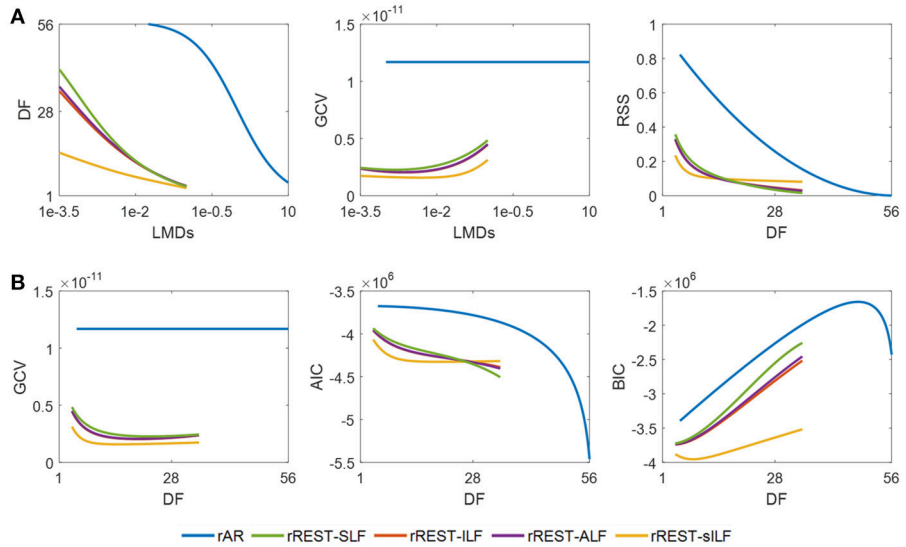

FIGURE 5 | Model selection with simulated data. DF, RSS, GCV, AIC, and BIC are the average over the 89 EEG data samples individually simulated with a different SNR among [5 20] dB. **(A)**, DF and GCV against LMD, and RSS varying with DF; **(B)**, model selection criteria (GCV, AIC, and BIC) against DF. DF, degree of freedom; RSS, residual sum square; GCV, generalized cross validation; AIC, Akaike information criteria; BIC, Bayesian information criteria; SLF, spherical lead field; ILF, individual realistic lead field; ALF, the average of realistic lead fields; sILF, sparse individual lead field.

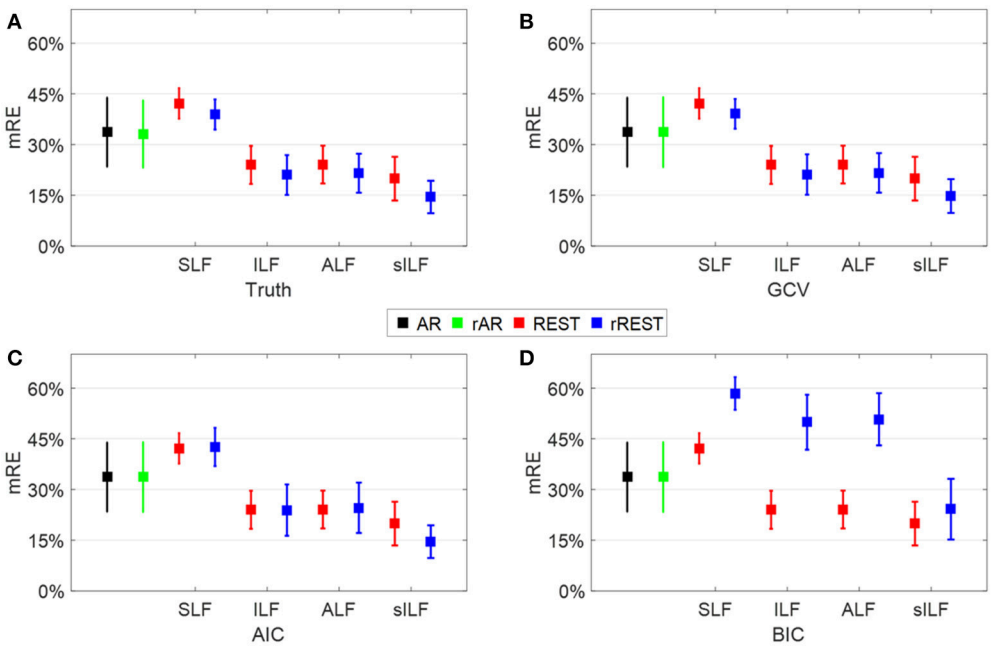

FIGURE 6 | Regularization parameter selection. Each square and the error bar are the mean relative error (mRE) and standard deviation over the 89 data samples individually simulated with a different SNR among [5 20] dB. **(A)**, The truth where the best λ is picked by the least RE; **(B–D)**, the results where the best λ is selected by the least GCV, AIC, and BIC values, respectively.

values of λ selected by the model selection criteria (GCV, AIC, and BIC) are close to the truth, that is, the oracle picked by the least RE based on the simulated dataset B. Note that the best λ identified by ground truth and the model selection criteria is in the individual data sample level rather than in the group level due to the averaged model selection criteria curves. Comparing the mean relative error (mRE) and the standard deviations in **Figures 6B–D** with those in **Figure 6A**, GCV is easily found

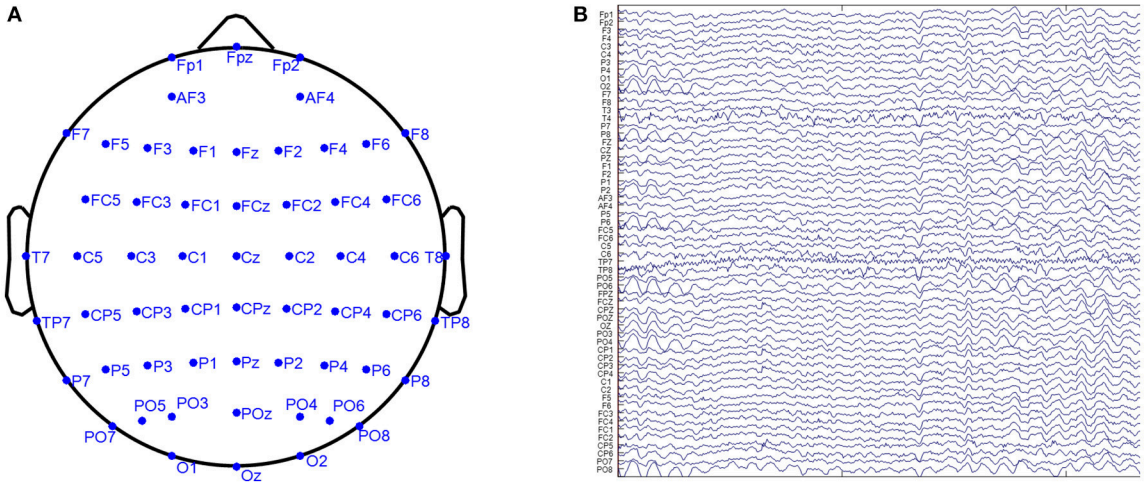

FIGURE 7 | The illustration of a real EEG data sample. **(A)** The electrodes position, **(B)** the waveform of one epoch.

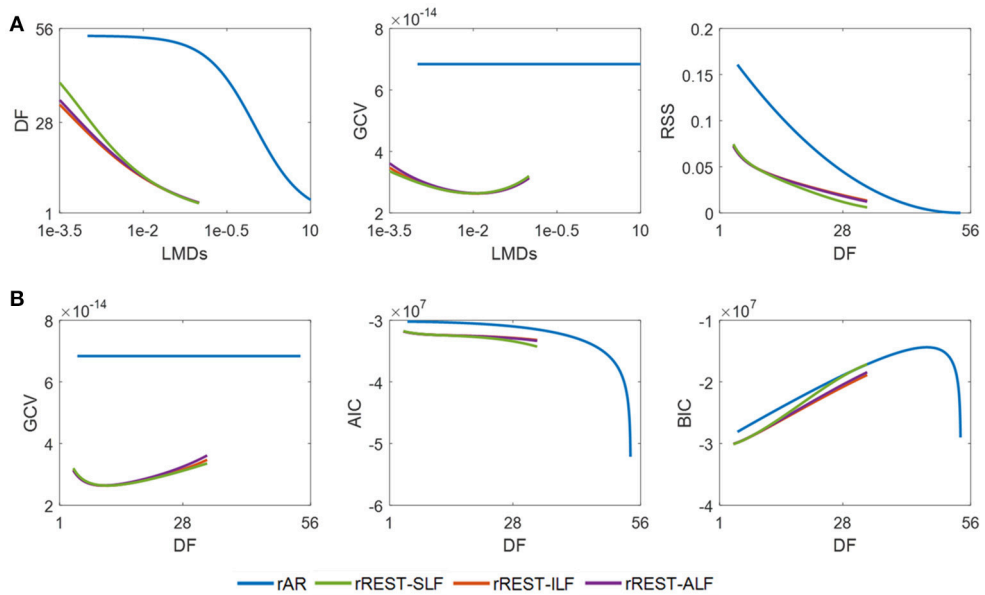

FIGURE 8 | Model selection with actual EEG. DF, RSS, GCV, AIC, and BIC are the average of them individually explored over the 89 real EEG recordings. **(A)** DF and GCV against LMD, and RSS varying with DF; **(B)**, model selection criteria (GCV, AIC, and BIC) against DF. DF, degree of freedom; RSS, residual sum square; GCV, generalized cross validation; AIC, Akaike information criteria; BIC, Bayesian information criteria; SLF, spherical lead field; ILF, individual realistic lead field; ALF, the average of realistic lead fields; sILF, sparse individual lead field.

as the best one to select the proper regularization parameter due to the almost same mRE and standard deviations to the truth; AIC is worse than GCV since except for the rREST by using sILF, the regularized reference (rAR, rREST) show the same or larger mRE and standard deviations than the ordinary reference (AR, REST); BIC is the worst one to select the proper regularization parameters because all the regularized references (rAR, rREST) present the larger mREs and standard deviations than the ordinary references (AR, REST).

Model Selection for Estimators With Real Data

We take the EEG of 89 subjects from the CHBMP database to evaluate the reference estimators. The EEG recordings were carried out in accordance with the recommendations of Ethics committees of Ministry of Public health and Cuban Neuroscience Center with written informed consent from all subjects. The EEG was acquired with 58 channels, 10–10 electrode placement system, sampling rate 200 Hz, recording period 2.5–5 minutes,

and with the resting-state of "eyes-closed-open" intermittently conditioned. **Figure 7** displays a real EEG data sample. To compare the performance of references over all subjects, we normalize the EEG data by

$$\mathbf{v}_r = \mathbf{v}_r^{raw} / \left\| \mathbf{v}_r^{raw} \right\|_F$$

The model selection criteria GCV, AIC, and BIC are calculated for each subject with the matched ILF, sILF, the identical ALF and SLF. The mean model selection criteria are averaged over 89 subjects.

To validate the preference of rREST over rAR, a similar analysis as descried before for simulations regarding performance is now applied to the realistic resting state EEG dataset of 89 subjects from the CHBMP database. The results in **Figure 8** show how the DF (degree of freedom) and GCV (generalized cross validation) change with the regularization parameter λ (i.e., LMD) and how the RSS (residual sum square) and model selection criteria (GCV, AIC, and BIC) vary with the DF. The plotted DF, RSS, and model selection criteria are the average of them individually explored over the 89 subjects. Since the reference transformation matrix **H** and the limits of regularization parameter λ (i.e., LMD) are the same as that in simulation, the curves of DF against LMDs in **Figure 8A** are identical to them in **Figure 5A**. The lower RSS and model selection criteria curves in **Figure 8B** confirm, for real data, our previous findings in simulations, that (1) the EEG signal reconstructed by rREST has lower RSS than that restored by rAR; (2) rREST has the smaller values of GCV, AIC, and BIC than rAR, except for the almost same BIC between rREST and rAR around DF = 28. Since GCV was found to be the best criteria to choose the proper regularization parameter λ in the simulation shown in **Figure 6**, we suggest adopting GCV to select the value of λ for each EEG recording in practice when the ground truth is unknown. The curves in the middle of **Figure 8A** shows how GCV varies with the values of λ (i.e., LMDs). For rREST, the global minimum of GCV occurs around λ = 1e-2 or DF = 10. We therefore conjecture that for the group analysis, it is possible to find the best regularization parameter by the lowest GCV which may offer an empirical example for the possible optimal LMD for rREST. However, it will be the safest to choose the regularizer parameter by using GCV for each individual recording as what we have shown in **Figure 6**. By contrast, GCV of rAR seems to be one constant which is caused by the nonconvex solution of rAR where it is hard to find the proper λ. These results indicate that the preference of rREST over rAR is validated for real EEG. Moreover, for rREST, the best regularization parameter can be picked at the global minimum of GCV curves.

DISCUSSION

Although the reference electrode standardization technique (REST) was put forward some time ago, its theoretical underpinnings have not been deeply studied, particularly from a mathematical statistics perspective. Prior to REST, the average reference (AR) had been broadly adopted, e.g., in the microstates analysis (Khanna et al., 2015), and as well offered as the final solution to "reference electrode problem" in the inverse solutions (Pascual-Marqui, 1999, 2002, 2007; Pascual-Marqui et al., 2011). Currently, both AR and REST are the main competing estimators (Nunez, 2010). Many comparative studies have been carried out, however, without providing the definitive evidence to prefer one over another (Qin et al., 2010; Chella et al., 2016, 2017; Lei and Liao, 2017). The need to settle this issue has been reinforced recently by the theoretical results of Yao, who demonstrated that the main assumption of AR—the cancelation of brain potentials averaged over the scalp is, in general, false (Yao, 2017). However, it is difficult to decide the reference issue solely by the biophysical interpretations. Empirical verification of the best reference using a full statistical model is also essential.

In this study, we propose to view the estimation of the potentials at infinity and the determination of reference as a linear inverse problem that can be attacked using well known Bayesian techniques. To our surprise, both AR and REST are two special cases with different prior distributions for the covariance of the EEG potentials referenced to infinity. By explicitly introduced the sensor noise term into the reference model, we combined the estimation of the potentials at infinity with denoising. The formulation, based on maximum a posterior estimation, leads to the regularized estimators, rAR and rREST. Finally, recognizing that the reference is a linear inverse problem leads to the use of model selection criteria to examine several issues. It is found, for both simulated and actual data, that (1) regularization is critical to solving the reference problem and denoising simultaneously; (2) the regularized reference (rAR/rREST) has a better performance than the ordinary reference (AR/REST), respectively; (3) rREST outperforms rAR; (4) to apply rREST to real EEG data, generalized cross-validation is recommended as an effective measure to select the optimal regularization parameter. In our opinion, the definitive argument in favor of rREST is that for 89 resting state EEGs it provides a smaller Generalized Cross Validation. This is the first empirical comparison of references using an information criterion that approximates the Bayesian model evidence.

We have demonstrated that AR is not "the final solution to the reference electrode problem" (Pascual-Marqui et al., 2011), but rather a special case of uncorrelated prior and noise-free of the unified reference estimator. Pascual-Marqui et al derived AR with the assumption of exact noise-free, or say, under the condition that the covariance matrix for the measurement noise is identity. Before the inverse solution, the reference problem is solved by the derived AR which is supposed to achieve the best fit for the reference process. However, in this study, if the reference process is also involved for the measurement noise but not only for the EEG signal, AR cannot be derived. Since the inverse solution does not depend on the reference electrode, both AR and the monopolar reference can be used to transform the lead fields and the EEG recordings with the same reference before the inverse solution. This is described as the stage 1 of the implementation of rREST following the Equation (9).

REST has attracted attention due to its theoretically sound basis (Yao, 2001; Kayser and Tenke, 2010; Nunez, 2010). However, some studies with ordinary REST suggest that it does not uniformly dominate AR (Yao, 2001; Hu et al., 2018). Though

ordinary REST was found to be more effective than AR for vertically oriented and shallow dipole sources, this was not so for transverse or deep dipoles. These findings, in our perspective, were due to that the covariance structure for ordinary REST is derived from the two factors, a spherical volume conductor, and limiting sources to the equivalent distributed dipoles layer (Yao and He, 2003), i.e., the sources over the 2D cortical sheet with radial orientation (Yao, 2001). By contrast, we tested here more realistic volume conduction models. Also, our simulations were based on multiple cortical patches. Our results indicate that more realistic volume conductor and source space do make the reference estimator better, and that in fact, REST does dominate AR in all cases.

We emphasize multi-possibilities of source modeling and restate the conception of the generalized inverse problem. As REST is a generalized inverse solution, the multipole sources (Daunizeau et al., 2006) and the general 3D distributed sources at each grid of brain volume (Michel et al., 2004) can be also be adopted for REST as well (Yao, 2000). We have shown that all generalized inverses are not equal and an interesting line of research will be to explore how different source model procedures can be translated into variants of REST.

The volume conduction model matching test showed that REST and rREST is volume conduction model dependent and the importance of the adequate volume conduction model. This is in agreement with the findings of Hu et al. (2018) and Liu et al. (2015). Liu et al reported that a realistic volume conduction model is critical to ordinary REST. Hu et al stated that ordinary REST is volume conduction model dependent but imprecise or slightly perturbated lead fields does not deteriorate ordinary REST much. This is in line with our simulation results that better estimates of both the volume conductor and source lead to better reference estimates. The result that sILF achieves the least relative errors among all the volume conduction models tested for rREST is obvious since the prior sILF matches the forward calculation. The only point of this simulation is to caution that the prior for rREST should be as close as possible to the actual. Of course, this can only be known to an actual approximation. In future, a promising way to account the uncertainty for a correct prior is to employ Bayesian Model Averaging (Trujillo-Barreto et al., 2004).

However, it is computational costly to estimate the individual lead field which requires the subject's sMRI—something not usual in many clinical settings. However, we found that the average lead field achieves the almost same performance as obtained with the exact individual lead field. This validates the proposal that approximate head models without individual MRI can be quite useful (Valdés-Hernández et al., 2009).

A critical point for rREST is to choose the optimal regularization parameter which has been the topic of intense research in statistics (Konishi and Kitagawa, 2008). Our simulations and validation on the real EEG recording suggest that the generalized cross validation criteria could be a simple and sensitive procedure to solve this issue. Once again, in practice, we recommend adopting the generalized cross validation criteria to select the regularization parameter for each individual EEG recording.

Main contributions of this paper are:

(1) We propose that reference estimation is a unified Bayesian linear inverse problem.
(2) This framework explicitly models sensor noise as a part of the EEG generative model.
(3) AR and REST are shown to be the special cases of the linear inverse problem, with a spatially independent prior for AR and a spatially correlated prior for REST due to volume conduction.
(4) Regularized estimators, rAR and rREST, are developed to implement reference estimation and denoising simultaneously.
(5) We adopted the model selection criteria (GCV, AIC, BIC) for not only to select the hyperparameter but also to compare model families. GCV was found to be the most useful indicator.
(6) We propose the average lead field as a practical substitute for the individual lead field to construct near optimal estimators.

Several extensions of this study are being explored:

- Artifact suppression may be incorporated together with reference estimation and denoising. For example, outliers can be eliminated by utilizing a likelihood function designed for robust statistics (Huber and Ronchetti, 2009).
- More biophysical information may be built into the prior distributions to more effectively differentiate the EEG signal from the sensor noise. Particularly, covariance matrices corresponding to different types of structured sparsity source models should be examined (Paz-Linares et al., 2017).
- We have dealt only with spatial priors for the covariance matrix of the EEG. Dynamical priors can easily be incorporated. Temporal autocorrelations may be modeled as state space models and estimated via the Kalman filter (Galka et al., 2004). Alternatively, formulations for the frequency, or time frequency domain are possible.
- The framework may be also extended to event related potentials incorporating prior work from our group in this direction (Carbonell et al., 2004).

CONCLUSION

We state the EEG reference problem as a unified inverse problem that can be solved via Bayesian techniques. To our best knowledge, this is a novel approach to the problem. This formulation allows us to:

- Adopt regularization methods to estimate the potential referenced to infinity.
- Demonstrate that REST and AR are the special cases of the unified estimator with different EEG spatial covariance priors.
- Simultaneously carry out denoising as part of the reference estimation procedure.
- Use model selection criteria to determine the optimal reference estimator. These results can be summarized as:
  - Regularized references (rREST or rAR) are superior to the ordinary REST or AR, with rREST having the overall best performance for both simulations and real data.

- The optimal choice of volume conductor model is the individual or averaged lead field.

Regularized REST (rREST) may be used in clinical settings, as an improved estimator of EEG potentials referenced to infinity.

AUTHOR CONTRIBUTIONS

SH developed the theories with PV-S, processed the data, and wrote the complete manuscript. DY made some valuable comments to this study. PV-S posed the scientific question to this study and polished the manuscript.

ACKNOWLEDGMENTS

The authors declare no conflict of interest. This research was co-funded by the National Natural Science Foundation of China projects (NSFC Grants No. 61673090, 81330032, and 81601585). We thank Esin Karahan and Pedro A. Valdes-Hernandez for their valuable technical assistance.

REFERENCES

Baksalary, J. K., Maria Baksalary, O., and Trenkler, G. (2003). A revisitation of formulae for the Moore–Penrose inverse of modified matrices. *Linear Algebra Appl.* 372, 207–224. doi: 10.1016/S0024-3795(03)00508-1

Bigdely-Shamlo, N., Mullen, T., Kothe, C., Su, K.-M., and Robbins, K. A. (2015). The PREP pipeline: standardized preprocessing for large-scale EEG analysis. *Front. Neuroinform.* 9:16. doi: 10.3389/fninf.2015.00016

Bosch-Bayard, J., Valdés-Sosa, P. A., Fernandez, T., Otero, G., Pliego Rivero, B., Ricardo-Garcell, J., et al. (2012). 3D Statistical Parametric Mapping of quiet sleep EEG in the first year of life. *Neuroimage* 59, 3297–3308. doi: 10.1016/j.neuroimage.2011.11.001

Carbonell, F., Galán, L., Valdés, P., Worsley, K., Biscay, R. J., Diaz-Comas, L., et al. (2004). Random Field–Union Intersection tests for EEG/MEG imaging. *Neuroimage* 22, 268–276. doi: 10.1016/j.neuroimage.2004.01.020

Chella, F., D'Andrea, A., Basti, A., Pizzella, V., and Marzetti, L. (2017). Non-linear analysis of scalp EEG by using bispectra: the effect of the reference choice. *Front. Neurosci.* 11:262. doi: 10.3389/fnins.2017.00262

Chella, F., Pizzella, V., Zappasodi, F., and Marzetti, L. (2016). Impact of the reference choice on scalp EEG connectivity estimation. *J. Neural Eng.* 13:36016. doi: 10.1088/1741-2560/13/3/036016

Chung, J., Español, M. I., and Nguyen, T. (2014). *Optimal Regularization Parameters for General-Form Tikhonov Regularization.* Available online at: http://arxiv.org/abs/1407.1911

Daunizeau, J., Mattout, J., Clonda, D., Goulard, B., Benali, H., and Lina, J. M. (2006). Bayesian spatio-temporal approach for EEG source reconstruction: conciliating ECD and distributed models. *IEEE Trans. Biomed. Eng.* 53, 503–516. doi: 10.1109/TBME.2005.869791

Ferree, T. C., Luu, P., Russell, G. S., and Tucker, D. M. (2001). Scalp electrode impedance, infection risk, and EEG data quality. *Clin. Neurophysiol.* 112, 536–544. doi: 10.1016/S1388-2457(00)00533-2

Galka, A., Yamashita, O., Ozaki, T., Biscay, R., and Valdés-Sosa, P. (2004). A solution to the dynamical inverse problem of EEG generation using spatiotemporal Kalman filtering. *Neuroimage* 23, 435–453. doi: 10.1016/j.neuroimage.2004.02.022

Goldman, D. (1950). The clinical use of the "average" reference electrode in monopolar recording. *Electroencephalogr. Clin. Neurophysiol.* 2, 209–212.

Guruvareddy, A. (2013). Artifact Removal from EEG Signals. *Int. J. Comput. Appl.* 77, 975–8887. doi: 10.5120/13543-1175

Hager, W. W. (1989). Updating the inverse of a matrix. *SIAM Rev.* 31, 221–239. doi: 10.1137/1031049

Hernandez-Gonzalez, G., Bringas-Vega, M. L., Galán-Garcia, L., Bosch-Bayard, J., Lorenzo-Ceballos, Y., Melie-Garcia, L., et al. (2011). Multimodal quantitative neuroimaging databases and methods: the cuban human brain mapping project. *Clin. EEG Neurosci.* 42, 149–159. doi: 10.1177/155005941104200303

Hoerl, A. E., and Kennard, R. W. (1970). Ridge regression: biased estimation for nonorthogonal problems. *Technometrics* 12, 55–67. doi: 10.1080/00401706.1970.10488634

Hu, S., Lai, Y., Valdes-Sosa, P. A., Bringas-Vega, M. L., and Yao, D. (2018). How do reference montage and electrodes setup affect the measured scalp EEG potentials? *J. Neural Eng.* 15:26013. doi: 10.1088/1741-2552/aaa13f

Huber, P. J., and Ronchetti, E. M. (2009). *Robust Statistics*. Hoboken, NJ: John Wiley and Sons, Inc.

Kaipio, J., and Somersalo, E. (2007). Statistical inverse problems: discretization, model reduction and inverse crimes. *J. Comput. Appl. Math.* 198, 493–504. doi: 10.1016/j.cam.2005.09.027

Kayser, J., and Tenke, C. E. (2010). In search of the Rosetta Stone for scalp EEG: converging on reference-free techniques. *Clin. Neurophysiol.* 121, 1973–1975. doi: 10.1016/j.clinph.2010.04.030

Khanna, A., Pascual-Leone, A., Michel, C. M., and Farzan, F. (2015). Microstates in resting-state EEG: current status and future directions. *Neurosci. Biobehav. Rev.* 49, 105–113. doi: 10.1016/j.neubiorev.2014.12.010

Konishi, S., and Kitagawa, G. (2008). *Information Criteria and Statistical Modeling*. New York, NY: Springer.

Kulaichev, A. P. (2016). Optimal choice of a reference electrode for EEG recording. *Moscow Univ. Biol. Sci. Bull.* 71, 145–150. doi: 10.3103/S0096392516030068

LaRiccia, V. N., and Eggermont, P. P. (2009). *Maximum Penalized Likelihood Estimation*. New York, NY: Springer.

Lei, X., and Liao, K. (2017). Understanding the influences of EEG reference: a large-scale brain network perspective. *Front. Neurosci.* 11:205. doi: 10.3389/fnins.2017.00205

Lemm, S., Curio, G., Hlushchuk, Y., and Müller, K.-R. (2006). Enhancing the signal-to-noise ratio of ICA-based extracted ERPs. *IEEE Trans. Biomed. Eng.* 53, 601–607. doi: 10.1109/TBME.2006.870258

Li, L., and Yao, D. (2007). A new method of spatio-temporal topographic mapping by correlation coefficient of K-means cluster. *Brain Topogr.* 19, 161–176. doi: 10.1007/s10548-006-0017-7

Liu, Q., Balsters, J. H., Baechinger, M., Van Der Groen, O., Wenderoth, N., and Mantini, D. (2015). Estimating a neutral reference for electroencephalographic recordings: the importance of using a high-density montage and a realistic head model. *J. Neural Eng.* 12:56012. doi: 10.1088/1741-2560/12/5/056012

MacKay, D. J. C. (1992). Bayesian Interpolation. *Neural Comput.* 4, 415–447. doi: 10.1162/neco.1992.4.3.415

Marzetti, L., Nolte, G., Perrucci, M. G., Romani, G. L., and Del Gratta, C. (2007). The use of standardized infinity reference in EEG coherency studies. *Neuroimage* 36, 48–63. doi: 10.1016/j.neuroimage.2007.02.034

Michel, C. M., Murray, M. M., Lantz, G., Gonzalez, S., Spinelli, L., and Grave De Peralta, R. (2004). EEG source imaging. *Clin. Neurophysiol.* 115, 2195–2222. doi: 10.1016/j.clinph.2004.06.001

Murphy, K. (2012). *Machine Learning: A Probabilistic Perspective*. Cambridge, MA: The MIT Press. Available online at: https://books.google.com/books?id=NZP6AQAAQBAJ&printsec=frontcover#v=onepage&q&f=false

Nunez, P. L. (2010). REST: a good idea but not the gold standard. *Clin. Neurophysiol.* 121, 2177–2180. doi: 10.1016/j.clinph.2010.04.029

Nunez, P. L., and Srinivasan, R. (2006). *Electric Fields of the Brain, 2nd Edn*. New York, NY: Oxford University Press.

Offner, F. F. (1950). The EEG as potential mapping: the value of the average monopolar reference. *Electroencephalogr. Clin. Neurophysiol.* 2, 213–214. doi: 10.1016/0013-4694(50)90040-X

Pascual-Marqui, R. D. (1999). Review of methods for solving the EEG inverse problem. *Int. J. Bioelectromagn.* 1, 75–86.

Pascual-Marqui, R. D. (2002). Standardized low-resolution brain electromagnetic tomography (sLORETA): technical details. *Methods Find. Exp. Clin. Pharmacol.* 24 (Suppl. D), 5–12.

Pascual-Marqui, R. D. (2007). Discrete, 3D distributed, linear imaging methods of electric neuronal activity. Part 1: exact, zero error localization. *Neurosci. Lett.* 485, 198–203.

Pascual-Marqui, R. D., Lehmann, D., Koukkou, M., Kochi, K., Anderer, P., Saletu, B., et al. (2011). Assessing interactions in the brain with exact low-resolution electromagnetic tomography. *Philos. Trans. R. Soc. A Math. Phys. Eng. Sci.* 369, 3768–3784. doi: 10.1098/rsta.2011.0081

Paz-Linares, D., Vega-Hernández, M., Rojas-López, P. A., Valdés-Hernández, P. A., Martínez-Montes, E., and Valdés-Sosa, P. A. (2017). Spatio temporal EEG source imaging with the hierarchical bayesian elastic net and elitist lasso models. *Front. Neurosci.* 11:635. doi: 10.3389/fnins.2017.00635

Phillips, C., Mattout, J., Rugg, M. D., Maquet, P., and Friston, K. J. (2005). An empirical Bayesian solution to the source reconstruction problem in EEG. *Neuroimage* 24, 997–1011. doi: 10.1016/j.neuroimage.2004.10.030

Phillips, C., Rugg, M. D., and Friston, K. J. (2002). Systematic regularization of linear inverse solutions of the EEG source localization problem. *Neuroimage* 17, 287–301. doi: 10.1006/nimg.2002.1175

Qin, Y., Xu, P., and Yao, D. (2010). A comparative study of different references for EEG default mode network: the use of the infinity reference. *Clin. Neurophysiol.* 121, 1981–1991. doi: 10.1016/j.clinph.2010.03.056

Robert, C. P. (2007). *The Bayesian Choice*. New York, NY: Springer New York.

Srinivasan, R. (1999). Methods to improve spatial resolution of EEG. *Int. J. Bioelectromagn.* 1, 102–111.

Srinivasan, R., Nunez, P. L., and Silberstein, R. B. (1998). Spatial filtering and neocortical dynamics: estimates of EEG coherence. *IEEE Trans. Biomed. Eng.* 45, 814–826. doi: 10.1109/10.686789

Stinstra, J. G., and Peters, M. J. (1998). The volume conductor may act as a temporal filter on the ECG and EEG. *Med. Biol. Eng. Comput.* 36, 711–716. doi: 10.1007/BF02518873

Tarantola, A. (2005). *Inverse Problem Theory and Methods for Model Parameter Estimation*. Philadelphia, PA: Society for Industrial and Applied Mathematics. doi: 10.1137/1.9780898717921

Teplan, M. (2002). Fundamentals of EEG measurement. *Meas. Sci. Rev.* 2, 1–11.

Tian, Y., and Yao, D. (2013). Why do we need to use a zero reference? Reference influences on the ERPs of audiovisual effects. *Psychophysiology* 50, 1282–1290. doi: 10.1111/psyp.12130

Trujillo-Barreto, N. J., Aubert-Vázquez, E., and Valdés-Sosa, P. A. (2004). Bayesian model averaging in EEG/MEG imaging. *Neuroimage* 21, 1300–1319. doi: 10.1016/j.neuroimage.2003.11.008

Uludag, K., Evans, A. C., Della-Maggiore, V., Kochen, S., Amaro, E., Sierra, O., et al. (2009). Latin American brain mapping network (LABMAN). *Neuroimage* 47, 312–313. doi: 10.1016/j.neuroimage.2009.03.030

Valdés-Hernández, P. A., Ojeda-González, A., Martínez-Montes, E., Lage-Castellanos, A., Virués-Alba, T., Valdés-Urrutia, L., et al. (2010). White matter architecture rather than cortical surface area correlates with the EEG alpha rhythm. *Neuroimage* 49, 2328–2339. doi: 10.1016/j.neuroimage.2009.10.030

Valdés-Hernández, P. A., von Ellenrieder, N., Ojeda-Gonzalez, A., Kochen, S., Alemán-Gómez, Y., Muravchik, C., et al. (2009). Approximate average head models for EEG source imaging. *J. Neurosci. Methods* 185, 125–132. doi: 10.1016/j.jneumeth.2009.09.005

Yasser Ad-Dab'bagh (2006). "The CIVET image-processing environment: a fully automated comprehensive pipeline for anatomical neuroimaging research," in *Proceedings 12th Annual Meeting Organization for Human Brain Mapping*, 2266.

Yao, D. (2000). High-resolution EEG mappings: a spherical harmonic spectra theory and simulation results. *Clin. Neurophysiol.* 111, 81–92. doi: 10.1016/S1388-2457(99)00205-9

Yao, D. (2001). A method to standardize a reference of scalp EEG recordings to a point at infinity. *Physiol. Meas.* 22, 693–711. doi: 10.1088/0967-3334/22/4/305

Yao, D. (2017). Is the surface potential integral of a dipole in a volume conductor always zero? A cloud over the average reference of EEG and ERP. *Brain Topogr.* 30, 161–171. doi: 10.1007/s10548-016-0543-x

Yao, D., and He, B. (2003). Equivalent physical models and formulation of equivalent source layer in high-resolution EEG imaging. *Phys. Med. Biol.* 48, 3475–3483. doi: 10.1088/0031-9155/48/21/002

Yao, D., Wang, L., Oostenveld, R., Nielsen, K. D., Arendt-Nielsen, L., and Chen, A. C. N. (2005). A comparative study of different references for EEG spectral mapping: the issue of the neutral reference and the use of the infinity reference. *Physiol. Meas.* 26, 173–184. doi: 10.1088/0967-3334/26/3/003

Zhai, Y., and Yao, D. (2004). A study on the reference electrode standardization technique for a realistic head model. *Comput. Methods Progr. Biomed.* 76, 229–238. doi: 10.1016/j.cmpb.2004.07.002

Conflict of Interest Statement: The authors declare that the research was conducted in the absence of any commercial or financial relationships that could be construed as a potential conflict of interest.

APPENDIX: DEMONSTRATION THAT $\mathbf{H}^{+}\mathbf{H} = \mathbf{I} - \mathbf{1}\mathbf{1}^{\mathbf{T}}/N_e$

Recall $\mathbf{f}^{\mathbf{T}}\mathbf{1} = 1$, $\mathbf{H} = \mathbf{I} - \mathbf{1}\mathbf{f}^{\mathbf{T}}$ (Hu et al., 2018) which reduces the matrix rank by one. Keeping same form with the formula (1.2) in Baksalary et al. (2003), we rewrite

$$\mathbf{M} = \mathbf{A} + \mathbf{b}\mathbf{c}^{\mathbf{T}}, \text{ with } \mathbf{M} = \mathbf{H}, \mathbf{A} = \mathbf{I}, \mathbf{b} = -\mathbf{1}, \mathbf{c} = \mathbf{f}$$

Referring to the **Theorem 1.1** in Baksalary et al. (2003), it follows that $rank(\mathbf{M}) = rank(\mathbf{A}) - 1$, since $\lambda = 1 + \mathbf{c}^{\mathbf{T}}\mathbf{A}^{+}\mathbf{b} = 1 + \mathbf{f}^{\mathbf{T}}(-1) = 0$ and both $\mathbf{b}$ and $\mathbf{c}$ belong to the column space of $\mathbf{A} = \mathbf{I}$. By utilizing the case ($\downarrow$) of **List 2** in **Theorem 2.1** in Baksalary et al. (2003) , we take

$$\mathbf{M}^{+}\mathbf{M} = \mathbf{A}^{+} - \delta^{-1}\mathbf{d}\mathbf{d}^{\mathbf{T}}$$

The formulas in (1.3) and (1.4) from Baksalary et al. (2003) are $\mathbf{d} = \mathbf{A}^{\mathbf{T}}\mathbf{b}$ and $\delta = \mathbf{d}^{\mathbf{T}}\mathbf{d}$. Applying these relations to our problem, it turns to be

$$\mathbf{H}^{+}\mathbf{H} = \mathbf{I} - \mathbf{1}\mathbf{1}^{\mathbf{T}}/N_e$$

which is the classical average reference.

frontiers in Neuroscience

ORIGINAL RESEARCH
published: 20 March 2019
doi: 10.3389/fnins.2019.00221

Graph Theoretical Characteristics of EEG-Based Functional Brain Networks in Patients With Epilepsy: The Effect of Reference Choice and Volume Conduction

Maria N. Anastasiadou[1], *Manolis Christodoulakis*[1], *Eleftherios S. Papathanasiou*[2], *Savvas S. Papacostas*[2], *Avgis Hadjipapas*[3] *and Georgios D. Mitsis*[4,5]*

[1] KIOS Research and Innovation Centre of Excellence, Faculty of Engineering, University of Cyprus, Nicosia, Cyprus, [2] Laboratory of Clinical Neurophysiology, Clinic B, Cyprus Institute of Neurology and Genetics, Nicosia, Cyprus, [3] University of Nicosia Medical School, Nicosia, Cyprus, [4] Department of Bioengineering, McGill University, Montreal, QC, Canada, [5] Department of Electrical and Computer Engineering, KIOS Research Center, University of Cyprus, Nicosia, Cyprus

OPEN ACCESS

Edited by:
Pedro Antonio Valdes-Sosa, Clinical Hospital of Chengdu Brain Science Institute, China

Reviewed by:
Dezhong Yao, University of Electronic Science and Technology of China, China
Jean-Marc Lina, École de Technologie Supérieure (ÉTS), Canada

***Correspondence:**
Georgios D. Mitsis
georgios.mitsis@mcgill.ca

Specialty section:
This article was submitted to Brain Imaging Methods, a section of the journal Frontiers in Neuroscience

Received: 20 November 2017
Accepted: 26 February 2019
Published: 20 March 2019

Citation:
Anastasiadou MN, Christodoulakis M, Papathanasiou ES, Papacostas SS, Hadjipapas A and Mitsis GD (2019) Graph Theoretical Characteristics of EEG-Based Functional Brain Networks in Patients With Epilepsy: The Effect of Reference Choice and Volume Conduction. Front. Neurosci. 13:221. doi: 10.3389/fnins.2019.00221

It is well-established that both volume conduction and the choice of recording reference (montage) affect the correlation measures obtained from scalp EEG, both in the time and frequency domains. As a result, a number of correlation measures have been proposed aiming to reduce these effects. In our previous work, we have showed that scalp-EEG based functional brain networks in patients with epilepsy exhibit clear periodic patterns at different time scales and that these patterns are strongly correlated to seizure onset, particularly at shorter time scales (around 3 and 5 h), which has important clinical implications. In the present work, we use the same long-duration clinical scalp EEG data (multiple days) to investigate the extent to which the aforementioned results are affected by the choice of reference choice and correlation measure, by considering several widely used montages as well as correlation metrics that are differentially sensitive to the effects of volume conduction. Specifically, we compare two standard and commonly used linear correlation measures, cross-correlation in the time domain, and coherence in the frequency domain, with measures that account for zero-lag correlations: corrected cross-correlation, imaginary coherence, phase lag index, and weighted phase lag index. We show that the graphs constructed with corrected cross-correlation and WPLI are more stable across different choices of reference. Also, we demonstrate that all the examined correlation measures revealed similar periodic patterns in the obtained graph measures when the bipolar and common reference (Cz) montage were used. This includes circadian-related periodicities (e.g., a clear increase in connectivity during sleep periods as compared to awake periods), as well as periodicities at shorter time scales (around 3 and 5 h). On the other hand, these results were affected to a large degree when the average reference montage was used in combination with standard cross-correlation, coherence, imaginary coherence, and PLI, which is likely due to the low number of electrodes and inadequate electrode coverage of the scalp. Finally, we demonstrate that the correlation between seizure onset and the brain network periodicities is preserved

when corrected cross-correlation and WPLI were used for all the examined montages. This suggests that, even in the standard clinical setting of EEG recording in epilepsy where only a limited number of scalp EEG measurements are available, graph-theoretic quantification of periodic patterns using appropriate montage, and correlation measures corrected for volume conduction provides useful insights into seizure onset.

Keywords: epilepsy, volume conduction, montage, scalp EEG, graph theory, periodicities

INTRODUCTION

The effect of reference choice and volume conduction on correlation measures obtained from scalp EEG is well-established; it has been shown that it may considerably influence measures of correlation in the time and frequency domains (Nunez et al., 1997). Specifically, both may introduce artificial zero-lag correlations: in the former case, referencing may result in the instantaneous subtraction of common signal components from different electrode time-series while in the latter case, instantaneous propagation of currents generated at a discrete source through the volume of the (head) conductor occurs (Nunez and Srinivasan, 2006; Christodoulakis et al., 2014). In turn, this makes the interpretation of EEG-based functional brain network characteristics more difficult. A number of correlation measures that attempt to reduce this influence have been proposed, including corrected cross-correlation, reduced/imaginary coherence as well as standard, and weighted phase lag index, which by construction are insensitive to instantaneous (zero-lag) correlations, and are in principle less susceptible to volume conduction and reference effects (Nunez et al., 1997, 1999; Guevara et al., 2005; Marzetti et al., 2007; Stam et al., 2007; Haufe et al., 2010; Vinck et al., 2011; Nevado et al., 2012; Peraza et al., 2012; Thatcher, 2012; Christodoulakis et al., 2014; Chella et al., 2016). So far, the effects of reference choice and volume conduction on functional brain network properties have been assessed using short-duration EEG recordings (up to several minutes; Marzetti et al., 2007; Qin et al., 2010; Xu et al., 2014; Chella et al., 2016).

The properties of brain networks over longer time scales (multiple hours to days) have been investigated to a lesser degree; however, they may also convey important information about the underlying physiological and neural processes. Pronounced fluctuations have been revealed in the temporal evolution of global network characteristics (clustering coefficient, average shortest path length, assortativity) in patients with epilepsy (Kuhnert et al., 2010; Kramer et al., 2011; Geier et al., 2015; Anastasiadou et al., 2016). These fluctuations exhibit some periodic temporal structure which can be largely attributed to circadian rhythms. Furthermore, global properties of epileptic networks around seizure onset have been characterized using the clustering coefficient and shortest path length/efficiency (Lehnertz et al., 2014). The importance of local network properties (e.g., individual nodes) in epilepsy has also been explored (Kramer et al., 2008; Wilke et al., 2011; Varotto et al., 2012; Burns et al., 2014; Zubler et al., 2014; Geier et al., 2015).

Using a unique dataset of long-term (days) continuous scalp EEG recordings in patients with epilepsy, we recently showed that the summative properties (degree, efficiency, clustering coefficient) and topology of the resulting functional brain networks exhibit robust long-term periodicities in addition to the well-known circadian 24 h period (Anastasiadou et al., 2016; Mitsis et al., 2018). Our results demonstrated that brain network periodicities (particularly around 3 and 5 h) are strongly correlated to seizure onset. Furthermore, we showed that the modulation of brain network properties by the seizure events were relatively minor compared to these concurrent long-term fluctuations of brain network properties. Collectively, these results have important implications for seizure pathophysiology and suggest the potential of quantifying the long-term properties of EEG–based brain functional networks and incorporating information regarding their correlations with seizure onset for achieving seizure detection and prediction with improved sensitivity and specificity. However, these results were obtained using the bipolar montage on the basis of our previous work (Christodoulakis et al., 2013) and the functional brain networks were constructed using a relatively limited set of correlation measures.

Therefore, in the current study, our main aim was to investigate the extent to which these key findings would be reproducible for different, commonly-used montage choices as well as when different correlation measures with varying sensitivity to volume conduction and zero-lag correlations are used to construct functional brain networks. Specifically, we considered the following three reference choices (montages): the common reference montage (Cz), the average reference montage and the bipolar montage. Signal correlation measures are affected by the choice of reference and also by volume conducted currents from common sources (Nunez et al., 1997; Stam et al., 2007). We also showed that the choice reference and correlation measures influence the properties of the resulting functional brain networks around seizure onset (Christodoulakis et al., 2014). Thus, we considered the following correlation measures: cross-correlation (CC) in the time domain and coherence (COH) in the frequency domain, as well as measures that account for volume conduction effects and zero-lag (instantaneous) correlations: corrected cross-correlation (corCC), imaginary coherence (IC), standard phase lag index (PLI), and weighted phase lag index (WPLI) (Nunez et al., 1997, 1999; Guevara et al., 2005; Stam et al., 2007; Haufe et al., 2010; Vinck et al., 2011; Nevado et al., 2012; Peraza et al., 2012; Thatcher, 2012; Christodoulakis et al., 2014). In order to construct brain networks, we used long duration scalp EEG recordings (ranging between 21 and 94 h; 23 channels) in

TABLE 1 | EEG recordings.

Patient	Length of recordings (h)	Number of seizures	Type of seizures
1	46	1	Focal
2	22	2	Focal
3	68	2	Focal
4	94	1	Generalized
5	36	1	Generalized
6	24	0	Psychogenic
7	21	1	Focal
8	71	2	Focal
9	27	6	Generalized
10	69	4	Focal

patients with epilepsy using all possible combinations between the above reference and correlation measure choices.

To our knowledge, this is the first study that investigates the influence of reference choice on the long-term periodic variations of scalp EEG-based functional brain networks. Furthermore, identifying the optimal combination between reference choice and correlation measure in the context of quantifying correlations between network properties and seizure onset is important as it may contribute to the design of improved detection/prediction algorithms which can take into account periodic variations in the state of the underlying functional brain networks.

EEG RECORDINGS AND PREPROCESSING

Long-term video-EEG recordings were collected from nine patients with epilepsy and one patient with psychogenic seizures in the Neurology Ward of the Cyprus Institute of Neurology and Genetics. The study was approved by the Cyprus National Bioethics Committee. All subjects gave written informed consent in accordance with the Declaration of Helsinki. Six patients were monitored using the an XLTek (Natus Medical Incorporated, CA, USA) scalp EEG recording system (Patients 1–6), while the remaining four were monitored with the Nicolet (Natus Medical Incorporated, CA, USA) system (Patients 7–10). **Table 1** summarizes the duration of the recordings, as well as the number and type of seizures of each patient. Seizures and sleep intervals were identified and marked by specialist neurophysiologists (coauthors ESP and SSP).

Twenty-one electrodes were placed according to the 10–20 international system with two additional anterotemporal electrodes. In addition, four electrodes were used to record electrooculogram (EOG) and electrocardiogram (ECG) signals, respectively. The data were recorded at a sampling rate of 200 and 500 Hz for the XLTek and Nicolet systems, respectively. The EEG and EOG signals were band-pass filtered between 1 and 45 Hz to remove line noise and muscle artifacts. Next, we applied Lagged Auto-Mutual Information Clustering (LAMIC) (Nicolaou and Nasuto, 2007), using simultaneous EOG recordings to remove ocular artifacts.

It has been demonstrated that the montage (i.e., the choice of reference) affects correlation measures (Nunez et al., 1997) and as a consequence it may affect the corresponding graph-theoretic measures. For this reason, we mathematically converted the input data, which were originally recorded relative to the common cephalic reference, to three different montages: the common reference (Cz), the average reference and the bipolar montage (see section Recording Montages). We obtained results employing all three montages.

Recording Montages

Scalp EEG recording devices use differential amplifiers in order to compute the voltage of each EEG channel. A differential amplifier takes as input the measurements of two electrodes and produces the corresponding EEG channel as the difference between the two inputs, after it has been amplified. The choice of input electrodes to each amplifier is known as montage.

The recordings obtained with our system is an example of common reference (Cz) where each amplifier takes as input one of the 10–20 system electrodes (Fp1, Fp2, F7, F3, Fz, F4, F8, T3, C3, Cz, C4, T4, T5, P3, Pz, P4, T6, O1, O2, A1, A2) and one reference electrode (REF) which is common to all amplifiers. This is an example of common reference (Cz) montage and we mathematically re-referenced the data to Cz, which is often the reference electrode of choice. The average reference montage subtracts the average signal over all channels (in our case, 19 scalp channels) or a carefully chosen subset of them from the signal at each channel. In this work, we used all 19 scalp channels to compute the average.

On the other hand, in the case of bipolar montage there is no input common to all the time-series but pairs of electrodes in nearby locations of the scalp are used to obtain the time-series by subtracting the corresponding measurements. Specifically, electrodes are taken in straight lines from the front to the back of the head, forming the pairs Fp1-F7, F7-T3, T3-T5, T5-O1, Fp2-F8, F8-T4, T4-T6, T6-O2, Fp1-F3, F3-C3, C3-P3, P3-O1, Fp2-F4, F4-C4, C4-P4, P4-O2, Fz-Cz, Cz-Pz.

Functional Brain Network Construction

After obtaining the artifact-free time series, we calculated pairwise correlation measures between all pairs of time series (EEG data converted to common reference (Cz), average reference and bipolar reference montages) using the correlation measures described in section Correlation Measures. Each time series in the common (Cz), average and bipolar montages corresponds to a node in the network, which does not change over time. The edges or connections between the nodes are then identified by computing correlation measures between the corresponding time series. Specifically, if the corresponding measure between each pair exceeded a pre-specified threshold, the value of which was dependent on the employed measure (section Correlation Measures), edges were added between node pairs. All the connections (edges) identified in this way form a binary graph, which we term the functional brain network. Common measures for estimating the correlation between pairs of time series include CC, COH, synchronization likelihood, Granger causality, directed coherence, mutual information, PLI,

and many more; see, e.g. (Pereda et al., 2005) for a review. The related changes in the brain network over time were tracked by using 5-s non-overlapping windows and quantifying the correlation between all time-series pairs, using the following measures: CC, corCC, COH, IC, PLI, and WPLI.

Correlation Measures

Cross correlation

Cross-correlation (CC) measures the similarity of two series as a function of the displacement of one relative to the other (Christodoulakis et al., 2014). For any pair of time series, $x(t)$, and $y(t)$, the normalized cross-correlation is calculated as follows:

$$C_{xy}(\tau) = \frac{1}{n-\tau}\sum_{t=1}^{n-\tau}\left(\frac{x(t)}{\sigma_x}\right)\left(\frac{y(t+\tau)}{\sigma_y}\right) \quad (1)$$

where σ_x and σ_y are the standard deviations of x and y, respectively. The normalized CC, C_{xy}, was computed for a range of values for the lag τ: a range of [−100 100] ms was examined here. C_{xy} takes values between −1 and 1, with 1 indicating perfect linear positive correlation, −1 perfect linear negative correlation and 0 no correlation. The maximum of the absolute value of CC, $max_\tau \left|C_{xy}\right|$, over the chosen range of τ values, was used to quantify the degree of correlation between the two signals within a given time window.

Corrected cross correlation

Corrected cross-correlation (corCC) is a measure that is used in the case of scalp EEG measurements as CC often attains its maximum value at zero lag and zero-lag correlations are largely due to volume conduction effects or reference choice. For instance, according to the common reference (Cz) montage, the same signal is subtracted from all other electrode time-series. In order to measure true interactions not occurring at zero lag, we calculated the corCC $\bar{C}_{xy}(\tau)$, which is a measure of the autocorrelation sequence asymmetry, as defined in Nevado et al. (2012), by subtracting the negative-lag part of $C_{xy}(\tau)$ from its positive-lag counterpart (Nevado et al., 2012):

$$\bar{C}_{xy}(\tau) = C_{xy}(\tau) - C_{xy}(-\tau) \quad \text{for } \tau > 0 \quad (2)$$

Note that $\bar{C}_{xy}(\tau)$ provides a lower bound estimate of the nonzero-lag cross-correlations and is notably smaller than C_{xy}. As in the case of CC, the maximum within the same range of time lags ([−100 100] ms) is taken as the measure of correlation.

Coherence

Coherency is a widely-used measure for characterizing linear dependence between a pair of stochastic processes, as well as a quantitative measure of their phase consistency and may be viewed as the equivalent measure of cross-correlation in the frequency domain. Coherence (COH - $k_{xy}(f)$), defined as the squared magnitude of coherency, is employed as a measure of correlation in the frequency domain (Pereda et al., 2005), i.e.:

$$k_{xy}(f) = \frac{\left|\langle S_{xy}(f)\rangle\right|}{\sqrt{\left|\langle S_{xx}(f)\right|\left|S_{yy}(f)\rangle\right|}} \quad (3)$$

The value of $k_{xy}(f)$ ranges between 0 and 1, with 1 indicating perfect linear correlation and 0 no correlation between x and y at frequency f. COH is a function of frequency; therefore, we calculated the maximum (with respect to frequency) COH value within the following frequency bands: broadband (1–45 Hz), delta (1–4 Hz), theta (4–8 Hz), alpha (8–13 Hz), beta (13–30 Hz), and gamma (30–45 Hz) in order to quantify the correlation between pairs of signals.

Imaginary coherence

The imaginary part of coherency (imaginary coherence—IC), as shown in Nolte et al. (2004), is less sensitive to volume conduction compared to its real part. Therefore, it can be used as a correlation measure to construct EEG-based functional brain networks:

$$IC_{xy}(f) = Imag\left(\Gamma_{xy}(f)\right) \quad (4)$$

Here, we used the maximum (with respect to frequency) absolute value of the IC for the broadband signal as well as within the aforementioned frequency bands to quantify the correlation between the two signals.

Phase lag index

The phase lag index (PLI) was introduced in Stam et al. (2007), aiming to obtain a measure that provides reliable estimates of phase synchronization between two signals and is insensitive to volume conduction. Here, the instantaneous phases were obtained by initially bandpass filtering the signals within the frequency bands defined above and subsequently using the Hilbert transform to obtain the phase of the corresponding analytic signal., Phase difference distribution ($\Delta\phi$) as an index of asymmetry between a given pair of channels, that were wrapped in the interval , can be obtained in the following way:

$$PLI_{xy} = \left|\langle sgn(\Delta\phi(\tau))\rangle\right| \quad (5)$$

PLI ranges between 0 and 1, with 0 indicating no correlation and 1 maximal correlation.

Weighted phase lag index

The weighted phase lag index (WPLI) was proposed in Vinck et al. (2011) as an improved measure of phase synchronization for electrophysiological signals in the presence of noise and volume conduction. PLI may be sensitive to both of these factors, mostly due to its discontinuity, as small perturbations may convert phase lags into leads and vice versa. In contrast with PLI, WPLI weights the contribution of the observed phase leads and lags by the magnitude of the imaginary component of the cross-spectrum (Vinck et al., 2011):

$$\begin{aligned} WPLI &= \frac{\left|\langle Imag(S_{xy}(f))\rangle\right|}{\langle\left|Imag(S_{xy}(f))\right|\rangle} \\ &= \frac{\left|\langle\left|Imag(S_{xy}(f))\right| \cdot sgn(Imag(S_{xy}(f))\rangle\right|}{\langle\left|Imag(S_{xy}(f))\right|\rangle} \end{aligned} \quad (6)$$

Similar to PLI, WPLI ranges between 0 and 1, with 0 indicating no correlation and 1 maximal correlation.

Network Binarization

We constructed binary (rather than weighted) networks, i.e., networks with connections only between strongly correlated nodes. To do so, a threshold was set, the value of which depends on the employed correlation measure. Edges with weight values larger than the specified threshold were included in the graph (weight: 1), while edges with values less than the threshold were removed (weight: 0). We examined various threshold values for all the considered correlation measures. In all cases, different values yielded very similar results in terms of the observed patterns in network properties, provided that the threshold value was not too high (e.g., close to one for CC)—which yields disconnected graphs -, or too low (close to zero)—which yields densely/fully connected graphs. Therefore, we selected threshold values between these two extremes. The threshold value determines the actual value of the graph theoretic measures, but did not affect our results otherwise, as we are interested in the variation of these measures over time and the resulting periodic patterns and not specifically in their absolute value. We also used the method of phase-randomized surrogate data to construct binary networks (Theiler et al., 1992); however, this approach yielded densely connected networks, i.e., degree values that were similar to those obtained by setting a fixed, low threshold value. Moreover, the temporal patterns of the network summative properties were found to be overall clearer when thresholding was used (Sections Network Binarization and Periodicities in Functional Brain Network Properties). Taking also into account that thresholding is much faster to implement, which is important for real-time seizure detection/prediction applications, we selected the thresholding method and we selected the threshold values so that similar average degree values were obtained for different correlation measures and montages. Specifically, we selected the following threshold values for the bipolar and common (Cz) reference; CC: 0.65, COH: 0.65, IC: 0.58, corCC: 0.1, PLI: 0.1, and WPLI: 0.45. For the average reference, the corresponding values were as follows; CC: 0.65, COH: 0.65, IC: 0.4, corCC: 0.1, PLI: 0.1, and WPLI: 0.45.

Graph Theoretic Measures

For each subject, the evolution of the functional brain network over time was monitored by observing how different measures of the corresponding graph changed over time: average degree, global efficiency, and clustering coefficient.

Average Degree

The degree k_i of a node i is defined as the number of connections or edges that this node has with other neighboring nodes in the network. The average degree of a network is the average value of the summary of degrees of a network and quantifies how well-connected the corresponding graph is (Rubinov and Sporns, 2010):

$$K = \frac{1}{n} \sum_{i \epsilon N} k_i \tag{7}$$

Global Efficiency

The shortest path length, d_{ij}, between a pair of nodes i and j is defined as the minimum number of edges that have to be traversed to get from node i to j. The characteristic path length is defined as the average shortest path length over all pairs of nodes in the network and is a measure of how efficient the information flow through the network is (Christodoulakis et al., 2014):

$$L = \frac{1}{n\,(n-1)} \sum_{i,j \epsilon N, i \neq j} d_{ij} \tag{8}$$

A limitation of the characteristic path length is that if any pair of nodes i and j is not connected through any path, the corresponding shortest path length value is $d_{ij} = \infty$. Therefore, the characteristic path length is well-defined only for pairs of nodes that are connected. To overcome this limitation, efficiency between a pair of nodes was defined as the inverse of the shortest distance between the nodes, $1/d_{ij}$ (Latora and Marchiori, 2001):

$$E = \frac{1}{n\,(n-1)} \sum_{i,j \epsilon N, i \neq j} \frac{1}{d_{ij}} \tag{9}$$

Global efficiency is defined as the average efficiency over all pairs of nodes (Latora and Marchiori, 2001).

Clustering Coefficient

A cluster in a graph is a group of nodes that is highly interconnected. The clustering coefficient C_i of a node i is defined as the fraction of existing edges between nodes adjacent to node i, over the maximum possible number of such edges (Watts and Strogatz, 1998).

$$C_i = \frac{2t_i}{k_i\left(k_i - 1\right)} \tag{10}$$

where k_i is the degree of node i, and t_i denotes the number of edges, $e_{jj'}$, between pairs of nodes, j and j', that are both connected to i. Consequently, the clustering coefficient of the network C is defined as the mean clustering coefficient among all network nodes.

$$C = \frac{1}{n} \sum_{i \epsilon N} C_i \tag{11}$$

Periodicity Estimation

One of our main aims was to characterize the periodicities that arise in functional brain network characteristics over a wide range of time scales. Each of the three network properties—average degree, global efficiency, and clustering coefficient, which were used for monitoring functional brain networks, provides a single value per network constructed from a 5-s window, thus forming a time series across the entire recording time. We utilized the Lomb-Scargle periodogram (Scargle, 1982) to obtain the power spectral density (PSD) of the time series for each network summative property (e.g., degree). This was done for all correlation measures and montages. The Lomb-Scargle periodogram is more appropriate for unevenly sampled data and in our case, we observed that in some patients we had small gaps in the signal measurements.

Circular Statistics

To investigate the relation of seizure onset to brain network periodicities and the influence of reference choice effect on these periodicities, we calculated the instantaneous phase at seizure onsets for each periodic component and obtained the corresponding phase distribution. Subsequently, we used circular statistics to examine whether seizure onsets occurred at specific/preferred phases, as opposed to random phases. To this end, we first performed zero-phase digital filtering of the average degree time series to obtain band limited signals around the main identified peaks on a subject-to-subject basis (± 0.5 h before and after the main peak of each periodic component). Specifically, we focused this analysis on the periodic components that were found to be consistent across patients. Significant peaks identified in individual subjects were deemed consistent if their location relative to the mean location across subjects was less or equal to half an hour. More details on the location of observed peaks are given in Section Periodicities in Functional Brain Network Properties.

Subsequently, we applied the Hilbert transform on the band limited signals to calculate the instantaneous phase of each periodic component (Klingspor, 2015). For all patients, the instantaneous phases at the onset of the seizure were collected and the obtained phase distribution were subsequently investigated using CircStat which is a Matlab (Math works, Natick MA) toolbox related to circular statistics (Berens, 2009). For more details, the reader is referred to Mitsis et al. (2018). To investigate whether phase values at seizure onset times were distributed uniformly around the circle from 0 to 2π, we applied the Rayleigh test with the null hypothesis (H_0) being that the population is distributed uniformly around the circle. The Rayleigh test computes the resultant vector length R that suggests a non-uniform distribution (Fisher, 1993) and is particularly suited for detecting a unimodal deviation from uniformity. To account for the fact that we had multiple seizures for some subjects, we created groups of nine samples (one seizure per patient) for all possible combinations to obtain the corresponding corrected p-values (Zar, 1999). Note that for the 24 h periodic (circadian) component, these groups included six samples only, since the recordings of six out of ten patients were longer than 24 h.

RESULTS

The results related to the time-resolved functional brain measures correspond to Patient 4, since the longest recording (94 h) was obtained from this patient. Similar results were obtained in all ten patients (see also **Supplementary Material**).

Network Binarization

As mentioned above, we selected the thresholds aiming to avoid extreme values and obtain similar average degree values among different correlation measures and montages. **Figure 1** illustrates the average network degree as obtained from CC using a bipolar montage for threshold values between 0.2 and 0.8, where it can be seen that the behavior for different threshold values is similar. It was found that the obtained network properties, e.g., average degree in this case, exhibit very similar patterns with respect to time, regardless of the threshold used. To provide comparisons with the surrogate data network binarization, we show the average degree obtained in the latter case in **Figure S1** for CC, where it can be seen that the resulting degree values are high and that the circadian periodicity is not as clear as in **Figure 1**.

Effect of Reference Choice on Network Measures and Their Periodicities

The choice of reference channel affects the local cortical estimates and their interactions with other locations. It is known that using a common reference (Cz) can substantially inflate coherence estimates, particularly at smaller distances (Nunez and Srinivasan, 2006) as a common signal is subtracted from all channels. On the other hand, the average reference is known to yield coherence estimates that are closer to coherence estimates obtained from reference-independent potentials (Nunez and Srinivasan, 2006). Note that the average reference is commonly used when a large number of electrodes with extensive coverage of the head is used. In our case, the standard 10–20 system was used, which may yield a poor approximation of the reference-free potentials (Nunez and Srinivasan, 2006; Christodoulakis et al., 2014). Furthermore, in the settings of a limited number of electrodes as in our case, the bipolar montage has been suggested for obtaining estimates of local superficial cortical generators (Nunez and Srinivasan, 2006; Christodoulakis et al., 2014).

Since the choice of montage influences the estimates of local activity (electrodes) and the interactions between them, it is also expected to influence the resulting graph theoretic measures and hence their periodic properties. We constructed functional networks using the correlation measures described in section Correlation Measures (CC, corCC, COH, IC, PLI, and WPLI) using long-term EEG data and all three montages [bipolar, common reference (Cz) and average reference]. Below, we study the effects of reference (montage) choice on the long-term properties of the resulting brain networks separately in the time and frequency domain, focusing on the emerging periodicities.

Time Domain

Figures 2, **3** show the time course of the average network degree using CC (**Figure 2**) and corCC (**Figure 3**) for all montages. The green, red and blue lines correspond to average, bipolar, and common (Cz) reference, respectively. In **Figure 2**, it is evident that the functional brain networks yielded by CC are less connected (lower degree) during the time when the patient is awake compared to sleep (gray shaded bars) in the case of bipolar and common reference (Cz) montage. In contrast, the average montage yields the opposite trend. In **Figure 3** it can be seen that, when corCC was used, the average reference yielded similar results to the other two montages (increased connectivity during sleep), suggesting that this measure is less susceptible to the choice of reference. In **Figure S1**, we can observe a similar 24 h periodic trend in the case of bipolar and common reference (Cz) montage for global network efficiency when CC was used. As before (**Figure 2**), the average reference montage yielded an opposite main periodic trend, which was however reversed when corCC was used (**Figure S2**). In **Figures S3**, **S4**,

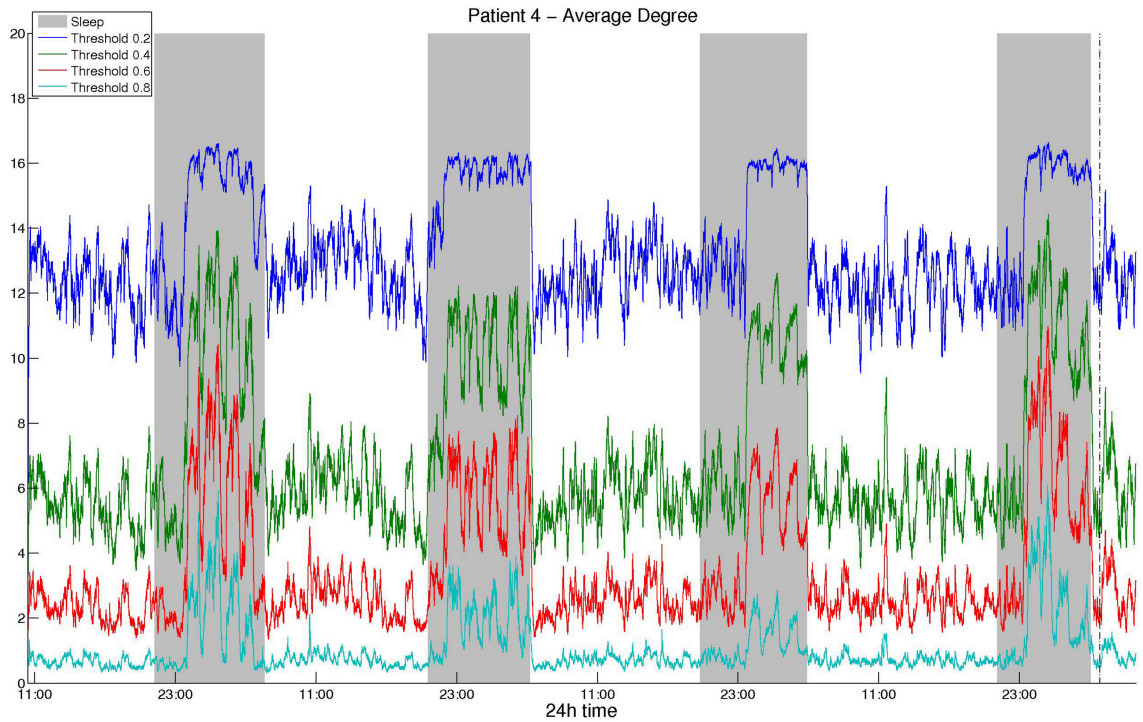

FIGURE 1 | Smoothed average degree of the functional brain network of Patient 4, constructed using cross-correlation, for various thresholds. For all thresholds, the 24 h period is visible and the resulting patterns are similar, although details for some intermediate periodicities may be lost.

we show the clustering coefficient patterns obtained with CC and corCC, respectively for all reference montages, whereby similar observations can be made. Therefore, corCC yielded overall more consistent patterns for different montages for all three network measures. Along with the dominant 24 h cycles, additional periodic components at shorter time scales co-exist; note, for example, the spikes that occur at both awake- and sleep-times separated on average by ∼75 min (e.g., **Figures 2**, **3**). These weaker periodicities are examined in detail in section Periodicities in Functional Brain Network Properties.

Frequency Domain

To investigate brain network properties in the frequency domain, we constructed functional networks using COH, IC, PLI, and WPLI. **Figures 4**, **5** show the average degree for the broadband signal obtained from COH and IC for all montages, respectively. **Figures 6**, **7** show the average degree obtained from PLI and WPLI for all montages, respectively. **Figures S5**, **S6** show the global efficiency and clustering coefficient, respectively when using WPLI for all montages. Note that the global efficiency and clustering coefficient are not shown separately for COH, IC, and PLI as they yielded similar periodic trends to the average degree for all montages. In **Figure 4** (COH), we observe that the average reference montage yields opposite periodic trends compared to the other two montages, similarly to CC (section Time Domain). Also, we observed that COH within all frequency bands (delta, theta, alpha, beta, and gamma) yielded similar periodic trends to the broadband signal (**Figure 4**) for both the bipolar and common (Cz) montages (results not shown separately). In the case of the average reference montage, the trend observed for the broadband signal was mostly determined by the delta, theta and alpha band, which yielded opposite periodic trends to the beta and gamma bands. It was found that functional brain networks obtained with COH were less connected during the time when the patient was awake compared to sleep (gray shaded bars), in the case of bipolar, and common (Cz) reference montage.

In **Figure 5** we can observe that IC exhibits a different behavior overall compared to COH and other correlation measures, with the bipolar and common (Cz) montages yielding opposite periodic trends. In contrast, the average reference montage yielded increased connectivity during sleep, exhibiting an opposite trend to the other two montages. The periodicities yielded by the broadband signal in the case of bipolar and common (Cz) montages were mostly determined by IC values in the beta and gamma bands and in the case of average reference montage they were mostly determined by IC values in the delta, theta and alpha bands, which yielded opposite periodic trends to the beta and gamma bands. The results suggest that IC and COH are influenced substantially by reference choice. As before, the main periodicity was the 24 h circadian cycle, which is evident in all the results.

In **Figure 6**, which shows the average degree obtained with the PLI for all montages, we can observe that the average reference yields opposite periodic trends compared to the other two montages. The functional brain networks using PLI are less connected during the time when the patient is awake compared

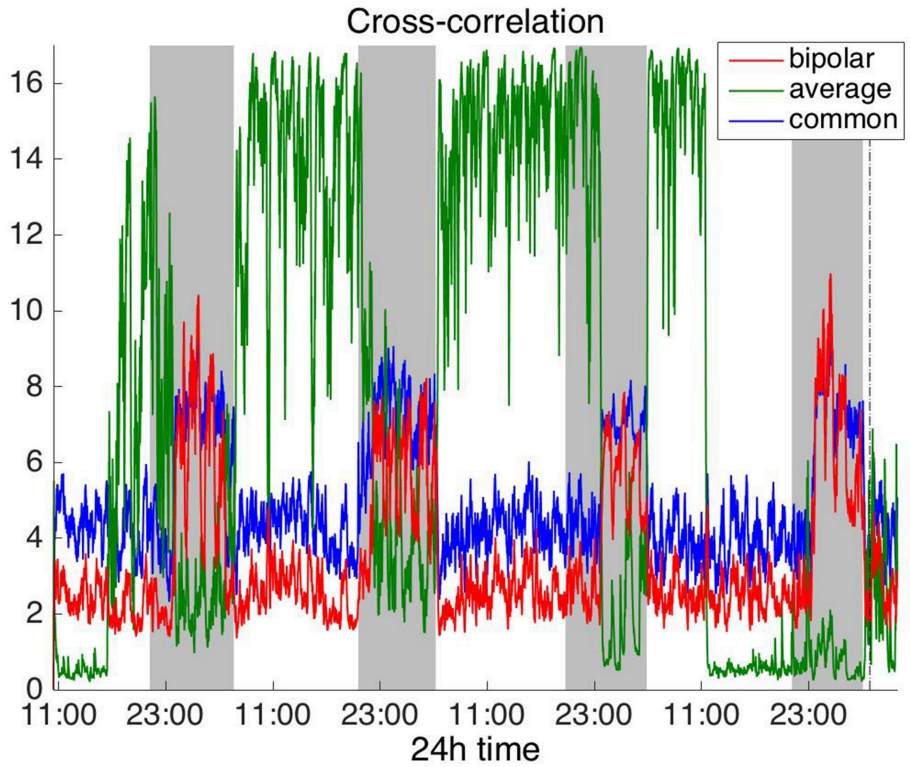

FIGURE 2 | Average degree of the functional brain networks of Patient 4 as a function of time, using cross correlation for assessing pairwise correlations. The vertical dashed line indicates seizure onset and the gray bars indicate sleep intervals. Cross correlation yields an opposite 24 h periodic pattern when using the average reference. However, we can clearly observe a periodic pattern with a main period equal to around 24 h for all montages.

to sleep in periodic cycles of ∼24 h, in the case of the bipolar and common (Cz) reference montages. In **Figure 7**, we show that the average degree obtained using WPLI was less affected by reference choice compared to the rest of the correlation measures. The same can be observed in **Figures S5**, **S6** for the efficiency and clustering coefficient, respectively. The WPLI-based functional brain networks were less connected during the time when the patient was awake compared to sleep for all montages. As before, along with the 24 h cycles, additional periodic components at shorter time scales co-exist in the time course of the average degree in the frequency domain (section Periodicities in Functional Brain Network Properties).

Periodicities in Functional Brain Network Properties

Apart from the dominant 24 h periodicity in network properties, periodicities at smaller time scales can also be observed (**Figures 2**–**7** and **Figures S2**–**S7**). In this section, we investigate these periodicities in more detail. **Figure 8** illustrates the periodogram of the average degree of the functional brain networks of Patient 4 constructed using all correlation measures for the bipolar (red) and common (Cz; blue) reference. The horizontal lines denote the statistical significance level ($p = 0.05$), above which spectral peaks can be considered as significant. In **Figure S8**, we also show the Lomb-Scargle periodogram of the average degree obtained using surrogate data network binarization for the bipolar montage (**Figure S1**). Similar periodic components can be observed; however, the circadian periodicity is not as clear as in **Figure 8**. The average reference montage yielded substantially noisier results for all subjects and is shown in **Figure S9**; however, the main peaks (e.g., at 24 h) are evident in this case as well. The green, red and blue lines indicate the average, bipolar, and common (Cz) reference, respectively. The peaks in the periodogram correspond to periods of 3.4, 5.9, 11.8, and 23.6 h and have been marked accordingly in the case of corCC (**Figure 8** and **Figure S9**). Similar peaks were observed for all other correlation measures. We observed four main peaks for all montages across patients, the location of which varied between 3.2 and 3.8 h (mean: 3.6 h), 4.9 and 5.9 h (mean: 5.4 h), 11.8 and 12.2 (mean:12 h), and 23.6 to 24.5 h (mean: 24 h). For simplicity, we refer to the main periodic peaks using these mean values from now on. The periodicity peaks at around 3.6, 5.4 h were observed in all subjects, while the peaks at around 12 and 24 h were identified in eight out of 10 subjects, and six out of six subjects, respectively (recall that recordings longer than 24 h were obtained for six subjects). In **Figure S9** we can observe that, in the case of the average reference montage, the peaks are located at slightly different frequencies compared to the other two montages, especially in the case of CC, COH, and IC, indicating that these correlation measures are influenced by reference choice to larger extent. On the other hand, corCC

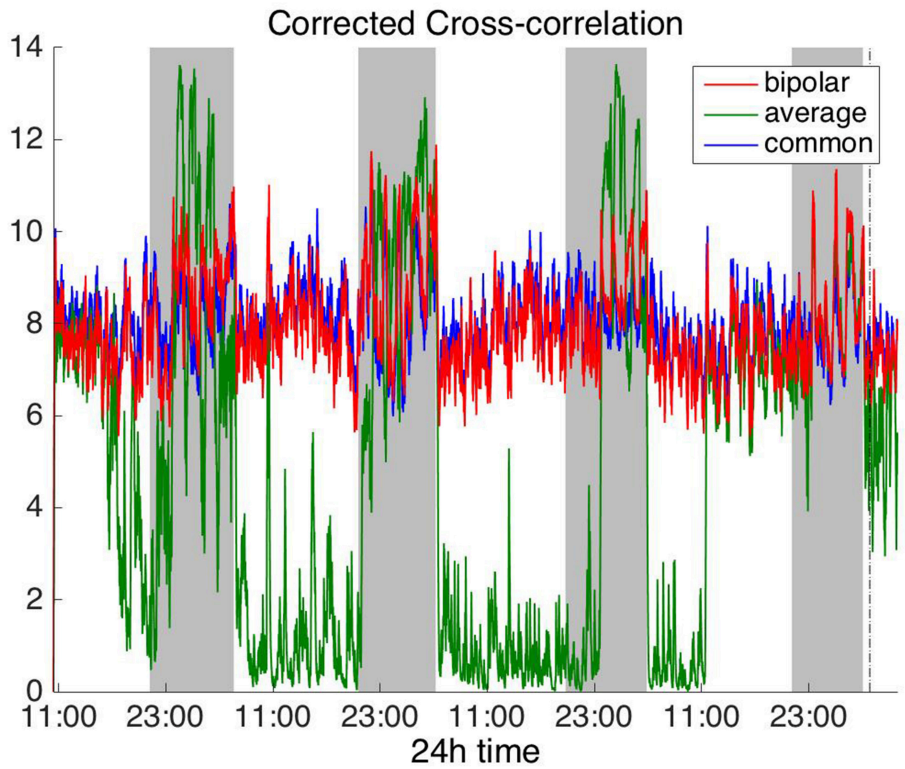

FIGURE 3 | Average degree of the functional brain networks of Patient 4 as a function of time, using corrected cross correlation for assessing pairwise correlations. The vertical dashed line indicates seizure onset and the gray bars indicate sleep intervals. In contrast to cross correlation (**Figure 2**), corrected cross correlation yields the same 24 h periodic pattern for all montages.

and WPLI are affected less by reference choice and yield the most consistent frequency peaks overall. **Figure S10** illustrates the Lomb-Scargle periodogram of the average degree of the functional brain networks obtained from Patient 6, who was the only psychogenic seizure patient in our cohort, constructed using all correlation measures for the bipolar (red) and common (Cz; blue) reference. The peaks in the periodogram correspond to periods of 3.4, 4.8, and 12.05 h and have been marked accordingly in the case of corCC (**Figure S10**). Note that the length of the recordings for this patient was 24 h; therefore, the peak at 24 h is not as clear as for subjects with longer recordings, except in the case of the corCC (**Figure S10**—top right panel).

Circular Statistics

The instantaneous phases of the main identified periodicities (mean across patients: 3.6, 5.4, 12, and 24 h) at seizure onset are shown in **Figures 9**, **10** respectively. These were obtained from all seizures from nine patients (i.e., except Patient 6) for the correlation measures that were less affected by reference choice, i.e., CorCC and WPLI (**Figure 8** and **Figure S9**). **Figures 9**, **10** show the instantaneous phases for the average network degree obtained using corCC and WPLI, respectively, for all montages, and peaks. The left panels show the instantaneous phases on the unit circle, while the right panels show the corresponding angular histograms. The green, red, and blue circles indicate the instantaneous phases obtained from the average, bipolar, and common (Cz) reference, respectively. The lines of the same color indicate the direction and magnitude of the mean resultant vector. The length of this vector is a crucial quantity for the measurement of circular spread and hypothesis testing in circular statistics. The closer the vector magnitude is to one, the more concentrated the data sample is around the mean direction. The instantaneous phases of the 3.6 h (**Figures 9A**, **10A**) and 5.4 h (**Figures 9B**, **10B**) periodicities were more concentrated around the mean direction and more consistent across montages. On the other hand, the instantaneous phases of the 12 h (**Figures 9C**, **10C**) and 24 h (**Figures 9D**, **10D**) periodicities were found to be less concentrated around the mean. Overall, corCC yielded the highest phase concentrations for the examined periodic components.

Table 2 shows the length of the mean resultant vector R and the corresponding *p*-values (Rayleigh test, max-values in groups) for the instantaneous phases of the average degree as obtained for all correlation measures and reference choices. It is evident from the **Figures 9**, **10** and **Table 2** that the instantaneous phases are not distributed uniformly, but seizures occur within specific phase ranges, especially for the 3.6 and 5.4 h periodicities. With regards to the slower periodicities (12 and 24 h), the phases were distributed more uniformly around the circle, yielding non-significant values in some cases (**Table 2**). Overall, the

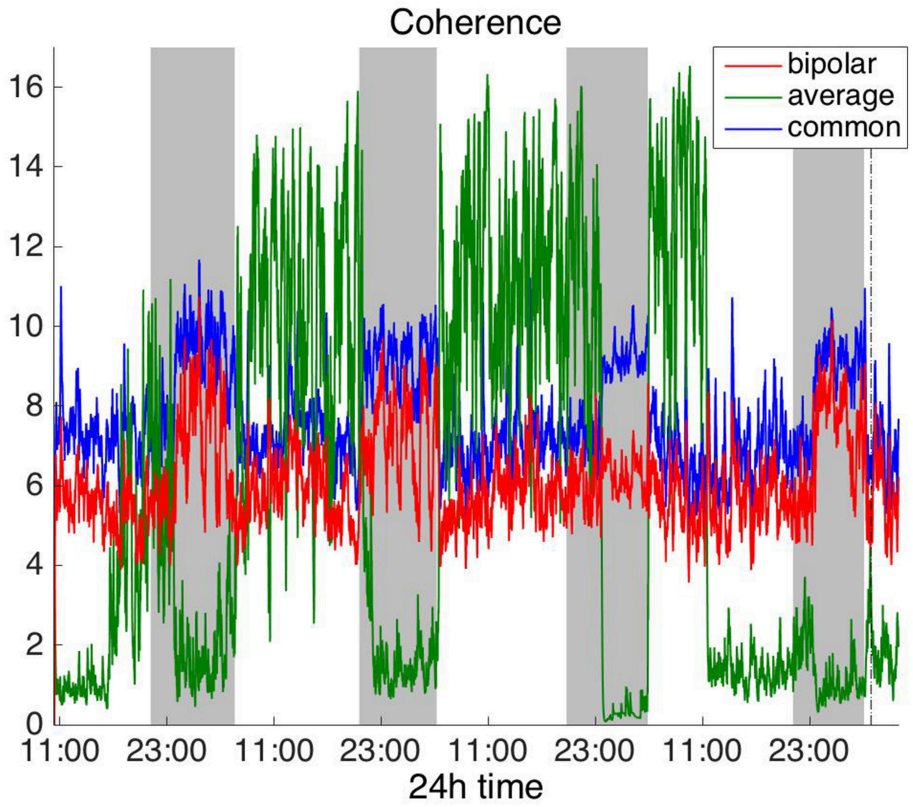

FIGURE 4 | Average degree of the functional brain networks of Patient 4 as a function of time (broadband signal), using coherence for assessing pairwise correlations. The vertical dashed line indicates seizure onset and the gray bars indicate sleep intervals. Similarly to correlation (**Figure 2**), coherence yields an opposite 24 h periodic pattern when using the average reference.

bipolar montage yielded the most consistent results across all correlation measures, with the corresponding *p*-values being significant in all cases (**Table 2**). Overall, the results of **Table 2** suggest that the coupling between seizure onset and network periodicities is detected for almost all combinations of reference and correlation measure. corCC yielded the most significant results across all periodic components followed by WPLI, while IC resulted in strong couplings for the shorter periodicities (3.6 and 5.4 h; **Table 2**).

DISCUSSION

Complex network analysis has recently emerged as a promising approach for studying brain dynamics and particularly functional connectivity. However, network analyses based on signal correlations of scalp EEG recordings are affected by the choice of reference electrode (montage), as well as volume conduction and more generally the fact that common signal is picked up by different electrodes leading to spurious correlations at zero lag. In this work, we investigated the effects of reference choice and volume conduction on the long-term properties of functional brain networks obtained from scalp EEG measurements using long duration data (between 22 and 94 h) from patients with epilepsy, extending our previous studies (Christodoulakis et al., 2013; Anastasiadou et al., 2016; Mitsis et al., 2018). To do so, we examined six bivariate signal correlation measures—CC, corCC, COH, IC, PLI, and WPLI, as well as three montages—common (Cz), average and bipolar. We quantified the long-term brain network properties using three widely used graph theoretic measures: average degree, efficiency, and clustering coefficient (Rubinov and Sporns, 2010).

Overall, the results obtained using the examined correlation measures and montages revealed consistent periodicities over different time scales in the obtained brain network properties, in agreement with (Anastasiadou et al., 2016; Mitsis et al., 2018). Specifically, in these papers the presence of a main 24 h circadian periodicity as well as periodicities around 3.6, 5.4, and 12 h (harmonically related to the 24 h periodicity on a subject-specific basis) were revealed for both network summative properties and topology (Mitsis et al., 2018). Here, we have extended the results by systematically examining the effects of correlation measure and montage choice. While the locations of the main periodicities were found to be overall consistent across these choices (**Figure 8** and **Figures S9**, **S10**), it was found that the choice of reference and correlation measure may have pronounced effects on the results (**Figures 2**–**7**). Specifically, the average reference was found to yield the most pronounced differences compared to the

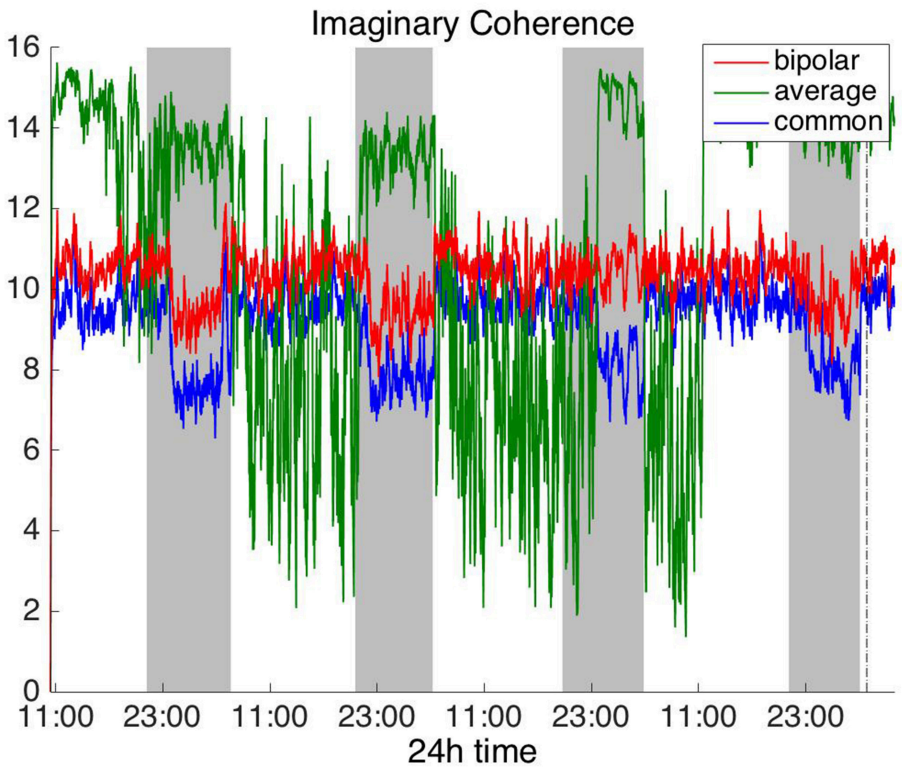

FIGURE 5 | Average degree of the functional brain networks of Patient 4 as a function of time (broadband signal), using imaginary coherence for assessing pairwise correlations. The vertical dashed line indicates seizure onset and the gray bars indicate sleep intervals. Similarly to correlation (**Figure 2**) and coherence (**Figure 4**), imaginary coherence yields an opposite 24 h periodic pattern when using the average reference.

other montages. This includes a reversal of the characteristics of the main 24 h periodicity (higher average degree, global efficiency and clustering coefficient during sleep; **Figures 2**, **4**–**6** and **Figures S2**, **S4**) as well as more variability with regards to the identified frequency peaks for a subset of the employed correlation measures (**Figures S9**,**S10**).

Ideally, the EEG referencing should be performed with respect to a reference electrode with zero voltage values. However, in practice the voltage values of the reference electrode are never zero. In addition to these reference effects, in practice the data and inferences from it are also affected by volume conduction, i.e., the fact that two or more sensors may instantaneously pick up a signal from the same source. Therefore, in practice, both volume conduction and reference electrode effects will occur inevitably. This is particularly true in the clinical setting examined in the present paper, where we had a standard 10–20 setup with a low number of electrodes. However, in such a setting of limited electrode numbers and limited head electrode coverage in an empirical dataset, is not possible to directly address the reference electrode and volume conduction effects. Therefore, the effects of volume conduction were *indirectly* assessed by using measures that are *differentially* sensitive to the influence of volume conduction. Both volume conduction and common (non-zero) reference effects can result in artifactual zero-time lag correlations. Various measures/correlation metrics have been proposed that are relatively insensitive to such zero-lag correlations including corCC, IC, PLI, and WPLI. Such measures (largely) account for volume conduction effects, which are necessarily zero-time lag but also for effects of non-zero and/or common reference.

Of the six correlation measures that we investigated, CC, and COH were affected by the choice of recording reference (montage) to the greatest degree, followed by IC and PLI. This was expected overall, as CC and COH are known to be influenced by zero-lag correlations (Nunez and Srinivasan, 2006). It should be noted that zero-lag correlations could be due to both artifactual (volume conduction/reference effects) and true correlations, whereas non-zero lag correlations are more likely to reflect true correlations of underlying sources (Eggermont and Smith, 1996; Stam et al., 2007). Thus, by quantifying correlations by measures that are less sensitive to volume conduction and active reference effects, one accepts the risk of missing functionally meaningful correlations at zero-lag, but at the same time, the most frequent artifacts for misinterpretation of correlations are very much reduced (Stam et al., 2007). CorCC and WPLI were the least affected correlation measures, as all three montages yielded similar network measure patterns (**Figures 3**, **6** and **Figures S3**, **S5**–**S7**). In addition to the aforementioned differences related to periodic peaks and reversal of the main circadian pattern, the average reference

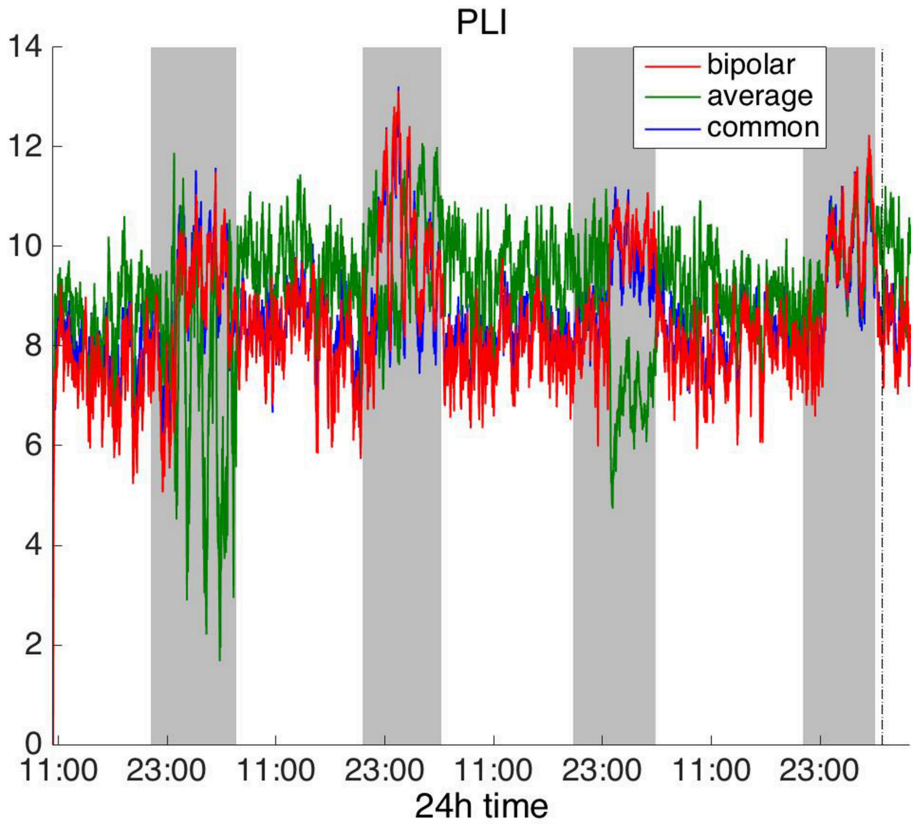

FIGURE 6 | Average degree of the functional brain networks of Patient 4 as a function of time (broadband signal), using PLI for assessing pairwise correlations. The vertical dashed line indicates seizure onset and the gray bars indicate sleep intervals. PLI yields a different 24 h periodic pattern when using the average reference.

yielded higher connectivity (as reflected on the average degree; **Figures 2–6**) compared to the other two montages for the same threshold value.

In our previous work, we have also assessed the effect of reference and correlation measure choice using relatively short data records (30 min) before and after seizure onset (Christodoulakis et al., 2014). Our results demonstrated that the graphs constructed with CC and COH were affected by volume conduction and montage more markedly; however, they exhibited a similar trend—decreasing connectivity at seizure onset, as well as during the ictal and early postictal periods, increasing again several minutes after the seizure has ended—with all the aforementioned measures accounting for volume conduction (corCC, PLI, WPLI) except IC. In particular, networks constructed using CC yielded a clearer discrimination between the pre-ictal and ictal periods than the measures less sensitive to volume conduction such as the PLI and IC. Thus, somewhat paradoxically, although removing the effects of volume conduction allows for a more accurate reconstruction of the true underlying networks this may come at the cost of discrimination ability with respect to brain state.

The average reference produces a good approximation of the reference-free potentials, given sufficient electrode coverage of the head (Nunez and Srinivasan, 2006; Nunez, 2011). However, the assumption underlying the average reference montage only holds for spherical volume conductors (Yao, 2017). As a standard 10–20 electrode system was used here, the average reference montage is likely to provide a poor approximation of the reference-free potentials (Nunez and Srinivasan, 2006, p. 295) as both the low number of electrodes and limited head coverage errors (only the upper part of the head was sampled) come into play. This is supported by our results, which suggest that using the average reference may result in considerable common signal being subtracted from each electrode, introducing artifactual correlation at zero-time lags. On the other hand, the bipolar montage yields better estimates of the local gradient of the potential along the scalp surface than a fixed reference at a remote distance. This increases sensitivity and spatial resolution for superficial generators but reduces the sensitivity to distant sources (Nunez and Srinivasan, 2006). Also, as we are assessing connectivity in the present study, the bipolar montage is a reasonable choice as it provides an estimate of local brain dynamics. When the effects of zero-time lag correlations are removed, for instance using corCC (**Figure 3**) or WPLI (**Figure 7**), the average reference montage results exhibited qualitatively similar trends to the bipolar [and common (Cz)] montage data. This supports the idea that there is possibly a remaining large common

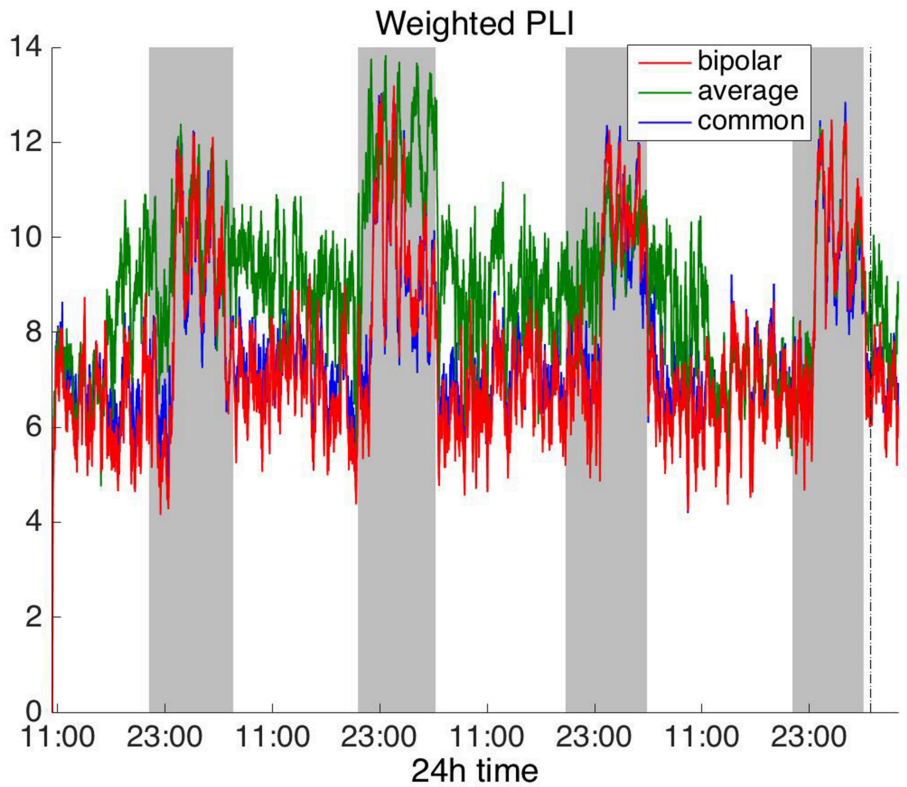

FIGURE 7 | Average degree of the functional brain networks of Patient 4 as a function of time (broadband signal), using WPLI for assessing pairwise correlations. The vertical dashed line indicates seizure onset and the gray bars indicate sleep intervals. Similarly to corrected cross-correlation (**Figure 3**), WPLI yields the same 24 h periodic pattern for all montages.

component in the average that is instantaneously subtracted from each channel.

The REST (reference electrode standardization technique) referencing method has recently been proposed to yield approximately reference-free potentials (Yao, 2001, 2017; Yao et al., 2005; Marzetti et al., 2007; Qin et al., 2010; Xu et al., 2014; Chella et al., 2016; Dong et al., 2017) and has been shown in simulations to outperform the average reference montage (Qin et al., 2010; Nunez, 2011). Ideally, the REST method is implemented by recording electrode positions and using individual head models but it can also be implemented using an average head template mode. A recent simulation study has suggested that REST outperforms average referencing even for a limited number of electrodes (Hu et al., 2018). In our experimental setting, due to that electrode positions were not recorded and the subsequent lack of an individual head model, as well as to the limited electrode density and coverage, which are typical in clinical settings, we did not implement REST. Also, we did not consider linked-ears or linked-mastoids referencing (physical or mathematical), as this approach has limited theoretical basis and may yield biased estimates of reference-free potentials (Nunez and Srinivasan, 2006).

Our results agree with previous studies (Nunez et al., 1997; Stam et al., 2007; Vinck et al., 2011; Peraza et al., 2012; Christodoulakis et al., 2014) in that corCC and WPLI were found to be less affected by reference choice. To our knowledge, our study is the first that demonstrates this for long-duration properties of the scalp EEG-based functional brain networks. Also, our results overall agree with previous studies applying graph-theoretic measures to intracranial recordings. Specifically, Kuhnert et al. (2010) recorded intracranial EEG data and constructed functional brain networks using mean phase coherence. They showed that functional brain networks change periodically over time, with prominent cycle around 24 h, and that seizures influence the brain networks significantly less compared to daily rhythms. In 2017, Geier and Lehnertz investigated the temporal and spatial variability of the importance regions in evolving epileptic brain networks and showed that the importance of brain regions fluctuates over time, with these fluctuations being mostly attributed to processes acting on timescales of hours to days.

We also assessed the effect of reference choice and correlation measure on the correlation strength between the instantaneous phase of the functional network periodicities in network properties (3.6, 5.4 and 12 h) with seizure onset revealed in our previous work (Anastasiadou et al., 2016; Mitsis et al., 2018). Importantly, in these studies we showed that connectivity-based markers are a more specific marker of seizure onset,

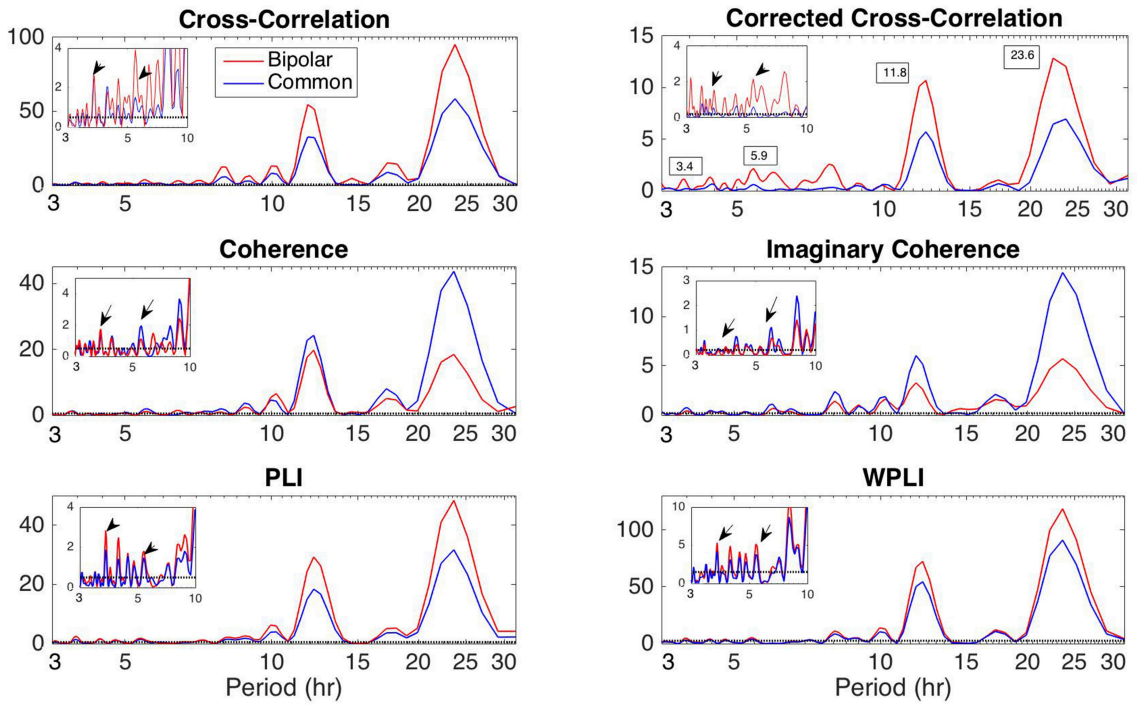

FIGURE 8 | Lomb-Scargle periodogram of the average degree of the functional brain network of Patient 4 using cross-correlation, corrected cross-correlation, coherence, imaginary coherence, PLI, and WPLI for common reference (blue line) and bipolar montage (red line). The dotted horizontal lines denote the statistical significance level ($p = 0.05$). The arrows in the inset figures denote the periods around 3.6 and 5.4 h, which were identified across all subjects along with the peaks around 12 and 24 h. Corrected cross correlation and WPLI were affected less by reference choice.

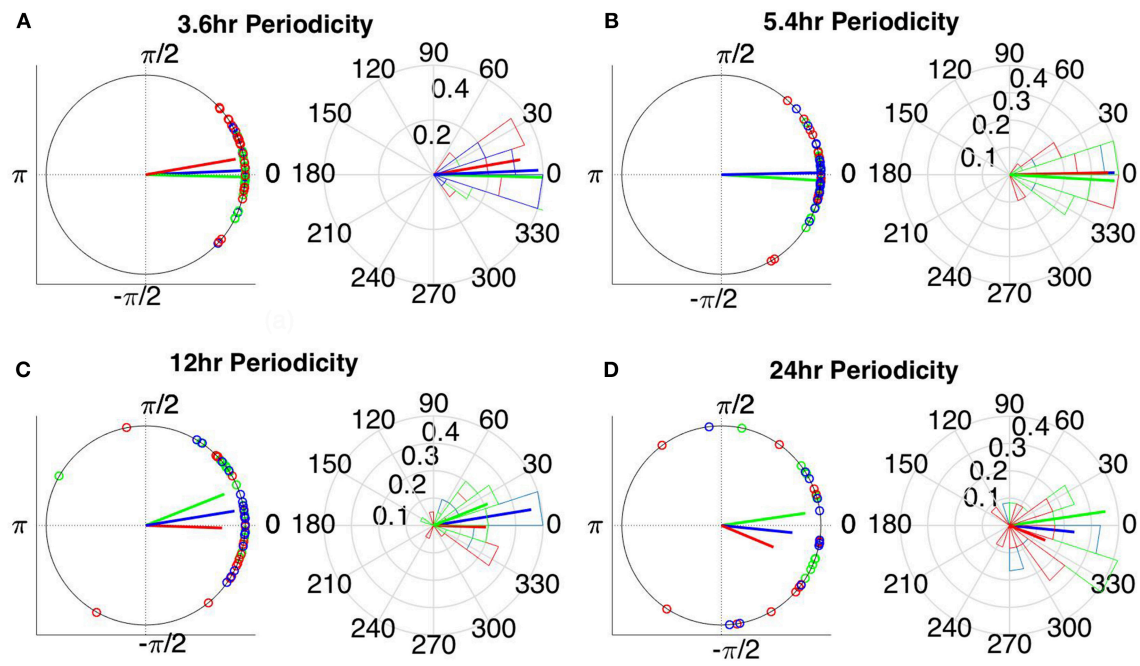

FIGURE 9 | Instantaneous phases of the network average degree at seizure onset for the **(A)** 3.6 h, **(B)** 5.4 h, **(C)** 12 h, and **(D)** 24 h periodicities of all patients for corrected cross correlation. The left panels present the unit circle and the phases as points for all seizures from all patients. The right panels show the angular histogram of the distribution as well as the corresponding probability values. Blue, common reference (Cz); green, average reference; red, bipolar reference.

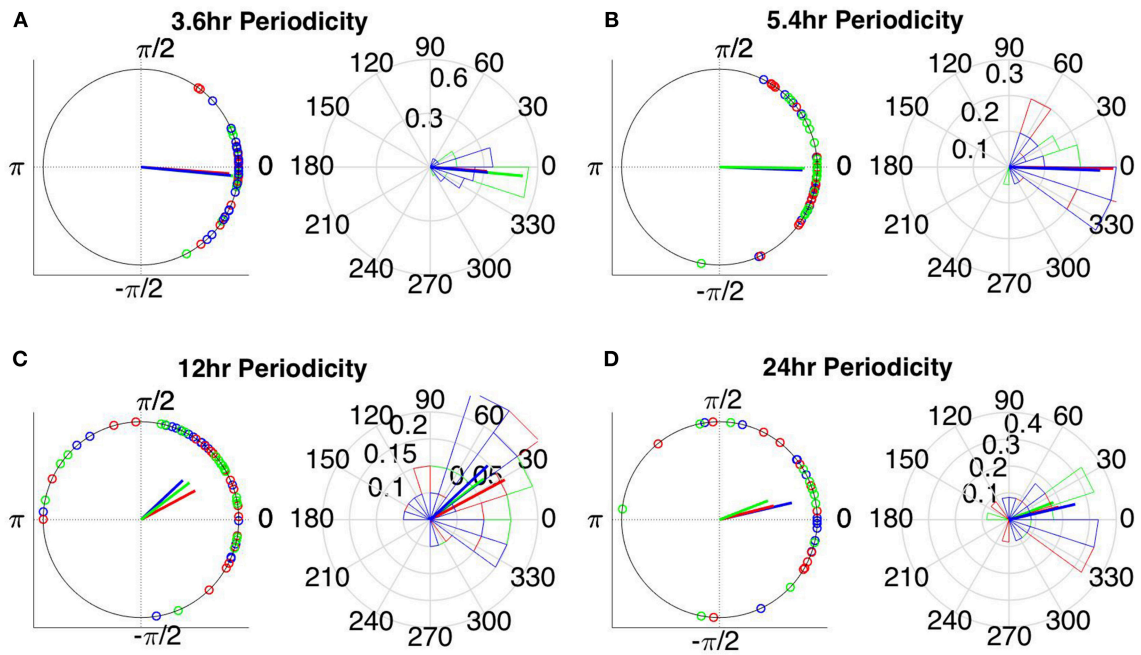

FIGURE 10 | Instantaneous phases of the network average degree at seizure onset for the **(A)** 3.6 h, **(B)** 5.4 h, **(C)** 12 h, and **(D)** 24 h periodicities of all patients for WPLI. The left panels present the unit circle and the phases as points for all seizures from all patients. The right panels show the angular histogram of the distribution as well as the corresponding probability values. Blue, common reference (Cz); green, average reference; red, bipolar reference.

TABLE 2 | The values for the mean resultant vector *R* and the *p*-values obtained with Rayleigh's test for uniform distribution of the main periodic component instantaneous phases at seizure onset for all correlation measures, montages, and patients.

Correlation measure and reference choice		R	*p*-value	R	*p*-value	R	*p*-value	R	*p*-value
		3.6 h		5.4 h		12 h		24 h	
CC	Average	0.82	0.004	0.86	0.001	0.59	0.15	0.29	0.9
	Bipolar	0.97	2.5e-5	0.97	2.4e-5	0.85	4.3e-4	0.72	0.02
	Common	0.95	2.6e-5	0.94	3.4e-5	0.73	0.02	0.73	0.03
corCC	Average	0.97	2.4e-5	0.96	2.2e-5	0.85	0.006	0.85	0.007
	Bipolar	0.92	7.9e-5	0.91	8.9e-4	0.87	0.005	0.77	0.01
	Common	0.96	2.6e-5	0.96	2.6e-5	0.96	6.8e-4	0.9	0.004
COH	Average	0.95	1.8e-5	0.91	1.7e-5	0.75	0.09	0.88	0.003
	Bipolar	0.95	6.1e-6	0.89	0.002	0.73	0.03	0.81	0.01
	Common	0.95	2.4e-5	0.89	2.2e-4	0.65	0.15	0.51	0.6
IC	Average	0.99	2.3e-5	0.98	2.6e-5	0.91	4.1e-4	0.84	0.02
	Bipolar	0.98	2.5e-5	0.97	2.6e-5	0.88	1.4e-4	0.87	0.006
	Common	0.97	2.6e-5	0.98	2.5e-5	0.82	9.6e-4	0.69	0.09
PLI	Average	0.94	4.11e-5	0.88	8.7e-4	0.47	0.5	0.68	0.2
	Bipolar	0.95	2.6e-5	0.90	1.6e-4	0.70	0.02	0.77	0.01
	Common	0.95	2.6e-5	0.94	2.5e-5	0.66	0.3	0.83	0.01
WPLI	Average	0.95	5.2e-5	0.87	0.002	0.72	0.5	0.73	0.8
	Bipolar	0.90	2.1e-4	0.83	0.003	0.73	0.03	0.70	0.02
	Common	0.92	1.4e-4	0.85	0.002	0.79	0.01	0.86	0.009

The p-values that are larger than 0.05, suggesting that the instantaneous phases are distributed uniformly around the circle, are indicated in red. CC, cross-correlation; corCC, corrected cross-correlation; COH, coherence; IC, imaginary coherence; PLI, phase lag index; and WPLI, weighted phase lag index.

as the couplings between long-term periodic components and seizure onset were not found to be present for the scalp EEG signals (Mitsis et al., 2018). The instantaneous phase of these periodicities (as obtained from the average degree time course) over different time scales was found to be correlated with seizure onset (**Figures 9**, **10** and **Table 2**) for almost all combinations of correlation measure and montage choices and that, overall, corCC, WPLI, and IC yielded the strongest coupling strengths (**Table 2**). In all cases, the instantaneous phase of the 3.6 and 5.4 h periodic components were more concentrated around the mean direction as compared to the 12 and 24 h components (**Figures 9C,D**, **10C,D**), in agreement with (Anastasiadou et al., 2016; Mitsis et al., 2018).

In the present paper, we assumed that the period of the identified network-related periodic components is constant over time. In principle, these periods may change over longer time periods (multiple days to weeks to even months). However, to observe such non-stationarities, particularly for the slower (e.g., circadian periodicities) would require very long duration data. We are aware of only one study of this kind that used intracranial data collected over weeks/months using an implantable deep brain stimulation system, where it was shown that subject-specific multi-dien rhythms in the intracranial EEG signal properties were correlated to seizures (Baud et al., 2018). The authors of that paper did not examine network properties as brain coverage was more limited. However, as the main circadian periodicity remains approximately constant over time (around 24 h) and the shorter periodicities that were found to be correlated to seizure onset hereby were mostly harmonics of the circadian periodicity, it is expected that even if time-frequency analysis is implemented, the results would not change substantially.

In conclusion, the present study suggests that the choice of reference may considerably affect the estimated long-term properties of graph theoretic analysis of scalp EEG functional brain networks and that, for the relatively low number of electrodes examined hereby, the bipolar montage yielded the most consistent results, while corCC and WPLI were the correlation measures that were found to be least affected by reference choice. Therefore, using a bipolar montage combined with one of these correlation measures (corCC and WPLI) in similar studies may lead to a better understanding of long-term functional connectivity, as well as improved seizure prediction/detection algorithms that take into account the instantaneous phase of the underlying network periodicities.

AUTHOR CONTRIBUTIONS

GM, AH, and MA conceived and designed the study. EP and SP performed the experiments. MA, MC, GM, AH, EP, and SP analyzed the data. MA, GM, MC, and AH wrote the paper.

FUNDING

This work was partially supported by the European Regional Development Fund and Republic of Cyprus through the Research Promotion Foundation (Project ΥΓΕΙΑ/ΔΥΓΕΙΑ/0609(BE)/11).

SUPPLEMENTARY MATERIAL

The Supplementary Material for this article can be found online at: https://www.frontiersin.org/articles/10.3389/fnins.2019.00221/full#supplementary-material

Figure S1 | Average degree of the functional brain network of Patient 4 using cross-correlation and the bipolar montage, constructed using multivariate phase randomization surrogate data (blue line), and thresholding as in **Figure 2** (red line; threshold value: 0.65). The surrogate method yielded more densely connected networks. While the temporal patterns are similar, the circadian periodicity is less clear for the surrogate-obtained results.

Figure S2 | Efficiency of the functional brain networks of Patient 4 as a function of time, using cross correlation for assessing pairwise correlations. The vertical dashed line indicates seizure onset and the gray bars indicate sleep intervals. Cross correlation yields an opposite 24 h periodic pattern when using the average reference. However, we can clearly observe a periodic pattern with a main period equal to around 24 h for all montages.

Figure S3 | Efficiency of the functional brain networks of Patient 4 as a function of time, using corrected cross correlation for assessing pairwise correlations. The vertical dashed line indicates seizure onset and the gray bars indicate sleep intervals. In contrast to cross correlation (**Figure S2**), corrected cross correlation yields the same 24 h periodic pattern for all montages.

Figure S4 | Clustering coefficient of the functional brain networks of Patient 4 as a function of time using cross correlation for assessing pairwise correlations. The vertical dashed line indicates seizure onset and the gray bars indicate sleep intervals. Cross correlation yields an opposite 24 h periodic pattern when using the average reference, similarly in efficiency (**Figure S1**). However, we can clearly observe a periodic pattern with a main period equal to around 24 h for all montages.

Figure S5 | Clustering coefficient of the functional brain networks of Patient 4 as a function of time, using corrected cross correlation for assessing pairwise correlations. The vertical dashed line indicates seizure onset and the gray bars indicate sleep intervals. In contrast to cross correlation (**Figure S3**), corrected cross correlation yields the same 24 h periodic pattern for all montages similarly in efficiency (**Figure S2**).

Figure S6 | Efficiency of the functional brain networks of Patient 4 as a function of time (broadband signal), using WPLI for assessing pairwise correlations. The vertical dashed line indicates seizure onset and the gray bars indicate sleep intervals. Similarly, to corrected cross correlation (**Figures S2**, **S3**), WPLI yields the same 24 h periodic pattern for all montages.

Figure S7 | Clustering coefficient of the functional brain networks of Patient 4 as a function of time (broadband signal), using WPLI for assessing pairwise correlations. The vertical dashed line indicates seizure onset and the gray bars indicate sleep intervals. Similarly to corrected cross correlation (**Figures S2**, **S3**), WPLI yields the same 24 h periodic pattern for all montages as in **Figure S5** with efficiency.

Figure S8 | Lomb-Scargle periodogram of the average degree of the functional brain network of Patient 4 using cross-correlation, corrected cross-correlation, coherence, imaginary coherence, PLI, and WPLI for all montages. The dotted horizontal lines denote the statistical significance level ($p = 0.05$). The arrows in the inset figures denote the periods around 3.6 and 5.4 h, which were identified across all subjects along with the peaks around 12 and 24 h. Corrected cross correlation and WPLI were affected less by reference choice.

Figure S9 | Lomb-Scargle periodogram of the average degree of the functional brain network of Patient 4 obtained using cross-correlation and bipolar montage, whereby binarization was performed using surrogate data. As suggested in **Figure S2**, the circadian periodicity is less pronounced compared to networks obtained using thresholding.

Figure S10 | Lomb-Scargle periodogram of the average degree of the functional brain network of Patient 6 (psychogenic seizure patient) using cross-correlation, corrected cross-correlation, coherence, imaginary coherence, PLI, and WPLI for common reference (blue line) and bipolar montage (red line). The dotted horizontal lines denote the statistical significance level ($p = 0.05$). The arrows in the inset figures denote the periods around 3.6 and 5.4 h, which were identified across all subjects along with the peaks around 12 and 24 h. Corrected cross correlation and WPLI were affected less by reference choice.

REFERENCES

Anastasiadou, M., Hadjipapas, A., Christodoulakis, M., Papathanasiou, E. S., Papacostas, S. S., and Mitsis, G. D. (2016). "Epileptic seizure onset correlates with long term eeg functional brain network properties*," in *2016 IEEE 38th Annual International Conference of the Engineering in Medicine and Biology Society (EMBC)* (Orlando, FL), 2822–2825. doi: 10.1109/EMBC.2016.7591317

Baud, M. O., Kleen, J. K., Mirro, E. A., Andrechak, J. C., King-Stephens, D., Chang, E. F., et al. (2018). Multi-day rhythms modulate seizure risk in epilepsy. *Nat. Commun.* 9:88. doi: 10.1038/s41467-017-02577-y

Berens, P. (2009). CircStat : a MATLAB toolbox for circular statistics. *J. Stat. Softw.* 31, 1–21. doi: 10.18637/jss.v031.i10

Burns, S. P., Santaniello, S., Yaffe, R. B., Jouny, C. C., Crone, N. E., Bergey, G. K., et al. (2014). Network dynamics of the brain and influence of the epileptic seizure onset zone. *Proc. Natl. Acad. Sci. U.S.A.* 111, E5321–5330. doi: 10.1073/pnas.1401752111

Chella, F., Pizzella, V., Zappasodi, F., and Marzetti, L. (2016). Impact of the reference choice on scalp EEG connectivity estimation. *J. Neural Eng.* 13:36016. doi: 10.1088/1741-2560/13/3/036016

Christodoulakis, M., Hadjipapa, A., Papathanasiou, E. S., Anastasiadou, M., Papacostas, S. S., and Mitsis, G. D. (2013). "On the effect of volume conduction on graph theoretic measures of brain networks in epilepsy," in *Modern Electroencephalographic Assessment Techniques*. *Neuromethods*, ed V. Sakkalis (New York, NY: Humana Press), 103–130. doi: 10.1007/7657_2013_65

Christodoulakis, M., Hadjipapas, A., Papathanasiou, E. S., Anastasiadou, M., Papacostas, S., and Mitsis, G. (2014). "On the effect of volume conduction on graph theoretic measures of brain networks in epilepsy," in *Modern Electroencephalographic Assessment Techniques. Neuromethods*, ed V. Sakkalis (New York, NY: Springer), 103–30.

Dong, L., Li, F., Liu, Q., Wen, X., Lai, Y., Xu, P., et al. (2017). MATLAB toolboxes for reference electrode standardization technique (REST) of scalp EEG. *Front Neurosci.* 11:601. doi: 10.3389/fnins.2017.00601

Eggermont, J. J., and Smith, G. M. (1996). Neural connectivity only accounts for a small part of neural correlation in auditory cortex. *Exp. Brain Res.* 110, 379–91.

Fisher, N. I. (1993). *Statistical Analysis of Circular Data*. Cambridge: Cambridge University Press.

Geier, C., Bialonski, S., Elger, C. E., and Lehnertz, K. (2015). How important is the seizure onset zone for seizure dynamics'. *Seizure* 25, 160–166. doi: 10.1016/j.seizure.2014.10.013

Guevara, R., Velazquez, J. L., Nenadovic, V., Wennberg, R., Senjanovic, G., and Dominguez, L. G. (2005). Phase synchronization measurements using electroencephalographic recordings: what can we really say about neuronal synchrony? *Neuroinformatics* 3, 301–314. doi: 10.1385/NI:3:4:301

Haufe, S., Tomioka, R., Nolte, G., Müller, K. R., and Kawanabe, M. (2010). Modeling sparse connectivity between underlying brain sources for EEG/MEG. *IEEE Trans. Bio-Med. Eng.* 57, 1954–1963. doi: 10.1109/TBME.2010.2046325

Hu, S., Lai, Y., Valdés-Sosa, P. A., Brings-Vega, M. L., and Yao, D. (2018). How do the reference montage and electrodes setup affect the measured scalp EEG potentials? *J. Neural Eng.* 15:026013. doi: 10.1088/1741-2552/aaa13f

Klingspor, M. (2015). *Hilbert Transform : Mathematical Theory and Applications to Signal Processing*. Faculty of Science and Engineering, Linköping University.

Kramer, M. A., Eden, U. T., Lepage, K. Q., Kolaczyk, E. D., Bianchi, M. T., and Cash, S. S. (2011). Emergence of persistent networks in long-term intracranial {EEG} recordings. *J. Neurosci.* 31, 15757–15767. doi: 10.1523/JNEUROSCI.2287-11.2011

Kramer, M. A., Kolaczyk, E. D., and Kirsch, H. E. (2008). Emergent network topology at seizure onset in humans. *Epilepsy Res.* 79, 173–186. doi: 10.1016/j.eplepsyres.2008.02.002

Kuhnert, M. T., Elger, C. E., and Lehnertz, K. (2010). Long-term variability of global statistical properties of epileptic brain networks. *Chaos* 20:43126. doi: 10.1063/1.3504998

Latora, V., and Marchiori, M. (2001). Efficient behavior of small-world networks. *Phys. Rev. Lett.* 87:198701. doi: 10.1103/PhysRevLett.87.198701

Lehnertz, K., Ansmann, G., Bialonski, S., Dickten, H., Geier, C., and Porz, S. (2014). Evolving networks in the human epileptic brain. *Physica D* 267, 7–15. doi: 10.1016/j.physd.2013.06.009

Marzetti, L., Nolte, G., Perrucci, M. G., Romani, G. L., and Del Gratta, C. (2007). The use of standardized infinity reference in EEG coherency studies. *NeuroImage* 36, 48–63. doi: 10.1016/j.neuroimage.2007.02.034

Mitsis, G. D., Anastasiadou, M. N., Christodoulakis, M., Papathanasiou, E. S., Papacostas, S. S., and Hadjipapas, A. (2018). Multi-scale periodicities in the functional brain networks of patients with epilepsy and their effect on seizure detection. *bioRxiv[preprint]. bioRxiv:* 221036. doi: 10.1101/221036

Nevado, A., Hadjipapas, A., Kinsey, K., Moratti, S., Barnes, G. R., Holliday, I. E., et al. (2012). Estimation of functional connectivity from electromagnetic signals and the amount of empirical data required. *Neurosci. Lett.* 513, 57–61. doi: 10.1016/j.neulet.2012.02.007

Nicolaou, N., and Nasuto, S. J. (2007). Automatic artefact removal from event-related potentials via clustering. *J. VLSI Signal Process. Syst. Signal Image Video Technol.* 48, 173–183. doi: 10.1007/s11265-006-0011-z

Nolte, G., Bai, O., Wheaton, L., Mari, Z., Vorbach, S., and Hallett, M. (2004). Identifying true brain interaction from EEG data using the imaginary part of coherency. *Clin Neurophysiol.* 115, 2292–2307. doi: 10.1016/j.clinph.2004.04.029

Nunez, P. L. (2011). REST: a good idea but not the gold standard. *Clin. Neurophysiol.* 121, 2177–2180. doi: 10.1016/j.clinph.2010.04.029

Nunez, P. L., Silberstein, R. B., Shi, Z., Carpenter, M. R., Srinivasan, R., Tucker, D. M., et al. (1999). EEG coherency II: experimental comparisons of multiple measures. *Clin. Neurophysiol.* 110, 469–486. doi: 10.1016/S1388-2457(98)00043-1

Nunez, P. L., and Srinivasan, R. (2006). *Electric Fields of the Brain: The Neurophysics* of EEG. New York, NY: Oxford University Press.

Nunez, P. L., Srinivasan, R., Westdorp, A. F., Wijesinghe, R. S., Tucker, D. M., Silberstein, R. B., et al. (1997). EEG coherency. I: statistics, reference electrode, volume conduction, Laplacians, cortical imaging, and interpretation at multiple scales. *Electroencephalogr. Clin. Neurophysiol.* 103, 499–515. doi: 10.1016/S0013-4694(97)00066-7

Peraza, L. R., Asghar, A. U., Green, G., and Halliday, D. M. (2012). Volume conduction effects in brain network inference from electroencephalographic recordings using phase lag index. *J. Neurosci. Methods* 207, 189–199. doi: 10.1016/j.jneumeth.2012.04.007

Pereda, E., Quiroga, R. Q., and Bhattacharya, J. (2005). Nonlinear multivariate analysis of neurophysiological signals. *Prog. Neurobiol.* 77, 1–37. doi: 10.1016/j.pneurobio.2005.10.003

Qin, Y., Xu, P., and Yao, D. (2010). A comparative study of different references for EEG default mode network: the use of the infinity reference. *Clin. Neurophysiol.* 121, 1981–1991. doi: 10.1016/j.clinph.2010.03.056

Rubinov, M., and Sporns, O. (2010). Complex network measures of brain connectivity: uses and interpretations. *NeuroImage* 52, 1059–1069. doi: 10.1016/j.neuroimage.2009.10.003

Scargle, J. D. (1982). Studies in astronomical time series analysis. II. Statistical aspects of spectral analysis of unevenly spaced data. *Astrophys. J.* 263, 835–853. doi: 10.1086/160554

Stam, C. J., Nolte, G., and Daffertshofer, A. (2007). Phase lag index: assessment of functional connectivity from multi channel EEG and MEG with diminished bias from common sources. *Hum. Brain Mapp.* 28, 1178–1193. doi: 10.1002/hbm.20346

Thatcher, R. W. (2012). Coherence, phase differences, phase shift, and phase lock in EEG/ERP analyses. *Dev. Neuropsychol.* 37, 476–496. doi: 10.1080/87565641.2011.619241

Theiler, J., Eubank, S., Longtin, A., Galdrikian, B., and Farmer, J. D. (1992). Testing for nonlinearity in time series: the method of surrogate data. *Physica D* 58, 77–94. doi: 10.1016/0167-2789(92)90102-S

Varotto, G., Tassi, L., Franceschetti, S., Spreafico, R., and Panzica, F. (2012). Epileptogenic networks of type II focal cortical dysplasia: a stereo-EEG study. *NeuroImage* 61, 591–598. doi: 10.1016/j.neuroimage.2012.03.090

Vinck, M., Oostenveld, R., van Wingerden, M., Battaglia, F., and Pennartz, C. M. (2011). An improved index of phase-synchronization for electrophysiological data in the presence of volume-conduction, noise and sample-size bias. *NeuroImage* 55, 1548–1565. doi: 10.1016/j.neuroimage.2011.01.055

Watts, D. J., and Strogatz, S. H. (1998). Collective dynamics of "small-world" networks. *Nature* 393, 440–442.

Wilke, C., Worrell, G., and He, B. (2011). Graph analysis of epileptogenic networks in human partial epilepsy. *Epilepsia* 52, 84–93. doi: 10.1111/j.1528-1167.2010.02785.x

Xu, P., Xiong, X. C., Xue, Q., Tian, Y., Peng, Y., Zhang, R., et al. (2014). Recognizing mild cognitive impairment based on network connectivity analysis of resting EEG with zero reference. *Physiol. Measure.* 35:1279. doi: 10.1088/0967-3334/35/7/1279

Yao, D. (2001). A method to standardize a reference of scalp EEG recordings to a point at infinity. *Physiol Meas.* 22, 693–711. doi: 10.1088/0967-3334/22/4/305

Yao, D. (2017). Is the surface potential integral of a dipole in a volume conductor always zero? a cloud over the average reference of EEG and ERP. *Brain Topogr.* 30, 161–171. doi: 10.1007/s10548-016-0543-x

Yao, D., Wang, L., Oostenveld, R., Nielsen, K. D., Arendt-Nielsen, L., and Chen, A. C. (2005). A comparative study of different references for EEG spectral mapping: The issue of the neutral reference and the use of the infinity reference. *Physiol. Measure.* 26, 173–184. doi: 10.1088/0967-3334/26/3/003

Zar, J. H. (1999). *Biostatistical Analysis*. Upper Saddle River, NJ: Prentice Hall.

Zubler, F., Gast, H., Abela, E., Rummel, C., Hauf, M., Wiest, R., et al. (2014). Detecting functional hubs of ictogenic networks. *Brain Topogr.* 28, 305–317. doi: 10.1007/s10548-014-0370-x

Conflict of Interest Statement: The authors declare that the research was conducted in the absence of any commercial or financial relationships that could be construed as a potential conflict of interest.

Advantages of publishing in Frontiers

OPEN ACCESS
Articles are free to read for greatest visibility and readership

FAST PUBLICATION
Around 90 days from submission to decision

HIGH QUALITY PEER-REVIEW
Rigorous, collaborative, and constructive peer-review

TRANSPARENT PEER-REVIEW
Editors and reviewers acknowledged by name on published articles

Frontiers
Avenue du Tribunal-Fédéral 34
1005 Lausanne | Switzerland

Visit us: www.frontiersin.org
Contact us: info@frontiersin.org | +41 21 510 17 00

REPRODUCIBILITY OF RESEARCH
Support open data and methods to enhance research reproducibility

DIGITAL PUBLISHING
Articles designed for optimal readership across devices

FOLLOW US
@frontiersin

IMPACT METRICS
Advanced article metrics track visibility across digital media

EXTENSIVE PROMOTION
Marketing and promotion of impactful research

LOOP RESEARCH NETWORK
Our network increases your article's readership